p-ISSN 1607-3274
e-ISSN 2313-688X

Радіоелектроніка Інформатика Управління

Radio Electronics Computer Science Control

2025/2

Науковий журнал «Радіоелектроніка, інформатика, управління» (скорочена назва – РІУ) видається Національним університетом «Запорізька політехніка» (НУ «Запорізька політехніка») з 1999 р. періодичністю чотири номери на рік.

Реєстрація суб'єкта у сфері друкованих медіа: Рішення Національної ради України з питань телебачення і радіомовлення № 3040 від 07.11.2024 року. Ідентифікатор медіа: R30-05582.

ISSN 1607-3274 (друкований), **ISSN** 2313-688X (електронний).

Наказом Міністерства освіти і науки України № 409 від 17.03.2020 р. «Про затвердження рішень Атестаційної колегії Міністерства щодо діяльності спеціалізованих вчених рад від 06 березня 2020 року» **журнал включений до переліку наукових фахових видань України в категої «А» (найвищій рівень),** в яких можуть публікуватися результати дисертаційних робіт на здобуття наукових ступенів доктора наук і доктора філософії (кандидата наук).

Журнал включений до польського Переліку наукових журналів та рецензованих матеріалів міжнародних конференцій з присвоєною кількістю балів (додаток до оголошення Міністра науки та вищої освіти Республіки Польща від 31 липня 2019 р.: № 16981).

В журналі безкоштовно публікуються наукові статті англійською, російською та українською мовами.

Правила оформлення статей подано на сайті: http://ric.zntu.edu.ua/information/authors.

Журнал забезпечує **безкоштовний відкритий он-лайн доступ** до повнотекстових публікацій.

Журнал дозволяє авторам мати авторські права і зберігати права на видання без обмежень. Журнал дозволяє користувачам читати, завантажувати, копіювати, поширювати, друкувати, шукати або посилатися на повні тексти своїх статей. Журнал дозволяє повторне використання його вмісту у відповідності Creative Commons ліцензією CC BY-SA..

Опублікованим статтям присвоюється унікальний ідентифікатор цифрового об'єкта DOI.

Журнал входить до наукометричної бази Web of Science.

Журнал реферується та індексується у провідних міжнародних та національних реферативних журналах і наукометричних базах даних, а також розміщується у цифрових архівах та бібліотеках з безкоштовним доступом у режимі on-line, повний перелік яких подано на сайті: http://ric.zntu.edu.ua/about/editorialPolicies#custom-0.

Тематика журналу: телекомунікації та радіоелектроніка, програмна інженерія (включаючи теорію алгоритмів і програмування), комп'ютерні науки (математичне і комп'ютерне моделювання, оптимізація і дослідження операцій, управління в технічних системах, міжмашинна і людино-машинна взаємодія, штучний інтелект, включаючи системи, засновані на знаннях, і експертні системи, інтелектуальний аналіз даних, розпізнавання образів, штучні нейронні і нейро-нечіткі мережі, нечітку логіку, колективний інтелект і мультиагентні системи, гібридні системи), комп'ютерна інженерія (апаратне забезпечення обчислювальної техніки, комп'ютерні мережі), інформаційні системи та технології (структури та бази даних, системи, засновані на знаннях та експертні системи, обробка даних і сигналів).

Усі статті, пропоновані до публікації, одержують **об'єктивний розгляд**, що оцінюється за суттю без урахування раси, статі, віросповідання, етнічного походження, громадянства або політичної філософії автора(ів).

Усі статті проходять двоступінчасте закрите (анонімне для автора) **резензування** штатними редакторами і незалежними рецензентами – провідними вченими за профілем журналу.

РЕДАКЦІЙНА КОЛЕГІЯ

РЕДАКЦІЙНО-КОНСУЛЬТАТИВНА РАДА

Рекомендовано до видання Вченою радою НУ «Запорізька політехніка», протокол № 10 від 27.05.2025.

Журнал зверстаний редакційно-видавничим відділом НУ «Запорізька політехніка».

Веб-сайт журналу: http://ric.zntu.edu.ua.

Адреса редакції: Редакція журналу «РІУ», Національний університет «Запорізька політехніка», вул. Жуковського, 64, м. Запоріжжя, 69063, Україна.

Тел: (061) 769-82-96 – редакційно-видавничий відділ Факс: +38-061-764-46-62

E-mail: rvv@zntu.edu.ua

The scientific journal Radio Electronics, Computer Science, Control is published by the National University Zaporizhzhia Polytechnic NU Zaporizhzhia Polytechnic since 1999 with periodicity four numbers per year.

Registration of an entity in the field of print media: Decision of the National Council of Ukraine on Television and Radio Broadcasting No. 3040 of November 7, 2024. Media ID: R30-05582.

ISSN 1607-3274 (print), **ISSN** 2313-688X (on-line).

By the Order of the Ministry of Education and Science of Ukraine from 17.03.2020 № 409 "On approval of the decision of the Certifying Collegium of the Ministry on the activities of the specialized scientific councils dated 06 March 2020" **journal is included in the list of scientific specialized periodicals of Ukraine in category "A" (highest level),** where the results of dissertations for Doctor of Science and Doctor of Philosophy may be published.

The journal is included to tne Polish List of scientific journals and peer-reviewed materials from international conferences with assigned number of points (Annex to the announcement of the Minister of Science and Higher Education of Poland from July 31, 2019: Lp. 16981).

The journal publishes scientific articles in English, Russian, and Ukrainian free of charge.

The **article formatting rules** are presented on the site: http://ric.zntu.edu.ua/information/authors.

The journal provides policy of **on-line open (free of charge) access** for full-text publications. The journal allow the authors to hold the copyright without restrictions and to retain publishing rights without restrictions. The journal allow readers to read, download, copy, distribute, print, search, or link to the full texts of its articles. The journal allow reuse and remixing of its content, in accordance with Creative Commons license CC BY-SA.

Published articles have a unique digital object identifier (DOI).

The journal is included into Web of Science.

The journal is abstracted and indexed in leading international and national abstractig journals and scientometric databases, and also placed to the digital archives and libraries with a free on-line access, full list of which is presented at the site: http://ric.zntu.edu.ua/about/editorialPolicies#custom-0.

The journal scope: telecommunications and radio electronics, software engineering (including algorithm and programming theory), computer science (mathematical modeling and computer simulation, optimization and operations research, control in technical systems, machine-machine and man-machine interfacing, artificial intelligence, including data mining, pattern recognition, artificial neural and neuro-fuzzy networks, fuzzy logic, swarm intelligence and multiagent systems, hybrid systems), computer engineering (computer hardware, computer networks), information systems and technologies (data structures and bases, knowledge-based and expert systems, data and signal processing methods).

All articles proposed for publication receive an **objective review** that evaluates substantially without regard to race, sex, religion, ethnic origin, nationality, or political philosophy of the author(s).

All articles undergo a two-stage **blind peer review** by the editorial staff and independent reviewers – the leading scientists on the profile of the journal.

EDITORIAL BOARD

EDITORIAL-ADVISORY COUNCIL

Recommended for publication by the Academic Council of NU Zaporizhzhia Polytechnic, protocol № 10 dated 27.05.2025.

The journal is imposed by the editorial-publishing department of NU Zaporizhzhia Polytechnic.

The journal web-site is http://ric.zntu.edu.ua.

The address of the editorial office: Editorial office of the journal Radio Electronics, Computer Science, Control, National University Zaporizhzhia Polytechnic, Zhukovskiy street, 64, Zaporizhzhia, 69063, Ukraine.

Tel.: +38-061-769-82-96 – the editorial-publishing department. Fax: +38-061-764-46-62

E-mail: rvv@zntu.edu.ua

ЗМІСТ

CONTENTS

РАДІОЕЛЕКТРОНІКА ТА ТЕЛЕКОМУНІКАЦІЇ

RADIO ELECTRONICS AND TELECOMMUNICATIONS

UDC 621.39

EVALUATING THE EFFICIENCY OF MECHANISMS FOR FRAME BLOCKS TRANSMISSION IN NOISY CHANNELS OF IEEE 802.11 NETWORKS

Khandetskyi V. S. – Dr. Sc., Professor, Head of the Department of Electronic Computing Machinery, Oles Honchar Dnipro National University, Dnipro, Ukraine.

Karpenko N. V. – PhD, Associate Professor of the Department of Electronic Computing Machinery, Oles Honchar Dnipro National University, Dnipro, Ukraine.

Gerasimov V.V. – PhD, Head of the Department of Computer Science and Information Technologies, Oles Honchar Dnipro National University, Dnipro, Ukraine.

ABSTRACT

Context. Aggregating frames into blocks when transmitting information in wireless IEEE802.11 networks helps to significantly reduce overhead costs and increase the transmission rate. However, the impact of noise reduces the efficiency of such transmission due to an increased probability of distortion of longer messages. We compared the efficiency of data transmission by variable and constant size blocks formed from frames using VBS and FBS mechanisms correspondingly under conditions of noise varying intensity.

Objective. The purpose of this article is a comparative study of VBS and FBS mechanisms used for the formation and transmission of different sizes frame blocks under medium and high noise intensity.

Method. A simple model used in IEEE 802.11 networks to determine the DSF throughput for transmitting frames in infrastructure domains was modified by us to transmit frame blocks of different sizes under conditions of medium and high intensity noise affecting the transmission process. We use for transmission a discrete in time Gaussian channel without memory. In such a channel, bit errors are independent and equally distributed over the bits of the frame. The scale factors of the model for the number of frames in a block k = 6–40 at an average noise level corresponding to BER = 10^{-6} and k = 4–15 for high-intensity noise at BER = 10^{-5} are determined. The algorithm for calculation of the network throughput has been generalized. The investigation of the dependences of the throughput on the number of frames in the VBS blocks showed the presence of local maxima in dependences, located in the region of average values of the frames number. These maxima are more pronounced at increased data transfer rates.

Results. It is shown that with a small number of frames in a block (k = 6–9) and high-intensity noise, the efficiency of the FBS mechanism exceeds the efficiency of the VBS block formation mechanism. However, at the same noise level, an increase in the number of frames in a block ($k \geq 10$) makes the use of the VBS mechanism more preferable. This advantage is explained by the fact that the VBS mechanism at each subsequent stage of transmission forms a block from frames distorted at the previous stage, therefore the size of the blocks at subsequent stages decreases, increasing the number of frames successfully transmitted to the AP (due to the increase in the probability of transmitting shorter blocks). At the same time, the constant and small probability of successful transmission of a constant size block at each stage makes the probability of transmission of frames distorted at the previous stages low. The situation changes for noise of medium intensity. Here the transmission of each subsequent block in the range of up to 25 frames per block using the VBS method requires the use of two stages. The application of the FBS method in these conditions shows that only the first set of frames requires the use of two stages for its complete transmission. Then, due to the accumulation of frames at the previous stages, each subsequent stage of transmission completes the formation of the corresponding set in the memory of AP. Thus, when the noise intensity decreases to BER = 10^{-6} and below, the use of the FBS mechanism becomes more effective. The obtained results are illustrated with specific examples characterizing the formation and transmission of various frame blocks.

Conclusions. In this article, using a mathematical model modified by us, a comparative study was conducted on the efficiency of various mechanisms for forming and transmitting a frame block of different sizes under conditions of the impact of different intensity noise on the transmission process. The algorithm for calculating the network throughput was generalized, and the values of the throughput were determined when using the VBS and FBS network functioning mechanisms.

KEYWORDS: IEEE 802.11 wireless networks, throughput, noise intensity, BER, frame blocks, VBS and FBS mechanisms.

ABBREVIATIONS

AP is an access point;
STA is a station;
BER is a bit error rate;
FER is a frame error rate;
BFER is a block frames error rate;
DCF is a Distributed Coordination Function;
ACK is a frame acknowledgment;
DIFS is an inter-frame space;
SIFS is a short inter-frame space;

DOI 10.15588/1607-3274-2025-2-1

MAC is a Medium Access Protocol;
BAR is a Block ACK Request;
BA is a Block ACK;
TCP is a Transfer Control Protocol;
EDCA is an Enhanced Distributed Channel Access;
VBS is a variable block size;
FBS is a fixed block size;
WLAN is a Wireless Local Area Network.

NOMENCLATURE

bE is a number of erroneous bits;
R is a data transfer rate;
t is a transmission time;
L_{data} is a length of the frame data field in bits;
E_b is an energy per bit;
N_0 is a noise power spectral density;
P_b is a bit error probability;
P_f is a frame error probability;
P_C is a probability of a data block collision in ideal channel;
P_B is a probability of a data block corruption by interference during transmission;
P_{Sr} is a relative probability of successful block transmission;
P_S is a probability of successful block transmission;
k is a number of frames in a block;
T_{DIFS} is an inter-frame space duration;
T_{SIFS} is a short inter-frame space duration;
T_{PHYhdr} is a transmission time of the frame's physical layer header;
$T_{\overline{CW}}$ is an average length of the backoff;
$CW_{\min}$ is a minimum contention window length;
T_{ACK} is an acknowledgment frame duration;
S_{id} is an ideal DCF throughput;
S_k is a real throughput when using block transmission;
δ is a propagation delay;
σ is a duration of one slot.

INTRODUCTION

The share of traffic transmitted by Wi-Fi devices in the total traffic of wireless networks over the past decade is approximately half. Wi-Fi technologies are rapidly developing, maintaining their positions in competitive activity [1, 2].

Despite significant progress in solving WLANs problems, achieved in the development of modern networks such as IEEE 802.11ac and 802.11ax, the effective throughput increases slowly, especially in dense networks operating under conditions of high external and internal noise intensity [3–5].

As noted by US Federal Communications Commission (FCC), an urgent problem for technologies using wide frequency channels (Δf = 160 MHz) is "clearing the frequency range". The effect of increasing interference is also observed with a decrease in the inter-symbol interval of transmitted data and with an increase in the number of subcarrier frequencies. The concentration of several spatial streams in one region of the channel leads to an increase in the mutual influence of signals too. This effect is further enhanced with an increase in the intensity of external noise, blurring the distinctive features of signals of different streams. Another challenge in wireless networks is the handover, which is the process of switching users from one AP to other [6].

Electromagnetic interference increases significantly when wireless networks operate in industrial environments. Sources of electromagnetic radiation such as vehicles, industrial equipment, electric motors, switching devices, high-voltage equipment, and fluorescent lamps produce intense noise.

High level of industrial interference increases BER (bit error rate) in transmission channel [7, 8]. The result is an increased loss of frames during transmission, retransmission of frame copies which in turn decreases the network throughput.

To reduce the overhead costs when transmitting data in separate frames, a block transfer mechanism was proposed [9–11]. This mechanism provides that a block of frames from one flow can be sent without acknowledging that the AP has correctly received each individual frame. After the block transmission the STA initiates a BAR frame to enquire the number of frames that have been received successfully. The AP then responds with a BA frame. The efficiency of this scheme comes from the fact that the overhead is greatly reduced, because DIFS and backoff intervals only occur before the first frame of the block and only one acknowledgment is used for all frames in the block (BA).

A similar principle is used by the TCP transport protocol when transmitting data segments in wired networks [12, 13].

The concept of EDCA used in IEEE 802.11e [14–16] provides two mechanisms for composition of frame blocks during the transmission process. A block of data can be formed using only those frames that were corrupted during the transmission of the previous block. In such a case referred to as VBS, data frames block size varies over time from one transmission stage to next. In other cases, a data block can also be composed on corrupted frames as well as newly transmitted frames, so that the data frames block size is kept at the maximum size specified at the initial stage. Thus, the data block size does not change over time and refers to this as FBS.

The object of study is the process of transmitting information in wireless networks using VBS and FBS mechanisms for the formation and transmission of frame blocks under conditions of medium and high intensity external noise.

The subject of study is the mathematical models of IEEE.802.11 BA networks using VBS and FBS operating mechanisms under conditions of noise influence on the transmission process.

The purpose of the paper is a comparative study of the efficiency of frame blocks transmission formed using the VBS and FBS mechanisms under the influence of variable intensity noise.

DOI 10.15588/1607-3274-2025-2-1

1 PROBLEM STATEMENT

Interferences that have various physical natures differ in their spectral composition. At the same time, it is important to study the general patterns of the interference influence on data transmitted in wireless networks over a radio channel. For this purpose, it is advisable to use Gaussian noise as the most general noise model that describes a wide range of noise sources and their superposition quite well [8, 17]. An example of a simple channel model that is widely used in information theory is additive white Gaussian noise channel without fading [18].

One of the changes that modern digital communication systems have brought to radio engineering is the need to end-to-end performance evaluations. The measure of that performance is usually bit error rate (BER), which quantified the reliability of the radio system from "bits in" to "bits out" [19]:

$$\mathrm{BER} = \frac{\text{number of corrupted bits}}{\text{total number of bits}} = \frac{bE}{R \cdot t}, \qquad (1)$$

where bE is the number of erroneous bits, R is the data transfer rate, t is the transmission time.

In a noisy channel, the BER is often expressed as a function of the normalized carrier-to-noise ratio denoted E_b/N_0. The Gaussian approximation of the noise in determining the BER is used to estimate the number of iterations needed to the convergence of the parity code decoder in function of the level of noise power [20]. Bit-error rate analysis of low-density parity-check codes using Gaussian approximation of a channel is considered in [21].

In general, errors at different locations of an information sequence of length L can occur with different probabilities. In this article, we use for transmission a time-discrete channel without memory with white Gaussian noise. A channel of this type is characterized by the fact that the bit errors in it are independent and equally distributed over the bits of the frame data [22, 23].

Let L and P_b correspond the frame length and bit error rate (BER), respectively, and P_f correspond the frame error rate (FER). Then the probability that a frame of length L will be transmitted undistorted is equal:

$$q = (1-P_{b1})(1-P_{b2})(1-P_{b3})...(1-P_{bL}) = (1-P_b)^L, \qquad (2)$$

where $P_{b1}= P_{b2}= P_{b3}=\ldots= P_{bL}= P_b$. In this case, the probability of frame distortion is equal to

$$P_f = 1-(1-P_b)^L. \qquad (3)$$

The probability of successful (error-free) transmission of a data block by the STA to AP can be expressed as follows:

$$P_S = (1-P_C)(1-P_B) = (1-P_C)(1-P_b)^{k \cdot L}. \qquad (4)$$

The P_C is traditionally determined using Markov-chain models [24–26].

Let us analyze the influence of the intensity of external interference or, in other words, the noise level in the communication channel on the probability of the block successful transmission. At the same time, since in accordance with (4) the influence of the collision's intensity P_C and external interference P_b is carried out on P_S separately [27], it is possible, without reducing the reliability of the analysis, to fix P_C at the certain level and consider the influence P_b on the relative value of $P_{Sr}= P_S/(1–P_C)$.

Table 1 shows the dependence of P_{Sr} on k (L=12000 bits) for three levels P_b=BER=10^{-7}, 10^{-6}, 10^{-5}.

If we assume that P_C is zero, then $P_{Sr}= P_S$ and from Table 1 it follows that the probability of a block successful transmission in case BER=P_b=10^{-5} decreases significantly with increasing k.

In the ideal case, the channel is regarded as perfect, i.e. neither error not collisions occur, and in any transmission cycles there is only one active STA which always has backlogged frame in queue between the MAC and its upper layer waiting to be transmitted. The receiver (AP – in infrastructure network) only responds with ACK (AC-Knowledgment) and the other STAs just sense the channel and wait. Then the ideal DCF throughput S_{id} taking into account [9, 28] can be defined as

$$S_{id} = \frac{L_{data}}{T_{DIFS} + T_{C\overline{W}} + T_F + T_{ACK} + 2\delta}, \qquad (5)$$

where $T_{C\overline{W}} = \frac{\sigma \cdot (CW_{\min} - 1)}{2}$ and $T_F = T_{PHYhdr} + \frac{L_{data}}{R} + T_{SIFS}$.

Each frame includes a common physical header whose duration T_{PHYhdr} has to be added to the frame transmission time [10].

The block transmission scheme in protected mode is illustrated in Fig. 1.

Table 1 – Dependences of P_{Sr} on k for different values of noise intensity P_b

BER=P_b=10^{-7}											
P_{Sr}	0.999	0.998	0.996	0.995	0.994	0.993	0.990	0.988	0.982	0.976	0.965
k	1	2	3	4	5	6	8	10	15	20	30
BER=P_b=10^{-6}											
P_{Sr}	0.988	0.976	0.965	0.953	0.942	0.931	0.908	0.887	0.835	0.787	0.697
k	1	2	3	4	5	6	8	10	15	20	30
BER=P_b=10^{-5}											
P_{Sr}	0.887	0.787	0.697	0.619	0.549	0.487	0.383	0.301	0.165	0.09	0.03
k	1	2	3	4	5	6	8	10	15	20	30

DOI 10.15588/1607-3274-2025-2-1

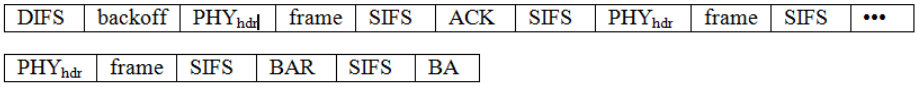

Figure 1 – The scheme of data frames block transmission

The transmission speed can be significantly increased by combining frames into blocks and transmitting them using the VBS and FBS mechanisms. It is of considerable interest to conduct a comparative analysis of the efficiency of these mechanisms when changing the sizes of transmitted blocks and in the presence of Gaussian noise of varying intensity in the transmission channel.

2 REVIEW OF THE LITERATURE

Supporting real-time communications over IEEE 802.11 WLANs is very important yet challenging due to limited channel capacity, unstable channel conditions and a low transmission delay requirement of real-time traffic [29]. In [30] the authors provided a closed formula, based on some approximations, for the configuration of the parameters $CW_{\min}$ and $CW_{\max}$, where CW is the contention window in backoff mechanism of a frame transmission. In [31] the authors built an analytical model to derive an average delay estimate for the traffic of different priorities in the unsaturated 802.11e WLANs.

The majority of analytical works on the delay performance of IEEE 802.11 focuses on predicting only the mean MAC delay, although higher layer application and protocols are interested in the total performance of the MAC layer. The analysis presented in [32] applies to the priority schemes of the of the EDCA mechanism of the IEEE 802.11e standard. However, by using an appropriate parameter setting, the results presented are also applicable to the legacy 802.11 DCF. In [33] authors note that for analytical tractability and simplicity, most exiting performance models of transmission opportunity (TXOP) have been restricted to unrealistic working scenarios where the traffic follows a Poisson process, which is unable to capture to heterogeneous characteristics of multimedia traffic. IEEE 802.11e EDCA induces service differentiation by appropriate joint turning of for adjustable contention parameters.

In [3] authors consider the situation in which a transmitter attempts to communicate reliably over a discrete memoryless channel. In [34] authors analyze additive white Gaussian noise at both the receiver and the warden for covert communication. The next generation of wireless communication technologies is accelerating the transformation of industrial Internet of things (IIoT) [4]. In [5] authors consider adversary's noise and channel uncertainties and analyze their impact on throughput of covert messages.

Congestion is the main cause of losses in wired networks, but in today's heterogeneous networks, loss events can also be introduced due to higher error rates on wireless channels, host mobility and frequent handovers [35]. Interference is the main performance-limiting factor in most wireless networks [36]. The interference ranges in a mentioned literature are set without fully considering the effect of the networks. The setting of the interference range is rather heuristic and remains an open problem [37].

In the case of collision, at least two stations (STAs) start transmission in the same slot, each of them sends out a whole block and BAR frame and then waits for the BA frame. The access point (AP) shall not send back the BA frames when it detects a collision. The STAs can't receive the BA frames successfully, and then they have to retry their transmission again.

In the erroneous case due to interference STA sends to AP a whole block and BAR frame as usual. The AP then sends back a BA frame to indicate which frames are corrupted.

The authors of article [10] justify the expediency of using the frame block protection mechanism during transmission. In this case, successful transmission of the first frame in a block is notified via immediate ACK. Otherwise, even if the first frame in a block collides with other frames transmitted by other stations, the transmitting station will continue to transmit the next frames in a block since it cannot determine such a collision. This can lead to severe performance degradation.

The BA frame contains information about the reception of the whole block through a corresponding bitmap. Both the BAR and BA frames are transmitted at the same rate used for the data frame transmission. After each BA the STA transmits the corrupted frames composed in a subsequent block.

Network performance is affected by two different states: the probability of having successful channel access and the channel utilization efficiency [24]. The first state depends on the number of competing stations. The second state depends on the overhead, in terms of headers, control frames and retransmissions required for the data delivery, and it is a function of the frame error rate.

3 MATERIALS AND METHODS

If the mechanism of variable blocks size (VBS) is used when transmitting data, then after receiving frame BA the next block is formed only from frames distorted at the previous state. Let's analyze the operation of this mechanism at average noise intensity BER=P_b=10^{-6} using the example of a block with k=20. The corresponding transmission scheme using the protection mode is shown in Fig.2.

In the fields of the scheme in Fig. 2, designated by the letter F, we integrate the physical layer header PHY_{hdr}, the frame itself and the short inter-frame interval SIFS.

The probability of successful transmission of a separate frame F1, which performs the block protection function, is equal to P_S=0.988, and we assume that this frame will be successfully transmitted. The probability of suc-

DOI 10.15588/1607-3274-2025-2-1

cessful transmission of an entire block consisting of 20 frames at BER=P_b=10^{-6} is equal to

$$P_{S,k=20} = (1-P_b)^{L_0 \cdot k} = 0.787\,, \qquad (6)$$

that is, we can assume that statistically approximately 16 frames from a block successfully passed to the AP, and 4 distorted frames (for example F3, F7, F11, F15), as shown in Fig.2, are transmitted at the second stage. In this case, taking into account (5), the throughput is

$$S_{k=20} = \frac{21 \cdot L_{data}}{2(T_{DIFS} + T_{\overline{CW}} + T_{ACK}) + 4T_{SIFS} + 25 \cdot T_F + 2T_{BAR} + 2T_{BA} + 8\delta}\,. \qquad (7)$$

DIFS	backoff	F1	ACK	SIFS	F2	F3	F4	F5	F6	F7	•••	F21	BAR	SIFS	BA

DIFS	backoff	F3	ACK	SIFS	F7	F11	F15	BAR	SIFS	BA

Figure 2 – The VBS transmission scheme for a block containing k = 20 frames at BER = P_b = 10^{-6}

For forty frames in a block (k = 40) with the same level of interference in the channel (BER = P_b = 10^{-6}), the transmission scheme is shown in Fig. 3.

DIFS	backoff	F1	ACK	SIFS	F2	F3	F4	F5	F6	F7	•••	F41	BAR	SIFS	BA

DIFS	backoff	F2	ACK	SIFS	F4, F7, F10, F13, F16, F19, F21, F24, F27, F30, F33, F36, F38, F40	BAR	SIFS	BA

DIFS	backoff	F4	ACK	SIFS	F21	BAR	SIFS	BA

Figure 3 – The VBS transmission scheme for a block containing k = 40 frames at BER = P_b = 10^{-6}

The probability of successful transmission of a block, consisting of k = 40 frames, calculated similarly to (6), is equal to $P_{S,k=40}$ = 0.619. Thus, it can be assumed that statistically approximately 25 frames from a block successfully passed to the access point, and 15 frames (for example F2, F4, F7, F10, F13, F16, F19, F21, F24, F27, F30 F33, F36, F38 and F40), as shown in Fig. 3, are transmitted at the second stage. The probability of successful transmission of a block formed at the second stage and containing 14 frames at BER=P_b=10^{-6} is $P_{S,k=14}$=0,845. From this number, statistically 12 frames will successfully reach the access point, and 2 frames (for example F4, F21) will be distorted and will be transmitted already at the third stage. In this case, the throughput is

$$S_{k=40} = \frac{41 \cdot L_{data}}{3(T_{DIFS} + T_{\overline{CW}} + T_{ACK}) + 6T_{SIFS} + 58 \cdot T_F + 3T_{BAR} + 3T_{BA} + 12\delta}\,. \qquad (8)$$

Similar calculations were carried out for blocks with k = 6, 10, 15, 25 and 30. The resulting throughput values for blocks of different lengths when changing the data transfer rate R are shown in Table 2. The following parameters were used in the calculations [9, 38]: T_{SIFS}=16 μs, σ = 9 μs, T_{DIFS}=34 μs, T_{PHYhdr} = 20 μs, $CW_{\min}$=16, 2δ=0,7 μs, T_{BAR}=21,8 μs, T_{BA}=31 μs, L_{data}=12000 bit.

Graphical dependencies of throughput S_k on the number of frames in a block k at different data transfer rates R are shown in Fig.4. As can be seen from the figure, the curves are characterized by the presence of a maximum in the area of average k values. As data rates increase, these maximums become more pronounced.

Let's analyze the effect of high-intensity noise with BER=P_b=10^{-5} on the process of block data transmission using the VBS mechanism. The process of transmitting a block with k=15 frames in protected mode is described schematically in Fig. 5.

Table 2 – The throughput values S_k at different k and R when BER=P_b=10^{-6}

k	S_k							
	R, Mbps							
	108	162	216	270	324	378	432	486
6	67.8	85.8	98.9	108.8	116.7	123.0	128.2	132.6
10	63.0	79.9	92.3	101.8	109.3	115.4	120.4	124.6
15	62.6	80.0	93.0	102.9	110.9	117.3	122.7	127.2
20	61.5	79.5	93.1	103.8	112.3	119.4	125.3	130.3
25	60.9	79.2	93.2	104.3	113.3	120.7	126.9	132.2
30	56.6	73.6	86.6	96.9	105.2	112.1	117.9	122.8
40	53.7	70.2	82.9	93.0	101.2	108.0	113.8	118.7

DOI 10.15588/1607-3274-2025-2-1

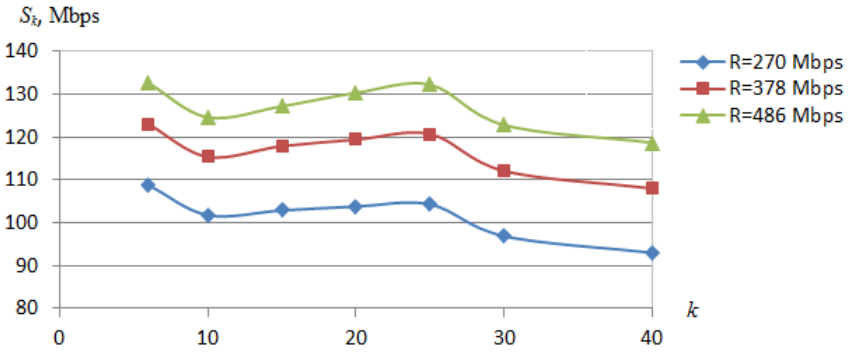

Figure 4 – Dependence of network throughput S_k on the number of frames k in a block. Data transfer is carried out using the VBS method at BER=P_b=10^{-6}

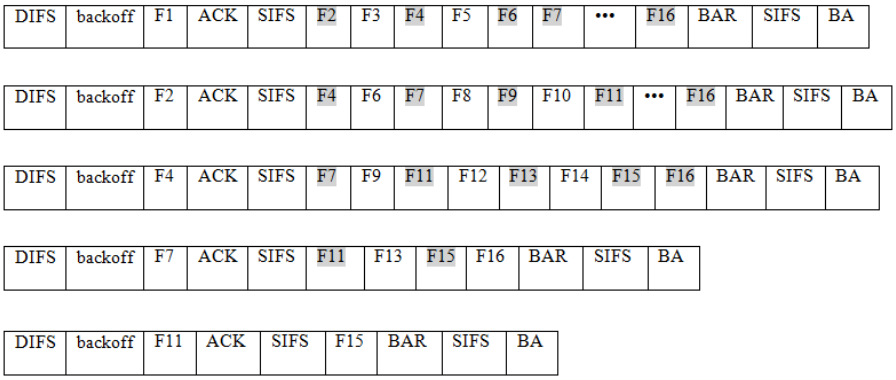

Figure 5 – The VBS transmission scheme for a block containing k = 15 frames at high interference intensity (BER=P_b=10^{-5})

The probability of successful transmission of a fifteen frames block when BER=P_b=10^{-5} is equal to

$$P_{S,k=15} = (1 - P_b)^{L_0 \cdot k} = 0.165, \quad (9)$$

that is, at the first stage statistically 2 frames successfully pass through the channel, and 13 are distorted (F2, F4, F6, F7, F8, F9, F10, F11, F12, F13, F14, F15, F16 in the designation of the blocks of the scheme in Fig. 5).

These frames are transmitted at the second stage, with F2 acting as a diagnostic frame, and a last 12 forming a block. The probability of successful transmission of this block is 0,237, therefore we assume that at this stage 3 frames successfully pass through the channel (F6, F8 and F10), and 9 are distorted (F4, F7, F9, F11, F12, F13, F14, F15, F16).

The indicated 9 frames are transmitted at the third stage, with F4 acting as a diagnostic frame, and a last 8 forming a block. The probability of successful transmission of this block is 0.383, so we assume that at this stage on average 3 frames successfully pass through the channel (F9, F12 and F14), and 5 are distorted (F7, F11, F13, F15, F16).

These frames are transmitted at the fourth stage, with F7 acting as a diagnostic frame, and a last 4 forming a block. The probability of successful transmission of this block is 0,619, therefore we assume that at this stage on average 2 frames successfully pass to the access point (F13 and F16), and 2 are distorted (F11 and F15). As shown in the scheme, they are successfully transmitted at the fifth stage.

In this case, the network throughput is calculated as follows:

$$S_{k=15} = \frac{13 \cdot L_{data}}{5(T_{DIFS} + T_{C\overline{W}} + T_{ACK}) + 10T_{SIFS} + 45 \cdot T_F + 5T_{BAR} + 5T_{BA} + 20\delta}. \quad (10)$$

Similar calculations were carried out for blocks with k = 4, 6, 8, 10, and 12. The throughput values for all these blocks when changing the data transfer rate R are shown in Table 3.

Graphs of the throughput S_k on k dependences for R = 270, 378, and 436 Mbps are shown in Fig. 6.

As can be seen from figure 6, the curves characterized by the presence of a local maximum in the vicinity of k=10. The values of these maxima, as well as the absolute values of the throughput at high noise level BER=P_b=10^{-5} are significantly smaller compared to the previous case described in section 4.1 where BER=P_b=10^{-6}.

DOI 10.15588/1607-3274-2025-2-1

Table 3 – The throughput values S_k at different k and R when BER=P_b=10^{-5}

k	S_k							
	R, Mbps							
	108	162	216	270	324	378	432	486
4	41.5	50.5	56.7	61.2	64.6	67.3	69.5	71.3
6	38.9	48.0	54.3	58.9	62.5	65.3	67.6	69.5
8	36.2	45.2	51.7	56.5	60.2	63.2	65.6	67.6
10	35.5	44.9	51.8	57.0	61.1	64.4	67.2	69.5
12	32.0	40.2	46.2	50.7	54.2	57.0	58.1	61.3
15	25.1	32.0	37.2	41.2	44.3	46.9	49.1	50.9

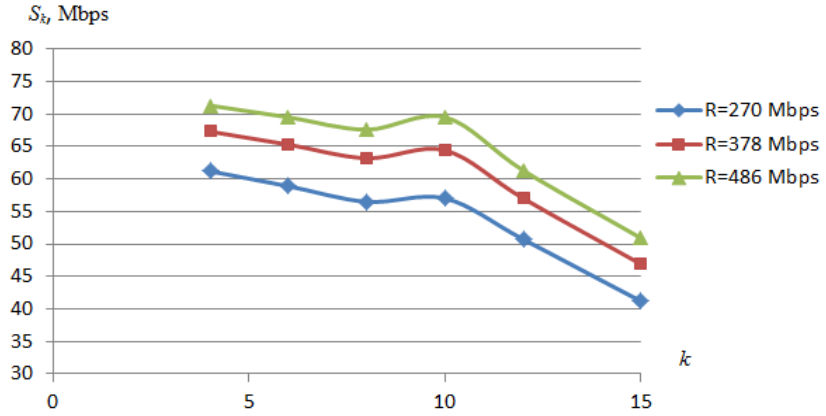

Figure 6 – Dependence of network throughput S_k on the number of frames k in a block. Data transfer is carried out using the VBS method at BER = P_b = 10^{-5}

In this work, to study the efficiency of data transmission using the VBS method under noise, we modified expression (1), which was originally proposed to calculate the throughput of a WLAN in ideal case of no noise. Keeping the simplicity of the original model, we propose to determine the influence of noise within the framework of the following model:

$$S_k = \frac{(k+1)\cdot L_{data}}{\alpha(T_{DIFS} + T_{\overline{CW}} + T_{ACK}) + \beta T_{SIFS} + \gamma T_F + \eta(T_{BAR} + T_{BA}) + \lambda\delta}. \quad (11)$$

The values of the coefficients α, β, γ, η, and λ for all k involved in calculation and two noise levels (BER) are collected in Tab.4. The dependences of the coefficient γ on k for different noise levels are shown in Fig. 7.

Table 4 – Values of coefficients in model (11)

Noise level, BER	Number of frames in each block k	Model coefficients				
		α	β	γ	η	λ
10^{-6}	6	1	2	7	1	4
	10	2	2	12	1	6
	15	2	4	18	2	8
	20	2	4	25	2	8
	25	2	4	32	2	8
	30	3	4	41	2	10
	40	3	6	58	3	12
10^{-5}	4	2	4	7	2	4
	6	3	4	11	2	10
	8	3	6	16	3	12
	10	3	6	21	3	12
	12	4	8	29	4	16
	15	5	10	45	5	20

DOI 10.15588/1607-3274-2025-2-1

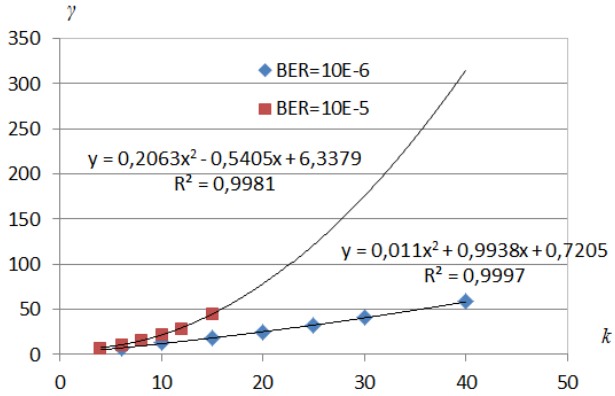

Figure 7 – Dependences of coefficient γ in (11) on the number of frames in block k for different noise levels

Let us generalize the algorithm for determining the network throughput.

1. At the first stage, using the noise level BER=P_b and the total data length of the frame's block $L_0 \cdot k$ we calculate the probability of successful block transmission $P_S^{(1)}$ using formulas (6). By multiplying the resulting probability $P_S^{(1)}$ by the number of frames in the block k and going to the nearest integer, we will obtain the average number of frames that will be successfully transmitted to the access point AP:

$$k_{AP}^{(1)} = [k \cdot P_S^{(1)}], \tag{12}$$

where [] denotes going to the nearest integer value.

If the number of frames $k_{AP}^{(1)}$ is less, than the number of frames in the block k, then they difference indicates frames distorted by interference, which, in accordance with the VBS method, will form a new block for transmission in the second stage:

$$k_D^{(2)} = [(k - k_{AP}^{(1)})]. \tag{13}$$

2. One is subtracted from the obtained value $k_D^{(2)}$ (10) (one frame performing the channel diagnostic function is transmitted before the block and its delivery is confirmed by a separate receipt ACK), the remaining number of frames is subjected to a procedure similar to (12):

$$k_{AP}^{(2)} = [(k_D^{(2)} - 1) \cdot P_S^{(2)}] = [(k_D^{(2)} - 1) \cdot (1 - P_b)^{L_0 \cdot (k_D^{(2)} - 1)}]. \tag{14}$$

In this case, the number of frames distorted during transmission at the second stage and intended for transmission at the third stage is

$$k_D^{(3)} = (k_D^{(2)} - 1) - k_{AP}^{(2)}. \tag{15}$$

3. These frames form the corresponding block at the third stage and the procedure is repeated:

$$k_{AP}^{(3)} = [(k_D^{(3)} - 1) \cdot P_S^{(3)}] = [(k_D^{(3)} - 1) \cdot (1 - P_b)^{L_0 \cdot (k_D^{(3)} - 1)}], \tag{16}$$

$$k_D^{(4)} = (k_D^{(3)} - 1) - k_{AP}^{(3)}. \tag{17}$$

Continuing this algorithm, we obtain its generalization in the following form:

$$k_{AP}^{(i)} = [(k_D^{(i)} - 1) \cdot P_S^{(i)}] = [(k_D^{(i)} - 1) \cdot (1 - P_b)^{L_0 \cdot (k_D^{(i)} - 1)}], \tag{18}$$

$$k_D^{(i+1)} = (k_D^{(i)} - 1) - k_{AP}^{(i)}. \tag{19}$$

Here symbol i denotes the number of transmission stages in the VBS method.

4 EXPERIMENTS

Let us first consider the transmission of blocks of a fixed size under conditions of high-intensity noise BER=P_b=10^{-5}. Let's assume that the transmitted block contains 6 frames of standard length (see section 3). The probability of successful transmission of the entire block is equal to $P_{S,k=6}$ =0.487, that is, approximately half of the frames of this block will be distorted (for example F2, F4, and F6).

But, unlike the VBS method, now, in order to maintain the constant block size, these frames are complemented with four new frames with the following numbers in order, forming the block – $F2_d$, $F4_d$, $F6_d$, F8, F9, F10, and F11 (the symbol d hereinafter denotes distorted frames; at the first stage, frames from 1 to 7, inclusive, took part in the transmission process and F1 diagnoses transmission environment). From the frames distorted at the first stage of transmission, we select a frame that will be diagnostic at the second stage, for example $F2_d$. This frame is separately confirmed by a receipt, and according to Section 3.2, the probability of its successful transmission is 0,887, that is, it is sufficiently high. Thus, at the second stage, the following block is formed for transmission: $F4_d$, $F6_d$, F8, F9, F10, and F11.

We assume that, as in the first stage, three frames are successfully transmitted to the access point, and three are distorted. Let's estimate the probability that copies of frames $F4_d$, $F6_d$ will be included in the number of successfully transmitted frames at the second stage. For this,

DOI 10.15588/1607-3274-2025-2-1

we will use the well-known formula of a probability theory [17]:

$$P_A = \frac{C_M^m \cdot C_{N-M}^{n-m}}{C_N^n}. \quad (20)$$

Here

$$C_N^n = \frac{N(N-1)(N-2)...1}{[n(n-1)(n-2)...1]\cdot[(N-n)(N-n-1)(N-n-2)...1]}. \quad (21)$$

In these formulas N is the number of frames in the sent block ($N = 6$); n is the total number of frames that were distorted during transmission ($n = 3$); M is the number of copies of distorted frames included in the block for transmission at the second stage ($M = 2$); m is the number of frame copies that are planned as successfully transmitted to the AP. In our case, for $m = 2$, $P_A = 0.2$, i.e. successful transfer at the second stage of copies $F4_d$ and $F6_d$ is the rare event. However, for $m = 1$, $P_A = 0.6$, i.e. successful transmission of $F4_d$ or $F6_d$ can be accepted. Let's assume that it is $F4_d$.

Thus, frame $F6_{dd}$ is included in the block for transmission at the third stage, as well as, for example, frames $F8_d$ and $F10_d$. From among these frames, a frame diagnosing the transmission environment in protected mode is selected. The probability of choosing the $F6_{dd}$ frame out of three is 1/3, and the total probability for the third and fourth stages of transmission is 2/3. Therefore, it can be assumed that the $F6_{dd}$ frame will be sent at one of these stages, and all 7 frames of the first set (F1 – F7) will finally be collected in the buffer memory of the AP. At the same time, it will be possible to form this set of frames in the required sequence and send it to the network. In the best case, this will be done after the third stage of transfer, in more likely – after the fourth stage. In the case of using the VBS method (see subsection 3.2), the formation of the entire first set in the desired sequence of frames took place immediately after the third stage of transmission.

But it should be taken into account that in the third and fourth stages, the frames of other sets will also be stored in the memory of the AP, which characterizes the potential possibility of forming complete sets for transmission over the network in the following stages. Let's consider this.

After the first stage of transmission, the access point will receive frames $F1_1$, $F3_1$, $F5_1$, $F7_1$, from the first set. It will not be able to send these frames to the network until this set is received completely and its frames are formed in the required sequence.

After the second stage of transmission, copies of frames $F2_d$ and $F4_d$ are added to the first set, and frames F9 and F11 from the second set are added to the access point.

After the third stage of transfer, frame $F6_{dd}$ is not added to the first set (the most realistic option is selected), and 3 frames are added to the second and third sets, for example $F10_d$, F13 to the second and F15 to the third block.

After the fourth stage of transmission, a copy of the $F6_{ddd}$ frame is finally added to the first set, completing its formation, and two more frames enter the memory of the AP, for example, $F14_d$ to the second block and F17 to the third block.

As a result, after the end of the fourth stage of transmission, the access point contains: a fully formed first set of frames (F1 – F7), as well as 5 frames of the second and 2 frames of the third set, which in total is equivalent to a complete set of frames.

Thus, under the considered conditions: a significant intensity of external noise – BER =10^{-5} and a small block length (k = 6–9 frames), it can be assumed that the efficiency of the FBS method exceeds the efficiency of the VBS method, which was studied in the previous section.

Let's analyze for comparison the option of transmitting longer blocks of frames (k =10) with the same significant noise intensity BER=10^{-5}.

At the first stage, the following set of frames is prepared for transmission: F1, F2, F3, F4, F5, F6, F7, F8, F9, F10, F11. The probability of successful transmission of a ten frames block (F2–F11) is $P_{S,k=10}$=0.301, which assumes the successful delivery of three frames plus a diagnostic frame F1. Suppose it will be F3, F5, F7.

Then, in the second stage, frames $F2_d$, $F4_d$, $F6_d$, $F8_d$, $F9_d$, $F10_d$, $F11_d$, F12, F13, F14, F15 will be prepared for transmission. Seven frames from this set were distorted in the process of the first stage of transmission, so copies of they were prepared for transmission, which were supplemented to a complete block by four new frames with consecutive numbers. A copy of the distorted frame is chosen as the diagnostic frame due to the higher probability of such a choice.

From the composition of this block, three frames will be successfully delivered to the access point. Due to the large number of the frame's copies in the set, we believe that there will be two copies and one frame from among the added ones, for example $F4_d$, $F8_d$ and F13. Thus, after the second stage of transmission, frames F1, $F2_d$, F3, $F4_d$, F5, F7, $F8_d$ from the first block and F13 from the second block will be accumulated in the buffer memory of the access point.

At the third stage of transmission, copies of distorted frames $F6_{dd}$, $F9_{dd}$, $F10_{dd}$, $F11_{dd}$, $F12_d$, $F14_d$, $F15_d$ will be used to form a block, which will be supplemented with frames F16, F17, F18, F19. The BA frame sent by the AP will contain information about distorted frames. Considering, that 4 out of 7 frames were distorted in the first stage, and in the second it was repeated with their copies, it is reasonable to choose a diagnostic frame from among them, let it be $F6_{dd}$. Then, in the third stage, will be sent the next set of frames: $F6_{dd}$_ $F9_{dd}$, $F10_{dd}$, $F11_{dd}$; $F12_d$, $F14_d$, $F15_d$; F16, F17, F18, F19. Three groups of frames, separated by the sign ";" are approximately equal in number, so let's assume that frames $F10_{dd}$, $F14_d$, F17, one from each group, will reach the AP undistorted. Thus, after the third stage of transmission, 9 frames of the first set will be accumulated in the memory of AP (two frames are missing from the full set, according to our example,

DOI 10.15588/1607-3274-2025-2-1

these are F9 and F11), as well as frames F13, F14, F17 from the second set.

Copies of frames $F9_{ddd}$, $F11_{ddd}$; $F12_{dd}$, $F15_{dd}$; $F16_{d}$, $F18_{d}$, $F19_{d}$ will be included to block in the fourth stage of transmission; which will be supplemented with frames F20, F21, F22, F23. The distorted frames form three, approximately equal groups, so it is more reasonable to expect that $F9_{ddd}$ or $F11_{ddd}$ will be used as a diagnostic frame at the fifth stage. The probability of successful delivery of one of these frames to the AP is 1/10, that is, it should not be expected to be delivered in the near stages. Replenishment of the second set of frames in the memory of the AP at the fourth stage will most likely take place with three frames; at the fifth stage a maximum of two is possible. The process then becomes more and more delayed, since the fewer unsent frames of a given set remain, the less likely it is that they will be among those successfully delivered.

At the same time, it should be noted that according to the calculation carried out when $k = 10$, using the VBS method allows us to fully form the first set in AP after the third stage of transmission.

5 RESULTS

Thus, it can be concluded that in conditions of significant interference intensity (BER = 10^{-5}) and an increase in the length of the transmitted block beyond $k = 10$, the VBS method is preferable for use. This advantage is due to the fact that when using the VBS method, at each subsequent stage of transmission, the length of the transmitted block is reduced and, accordingly, the absolute number of successfully delivered frames increases (due to the increase in the probability of delivery) from this already reduced block. The convergence of the algorithm is accelerated.

In the case of FBS, the large block length results in a low delivery probability value that remains constant at each transfer stage. Therefore, the number of successfully delivered frames at each stage of transmission is small and, as calculations show, this is not compensated by the successful delivery and accumulation of frames from subsequent sets.

Let's compare these two methods when working in conditions of medium interference intensity (BER = 10^{-6}).

According to subsection 4.1, when VBS mechanism works for $k = 10$, the completion of the first set formation in access point is observed after the second stage of transmission. And then the transmission of the frames of the second set begins. The same is true for subsequent sets of frames. Two stages of transmission are required to transmit each block here. A similar situation is observed for blocks containing up to $k = 25$ frames.

For the FBS method at the first stage of transmission, the set of frames looks like: F1_F2, F3, F4, F5, F6, F7, F8, F9, F10, F11. The probability of successful block transfer is $P_{S,k=10}$=0.887, so statistically approximately 9 frames from the set F2–F11 will be successfully delivered, and, for example, F3 will be unsuccessful.

At the second stage we will receive the following set: $F3_{d}$_F12, F13, F14, F15, F16, F17, F18, F19, F20, F21 and from this block (F12–F21) approximately 9 frames will be successfully delivered to the AP too.

Thus, if we use the FBS method in these conditions, after the second stage in memory of the AP the first complete set of frames F1–F11 will be located, as well as 9 frames of the following second set, which will be formed on the third stage. By conducting a similar analysis, we find that sets 1, 2 and 3 will be formed in the AP after the fourth stage of transmission, and the entire set 4 will be added to them after the fifth stage, and so on.

Under these conditions, the use of the FBS method is more preferable.

6 DISCUSSION

We compared the efficiency of data transmission by variable and constant size blocks formed from frames using VBS and FBS mechanisms under conditions of noise varying intensity. It is shown that with a small number of frames in a block ($k = 6$) and high-intensity noise (BER = 10^{-5}), the efficiency of the FBS mechanism exceeds the efficiency of the VBS block formation mechanism. However, at the same noise level, an increase in the number of frames in a block ($k \geq 10$) makes the use of the VBS mechanism more preferable. This advantage is explained by the fact that the VBS mechanism at each subsequent stage of transmission forms a block from frames distorted at the previous stage, therefore the size of the blocks at subsequent stages decreases, increasing the number of frames successfully transmitted to the access point (due to the increase in the probability of transmitting shorter blocks). At the same time, the constant and small probability of successful transmission of a constant size block at each stage makes the probability of transmission of frames distorted at the initial stages low. This is due to both the low probability of transmission of the rather long blocks themselves and the relatively small number of copies of frames in the block that have already been distorted several times at previous stages of transmission. The above factors complicate the formation of a correct and complete sequence of frames of a given information message, significantly slowing down this process.

For medium-intensity noise (BER = 10^{-6}), the transmission of each subsequent block in the range of up to 25 frames per block using the VBS method requires the use of two stages. The application of the FBS method in these conditions shows that only the first set of frames requires the use of two stages for its complete transmission. Then, due to the accumulation of frames at the previous stages, each subsequent stage of transmission completes the formation of the corresponding set in the memory of access point. Thus, when the noise intensity decreases to BER = 10^{-6} and below, the use of the FVS mechanism becomes more effective.

The obtained results are illustrated with specific examples characterizing the formation and transmission of various frame blocks.

DOI 10.15588/1607-3274-2025-2-1

These studies were conducted under the condition of a fixed probability of collisions. In the future, it is planned to continue comparing the efficiency of various mechanisms for forming frame blocks under conditions of different noise intensities, taking into account the change in the number of collisions in 802.11 networks.

CONCLUSIONS

1. A simple model used in IEEE 802.11 networks to determine the DSF throughput for transmitting frames in infrastructure domains was modified by us to transmit frame blocks of different sizes under conditions of medium and high intensity noise affecting the transmission process. The scale factors of the model for the number of frames in a block k = 6–40 at an average noise level corresponding to BER = 10^{-6} and k = 4–15 for high-intensity noise at BER = 10^{-5} are determined. The algorithm for calculation the network throughput has been generalized.

2. For the first time, comparative studies of VBS and FBS mechanisms used for the formation and transmission of different sizes frame blocks under medium and high noise intensity were conducted.

3. The process of step-by-step dynamic transmission of blocks with a decreasing number of frames from stage to stage, formed within the VBS mechanism, in an environment with medium and high noise intensity was studied.

The investigation of the throughput dependences on the number of frames in the FBS blocks showed the presence of local maxima, located in the region of average values of the frames number. These maxima are more pronounced at increased data transfer rates.

4. It is shown that with a small number of frames in a block (k = 6) and high-intensity noise (BER = 10^{-5}), the efficiency of the FBS mechanism exceeds the efficiency of the VBS block formation mechanism. However, at the same noise level, an increase in the number of frames in a block ($k \geq 10$) makes the use of the VBS mechanism more preferable. When the noise intensity decreases to BER = 10^{-6} and below, due to the accumulation of frames at the previous stages of transmission the use of the FVS mechanism provides a wider throughput and therefore becomes more effective.

The scientific novelty of obtained results consists in determining the throughput of wireless computer networks IEEE 802.11 using the mechanisms of VBS and FBS for the formation and transmission of frame blocks under the influence of variable-intensity noise on the transmission process. The study of the dependence of through put on the number of frames in VBS blocks showed the presence of local maxima of the dependences, which are located in the region of average values of the frames number. These maximums are observed in the range of medium and high noise intensities and are more pronounced at higher data transfer rates.

The practical significance of obtained results consists in the possibility of a reasonable choice of a suitable mechanism for the formation and transmission of frame blocks in accordance with the noise level in the data transmission environment and the determination of the optimal number of frames in the block corresponding to the maximum throughput under given transmission conditions.

Prospects for further research are to study the possibility of using congestion control algorithms in fiber-optic TCP networks, when transmitting data segments using sliding windows, for use in wireless networks with the implementation of automatic regulation of the length of transmitted frame blocks and adaptation to the noise level in the transmission medium. The model created by these studies must also take into account the impact of collisions caused by active frame generation by other stations in the wireless domain.

ACKNOWLEDGEMENTS

The work was carried out at the Department of Electronic Computing Machinery of the Oles Honchar Dnipro National University within the framework of research project “Improving the efficiency of information processing in the process of its formation and transmission using modern computer systems and networks”, No 0122U001400.

REFERENCES

1. IEEE Standard for Local and metropolitan area networks – Media Access Control (MAC) Service Definition, IEEE 802.1AC-2016, 2016.
2. IEEE Standard for Local and metropolitan area networks, IEEE 802.1AX-2020, 2020.
3. Bloch M. R. Covert communication over noisy channels: A resolvability perspective, *IEEE Transactions on Information Theory*, 2016, Vol. 62, № 5, P. 2334–2354. DOI: 10.1109/TIT.2016.2530089
4. Wang H., Li X., Jhaveri R. H. et al. Sparse Bayesian learning based channel estimation in FBMS/OQAM industrial IoT networks, *Computer Communications*, 2021, Vol. 176, № 1, pp. 40–45. DOI: 10.1016/j.comcom.2021.05.020
5. Hien Q. Ta., Quoc-Viet Pham, Khuong Ho-Van et al. Covert communication with noise and channel uncertainties, *Wireless Networks*, 2022, Vol. 28, № 1, pp. 161–172. DOI: 10.1007/s11276-021-02828-3
6. Aldbaibani Omar A., Raschella G. Mohi-Ud-Din, Mackay M. User Prioritisation Algorithm for Horizontal Handover in Dense WLANs, *International Journal of Wireless Information Networks*, 2022, Vol. 29, pp. 130–142. DOI: 10.1007/s10776-021-00544-5
7. Gast M. 802.11 Wireless Networks: The Definitive Guide, O’ Reilly Media, Inc., 2005, 630 p.
8. Proakis J. G., Salehi M. Digital Communications. Fifth Edition, McGrow-Hill Education, 2007, 150 p.
9. Li T., Ni Q., Turletti T. et al. Performance analysis of the IEEE 802.11e block ACK scheme in a noisy channel, *Proc. of Broadnet IEEE International Conference, Boston, Oct. 2005*, Vol. 1, pp. 511–517. DOI: 10.1109/ICBN.2005.1589655
10. Lee H., Tinnirello I., Yu J. et al. Throughput and delay analysis of IEEE 802.11e Block ACK with channel errors, *Proc. of 2nd International Conference on Communication Systems Software and Middleware, Jan. 2007*, pp. 406–414. DOI: 10.1109/COMSWA.2007.382498

DOI 10.15588/1607-3274-2025-2-1

11. IEEE. IEEE standard for information technology–telecommunications and information exchange between systems – Local and metropolitan area networks – Specific requirements – Part II: Wireless LAN medium access control (MAC) and physical layer (PHY) specifications : IEEE standard 802.11-2012. New York: Institute of Electrical and Electronics Engineers, 2012. (Revision of IEEE standard 802.11-2007).
12. Tanenbaum A., Wetherall D. Computer Networks. New Jersey, Pearson Prentice Hall, 2011, 960 p.
13. Kurose James F., Keith W. Computer Networking. A Top-Down Approach. Kurose, Keith W. Ross New Jersey, Pearson Education Inc., 2013, 889 p.
14. Kim T. O., Kim J. K., Choj B. D. Performance analysis of IEEE 802.11 DCF and IEEE 802.11 EDCA in non-saturation condition, *IEICE Transactions on Communications*, 2008, Vol. E91.B, № 4, pp. 1122–1131. DOI: 10.1093/ietcom/e91-b.4.1122
15. Zhao Q., Tsang D. H. K., Sakurai T. A Scalable and Accurate Nonsaturated IEEE 802.11e EDCA Model for an Arbitrary Buffer Size, *IEEE Transactions on Mobile Computing*, 2013, Vol. 12, № 12, pp. 2455–2469. DOI: 10.1109/TMC.2012.211
16. Wei F. Performance analysis of IEEE 802.11e EDCA wireless networks under finite load, *Wireless Networks*, 2020, Vol. 26, № 11, pp. 4431–4457. DOI: 10.1007/s11276-020-02324-0
17. Cover T. M., Thomas J. A. Elements of Information Theory. Second Edition. Hoboken, New Jersey, Wiley, 2006, 774 p.
18. Ghani B., Launay F., Pousset Y.et al. Low-complexity hybrid interference cancellation for sparse code multiple access, *J Wireless Com Network*, 2022, 95 (2022). DOI: 10.1186/s13638-022-02162-y
19. Breed G. Bit error rate: fundamental concepts and measurement issues, High Frequency Design. Summit Technical Media LLC, January 200, pp. 46–48.
20. Castro P. M., González-Coma J. P., García-Naya J. A. et al. Performance of MIMO systems in measured indoor channels with transmitter noise, *J Wireless Com Network*, 2012, 109 (2012). DOI: 10.1186/1687-1499-2012-109
21. Studer C., Wenk M., Burg A. MIMO transmission with residual transmit-RF impairments, *2010 International ITG Workshop on Smart Antennas (WSA). Bremen*, Germany, 2010, pp. 189–196. DOI: 10.1109/WSA.2010.5456453
22. Tinnirello I., Choi S. Efficiency analysis of burst transmissions with block ACK in contention-based 802.11e WLANs, *IEEE International Conference on Communications, Seoul*, 2005, ICC 2005, Vol. 5, pp. 3455–3460. DOI: 10.1109/ICC.2005.1495062
23. Khandetskyi V. S., Karpenko N. V. Modeling of IEEE 802.11 computer networks at increased interference intensity, *Radio Electronics, Computer Science, Control*, 2022, Vol. 61, № 2, pp.132–139. DOI: 10.15588/1607-3274-2022-2-13
24. Tinnirello I., Bianchi G., Xiao Y. Refinements on IEEE 802.11 Distributed Coordination Function Modeling Approaches, *IEEE Transactions on Vehicular Technology*, 2010, Vol. 59, № 3, pp. 1055–1067. DOI: 10.1109/TVT.2009.2029118
25. Bianchi G. Performance analysis of the IEEE 802.11 distributed coordination function, *IEEE Journal on Selected Areas in Communications*, 2000, Vol. 18, № 3, pp. 535–547. DOI: 10.1109/49.840210
26. Patidar R., Roy S., Henderson T.R.et al.Validation of Wi-Fi network simulation on ns-3, *University of Washington Technical Report: August 7, 2017*. Seattle, WA, 98195, 13 p.
27. Ouyang M., Shi W., Zhang R. et al. Optimal interference range for minimum Bayes risk in binomial and Poisson wireless networks, *J Wireless Com Network*, 2019, 247 (2019). DOI: 10.1186/s13638-019-1585-z
28. Shi Y., Hou T., Liu J. et al. Bridging the gap between protocol and physical models for wireless networks, *IEEE Transactions on Mobile Computing*, 2013, 12(7), pp. 1404–1416. DOI: 10.1109/TMC.2012.118
29. Bazkurt A. Optimal delay analysis for real-time traffics over IEEE 802.11 wireless LANs, *EURASIP Journal of Wireless Communications and Networking*, 2016, 52 (2016). DOI: 10.1186/s13638-016-0545-0
30. Banchs A., Vollero L.Throughput analysis and optimal configuration of 802.11e EDCA, *Computer Networks*, 2006, Vol. 50, № 11, pp.1749–1768. DOI: 10.1016/j.comnet.2005.07.008
31. Chen X., Zhai H., Tian X. et al. Supporting QoS in IEEE 802.11e wireless LANs, *IEEE Transactions on Wireless Communications*, 2006, Vol. 8, № 5, pp. 2217–2227. DOI: 10.1109/TWC.2006.1687738
32. Engelstad P. E., Osterbo O. N. Analysis of the Total Delay of IEEE 802.11e EDCA and 802.11 DCF, *2006 IEEE International Conference on Communications.* Istanbul, Turkey, 2006, pp. 552–559. DOI: 10.1109/ICC.2006.254853
33. Min G., Hu J., Woodward M. E. Performance modelling and analysis of the TXOP scheme in wireless multimedia networks with heterogeneous stations, *IEEE Transactions on Wireless Communications*, 2011, Vol. 12, № 10, pp. 4130–4139. DOI: 10.1109/TWC.2011.093011.101387
34. Yan S., Cong Y., Hanly S. V. et al. Gaussian signaling for cover communications, *IEEE Transactions for Cover Communications*, 2019, Vol. 18, № 7, pp. 3542–3553. DOI: 10.1109/TWC.2019.2915305
35. Andreadis A., Risutto S., Zambon R. A cross-layer jitter-based TCP for wireless networks, *Journal of Wireless Communications and Networking*, 2016, 191(2016). DOI: 10.1186/s13638-016-0695-0
36. Khandetskyi V. S., Gerasimov V. V., Karpenko N. V. Performance analysis of wireless computer networks in conditions of high interference intensity, *Radio Electronics, Computer Science, Control*, 2023, Vol. 66, № 3, pp. 148–159. DOI: 10.15588/1607-3274-2023-3-15
37. Xiao Y., Rosdahl J. Performance analysis and enhancement for the current and future IEEE 802.11 MAC protocols, *ACM SIGMOBILE. Mobile Computing and Communications Review (MC2R), special issue on Wireless Home Networks*, 2003, Vol. 7, № 2, pp. 6–19. DOI: 10.1145/950391.950396
38. Chang Z. et al. Performance Analysis of IEEE 802.11ac DCF with Hidden Nodes, *2012 IEEE 75th Vehicular Technology Conference (VTC Spring)*. Yokohama, Japan, 2012, pp. 1–5. DOI: 10.1109/VETECS.2012.6240054

Received 18.01.2025.
Accepted 20.04.2025.

DOI 10.15588/1607-3274-2025-2-1

УДК 621.39

ОЦІНКА ЕФЕКТИВНОСТІ МЕХАНІЗМІВ ПЕРЕДАЧІ БЛОКІВ ФРЕЙМІВ В ЗАШУМЛЕНИХ КАНАЛАХ IEEE 802.11 МЕРЕЖ

Хандецький В. С. – д-р техн. наук, професор, завідувач кафедри електронних обчислювальних машин Дніпровського національного університету імені Олеся Гончара, Дніпро, Україна.

Карпенко Н. В. – канд. фіз.-мат. наук, доцент, доцент кафедри електронних обчислювальних машин Дніпровського національного університету імені Олеся Гончара, Дніпро, Україна.

Герасимов В. В. – канд. техн. наук, доцент, завідувач кафедри комп'ютерних наук та інформаційних технологій Дніпровського національного університету імені Олеся Гончара, Дніпро, Україна.

АНОТАЦІЯ

Актуальність. Об'єднання фреймів у блоки при передаванні інформації в бездротових мережах IEEE 802.11 допомагає суттєво зменшити накладні витрати і підвищити швидкість передачі. Одночасно з цим, вплив шуму зменшує ефективність такої передачі внаслідок підвищення імовірності викривлення більш довгих повідомлень. Ми порівнювали ефективність передачі даних з використанням змінного та постійного розмірів блоків з фреймів, що формуються з використанням VBS та FBS механізмів, в умовах дії шуму змінної інтенсивності.

Мета роботи. Метою цієї статті є порівняльні дослідження VBS та FBS механізмів, що використовуються для формування і передачі блоків фреймів різного розміру в умовах середньої та високої інтенсивності шуму.

Метод. Проста модель, що використовується в IEEE 802.11 мережах для визначення DCF пропускної здатності при передаванні фреймів в інфраструктурних доменах була модифікована нами для передачі блоків фреймів різного розміру в умовах середньої та високої інтенсивності шуму, що впливає на процес передачі. Ми використовуємо для передачі дискретний у часі Гаусовий канал без пам'яті. У такому каналі бітові помилки є незалежними і рівномірно розподіленими серед бітів фрейму. Визначені масштабуючі коефіцієнти моделі для кількості фреймів в блоці k = 6–40 при середньому рівні шуму, що відповідає BER = 10^{-6}, і k = 4–15 для високого рівня шуму при BER = 10^{-5}. Узагальнено алгоритм для розрахунку пропускної здатності мережі. Дослідження залежностей пропускної здатності від кількості фреймів у VBS блоках показало наявність локальних максимумів залежностей, які розташовані в області середніх значень кількості фреймів. Ці максимуми є більш вираженими при підвищених швидкостях передачі даних.

Результати. Показано, що при невеликій кількості фреймів в блоці (k = 6–9) і високоінтенсивному шумі ефективність FBS механізму перевищує ефективність VBS механізму формування блоків. Проте, при такому ж рівні шуму, підвищення кількості фреймів в блоці ($k \geq 10$) робить використання VBS механізму кращим. Ця перевага пояснюється тим фактом, що VBS механізм на кожній наступній стадії передачі формує блок з фреймів, викривлених на попередній стадії, при цьому розмір блоків на наступних стадіях передачі зменшується, підвищуючи число фреймів, успішно переданих AP (внаслідок підвищення імовірності передачі більш коротких блоків). Одночасно з цим, постійна і невелика імовірність успішної передачі блоків постійного розміру на кожній стадії робить імовірність передачі фреймів, пошкоджених на попередніх стадіях, низькою. Ситуація змінюється для шуму середньої інтенсивності. Тут передача кожного наступного блоку в діапазоні до 25 фреймів на блок з використанням методу VBS потребує двох етапів. Застосування ж методу FBS в цих же умовах показує, що тільки перший набір фреймів потребує використання двох стадій для його повної передачі. Потім, внаслідок накопичення фреймів попередніх стадій, на кожній наступній стадії передачі завершується повне формування відповідного набору в пам'яті AP. Таким чином, коли інтенсивність шуму зменшується до BER = 10^{-6} і нижче, використання FBS механізму стає більш ефективним. Одержані результати ілюструються специфічними прикладами, які характеризують формування і передачу різних блоків фреймів.

Висновки. У цій статті, використовуючи модифіковану нами математичну модель, проведені порівняльні дослідження ефективності механізмів формування і передачі блоків фреймів різного розміру в умовах впливу шуму різної інтенсивності на процес передачі. Узагальнено алгоритм для розрахунку пропускної здатності, визначені величини пропускної здатності при використанні VBS та FBS механізмів функціонування мережі.

КЛЮЧОВІ СЛОВА: IEEE 802.11 бездротові мережі, пропускна здатність, інтенсивність шуму, BER, блоки фреймів, VBS та FBS механізми.

ЛІТЕРАТУРА

1. IEEE Standard for Local and metropolitan area net-works – Media Access Control (MAC) Service Definition : IEEE 802.1AC-2016. – 2016.
2. IEEE Standard for Local and metropolitan area networks : IEEE 802.1AX-2020. – 2020.
3. Bloch M. R. Covert communication over noisy channels: A resolvability perspective / M. R. Bloch // IEEE Transactions on Information Theory. – 2016. – Vol. 62, № 5. – P. 2334–2354. – DOI: 10.1109/TIT.2016.2530089
4. Sparse Bayesian learning based channel estimation in FBMS/OQAM industrial IoT networks / [H. Wang, X. Li, R. H. Jhaveri et al.] // Computer Communications. – 2021. – Vol. 176, № 1. – P. 40–45. – DOI: 10.1016/j.comcom.2021.05.020
5. Covert communication with noise and channel uncertainties / [Q. Ta. Hien, Pham Quoc-Viet, Ho-Van Khuong et al.] // Wireless Networks. – 2022. – Vol. 28, № 1. – P. 161–172. – DOI: 10.1007/s11276-021-02828-3
6. Aldbaibani Omar A. User Prioritisation Algorithm for Horizontal Handover in Dense WLANs / Omar A. Aldbaibani, G. Mohi-Ud-Din Raschella, M. Mackay // International Journal of Wireless Information Networks. – 2022. – Vol. 29. – P. 130–142. – DOI: 10.1007/s10776-021-00544-5
7. Gast M. 802.11 Wireless Networks: The Definitive Guide / M. Gast. – O' Reilly Media, Inc., 2005. – 630 p.
8. Proakis J. G. Digital Communications. Fifth Edition / J. G. Proakis, M. Salehi. – McGrow-Hill Education, 2007. – 1150 p.
9. Performance analysis of the IEEE 802.11e block ACK scheme in a noisy channel / [T. Li, Q. Ni, T. Turletti et al.] // Proc. of

DOI 10.15588/1607-3274-2025-2-1

Broadnet IEEE International Conference, Boston, Oct. 2005. – Vol. 1. – P. 511–517. DOI: 10.1109/ICBN.2005.1589655
10. Throughput and delay analysis of IEEE 802.11e Block ACK with channel errors / [H. Lee, I. Tinnirello, J. Yu et al.] // Proc. of 2nd International Conference on Communication Systems Software and Middleware, Jan. 2007. – P. 406–414. DOI: 10.1109/COMSWA.2007.382498
11. IEEE. IEEE standard for information technology–telecommunications and information exchange between systems-Local and metropolitan area networks-Specific requirements-Part II: Wireless LAN medium access control (MAC) and physical layer (PHY) specifications : IEEE standard 802.11–2012. – New York: Institute of Electrical and Electronics Engineers, 2012. (Revision of IEEE standard 802.11–2007).
12. Tanenbaum A. Computer Networks / A. Tanenbaum, D. Wetherall. – New Jersey: Pearson Prentice Hall, 2011. – 960 p.
13. Kurose James F. Computer Networking. A Top-Down Approach / James F. Kurose, Keith W. –Ross New Jersey: Pearson Education Inc., 2013. – 889 p.
14. Kim T. O. Performance analysis of IEEE 802.11 DCF and IEEE 802.11 EDCA in non-saturation condition / T. O. Kim, J. K. Kim, B. D. Choj // IEICE Transactions on Communications. – 2008. – Vol. E91.B, № 4. – P. 1122–1131. DOI: 10.1093/ietcom/e91-b.4.1122
15. Zhao Q. A Scalable and Accurate Nonsaturated IEEE 802.11e EDCA Model for an Arbitrary Buffer Size / Q. Zhao, D. H. K. Tsang, T. Sakurai // IEEE Transactions on Mobile Computing. – 2013. – Vol. 12, № 12. – P. 2455–2469. DOI: 10.1109/TMC.2012.211
16. Wei F. Performance analysis of IEEE 802.11e EDCA wireless networks under finite load / F. Wei // Wireless Networks. – 2020. – Vol. 26, № 11. – P. 4431–4457. DOI: 10.1007/s11276-020-02324-0
17. Cover T. M. Elements of Information Theory. Second Edition / T. M. Cover, J. A. Thomas. – Hoboken, New Jersey: Wiley, 2006. – 774 p.
18. Low-complexity hybrid interference cancellation for sparse code multiple access / [B. Ghani, F. Launay, Y. Pousset et al.] // J Wireless Com Network. – 2022. – 95 (2022). DOI: 10.1186/s13638-022-02162-y
19. Breed G. Bit error rate: fundamental concepts and measurement issues / G. Breed // High Frequency Design. Summit Technical Media LLC, January 2003. – P. 46–48.
20. Performance of MIMO systems in measured indoor channels with transmitter noise / [P. M. Castro, J. P. González-Coma, J. A. García-Naya et al.] // J Wireless Com Network. – 2012. – 109 (2012). DOI: 10.1186/1687-1499-2012-109
21. Studer C. MIMO transmission with residual transmit-RF impairments / C. Studer, M. Wenk, A. Burg // 2010 International ITG Workshop on Smart Antennas (WSA), Bremen, Germany. – 2010. – P. 189–196. DOI: 10.1109/WSA.2010.5456453
22. Tinnirello I. Efficiency analysis of burst transmissions with block ACK in contention-based 802.11e WLANs / I. Tinnirello, S. Choi // IEEE International Conference on Communications, Seoul, 2005. – ICC 2005. – Vol. 5. – P. 3455–3460. DOI: 10.1109/ICC.2005.1495062
23. Khandetskyi V. S. Modeling of IEEE 802.11 computer networks at increased interference intensity / V. S. Khandetskyi, N. V. Karpenko // Radio Electronics, Computer Science, Control. – 2022. – Vol. 61, № 2. – P.132–139. DOI: 10.15588/1607-3274-2022-2-13
24. Tinnirello I. Refinements on IEEE 802.11 Distributed Coordination Function Modeling Approaches / I. Tinnirello, G. Bianchi, Y. Xiao // IEEE Transactions on Vehicular Technology. – 2010. – Vol. 59, № 3. – P. 1055–1067. DOI: 10.1109/TVT.2009.2029118
25. Bianchi G. Performance analysis of the IEEE 802.11 distributed coordination function / G. Bianchi // IEEE Journal on Selected Areas in Communications. – 2000. – Vol. 18, № 3. – P. 535–547. DOI: 10.1109/49.840210
26. Validation of Wi-Fi network simulation on ns-3 / [R. Patidar, S. Roy, T. R. Henderson et al.] // University of Washington Technical Report: August 7, 2017. – Seattle, WA, 98195. – 13 p.
27. Optimal interference range for minimum Bayes risk in binomial and Poisson wireless networks / [M. Ouyang, W. Shi, R. Zhang et al.] // J Wireless Com Network. – 2019. – 247 (2019). DOI: 10.1186/s13638-019-1585-z
28. Bridging the gap between protocol and physical models for wireless networks / [Y. Shi, T. Hou, J. Liu et al.] // IEEE Transactions on Mobile Computing. – 2013. – 12(7). – P. 1404–1416. DOI: 10.1109/TMC.2012.118
29. Bazkurt A. Optimal delay analysis for real-time traffics over IEEE 802.11 wireless LANs / A. Bazkurt // EURASIP Journal of Wireless Communications and Networking. – 2016. – 52 (2016). DOI: 10.1186/s13638-016-0545-0
30. Banchs A. Throughput analysis and optimal configuration of 802.11e EDCA / A. Banchs, L. Vollero // Computer Networks. – 2006. – Vol. 50, № 11. – P. 1749–1768. DOI: 10.1016/j.comnet.2005.07.008
31. Supporting QoS in IEEE 802.11e wireless LANs / [X. Chen, H. Zhai, X. Tian et al.] // IEEE Transactions on Wireless Communications. – 2006. – Vol. 8, № 5. – P. 2217–2227. DOI: 10.1109/TWC.2006.1687738
32. Engelstad P. E. Analysis of the Total Delay of IEEE 802.11e EDCA and 802.11 DCF / P. E. Engelstad, O. N. Osterbo // 2006 IEEE International Conference on Communications, Istanbul, Turkey, 2006. – P. 552–559. DOI: 10.1109/ICC.2006.254853
33. Min G. Performance modelling and analysis of the TXOP scheme in wireless multimedia networks with heterogeneous stations / G. Min, J. Hu, M.E. Wood-ward // IEEE Transactions on Wireless Communications. – 2011. – Vol. 12, № 10. – P. 4130–4139. DOI: 10.1109/TWC.2011.093011.101387
34. Gaussian signaling for cover communications / [S. Yan, Y. Cong, S. V. Hanly et al.] // IEEE Transactions for Cover Communications. – 2019. – Vol. 18, № 7. – P. 3542–3553. DOI: 10.1109/TWC.2019.2915305
35. Andreadis A. A cross-layer jitter-based TCP for wireless networks / A. Andreadis, S. Risutto, R. Zambon // Journal of Wireless Communications and Networking. – 2016. – 191(2016). DOI: 10.1186/s13638-016-0695-0
36. Khandetskyi V.S. Performance analysis of wireless computer networks in conditions of high interference intensity / V. S. Khandetskyi, V. V. Gerasimov, N. V. Karpenko // Radio Electronics, Computer Science, Control. – 2023. – Vol. 66, № 3. – P. 148–159. DOI: 10.15588/1607-3274-2023-3-15
37. Xiao Y. Performance analysis and enhancement for the current and future IEEE 802.11 MAC protocols / Y. Xiao, J. Rosdahl // ACM SIGMOBILE. Mobile Computing and Communications Review (MC2R), special issue on Wireless Home Networks. – 2003. – Vol. 7, № 2. – P. 6–19. DOI: 10.1145/950391.950396
38. Performance Analysis of IEEE 802.11ac DCF with Hidden Nodes / [Z. Chang et al.] // 2012 IEEE 75th Vehicular Technology Conference (VTC Spring), Yokohama, Japan, 2012. – P. 1–5. DOI: 10.1109/VETECS.2012.6240054

DOI 10.15588/1607-3274-2025-2-1

UDC 621.3.049

THE SELECTION OF INFORMATION-MEASURING MEANS FOR THE ROBOTOTECHNICAL COMPLEX AND THE RESEARCH OF THEIR WORKER CHARACTERISTICS

Mammadov J. F. – Dr. Sc., Professor, Head of the Department of Automatic and mechanic, Sumgait State University, Sumgait, Azerbaijan.

Ahmadova T. A. – Dr. Sc., Professor of the Department of Energetic, Sumgait State University, Sumgait, Azerbaijan.

Huseynov A. H. – Dr. Sc., Professor of the Department of Automatic and mechanic, Sumgait State University, Sumgait, Azerbaijan.

Talibov N. H. – PhD, Associate Professor, Head of the Department of Information technology, Sumgait State University, Sumgait, Azerbaijan.

Hashimova H. M. – Assistant of the Department of Automatic and mechanic, Sumgait State University, Sumgait, Azerbaijan.

Ahmadov A. A. – SOCAR Polimer engineer, Azerbaijan.

ABSTRACT

Context. The topic of the article is devoted to the issue selection of the means of the information-measurement system (IMS) for automation of robototechnical complexes (RTC) of flexible production systems applied in various fields of industry, and the research of their technological characteristics.

Objective. The goal is using the mathematical models to researching of the working characteristics of the new construction transmitters for information – measurement and automated control of robototechnical complex in flexible production areas.

Method. In the article, the following issues were set and solved: the analysis of the application object, the selection of the types of information-measurement and management elements of RTC creation and structure scheme; research of the characteristics of the information-measuring transmitter for managing the active elements of the RTC; determining the error of the analog output transmitter of the information-measurement system of RTC active elements.

Based on the analysis of the application object, it was determined that the structure scheme of the RTC at the flexible production system includes complex technological, functionally connected production areas, modules and robotic complexes, their automated control system IMS, regulation, execution, microprocessor control system and devices and devices of the industrial network. includes The functional block diagrams of the IMS of RTCi of the flexible production system are given. Based on research, it was found that it is convenient to use a magnetoelastic transducer with a ring sensitive element to measure the mechanical force acting on the working organs of an industrial robot (IR). For this, unlike existing transmitters, the core of this transmitter is made of whole structural steel. The inductive coil of the proposed transmitter is included in the LC circuit of the autogenerator. The magnetoelastic emitter semiconductor is assembled at the base of the transistor. The cross-section of its core is calculated for the mechanical stress that can be released for the steel. The block-scheme of the inductive transmitter is proposed. The proposed transmitters work on the principle of an autogenerator assembled on an operational amplifier. A mathematical expression is defined for determining the output frequency of the autogenerator. The model of the autogenerator consists of a dependent source, the transmission coefficient is determined.

Results. A new transmitter is proposed to measure the information of the manipulator to perform special technological operations synchronously.

Conclusions. A mathematical model was developed to determine the error of the analog output transmitter of the information-measurement system of RTC active elements. The expression ehq is used to determine the error of the transmitter whose output is analog during the measurement of the current technological operation. It was determined that in practice, the geometric dimensions of the transmitter and the number of windings remain unchanged during the work process, where it is changed due to the influence of the environment. Considering this variation, a mathematical model was developed to determine the transmitter error.

KEYWORDS: Robototechnical complex, information-measuring system, transmitter, inductive sensor, autogenerator, LC motor, semiconductor commutator, analog output transmitter, transmitter error.

ABBREVIATIONS

IMM is information-measurement and management;
RTC is robototechnical complex;
FMS is flexible manufacturing system;
IMS is information-measurement system;
MCS is microprocessor control system;
IND is industrial network devices;
IT is intelligent transmitter;
IR is industrial robot;
TEPM is technological equipment of production module; MT is machine tool;
F is furnaces;
PQCT is products quality control tool;
IT is intelligent transmitter.

NOMENCLATURE

δ is a proportion;
L_1 is an inductance of the oscillation circuit;
L_2 is an inductance of the oscillation circuit;

DOI 10.15588/1607-3274-2025-2-2

r_e is an emitter switching resistance of the transistor;
r_b is a base switching resistance of the transistor;
r_k is a collector switching resistances of the transistor;
r_2 is an ohmic resistance of the oscillation circuit;
K_u is a load factor;
K is a transmission factor;
R is a resistance;
R_1 is an active resistance;
R_2 is an active resistance;
R_{out} is an output resistance;
ω is an angular frequency of the induced current;
L is an inductive;
α is a current amplification factor of the transistor;
ω_0 is a specific frequency of the oscillation contour of the autogenerator;
f_0 is an autogenerator frequency;
z is a k load resistance;
ΔU is a displacement of power;
X_m is a maximum displacement;
X is a current value of displacement;
k is a proportionality coefficient;
W_1 is a number of affected laps;
W_2 is a number of section laps;
h is a depth of the slot;
a is a width of the slot;
δ is a length of the air gap between the housing and the rotating cylinder;
μ is a corresponding to the equivalent extinction depth of the core;
μ_0 is corresponding to the equivalent extinction depth of the core;
$\dot{I}_T$ – is a complex value of induced current;
M is a mutual induction;
L_T is an induction of section windings;
r_T is an active resistance in section windings;
$\dot{E}$ is an induction ehq in section windings;
C_1 is a constant factor;
C_2 is a constant factor;
N is a speed of rotation;
S is an elative magnetic permeability of the core and absolute magnetic permeability of the cavity, respectively;
d is an equivalent depth of the magnetic flux in the core;
l is a length of the core.

INTRODUCTION

The many different types of mechanical quantity transmitters, transmitters based on magnetic systems are of great interest. However, numerous constructive options do not reflect their quality indicators, but reflect their technical and economic indicators. Structurally, the magnetic system of existing transmitters is rectangular, cylindrical, etc. is prepared in the form [1, 2]. Cylindrical magnetic systems are highly resistant to obstacles, have low scattered magnetic flux, high sensitivity, and simple manufacturing technology.

DOI 10.15588/1607-3274-2025-2-2

The magnetic system of the transmitters in this form is made of a material called ferrite, which is fragile due to mechanical shocks and vibrations, so it quickly breaks down and loses its working capacity. Thus, on the basis of a long-term study, it was determined that when the core of the magnetic system of the existing inductive transmitters is made of ordinary structural steel, the above-mentioned shortcomings are reduced, that is, their sensitivity increases, they are resistant to mechanical shocks, reliable operation is ensured, and quality indicators increase. In this regard, many Azerbaijani and Russian scientists, including academician Aliyev R.A., Aliyev T.M., Mammadov F.I., Nabiyev M.A., Mostovoy B.H., Ahmadova T.A. in their research, they used structural steel in the preparation of transmitters [3, 4, 5].

The comparative analysis of magnetic circuits of different designs allows such transmitters to be used in the measurement of mechanical quantities. According to the setting conditions of the magnetic system, make it consist of a high-grade homogeneous magnetic field of the magnetic system and calculate the high-precision displacement, speed, oscillation, acceleration, force, pressure, torque, etc. at the base of this system. it is necessary to create transmitters that measure quantities. Thus, it is necessary to unify different types of magnetic systems. The mass, dimensions, energy demand, structural simplicity, and manufacturing technology of the transmitters are considered to be one of the main important issues [6, 7, 8, 9].

The object of study.

Nowadays, every RTC and FMS systems are widely used, and they contain numerous non-contact transmitters, and with their help, various physical quantities are converted into electrical quantities and provide information about the technological process [10–16]. Because, as an object os study, it was chosen the RTC in FMS, where for its effective control and automation, information-measuring, processing and executing elements characteristics must be researched.

The subject of study is based on the methods for researching energetically characteristics of the inductive transmitter for the converting manipulator and industrial robot served the active elements at RTC.

The analyze of the known methods [1–27] shown that have the non solved problems at complex design of information measure systems applied to robototechnical and manipulator of FMS, and at that needs to decision these tasks.

The purpose of the work – using the mathematical models to researching of the working characteristics of the new construction transmitters for information-measurement and automated control of robototechnical complex in flexible production areas. In order to achieve the set goal, the following issues should be solved:

– analysis of the application object, selection of types of information-measuring and control elements of the robotic complex and creation of a structural scheme;

– study of the characteristics of the information-measuring transmitter for the management of the active elements of the robotic complex;

– determining the error of the transmitter with analog output of the information-measurement system of active elements of RTC.

1 PROBLEM STATEMENT

Let us consider the issue of developing an algorithm for improving static characteristics, which include correction of the initial offset, increase in the slope of the linear static characteristic, correction of the scale of the measuring path, linearization of the static characteristic and approximation using a polynomial. In this regard, in accordance with the above-presented static characteristics, we will present the input data as follows:

1. Bridge-type measuring transducers based on strain gauges have an initial offset of the output signal, which can reach 15 mV/V with a sensitivity of the primary transducer of 2 ... 4 mV/V.

2. The slope coefficient is the partial derivative of the power with respect to the corresponding parameters.

3. All errors of the measuring path can be legitimately considered as a single centered random variable and characterized by a single indicator – the second central moment (variance) – as the average value of the power of the error change curve.

4. The small deviation method is used to linearize the characteristics of the measuring path.

In Figure 1 the block diagram of the inductive transmitter is given.

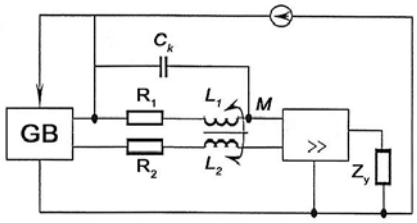

Figure 1 – Inductive substitution block-scheme

In the block-scheme, GB-voltage divider; z_y is the load resistance. By that, an operational amplifier is taken as an amplifier. Such an amplifier has strong feedback. In ideal operational amplifiers $R_g = \infty$, and accordingly, the voltage gain is also $K_u = \infty$ obtained. The output resistance of such amplifiers is close to zero.

For solution of the task of definition of output frequency of the autogenerator, let the given list of the following input variables:

1. ω_0 – the specific frequency of the oscillation contour of the autogenerator;

2. L_1, L_2 – the inductances of the oscillation circuit;

3. r_e – the emitter switching resistance of the transistor;

4. r_b – the base switching resistance of the transistor;

5. r_k – the collector switching resistances of the transistor;

6. r_2 –ohmic resistance of the oscillation circuit;

7. α – current amplification factor of the transistor.

Then the task consists of determination of output frequency of the autogenerator worked on the principle of an autogenerator assembled on an operational amplifier. Thus output frequency of the autogenerator is determined as follows:

$$\omega = \omega_0 \sqrt{\frac{L_1\left[r_e + (r_2 + r_b)(1-\alpha)\right]}{L_1\left[r_e + (r_e + r_b)(1-\alpha)\right] + L_2 r_k (1-\alpha)}}. \qquad (1)$$

2 REVIEW OF THE LITERATURE

Automation of various technological processes, effective management of aggregates, machines, and mechanisms require the measurement of many different physical quantities. All the requirements for the elements of automation to increase the reliability, quality and economic efficiency, the increase of all the requirements for the information-measurement and management (IMM) technique require new developments, extensive field research. In this field, great attention is paid to the development of electromagnetic elements, including their reliability, simplicity of technology and low cost.

Some of the converters used in FMS and RTC[s] work mainly in relay mode. In such systems, in addition to transmitters working in relay mode, measuring transmitters that can measure technological parameters with high accuracy or various vision devices are also used [17, 18]. In the technological lines of FMS and RTC systems, the product is moved along the line and is subjected to certain technological operations in different parts of this line. In this regard, in order to ensure continuity and consistency in the technological line, it is necessary to use devices that indicate the presence of products in one or more places of the line. For this purpose, electromagnetic inductive transmitters are used in the IMM systems.

Research of information and measuring systems applied to robotic systems of mechanical engineering flexible production have shown that the used sensors belong to the areas measuring mechanical states of the industrial robot in the environment. At the same time, the main elements of the information and measuring systems of robotic complexes – sensors, receive a wide range of data about the environment, such as position, size, orientation, speed, distance, temperature, weight, force, etc. [19, 20, 21]. This information allows industrial robots and mechatronic means to function effectively, interacting with the environment, while performing complex manipulation, operational and planned production tasks.

The used sensors of industrial robots and mechatronic means of the robotic complex are based on the principle of energy conversion, also known as transduction [22]. Given the complexity and presence of a large number of standard industrial robots, process equipment, logistics and transport technologies, different sensors are required to improve efficiency, measurement accuracy, control

DOI 10.15588/1607-3274-2025-2-2

reliability, monitoring and flexible response in the working environment of the robotic complex. Complex in structure industrial robotic sections, manipulation of hands, gripping devices and transportation industrial robots require contact sensors [23], which function when changing the speed, position, acceleration, torque or force in the links of the manipulator and the working body of industrial robots. Insufficient research in this direction requires careful consideration of the issue of determining the parameters that arise during physical contact in order to effectively direct the industrial robot to appropriate actions in the robotic complex. In this case, the sensors used to measure contact are performed using various switches, such as a limit switch, a push-button switch and a tactile bumper switch. In the works [24, 25], the contact sensors under consideration are used to avoid obstacles encountered in the robotic complex. When any obstacle is detected, it transmits a signal to the robot so that it can perform various actions, such as reversing, turning or simply stopping. Special research requires the issue of measuring sensors for detecting objects, which are considered in the work [26, 27]. In this paper, using the capabilities of a magnetic field to detect the objects in question, the required energy characteristics of ultrasonic sensors are determined, which measure distances to a certain object by emitting ultrasonic sound waves and converting the reflected sound into an electrical signal. However, obtaining large errors when using such technology requires the use of a new approach to accurately determine the distance from one object to another object without the need for physical contact [28]. On the review of the literature can do conclusion that the primary elements of the existing information-measurement and management systems – transmitters have low reliability. They fail quickly due to the corresponding mechanical vibration and shocks under heavy duty conditions. Measuring transmitters, technical vision systems and other control and regulatory devices working in such harsh conditions work unsteadily [29]. Thus, it is necessary to increase the stability of the transmitters and the IPC. This remains a problem in production.

3 MATERIALS AND METHODS

The autogenerator model consists of a dependent source $K_u^0 u_{y.i} = u_0$, where the transmission factor is written as follows [30]:

$$K = \frac{R}{(1+j\omega CR)\left[\frac{R}{1+j\omega CR} + R_2 + j(\omega L - \frac{1}{\omega C})\right]}, \qquad (2)$$

Fig. 2 shows the replacement scheme of the autogenerator built on the basis of the EP scheme. When creating an autogenerator, it is convenient to choose its active resistance, i.e $R_1 = R_2 = R_{or}$

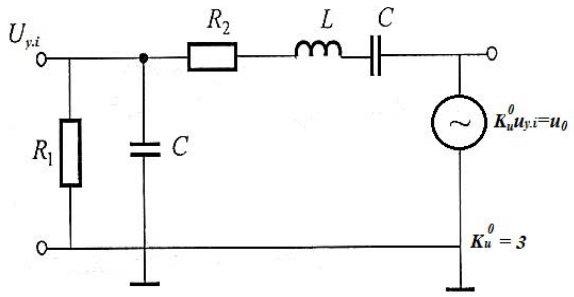

Figure 2 – Autogenerator replacement scheme

(1) for the resonant condition of the autogenerator by slightly changing the expression

$$\omega_0^2 C^2 R^2 + \omega_0^2 C L - 1 = 0. \qquad (3)$$

From the solution of this equation

$$\omega_0 = \pm\sqrt{\frac{1}{C(R^2C + L)}}. \qquad (4)$$

For the real circuit, the following equation is satisfied in the autogenerator

$$L = R^2 C. \qquad (5)$$

Real operational amplifiers are designed to have an infinitely large input resistance and a minimum output resistance. It happens because it is accepted $\omega = \omega_0 = 2\pi f_0$ where $d \approx 1$. That is

$$f_0 = \frac{1}{2\pi\sqrt{LC}}. \qquad (6)$$

From the last statement, it can be seen that when the frequency of the autogenerator is high, it is more sensitive to the change of inductance and to the change of capacitance at low frequency.

It should be noted that the voltage change obtained at the final resistance

$$\Delta U = \frac{k}{X_m} X. \qquad (7)$$

The proportionality factor k is obtained from the interaction of the influence loop located in the transmitter housing and the section loops [31]. Let's assume that the transmitter is fed from an alternating current source with a frequency of 400 Hz, and in this case the magnetic field around the slot 5 is extinguished at a depth of about 1 mm. In this regard, the magnetic field at that depth of the core is considered homogeneous. According to the same

DOI 10.15588/1607-3274-2025-2-2

rule, the extinction depth of the magnetic flux in each section is assumed to be close to 1mm. If we consider all the above for the magnetic field generated around the induced loop, the mutual magnetic induction

$$M = \frac{W_1 W_2 \mu \mu_0 S}{2\left[h + a + \mu\delta\right]} \quad (8)$$

happens. Where $W_1, W_2 -$, the number of affected and section laps, respectively, $h, a -$ the depth and width of the slot; $\delta -$ the length of the air gap between the housing and the rotating cylinder; $S -$ cross-sectional area $\mu, \mu_0 -$ corresponding to the equivalent extinction depth of the core; $S = dl$ relative magnetic permeability of the core and absolute magnetic permeability of the cavity, respectively; $d -$ the equivalent depth of the magnetic flux in the core; $l -$ is the length of the core. Induction ehq in section windings is defined by the expression

$$\dot{E} = -j\omega M \dot{I}_T, \quad (9)$$

where, $\omega -$ the angular frequency of the induced current; $\dot{I}_T -$ complex value of induced current; $M -$ is mutual induction.

The complex value of the current flowing through the excitation loop

$$\dot{I}_T = \frac{\dot{U}}{r_T + j\omega L_T} \quad (10)$$

is defined by the expression If we consider expression (4) in (3) and make some transformation:

$$\dot{E} = \frac{\omega M \dot{U}}{\sqrt{r_T^2 + (\omega L_T)^2}} e^{j\varphi}. \quad (11)$$

Inductance obtained from the study of the magnetic system of the inverter

$$L_T = \frac{W_2^2 \mu\mu_0 S}{2(h + a + \mu\delta)} \quad (12)$$

is defined as If we substitute expressions (8) and (12) in (10) and carry out a transformation, we get for the modulus or k coefficient of ehq:

$$E_m = k = \frac{\omega W_1 W_2 \mu\mu_0 S}{2(K + a + \mu\delta)} \cdot \frac{U}{\sqrt{r_1^2 + \left(\omega \frac{W_2^2 \mu\mu_0 S}{2(h + a + \mu\delta)}\right)^2}}. \quad (13)$$

If we write the last expression in formula (7):

$$\Delta U = \frac{\omega W_1 W_2 \mu\mu_0 S U}{\sqrt{4(h + a + \mu\delta)^2 r_T^2 + (\omega W_2^2 \mu\mu_0 S)^2}} \frac{X}{X_m}. \quad (14)$$

The obtained expression (14) allows to find the operating characteristic of the transmitter. Where, a motor is used as an actuator for the manipulator to perform angular rotation. The scheme of connecting such an execution engine to the circuit is shown in Figure 3. Where, the normally open and normally closed contacts K_3, K_4 used in the system K_1, K_2 are used. Contacts electric motor is influenced by a permanent magnet and consists of an angle transmitter indicating the position of the rotor and a semiconductor commutator [32].

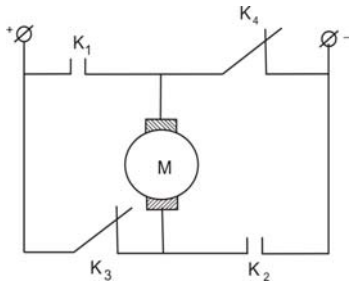

Figure 3 – Scheme of connecting the motor to the circuit through contacts

In a contactless motor, the motor and the commutator are placed in one housing or they are installed in separate housings, connected to each other by a cable. The principle of operation of this motor is as follows: the interaction between the armature current and the magnetic flux in the poles creates a torque, which rotates the armature and the poles in different directions (Fig. 9). Due to this, the torque maintains its direction, and the motor continues the direction of rotation.

Due to the effect of the torque, the rotor rotation speed n increases. In this regard, the ehq generated in the anchor

$$E = C_1 n \Phi \quad (15)$$

happens.

In the active resistance l of the armature and the corresponding armature rotation speed

$$n = \frac{(u - lr)}{C_m \Phi} \quad (16)$$

happens.

In the model shown in Fig. 4, the brush acts as a commutator and synphase works with the rotation of the rotor. Where, the sections of the windings of the rotor are connected in such a way that the current in the windings is always in the same direction [33].

DOI 10.15588/1607-3274-2025-2-2

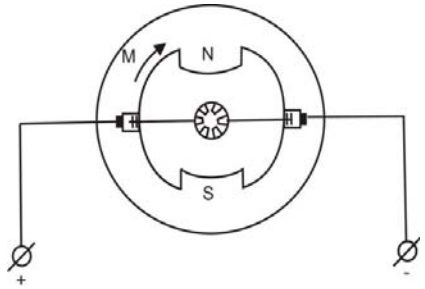

Figure 4 – DC motor connection diagram

4 EXPERIMENTS

A contactless of the motor consists of three main parts: 1) in the stator *m* – phase winding and affected rotor; 2) rotor status transmitter; 3) contactless switch. Here, the currents flowing through the stator windings are switched from the status transmitter signals. An angle transmitter is used as a transmitter to indicate the position of the rotor. Through this, the control signal is processed, and the windings of the motor determine the sequence of switching.

The technical parameters of the contactless direct current motor are shown in Table 1.

Table 1 – technical parameters of the contactless direct current motor

№	The name of the indicators	Unit of measure	The value
1	Nutritional stress	V	27
2	Useful power	Vt	14
3	Rotational frequency	Cycle/min	4500
4	Ambient temperature	^{0}C	–10 ÷+40
5	The relative humidity of the air at a temperature of 25^0 C	%	98
6	Required current	A	1.1
7	Useful work factor	%	60
8	Mass Engine Switch	kg	0.58 0.4
9	Overall dimensions of the switch	mm.mm.mm	0 x 64 x 81

For accurate and reliable management of complex technological operations in RTC, precise analog signals of the measured parameters must be received and processed from the information-measuring transmitters used at the 1st level of the automated control system to the input of the microprocessor control system and the programmable logic controller [34]. When measuring the current technological operation, it is necessary to use the expression ehq to determine the error of the transmitter whose output is analog. The modulus of this expression is written as follows:

$$E = \frac{\omega W_1 W_2 \mu\mu_0 S u}{2(h+a+\mu\delta)\sqrt{r_1^2+\left(\frac{\omega W_2^2 \mu\mu_0 S}{2(h+a+\mu\delta)}\right)^2}}. \quad (17)$$

In practice, it appears that the geometric dimensions of the transmitter and the number of windings remain unchanged during the work process. Where, $\omega, \mu, u, \delta, r$ it is changed due to the influence of the environment. Given this change,

$$E_{ao}\left(1\pm\frac{\Delta E}{E_{ao}}\right)=\frac{W_1W_2\mu_0S\omega_{ao}\left(1\pm\frac{\Delta\omega}{\omega_{ao}}\right)\left(1\pm\frac{\Delta\mu}{\mu_{ao}}\right)}{2\left[\left(h+a+\mu_{ao}\left(1\pm\frac{\Delta\mu}{\mu_{ao}}\right)\delta_{ao}\left(1\pm\frac{\Delta\delta}{\delta_{ao}}\right)\right)\right]}\times$$

$$\times\frac{1}{\sqrt{r_{1ao}^2\left(1\pm\frac{\Delta r}{r_{1ao}}\right)^2+\left(\frac{\omega_{ao}\left(1\pm\frac{\Delta\omega}{\omega_{ao}}\right)W_2^2\mu_0S\mu_{ao}\left(1+\frac{\Delta\mu}{\mu_{ao}}\right)}{2\left(h+a+\mu_{ao}\left(1\pm\frac{\Delta\mu}{\mu_{ao}}\right)\delta_{ao}\left(1\pm\frac{\Delta\delta}{\delta_{ao}}\right)\right)}\right)^2}}. \quad (18)$$

If we raise the numerator and denominator of the obtained fraction to a power and consider the quantities whose degree is greater than unity, the expression (18) is written as follows:

$$E_{ao}\left(1\pm\frac{\Delta E}{E_{ao}}\right)=\frac{W_1W_2\mu_0S\omega_{ao}U_{ao}\left(1\pm\frac{\Delta\omega}{\omega_{ao}}\pm\frac{\Delta U}{U_{ao}}\pm\frac{\Delta\mu}{\mu_{ao}}\right)\mu_{ao}}{2\left[\left(h+a+\mu_{ao}\delta_{ao}\left(1\pm\frac{\Delta\delta}{\delta_{ao}}\pm\frac{\Delta\mu}{\mu_{ao}}\right)\right)\right]}\times$$

$$\times\frac{1}{\sqrt{r_{ao}^2\left(1\pm2\frac{\Delta r}{r_{1ao}}\right)+\left(\frac{\omega_{ao}W_2^2\mu_0S\mu_{ao}\left(1\pm\frac{\Delta\omega}{\omega_{ao}}\pm\frac{\Delta\mu}{\mu_{ao}}\right)}{2\left(h+a+\mu_{ao}\delta_{ao}\left(1\pm\frac{\Delta\mu}{\mu_{ao}}\pm\frac{\Delta\delta}{\delta_{ao}}\right)\right)}\right)^2}}. \quad (19)$$

If we have considered the second, third and fourth order variables in the expression (19), we can write the changed form of the expression (19) as follows:

$$E_{ao}\left(1\pm\frac{\Delta E}{E_{ao}}\right)=\frac{W_1W_2'\mu_0S\omega_{ao}'U_{ao}\mu_{ao}\left(1\pm\frac{\Delta\omega}{\omega_{ao}}\pm\frac{\Delta U}{U_{ao}}\pm\frac{\Delta\mu}{\mu_{ao}}\right)}{2\left[\left(h+a+\mu_{ao}\delta_{ao}\left(1\pm\frac{\Delta\delta}{\delta_{ao}}\pm\frac{\Delta\mu}{\mu_{ao}}\right)\right)\right]}\times$$

$$\times\frac{1}{\sqrt{r_{ao}^2\left(1\pm2\frac{\Delta r}{r_{ao}}\right)+\frac{\omega_{ao}^2W_2^4\mu^2{}_0S^2\mu^2{}_{ao}\left(1\pm\frac{\Delta\omega}{\omega_{ao}}\pm\frac{\Delta\mu}{\mu_{ao}}\right)^2}{\left[4(h+a+\mu_{ao}\delta^2{}_{ao})^2\left(1\pm\frac{\Delta\mu}{\mu_{ao}}\pm\frac{\Delta\delta}{\delta_{ao}}\right)\right]^2}}}. \quad (20)$$

DOI 10.15588/1607-3274-2025-2-2

$K_1 = \frac{\mu_0 \mu_{ao}}{(h + a + \delta + \mu_{ao})}$ if we consider that we have divided the first part of the received fraction into its first-order variables

$$E_{ao}\left(1 \pm \frac{\Delta E}{E_{ao}}\right) = \frac{W_1 W_2 \mu_o S U_a \omega_{ao} \mu_{ao} \left(1 \pm \frac{\Delta\omega}{\omega_{ao}} \pm \frac{\Delta U}{U_{ao}} \pm \frac{\Delta\mu}{\mu_{ao}}\right)}{2(h + a + \mu_{ao}\delta_o)} \times$$
$$\times \left(1 \pm \frac{\Delta\omega}{\omega_{ao}} \pm \frac{\Delta U}{U_{ao}} \pm I \pm K_1 \Delta\mu\mu\omega_0 \mp \frac{\Delta\delta}{\delta_{ao}}\right) \times$$
$$\times \frac{1}{\sqrt{r_{ao}^2\left(1 \pm 2\frac{\Delta r}{r_{ao}}\right) + \frac{\omega^2{}_{ao} W_2^4 \mu^2{}_0 S^2 \mu^2{}_{ao}\left(1 \pm \frac{\Delta\omega}{\omega_{ao}} \pm \frac{\Delta\mu}{\mu_{ao}}\right)^2}{4(h + a + \mu_{ao})^2\left(1 \pm \frac{\Delta\mu}{\mu_{ao}} \pm \frac{\Delta\delta}{\delta_{ao}}\right)}}}. \quad (21)$$

(21) to the power, and consider the second and third and higher-order expressions,

$$\left(1 \pm K_1 \frac{\Delta\mu}{\mu_{ao}} \pm K_1 \frac{\Delta\delta}{\delta_{ao}}\right) \text{ and } \left(1 \pm \frac{\Delta\omega}{\omega_{ao}} \pm \frac{\Delta\mu}{\mu_{ao}}\right) \quad (22)$$

we will get that. Where, if we multiply $\left(1 \pm K_1 \frac{\Delta\mu}{\mu_{ao}} + K_1 \frac{\Delta\delta}{\delta_{ao}}\right)$ the inverse of the expression $\left(1 \pm \frac{\Delta\omega}{\omega_{ao}} \pm \frac{\Delta\mu}{\mu_{ao}}\right)$ by the expression and keep the first-order quantities, then their product is in the following form

$$\left(1 \pm \frac{\Delta\omega}{\omega_{a0}} \pm \frac{\Delta\mu}{\mu_{a0}}\right)\left(1 \mp K_1 \frac{\Delta\mu}{\mu_{a0}} \mp K_1 \frac{\Delta\delta}{\delta_{a0}}\right) = 1 \mp K_1 \frac{\Delta\mu}{\mu_{a0}} \mp K_1 \frac{\Delta\delta}{\delta_{a0}} + 1 \pm \frac{\Delta\omega}{\omega_{b0}} \pm \frac{\Delta\mu}{\mu_{b0}} =$$
$$= 2 \pm (1 - K_1)\frac{\Delta\mu}{\mu_{a0}} \pm \frac{\Delta\omega}{\omega_{b0}} \pm \frac{\Delta\delta}{\delta_{a0}}(1 - K_1) = 2 \pm (1 - K_1)\left(\frac{\Delta\mu}{\mu_{a0}} + \frac{\Delta\delta}{\delta_{a0}}\right) \pm \frac{\Delta\omega}{\omega_{b0}}. \quad (23)$$

Thus,

$$\frac{1}{\sqrt{r_{a0}^2 \pm 2\frac{\Delta r}{r_{a0}} + K_2^2\left[2 \pm (1 - K_1)\left(\frac{\Delta\mu}{\mu_{a0}} + \frac{\Delta\delta}{\delta_{a0}}\right) \pm \frac{\Delta\omega}{\omega_{a0}}\right]}} =$$
$$= \frac{1}{\sqrt{r_{a0}^2 + K_2^2}\sqrt{3 \pm 2\frac{\Delta r}{r_{a0}} \pm (1 - K_1)\left(\frac{\Delta\mu}{\mu_{a0}} + \frac{\Delta\delta}{\delta_{a0}}\right) \pm \frac{\Delta\omega}{\omega_{a0}}}}, \quad (24)$$

where

$$K_2^2 = \frac{\omega_{ao}^2 W_2^4 \mu_0^2 S^2 \mu_{ao}^2}{4(h + a + \mu_{ao}\delta_{ao})},$$
$$K_3 = \sqrt{r_{ao}^2 + K_2^2},$$
$$K_4 = \frac{W_1 W_3 \mu_0 S U_{ao} \omega_{ao} \mu_{ao}}{2(h + a + \mu_{ao}\delta_{ao})}.$$

(24) and multiply it by the $\sqrt{3 \pm 2\frac{\Delta r}{r_{a0}} \pm (1 - K_1)\left(\frac{\Delta\mu}{\mu_{a0}} + \frac{\Delta\delta}{\delta_{a0}}\right) \pm \frac{\Delta\omega}{\omega_{a0}}}$ inverse of the expression (23).

$$\left[1 \pm \frac{\Delta\omega}{\omega_{ao}} \pm \frac{\Delta U}{U_{ao}} \pm (1 - K_1)\left(\frac{\Delta\mu}{\mu_{ao}} + \frac{\Delta\delta}{\delta_{ao}}\right)\right]\left[3 \mp 2\frac{\Delta r}{r_{ao}} \mp (1 - K_1)\left(\frac{\Delta\mu}{\mu_{ao}} + \frac{\Delta\delta}{\delta_{ao}}\right) \pm \frac{\Delta\omega}{\omega_{ao}}\right] \quad (25)$$

is taken.

At the opening of the last statement

$$3 \pm 3\frac{\Delta\omega}{\omega_{b0}} \pm 3\frac{\Delta U}{U_{ao}} \pm 3(1 - K_1)\left(\frac{\Delta\mu}{\mu_{ao}} + \frac{\Delta\delta}{\delta_{ao}}\right) \mp 3 \mp 2\frac{\Delta r}{r_{ao}} \mp (1 - K_1)\left(\frac{\Delta\mu}{\mu_{ao}} + \frac{\Delta\delta}{\delta_{ao}}\right) \pm \frac{\Delta\omega}{\omega_{ao}} \quad (26)$$

we will get that. If we consider the high rates of growth where,

$$E_{ao}\left(1 \pm \frac{\Delta E}{E_{ao}}\right) = K_4\left[2 \pm 2\frac{\Delta\omega}{\omega_{ao}} \pm 3\frac{\Delta U}{U_{ao}} \pm 2(1 - K_1)\left(\frac{\Delta\mu}{\mu_{ao}} + \frac{\Delta\delta}{\delta_{ao}}\right) \mp 2\frac{\Delta r}{r_{ao}}\right] \quad (27)$$

is taken.
Where

$$\pm\frac{\Delta E}{E_{ao}} = 1 \pm 2\frac{\Delta\omega}{\omega_{ao}} \pm 3\frac{\Delta U}{U_{ao}} \pm (1 - K_1)\left(\frac{\Delta\mu}{\mu_{ao}} + \frac{\Delta\delta}{\delta_{ao}}\right) \pm 2\frac{\Delta r}{r_{ao}}. \quad (28)$$

Let us denote the right side of the obtained equation by β_0

$$\beta_0 = 1 \pm 2\frac{\Delta\omega}{\omega_{a0}} \pm 3\frac{\Delta U}{U_{a0}} \pm (1 - K_1)\left(\frac{\Delta\mu}{\mu_{a0}} + \frac{\Delta\delta}{\delta_{a0}}\right) \mp 2\frac{\Delta r}{r_{a0}}. \quad (29)$$

5 RESULTS

From the last expression it is clear that the largest error is obtained from the change in voltage, the second error is obtained from the change in network frequency, and the third error is obtained due to the change in the active resistance in the opposite direction. The smallest error is obtained by multiplying $(1 - K_1)$ the expression by the expression $\frac{\Delta\mu}{\mu_{ao}} + \frac{\Delta\delta}{\delta_{ao}}$.

Computer experiments were conducted to construct the asymptotic diagram (Figure 5).

DOI 10.15588/1607-3274-2025-2-2

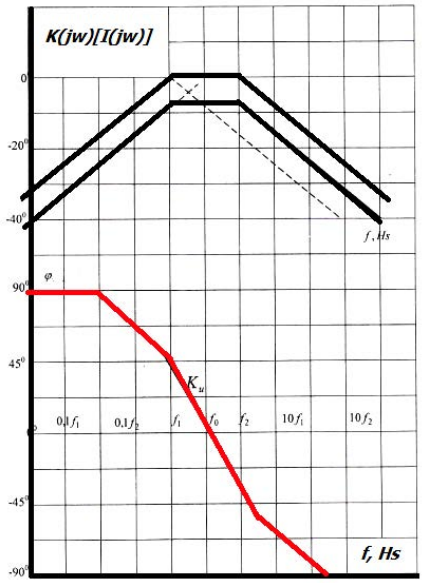

Figure 5 – The asymptotic diagram got by means of computer experiment

The feedback loop assumed in the asymptotic diagram is determined as a function of the RC resistance of the filter.

6 DICUSSION

Based on the analysis of the application object, it was determined that the structure scheme of the RTC at the flexible production system includes complex technological, functionally connected production areas, modules and robotic complexes, their automated control system IMS, regulation, execution, microprocessor control system and devices and devices of the industrial network. includes The functional block diagrams of the IMS of RTCi of the flexible production system are given. Based on research, it was found that it is convenient to use a magnetoelastic transducer with a ring sensitive element to measure the mechanical force acting on the working organs of an industrial robot (IR). For this, unlike existing transmitters, the core of this transmitter is made of whole structural steel. The inductive coil of the proposed transmitter is included in the LC circuit of the autogenerator. The magnetoelastic emitter semiconductor is assembled at the base of the transistor. The cross-section of its core is calculated for the mechanical stress that can be released for the steel. The block-scheme of the inductive transmitter is proposed. The proposed transmitters work on the principle of an autogenerator assembled on an operational amplifier. A mathematical expression is defined for determining the output frequency of the autogenerator. The model of the autogenerator consists of a dependent source, the transmission coefficient is determined.

It is clear from the last expression that the largest error is obtained from the change in voltage, the second error is obtained from the change in the frequency of the network, the 3rd error is obtained due to the change in the active resistance in the opposite direction, and the smallest error $(1-K_1)$ is obtained from the product of the expression of $\frac{\Delta\mu}{\mu_{ao}}+\frac{\Delta\delta}{\delta_{ao}}$.

CONCLUSION

Based on the conducted research, the following results were **the scientific novelty** obtained:

1. The issues of constructor design of transmitters of new construction for the active elements of the robotic complex have been resolved, and the increase in their technical characteristics has been justified.

2. Mathematical models were built for determining the functional parameters of electromagnetic type transmitters with a core made of structural steel, and the advantages of these transmitters were justified.

The practical significance of obtained result is that a replacement circuit that keeps the output frequency of transmitters stable at the information-measurement level of the automated control system in robotics complexes has been established and a research model.

ACKNOWLEDGEMENTS

The work is supported by the state budget scientific research project of the department “Automatic and mechanic” of Sumgait State University “Intellectual control for technology process automation”.

REFERENCES

1. Fujisaki K. High accuracy electromagnetic sensor, *IEEE International Magnetics Conference*, 2002, pp. 123–134. doi: 10.1109/INTMAG.2002.1001384
2. Guo Zhaoyu, Shao Lai, Longfei Xu, Lingling Li Differential Structure of Inductive Proximity Sensor, *Sensors*, 2019, No. 19, pp. 221–230. doi: 10.3390/s19092210
3. Asadova R. Sh., Mamedov F. I., Asadova K. F. Inductive transformer of linear and angular transference, *Patent of the Azerbaijan Republic*. Baku, 2008, 005.
4. Mamedov F. I., Asadova R. Sh. Analytical investigation of optimal parameters of two – functional electromagnetic transducers with continuous magnet conductor, *Works of II International Symposium “Problems of mathematical modeling, controlling and information technologies in oil-gas industry”, News of National Academy Of Sciences Of Baku*, September 21–26, 2008, pp. 101–103.
5. Mamedov F. I., Asadova R. Sh., Sattarov V. K., Mamedov J. F. Two-functional inductive transducer of linear and angular transfers, *Patent of the Azerbaijan Republic, 990049*. Baku, Printed in BI, 1998.
6. Ji Wu., He Xiao-Ting, Sun Jun-Yi A Theoretical Study on Static Gas Pressure Measurement via Circular Non-Touch Mode Capacitive Pressure Sensor, *Sensors*, 2024, №24 (16), pp. 3–14. https://doi.org/10.3390/s24165314
7. Molla-Alipour M., Ganji B. A. Analytical analysis of mems capacitive pressure sensor with circular diaphragm under dynamic load using differential transformation method (DTM), *Acta Mech. Solid Syn.*, 2015, No. 28,

DOI 10.15588/1607-3274-2025-2-2

pp. 400–408. https://doi.org/10.1016/S0894-9166(15)30025-2
8. Lian Y. S., Sun J. Y., Ge X. M., Yang Z. X., He X. T., Zheng Z. L. A theoretical study of an improved capacitive pressure sensor: Closed-form solution of uniformly loaded annular membranes, *Measurement*, 2017, pp. 84–92. https://doi.org/10.1016/j.measurement.2017.07.025
9. Zhang D. Z., Jiang C. X., Tong J., Zong X. Q., Hu W. Flexible Strain Sensor Based on Layer-by-Layer Self-Assembled Graphene/Polymer Nanocomposite Membrane and Its Sensing Properties, *Journal Electron. Mater*. 2018, № 47, pp. 2263–2270. http https://link.springer.com/article/10.1007/s11664-017-6052-1
10. Kumar G. A., Jindal A. U., Sreekanth P. K. Capacitance response of concave well substrate MEMS double touch mode capacitive pressure sensor: Robust design, theoretical modeling, numerical simulation and performance comparison, *Silicon*, 2022, № 14, pp. 9659–9667. DOI: https://doi.org/10.1007/s12633-022-01693-9
11. Lian Y. S., Sun J. Y., Zhao Z. H., He X. T., Zheng Z. L. A revisit of the boundary value problem for Foppl – Hencky membranes: Improvement of geometric equations, *Mathematics*, 2020, № 8, 631 p. https://doi.org/10.3390/math8040631
12. Sun J. Y., Lian Y. S., Lee Z. L., He X. T., Zheng Z. L. Theoretical study on shaft-loaded blister test technique: Synchronous characterization of surface and interfacial mechanical properties, *International Journal of Adhesion and Adhesives*, 2014, № 51, pp. 28–39. https://doi.org/10.1016/j.ijadhadh.2014.03.004
13. Almeida Fernando. Designing and implementation of an intelligent manufacturing system, *Journal of Industrial Engineering and Management*, 2011, № 4, pp. 45–61. http://dx.doi.org/10.3926/jiem.371
14. Akhmedova T. A. Intellectual control of flexible manufacturing module with over manipulator and step conveyor, *American Journal of Computation and Control*, 2015, № 2, pp. 12–15. http://article.aascit.org/file/pdf/9010916.pdf
15. Akhmedova T. A., Guliyev H. B. Fuzzy Logic Controller to Control Voltage and Reactive Power Flow at the Network with Distributed Generation, *Proceedings of the Tenth International Conference on Management Science and Engineering*. Management, Springer, 2017, pp. 329–341. DOI https://doi.org/10.1007/978-981-10-1837-4_29
16. Bakakeu Romuald, Bär, Schirin, Bauer, Jochen et al. An Artificial Intelligence Approach for Online Optimization of Flexible Manufacturing Systems, *Applied Mechanics and Materials*, 2018, № 882, pp. 96–108. doi.org/10.4028/www.scientific.net/AMM.882.96
17. Conrad K., Shiakolas P. Robot calibration issue: ac curacy, repeatability and calibration, The University of Texas at Arlington. USA, 2003, pp. 34–45. https://www.researchgate.net/publication/228686936_Robotic_calibration_issues_Accuracy_repeatability_and_calibration
18. Kumar Manish, Garg D. P. Intelligent multi-sensor fusion techniques in flexible manufacturing work cells, *Proceedings of the American Control Conference*, 2004, Vol. 6, pp. 5375–5380. DOI: 10.23919/ACC.2004.1384707
19. Kolhe J. P., Shaheed M., Chandar T. S., Talole S. E. Robust control of robot manipulators based on uncertainty and disturbance estimation, *International Journal of Robust and Nonlinear Control*, 2013, Vol. 23, № 1, pp. 104–122. https://doi.org/10.1002/rnc.1823
20. Kuo T.C. Trajectory control of a robotic manipulator utilizing an adaptive fuzzy sliding mode, *World Academy of Science, Engineering and Technology*, 2010, Vol. 65, pp. 913–917. https://www.researchgate.net/publication/289291312_Trajectory_control_of_a_robotic_manipulator_utilizing_an_adaptive_fuzzy_sliding_mode
21. Li R., Anwar A. Parsa, Anwar A. M., Lu T. Dynamic Modeling of Underwater Manipulator and its Simulation, *World Academy of Science, Engineering and Technology International Journal of Mechanical, Aerospace, Industrial, Mechatronic and Manufacturing Engineering*, 2012, Vol. 6, № 12, pp. 23–31. https://zenodo.org/record/1078028/files/11836.pdf
22. Manu G., Kumar M., Vijay & Nagesh H. & Jagadeesh D. & Gowtham M. B. Flexible Manufacturing Systems (FMS), A Review, *International Journal of Mechanical and Production Engineering Research and Development*, 2018, pp. 323–336. DOI:10.24247/ijmperdapr201836
23. Pinto Rui. Smart Sensing Components in Advanced Manufacturing Systems, *International Journal on Advances in Intelligent Systems*, 2016, No. 9, pp. 181–198. https://core.ac.uk/download/pdf/148428405.pdf
24. Mammadov J. F., Huseynov E. B., Talibov N. H., Akhmedova T. A., Genjeliyeva G. Q. Development of program tool for expert assessment of innovation projects in the scientific technopark, *IFAC Papers Online Conference paper archive, Science Direct*, 2018, pp. 135–142.
25. Mamedov J. F., Akhmedova T. A. Algorithm of elements option of control systems of flexible manufacturing system, *International Journal of Current Research*, 2015,Vol. 7, Issue 03, March, pp. 13779–13783. www.journalcra.com/sites/default/files/issue-pdf/7989.pdf
26. Mamedov F.I. Provision of Turow over manipulator and stop conveyor with sensor coltrols PC1, *2012 Inwinter National conference Problems of constnetistics and informatics*. Baku, Azerbaijan, 2012, Vol. 1, September 12–14, pp. 237–239. http://dx.doi.org/10.1109/ICPCI.2012.6486330
27. Mamedov J. F., Huseynov A. H., Taghiyeva T. A. Functional and Programmatic Simulation of Architecture for Computing Design of Flexible Manufacture, *American Journal of Computer Science and Information Engineering*. 2014, Vol. 1, № 1, pp. 6–9. http://article.aascit.org/file/pdf/9120727.pdf
28. Lee M., Choi H. S. A Robust Neural Controller for Underwater Robot Manipulators, *IEEE Transactions on Neural Networks*, 2000, Vol. 11, pp. 1465–1470. DOI: 10.1109/IJCNN.1998.687183
29. Piltan F., Sulaiman N., Allahdadi S., Dialame M., Zare A. Position control of robot manipulator: design a novel SISO adaptive sliding mode fuzzy PD fuzzy sliding

DOI 10.15588/1607-3274-2025-2-2

mode control, *International Journal of Artificial Intelligence and Expert System*, 2011, Vol. 2, № 5, pp. 208–228. https://www.cscjournals.org/library/manuscriptinfo.php?mc=IJAE-79
30. Vidakovic J., Lazarevic M., Kvrgic V., Dancuo Z., Ferenc G. Advanced Quaternion Forward Kinematics Algorithm Including Overview of Different Methods for Robot Kinematics, *FME Transactions, Belgrade University*, 2014, Vol. 42, № 3, pp. 189–199. DOI:10.5937/fmet1403189v.
31. Shishaev M. G., Dikovitsky V. V., Nikulina N. V. Architecture and Technologies of Knowledge-Based Multidomain Information Systems for Industrial Purposes, *Computer Science On-line Conference*. Springer, Cham. 27.04.2016, pp. 201–209. https://link.springer.com/chapter/10.1007/978-3-319-33389-2_34
32. Sahu B., Subudhi B. The State of Art of Autonomous Underwater Vehicles in Current and Future Decades, *2014 First International Conference on Automation, Control, Energy and Systems (ACES)*. Hooghy, 2014, pp. 1–6. DOI: 10.1109/ACES.2014.6808014
33. Timashova L. A. Problems of Intellectualization of the Solution of the Problems of Modeling and Control of Production Processes, *USIM*, 2016, №4, pp. 16–26.
34. Timashova L.A., Morozova A. I., Leschenko V. A. and Taran L. Yu. Models of knowledge extraction and structuring, *Inductive modeling of folding systems: Proc., MNNC 1T and S*. Kiev, 2015, pp. 132–151.

Received 12.01.2025.
Accepted 25.04.2025.

УДК 621.3.049

ВИБІР ІНФОРМАЦІЙНО-ВИМІРЮВАЛЬНИХ ЗАСОБІВ ДЛЯ РОБОТОТЕХНІЧНОГО КОМПЛЕКСУ ТА ДОСЛІДЖЕННЯ ЇХНІХ РОБОЧИХ ХАРАКТЕРИСТИК

Мамедов Я. Ф. – д-р техн. наук, професор, завідувач кафедри автоматики і механіки Сумгаїтського державного університету, м. Сумгаїт, Азербайджан.

Ахмадова Т. А. – д-р техн. наук, професор кафедри енергетики Сумгаїтського державного університету, м. Сумгаїт, Азербайджан.

Гусейнов А. Х. – д-р техн. наук, професор кафедри автоматики і механіки Сумгаїтського державного університету, м. Сум-Гайт, Азербайджан.

Талібов Н. Г. – канд. техн. наук, доцент, завідувач кафедри інформаційних технологій Сумгаїтського державного університету, м. Сумгаїт, Азербайджан.

Хашімова Х. М. – асистент кафедри автоматики і механіки Сумгаїтського державного університету, м. Сумгаїт, Азербайджан.

Ахмедов А. А. – інженер, SOCAR Polimer, Азербайджан.

АНОТАЦІЯ

Актуальність. Стаття присвячена питанням вибору засобів інформаційно-вимірювальної системи (ІВС) для автоматизації робототехнічних комплексів (РТК) гнучких виробничих систем, що застосовуються в різних галузях промисловості, та дослідженню їхніх технологічних характеристик.

Мета. Мета – використання математичних моделей для дослідження робочих характеристик передавачів нової конструкції для інформаційно-вимірювального та автоматизованого керування робототехнічним комплексом у гнучких виробничих зонах.

Метод. У статті були поставлені та вирішені наступні питання: аналіз прикладного об’єкта, вибір типів інформаційно – вимірювальних та керуючих елементів створення та структури РТК; дослідження характеристик інформаційно-вимірювального передавача для керування активними елементами РТК; визначення похибки аналогового виходу передавача інформаційно-вимірювальної системи активних елементів РТК.

На основі аналізу об’єкта застосування встановлено, що структурна схема РТК на гнучкій виробничій системі включає складні технологічні, функціонально пов’язані виробничі ділянки, модулі та робототехнічні комплекси, автоматизовану систему керування ними ІСУ, регулювання, виконання, мікропроцесорну систему керування та пристрої та пристрої промислової мережі. включає в себе Наведено функціональні блок-схеми ІВС РТК і гнучкої виробничої системи. На основі досліджень встановлено, що для вимірювання механічної сили, яка діє на робочі органи промислового робота, зручно використовувати магнітопружний перетворювач з кільцевим чутливим елементом. Для цього, на відміну від існуючих передавачів, серцевина цього передавача виготовлена з цільної конструкційної сталі. Індуктивна котушка запропонованого передавача включена в LC-ланцюг автогенератора. На базі транзистора зібраний магнітопружний емітерний напівпровідник. Поперечний переріз його серцевини розрахований на механічне навантаження, яке може вивільнити сталь. Запропоновано блок-схему індукційного передавача. Пропоновані передавачі працюють за принципом автогенератора, зібраного на операційному підсилювачі. Визначено математичний вираз для визначення вихідної частоти автогенератора. Модель автогенератора складається із залежного джерела, визначений коефіцієнт передачі.

Результати. Пропонується новий передавач для вимірювання інформації маніпулятора для синхронного виконання спеціальних технологічних операцій.

DOI 10.15588/1607-3274-2025-2-2

Висновки. Розроблено математичну модель визначення похибки аналогового вихідного передавача інформаційно-вимірювальної системи активних елементів РТК. Вираз ehq використовується для визначення похибки передавача, вихід якого є аналоговим, під час вимірювання поточної технологічної операції. Встановлено, що на практиці геометричні розміри передавача та кількість обмоток залишаються незмінними в процесі роботи, де вона змінюється через вплив зовнішнього середовища. Враховуючи цей варіант, була розроблена математична модель для визначення помилки передавача.

КЛЮЧОВІ СЛОВА: робототехнічний комплекс, інформаційно-вимірювальна система, передавач, індуктивний датчик, автогенератор, LC двигун, напівпровідниковий комутатор, аналоговий вихідний передавач, помилка передавача.

REFERENCES

1. Fujisaki K. High accuracy electromagnetic sensor / K. Fujisaki // IEEE International Magnetics Conference. – 2002. – P. 123–134. doi: 10.1109/INTMAG.2002.1001384
2. Differential Structure of Inductive Proximity Sensor / [Guo Zhaoyu, Lai Shao, Xu Longfei, Li Lingling] // Sensors. 2019. – No. 19. – P. 221–230. doi: 10.3390/s19092210
3. Asadova R. Sh. Inductive transformer of linear and angular transference / R. Sh. Asadova, F. I. Mamedov, K. F. Asadova // Patent of the Azerbaijan Republic. – Baku, 2008. – 005.
4. Mamedov F.I. Analytical investigation of optimal parameters of two – functional electromagnetic transducers with continuous magnet conductor / F. I. Mamedov, J. F. Mamedov, R. Sh. Asadova // Works of II International Symposium “Problems of mathematical modeling, controlling and information technologies in oil-gas industry”, News of National Academy Of Sciences Of Baku, September 21–26, 2008. – P. 101–103.
5. Two-functional inductive transducer of linear and angular transfers / [F. I. Mamedov, R. Sh. Asadova, V. K. Sattarov, J. F. Mamedov] // Patent of the Azerbaijan Republic, 990049. – Baku, Printed in BI, 1998.
6. Ji Wu. A Theoretical Study on Static Gas Pressure Measurement via Circular Non-Touch Mode Capacitive Pressure Sensor // Ji Wu, Xiao-Ting He, Jun-Yi Sun // Sensors. – 2024. – № 24 (16). – P. 3–14. https://doi.org/10.3390/s24165314
7. Molla-Alipour M. Analytical analysis of mems capacitive pressure sensor with circular diaphragm under dynamic load using differential transformation method (DTM) / M. Molla-Alipour, B. A. Ganji // Acta Mech. Solid Syn. – 2015. – No. 28. – P. 400–408. https://doi.org/10.1016/S0894-9166(15)30025-2
8. A theoretical study of an improved capacitive pressure sensor: Closed-form solution of uniformly loaded annular membranes / [Y. S. Lian, J. Y. Sun, X. M. Ge et al.] // Measurement. – 2017. – P. 84–92. https://doi.org/10.1016/j.measurement.2017.07.025
9. Flexible Strain Sensor Based on Layer-by-Layer Self-Assembled Graphene/Polymer Nanocomposite Membrane and Its Sensing Properties / [D. Z. Zhang, C. X. Jiang, J. Tong et al.] // Journal Electron. Mater. – 2018. – № 47. – P. 2263–2270. http https://link.springer.com/article/10.1007/s11664-017-6052-1
10. Kumar G. A. Capacitance response of concave well substrate MEMS double touch mode capacitive pressure sensor: Robust design, theoretical modeling, numerical simulation and performance comparison / G. A. Kumar, A. U. Jindal, P. K. Sreekanth // Silicon. – 2022. – № 14. – P. 9659–9667. DOI: https://doi.org/10.1007/s12633-022-01693-9
11. A revisit of the boundary value problem for Foppl – Hencky membranes: Improvement of geometric equations / [Y. S. Lian, J. Y. Sun, Z. H. Zhao et al.] // Mathematics. – 2020. – № 8. – 631 p. https://doi.org/10.3390/math8040631
12. Theoretical study on shaft-loaded blister test technique: Synchronous characterization of surface and interfacial mechanical properties / [J. Y. Sun, Y. S. Lian, Z. L. Lee et al.] // International Journal of Adhesion and Adhesives. – 2014. – № 51. – P. 28–39. https://doi.org/10.1016/j.ijadhadh.2014.03.004
13. Almeida Fernando. Designing and implementation of an intelligent manufacturing system / Almeida Fernando // Journal of Industrial Engineering and Management. – 2011. – № 4. – P. 45–61. http://dx.doi.org/10.3926/jiem.371
14. Akhmedova T. A. Intellectual control of flexible manufacturing module with over manipulator and step conveyor / T. A. Akhmedova // American Journal of Computation and Control. – 2015. – № 2. – P. 12–15. http://article.aascit.org/file/pdf/9010916.pdf
15. Akhmedova T. A. Fuzzy Logic Controller to Control Voltage and Reactive Power Flow at the Network with Distributed Generation / T. A. Akhmedova, H. B. Guliyev // Proceedings of the Tenth International Conference on Management Science and Engineering. – Management, Springer, 2017. – P. 329–341. DOI https://doi.org/10.1007/978-981-10-1837-4_29
16. An Artificial Intelligence Approach for Online Optimization of Flexible Manufacturing Systems / [Bakakeu Romuald, Bär, Schirin, Bauer, Jochen et al.] // Applied Mechanics and Materials. – 2018. – №. 882. – P. 96–108. doi.org/10.4028/www.scientific.net/AMM.882.96
17. Conrad, K., Robot calibration issue: ac curacy, repeatability and calibration / K. Conrad, P. Shiakolas. – The University of Texas at Arlington, USA, 2003. – P. 34–45. https://www.researchgate.net/publication/228686936_Robotic_calibration_issues_Accuracy_repeatability_and_calibration
18. Kumar Manish Intelligent multi-sensor fusion techniques in flexible manufacturing work cells / Manish Kumar, D. P. Garg // Proceedings of the American Control Conference. 2004. – Vol. 6. – P. 5375–5380. DOI: 10.23919/ACC.2004.1384707
19. Robust control of robot manipulators based on uncertainty and disturbance estimation / [J. P. Kolhe, M. Shaheed, T. S. Chandar, S. E. Talole] // International

DOI 10.15588/1607-3274-2025-2-2

Journal of Robust and Nonlinear Control. – 2013. – Vol. 23, № 1. – P. 104–122. https://doi.org/10.1002/rnc.1823
20. Kuo T. C. Trajectory control of a robotic manipulator utilizing an adaptive fuzzy sliding mode / T. C. Kuo // World Academy of Science, Engineering and Technology. – 2010. – Vol. 65. – P. 913–917. https://www.researchgate.net/publication/289291312_Trajectory_control_of_a_robotic_manipulator_utilizing_an_adaptive_fuzzy_sliding_mode
21. Dynamic Modeling of Underwater Manipulator and its Simulation / [R. Li, Anwar A. Parsa, Anwar A. M, Lu T.] // World Academy of Science, Engineering and Technology International Journal of Mechanical, Aerospace, Industrial, Mechatronic and Manufacturing Engineering. – 2012. – Vol. 6, № 12. – P. 23–31. https://zenodo.org/record/1078028/files/11836.pdf
22. Flexible Manufacturing Systems (FMS), A Review / [G. Manu, M. Kumar, Vijay & Nagesh H. & Jagadeesh D. & Gowtham M. B.] // International Journal of Mechanical and Production Engineering Research and Development. – 2018. – P. 323–336. DOI:10.24247/ijmperdapr201836
23. Pinto Rui. Smart Sensing Components in Advanced Manufacturing Systems / Pinto Rui // International Journal on Advances in Intelligent Systems. – 2016. – No. 9. – P. 181–198. https://core.ac.uk/download/pdf/148428405.pdf
24. Development of program tool for expert assessment of innovation projects in the scientific technopark / [J. F. Mammadov, Huseynov E. B., Talibov N. H. et al.] // IFAC Papers Online Conference paper archive, Science Direct. – 2018. – P. 135–142.
25. Mamedov J. F. Algorithm of elements option of control systems of flexible manufacturing system / J. F. Mamedov, T. A. Akhmedova // International Journal of Current Research. – 2015. –Vol. 7, Issue 03, March. – P. 13779–13783. www.journalcra.com/sites/default/files/issue-pdf/7989.pdf
26. Mamedov F.I. Provision of Turow over manipulator and stop conveyor with sensor coltrols PC1 / F. I. Mamedov, T. A. Akhmedova // 2012 Inwinter National conference Problems of constnetistics and informatics. – Baku: Azerbaijan. – 2012. – Vol. 1, September 12–14. – P. 237–239. http://dx.doi.org/10.1109/ICPCI.2012.6486330
27. Mamedov J.F., Functional and Programmatic Simulation of Architecture for Computing Design of Flexible Manufacture / J. F. Mamedov, A. H. Huseynov, T. A. Taghiyeva // American Journal of Computer Science and Information Engineering. – 2014. – Vol. 1, № 1. – P. 6–9. http://article.aascit.org/file/pdf/9120727.pdf
28. Lee M. A Robust Neural Controller for Underwater Robot Manipulators / M. Lee, H. S. Choi // IEEE Transactions on Neural Networks.– 2000. – Vol. 11. – P. 1465–1470. DOI: 10.1109/IJCNN.1998.687183
29. Position control of robot manipulator: design a novel SISO adaptive sliding mode fuzzy PD fuzzy sliding mode control / [F. Piltan, N. Sulaiman, S. Allahdadi et al.] // International Journal of Artificial Intelligence and Expert System. – 2011. – Vol. 2, № 5. – P. 208–228. https://www.cscjournals.org/library/manuscriptinfo.php?mc=IJAE-79
30. Advanced Quaternion Forward Kinematics Algorithm Including Overview of Different Methods for Robot Kinematics / [J. Vidakovic, M. Lazarevic, V. Kvrgic et al.] // FME Transactions, Belgrade University. – 2014. – Vol. 42, № 3. – P. 189–199. DOI:10.5937/fmet1403189v.
31. Shishaev M. G. Architecture and Technologies of Knowledge-Based Multi-domain Information Systems for Industrial Purposes / M. G. Shishaev, V. V. Dikovitsky, N. V. Nikulina // Computer Science On-line Conference. – Springer, Cham. 27.04.2016. – P. 201–209. https://link.springer.com/chapter/10.1007/978-3-319-33389-2_34
32. Sahu B. The State of Art of Autonomous Underwater Vehicles in Current and Future Decades / B. Sahu, B. Subudhi // 2014 First International Conference on Automation, Control, Energy and Systems (ACES), Hooghy. – 2014. – P. 1–6. DOI: 10.1109/ACES.2014.6808014
33. Timashova L. A. Problems of Intellectualization of the Solution of the Problems of Modeling and Control of Production Processes / L. A. Timashova // USIM. – 2016. – № 4. – P. 16–26.
34. Models of knowledge extraction and structuring / [L. A. Timashova, A. I. Morozova, V. A. Leschenko and L. Yu. Taran] // Inductive modeling of folding systems: Proc., MNNC 1T and S, Kiev, 2015. – P. 132–151.

DOI 10.15588/1607-3274-2025-2-2

UDC 621.391.2:004.31

DEVELOPMENT OF A RANGE MEASUREMENT MODULE ON AN ULTRASONIC SENSOR WITH A GSM MODULE

Sotnik S. V. – PhD, Associate Professor, Associate Professor of Department of Computer-Integrated Technologies, Automation and Robotics, Kharkiv, Ukraine.

ABSTRACT

Context. The development of a range measurement module based on an ultrasonic sensor with a Global System for Mobile Communications (GSM) module is extremely relevant in the field of telecommunications and radio electronics. In today's world, an increasing number of devices are integrated into Internet of Things (IoT) systems, where long-distance data transmission is provided by telecommunication technologies. The use of the GSM module allows real-time transmission of information from the measuring device to remote servers or end users, which is critical for remote monitoring and control solutions.

Ultrasonic sensors in combination with a GSM module can automate measurement processes in hard-to-reach or hazardous environments, which increases the efficiency and safety of systems. The use of radio electronic technologies for real-time transmission of measurement data can significantly expand the functionality of devices and facilitate their integration into existing telecommunications systems, particularly in the industrial, transportation, and infrastructure sectors.

Thus, the development of this module with precise measurements contributes to the development of innovations in the field of telecommunications and radio electronics, providing fast and reliable data transmission, which is an important component of modern information systems.

Objective. Development of a range measurement module based on an ultrasonic sensor with a GSM module and improving the accuracy of measurements by implementing the proposed mathematical model of ultrasonic sensor autocalibration.

Method. To achieve this goal, an integrated range measurement module was developed, which combines the HC-SR04 ultrasonic sensor with a GSM module. The method of improving accuracy is based on the proposed mathematical model of ultrasonic sensor autocalibration.

Results. The task was stated, and a range measurement module based on an ultrasonic sensor with an integrated GSM module was developed. In the course of the study, an electrical schematic diagram of the device was created using DipTrace software. An algorithm for the operation of the module has been developed, which optimizes the interaction between the ultrasonic sensor. A printed circuit board has been created. A mathematical model of autocalibration of an ultrasonic sensor to improve measurement accuracy has been proposed. A series of experimental studies were carried out to assess accuracy. The results of the experiments confirmed the effectiveness of the developed module for measuring distances.

Conclusions. The developed range measurement module based on an ultrasonic sensor with a GSM module is an innovative solution that meets the modern requirements of telecommunication and radio engineering systems. The integration of accurate distance measurement based on the proposed mathematical model of autocalibration of an ultrasonic sensor with the possibility of remote data transmission opens up new prospects for remote monitoring and automation of processes. Experimental studies have confirmed the accuracy and reliability of the device, and comparative analysis with analogs has demonstrated its competitive advantages. The cost-effectiveness and energy efficiency of the developed module make it attractive to a wide range of users, from individual developers to industrial enterprises. Further research can be aimed at improving data processing algorithms and expanding the functionality of the device, which will contribute to the development of innovative technologies in the field of radio electronics and telecommunications.

KEYWORDS: range, measurement, module, ultrasonic sensor, GSM module.

ABBREVIATIONS

AT – attention command;
FFBPN – feedforward backpropagation neural network;
GSM – global system for mobile communications;
ICSPCLK – in-circuit serial programming clock;
ICSPDAT – in-circuit serial programming data;
IoT – internet of things;
LVP – low voltage programming;
MCLR – master clear (reset);
PCB – printed circuit board;
PGC – programming clock;
PGD – programming data;
PGM – programming;
PIC – peripheral interface controller;
RA0/AN0 – analog input 0;
RA1/AN1 – analog input 1;
RAM – random access memory;
RB0/INT – transition / interruption;
RB1/RX/DT – receiver / data transmission;
SIM – subscriber identity module;
TTL – transistor-transistor logic;
UART – universal asynchronous receiver-transmitter;
UIPS – ultra-wideband indoor positioning system;
Vdd – positive supply voltage;
Vpp – programming voltage;
Vss – ground (grounding).

NOMENCLATURE

E – multitude of external influencing factors;
E_b – bit energy;
E_m – energy spent on measurement;
E_{pr} – energy spent on data processing;
E_{tot} – total energy consumption of the system;

DOI 10.15588/1607-3274-2025-2-3

E_{tr} – energy spent on data transmission;

f_s – sampling frequency, which determines the number of signal samples per unit of time;

H – relative humidity at the measurement site;

K_{cor} – coefficient to compensate for systematic error;

K_{rce} – correction coefficient of compensation for the random component of the error;

L – distance, m;

L_A – acoustic interference level;

L_m – measured distance value;

L_{tr} – true value of the distance;

m – total number of measurements;

N – total number of counts that have been made;

N_0 – noise power spectral density;

t – time of the reflected pulse per second;

$s[n]$ – discrete signal samples;

P – calibration options;

P_e – probability of error;

P_{noi} – noise power in the communication channel;

P_{sig} – power of the useful signal;

p_{SW} – Shapiro-Wilk criterion;

R^2 – coefficient of determination;

$RMSE$ – root mean square error;

$Q(\ )$ – function;

SNR – signal-to-noise ratio;

T – air temperature or directly temperature in the measurement environment of the HC-SR04 ultrasonic sensor, °C;

T_s – sampling period, which determines the time interval at which samples are taken;

$Y_{cal,i}$ – calibrated value for the *i*-th measurement;

$Y_{mes,i}$ – measured value for the *i*-th measurement;

Y_{pr} – primary measurement;

$Y_{ref,i}$ – reference value for the *i*-th measurement;

α – coefficient that determines the effect of temperature in a systematic error;

β – coefficient that determines the effect of humidity in a systematic error;

γ – coefficient that determines the influence of the level of acoustic interference in the systematic error;

δ – relative error;

θ – coefficient that determines the influence of the primary measurement into a systematic error;

ε – measurement error, m;

ε_{sys} – systematic error;

μ – average error value, m;

σ – variance, which characterizes the spread of errors around the mean value;

ν – ultrasonic speed, m/s.

DOI 10.15588/1607-3274-2025-2-3

INTRODUCTION

As the coverage of mobile networks increases, GSM modules are becoming increasingly popular. They allow efficient transmission of data or other information. This approach provides convenience and speed of information transfer in real time. This trend is especially relevant in an environment where automation and remote monitoring are becoming an integral part of modern technological systems [1–4].

Automated control allows precise control of process parameters such as temperature and metal casting speed, ensuring stable production conditions and preventing defects. In addition, the automated system records data in real time, which simplifies the maintenance of technical documentation and allows you to quickly respond to changes in process parameters.

Ultrasonic sensors are one of the most effective tools for precise distance measurement in various media. The combination of ultrasonic sensors with GSM modules opens up new possibilities for creating autonomous measurement systems that can transmit measurement results over long distances. This is especially important for applications where traditional methods of data collection and transmission are not efficient or possible.

The development of a range measurement module based on an ultrasonic sensor with the integration of a GSM module is aimed at creating a universal device that will provide accurate distance measurements and the ability to transmit them to remote servers or end users. This will significantly increase the efficiency in the field of radio engineering and telecommunications by improving the collection and processing of data in real time. The integration of the GSM module ensures stable communication over long distances, which reduces delays in data transmission. This allows you to improve monitoring systems, controlling remote devices and networks, especially in environments where the use of advanced technologies is difficult or impossible.

The research objectives include the development of an integrated module that combines the HC-SR04 ultrasonic sensor with a GSM module for remote monitoring and real-time data transmission. In addition, it is necessary to identify and analyze modern distance measurement devices, their characteristics, advantages and disadvantages, and develop an algorithm for the module to ensure measurement accuracy and reduce power consumption. These tasks are aimed at creating and implementing an innovative, energy-efficient and cost-effective solution for remote distance measurement with real-time data transmission to expand the capabilities of telecommunication systems, improve remote monitoring technologies in various industries and science, and develop applied aspects of radio engineering in the field of measurement systems and wireless data transmission. Practical tasks include the implementation of an algorithm and the creation of a remote distance measurement module that integrates an inexpensive HC-SR04 ultrasonic sensor with a GSM module, which allows for remote measurements at an affordable price.

Since one of the main problems that exist in the development and use of remote distance measurement systems is to ensure high accuracy of measurements in various operating conditions, improving the accuracy of distance measurement becomes a key task for improving such systems. This is especially important for applications where even small errors can have a significant impact on the results of the entire system, which is why this is the topic of our research.

The initial data include the results of previous studies, technical requirements for creating a distance measurement module [5–7].

The object of research is the distance measurement process and the GSM module for data transmission.

The subject of research is a distance measurement module.

The purpose of the research is to development of a range measurement module based on an ultrasonic sensor with a GSM module and increasing the accuracy of measurements by implementing the proposed mathematical model of ultrasonic sensor autocalibration.

1 PROBLEM STATEMENT

In the context of the rapid development of telecommunication technologies and the expansion of the application areas of radio systems, the issue of effective integration of measuring devices with data transmission systems is becoming particularly relevant. Modern radio engineering and telecommunications require reliable, accurate and cost-effective solutions for remote measurement and monitoring of various parameters, including distance.

Existing distance measurement systems in radio engineering applications often face accuracy and reliability issues, especially in variable electromagnetic environments or when working with different types of surfaces. These limitations have a significant impact on the efficiency and reliability of telecommunications' systems that use distance data to optimize signal transmission or antenna system setup.

Integration of measuring devices with modern telecommunications networks, in particular with mobile communication systems, remains a challenge. Many existing solutions do not have effective means for long-distance data transmission, which limits their use in distributed radio systems and networks. This problem is particularly acute in the context of the development of IoT technologies and the expansion of mobile network coverage, where efficient data transmission from remote sensors is critical.

In light of these challenges, there is an urgent need to develop an integrated range measurement module that would combine high measurement accuracy with the ability to efficiently transmit data over mobile networks. Such a module should be energy-efficient with the ability to operate autonomously, affordable, and able to operate in a variety of operating conditions typical of telecommunications systems.

The development of a module based on the HC-SR04 ultrasonic sensor with the integration of a GSM module seems to be a promising solution that can meet the above requirements.

The mathematical formulation includes in the model the measurement of distance by an ultrasonic sensor: $L = (\nu \cdot t)/2$. Taking into account the effect of temperature on the speed of sound: $L = 331{,}3 + 0{,}606 \cdot T$. Model of measurement error: $L_m = L_{tr} + \varepsilon$. While the measurement error can be modeled as a random variable with a normal distribution $N(\mu, \sigma^2)$, the average error value is zero, i.e., $\mu = 0$ on average, the error will not bias the result in a certain direction (no systematic error). Dispersion, which characterizes the spread of errors around the mean value. The larger the value σ, the more errors can deviate from zero.

Sampling of a signal for digital processing: $s[n] = s(T_s), n = 1, 2, ..., N-1$. The sampling period that determines at what interval samples are taken $f_s = 1/T_s$. It can be thought of as the inverse of the sampling rate Data transmission model via a GSM module: $SNR = P_{sig} / P_{noi}$. The probability of error when transmitting a bit of information: $P_e = Q(\sqrt{2E_b / N_0})$. Energy efficiency of the system: $E_{tot} = E_m + E_{pr} + E_{tr}$.

This mathematical formulation covers the main aspects of the developed module, including distance measurement, signal processing, data transmission, and energy efficiency of the system. It allows for a theoretical analysis and optimization of system parameters to achieve the best measurement accuracy and data transmission reliability.

2 REVIEW OF THE LITERATURE

Today, many authors have studied in detail the areas of application and various aspects of distance measurement technologies. In particular, numerous scientific publications and technical reports focus on analyzing the effectiveness of various distance measurement methods, their accuracy, speed, and adaptation to different conditions.

Thus, the ultrasonic method of measurement, namely sensors, is one of the most effective tools for accurate distance measurement. A striking example of the synergy of radio engineering and telecommunications is the development and implementation of an UIPS, presented in [8]. This system demonstrates how technologies traditionally associated with radio engineering (ultrasonic signals, specialized signal processing methods) are integrated with modern telecommunications solutions (Wi-Fi, wireless sensor networks) to create an effective positioning system.

Another important study [9] presents an innovative assistive device for navigation for blind and visually impaired people, which, although it has wide practical application, is based on the principles of radio engineering and telecommunications. This device combines radio engineering components (ultrasonic sensors for detecting obstacles, signal processing and analysis) with telecommu-

DOI 10.15588/1607-3274-2025-2-3

nications and information technologies (integration of a smartphone and its camera, visual information processing). These studies clearly demonstrate that modern developments in distance measurement and positioning lie at the intersection of radio engineering and telecommunications, combining signal processing principles with advanced data transmission methods.

In modern radio engineering and telecommunications, there is a wide range of technologies for measuring distance. Each of these technologies has its own advantages and limitations that determine their areas of application.

Ultrasonic and infrared technologies for detecting various objects on flat surfaces and from different materials are described in [10]. The focus is on measurements at short distances within useful ranges.

A study of the operation of an ultrasonic sensor that measures distance by the threshold method is presented in [11]. To improve the accuracy of distance measurement, the authors used the least-squares method, the piecewise method, and the Vandermonde method. The principle of operation of these sensors is based on measuring the time required for the reflection of an ultrasonic pulse from an object. Research shows that ultrasonic sensors are particularly effective for measurements up to 4 meters away, making them ideal for many industrial and domestic applications.

Paper [12] describes research in the field of laser sensors for movement, distance, and position. Laser distance measurement technologies are used in robotics, surveillance, autonomous driving, and biomedicine. Laser sensors are based on various optical methods, such as triangulation, time-of-flight, confocal and interferometric sensors.

Optical sensors use infrared radiation to measure distance [13, 14]. These sensors have the advantage of being fast and able to work with transparent objects.

In [14], a device was developed to measure the exact distance from 5 to 400 cm using three sensors using the proposed online FFBPN. The field of application of the device is in robotics and radar for accurate object detection in robotics and radar, as this device successfully detects close and distant objects.

The use of GSM modules to transmit measurement data is becoming increasingly popular due to the wide coverage of mobile networks [15]. This makes it possible to create autonomous monitoring systems that can operate over long distances without the need for additional communications. The authors in [15] describe the experimental setup and discuss the measurement principle. To calculate the distance using this device, the target, the distance to which is to be measured, should always be perpendicular to the plane of propagation of ultrasonic waves. Thus, the target orientation is a limitation of this system. The paper describes the device in some detail but does not pay much attention to studies on accuracy and energy efficiency.

Paper [16] is devoted to the use of ultrasonic sensors to measure the distance to objects without physical contact. The device includes a built-in temperature compensation sensor to improve measurement accuracy because temperature changes affect the propagation speed of ultrasonic waves. The work uses an ATmega32 and an ultrasonic transmitter and receiver operating at 40 kHz, generating and receiving ultrasonic pulses and calculating the time of their reflection from the obstacle. The authors also used the HC-SR04 sensor. Although the distance to the object can be measured up to 60 meters and the measurement results are displayed on an LCD screen, it is worth noting that our choice of the PIC16F628A may be more efficient because it has a power consumption advantage for battery-powered devices.

In [17], distance measurement methods are considered, in particular, the non-contact method that uses an ultrasonic sensor. An ultrasonic transducer uses the time-of-flight technique to determine distance. This method calculates the time interval between the transmitted and reflected signal, which allows for distance determination. Although the tests have shown successful results in measuring the distance to an object up to 5 meters, as well as calculating the corresponding area and volume, the described methods and results could be compared with analogs, as we have done in our work, to prove the effectiveness of the work. In addition, the article does not provide a detailed analysis of the impact of different environmental conditions on the accuracy of measurements, which is an important aspect to improve the overall performance of the system.

Measurements using ultrasonic sensor probes are among the cheapest of the various options. Such sensors are considered to be one of the most efficient and cost-effective methods of distance measurement, although there is potential for further development of this technology for longer distances. This paper describes measuring the distance to an obstacle using such a sensor.

The general trend of these scientific works is a great interest in the development and improvement of non-contact distance measurement methods using ultrasonic and other types of sensors. Researchers focus on improving the accuracy and range of measurements, as well as on integrating these technologies with various electronic systems to achieve better results in practical applications.

Therefore, in this work, emphasis is placed on the development of a range measurement module on an ultrasonic sensor with a GSM module and to increase the accuracy of distance measurement, and in addition, it will be possible to transmit the obtained values to remote servers or end users.

3 MATERIALS AND METHODS

To begin with, let’s justify the choice of technical means for the distance measurement module.

For this study, we chose the HC-SR04 ultrasonic sensor developed by RoboBox because it is (Fig. 1) [18]:

– is widespread and easily available on the market of electronic components;

– is one of the most cost-effective solutions for distance measurement;

DOI 10.15588/1607-3274-2025-2-3

– has a simple interface that facilitates its integration with various microcontrollers;

– HC-SR04 measurement accuracy (usually ±3 mm) is quite acceptable;

– no blind spots;

– the sensor is capable of measuring distances from 2 cm to 400 cm, which is suitable for many projects;

– consumes little power, which is important for mobile or autonomous devices;

– small dimensions of the sensor make it easy to integrate into various projects;

– less sensitive to light and color of objects compared to optical sensors.

Figure 1 – HC-SR04 sensor

To generate ultrasonic waves on the transducer, a TTL pulse of 10 μs duration must be applied to the Trig pin.

When the pulse arrives, the circuit generates 8 pulses with a frequency of 40 kHz, which activate the piezoresistive transducer. This creates ultrasonic waves that propagate in the direction of the obstacle. The reflected waves are captured by a second piezoelectric transducer. By comparing the time between sending and receiving pulses, the circuit generates a TTL-level Echo pulse whose duration is proportional to the distance to the object.

After determining the width of the Echo pulse, you can calculate the distance to the reflected surface using the following formula: pulse width equals distance.

The PIC16F628A microcontroller is used to convert the duration of the signal generated by the ultrasonic sensor into a distance value and then transmit it to the SIM module. This microcontroller is part of the widely used PIC series. The choice of this microcontroller is due to the presence of a built-in timer and a UART interface, which allows you to transfer data and commands such as AT, which are recognized by the SIM module.

PIC16F628A is the best choice for developing a range measurement module with an ultrasonic sensor and GSM module because:

– PIC16F628A offers a good feature set at an affordable price;

– the small size of the microcontroller (18-pin DIP or SOIC package) allows you to create compact devices;

– PIC16F628A has power-saving modes, which is important for standalone devices;

– clock frequency up to 20 MHz provides sufficient performance for processing data from the ultrasonic sensor and GSM module;

– 2048 words of program Flash memory and 224 bytes of RAM are enough to implement the required functionality;

– the presence of UART, timers, and comparators simplifies the work with external devices;

– PIC series microcontrollers are known for their stability and resistance to interference.

The location of the pins of the microcontroller PIC16F628A in Fig. 2.

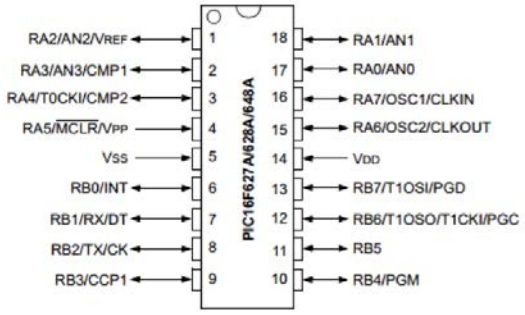

Figure 2 – Diagram of the location of the pins of the microcontroller PIC16F628A

In Fig. 2 the diagram shows the purpose of each of the 18 pins of the microcontroller, such as RA0/AN0, RA1/AN1, RB0/INT, RB1/RX/DT, etc. This information is important for the correct connection of the microcontroller to other components of the circuit, for example, to connect an ultrasonic sensor, GSM module, and other devices within the developed range measurement module.

Next, let's move on to the development of a diagram of an electrical circuit device for measuring distance.

In this study, a distance measurement module was developed using the DipTrace software.

DipTrace was chosen for designing component packages and creating PCB layouts due to its ease of use, intuitive interface, and powerful set of design tools. This program provides high accuracy when working with various components, which allows you to create complex electronic circuits and layouts with minimal errors. In addition, DipTrace supports a wide range of file formats, which facilitates integration with other tools and systems, making it a universal solution for PCB designers. The electrical schematic diagram of the device was created using the DipTrace Schematic module (Fig. 3).

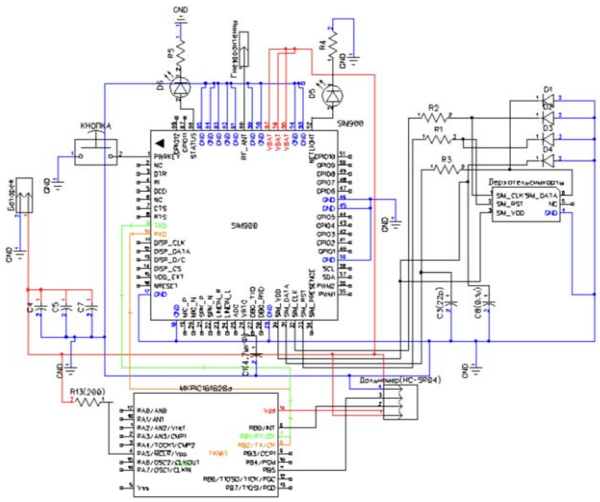

Figure 3 – Schematic diagram of the distance measurement module of the microcontroller PIC16F628A

DOI 10.15588/1607-3274-2025-2-3

First, the matching elements were removed from the antenna circuit. It is allowed to use a short connection between RF_ANT(60) and the antenna at short distances. The PWRKEY(1) pin has a button, which, when pressed for 0,5 seconds, turns on the module.

The LED indicators are connected via resistors. When the module is turned on, the LED connected to the STATUS(66) pin should light up.

The NETLIGHT(52), which shows the network status, operates in glow and non-beam modes.

The TX(9) and RX(10) pins of the module are connected to the PIC16F628A microcontroller, providing data exchange via a serial UART interface using AT commands.

Resistors R4 and R5 limit the current supplied to LED indicators set to 300 ohms.

Any antenna in the GSM band with an SMA-F connector is used.

Capacitors: C1–4,7 μF, C3–22 pF, C4–100 μF, C5–104 nF, C7–10 pF, C8–0.47 μF.

The SIM cardholder is installed with protective diodes.

It is recommended to use a powerful power supply since, when searching for a network, the peak current can reach 1.5 A.

Now, let's move on to the development of the module's algorithm. Consider the principle of operation of the distance measurement module.

When idle, the module goes into sleep mode.

The microcontroller is configured in such a way that it automatically activates when it is in idle mode. The wake-up of the microcontroller is due to a signal from the SIM900, specifically from the RI pin (4), which is connected to the RB4 pin of the microcontroller.

When an incoming call or SMS is received at the RI(4) input of the SIM900, the logical level on this pin is lowered to 0, which causes an interrupt in the microcontroller and activates it.

After waking up, the device is configured so that when receiving an incoming call, the microcontroller sends a pulse of 10 μs to the HC-SR04 ultrasonic sensor.

After receiving a signal from the sensor, the microcontroller calculates the distance (in centimeters) and transmits this data via AT commands to the communication module.

The general algorithm of the program is shown in Figure 4.

Declaring variables is the first step in executing a program.

Next, the microcontroller timers are configured.

After that, it is necessary to implement the output of the AT command to configure the operation of SMS transmission, so the program outputs the AT command for the configuration of SMS transmission. AT commands allow: to configure communication parameters, initiate a connection, send and receive data (in this case, SMS), control the functions of a modem or GSM module.

At the stage "Output of AT commands to configure the operation of SMS transmission", the program probably sends one or more AT commands to the GSM module for its configuration before sending SMS.

Next, the program waits for an incoming call, which is marked as "Ring" on the diagram – this is a special signal. This call serves as a trigger or signal to activate the measuring process. It is not designed for voice communication.

Advantages of this approach:

– the system does not carry out constant measurements but is activated only when necessary;

– access control, because only authorized numbers can initiate measurements;

– remote control: the ability to start measuring remotely.

If the "Ring" call is received, the following steps are performed:

– measuring the time around the input signal, that is, the program measures the duration of the input signal, so the trigger for the HC-SR04 is triggered, the sensor generates 8 pulses for transmission, and the displayed signal will be sent to the microcontroller;

– converting them into centimeters, that is, the measured time is converted into distance (centimeters);

– sending SMS, here the program generates and sends SMS messages.

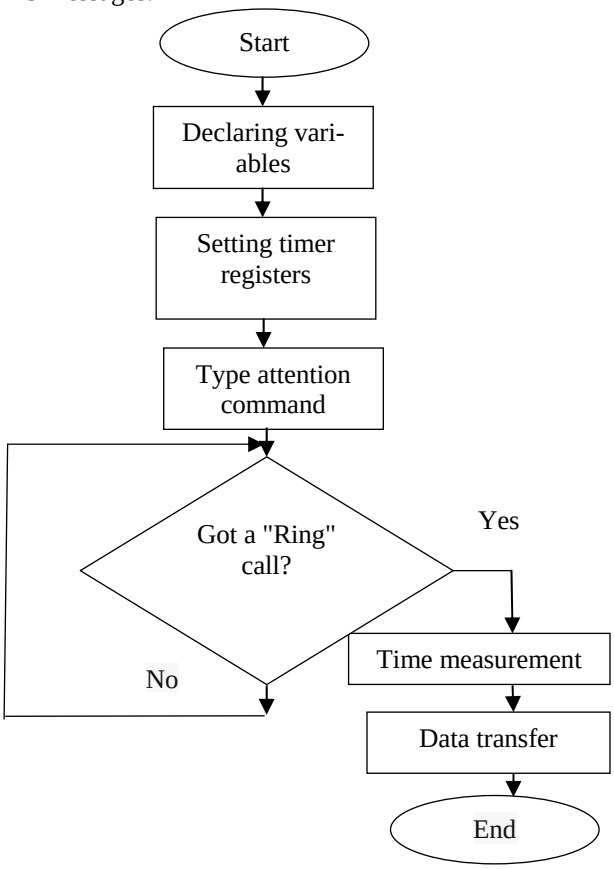

Figure 4 – Algorithm of the distance measurement module program

The "Ring" call does not require an answer or connection. The very fact of its receipt is a signal to start work.

DOI 10.15588/1607-3274-2025-2-3

The sensor data is sent to the user's landline number.

Thus, the microcontroller is in sleep mode while waiting for the "Ring" call and will "wake up" when interruptions occur from the contact of the module UART_RI(4), which reduces the power consumption of the device.

The application for the PIC16F628A microcontroller was downloaded using the PICkit 2v2.61 utility and the PICkit 2 programmer. Next, we describe which microcontroller pins should be connected to the outputs of the programmer for flashing the program:

1 – MCLR/Vpp;
2 – Vdd Target;
3 – Vss (ground);
4 – PGD (ICSPDAT);
5 – PGC (ICSPCLK);
6 – PGM (LVP).

3.4 Creating a PCB for the distance measurement module

For this device, according to the above scheme (Fig. 3), a printed circuit board was created using laser-iron technology. The board drawing was made using the DipTrace PCB program, which has auto-positioning and auto-trace functions. The circuit board diagram is depicted in DipTrace (Fig. 5 a).

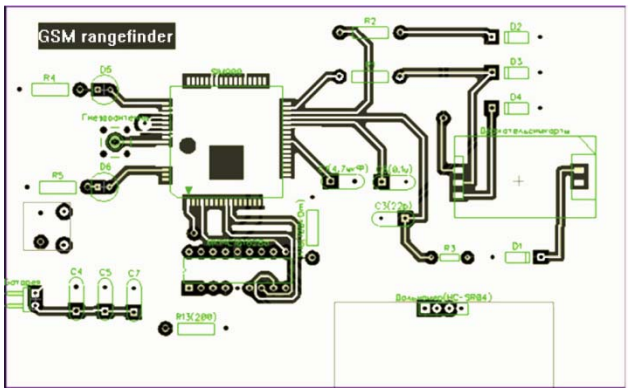

a

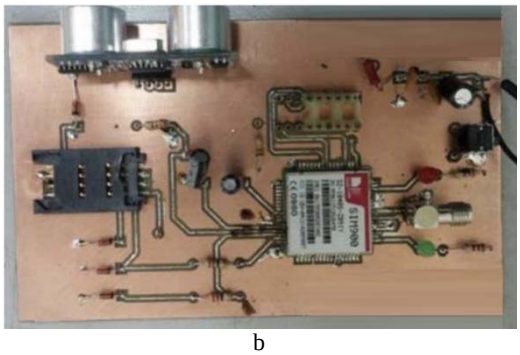

b

Figure 5 – Range measurement module PCB

Fiberglass board of the range measurement module measuring 13 cm × 8 cm in size (Fig. 5 b).

Images of the tracks, pins, and board elements were generated as a template using PCB design programs such as DipTrace and then printed on A4 glossy paper for transfer to fiberglass during board manufacturing.

After that, the workpiece was prepared, namely, the surface of the fiberglass was cleaned with fine sandpaper and degreased with lotexolite, carefully placing it on the workpiece and smoothing it with an iron for 3–5 minutes. Then the paper is moistened with water and carefully removed. The workpiece was etched in a solution of ferric chloride prepared in a ratio of 1:1 with water.

Therefore, to increase accuracy, it is proposed to formalize the process of correcting measurements.

A mathematical model of autocalibration is proposed, which will be based on a statistical analysis of the discrepancies between the measured and reference values. The key idea is to determine the systematic error of the sensor and its subsequent compensation.

Therefore, the mathematical model of autocalibration of an ultrasonic sensor is a multicomponent approach to improving the accuracy of measurements by statistically correcting systematic errors.

The concept of the model is:

– analysis of discrepancies between measured and reference values;

– formalization of the process of determining errors;

– development of a mechanism for adaptive correction of measurements;

– taking into account the influence of external factors on the accuracy of measurements.

The experiments section presents the results of the measurements made with HC-SR04 and the reference values that were compared. These comparisons are the basis for the development of the autocalibration method.

The general mathematical model can be represented as a functional mapping:

$$Y_{cal} = F(Y_{pr}, E, T, H, L_A). \quad (1)$$

External conditions E include: atmospheric parameters (air pressure, density of the medium, presence of air currents); geometric characteristics of the environment (presence of physical obstacles, distance to objects, configuration of space); external physical influences (electromagnetic fields, acoustic background, vibrations).

Let's formalize the process of determining errors. The component of systematic error can be represented as:

$$\varepsilon_{sys} = f(Y_{pr}, T, H, L_A) = \\ = \alpha \cdot T + \beta \cdot H + \gamma \cdot L_A + \theta \cdot Y_{pr}. \quad (2)$$

The accuracy of the HC-SR04 ultrasonic sensor is key to its effective use in real-world applications. Minor errors in the operation of the sensor can accumulate, affecting the overall quality of the system. To ensure reliable operation of the system, it is important to take into account the errors (systematic or random) that occur during measurements. Therefore, systematic errors can be presented in the form of:

DOI 10.15588/1607-3274-2025-2-3

$$\sigma(\varepsilon) = \sqrt{\sum_{i=1}^{m} (Y_{mes,i} - Y_{ref,i})^2 \cdot w(T, H, L_A) / m}. \quad (3)$$

We will take into account the weight function of external factors $w(T, H, L_A)$, which allows us to estimate their influence on the variance of errors

The algorithm for the process of correcting ultrasonic sensor measurements is shown in Fig. 6.

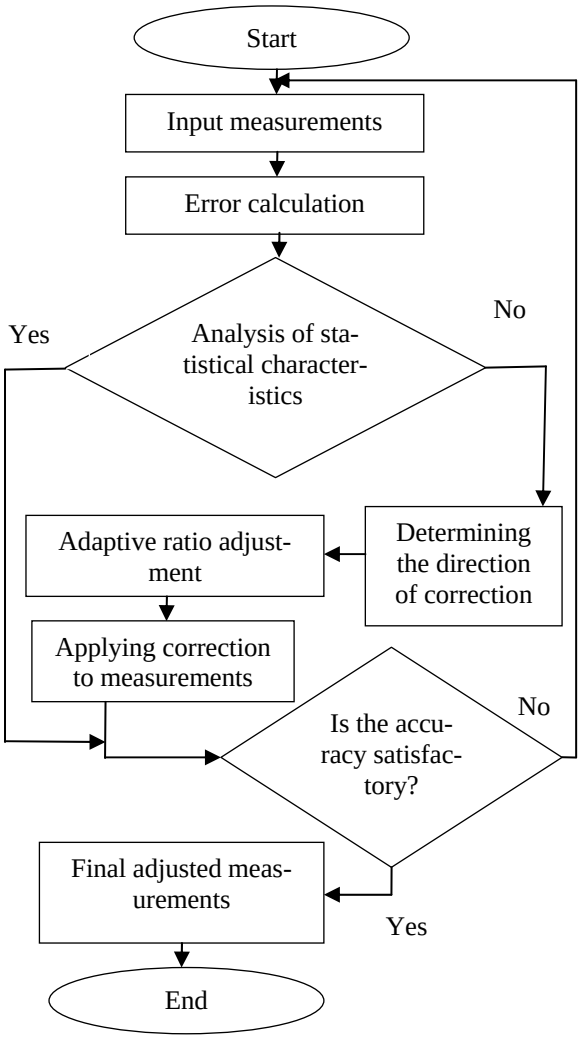

Figure 6 – Algorithm of the ultrasonic sensor measurement correction process

Step 1. Input measurements.
Step 2. Calculation of errors.
Розрахунок абсолютної похибки:

$$\varepsilon = \left| Y_{mes} - Y_{ref} \right|. \quad (4)$$

The relative error can be determined:

$$\delta = \left(\left| Y_{mes} - Y_{ref} \right| \right) / Y_{ref} \cdot 100\%. \quad (5)$$

Step 3. Analysis of statistical characteristics includes verification:

– the average value of the error > 0.1, then the systematic error. If the average error value is <= 0.1, then the error is within the normal range;

– variance of errors > critical value, then this is a significant random error. If the variance <= of a critical value, then the stability of the measurements;

– distribution asymmetry != 0, then, nonlinearity of errors. If the distribution asymmetry = 0, then the symmetric error distribution;

– the Shapiro-Wilk criterion p_{SW} < 0.05, then there is a deviation from the normal distribution. If the Shapiro-Wilk criterion p_{SW} > = 0.05, then the normal error distribution.

Step 4. If the analysis of statistical characteristics showed that the obtained values of the monitored parameters (average error value, etc.) are not within the normal range, then the direction of correction is determined. This stage involves an analysis of the nature of the detected errors in order to choose the optimal approach to their compensation:

– if the average value of the error exceeds the norm, this indicates the presence of a systematic error. The direction of correction will be aimed at reducing this systematic component;

– if the error variance is too high, this indicates a significant random error. In this case, the direction of correction will be aimed at reducing the influence of random factors;

– analysis of the asymmetry of the error distribution helps to identify the presence of nonlinearities, which is also taken into account when determining the direction of correction;

– if the Shapiro-Wilk criterion < 0.05, then there is a deviation from the normal distribution. In this case, it is necessary to apply other approaches to modeling and compensation for errors that are not based on the assumption of a normal distribution. For example, robust statistical methods can be used, which are less sensitive to deviations from normality. This will allow you to correctly take into account the peculiarities of the real distribution of errors when developing an automatic calibration algorithm.

If the statistical characteristics of the errors are within the normal range, that is, they show the stability of the measurements, then the next step should be to check the accuracy. The application of additional correction will not be necessary. After checking the accuracy, if it meets the requirements, it will be possible to complete the autocalibration process.

Step 5. Adaptive adjustment of correction coefficients based on the analysis of errors. This stage is key, as it allows you to dynamically adjust the compensation parameters depending on the current state of the measuring system.

The concept of adaptive coefficient adjustment will take into account the following factors:

DOI 10.15588/1607-3274-2025-2-3

– current statistical characteristics of errors (mean, variance, asymmetry);

– changes in external conditions that affect the sensor.

For example, if the analysis revealed the presence of a systematic component of error, the compensation coefficient will be increased to reduce this component.

Thus, the adaptive approach allows you to flexibly respond to changes in the operation of the sensor and optimally adjust the correction parameters to ensure high accuracy of measurements in real operating conditions.

Step 6. Step 6 consists of applying the calculated correction to the sensor's output measurements. At this stage, the adaptive correction coefficients determined in the previous step are used to compensate for systematic and random errors.

Thus, the initial uncorrected sensor readings are processed using the calculated correction coefficients, which allows you to obtain corrected, more accurate measurement values. This step completes the autocalibration process, providing an increase in the overall accuracy of the ultrasonic sensor.

Let the systematic error of the sensor be represented by the formula (2). Then the adjustment factor to compensate for the systematic error is calculated as:

$$K_{cor} = 1/(1+\varepsilon_{sys}). \quad (6)$$

To compensate for the random component of the error, the correction factor is determined based on the variance of the errors:

$$K_{rce} = 1/\sqrt{\sigma}. \quad (7)$$

If the analysis shows the presence of nonlinearities in the error distribution, i.e. asymmetry, or deviations from the normal distribution according to the Shapiro-Wilk criterion, this means that the errors cannot be compensated by linear correction coefficients alone. In general, deviation from normality requires the use of robust statistical analysis methods and appropriate nonlinear error-side compensation algorithms. This will allow you to more effectively take into account the real features of the distribution of sensor errors.

Step 7. Accuracy check. Accuracy verification is the final stage of the autocalibration process and is aimed at evaluating the effectiveness of the developed error correction methods. The main goal of this stage is to confirm that the applied correction algorithms have improved the accuracy of the ultrasonic sensor measurements. The procedure for checking accuracy usually consists of the following sub-stages:

1. Collection of new test data. At this stage, new measurements are made using the sensor after making adjustments. These measurements are compared with reference values. Reference values are usually obtained from high-precision systems or using special calibration equipment.

2. The residual errors are calculated after applying the correction factors:

$$\varepsilon_{res} = Y_{cal} - Y_{ref}. \quad (8)$$

3. Analysis of statistical characteristics of residual errors.

First, key parameters are evaluated, namely:

– average value of residual errors ($\bar{\varepsilon}$). If $\bar{\varepsilon} \approx 0$, this indicates the minimization of the systematic error;

– dispersion of residual errors (σ^2). If σ^2 has decreased significantly compared to the initial data, this means effective compensation for random errors;

– asymmetry (Skewness) and excess (Kurtosis). If the asymmetry (Skewness) is close to 0, and the excess (Kurtosis) is 3 (or close to 3), this confirms the normal distribution of residual errors;

– Shapiro-Wilk criterion p_{SW}. If $p_{SW} \geq 0.05$, the residual errors are normally distributed, which is a good indicator.

4. Comparison before and after correction. The key accuracy metrics before and after the application of correction algorithms are compared:

– standard error (RMSE):

$$RMSE = \sqrt{\frac{1}{m}\sum_{i=1}^{m}(Y_{cal,i} - Y_{ref,i})^2}. \quad (9)$$

A decrease in $RMSE$ confirms the success of the correction.

The coefficient of determination (R^2) analyzes how much the adjusted values correspond to the reference values.

5. Assessment of the admissibility of residual errors. It is checked whether the residual errors are within the permissible range. If they go beyond these limits, it is necessary to reconfigure the correction algorithm.

Thus, the accuracy check covers the calculation of residual errors, their statistical analysis, visualization and comparison of results before and after correction. This allows you to evaluate the effectiveness of autocalibration and confirm the achievement of the required level of accuracy.

Step 8. Obtaining final corrected measurements.

A more in-depth analysis of the mathematical model of autocalibration will be presented in this paper.

4 EXPERIMENTS

A series of experimental studies were carried out to evaluate the accuracy and reliability of the developed distance measurement module. The main purpose of the experiments was to compare the indicators of the HC-SR04 ultrasonic sensor with reference measurements made using a ruler.

The methodology of the experiment included the following stages:

DOI 10.15588/1607-3274-2025-2-3

– preparation of an experimental bench consisting of a developed distance measurement module and a reference ruler;

– installation of the measuring object at different distances in the range of up to 15 cm;

– distance measurements using the HC-SR04 ultrasonic sensor;

– parallel distance measurement using a ruler to obtain reference values;

– distance measurements using the Sharp GP2Y0A21YK0F optical sensor;

– recording and comparing the results obtained;

– analysis of the obtained data: plotting the presence of the measured distance from the real one for both sensors and determining the ranges of greatest accuracy for each type of sensor.

It is necessary to take into account the influence of various environmental conditions on the accuracy of distance measurement:

– in environments with a high noise level, false alarms are possible;

– the sensor can be sensitive to changes in temperature and humidity, which can affect the speed of propagation of ultrasonic waves;

– measurement efficiency may decrease when working with soft or porous surfaces that reflect ultrasonic waves worse;

– the accuracy of measurements can be affected by the angle of inclination of the surface relative to the sensor;

– the presence of other ultrasonic sources nearby can create interference and lead to inaccurate measurements;

– the sensor has a “blind spot” at very close distances (usually less than 2 cm), where it cannot accurately measure the distance.

5 RESULTS

The measured distance of the HC-SR04 was compared with the ruler and the Sharp GP2Y0A21YK0F, the results were entered in Table 1.

Table 1 – Measurement results

Measured distance on HC-SR04, cm	Distance on the ruler, cm	Measured percentage on Sharp GP2Y0A21YK0F, cm
2	2	2
3	3	3
4	4	4
6	5	5
6	6	6
7	7	7
8	8	8
9	9	9
10	10	11
12	11	12,1
12	12	13
13	13	14,3
15	14	15,4
15	15	16

Graphs of the dependence of the measured distance on the real one for both sensors are plotted in Fig. 6.

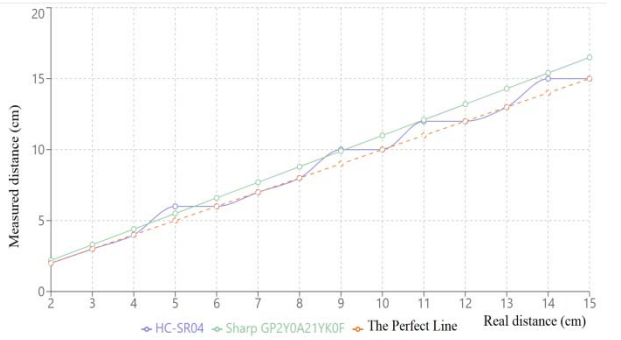

Figure 6 – Graph of the dependence of the measured distance on the real distance for HC-SR04 and Sharp GP2Y0A21YK0F

The analysis of the results of experiments showed that the accuracy of measurements depends on several factors:

1. The characteristics of the reflective surface because different materials can reflect ultrasonic waves differently, which affects the accuracy of measurements.

2. Measurement mediums because the speed of sound can vary depending on temperature, humidity and other environmental parameters.

3. Measurement errors. The measurement error of this range meter device on an ultrasonic sensor is ± 1 cm.

The results obtained confirm the high accuracy and reliability of the developed module based on the HC-SR04 for measuring distances in the range of up to 15 cm.

Comparison with the Sharp GP2Y0A21YK0F optical sensor demonstrates the advantages of the ultrasonic method in the context of measurement stability and less sensitivity to external factors.

6 DISCUSSION

The results of experiments carried out with the developed distance measurement module based on the HC-SR04 ultrasonic sensor demonstrate the high accuracy and reliability of the device. However, the data obtained require detailed analysis and interpretation in the context of potential applications and limitations of the technology.

Comparison of the readings of the ultrasonic sensor with the reference measurements with the ruler showed that the measurement accuracy is within ±1 cm. This is an acceptable result for many practical applications, especially given the low cost and ease of implementation of the device.

However, it is worth noting that at distances of 9–11 cm, some deviations were observed. This may be due to the peculiarities of the propagation of ultrasonic waves or the specifics of a particular sensor sample. To increase accuracy at these distances, you can consider calibrating the sensor or using additional data processing algorithms.

Let’s compare with other analogs. For example, compared to optical sensors such as infrared distance sensors, the HC-SR04 ultrasonic sensor has the advantage that it is less sensitive to the illumination and color of objects. This makes it more versatile for a variety of applications.

However, laser rangefinders usually provide higher measurement accuracy. However, they are significantly

DOI 10.15588/1607-3274-2025-2-3

more expensive and may have limitations when working with transparent or mirrored surfaces.

For a more detailed analysis, consider comparing the HC-SR04 with the common Sharp GP2Y0A21YK0F optical sensor.

Table 2 – Comparison of HC-SR04 and Sharp GP2Y0A21YK0F

Characteristic	HC-SR04 (Ultrasonic) [12, 13]	Sharp GP2Y0A21YK0F (Optical) [12, 13]
Measurement range	2 cm – 400 cm	10 cm – 80 cm
Accuracy	±3 mm	±10 % of the measured distance
Response time	~60 ms	~39 ms
Supply voltage	5V	4.5 V – 5.5 V
Current consumption	~15 mA (active mode)	~30 mA
Object color sensitivity	Low	High
Sensitivity to transparent objects	High	Low
Exposure to outdoor lighting	Low	High
Sizes	45 x 20 x 15 mm	29.5 x 13 x 13.5 mm
Price (approx.)	$2–$5	$10–$15

Analyzing the data from the table, the following conclusions can be drawn:

– the measurement range of the HC-SR04 is a much wider measurement range, which makes it more versatile for different applications;

– the accuracy of the HC-SR04 is higher, especially at longer distances.

– the speed of the optical sensor has a slightly better response time, which can be critical for some applications;

– the HC-SR04 has low power consumption, making it an ideal choice for energy-efficient and stand-alone devices. This allows the sensor to be used in battery-powered systems, ensuring long-term operation without the need for frequent maintenance or recharging. Thanks to this, the device can function effectively in remote places or in conditions where there is no constant power source;

– sensitivity to external factors in HC-SR04 it is less to the color of the object and ambient light, but it may have problems detecting transparent objects;

– dimensions and cost. The HC-SR04 is somewhat larger in size, but significantly cheaper.

The choice between these two types of sensors depends on the specific application. The HC-SR04 is the preferred choice for general use, especially in variable lighting environments or when working with objects of different colors. However, for applications that require high performance or working with transparent objects, an optical sensor may be the preferred choice.

Despite the overall effectiveness of the developed module, there are certain limitations that should be taken into account:

1. The maximum measurement distance is limited to 4 meters, which may not be sufficient for some applications.

2. Ultrasonic waves may not bounce off soft or porous surfaces as efficiently, which may affect the accuracy of measurements.

3. Influence of various environmental conditions on the accuracy of measurements In environments with a high noise level, false positives are possible.

Overall, the developed distance measurement module demonstrates high potential for practical applications, providing a balance between accuracy, ease of implementation and cost-effectiveness.

CONCLUSIONS

An urgent problem has been solved: the development of a range measurement module on an ultrasonic sensor with a GSM module, which allows for accurate distance measurement and transmission of results to remote servers or directly to end users.

The scientific novelty of the results obtained lies in the fact that a mathematical model of autocalibration of an ultrasonic sensor has been proposed. The key benefits of this approach are:

1. Comprehensive statistical error analysis, since the model allows you to detect and compensate for both systematic and random errors of the sensor based on the analysis of discrepancies between measured and reference values.

2. Adaptive correction because the proposed mechanism for adaptive adjustment of correction coefficients provides a flexible response to changes in external conditions that affect the accuracy of measurements.

3. Taking into account the influence of factors, because the model takes into account the influence of temperature, humidity, interference, etc., on sensor errors, which increases the efficiency of compensation.

4. Formalization of the process, since the presentation of a mathematical model in the form of clear equations and algo-rhythmic steps provides structure and the possibility of further improvement of the method.

In general, this approach allows you to significantly increase the accuracy of the ultrasonic sensor in real operating conditions due to comprehensive statistical error correction. The formalization of the model in mathematical form is an innovative step that contributes to the effective practical application of the method.

The practical value of the results obtained lies in the creation of a cost-effective solution for remote distance measurement, because the developed module combines an inexpensive HC-SR04 ultrasonic sensor with a GSM module, which allows remote measurements at an affordable price. This is especially useful for small businesses and individual developers in the field of radio electronics. The development can expand the capabilities of telecommunication systems because the integration of the GSM module allows you to transmit measurement data over a cellular network, expanding the scope of application of the device in telecommunication systems. This makes it

DOI 10.15588/1607-3274-2025-2-3

possible to monitor over long distances without the need for additional communications. Optimization of power consumption lies in the fact that the developed algorithm of the module, which provides for sleep mode and activation on an incoming call, can significantly reduce the power consumption of the device. This is crucial for autonomous systems in radio electronics and telecommunications.

Thus, an integrated range measurement module has been developed, which combines the HC-SR04 ultrasonic sensor with a GSM module, which allows for accurate remote measurement and data transmission in real time.

The experiments carried out using real data demonstrate the effectiveness of the developed module. A comparative analysis with an optical sensor showed that the developed module based on HC-SR04 is less sensitive to external factors (lighting, object color), which increases the reliability of measurements in various operating conditions.

A wide range of measurements (up to 4 m) and the ability to work with different types of surfaces makes the module versatile for many tasks in radio electronics, from industrial automation to security systems. Therefore, the results obtained make a significant contribution to the development of radio electronics.

Prospects for further research are as follows:

1. Integration of additional sensors (e.g. infrared) to increase the reliability of measurements.

2. Develop machine learning algorithms to improve accuracy and noise filtering.

3. Optimization of power consumption to increase the autonomy of the device

REFERENCES

1. Sotnik S. V., Redkin K. S. Design features of control panels and consoles in automation systems, *The 9th International scientific and practical conference "Science and innovation of modern world" (May 18–20, 2023) Cognum Publishing House.* London, United Kingdom. – 2023. – P. 201–205
2. Sotnik S. V. Development of automated control system for continuous casting, *Radio Electronics, Computer Science, Control*, 2024, № 2(69), pp. 181–189. DOI: 10.15588/1607-3274-2024-2-18
3. Polikanov K. et al. Smart home with house module: overview of automation technologies / K. Polikanov // I*nternational Conference "DIGITAL INNOVATION & SUSTAINABLE DEVELOPMENT 2024"*, 2024, pp. 20–21
4. Sukhno P. et al. Critical review of GSM network structure, *Manufacturing & Mechatronic Systems 2024: Proceedings of VIII st International Conference*. Kharkiv, October 25–26, 2024, 2024, pp. 37–41
5. Abdulkhaleq N. I., Hasan I. J., Salih N. A. J. Investigating the resolution ability of the HC-SRO4 ultrasonic sensor, *IOP Conference Series: Materials Science and Engineering*, 2020, T. 745, №. 1, pp. 1–8. DOI: 10.1088/1757-899X/745/1/012043
6. Al Tahtawi A. R. Kalman filter algorithm design for hc-sr04 ultrasonic sensor data acquisition system, *IJITEE (International Journal of Information Technology and Electrical Engineering)*, 2018, T. 2, №. 1, pp. 15–19
7. Rihmi M. K. et al Accuracy Analysis of Distance Measurement Using Sonar Ultrasonic Sensor HC-SR04 on Several Types of Materials, *Journal of Environmental Engineering and Sustainable Technology*, 2024, T. 11, № 01, pp. 10–13
8. Qi J., Liu G. P. A robust high-accuracy ultrasound indoor positioning system based on a wireless sensor network, *Sensors*, 2017, No. 17(11), pp. 1–17. DOI: 10.3390/s17112554
9. Mocanu B., Tapu R., Zaharia T. When ultrasonic sensors and computer vision join forces for efficient obstacle detection and recognition, *Sensors*, 2016, No. 16 (11), pp. 1–23. DOI: 10.3390/s16111807
10. Mohammad T. Using ultrasonic and infrared sensors for distance measurement, *World academy of science, engineering and technology*, 2009, T. 51, pp. 293–299
11. Aliew F. An approach for precise distance measuring using ultrasonic sensors, *Engineering Proceedings*, 2022, T. 24, № 1, pp. 1–9. DOI: 10.3390/IECMA2022-12901
12. Suh Y. S. Laser sensors for displacement, distance and position, *Sensors*, 2019, T. 19, №. 8, pp. 1–4. DOI: 10.3390/s19081924
13. de Bakker B. How to use a SHARP GP2Y0A21YK0F IR Distance Sensor with Arduino, *Makerguides. com.*, 2019, pp. 1–20
14. Khaleel H. Z., Raheem F. A. Design and Implementation Accurate Three Distance Sensors Device Using Neural Network, *Tikrit Journal of Engineering Sciences*, 2024, T. 31, №. 2, pp. 138–147. DOI: 10.25130/tjes.31.2.13
15. Soni A., Aman A. Distance Measurement of an Object by using Ultrasonic Sensors with Arduino and GSM Module, *International Journal of Science Technology & Engineering*, 2018, T. 4, №. 11, pp. 23–28
16. Gbotoso G. A. Development of distance measurement using ultrasonic based sensors, *International Journal of Engineering Research Updates*, 2024, No. 06(02), pp. 35–40. DOI: 10.53430/ijeru.2024.6.2.0028
17. Sharma J., Abrol P. Design and Implementation of digital distance measurement system using ultrasonic sensor, *International journal of research in electronics and computer engineering*, 2014, No. 2(3), pp. 27–30
18. Morgan E. J. HC-SR04 ultrasonic sensor. Nov., 2014, pp. 1–6

Received 03.02.2025.
Accepted 19.04.2025.

DOI 10.15588/1607-3274-2025-2-3

УДК 621.391.2:004.31

РОЗРОБКА МОДУЛЯ ВИМІРЮВАННЯ ДАЛЬНОСТІ НА УЛЬТРАЗВУКОВОМУ ДАТЧИКУ З GSM МОДУЛЕМ

Сотник С. В. – канд. техн. наук, доцент, доцент кафедри комп'ютерно-інтегрованих технологій, автоматизації та робототехніки Харківського національного університету радіоелектроніки, Харків, Україна.

АНОТАЦІЯ

Актуальність. Розробка модуля вимірювання дальності на основі ультразвукового датчика з GSM модулем є надзвичайно актуальною у сфері телекомунікацій та радіоелектроніки. У сучасному світі все більша кількість пристроїв інтегрується в системи Інтернету речей (IoT), де передачу даних на великі відстані забезпечують телекомунікаційні технології. Використання GSM модуля дозволяє в режимі реального часу передавати інформацію з вимірювального пристрою на віддалені сервери або кінцевим користувачам, що є критичним для рішень у сфері дистанційного моніторингу та контролю.

Ультразвукові датчики у поєднанні з GSM модулем можуть дозволять автоматизувати процеси вимірювання у важкодоступних або небезпечних для людини умовах, що підвищує ефективність та безпеку систем. Застосування радіоелектронних технологій для передачі вимірювальних даних у реальному часі дозволяє значно розширити функціональність пристроїв, полегшити їхню інтеграцію у вже існуючі системи телекомунікацій, зокрема у промислових, транспортних, та інфраструктурних секторах.

Таким чином, розробка даного модуля з точними вимірами сприяє розвитку інновацій у галузі телекомунікацій та радіоелектроніки, забезпечуючи швидку та надійну передачу даних, що є важливою складовою сучасних інформаційних систем.

Мета. Розробка модуля вимірювання дальності на основі ультразвукового датчика з GSM-модулем та підвищення точності вимірювань шляхом впровадження запропонованої математичної моделі автокалібрування ультразвукового датчика.

Метод. Для досягнення поставленої мети був розроблений інтегрований модуль вимірювання дальності, який поєднує ультразвуковий датчик HC-SR04 з GSM-модулем. Метод підвищення точності базується на запропонованій математичній моделі автокалібрування ультразвукового датчика.

Результати. Здійснена постановка задачі та розроблено модуль вимірювання дальності на основі ультразвукового датчика з інтегрованим GSM-модулем. У ході дослідження було створено електричну принципову схему пристрою за допомогою програмного забезпечення DipTrace. Розроблено алгоритм роботи модуля, який оптимізує взаємодію між ультразвуковим датчиком. Створено друковану плату. Запропоновано математичну модель автокалібрування ультразвукового датчика для підвищення точності вимірювання. Проведено серію експериментальних досліджень для оцінки точності. Результати експериментів підтвердили ефективність розробленого модуля для вимірювання відстаней.

Висновки. Розроблений модуль вимірювання дальності на основі ультразвукового датчика з GSM-модулем представляє собою інноваційне рішення, що відповідає сучасним вимогам телекомунікаційних та радіотехнічних систем. Інтеграція точного вимірювання відстані на базі запропонованої математичної модель автокалібрування ультразвукового датчика з можливістю дистанційної передачі даних відкриває нові перспективи для дистанційного моніторингу та автоматизації процесів. Експериментальні дослідження підтвердили точність та надійність пристрою, а порівняльний аналіз з аналогами продемонстрував його конкурентні переваги. Економічна ефективність та енергоощадність розробленого модуля роблять його привабливим для широкого кола користувачів, від індивідуальних розробників до промислових підприємств. Подальші дослідження можуть бути спрямовані на вдосконалення алгоритмів обробки даних та розширення функціональних можливостей пристрою, що сприятиме розвитку інноваційних технологій у сфері радіоелектроніки та телекомунікацій.

КЛЮЧОВІ СЛОВА: дальність, вимірювання, модуль, ультразвуковий датчик, GSM модуль.

ЛІТЕРАТУРА

1. Sotnik S. V. Design features of control panels and consoles in automation systems / S. V. Sotnik, K. S. Redkin // The 9th International scientific and practical conference "Science and innovation of modern world" (May 18–20, 2023) Cognum Publishing House, London, United Kingdom. – 2023. – P. 201–205
2. Sotnik S. V. Development of automated control system for continuous casting / S. V. Sotnik // Radio Electronics, Computer Science, Control. – 2024. – № 2(69). – P. 181–189. DOI: 10.15588/1607-3274-2024-2-18
3. Polikanov K. Smart home with house module: overview of automation technologies / [K. Polikanov et al.] // International Conference "DIGITAL INNOVATION & SUSTAINABLE DEVELOPMENT 2024". – 2024. – P. 20–21
4. Sukhno P. Critical review of GSM network structure / [P. Sukhno et al.] // Manufacturing & Mechatronic Systems 2024: Proceedings of VIII st International Conference, Kharkiv, October 25–26, 2024. – 2024. – P. 37–41
5. Abdulkhaleq N. I. Investigating the resolution ability of the HC-SRO4 ultrasonic sensor / N. I. Abdulkhaleq, I. J. Hasan, N. A. J. Salih // IOP Conference Series: Materials Science and Engineering. – 2020. – T. 745, №. 1. – P. 1–8. DOI: 10.1088/1757-899X/745/1/012043
6. Al Tahtawi A. R. Kalman filter algorithm design for hc-sr04 ultrasonic sensor data acquisition system / A. R. Al Tahtawi // IJITEE (International Journal of Information Technology and Electrical Engineering). – 2018. – T. 2, №. 1. – P. 15–19
7. Rihmi M. K. Accuracy Analysis of Distance Measurement Using Sonar Ultrasonic Sensor HC-SR04 on Several Types of Materials / [M. K. Rihmi et al.] // Journal of Environmental Engineering and Sustainable Technology. – 2024. – T. 11, №. 01. – P. 10–13
8. Qi J. A robust high-accuracy ultrasound indoor positioning system based on a wireless sensor network / J. Qi, G. P. Liu // Sensors. – 2017. – No. 17(11). – P. 1–17. DOI: 10.3390/s17112554
9. Mocanu B. When ultrasonic sensors and computer vision join forces for efficient obstacle detection and recognition / B. Mocanu, R. Tapu, T. Zaharia // Sensors. – 2016. – No. 16 (11). – P. 1–23. DOI: 10.3390/s16111807
10. Mohammad T. Using ultrasonic and infrared sensors for distance measurement / T. Mohammad // World academy of science, engineering and technology. – 2009. – T. 51. – P. 293–299
11. Aliew F. An approach for precise distance measuring using ultrasonic sensors / F. Aliew // Engineering Proceedings. – 2022. – T. 24, №. 1. – P. 1–9. DOI: 10.3390/IECMA2022-12901
12. Suh Y. S. Laser sensors for displacement, distance and position / Y. S. Suh // Sensors. – 2019. – T. 19, №. 8. – P. 1–4. DOI: 10.3390/s19081924
13. de Bakker B. How to use a SHARP GP2Y0A21YK0F IR Distance Sensor with Arduino / B. de Bakker // Makerguides. com. – 2019. – P. 1–20.
14. Khaleel H. Z. Design and Implementation Accurate Three Distance Sensors Device Using Neural Network / H. Z. Khaleel, F. A. Raheem // Tikrit Journal of Engineering Sciences. – 2024. – T. 31, №. 2. – P. 138–147. DOI: 10.25130/tjes.31.2.13
15. Soni A. Distance Measurement of an Object by using Ultrasonic Sensors with Arduino and GSM Module / A. Soni, A. Aman // International Journal of Science Technology & Engineering. – 2018. – T. 4, №. 11. – P. 23–28.
16. Gbotoso G. A. Development of distance measurement using ultrasonic based sensors / G. A. Gbotoso // International Journal of Engineering Research Updates. – 2024. – No. 06(02). – P. 35–40. DOI: 10.53430/ijeru.2024.6.2.0028
17. Sharma J. Design and Implementation of digital distance measurement system using ultrasonic sensor / J. Sharma, P. Abrol // International journal of research in electronics and computer engineering. – 2014. – No. 2(3). – P. 27–30.
18. Morgan E. J. HC-SR04 ultrasonic sensor / E. J. Morgan. – Nov. – 2014. – P. 1–6.

DOI 10.15588/1607-3274-2025-2-3

МАТЕМАТИЧНЕ ТА КОМП'ЮТЕРНЕ МОДЕЛЮВАННЯ

MATHEMATICAL AND COMPUTER MODELING

UDC 004.93

THE INTELLECTUAL ANALYSIS METHOD OF COLOR IMAGES

Fedorov E. E. – Dr. Sc., Professor, Professor of Department of Statistics and Applied Mathematics, Cherkassy State Technological University, Cherkassy, Ukraine.

Khramova-Baranova O. L. – Dr. Sc., Professor, Head of the Department of Graphic Design, Fashion and Style, Cherkassy State Technological University, Cherkassy, Ukraine.

Utkina T. Y. – PhD, Associate Professor, Associate Professor of Department of Robotics and Specialized Computer Systems, Cherkassy State Technological University, Cherkassy, Ukraine.

Kozhushko Ya. M. – PhD, Senior Researcher, Leading Researcher of the Scientific Research Department of Testing Automated, Information Systems and Communication Equipment, State Scientific Research Institute of Armament and Military Equipment Testing and Certification, Cherkasy, Ukraine.

Nesen I. O. – PhD, Senior Lecturer of Department of Information Systems and Organization of Civil Protection Measures, Educational and Research Institute of Civil Protection, National University of Civil Protection of Ukraine, Major of Civil Protection Service of Ukraine, Cherkassy, Ukraine.

ABSTRACT

Context. Automatic and automated image analysis methods used in computer graphic design, biometric identification, and military target search are now widespread. The object of the research is the process of color image analysis.

Objective. The goal of the work is to create an intelligent method of image analysis based on quantization, binarization and clustering.

Method. The proposed method for intelligent color image analysis consists of the following techniques. The technique of reducing the number of colors based on the conversion of a color image into a gray-scale image and quantization of the resulting gray-scale image improves the accuracy of image feature extraction by preventing the appearance of an excessive number of image clusters. The technique of creating a set of binary images based on binarization of a quantized gray-scale image allows increasing the speed of subsequent clustering by replacing sequential extraction of all elements of a quantized gray-scale image with parallel extraction of binary image elements, as well as separating clusters obtained during subsequent clustering by color due to image membership. The technique of determining the highest priority binary images based on the probability of occurrence of each color in the quantized gray-scale image improves the speed of image structure synthesis based on the analysis results by considering the most informative binary images. The technique of extracting binary image elements on the basis of its clustering allows to increase the accuracy of extracting binary image elements by improving the method of forming the neighborhoods of points (no radius of empirically determined neighborhood is needed), detecting random outliers and noise, extracting image elements of different shapes and sizes without specifying the number of extracted binary image elements, as well as increasing the speed of extracting binary image elements by forming the neighborhoods of white points only. The technique of determining the higher priority parts of the binary image based on the power of image clusters allows increasing the accuracy of image structure synthesis based on the analysis results by omitting noise and random outliers.

Results. The proposed method for intelligent analysis of color images was programmatically implemented using Parallel Computing Toolbox of Matlab package and investigated for the task of image feature extraction on the corresponding database. The results obtained allowed to compare the traditional and proposed methods.

Conclusions. The proposed method allows to expand the application area of color image analysis based on color-to-gray-scale image conversion, quantization, binarization, parallel clustering and contributes to the efficiency of computer systems for image classification and synthesis. Prospects for further research investigating the proposed method for a wide class of machine learning tasks.

KEYWORDS: intelligent image analysis, quantization, binarization, image feature extraction, clustering.

ABBREVIATIONS

EM is an expectation-maximization algorithm;

PAM is a partitioning around medoids algorithm;

ISODATA is an iterative self-organizing data analysis technique algorithm;

FCM is ae fuzzy classifier means algorithm;

OPTICS is an ordering points to identify the clustering structure algorithm;

DBSCAN is a density-based spatial clustering of applications with noise algorithm;

DISMEA is a divisive hierarchical clustering algorithm that uses the k-means algorithm to subdivide a cluster into two;

DIANA is a divisive analysis algorithm.

NOMENCLATURE

$A = \{A_1, ..., A_c\}$ is a correct set of image elements;

DOI 10.15588/1607-3274-2025-2-4

T is a time;

n_1 is a line number of the image;

n_2 is a column number of the image;

N_1 is an end of the current row of the image;

N_2 is an end of the current column of the image;

$R(n_1, n_2)$ is a red color component;

$G(n_1, n_2)$ is a green color component;

$B(n_1, n_2)$ is a blue color component;

$y(n_1, n_2)$ is an 8-bit gray-scale image;

k is a color number;

Δ is a quantization step;

$s(n_1, n_2)$ is a quantized gray-scale image;

$M_k(n_1, n_2)$ is a point label matrix;

c_k is a counter of the number of connected regions;

i is a current point of the image;

$U_{i,\varepsilon}$ is a neighborhood of the i-th point;

v is a first element from the set S, i.e. $S = U_{i,\varepsilon}$, $v = s_1$;

m_1, m_2 are the coordinates of the v-th point in the image;

$U_{v,\varepsilon}$ is a neighborhood of the v-th point;

$z_k(n)$ is a power vector of clusters;

$Q_k(n_1, n_2)$ is a k-th binary image;

p_k is a probability of occurrence of a point with color with number k;

D is a size of Moore's neighborhood of the point;

$p_k \times N_1 \times N_2$ is a number of white dots in k-th binary image;

mod is a modulo division;

$[\ ]$ is taking the integer part of the number.

INTRODUCTION

The rapid development of computing and information technology has provided automatic or automated processing and analysis of visual information.

One of the applications of visual information analysis has become computer graphic design. To synthesize new images, components of already existing images are often used, so the problem of accurate and fast extraction of required elements of previous images is relevant [1–3].

Another application of visual information analysis was the creation of biometric personal identification systems to solve the problems of differentiating the access of users of software and hardware objects, identifying intruders and others. In this case, one of the most popular and simple in terms of technical means of identification is identification by face [4–6].

Another application of visual information analysis is the detection of military targets. Currently, the problem of accurate and fast decision making about ground targets for drones is relevant.

Nowadays, methods of automatic and automated image analysis, which use machine learning algorithms, are widespread.

The object of study is the process of color image analysis.

The subject of study is the methods for color image analysis based on digital image processing and machine learning.

The purpose of the work is to create an intelligent method of image analysis based on quantization, binarization, and clustering.

In order to achieve the goal, the following objectives were set and solved:

1) to create a technique to reduce the number of colors based on color-to-gray-scale image conversion and quantization;

2) to develop a technique for creating a set of binary images based on the binarization of a quantized gray-scale image;

3) to create a technique for determining the highest priority binary images based on the probability of occurrence of each color in the quantized gray-scale image;

4) to develop a technique for image feature extraction based on clustering of binary image;

5) to create a technique for determining the highest priority elements of a binary image based on the clustering power of that image;

6) to conduct a numerical study of the proposed method.

1 PROBLEM STATEMENT

The problem of improving the efficiency of image analysis based on clustering is represented as the problem of finding such an ordered set of image elements $A^* = \{A_1^*, ..., A_c^*\}$ in time T, at which

$$F = \sum_{k=1}^{c} \left\| A_i - A_i^* \right\| \to \min \text{ and } T \to \min.$$

2 REVIEW OF THE LITERATURE

For automatic and automated image classification and synthesis, image feature extraction plays an important role, for which quantization, binarization, and image segmentation techniques can be used.

For image binarization, the approaches commonly used are [7]:

– automatic selection of a single-level local threshold (e.g., Eikwel, Bernsen, Sauvola, Niblack, Christian methods) [9];

DOI 10.15588/1607-3274-2025-2-4

– automatic selection of a single-level global threshold (e.g., Otsu's method) [8].

The above methods have one or more of the following disadvantages:

– require a time-consuming thresholding procedure;

– do not perform binarization accurately enough;

– require a labor-intensive procedure for determining additional parameters.

In this regard, it is relevant to create a method of image binarization that will eliminate the mentioned disadvantages.

For image segmentation usually use such approaches as [7]:

– Markov random field based [17];

– region detection (region sprawl, region splits and merges, watershed) [11];

– definition of region boundaries (pixels with a large intensity gradient and also differing in color are selected as region boundaries) [10];

– taxonomic [12];

– based on partial derivative equations [14].

– histogram [13];

– graph-based [16];

– variational [15].

The most popular of them is the taxonomic approach.

The traditional methods of the taxonomic approach are:

1. Model mixture or model-based (e.g., EM [21]) or distribution-based methods.

2. Partitioning-based (partitioning-based, partition-based) or center-based (center-based) methods (e.g., PAM (k-medoids) [18], *k*-means [18], ISODATA [20], FCM [19] algorithms).

3. Methods are hierarchical (hierarchal).

4. Density-based methods (e.g., OPTICS [23], DBSCAN [22] algorithms).

5. Divisive or top-down (e.g., DISMEA, DIANA methods) [25].

6. Agglomerative or bottom up (e.g., Ward's methods, centroidal linkage, full linkage, single linkage, group mean) [24].

Taxonomy-based methods can also be based on metaheuristics [26] and artificial neural networks [27].

The above methods have one or more of the following disadvantages:

– require the definition of parameter values;

– do not allow to separate noise and random outliers;

– have high computational complexity;

– require specifying the number of clusters;

– clusters cannot have different shapes and sizes.

In this regard, it is relevant to create an image segmentation method that will eliminate the above disadvantages.

One of the ways to speed up segmentation is to pre-transform a color image into a gray-scale image and quantization, which reduce the number of colors [28–30].

3 MATERIALS AND METHODS

The method of intellectual analysis of a color image based on parallel clustering includes six stages (the first two stages correspond to the technique of image color reduction, the third stage corresponds to the technique of creating a set of binary images, the fourth stage corresponds to the technique of determining the highest priority binary images, the fifth stage corresponds to the technique of extracting elements of a binary image, the sixth stage corresponds to the technique of determining the highest priority elements of a binary image):

Stage 1. Converting the color image into a gray-scale image

The conversion of a color image $R(n_1, n_2), G(n_1, n_2), B(n_1, n_2)$ into an 8-bit gray-scale image $y(n_1, n_2)$ is performed using the YCrCb color space

$$y(n_1, n_2) = 0.2989 \cdot R(n_1, n_2) + \\ + 0.5870 \cdot G(n_1, n_2) + 0.1140 \cdot B(n_1, n_2),$$
$$n_1 \in \overline{1, N_1},\ n_2 \in \overline{1, N_2}.$$

Step 2. Quantization of gray image

1. Set the 8-bit gray-scale image $y(n_1, n_2)$, $n_1 \in \overline{1, N_1}$, $n_2 \in \overline{1, N_2}$. Set the quantization step Δ.

2. Set the line number of the image $n_1 = 1$.

3. Set the column number of the image $n_2 = 1$.

4. Set the color number $k = 1$.

5. If $k\Delta - \Delta \le y(n_1, n_2) \wedge y(n_1, n_2) < k\Delta$, then $s(n_1, n_2) = k\Delta - \Delta / 2$.

6. If not the last color, i.e. $k < 256/\Delta$ then increase the color number, i.e. $k = k + 1$, then go to step 5.

7. If $y(n_1, n_2) = 255$, then $s(n_1, n_2) = 256 - \Delta / 2$.

8. If not the end of the current row of the image, i.e. $n_2 < N_2$, then increase the column number of the current row, i.e. $n_2 = n_2 + 1$, then go to step 4.

9. If not the last row of the image, i.e. $n_1 < N_1$, then increase the row number of the current row, i.e. $n_2 = n_2 + 1$, then go to step 3.

Step 3. Binarization of quantized gray-scale image (creation of the k-th binary image)

1. Set the quantized gray-scale image $s(n_1, n_2)$, $n_1 \in \overline{1, N_1}$, $n_2 \in \overline{1, N_2}$.

2. Perform binarization of the image in the form

DOI 10.15588/1607-3274-2025-2-4

$$Q_k\left(n_1, n_2\right)=\begin{cases}1, & s\left(n_1, n_2\right)=k\Delta-\Delta/2\\ 0, & s\left(n_1, n_2\right)\neq k\Delta-\Delta/2\end{cases},$$

$$n_1\in\overline{1, N_1},\ n_2\in\overline{1, N_2}.$$

Step 4. Calculate the probability of appearance of a point with color with number k in the quantized gray image

1. Set the k-th binary image $Q_k\left(n_1, n_2\right)$, $n_1\in\overline{1, N_1}$, $n_2\in\overline{1, N_2}$.

2. Calculate the probability of appearance of a point with color with number k

$$p_k=\frac{1}{N_1N_2}\sum_{n_1=1}^{N_1}\sum_{n_2=1}^{N_2}Q_k\left(n_1, n_2\right).$$

Step 5. Clustering of the k-th binary image

1. Set the image $s\left(n_1, n_2\right)$, $n_1\in\overline{1, N_1}$, $n_2\in\overline{1, N_2}$. Set the k-th binary image $Q_k\left(n_1, n_2\right)$, $n_1\in\overline{1, N_1}$, $n_2\in\overline{1, N_2}$. Set the size of the Moore neighborhood of the point D. Set the point label matrix $M_k\left(n_1, n_2\right)=0$, $n_1\in\overline{1, N_1}$, $n_2\in\overline{1, N_2}$. Set the count of the number of clusters $c_k=0$.

2. Set the row number of the image $n_1=1$.

3. Set the image column number $n_2=1$.

4. Define the number of the current point of the image $i=\left(n_1-1\right)N_2+n_2$.

5. If the i-th point is already marked, i.e. $M_k\left(n_1, n_2\right)\neq 0$, then go to step 20.

6. Determine the neighborhood of the i-th point

$$U_{i,\varepsilon}=\left\{e\,|\,Q_k\left(l_1+n_1, l_2+n_2\right)=1\right\},$$

$$e=\left(l_1+n_1-1\right)N_2+l_2+n_2,\ l_1, l_2\in\left\{-1, 0, 1\right\}.$$

7. If not all the neighbors of the i-th point fall in its neighborhood, i.e. $\left|U_{i,\varepsilon}\right|<D$, then mark the i-th point as a random outlier or a noise, i.e. $M_k\left(n_1, n_2\right)=-1$, go to step 20.

8. Increment the counter of the number of connected regions, i.e. $c_k=c_k+1$.

9. Label the i-th point as the c_k-th cluster, i.e. $M_k\left(n_1, n_2\right)=c_k$.

10. Create the set $S=U_{i,\varepsilon}$.

11. Remove the first element from the set S, i.e. $v=s_1$, and remove it from the set S, i.e. $S=S\setminus\{v\}$.

12. Determine the coordinates of the v-th point in the image

$$m_2=v\bmod N_2,\ m_1=\left[\left(v-m_2\right)/N_2\right].$$

13. If the v-th point was labeled as a random outlier or noise, i.e. $M_k\left(m_1, m_2\right)=-1$, then label it as the c_k-th cluster, i.e. $M_k\left(m_1, m_2\right)=c_k$.

14. If the v-th point is already labeled, i.e. $M_k\left(m_1, m_2\right)\neq 0$, then proceed to step 19.

15. Label the v-th point, i.e. $M_k\left(m_1, m_2\right)=c_k$.

16. Determine the neighborhood of the v-th point

$$U_{v,\varepsilon}=\left\{e\,|\,Q_k\left(l_1+m_1, l_2+m_2\right)=1\right\},$$

$$e=\left(l_1+m_1-1\right)N_2+l_2+m_2,\ l_1, l_2\in\left\{-1, 0, 1\right\}.$$

17. If not all neighbors of the v-th point fall in its neighborhood, i.e. $\left|U_{v,\varepsilon}\right|<D$, then go to step 19.

18. Merge the set S with the neighborhood of the v-th point, i.e. $S=S\bigcup U_{v,\varepsilon}$.

19. If the set S is not empty, i.e. $|S|>0$, then go to step 11.

20. If not the end of the current row of the image, i.e. $n_2<N_2$, then increase the column number of the current row, i.e. $n_2=n_2+1$, then go to step 4.

21. If not the last row of the image, i.e. $n_1<N_1$, then increase the row number of the current row, i.e. $n_2=n_2+1$, move to step 3.

Step 6. Computing the power of clusters of the k-th binary image

1. Set the point label matrix $M_k\left(n_1, n_2\right)$, $n_1\in\overline{1, N_1}$, $n_2\in\overline{1, N_2}$. Set the number of clusters c_k. Set the power vector of clusters $z_k\left(n\right)=0$, $n\in\overline{1, c_k}$.

2. Set the row number of the image $n_1=1$.

3. Set the image column number $n_2=1$.

4. If a point belongs to a cluster, i.e. $M_k\left(n_1, n_2\right)>0$, then increase the power of the clusters, i.e. $z_k\left(M_k\left(n_1, n_2\right)\right)=z_k\left(M_k\left(n_1, n_2\right)\right)+1$.

5. If not the end of the current row of the image, i.e. $n_2<N_2$, then increase the column number of the current row, i.e. $n_2=n_2+1$, then go to step 4.

6. If not the last row of the image, i.e. $n_1<N_1$, then increase the row number of the current row, i.e. $n_2=n_2+1$, then go to step 3.

7. Sort the power vector of clusters in descending order, i.e. $z_k\left(n\right)\geq z_k\left(n+1\right)$.

4 EXPERIMENTS

Numerical study of the proposed method of intelligent color image analysis was carried out using Parallel Computing Toolbox of Matlab package on the basis of theatrical playbill data.

DOI 10.15588/1607-3274-2025-2-4

In this work the image sizes $N_1 = 228$ and $N_2 = 165$, the quantization step $\Delta = 16$, for the white point the Moore neighborhood of size $1 \le D \le 9$.

5 RESULTS

In Fig. 1, a, the original color image is shown. According to the first step, the color image is converted to gray-scale image.

According to the second stage, in Fig. 1, b, the gray-scale image is quantized with quantization step $\Delta = 16$, i.e., the possible colors are 8, 24, 40, 56, 72, 72, 88, 104, 120, 136, 136, 152, 152, 168, 184, 200, 216, 232, 248.

According to the third stage quantized gray-scale image can be divided into $256/\Delta = 16$ binary images.

According to the fourth step the probabilities of color appearance are calculated.

In Fig. 3 binary images corresponding to colors with the highest probability of occurrence are presented with indication of their number k, color and probability of occurrence p_k.

Figure 1 – The color image

Figure 2 – The gray image from $\Delta = 16$

a

b

c

d

Figure 3 – The binary image: a – $k = 1$ (color 8, $p_1 = 0.467$); b – $k = 11$ (color 168, $p_{11} = 0.126$); c – $k = 13$ (color 200, $p_{13} = 0.062$); d – $k = 16$ (color 248, $p_{16} = 0.159$)

DOI 10.15588/1607-3274-2025-2-4

In accordance with the fifth stage, parallel clustering of binary images is performed. The binary image corresponding to the color with the highest probability of occurrence, which is shown in Fig. 3a, was chosen as an example.

According to the sixth step, the power of clusters is calculated. In Fig. 4 the most powerful clusters are presented with their number n and power $z_k(n)$ with the size of Moore's neighborhood $D = 4.5$.

In Fig. 5, the most powerful clusters are shown with their number n and power $z_k(n)$ with the size of the cluster Moore's neighborhood $D = 9$ stands out more accurately.

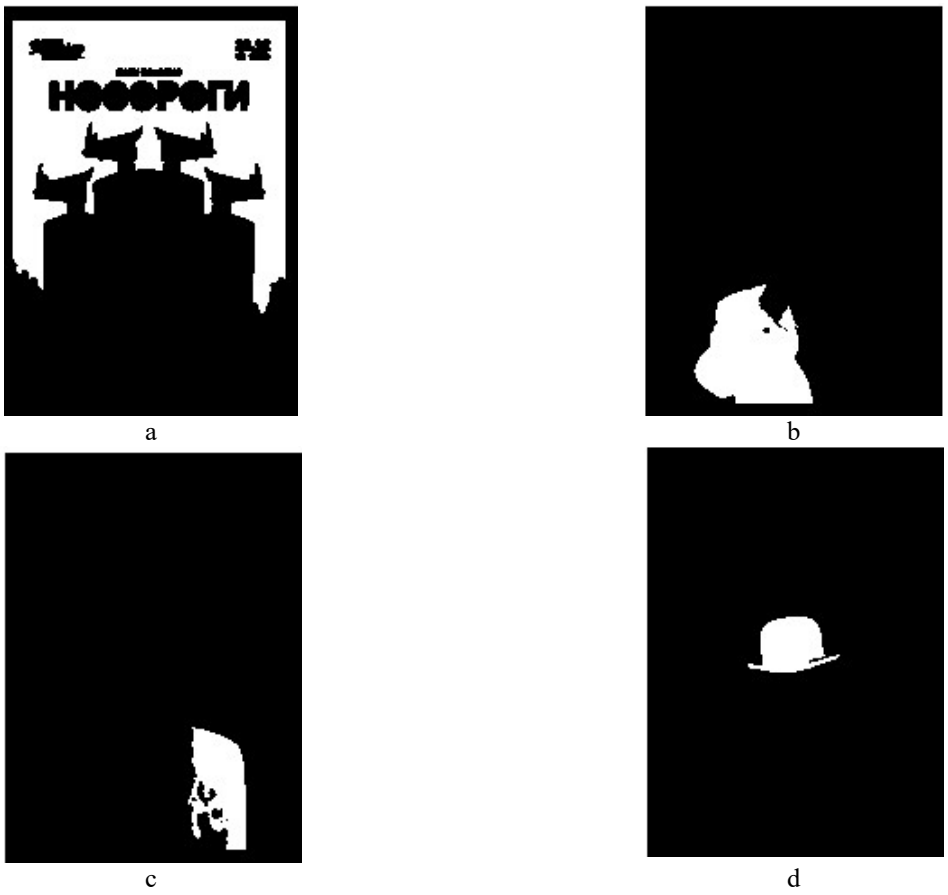

a b c d

Figure 4 – The cluster:
a – $n = 1$ ($D = 4.5$, $z_1(1) = 11921$) ; b – $n = 2$ ($D = 4.5$, $z_1(2) = 2829$) ;
c – $n = 3$ ($D = 4.5$, $z_1(3) = 1454$) ; d – $n = 4$ ($D = 4.5$, $z_1(4) = 973$)

DOI 10.15588/1607-3274-2025-2-4

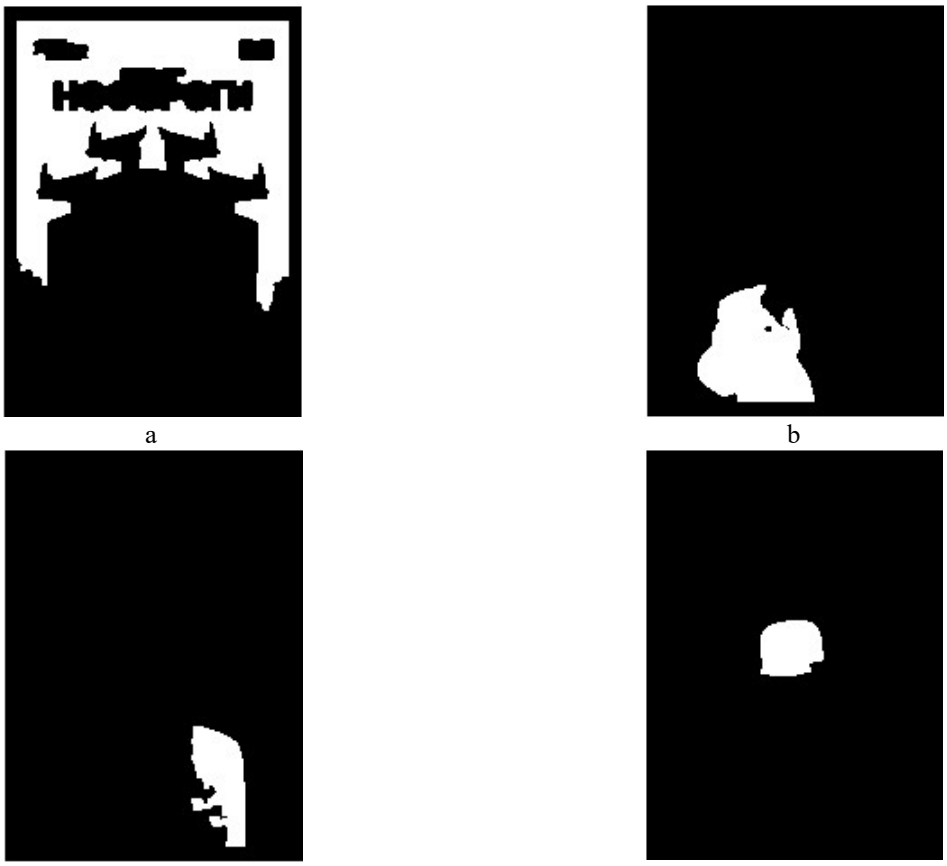

Figure 5 – The cluster:
a – $n = 1$ ($D = 9$, $z_1(1) = 11564$) ; b – $n = 2$ ($D = 9$, $z_1(2) = 2817$) ;
c – $n = 3$ ($D = 4.5$, $z_1(3) = 1341$) ; d – $n = 4$ ($D = 9$, $z_1(4) = 920$)

The comparison results of the proposed parallel clustering based intelligent image analysis method with the existing DBSCAN method are shown in Table 1.

Table 1 – Comparison of the proposed intelligent image analysis method based on parallel clustering with the existing DBSCAN method

Accuracy		Computational complexity	
proposed	existing	proposed	existing
0.98	0.85	$(p_k \times N_1 \times N_2)^2$	$(N_1 \times N_2)^2$

6 DISCUSSION

The existing DBSCAN method, which refers to density clustering and extracts connected regions:

– has high computational complexity;

– does not allow parallel processing;

– does not guarantee strict partitioning of image clusters by color;

– can lead to an excessive number of clusters in case of a large variety of image colors;

– requires setting the neighborhood radius, incorrect setting of which may reduce the clustering accuracy.

Therefore, in this paper we proposed a method for intelligent analysis of color images, which instead of a long clustering of a single image goes to a set of binary images (each binary image contains only elements of the quantized gray image with the same color, and these elements in the binary image are highlighted in white), the extraction of elements of which during clustering occurs in parallel, and during clustering the formation of neighborhoods only points of white color are checked. Since the clusters associated with a single binary image correspond to a certain color of the quantized gray image, there is a partitioning of clusters by color. Since in the proposed method there is a preliminary conversion of color image to gray-scale image and then the gray-scale image is quantized, i.e., the number of colors is reduced, there is

DOI 10.15588/1607-3274-2025-2-4

no excessive number of image clusters. Since the proposed method clusters binary images and only white color points are considered, instead of neighborhood radius, white color check of neighborhood points is used, which improves the accuracy of clustering.

Thus, the proposed method eliminates the mentioned disadvantages of the existing method.

The selected parameter values of the proposed method of intelligent color image analysis provide high accuracy of image elements extraction (Fig. 3a) and speed of this extraction (Fig. 3a), compared to the existing DBSCAN method.

According to Fig. 4 and Fig. 5 in case of Moore's neighborhood size $D = 4.5$, the elements of binary image are extracted more accurately.

CONCLUSIONS

The actual problem of improving the efficiency of color image analysis methods was solved by creating a method based on digital image processing and clustering algorithms.

The scientific novelty.

1. The proposed method of intelligent analysis of color images allows to increase the accuracy and speed of image elements extraction due to digital pre-processing and parallel clustering.

2. The technique of reducing the number of colors on the basis of color image conversion to gray-scale and quantization of the resulting gray-scale image allows increasing the accuracy of image elements extraction by preventing the appearance of an excessive number of image clusters.

3. The technique of creating a set of binary images on the basis of quantized gray image binarization (each binary image contains only elements of the quantized gray image with the corresponding same color, and these elements in the binary image are highlighted in white) allows to increase the speed of further clustering by replacing the sequential extraction of all elements of the quantized gray image by parallel extraction of elements of binary images, as well as to break the clusters obtained in the course of further clustering of the quantized gray image.

4. The technique of determining the highest priority binary images based on the probability of occurrence of each color in the quantized gray-scale image allows increasing the speed of image structure synthesis from the analysis results by considering the most informative binary images.

5. The technique of extracting binary image elements on the basis of its clustering allows to increase the accuracy of extracting binary image elements by improving the method of point neighborhood formation (to include a white point in the neighborhood of the point, the points nearest to it are simply checked for white color, so no empirically determined neighborhood radius is required). detecting random outliers and noise (minimum power cluster), extracting image elements of different shapes and sizes (due to connectivity), not specifying the number of and

6. The technique of determining the highest priority elements of a binary image based on the power of clusters of this image allows increasing the accuracy of image structure synthesis based on the analysis results by omitting noise and random outliers.

The practical significance. The proposed method extends the application area of color image analysis based on color-to-gray-scale image conversion, quantization, binarization, parallel clustering, and contributes to the efficiency of computer-based image classification and synthesis systems.

Prospects for further research are the study of the proposed method for a wide class of artificial intelligence tasks.

ACKNOWLEDGEMENTS

The studies were carried out in accordance with the priority direction of the development of science and technology in Ukraine "Information and Communication Technologies" and contain some results of the state scientific research project "Development of Models and Methods of Biometric Human Identification" (state registration number 0119U002860).

REFERENCES

1. Son X. The Application of Computer Post-Processing Technique in the Abstract Photography Art Expression, *2015 International Conference on Education Technology, Management and Humanities Science : proceedings.* Amsterdam, Atlantis Press, 2015, pp. 1340–1343. DOI: 10.2991/etmhs-15.2015.296
2. Khramova-Baranova O. L., Savanchuk O. S. Photography as a Means of Creating an Artistic Image in Graphic Design, *Synergy of science and business in the post-war reconstruction of the Kherson Region : Materials of the international scientific and practical conference*. Odesa, Oldi+, 2023, pp. 36–39.
3. Khramova-Baranova O. L., Kudrevich V. V., Baranov H., H. Zvonkova Emergence and Evolution of Computer Design in Ukraine and the World, *2023 IEEE International Conference on Information and Telecommunication Technologies and Radio Electronics (UkrMiCo) : proceedings*. Kyiv, Ukraine, 2023, pp. 364–368. DOI: 10.1109/UkrMiCo61577.2023.10380346
4. Li S. Z., Jain A. K. Handbook of Face Recognition. London, Springer, 2011, 699 p. DOI: 10.1007/978-0-85729-932-1
5. Nechyporenko O. V., Korpan Ya. V. Biometric Identification and Authentication of Persons for Geometry Face, *Herald of Khmelnytskyi National University*, 2016, No. 4 (239), pp. 133–138. URL: http://journals.khnu.km.ua/vestnik/pdf/tech/pdfbase/2016/2016_4/(239)%202016-4-t.pdf
6. Nechyporenko O., Korpan Y. Analysis of Methods and Technologies of Human Face Recognition, *Technology Audit and Production Reserves,* 2017, Vol. 5, № 2 (37), pp. 4–10. DOI: 10.15587/2312-8372.2017.110868
7. Fedorov E. E. , O. V. Nechyporenko, T. Yu. Utkina, Ya. V. Korpan Models and Methods of Computer Systems for Visual Image Recognition. Cherkasy, Cherkasy State Technological University, 2021, 482 p.

DOI 10.15588/1607-3274-2025-2-4

8. Bow S. T. (eds)Pattern Recognition and Image Preprocessing, 2nd ed. CRC Press, 2002. DOI: 10.1201/9780203903896
9. Gonzalez R., Woods R. Digital Image Processing ; 4th ed. Pearson International, 2017, 1024 p. URL: https://elibrary.pearson.de/book/99.150005/9781292223070
10. Martin D. R., Fowlkes C. C., Malik J. Learning to Detect Natural Image Boundaries using Local Brightness, Color, and Texture Cues, *IEEE Transactions on Pattern Analysis and Machine Intelligence*, 2004, Vol. 26, № 5, pp. 530–549. DOI: 10.1109/TPAMI.2004.1273918
11. Ballard D. H., Brown C. M. Computer Vision, Prentice-Hall, 1982, 523 p. URL: http://homepages.inf.ed.ac.uk/rbf/BOOKS/BANDB/Ballard__D._and_Brown__C._M.__1982__Computer_Vision.pdf
12. Dorin C., Meer P. Mean Shift: A Robust Approach toward Feature Space Analysis, *IEEE Transactions on Pattern Analysis and Machine Intelligence*, 2002. Vol. 24, Issue 5, P. 603–619. URL: https://courses.csail.mit.edu/6.869/handouts/PAMIMeanshift.pdf
13. Shapiro L. G., Stockman G. C. Computer Vision. New Jersey, Prentice-Hall, 2001, pp. 279–325. URL: https://cdn.preterhuman.net/texts/science_and_technology/artificial_intelligence/Computer%20Vision%20-%20Linda%20Shapiro.pdf
14. Kass M., Witkin A., Terzopoulos D. Snakes: Active Contour Models, *IJCV,* 1988, Vol. 1, Issue 4, pp. 321–331. URL: http://www.cs.ait.ac.th/~mdailey/cvreadings/Kass-Snakes.pdf
15. Chan T. F., Vese L. Active Contours without Edges, *IEEE Transactions on Image Processing,* 2001, Vol. 10, Issue 2, pp. 266–277. URL: https://www.math.ucla.edu/~lvese/PAPERS/IEEEIP2001.pdf
16. Wu Z., Leahy R. An Optimal Graph Theoretic Approach to Data Clustering: Theory and its Application to Image Segmentation, *IEEE Transactions on Pattern Analysis and Machine Intelligence*, 1993, Vol. 15, Issue 11, pp. 1101–1113. URL: https://cse.sc.edu/~songwang/csce790/Suppl/WuLeahy.pdf
17. Geman S., Geman D. Stochastic Relaxation, Gibbs Distributions and Bayesian Restoration of Images, *IEEE Transactions on Pattern Analysis and Machine Intelligence.* – 1984, Vol. 6, Issue 6, pp. 721–741. URL: http://image.diku.dk/imagecanon/material/GemanPAMI84.pdf
18. Brusco M. J. Shireman E. , Steinley D. A Comparison of Latent Class, K-means, and K-median Methods for Clustering Dichotomous Data, *Psychological Methods,* 2017, Vol. 22, Issue 3, pp. 563–580. DOI: 10.1037/met0000095
19. Bezdek J. C. Pattern Recognition with Fuzzy Objective Function Algorithms. New York, Plenum Press, 1981, 256 p. DOI: 10.1007/978-1-4757-0450-1
20. Ball G. H. Hall D. J. A Novel Method of Data Analysis and Pattern Classification. Technical Report. Menlo Park, CA : Stanford Research Institute, 1965, 79 p. DOI: 10.4236/ojml.2014.42028
21. Fu Z., Wang L. Color Image Segmentation Using Gaussian Mixture Model and EM Algorithm, *Multimedia and Signal Processing,* 2012, pp. 61–66. DOI: 10.1007/978-3-642-35286-7_9
22. Ester M., Kriegel H.-P., Sander J., Xu X. A Density-based Algorithm for Discovering Clusters in Large Spatial Databases with Noise, *The International Conference on Knowledge Discovery and Data Mining (KDD'1996) : proceedings,* 1996, pp. 226–231. URL: https://www.aaai.org/Papers/KDD/1996/KDD96-037.pdf
23. Ankerst M. , Breunig M. M. , Kriegel H.-P. , Sander J. OPTICS: Ordering Points to Identify the Clustering Structure, *SIGMOD Conference : proceedings,* 1999, pp. 49–60. URL: https://www.dbs.ifi.lmu.de/Publikationen/Papers/OPTICS.pdf
24. Mirkin B. G. Clustering for Data Mining: A Data Recovery Approach. Boca Raton, FL, CRC Press, 2005, 277 p. URL: http://www.dcs.bbk.ac.uk/~mirkin/papers/n.pdf
25. Aggarwal C. C. Reddy C. K. Data Clustering: Algorithms and Applications. Boca Raton, FL, CRC Press, 2014, 620 p. URL: https://people.cs.vt.edu/~reddy/papers/DCBOOK.pdf
26. Fedorov E., Utkina T., Nechyporenko O., Korpan Y. Development of Technique for Face Detection in Image Based on Binarization, Scaling and Segmentation Methods, *Eastern-European Journal of Enterprise Technologies,* 2020, № 1 (9–103), pp. 23–31. DOI: 10.15587/1729-4061.2020.195369
27. Fedorov E., Lukashenko V., Patrushev V., Lukashenko A., Rudakov K., Mitsenko S. The Method of Intelligent Image Processing Based on a Three-Channel Purely Convolutional Neural, *CEUR Workshop Proceedings,* 2018, Vol. 2255, pp. 336–351. URL: http://ceur-ws.org/Vol-2255/paper30.pdf
28. Bannore V. Iterative-Interpolation Super-Resolution Image Reconstruction. A Computationally Efficient Technique. Berlin, Springer-Verlag, 2009, 113 p. DOI: 10.1007/978-3-642-00385-1
29. Friedland G., Jain R. Multimedia Computing. Cambridge, Cambridge University Press, 2014, 368 p.
30. O'Gorman L., Sammon M. J., Seul. M. Practical Algorithms for Image Analysis with CD-ROM. Cambridge, Cambridge University Press, 2008, 360 p.

Received 05.01.2025.
Accepted 27.04.2025.

DOI 10.15588/1607-3274-2025-2-4

УДК 004.93

МЕТОД ІНТЕЛЕКТУАЛЬНОГО АНАЛІЗУ КОЛЬОРОВИХ ЗОБРАЖЕНЬ

Федоров Є. Є. – д-р техн. наук, професор, професор кафедри статистики та прикладної математики Черкаського державного технологічного університету, Черкаси, Україна.

Храмова-Баранова О. Л. – д-р іст. наук, професор, завідувачка кафедри графічного дизайну, моди та стилю Черкаського державного технологічного університету, Черкаси, Україна.

Уткіна Т. Ю. – канд. техн. наук, доцент, доцент кафедри робототехніки та спеціалізованих комп'ютерних систем Черкаського державного технологічного університету, Черкаси, Україна.

Кожушко Я. М. – канд. техн. наук, старший дослідник, провідний науковий співробітник науково-дослідного відділу автоматизованих, інформаційних систем та засобів зв'язку, Державний науково-дослідний інститут випробувань і сертифікації озброєння та військової техніки, м. Черкаси, Україна.

Несен І. О. – канд. техн. наук, старший викладач кафедри інформаційних систем та організації заходів цивільного захисту Навчально-наукового інституту цивільного захисту Національного університету цивільного захисту України, майор служби цивільного захисту України, Черкаси, Україна.

АНОТАЦІЯ

Актуальність. В даний час широкого поширення набули методи автоматичного та автоматизованого аналізу зображень, які використовуються в комп'ютерному графічному дизайні, біометричній ідентифікації, пошуку військових цілей. Об'єктом дослідження є процес аналізу кольорових зображень.

Метою роботи є створення інтелектуального методу аналізу зображення на основі квантування, бінаризації та кластеризації.

Метод. Запропонований метод інтелектуального аналізу кольорових зображень складається з таких методик. Методика зменшення кількості кольорів на основі перетворення кольорового зображення в сіре та квантування отриманого сірого зображення дозволяє підвищити точність вилучення елементів зображення за рахунок запобігання появі надлишкової кількості кластерів зображення. Методика створення набору бінарних зображень на основі бінаризації квантованого сірого зображення дозволяє підвищити швидкість подальшої кластеризації за рахунок заміни послідовного вилучення всіх елементів квантованого сірого зображення паралельним вилученням елементів бінарних зображень, а також розбити кластери, отримані в ході подальшої кластеризації, за кольором за рахунок належності різним бінарним зображенням. Методика визначення найбільш пріоритетних бінарних зображень на основі ймовірності появи кожного кольору в квантованому сірому зображенні дозволяє підвищити швидкість синтезу структури зображення за результатами аналізу за рахунок розгляду найбільш інформативних бінарних зображень. Методика вилучення елементів бінарного зображення на основі його кластеризації дозволяє підвищити точність вилучення елементів бінарного зображення за рахунок поліпшення способу формування околиць точок (не потрібний радіус околиці, що емпірично визначається), виявлення випадкових викидів і шуму, видобування елементів зображення різної форми та розміру, не вказуючи кількість видобутих елементів бінарного зображення, а також підвищення швидкості вилучення елементів бінарного зображення за рахунок формування околиць тільки точок білого кольору. Методика визначення найбільш пріоритетних елементів бінарного зображення на основі потужності кластерів зображення дозволяє підвищити точність синтезу структури зображення за результатами аналізу за рахунок пропуску шуму і випадкових викидів.

Результати. Запропонований метод інтелектуального аналізу кольорових зображень був програмно реалізований за допомогою Parallel Computing Toolbox пакету Matlab і досліджений для завдання вилучення елементів зображень на відповідній базі даних. Отримані результати дозволили порівняти традиційний та запропонований методи.

Висновки. Запропонований метод дозволяє розширити область застосування аналізу кольорових зображень на основі перетворення кольорового зображення в сіре, квантування, бінаризації, паралельної кластеризації, та сприяє підвищенню ефективності комп'ютерних систем класифікації та синтезу зображень. Перспективами подальших досліджень є дослідження запропонованого методу для широкого класу задач машинного навчання.

КЛЮЧОВІ СЛОВА: інтелектуальний аналіз зображення, квантування, бінаризація, вилучення елементів зображення, кластеризація.

ЛІТЕРАТУРА

1. Son X. The Application of Computer Post-Processing Technique in the Abstract Photography Art Expression / X. Son // 2015 International Conference on Education Technology, Management and Humanities Science : proceedings. – Amsterdam : Atlantis Press, 2015. – P. 1340–1343. DOI: 10.2991/etmhs-15.2015.296
2. Khramova-Baranova O. L. Photography as a Means of Creating an Artistic Image in Graphic Design / O. L. Khramova-Baranova , O. S. Savanchuk // Synergy of science and business in the post-war reconstruction of the Kherson Region : Materials of the international scientific and practical conference. – Odesa : Oldi+, 2023. – P. 36–39.
3. Emergence and Evolution of Computer Design in Ukraine and the World / [O. L. Khramova-Baranova, V. V. Kudrevich, H. Baranov, H. Zvonkova] // 2023 IEEE International Conference on Information and Telecommunication Technologies and Radio Electronics (UkrMiCo) : proceedings. – Kyiv, Ukraine, 2023. – P. 364–368. DOI: 10.1109/UkrMiCo61577.2023.10380346
4. Li S. Z. Handbook of Face Recognition / S. Z. Li, A. K. Jain. – London : Springer, 2011. 699 p. DOI: 10.1007/978-0-85729-932-1
5. Nechyporenko O. V. Biometric Identification and Authentication of Persons for Geometry Face / O. V. Nechyporenko, Ya. V. Korpan // Herald of Khmelnytskyi National University. – 2016. – No. 4 (239). – P. 133–138. URL: http://journals.khnu.km.ua/vestnik/pdf/tech/pdfbase/2016/2016_4/(239)%202016-4-t.pdf

DOI 10.15588/1607-3274-2025-2-4

6. Nechyporenko O. Analysis of Methods and Technologies of Human Face Recognition / O. Nechyporenko, Y. Korpan // Technology Audit and Production Reserves. – 2017. – Vol. 5, № 2 (37). – P. 4–10. DOI: 10.15587/2312-8372.2017.110868
7. Models and Methods of Computer Systems for Visual Image Recognition / [E. E. Fedorov, O. V. Nechyporenko, T. Yu. Utkina, Ya. V. Korpan]. – Cherkasy : Cherkasy State Technological University, 2021. – 482 p.
8. Bow S. T. Pattern Recognition and Image Preprocessing / S. T. Bow (eds) ; 2nd ed. – CRC Press, 2002. DOI: 10.1201/9780203903896
9. Gonzalez R., Woods R. Digital Image Processing ; 4th ed. / R. Gonzalez, R. Woods. – Pearson International, 2017. – 1024 p. – URL: https://elibrary.pearson.de/book/99.150005/9781292223070
10. Martin D. R. Learning to Detect Natural Image Boundaries using Local Brightness, Color, and Texture Cues / D. R. Martin, C. C. Fowlkes, J. Malik // IEEE Transactions on Pattern Analysis and Machine Intelligence. – 2004. – Vol. 26, № 5. – P. 530–549. DOI: 10.1109/TPAMI.2004.1273918
11. Ballard D. H. Computer Vision / D. H. Ballard, C.M. Brown. – Prentice-Hall, 1982. – 523 p. URL: http://homepages.inf.ed.ac.uk/rbf/BOOKS/BANDB/Ballard__D._and_Brown__C._M.__1982__Computer_Vision.pdf
12. Dorin C. Mean Shift: A Robust Approach toward Feature Space Analysis / C. Dorin, P. Meer // IEEE Transactions on Pattern Analysis and Machine Intelligence. – 2002. – Vol. 24, Issue 5. – P. 603–619. URL: https://courses.csail.mit.edu/6.869/handouts/PAMIMeanshift.pdf
13. Shapiro L. G. Computer Vision / L. G. Shapiro, G. C. Stockman. – New Jersey : Prentice-Hall, 2001. – P. 279–325. URL: https://cdn.preterhuman.net/texts/science_and_technology/artificial_intelligence/Computer%20Vision%20-%20Linda%20Shapiro.pdf
14. Kass M. Snakes: Active Contour Models / M. Kass, A. Witkin, D. Terzopoulos // IJCV. – 1988. – Vol. 1, Issue 4. – P. 321–331. URL: http://www.cs.ait.ac.th/~mdailey/cvreadings/Kass-Snakes.pdf
15. Chan T. F. Active Contours without Edges / T. F. Chan, L. Vese // IEEE Transactions on Image Processing. – 2001. – Vol. 10, Issue 2. – P. 266–277. URL: https://www.math.ucla.edu/~lvese/PAPERS/IEEEIP2001.pdf
16. Wu Z. An Optimal Graph Theoretic Approach to Data Clustering: Theory and its Application to Image Segmentation / Z. Wu, R. Leahy // IEEE Transactions on Pattern Analysis and Machine Intelligence. – 1993. – Vol. 15, Issue 11. – P. 1101–1113. URL: https://cse.sc.edu/~songwang/csce790/Suppl/WuLeahy.pdf
17. Geman S. Stochastic Relaxation, Gibbs Distributions and Bayesian Restoration of Images / S. Geman, D. Geman // IEEE Transactions on Pattern Analysis and Machine Intelligence. – 1984. – Vol. 6, Issue 6. – P. 721–741. URL: http://image.diku.dk/imagecanon/material/GemanPAMI84.pdf
18. Brusco M. J. A Comparison of Latent Class, K-means, and K-median Methods for Clustering Dichotomous Data / M. J. Brusco, E. Shireman, D. Steinley // Psychological Methods. – 2017. – Vol. 22, Issue 3. – P. 563–580. DOI: 10.1037/met0000095
19. Bezdek J. C. Pattern Recognition with Fuzzy Objective Function Algorithms / J. C. Bezdek. – New York : Plenum Press, 1981. – 256 p. DOI: 10.1007/978-1-4757-0450-1
20. Ball G. H. A Novel Method of Data Analysis and Pattern Classification. Technical Report / G. H. Ball, D. J. Hall. – Menlo Park, CA : Stanford Research Institute, 1965. – 79 p. DOI: 10.4236/ojml.2014.42028
21. Fu Z. Color Image Segmentation Using Gaussian Mixture Model and EM Algorithm / Z. Fu, L. Wang // Multimedia and Signal Processing. – 2012. – P. 61–66. DOI: 10.1007/978-3-642-35286-7_9
22. A Density-based Algorithm for Discovering Clusters in Large Spatial Databases with Noise / [M. Ester, H.-P. Kriegel, J. Sander, X. Xu] // The International Conference on Knowledge Discovery and Data Mining (KDD'1996) : proceedings. – 1996. – P. 226–231. URL: https://www.aaai.org/Papers/KDD/1996/KDD96-037.pdf
23. OPTICS: Ordering Points to Identify the Clustering Structure / [M. Ankerst, M. M. Breunig, H.-P. Kriegel, J. Sander] // SIGMOD Conference : proceedings. – 1999. – P. 49–60. URL: https://www.dbs.ifi.lmu.de/Publikationen/Papers/OPTICS.pdf
24. Mirkin B. G. Clustering for Data Mining: A Data Recovery Approach / B. G. Mirkin. – Boca Raton, FL : CRC Press, 2005. – 277 p. URL: http://www.dcs.bbk.ac.uk/~mirkin/papers/n.pdf
25. Aggarwal C. C. Data Clustering: Algorithms and Applications / C. C. Aggarwal, C. K. Reddy. – Boca Raton, FL : CRC Press, 2014. – 620 p. URL: https://people.cs.vt.edu/~reddy/papers/DCBOOK.pdf
26. Development of Technique for Face Detection in Image Based on Binarization, Scaling and Segmentation Methods / [E. Fedorov, T. Utkina, O. Nechyporenko, Y. Korpan] // Eastern-European Journal of Enterprise Technologies. – 2020. № 1 (9–103). – P. 23–31. DOI: 10.15587/1729-4061.2020.195369
27. The Method of Intelligent Image Processing Based on a Three-Channel Purely Convolutional Neural / [E. Fedorov, V. Lukashenko, V. Patrushev et al.] // CEUR Workshop Proceedings. – 2018. – Vol. 2255. – P. 336–351. URL: http://ceur-ws.org/Vol-2255/paper30.pdf
28. Bannore V. Iterative-Interpolation Super-Resolution Image Reconstruction. A Computationally Efficient Technique / V. Bannore. – Berlin : Springer-Verlag, 2009. – 113 p. DOI: 10.1007/978-3-642-00385-1
29. Friedland G. Multimedia Computing / G. Friedland, R. Jain. – Cambridge : Cambridge University Press, 2014. – 368 p.
30. O'Gorman L. Practical Algorithms for Image Analysis with CD-ROM / L. O'Gorman, M. J. Sammon, M. Seul. – Cambridge : Cambridge University Press, 2008. – 360 p.

DOI 10.15588/1607-3274-2025-2-4

UDC 004.93

PREDICTION THE ACCURACY OF IMAGE INPAINTING USING TEXTURE DESCRIPTORS

Kolodochka D. O. – Post-graduate student of the Institute of Computer Systems, Odesa Polytechnic National University, Odesa, Ukraine.

Polyakova M. V. – Dr. Sc., Associate Professor, Professor of the Department of Applied Mathematics and Information Technologies, Odesa Polytechnic National University, Odesa, Ukraine.

Rogachko V. V. – Student of the Institute of Computer Systems, Odesa Polytechnic National University, Odesa, Ukraine.

ABSTRACT

Context. The problem of filling missing image areas with realistic assumptions often arises in the processing of real scenes in computer vision and computer graphics. To inpaint the missing areas in an image, various approaches are applied such as diffusion models, self-attention mechanism, and generative adversarial networks. To restore the real scene images convolutional neural networks are used. Although convolutional neural networks recently achieved significant success in image inpainting, high efficiency is not always provided.

Objective. The paper aims to reduce the time consumption in computer vision and computer graphics systems by accuracy prediction of image inpainting with convolutional neural networks.

Method. The prediction of image inpainting accuracy can be done by an analysis of image statistics without the execution of inpainting itself. Then the time and computer resources on the image inpainting will not be consumed. We have used a peak signal-to-noise ratio and a structural similarity index measure to evaluate an image inpainting accuracy.

Results. It is shown that a prediction can perform well for a wide range of mask sizes and real-scene images collected in the Places2 database. As an example, we concentrated on a particular case of the LaMa network versions although the proposed method can be generalized to other convolutional neural networks as well.

Conclusions. The results obtained by the proposed method show that this type of prediction can be performed with satisfactory accuracy if the dependencies of the SSIM or PSNR versus image homogeneity are used. It should be noted that the structural similarity of the original and inpainted images is better predicted than the error between the corresponding pixels in the original and inpainted images. To further reduce the prediction error, it is possible to apply the regression on several input parameters.

KEYWORDS: image inpainting, accuracy prediction, LaMa network, texture descriptor, co-occurence matrix.

ABBREVIATIONS

CNN is a convolutional neural network;
LaMa is a Large Mask Inpainting;
ReLU is a Rectified Linear Unit;
GLCM is a gray-level co-occurrence matrix;
PSNR is a peak signal-to-noise ratio;
SSIM is a structural similarity index measure;
MSE is a mean squared error;
MAE is a mean absolute error.

NOMENCLATURE

n is a number of image rows;
m is a number of image columns;
(x,y) are coordinates of the image pixel;
$\mathbf{I}(x,y)$ is a vector function representing an image by color channels;
$I_R(x,y)$ is a red channel of an image;
$I_G(x,y)$ is a green channel of an image;
$I_B(x,y)$ is a blue channel of an image;
$M(x,y)$ is a binary mask;
$\circ$ is an element-by-element product of matrices;
f_θ is an inpainting network;
a_i is a coefficient of the polynomial of the 1st degree;
b_i is a coefficient of the polynomial of the 2nd degree;
d_i is a coefficient of the polynomial of the 3rd degree;
q_i is a coefficient of the inverse square root function;
r_i is a coefficient of a logarithmic function;
G is a gray-level co-occurrence matrix;
H is an image entropy;
W is an image homogeneity;
U is an image uniformity;
D_i is a texture descriptor;
P_i is a measure of image inpainting accuracy;
S is the size of the missing image area;
$h_i(\bullet)$ is a function of the dependence of P_i on D_i;
$\mathbf{W}_i$ is a vector of parameters of the function $h_i(\bullet)$;
L is a number of intensity levels in the image;
$I(v, w)$ is a luminance difference between images v, w;
$c(v, w)$ is a contrast difference between images v, w;
$s(v, w)$ is a structure difference between images v, w;
m_v is a local mean of image v;
σ_v is a standard deviation of image v;
σ_{vw} is a cross-covariance for images v and w.
C_i is a positive constant;
α is a positive constant;
β is a positive constant;
γ is a positive constant.

INTRODUCTION

Image inpainting means filling missing image areas with realistic assumptions in computer vision and computer graphics [1, 2]. Often, when photographing, users can encounter unwanted scene elements, for example, random persons or objects that need to be deleted. Before publishing the photo, you may want to make changes to correct the composition. In this case, image inpainting helps to remove unwanted objects and restore the image. Another case of application is the restoration of old photos that have been physically damaged.

DOI 10.15588/1607-3274-2025-2-5

The missing areas in an image can be inpainted by various approaches such as diffusion models (face and expressions inpainting [3, 4]) and self-attention mechanism (object removal in remote sensing images [2, 5, 6]). Generative adversarial networks are used for general image object removal and image desensitization which replaces sensitive information in images [2, 7]. To restore modern life and industrial images single- and multi-subnet CNNs are applied [8–10].

When filling an image area, it is necessary to select an inpainting method depending on the size of the missing area and the properties of the image. The CNNs known from the literature do not always provide high efficiency [1, 2, 8–10]. The question arises about the advisability of using a particular CNN and, accordingly, the consumption the time and computer resources on the image inpainting. Therefore, it is desirable to predict the accuracy of the filling of an image area of a certain size. It is supposed that the selected CNN is applied to the specific type of researched images.

The object of study is inpainting of real scene images in computer vision and computer graphics systems.

The subject of the study is methods of accuracy prediction of image inpainting using CNNs.

The paper aims to reduce the time consumption in computer vision and computer graphics systems by accuracy prediction of image inpainting with CNNs.

1 PROBLEM STATEMENT

The three-channels real scene image is defined as $\mathbf{I}(x,y)=(I_R(x,y), I_G(x,y), I_B(x,y))$, where $x=1, \ldots, n$; $y=1, \ldots, m$. To represent the missing areas of the image a mask is introduced. It is a binary image $M(x, y)$ of the same size as each channel of the original image. The mask is element-by-element multiplied by image channels, and the image with missing areas is represented as $\mathbf{I_M}(x,y)=(I_R(x,y)\circ M(x, y), I_G(x,y)\circ M(x, y), I_B(x,y)\circ M(x, y))$ [8–9, 11].

Let us suppose that the CNN $f_\theta(\bullet)$ with parameters θ was preliminarily trained to inpaint the images. It outputs the image $\mathbf{I_{in}}(x,y) = f_\theta(\mathbf{I_M}(x,y))$ which approximates the original image $\mathbf{I}(x,y)$ in the sense of some criterion [8].

To predict the accuracy of the image inpainting by the considered network, an image feature (one or more) is selected. To evaluate this feature, descriptors D_1, D_2, ..., D_k are formed. They will be used as independent variables representing the input information for the prediction. Besides, the prediction can be significantly influenced by additional factors. In our case, this is the size of the missing image area S.

Next, the output variables are selected. These are measures evaluating the accuracy of the image inpainting by the selected network: P_1, P_2, ..., P_l. It is necessary to define the dependence of measures P_1, P_2, ..., P_l on descriptors D_1, D_2, ..., D_k and factor S :

$$P_i=h_1(D_1, \mathbf{W}_1, S), P_i=h_2(D_2, \mathbf{W}_2, S), \ldots, \quad P_i=h_k(D_k, \mathbf{W}_k, S), \ i=1, \ldots, l; \qquad (1)$$

and to estimate vectors of parameters $\mathbf{W}_1$, $\mathbf{W}_2$, ..., $\mathbf{W}_k$ of these dependences. Further for each P_i, $i=1, ..., l$, we determine from a set of dependencies (1) the dependency $P_i=h_{j(i)}(D_{j(i)}, \mathbf{W}_{j(i)}, S)$, $j(i)\in\{1, ..., k\}$, with the highest value of the selected measure of approximation accuracy. Interpolation or extrapolation of the functions, $P_i=h_{j(i)}(D_{j(i)}, \mathbf{W}_{j(i)}, S)$, $i=1, ..., l$; will predict the accuracy of image inpainting by the network $f_\theta(\bullet)$.

In this paper we propose a method to predict the accuracy of the real scene image inpainting with the selected neural network. To obtain the solution to this problem we determined the factors that influenced the inpainting accuracy measures. Based on these factors we selected the predictors and determined the structure of dependence between the predictors and the measures of inpainting accuracy. After the estimation of the parameters of such dependence and the approximation accuracy evaluation, we can calculate an input parameter and predict the output parameter based on the dependence existing between them. Having this prediction, one can decide by a human or automatically using certain rules whether to apply considered CNN for image inpainting.

To research the proposed method experimentally we used the selected LaMa convolutional network and varied the size of the missing area which must be inpainted. The size of the missing area defines the complexity of image inpainting and determines the effectiveness of the prediction for the selected network. We also evaluated the accuracy of prediction for the different spectral transforms consisted the LaMa network and for different image inpainting measures. The experimental results presented in this article were obtained using the Places365 dataset [12].

2 REVIEW OF THE LITERATURE

In the literature the ability to predict the CNN efficiency was researched for classification problems in [13]. The prediction of the image denoising efficiency based on the discrete cosine transform was considered in [14–16]. The paper [17] is devoted to the prediction of the dynamics of the signals describing a signature using the CNN. It is needed to detect potential forgeries by identity verification systems. However, the network efficiency has not been predicted for the problem of image inpainting. The recommendations for the selection of image inpainting methods are mostly qualitative. The evaluation of the accuracy of the filling of missing image areas is provided after image inpainting which is time and resource-consuming.

The existing image inpainting approaches are influenced by the content of input images, missing area size, and the ill-posedness of image inpainting problem. The deep learning-based methods in image inpainting allow for improving results by capturing image features and semantic on different scales [18]. Despite the similarity of deep learning methods, they differ in inpainting approaches, network architecture, loss function, etc. To construct the model for inpainting

DOI 10.15588/1607-3274-2025-2-5

accuracy prediction it is advisable to take into account the following four image inpainting approaches [1].

The progressive inpainting fills missing image areas step by step. Specifically, coarse-to-fine, low-to-high-resolution, and structure-to-content inpainting are used. This approach supposes that available information is not sufficient to reconstruct all missing pixels in one step [5, 18].

The structural information-guided inpainting is based on the structure of the known regions, such as segmentation results, edges, depth maps, gradient of color or intensity, etc. These auxiliary cues facilitate the recovery of sharp details and fine structure of the missing areas [19–21].

The convolutions-aware inpainting applies different convolution operators for the generation of missing pixels. For example, the traditional convolution operates by valid pixels as well as by substitute values in the missing areas, which leads to color discrepancy and blurring [22]. To avoid the disadvantages, partial convolution, gated convolution, and bidirectional convolution are used [22–24].

The attention-based inpainting uses the image content from distant spatial locations when CNNs are ineffective for the filling of missing areas. The additional information can be obtained from contextual patches, feature maps, searching for the most similar patch, or the modeling of the underlying distribution of reconstructed images [6, 7, 25].

Let us review these approaches in light of the possibility of their applying to the prediction of image inpainting accuracy. So, progressive inpainting is not well suited for inpainting accuracy prediction due to its generality. Almost all the CNNs based on the convolutions-aware approach due to their architecture. If we will use the same approach to predict the accuracy of the image inpainting by the CNN we can obtain the overtrained prediction model. The attention-based approach uses local patterns of the original image and similar images. It is not clear how these local patterns can influence image inpainting in general and how to elaborate a predictive model based on such a representation. However, the attention-based approach can be used to obtain additional information for image inpainting accuracy prediction, specifically, the properties of the distribution of image colors or intensities.

It should be noticed that the image content and fine structure influence the image inpainting accuracy. Therefore, it is advisable to predict the image inpainting accuracy based on a structural information-guided approach which allows to extraction of the image features and to estimate the feature descriptors.

3 MATERIALS AND METHODS

The proposed method of predicting the accuracy ofThe proposed method of predicting the accuracy of the image inpainting by CNN applies the regression on initial image descriptors. The general idea of the proposed method can be described by the following steps.

Step 1. Preparing the data.

The datasets for image inpainting are selected. The range of sizes and the form of the image missing areas are determined. Then the binary masks modeling the image's missing areas are formed and superimposed on images.

Step 2. The tuning of the CNN.

As a result of the literature review, we choose CNN for image inpainting. If a pre-trained network is used then the parameters of such network are loaded. Otherwise, the training and test sets of images are formed from the selected datasets. The researched network is trained to inpaint the missing areas modeled with binary masks on the images of the training set.

Step 3. The determining of the prediction model variables.

To obtain the output variables of a prediction model, the measures of image inpainting accuracy are selected. The trained network is applied to test set images with missing areas. The inpainting accuracy is evaluated by the selected measures depending on the size of the missing areas of the image.

Next, we choose the image descriptors that estimate the image features influencing the inpainting accuracy. They will be used as input variables of the model. Values of these descriptors are calculated based on original images from the test set.

Step 4. The prediction model selection and model parameters estimation.

The regression model that connects output and input variables is constructed using the fitting of the curves to data points in scatter plots. While scatter plots are created we take into account that original images may have different properties or content of missing areas differs from one image to the other. The regression model parameters are estimated on a training set of images by the least squares approach.

Step 5. The prediction model evaluation and the image inpainting accuracy prediction.

To evaluate the prediction model performance the accuracy of curve fitting is estimated based on the values of input and output variables obtained on the test set images. The regression interpolation or extrapolation predicts the values of the image inpainting accuracy measures relying on the values of descriptors. The obtained results are analyzed to conclude the appropriateness of the considered CNN to inpaint the specific image.

In this paper, we provide prerequisites for decision-making based on the specifics of image inpainting methods. In the following research, we concentrate on a particular case of versions of the LaMa network although the proposed method can be generalized to other CNNs as well.

The LaMa network is considered here to inpaint the images for the following reasons.

(1) This CNN has a simpler architecture than many of the other state-of-the-art networks for image inpainting. In particular, the LaMa network consists of one subnet rather than an ensemble of subnets and has fewer parameters.

DOI 10.15588/1607-3274-2025-2-5

(2) It can implement data processing with fast Fourier transform or discrete wavelet transform leading to several benefits:

a) a higher speed of image processing and network training;

b) successful inpainting of large missing areas of spectral textures;

c) high-quality inpainting of fine details of images and edges of objects.

Let us describe the architecture of the LaMa network (Fig. 1) [8, 9, 11]. This network has inputted an image with an overlayed mask denoting the pixels that need to be inpainted. At first, the initial image is downscaled by a factor of 3. Then the local and global textures are extracted from the obtained image. These global and local features are further passed through convolution layers. Then spectral transform block is additionally applied to global texture channels. The fast Fourier transform or the discrete wavelet transform is implemented in this block. The features of using these transforms in the LaMa network are described and studied in detail in [8, 9, 11]. The outputs of the convolution layers are added up crosswise. Then after batch normalization and ReLU activation, the results of local and global texture processing are concatenated. The described layers excluded from the downscale are repeated and added up with the downscaled image. The LaMa network module embedded between downscaling and upscaling is also repeated nine times. After that, the image is upscaled to its initial size and outputted [8, 9].

Despite the relatively simple LaMa network architecture, the learning of this network is time-consuming. The image impainting by this trained network also requires a lot of time. For example, in the Google Colab environment with a pre-configured NVIDIA Tesla T4 GPU, which has 16 GB of GDDR6 memory and 2,560 CUDA cores it took us 2 to 7 seconds to inpaint an image of size 1024x1024 pixels. At the same time although the LaMa network has demonstrated a high inpainting accuracy, some of the restored images are of insufficient quality. In particular, this is the case of the inpainting of statistical textures and detail-rich images. In [11] it was noted that the quality of the images inpainted with the LaMa network is influenced by the initial image textures. To avoid wasting time and resources we propose to previously evaluate the accuracy of image inpainting by the LaMa network.

Let us define the output variables of a prediction model. We propose to use PSNR and SSIM which estimate the inpainting accuracy in terms of edge quality and structural integrity [26]. Let us suppose that the lowest image intensity level is equal to zero. Then PSNR is evaluated as the ratio between the highest squared intensity $(L-1)$ of the initial image and MSE between the initial and inpainted images [26]:

$$PSNR = 10\times\log_{10}((L-1)^2/MSE).$$

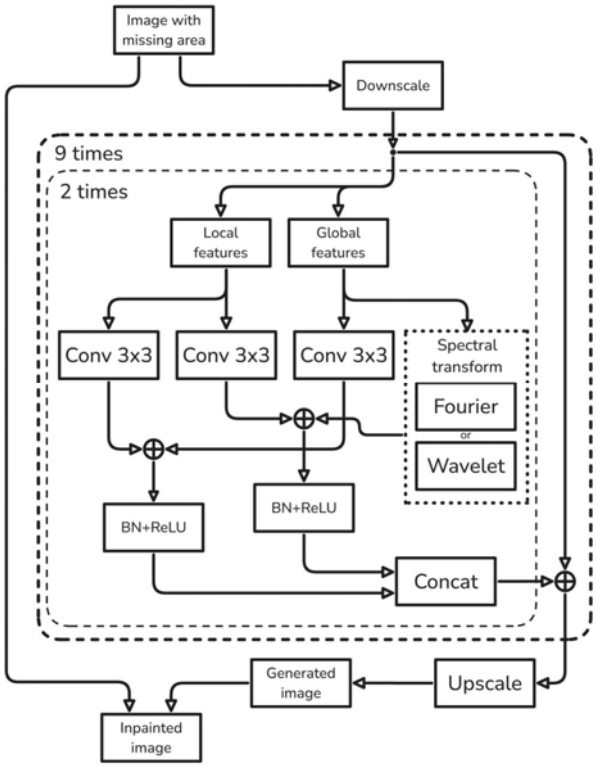

Figure 1 – LaMa network architecture [8, 9]

PSNR compares the edges and fine details in the original and inpainted image and determines differences between them at the pixel level.

Another considered measure is SSIM evaluates the inpainted image in terms of restoring the natural appearance of textures and edges. It estimates the differences in texture, contrast, and structure of the initial and reconstructed images [26]:

$$SSIM(v, w)=l\,(v, w)^{\alpha}\; c\,(v, w)^{\beta}\; s\,(v, w)^{\gamma},$$
$$l\,(v, w) = (2m_v m_w + C_1)/(m_v^2 + m_w^2 + C_1),$$
$$c\,(v, w) = (2\sigma_v \sigma_w + C_2)/(\sigma_v^2 + \sigma_w^2 + C_2),$$
$$s\,(x, y)=(\sigma_{vw} + C_3)/(\sigma_v \sigma_w + C_3).$$

We suppose that $\alpha=\beta=\gamma=1$, then the SSIM values range between 0 to 1.

Selecting the input variables of the prediction model we observed that the accuracy of image inpainting weakly depends on the texture measures based on the color or intensity histograms. They ignore the spatial relations between pixels, which is important when a texture is described. To avoid the shortcoming it can be taken into consideration not only the distribution of intensities but also the relative positions of pixels in an image. In this way in [27] an operator Q is defined which evaluates the relation between the intensities of two pixels. Based on this operator a GLCM G is determined for a gray-scale image $I(x, y)$ with L possible intensity levels. Each element g_{ij} of the matrix G is the number of times that the pixel pair with intensities l_i and l_j is found in the image in the relation Q, where $1 \le i, j \le L$.

DOI 10.15588/1607-3274-2025-2-5

Based on a GLCM the texture descriptors are introduced in [27]. When the LaMa network efficiency was tested, we observed that the texture descriptors such as uniformity, homogeneity, and entropy changed for different values of the PSNR and SSIM [11]. Therefore, we can to use these texture descriptors as the input variables of the prediction model because their computation is time-saving compared to the image inpainting by CNN.

The uniformity determines the pixel intensity randomness and takes values from the range [0, 1]:

$$U = \frac{1}{n_Q^2} \sum_{i=1}^{L} \sum_{j=1}^{L} g_{ij}^2 ,$$

where n_Q is the number of pixel pairs in the relation Q. Uniformity increases as the square of the probability values, so the less random an image is, the higher its uniformity. The uniformity is equal to 1 for a constant image.

Homogeneity measures the concentration of GLCM element values near the main diagonal by expression

$$W = \frac{1}{n_Q} \sum_{i=1}^{L} \sum_{j=1}^{L} \frac{g_{ij}}{1+|i-j|} .$$

The value of the denominator $(1 + |i – j|)$ decreases as the values of i and j get closer, i.e., as they approach the main diagonal. The range of homogeneity values is [0, 1], with the maximum being achieved when G is a diagonal matrix. The GLCM with the highest values of elements near the main diagonal will correspond to images with a variety of gray-level content and areas of slowly varying intensity values.

Entropy measures the randomness of the elements of GLCM which, in turn, is determined by the randomness of the initial image:

$$H = -\sum_{i=1}^{L} \sum_{j=1}^{L} \frac{g_{ij}}{n_Q} \log_2 \frac{g_{ij}}{n_Q} .$$

The highest value $2\times\log_2 L$ is achieved for matrix GLCM, obtained from an image that is formed by uniform noise then all image intensities are approximately equally probable. The entropy is equal to zero for a constant-intensity image.

4 EXPERIMENTS

Let us consider the construction of the scatter plots for the image inpainting accuracy prediction. To obtain the regression function that describes the dependence between output and input variables, the curve fitting of scatter plots is applied. To take into consideration the different properties of inpainted images the simulation of missing areas of the different sizes is needed. That is why we have formed three separate categories of masks, modeling different levels of image inpainting complexity. These masks randomly uniformly cover 25%, 50%, and 75% of the image area, and are named as narrow, medium, and large, respectively.

We constructed masks of 1–5 straight lines with a slope from 0 to 2π, 1–100 pixels wide, and 10–200 pixels long. As an alternative, masks of 1–4 rectangles with sides of 30–150 pixels were generated with a probability of 0.5. Then the test set included 2,000 images from the Places2 dataset [12]. The missing areas of these images covered by generated masks were reconstructed by the LaMa network. As spectral transform fast Fourier transform or discrete wavelet transform were included in LaMa network architecture. The LaMa-Fourier and LaMa-Wavelet networks are obtained [8, 9]. The results of image inpainting were evaluated with PSNR and SSIM.

Further, the GLCM has been determined and the image uniformity, homogeneity, and entropy have been calculated based on the obtained GLCM for each test image. Next, one mask from each category was generated for each image. After element-by-element multiplication of images on masks, the inpainting was performed using LaMa-Fourier and LaMa-Wavelet networks. In Figure 2 the scatter plots SSIM and PSNR versus uniformity, homogeneity and entropy are shown.

As a basis for prediction, the data points in the obtained scatter plots indicate the main trends. Specifically, the PSNR and SSIM decrease if entropy increases and uniformity and homogeneity decrease. Data for different mask categories are shown in the different scatter plots. The results related to the image inpainting by the LaMa-Wavelet and LaMa-Fourier networks denoted with different symbols.

Next, we consider the estimation of the parameters of the image inpainting accuracy prediction model. The following functions for the scatter-plot fitting were selected.

1. Polynomials of the first, second and third degree $y(x)=a_1x+a_0$, $y(x)=b_2x^2+b_1x+b_0$, $y(x)=d_3x^3+d_2x^2+d_1x+d_0$.
2. Inverse square root function $y(x) = q_1x^{-1/2} + q_0$.
3. Logarithmic function $y(x) = r_1\ln x + r_0$.

The parameters of the mentioned functions were estimated by the fitting of the scatter plots using the least squares approach. To evaluate the curve fitting results we have selected a curve fitting accuracy measure. This is the R-squared (R^2) value which is estimated as the proportion of the variance in the dependent variable explained by the independent variable in the considered model. The R-squared values lie between 0 and 1, where higher R^2 relates to better curve fitting. To estimate the approximation error the mean squared error (MSE) is used. It estimates the average squared difference between the actual and predicted values of the dependent variable. Lower MSE indicates that the selected model better approximates the actual values. MSE is bounded below by zero and has no higher limit.

DOI 10.15588/1607-3274-2025-2-5

5 RESULTS

The obtained values of *R*-squared are shown in Tables 1nand 2. We have discarded the low-valued outliers of entropy (2.5% for narrow and medium masks, 5% for large masks), and the high-valued outliers of uniformity (10% for narrow masks, 15% for medium masks, 20% for large masks) to increase the approximation accuracy. As a result, the R-squared values were increased by an average of 7–8%. The best R-squared values were mostly obtained on polynomials of the third order but the other functions used for scatter-plot fitting in the paper have shown similar results.

In Table 3 the MSEs related to SSIM and corresponding to the R-squared from Table 1 are presented without the brackets. The MSEs related to PSNR and corresponding to the R-squared from Table 2 are shown in brackets.

Table 1 – The *R*-squared for polynomial regression degree 3, the dependent variable is SSIM

Input variable	Narrow masks	Medium masks	Large masks
	LaMa-Fourier		
Entropy	0.3950	0.4192	0.4241
Homogeneity	0.7007	0.7098	0.6920
Uniformity	0.4408	0.4641	0.4500
	LaMa-Wavelet		
Entropy	0.4151	0.4277	0.4257
Homogeneity	0.7203	0.7267	0.7090
Uniformity	0.4541	0.4630	0.4489

The obtained dependencies of PSNR versus homogeneity W for narrow masks are expressed for LaMa-Fourier and LaMa-Wavelet as

$$PSNR=24.3653+14.9912W-2.4763W^2+4.7581W^3;$$
$$PSNR=24.1664+18.0167W-11.4362W^2+13.5988W^3.$$

The SSIM versus homogeneity W for narrow masks is expressed for LaMa-Fourier and LaMa-Wavelet as

$$SSIM=0.8228+0.4694W-0.7282W^2+0.4640W^3;$$
$$SSIM=0.8199+0.4644W-0.7077W^2+0.4622W^3;$$

for medium masks as

$$SSIM=0.6341+0.8195W-1.0334W^2+0.6318W^3;$$
$$SSIM=0.6291+0.8284W-1.0622W^2+0.6838W^3;$$

for large masks as

$$SSIM=0.4112+1.1130W-1.1985W^2+0.7524W^3;$$
$$SSIM=0.3988+1.1170W-1.1921W^2+0.7549W^3.$$

Table 2 – The *R*-squared for polynomial regression, degree 3, the dependent variable is PSNR

Input variable	Narrow masks	Medium masks	Large masks
	LaMa-Fourier		
Entropy	0.3220	0.2707	0.1457
Homogeneity	0.4826	0.3496	0.1960
Uniformity	0.2720	0.1691	0.0600
	LaMa-Wavelet		
Entropy	0.3329	0.2691	0.1466
Homogeneity	0.5034	0.3523	0.1961
Uniformity	0.2831	0.1620	0.0603

Table 3 – The MSE for polynomial regression, degree 3, the dependent variable is SSIM (PSNR)

Input variable	Narrow masks	Medium masks	Large masks
	LaMa-Fourier		
Entropy	0.0004 (5.0254)	0.0019 (5.6551)	0.0048 (4.8962)
Homogeneity	0.0002 (4.0205)	0.0009 (5.0474)	0.0025 (4.9400)
Uniformity	0.0003 (5.5083)	0.0016 (5.6171)	0.0042 (4.7120)
	LaMa-Wavelet		
Entropy	0.0004 (5.0083)	0.0019 (5.7219)	0.0048 (4.7160)
Homogeneity	0.0002 (3.9224)	0.0009 (5.0739)	0.0025 (4.4509)
Uniformity	0.0004 (4.7620)	0.0017 (6.1228)	0.0043 (4.7074)

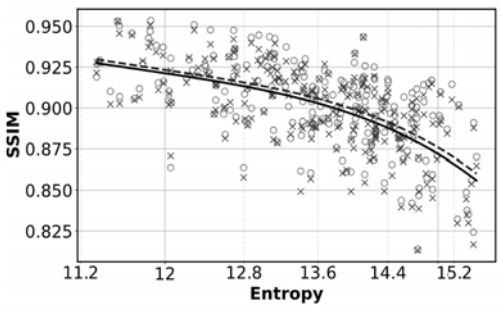

a

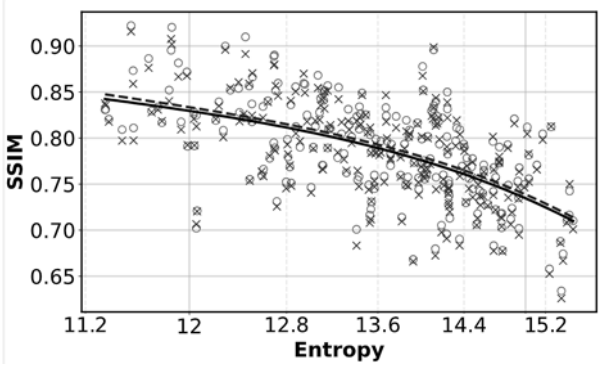

b

DOI 10.15588/1607-3274-2025-2-5

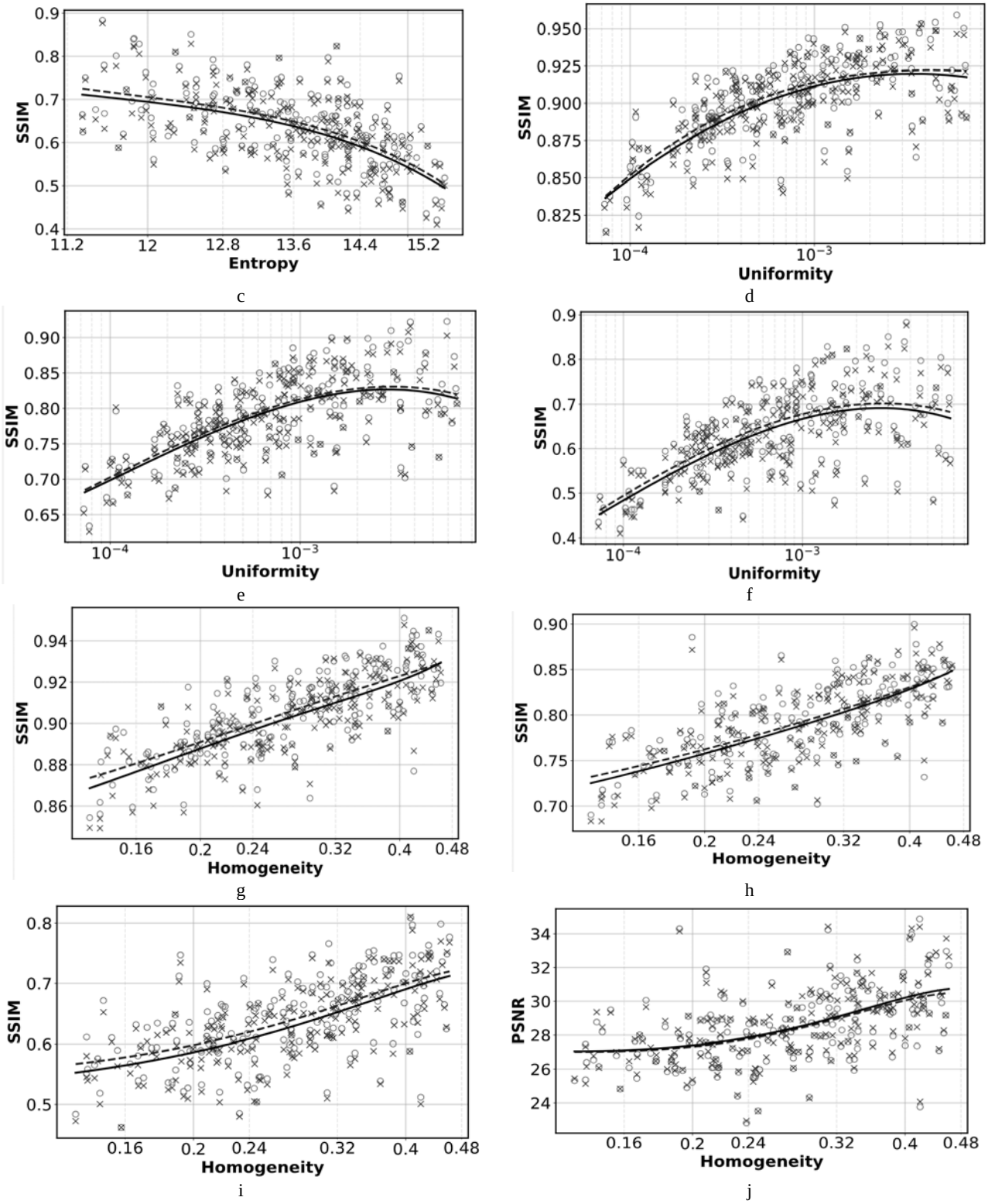

Figure 2 – The scatter-plots of SSIM vs entropy: a – narrow mask; b – medium mask; c – large mask; SSIM vs uniformity: d – narrow mask; e – medium mask; f – large mask; SSIM vs homogeneity: g – narrow mask; h – medium mask; i – large mask; PSNR vs homogeneity: j – narrow mask. The data points and the line of polynomial regression of 3rd degree related to LaMa-Fourier results are marked with a circle and dash line; the same objects related to LaMa-Wavelet are marked with a cross and solid line

DOI 10.15588/1607-3274-2025-2-5

6 DISCUSSIONS

Let us consider the dependencies of the SSIM from the texture descriptors if the LaMa-Fourier network is used. The best fitting is achieved for SSIM versus homogeneity (Table 1). Specifically, the approximation by a polynomial of degree 3 gives R^2 from 0.6920 to 0.7098 for different mask size. This indicates that considered model fits the data well. Others texture descriptors worse explain the dependent variable SSIM (R^2 varies from 0.3950 to 0.4241 for entropy and from 0.4508 to 4641 for uniformity). As one can see, the results do not appear to be affected by the mask size.

Now we analyze the dependences the PSNR from the texture descriptors if the LaMa-Fourier network is used (Table 2). The best fitting is again achieved for homogeneity versus PSNR. Specifically, the approximation by a polynomial of degree 3 gives R^2 from 0.1960 to 0.4826 for different mask size. Others texture descriptors even worse explain the PSNR (R^2 varies from 0.1457 to 0.3220 for entropy and from 0.0603 to 0.2831 for uniformity). Therefore, the PSNR can be only predicted from homogeneity and for narrow masks. As for the remaining scatter plots, the proportion of the PSNR variance that is explained by texture descriptors is very low to predict the actual PSNR values.

If the LaMa-Wavelet network is applied then the R-squared values are increased by 3–5% for considered dependencies and categories of masks (Tables 1, and 2). Therefore, the LaMa-Wavelet network is more acceptable for the prediction of the image inpainting accuracy.

The scatter plots for different mask sizes are presented in different figures (Figure 2). It can be observed that the LaMa network versions in general show similar results, i.e. the data points related to the LaMa-Fourier and LaMa-Wavelet do not create separate clusters. Moreover, the scatter plots of dependences of the texture descriptors on the SSIM obtained for the different mask sizes are also similar. However, in the scatter-plots of dependences of the texture descriptors on the PSNR, the compactness of data points is enlarged as the mask size is increased. The cluster of data points is “pressed” to the texture descriptor axis showing the significant lowering of the PSNR of inpainted images as the missing area size increases. It means that the accuracy of image detail in inpainting is decreased as mask size is increased.

The results of the prediction of the image inpainting accuracy on a test set of images from the Places2 dataset are presented in Table 4. MAE was estimated between the actual and predicted values of PSNR and SSIM. It should be noted that the lowest MAE of the prediction we have obtained for narrow mask inpainting. However, the highest MAE is obtained for medium masks. This fact can be explained by a high variety of medium-sized image details.

As an example, we have considered the results of the prediction of the inpainting accuracy for the images from Figure 3. The images from Figures 3, a, b are processed with narrow masks; the images from Figures 3, c, d are inpainted with medium and large masks, respectively. The PSNR was only predicted for images from Figure 3, a, b. The actual PSNR were 24.7131 dB and 30.6880 dB, the predicted PSNR were 30.5912 dB and 31.7558 dB. The SSIM was predicted for images from Figure 3, a–d. The actual values were 0.8926, 0.9281, 0.7819, and 0.5452; the predicted values were 0.9260, 0.9330, 0.8586, 0.6185; respectively.

Table 4 – The MAE of image inpainting accuracy prediction

Narrow masks, PSNR, dB	Narrow masks, SSIM	Medium masks, SSIM	Large masks, SSIM
LaMa-Fourier			
3.7359	0.0262	0.0960	0.0504
LaMa-Wavelet			
3.7443	0.0283	0.0966	0.0705

Finally, we note that computing the texture descriptors, specifically, entropy, homogeneity, and uniformity, took an average of 0.1139 sec per image of 1024x1024 pixels. The PSNR and SSIM calculation takes an average of 0.1605 sec per image of the same size. By comparison, we can mention that image inpainting by the LaMa-Wavelet network took an average of 6.6 sec per image. However, the network’s computations are predominantly GPU-accelerated, making heavy use of hardware-level parallelism, while the accuracy metrics evaluation is done on the CPU (Intel(R) Xeon(R) CPU 2.00GHz, total RAM 12.67 GB) relying on synchronous operations. It should be noted that because of inherent differences in the hardware architecture, the time of the computing of texture descriptors and calculations in the network should not be directly compared.

CONCLUSIONS

The scientific novelty is the proposed method of the prediction of the image inpainting accuracy. The method is based on the set of texture descriptors estimated using the gray-level co-occurrence matrix to predict the values of image inpainting accuracy measures, specifically, the PSNR and SSIM.

The practical significance of the research is in the results obtained for real scene images from the Places2 dataset with the LaMa network applied. These results show that the prediction of the image inpainting accuracy can be performed with satisfactory accuracy if the dependencies of the SSIM or PSNR versus homogeneity are used. The other considered texture descriptors such as entropy and uniformity can be only used to support the prediction. It should be noted that the structural similarity of the original and inpainted images is better predicted than the error between the corresponding pixels in the original and inpainted images. The better approximation accuracy was achieved with the polynomial of 3rd degree if data outliers have been removed. Better prediction accuracy was obtained if the missing areas could be modeled by a narrow mask.

DOI 10.15588/1607-3274-2025-2-5

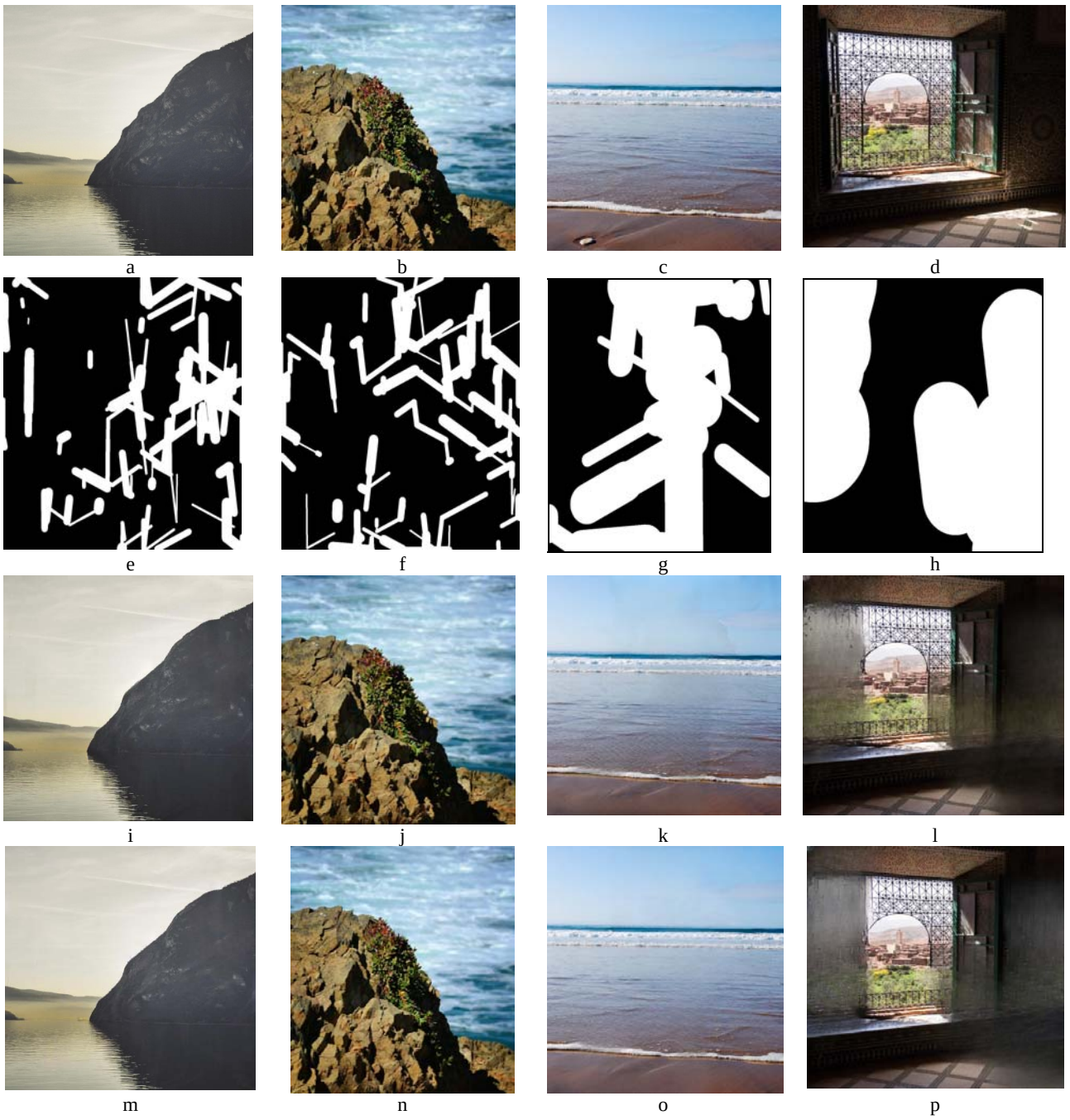

Figure 3 – The results of image inpainting with LaMa network: a, b, c, d – initial image; e, f – narrow mask; g – medium mask; h – large mask; i, j, k, l – images inpainted with LaMa-Fourier; m, n, o, p – images inpainted with LaMa-Wavelet

Prospect for further research is a reducing the prediction error. In this way, it is possible to apply the regression on several input parameters. To our opinion, the proposed method can be also applied to other CNNs trained to inpaint real scene images to decide about the advisability of the time and resource consumption needed for image inpainting.

ACKNOWLEDGEMENTS

The work was supported by the state budget research project of the Odessa Polytechnic National University "Modeling of self-organizing systems and controlled dynamic systems" (state registration number 0119U003520).

REFERENCES

1. Xiang H., Zou Q., Nawaz M. A. et al. Deep learning for image inpainting: a survey, *Pattern Recognition*, 2023, Vol. 134, Article 109046. DOI: 10.1016/j.patcog.2022.109046.
2. Xu Z., Zhang X., Chen W. et al. A review of image inpainting method based on deep learning, *Appl. Sci.*, 2023, Vol. 13, Article 11189. DOI: 10.3390/app132011189.

DOI 10.15588/1607-3274-2025-2-5

3. Ho J., Jain A., Abbeel P. Denoising diffusion probabilistic models, *Advances in Neural Information Processing Systems*, 2020, Vol. 33, pp. 6840–6851.
4. Lugmayr A., Danelljan M., Romero A. et al. Repaint: Inpainting using denoising diffusion probabilistic models, *Computer Vision and Pattern Recognition: IEEE/CVF Conference, New Orleans, LA, USA, 19–20 June 2022 : proceedings.* IEEE 2022, pp. 11451–11461. DOI: 10.1109/CVPR52688.2022.0111.
5. Yu J., Yang J., Shen X., Lu X., Huang T. S. Generative image inpainting with contextual attention. *Computer Vision and Pattern Recognition Workshops: IEEE/CVF Conference, CVPRW, Salt Lake City, UT, USA, 18–22 June, 2018 : proceedings.* IEEE, 2018, pp. 5505–5514. DOI: 10.1109/CVPRW.2018.00577.
6. Mohite T. A., Phadke G. S. Image inpainting with contextual attention and partial convolution, *Artificial Intelligence and Signal Processing: 2020 International Conference, AISP, Amaravati, India, 10–12 January 2020 : proceedings*. IEEE, 2020, pp. 1–6. DOI: 10.1109/AISP48273.2020.9073008.
7. Guo Q., Li X., Juefei-Xu F. et al. JPGnet: Joint predictive filtering and generative network for image inpainting, *Multimedia: 29th ACM International Conference, Chengdu, China, 20–24 October 2021 : proceedings.* ACM, 2021, pp. 386–394. DOI: 10.1145/3474085.3475170.
8. Suvorov R., Logacheva E., Mashikhin A. et al. Resolution-robust large mask inpainting with Fourier convolutions, *Applications of Computer Vision: IEEE Workshop/Winter Conference, WACV, Waikoloa, Hawaii, 4–8 January, 2022 : proceedings*. IEEE, 2022, pp. 2149–2159. DOI: 10.1109/WACV51458.2022.00323
9. Kolodochka D. O., Polyakova M. V. LaMa-Wavelet: image inpainting with high quality of fine details and object edges, *Radio Electronics, Computer Science, Control*, 2024, № 1, pp. 208–220. DOI: 10.15588/1607-3274-2024-1-19.
10. Jain S., Shivam V., Bidargaddi A. P., Malipatil S., Patil K. Image inpainting using YOLOv8 and LaMa model, *Emerging Technology: 5th International Conference (INCET), Belgaum, India, 24-26 May 2024 : proceedings.* IEEE, 2024, pp. 1–7. DOI: 10.1109/INCET61516.2024.10593536.
11. Kolodochka D., Polyakova M., Nesteriuk O., Makarichev V. LaMa network architecture search for image inpainting, *Information Control Systems & Technologies: 12th International Conference, ICST, Odesa, Ukraine, 23–25 September, 2024 : proceedings*. CEUR-WS, 2024, Vol. 3799, pp. 365 – 376.
12. Places365 Scene Recognition Demo [Electronic resource]. Access mode: http://places2.csail.mit.edu/
13. Mellor J., Turner J., Storkey A. J., Crowley E. J. Neural architecture search without training, *Machine Learning: 38th International Conference, PMLR, Virtual, 18–24 July 2021: proceedings*. IEEE, 2021, Vol. 139, pp. 7588–7598. DOI: 10.48550/arXiv.2006.04647.
14. Rubel O., Abramov S., Lukin V. et al. Is texture denoising efficiency predictable, *International Journal on Pattern Recognition and Artificial Intelligence*, 2018, Vol. 32, Article 1860005. DOI: 10.1142/S0218001418600054.
15. Rubel O. S., Lukin V. V., de Medeiros F. S. Prediction of despeckling efficiency of DCT-based filters applied to SAR images, *Distributed Computing in Sensor Systems: 2015 International Conference, (DCOSS), Fortaleza, Brazil, 10–12 June, 2015 : proceedings*. IEEE, 2015, pp. 159–168. DOI: 10.1109/DCOSS.2015.16.
16. Abramov S., Abramova V., Lukin V., Egiazarian K. Prediction of signal denoising efficiency for DCT-based filter, *Telecommunications and Radio Engineering*, 2019, Vol. 78, № 13, pp. 1129–114. DOI: 10.1615/TelecomRadEng.v78.i13.10.
17. Zalasiński M., Cader A., Patora-Wysocka Z., Xiao M. Evaluating neural network models for predicting dynamic signature signals, *Journal of Artificial Intelligence and Soft Computing Research*, 2024, Vol. 14, № 4, pp. 361–372. DOI: 10.2478/jaiscr-2024-0019.
18. Cao L., Yang T., Wang Y., Yan B., Guo Y. Generator pyramid for high-resolution image inpainting, *Complex & Intelligent Systems*, 2023, Vol. 9, Article 7553. DOI: 10.1007/s40747-023-01080-w.
19. Yamashita Y., Shimosato K., Ukita N. Boundary-aware image inpainting with multiple auxiliary cues, *Computer Vision and Pattern Recognition: IEEE/CVF Workshop/Conference, New Orleans, LA, USA, 19–20 June, 2022 : proceedings*. IEEE, 2022, pp. 618–628. DOI: 10.1109/CVPRW56347.2022.00077.
20. Nazeri K., Ng E., Joseph T., Qureshi F., Ebrahimi M. EdgeConnect: structure guided image inpainting using edge prediction, *Computer Vision Workshop: IEEE/CVF International Conference, ICCVW, Seoul, Korea (South), 27–28 October, 2019 : proceedings.* IEEE, 2019, pp. 2462–2468. DOI: 10.1109/ICCVW.2019.00408
21. Liao L., Xiao J., Wang Z., Lin C.-W., Satoh S. Guidance and evaluation: semantic-aware image inpainting for mixed scenes, *Computer Vision: 16th European Conference, ECCV, Glasgow, UK, 23–28 August 2020 : proceedings.* IEEE, 2020, pp. 683–700. DOI: 10.1007/978-3-030-58583-9_41.
22. Liu G., Reda F. A., Shih K. J. et al. Image inpainting for irregular holes using partial convolutions, *Computer Vision: European Conference, ECCV, Munich, Germany, 8–14 September, 2018 : proceedings.* IEEE, 2018, pp. 85–100. DOI: 10.1007/978-3-030-01252-6_6.
23. Yu J., Lin Z., Yang J. et al. Free-form image inpainting with gated convolution, *Computer Vision: IEEE/CVF International Conference, ICCV, Seoul, Korea (South), 27 October – 2 November, 2019 : proceedings*. IEEE, 2019, pp. 4471–4480. DOI: 10.1109/ICCV.2019.00457.
24. Xie C., Liu S., Li C. et al. Image inpainting with learnable bidirectional attention maps, *Computer Vision: IEEE/CVF International Conference, ICCV, Seoul, Korea (South), 27 October – 2 November 2019 : procedings.* IEEE, 2019, pp. 8857–8866. DOI: 10.1109/ICCV.2019.00895.
25. Wang X., Girshick R., Gupta A., He K. Non-local neural networks, *Computer Vision and Pattern Recognition: 2018 IEEE/CVF Conference, Salt Lake City, UT, USA, 18–22 June 2018 : proceedings*. IEEE, 2018, pp. 7794–7803. DOI: 10.1109/CVPR.2018.00813.
26. Sara U., Akter M., Uddin M. S. Image quality assessment through FSIM, SSIM, MSE and PSNR – a comparative study, *Journal of Computer and Communications*, 2019, Vol. 7, № 3, pp. 8–18. DOI: 10.4236/jcc.2019.73002.
27. Gonzalez R. C., Woods R. E. Digital Image Processing, NY: Pearson, 4th Edition, 2017, 1192 p.

Received 05.02.2025.
Accepted 22.04.2025.

DOI 10.15588/1607-3274-2025-2-5

УДК 004.93

ПРОГНОЗУВАННЯ ЯКОСТІ ВІДНОВЛЕННЯ ЗОБРАЖЕНЬ ІЗ ЗАСТОСУВАННЯМ ТЕСТУРНИХ ДЕСКРИПТОРІВ

Колодочка Д. О. – студент Інституту комп'ютерних систем Національного університету «Одеська політехніка», Одеса, Україна.

Полякова М. В. – д-р техн. наук, доцент, професор кафедри прикладної математики та інформаційних технологій Національного університету «Одеська політехніка», Одеса, Україна.

Рогачко В. В. – студент Інституту комп'ютерних систем Національного університету «Одеська політехніка», Одеса, Україна.

АНОТАЦІЯ

Актуальність. Проблема заповнення відсутніх областей зображення реалістичним контентом часто виникає при обробці реальних сцен у комп'ютерному зорі та комп'ютерній графіці. Щоб відновити відсутні області на зображенні, застосовуються різні підходи, такі як дифузійні моделі, механізм самоуважності, генеративні змагальні мережі. Для відновлення зображень реальних сцен використовуються згорткові нейронні мережі. Із застосуванням цих мереж останнім часом досягнуто значних успіхів у відновленні зображень. Але отримані відновлені зображення не завжди високої якості.

Мета роботи полягає у зменшенні витрат часу в системах комп'ютерної графіки та комп'ютерного зору шляхом прогнозування якості відновлення зображень згортковими нейронними мережами.

Метод. Прогноз точності відновлення зображення здійснено шляхом аналізу статистики зображення без виконання самої реконструкції і, отже, без витрачання зайвого часу та комп'ютерних ресурсів на відновлення зображення. Ми використали пікове відношення сигнал/шум і показник індексу структурної подібності для оцінки якості відновлення зображення.

Результати. Показано, що передбачення ефективне для широкого діапазону розмірів масок і зображень реальних сцен з бази даних Places2. У якості прикладу було зосереджено на окремих випадках версій мережі LaMa, хоча запропонований метод також можна узагальнити на інші згорткові нейронні мережі.

Висновки. Отримані результати показують, що прогноз якості відновлення зображень може бути виконаний із задовільною точністю, якщо використовувати залежності SSIM або PSNR від показника однорідності текстури зображень. Слід зазначити, що структурна подібність початкового та відновленого зображень краще передбачувана, ніж помилка між відповідними пікселями цих зображень. Щоб зменшити помилку прогнозування можна застосувати регресію за декількома вхідними змінними.

КЛЮЧОВІ СЛОВА: відновлення зображення, прогнозування точності, мережа LaMa, дескриптор текстури, матриця суміжності.

ЛІТЕРАТУРА

1. Deep learning for image inpainting: a survey / [H. Xiang, Q. Zou, M. A. Nawaz et al.] // Pattern Recognition. – 2023. – Vol. 134. – Article 109046. DOI: 10.1016/j.patcog.2022.109046.
2. A review of image inpainting method based on deep learning / [Z. Xu, X. Zhang, W. Chen et al.] // Applied Sciences. – 2023. – Vol. 13. – Article 11189. DOI: 10.3390/app132011189.
3. Ho J. Denoising diffusion probabilistic models / J. Ho, A. Jain, P. Abbeel // Advances in Neural Information Processing Systems. – 2020. – Vol. 33. – P. 6840–6851.
4. Repaint: Inpainting using denoising diffusion probabilistic models / [A. Lugmayr, M. Danelljan, A. Romero et al.] // Computer Vision and Pattern Recognition: IEEE/CVF Conference, New Orleans, LA, USA, 19–20 June 2022 : proceedings. – IEEE 2022. – P. 11451–11461. DOI: 10.1109/CVPR52688.2022.0111.
5. Generative image inpainting with contextual attention / [J. Yu, J. Yang, X. Shen et al.] // Computer Vision and Pattern Recognition Workshops: IEEE/CVF Conference, CVPRW, Salt Lake City, UT, USA, 18–22 June, 2018 : proceedings. – IEEE, 2018. – P. 5505–5514. DOI: 10.1109/CVPRW.2018.00577.
6. Mohite T. A. Image inpainting with contextual attention and partial convolution / T. A. Mohite, G. S. Phadke // Artificial Intelligence and Signal Processing: 2020 International Conference, AISP, Amaravati, India, 10–12 January 2020 : proceedings. – IEEE, 2020. – P. 1–6. DOI: 10.1109/AISP48273.2020.9073008.
7. JPGnet: Joint predictive filtering and generative network for image inpainting / [Q. Guo, X. Li, F. Juefei-Xu et al.] // Multimedia: 29th ACM International Conference, Chengdu, China, 20–24 October 2021 : proceedings. – ACM, 2021. – P. 386–394. DOI: 10.1145/3474085.3475170.
8. Resolution-robust large mask inpainting with Fourier convolutions / [Suvorov R., Logacheva E., Mashikhin A. et al.] // Applications of Computer Vision: IEEE Workshop/Winter Conference, WACV, Waikoloa, Hawaii, 4 – 8 January, 2022 : proceedings. – IEEE, 2022. – P. 2149–2159. DOI: 10.1109/WACV51458.2022.00323.
9. Kolodochka D. O. LaMa-Wavelet: image inpainting with high quality of fine details and object edges / D. O. Kolodochka, M. V. Polyakova // Radio Electronics, Computer Science, Control. – 2024. – № 1. – P. 208–220. DOI: 10.15588/1607-3274-2024-1-19.
10. Image inpainting using YOLOv8 and LaMa model / [S. Jain, V. Shivam, A. P. Bidargaddi et al.] // Emerging Technology: 5th International Conference (INCET), Belgaum, India, 24–26 May 2024 : proceedings. – IEEE, 2024. – P. 1–7. DOI: 10.1109/INCET61516.2024.10593536.
11. LaMa network architecture search for image inpainting / [D. Kolodochka, M. Polyakova, O. Nesteriuk, V. Makarichev] // Information Control Systems & Technologies: 12th International Conference Information, ICST, Odesa, Ukraine, 23–25 September, 2024 : proceedings. – CEUR-WS, 2024. – Vol. 3799. – P. 365 – 376.
12. Places365 Scene Recognition Demo [Electronic resource]. Access mode: http://places2.csail.mit.edu/

DOI 10.15588/1607-3274-2025-2-5

13. Neural architecture search without training / [J. Mellor, J. Turner, A. J. Storkey, E. J. Crowley] // Machine Learning: 38th International Conference, PMLR, Virtual, 18–24 July 2021: proceedings. – IEEE, 2021. – Vol. 139. – P. 7588–7598. DOI: 10.48550/arXiv.2006.04647.
14. Is texture denoising efficiency predictable / [O. Rubel, S. Abramov, V. Lukin et al.] // International Journal on Pattern Recognition and Artificial Intelligence. – 2018. – Vol. 32. – Article 1860005. DOI: 10.1142/S0218001418600054.
15. Rubel O. S. Prediction of despeckling efficiency of DCT-based filters applied to SAR images / O. S. Rubel, V. V. Lukin, F. S. de Medeiros // Distributed Computing in Sensor Systems: 2015 International Conference (DCOSS), Fortaleza, Brazil, 10 – 12 June, 2015 : proceedings. – IEEE, 2015. – P. 159–168. DOI: 10.1109/DCOSS.2015.16.
16. Prediction of signal denoising efficiency for DCT-based filter / [S. Abramov, V. Abramova, V. Lukin, K. Egiazarian] // Telecommunications and Radio Engineering. – 2019. – Vol. 78, № 13. – P. 1129–114. DOI: 10.1615/TelecomRadEng.v78.i13.10.
17. Evaluating neural network models for predicting dynamic signature signals / [M. Zalasiński, A. Cader, Z. Patora-Wysocka, M. Xiao] // Journal of Artificial Intelligence and Soft Computing Research. – 2024. – Vol. 14, № 4. – P. 361–372. DOI: 10.2478/jaiscr-2024-0019.
18. Generator pyramid for high-resolution image inpainting / [L. Cao, T. Yang, Y. Wang, B. Yan, Y. Guo] // Complex & Intelligent Systems. – 2023. – Vol. 9. – Article 7553. DOI: 10.1007/s40747-023-01080-w.
19. Yamashita Y. Boundary-aware image inpainting with multiple auxiliary cues / [Y. Yamashita, K. Shimosato, N. Ukita] // Computer Vision and Pattern Recognition: IEEE/CVF Workshop/Conference, New Orleans, LA, USA, 19 – 20 June, 2022 : proceedings. – IEEE, 2022. – P. 618–628. DOI: 10.1109/CVPRW56347.2022.00077.
20. EdgeConnect: structure guided image inpainting using edge prediction / [K. Nazeri, E. Ng, T. Joseph et al.]// Computer Vision Workshop: _IEEE/CVF International Conference, ICCVW, Seoul, Korea (South), 27–28 October, 2019 : proceedings. – IEEE, 2019. – P. 2462–2468. DOI: 10.1109/ICCVW.2019.00408.
21. Guidance and evaluation: semantic-aware image inpainting for mixed scenes / [L. Liao, J. Xiao, Z. Wang et al.] // Computer Vision: 16th European Conference, ECCV, Glasgow, UK, 23–28 August 2020 : proceedings. – IEEE, 2020. – P. 683–700. DOI: 10.1007/978-3-030-58583-9_41.
22. Image inpainting for irregular holes using partial convolutions / [G. Liu, F. A. Reda, K. J. Shih et al.] // Computer Vision: European Conference, ECCV, Munich, Germany, 8 – 14 September, 2018 : proceedings. – IEEE, 2018. – P. 85–100. DOI: 10.1007/978-3-030-01252-6_6.
23. Free-form image inpainting with gated convolution / [J. Yu, Z. Lin, J. Yang et al.] // Computer Vision: IEEE/CVF International Conference, ICCV, Seoul, Korea (South), 27 October – 2 November, 2019 : proceedings. – IEEE, 2019. – P. 4471–4480. DOI: 10.1109/ICCV.2019.00457.
24. Image inpainting with learnable bidirectional attention maps / [C. Xie, S. Liu, C. Li et al.] // Computer Vision: IEEE/CVF International Conference, ICCV, Seoul, Korea (South), 27 October – 2 November 2019 : procedings. – IEEE, 2019. – P. 8857–8866. DOI: 10.1109/ICCV.2019.00895.
25. Non-local neural networks / [X. Wang, R. Girshick, A. Gupta, K. He] // Computer Vision and Pattern Recognition: 2018 IEEE/CVF Conference, Salt Lake City, UT, USA, 18 – 22 June 2018 : proceedings. – IEEE, 2018. – P. 7794–7803. DOI: 10.1109/CVPR.2018.00813.
26. Sara U. Image quality assessment through FSIM, SSIM, MSE and PSNR — a comparative study / U. Sara, M. Akter, M. S. Uddin // Journal of Computer and Communications. – 2019. – Vol. 7, № 3. – P. 8–18. DOI: 10.4236/jcc.2019.73002.
27. Gonzalez R. C. Digital Image Processing / R. C. Gonzalez, R. E. Woods. – NY: Pearson, 4th Edition, 2017. – 1192 p.

DOI 10.15588/1607-3274-2025-2-5

UDC 519.8

MATHEMATICAL FOUNDATIONS OF METHODS FOR SOLVING CONTINUOUS PROBLEMS OF OPTIMAL MULTIPLEX PARTITIONING OF SETS

Koriashkina L. S. – Doctor of Science, Associate Professor, Associate Professor of the Department of System Analysis and Control, Dnipro University of Technology, Dnipro, Ukraine.

Lubenets D. E. – Postgraduate student of the Department of System Analysis and Control, Dnipro University of Technology, Dnipro, Ukraine.

Minieiev O. S. – PhD, Associate Professor, Associate Professor of the Department of System Analysis and Control, Dnipro University of Technology, Dnipro, Ukraine.

Sazonova M. S. – PhD, Associate Professor, Researcher in the Optimization and Systems Theory Section, Department of Mathematics, KTH Royal Institute of Technology, Stockholm, Sweden.

ABSTRACT

Context. The research object is the process of placing service centers (e.g., social protection services, emergency supply storage) and allocating demand for services continuously distributed across a given area. Mathematical models and optimization methods for location-allocation problems are presented, considering the overlap of service zones to address cases when the nearest center cannot provide the required service. The relevance of the study stems from the need to solve problems related to territorial distribution of logistics system facilities, early planning of preventive measures in potential areas of technological disasters, organizing evacuation processes, or providing primary humanitarian assistance to populations in emergencies.

Objective. The rational organization of a network of service centers to ensure the provision of guaranteed service in the shortest possible time by assigning clients to multiple nearest centers and developing the corresponding mathematical and software support.

Method. The concept of a characteristic vector-function of a *k*-th order partition of a continuous set is introduced. Theoretical justification is provided for using the LP-relaxation procedure to solve the problem, formulated in terms of such characteristic functions. The mathematical framework is developed using elements of functional analysis, duality theory, and nonsmooth optimization.

Results. A mathematical model of optimal territorial zoning with center placement, subject to capacity constraints, is presented and studied as a continuous problem of optimal multiplex partitioning of sets. Unlike existing models, this approach describes distribution processes in logistics systems by minimizing the distance to several nearest centers while considering their capacities. Several propositions and theorems regarding the properties of the functional and the set of admissible solutions are proven. Necessary and sufficient optimality conditions are derived, forming the basis for methods of optimal multiplex partitioning of sets.

Conclusions. Theoretical findings and computational experiment results presented in the study confirm the validity of the developed mathematical framework, which can be readily applied to special cases of the problem. The proven propositions and theorems underpin computational methods for optimal territorial zoning with center placement. These methods are recommended for logistics systems to organize the distribution of material flows while assessing the capacity of centers and the fleet of transportation vehicles involved.

KEYWORDS: continuous set, multiplex partitioning, optimization, LP-relaxation, optimality conditions, location-allocation problems.

ABBREVIATIONS

OMPS is an optimal multiplex partitioning of sets;

LP is Linear Programming.

NOMENCLATURE

Ω is a set being partitioned is bounded, closed, and Lebesgue measurable in the space E_2;

τ_i are points from Ω, which are called centers;

N is a number of centers;

k is an order of the partition of the set Ω;

N is a set of all center indices;

M is a set of all k-element subsets of the set **N**;

L is a number of all k-element subsets of the set **N**;

$\rho()$ is a non-negative function describing the demand for the service.

$c()$ is a cost function;

w_i is a proportionality coefficient;

a_i is a cost of establishing i-th center τ_i or upgrading an existing one, or its fixed operating costs calculated per unit of demand;

b_i is a capacity of i-th center, which defines the maximum volume of services the center can provide;

Ω_σ are areas covering clients who have the same k nearest neighboring service centers from N existing (possible);

σ is a set of indices of centers associated with the subset Ω_σ.

INTRODUCTION

The problems of efficient organization of logistics, production, and trade networks constitute one of the directions of modern optimization theory. The scientific literature contains numerous works devoted to the location-allocation problem – determining the best positions for service centers along with the most rational distribution of demand for the services they provide. A comprehensive review of location-allocation models and methods, as well as their practical applications, is presented in [1]. The paper [2] provides a history of location models over the past 50 years, though it is not exhaustive, as it

DOI 10.15588/1607-3274-2025-2-6

highlights the contributions of only some of the most active European operational research groups. A significant part of scientific research focuses not only on the analysis of object location but also on the evaluation of the market share they occupy, their attractiveness, and competitors' reactions to the appearance of new objects. In particular, [3] describes methods for finding the best locations for competing objects and significant modifications of the classical gravity model. The paper [4] presents mathematical models of optimal location of service centers and partitioning of the territory into service zones, considering the possibility of receiving services from any of the nearest centers. Overlapping zones are provided for cases when the nearest center is unable to provide the service. Centers can include, for example, social protection services, emergency supply warehouses, etc. The distribution of service consumers among service centers is described as optimal multiplex partitioning problems of continuous sets in various formulations – with predefined centers or the need for their location, with or without capacity constraints for service centers. Several possible optimality criteria for multiplex partitioning of sets are proposed. The applied aspects of these problems and related continuous multiple spheres covering problems are considered in [5].

This paper is devoted to the description and theoretical justification of the method for solving continuous problems of optimal multiplex partitioning of sets with center location and capacity constraints.

The object of study is the process of locating service centers and territorial zoning.

The subject of study is mathematical models and methods for optimal location of centers with the determination of their service zones.

The purpose of the work is to organize rationally a network of service centers by determining such locations and service zones to ensure the guaranteed provision of services to consumers in the shortest possible time by assigning them to several nearest centers.

1 PROBLEM STATEMENT

Lets Ω represents the territory of a region where a network of service enterprises operates; $\rho(x)$ is a function that describes the demand for a service at point x within the set Ω; τ_i are points from Ω, which are called centers, $\tau_i \in \Omega, i = 1,2,\ldots,N$; b_i is the capacity of the i-th center $i = 1,2,\ldots,N$; $c(x,\tau_i)$ is the cost of providing the service to a client at the point $x \in \Omega$ by center τ_i, which is considered proportional to the distance between the two points; a_i is the cost of establishing a new center or upgrading an existing one at point τ_i or its fixed organizational costs, calculated per unit of demand, for $i = 1,2,\ldots,N$.

We will consider the problem of optimal location of a certain number of service centers in a given area and assigning service zones to them in such a way that each service consumer (the residents of the area) is assigned to k nearest centers to ensure guaranteed service. The quality criterion is the minimization of transportation (time) and organizational costs, with the condition being the capacity constraints of the centers (the maximum volume of services that a center can provide).

2 REVIEW OF THE LITERATURE

Models of the location of one or several objects among a given set of demand points to achieve a particular goal are considered in [6]. In discrete models, a finite set of potential locations for the objects is given. In continuous models, objects can be located anywhere on the plane or within a region with an infinite number of potential locations. In paper [7], the use of professional optimization software (CPLEX and AIMMS packages) to solve the location-allocation problem is demonstrated, but only discrete models of problems are considered. In article [8], the problems of intermediate transportation hubs, transfer points, and collection warehouses are discussed, highlighting the difference between node location problems and classical object location problems, presenting the p-median problem with single and multiple allocations. Research [9] is aimed at solving continuous location problems for the *p*-center by repeated analysis. An algorithm based on model relaxation is presented here, enhanced by the addition of four mathematical improvements, which provide a significant reduction in computation time for large data sets (up to one and a half thousand nodes). The flexibility of the improved algorithm is demonstrated, as it can be easily adapted for the α-neighbor p-center problem and problems with constraints.

The features of most of the listed problems are the discrete demand for services, and the obtaining of service zones in the form of spatial monopolies. The classic p-median problem assumes that services are always provided to clients by the nearest facility, whereas in practice, clients often interact with several facilities for various reasons (not just the nearest one). In works [4, 10], distribution rules for modeling such flows are introduced. In [4], a mathematical model of the problem of locating service centers while simultaneously determining overlapping service zones is presented as an optimal multiplex partitioning problem. In [10], the so-called "distributed" p-median problem is formulated, and various types of allocation rules are investigated. For instance, if the weighting coefficients increase (i.e., the assigned flows are larger for objects located farther away), the problem can be solved in polynomial time as a *1*-median. For decreasing weights, a special case of which is the classical *p*-median, a generalization of standard continuous and discrete models is obtained, leading to a broader interpretation of median points. In work [11], the demand for service is continuously distributed over a certain area, as in the problems from [4, 12]. In these works, analytical or spatially interpolated functions are used for the approximate representation of demand, although the results of both methods are subject to significant errors and are characterized by uncertainty. For this reason, [11] introduces a general location model and a continuous Weber

DOI 10.15588/1607-3274-2025-2-6

problem, in which objects can be located anywhere in space to best meet the continuously distributed demand. Due to the complexity of assessing constant demand, it is proposed to integrate optimization methods with the functional capabilities of a geographic information system.

In [12, 13], an approach to developing methods for optimal multiplex partitioning of sets is presented, based on formulating problems in terms of characteristic functions, applying LP-relaxation for the obtained infinite-dimensional optimization problems with Boolean variables, and further using elements of duality theory. Although the relaxation procedure for discrete location-allocation problems is widely used (see, for example, [6, 9]), its application for multiplex partitioning problems in a continuous setting requires theoretical justification and has not been covered in the scientific literature so far. The goal of this work is to rigorously prove statements and theorems that underpin the methods and algorithms for solving continuous optimal multiplex partitioning problems.

3 MATERIALS AND METHODS

To formulate the mathematical model, we introduce some notations and concepts.

$\mathbf{N}$ is a set of all center indices, $\mathbf{N}=\{1,2,\ldots,N\}$; $\mathrm{M}(\mathbf{N},k)$ is a set of all k-element subsets of the set $\mathbf{N}$; L is a number of all k-element subsets of the set $\mathbf{N}$, $L=C_N^k$; Ω_{σ_l} are areas covering clients who have the same k nearest neighboring service centers $\{\tau_{j_1^l},\tau_{j_2^l},\ldots,\tau_{j_k^l}\}$ from N existing (possible), $l=\overline{1,L}$; σ_l is a set of indices $\{j_1^l, j_2^l,\ldots, j_k^l\}$ of centers associated with the subset Ω_{σ_l}.

Definition 1. A collection of subsets $\{\Omega_{\sigma_1},\Omega_{\sigma_2},\ldots,\Omega_{\sigma_L}\}$ from $\Omega\subset E^2$ is called a k-th order partition of the set Ω into its subsets $\Omega_{\sigma_1},\ldots,\Omega_{\sigma_L}$, if

$$\bigcup_{l=1}^{L}\Omega_{\sigma_l}=\Omega, \mathrm{mes}\left(\Omega_{\sigma_i}\cap\Omega_{\sigma_j}\right)=0;$$

$$\sigma_i,\sigma_j\in\mathrm{M}(\mathbf{N},k), i\neq j,\ i,\ j=\overline{1,L},$$

where $\mathrm{mes}(\cdot)$ – is the measure of the set. Ω_{σ_j} are k-th order subsets of the set Ω.

Let $\Sigma_\Omega^{N,k}$ – be the class of all possible k-th order partitions of the set Ω into its subsets $\Omega_{\sigma_1},\ldots,\Omega_{\sigma_L}$:

$$\Sigma_\Omega^{N,k}=\left\{\overline{\omega}=\{\Omega_{\sigma_1},\ldots,\Omega_{\sigma_L}\}:\bigcup_{l=1}^{L}\Omega_{\sigma_l}=\Omega,\right.$$

$$\left.mes\left(\Omega_{\sigma_i}\cap\Omega_{\sigma_j}\right)=0,\ \sigma_l,\sigma_j\in\mathrm{M}\left(\mathbf{N},k\right),\ i\neq j,\ i,\ j=\overline{1,L}\right\}.$$

Problem A. The problem of optimal k-th order partition of the continuous set Ω under constraints with location of centers:

$$F\left(\overline{\omega},\boldsymbol{\tau}^N\right)\to\min_{\overline{\omega}\in\Sigma_\Omega^{N,k};\boldsymbol{\tau}^N\in\hat{\Omega}^N}$$

$$F\left(\overline{\omega},\boldsymbol{\tau}^N\right)=\frac{1}{k}\sum_{l=1}^{L}\int_{\Omega_{\sigma_l}}\sum_{i\in\sigma_l}\left(c\left(x,\tau_i\right)/w_i+a_i\right)\rho\left(x\right)dx,$$

$$\sum_{\substack{l=1\\ l:\,i\in\sigma_l}}^{L}\int_{\Omega_{\sigma_l}}\gamma_i^l\rho(x)dx=b_i,\quad i=\overline{1,p};\tag{1}$$

$$\sum_{\substack{l=1\\ l:\,i\in\sigma_l}}^{L}\int_{\Omega_{\sigma_l}}\gamma_i^l\rho(x)dx\le b_i,\quad i=\overline{p+1,N}.\tag{2}$$

Here $x=\left(x^{(1)},x^{(2)}\right)\in\Omega$; $c\left(x,\tau_i\right)$, $i=\overline{1,N}$ are bounded functions defined on $\Omega\times\Omega$. The function $\rho\left(x\right)$ is bounded and non-negative on Ω; $w_i>0, a_i\ge 0, b_i\ge 0, i=\overline{1,N}$, are given constants. The coefficients γ_i^l define the share of the service market that the center τ_i occupies in the territory Ω_{σ_l}, among the facilities $\{\tau_{j_1^l},\tau_{j_2^l},\ldots,\tau_{j_k^l}\}$, serving this territory, such that for all $j=\overline{1,N}$, $l=\overline{1,L}$

$$0\le\gamma_j^l\le 1,\ \gamma_{j_1^l}^l+\gamma_{j_2^l}^l+\ldots+\gamma_{j_k^l}^l=1.\tag{3}$$

If we assume that the allocation of demand for services across the entire region Ω is proportional to the capacities of the centers, then for all $l=\overline{1,L}$ and for all $j=\overline{1,N}$, $j\in\sigma_l$, the values γ_j^l are given by the following expression: $\gamma_j^l=b_j/\sum_{q:\,q\in\sigma_l}b_q$. If the demand is distributed evenly among the centers, then $\gamma_j^l=\frac{1}{k}$, for all j and l.

Lemma 1 (see [13]). Let $S=\int_\Omega\rho(x)dx$ in problem **A**, and assume the conditions hold:

$$0\le b_i\le S,\quad i=1,\ldots,N;\ \sum_{i=1}^{p}b_i\le S\le\sum_{i=1}^{N}b_i.\tag{4}$$

Then, for any fixed vector $\tau^N\in\Omega^N$ the set of feasible partitions (satisfying conditions (1), (2)) is non-empty.

The method for solving Problem **A** involves expressing it in terms of characteristic vector-functions of the k-th order partition of the set Ω.

Definition 2. A characteristic vector-function of the k-th order partition $\overline{\omega}=\{\Omega_{\sigma_1},\ldots,\Omega_{\sigma_l},\ldots,\Omega_{\sigma_L}\}$ of the set Ω is the vector-function $\chi(\cdot)=\left(\chi_1(\cdot),\ldots,\chi_l(\cdot),\ldots,\chi_L(\cdot)\right)$, defined on Ω, which components are characteristic

DOI 10.15588/1607-3274-2025-2-6

functions of the subsets Ω_{σ_l} and are given by the formula (almost everywhere) for $x \in \Omega$

$$\chi_l(x) = \begin{cases} 1, & x \in \Omega_{\sigma_l}, \\ 0, & x \in \Omega \setminus \Omega_{\sigma_l}, \end{cases} \quad l = \overline{1, L}.$$

In [12, 13], to describe the *k*-th order partition of the set Ω, and *NL*-dimensional vector $\lambda(x)$ is introduced with coordinates

$$\lambda_i^l(x) = \begin{cases} 1, \text{ if } x \in \Omega_{\sigma_l} \text{ and } i \in \sigma_l, \\ 0 \text{ otherwise}, \end{cases} \quad i = \overline{1, N}, i = \overline{1, L}, \tag{5}$$

where $\sigma_l = \left\{ j_1^l, ..., j_k^l \right\}$ is the set of indices of the centers $\left\{ \tau_{j_1^l}, ..., \tau_{j_k^l} \right\}$, associated with Ω_{σ_l}.

Using (5), the coordinates of the function $\chi(\cdot)$ can be represented as $\chi_l(x) = \prod_{i \in \sigma_l} \lambda_i^l(x)$, $l = \overline{1, L}$. for each point $x \in \Omega$. Since each point $x \in \Omega$ belongs to only one of the subsets Ω_{σ_l}, among all components $\lambda_i^l(x)$ only *k* components for the same index *l* are equal to one. This means that the vector-functions $\lambda(\cdot)$ and $\chi(\cdot)$, which define the same *k*-th order partition $\bar{\omega}$ of the set Ω, satisfy the following conditions: for each point $x \in \Omega$

$$\chi_l(x) = 0 \vee 1, \ \lambda_i^l(x) = 0 \vee 1, \ i = \overline{1, N}, \ l = \overline{1, L},$$
$$\sum_{i=1}^{N} \lambda_i^l(x) = k\chi_l(x), \ l = \overline{1, L}; \sum_{l=1}^{L} \chi_l(x) = 1.$$

The relationship between $\lambda(\cdot)$ and $\chi(\cdot)$ is one-to-one. Indeed, if $x \in \Omega_{\sigma_l}$, i.e., $\chi_l(x) = 1$, then in the corresponding vector $\lambda(x)$ only *k* components will be equal to one:

$$\lambda_i^l = \begin{cases} 1, & i \in \sigma_l, \\ 0, i \in \mathrm{N} \setminus \sigma_l, \end{cases} \quad i = \overline{1, N}. \tag{6}$$

The remaining components $\lambda_i^t(x) = 0, \forall i = \overline{1, N}$, $t = \overline{1, L}, t \neq l$.

On the other hand, if a point $x \in \Omega$ is associated with a vector $\lambda(x) = \left(\lambda^1(x), \ldots, \lambda^l(x), \ldots, \lambda^L(x)\right)$, in which only *k* components are equal to one among $\lambda_1^l(x), \ldots, \lambda_N^l(x)$, and the rest are zero, this means that there exists a set $\sigma_l = \left\{ j_1^l, j_2^l, \ldots, j_k^l \right\}$, such that $x \in \Omega_{\sigma_l}$ and $\chi_l(x) = 1$. From a practical perspective, $\lambda_i^l(x)$, $i = \overline{1, N}$, serves as an indicator of whether a client at point *x* is served by center τ_i along with the remaining (*k*–1)-centers τ_j, where $j \in \sigma_l$.

To formulate the OMPS problem in terms of the characteristic functions of the partition, both vectors will be used, with the vector-function $\chi(\cdot)$ considered as the unknown (which distinguishes this work from [12, 13]). In the vector $\lambda^l(x) = \left(\lambda_1^l(x), \ldots, \lambda_N^l(x)\right)$, which corresponds to the component $\chi_l(x)$ of the characteristic vector-function of the partition, the argument will be omitted for compactness of notation. This vector defines the indicators of the indices in the set σ_l from the **N** (see formula (6)) and will therefore be used as a template.

Problem **A** is formulated in the following equivalent form.

Problem B.

$$\min_{(\chi(\cdot), \boldsymbol{\tau}^N) \in \Gamma^k \times \hat{\Omega}^N} I\left(\chi(\cdot), \boldsymbol{\tau}^N\right),$$

where

$$I\left(\chi(\cdot), \boldsymbol{\tau}^N\right) = \frac{1}{k} \int_{\Omega} \sum_{l=1}^{L} \left(\sum_{i=1}^{N} \left(c(x, \tau_i) / w_i + a_i \right) \lambda_i^l \right) \rho(x) \chi_l(x) dx$$

$$\Gamma^k = \Big\{ \chi(\cdot) : \chi(\cdot) \in \Gamma_0^k,$$

$$\int_{\Omega} \sum_{l=1}^{L} \gamma_i^l \lambda_i^l \rho(x) \chi_l(x) dx = b_i, \quad i = 1, \ldots, p,$$

$$\int_{\Omega} \sum_{l=1}^{L} \gamma_i^l \lambda_i^l \rho(x) \chi_l(x) dx \le b_i, \quad i = p+1, \ldots, N \Big\};$$

$$\Gamma_0^k = \Big\{ \chi(\cdot) = \left(\chi_1(\cdot), \ldots, \chi_L(\cdot)\right) : \chi_l(x) = 0 \vee 1,$$

$$l = \overline{1, L}, \sum_{l=1}^{L} \chi_l(x) = 1 \text{ a.e. } x \in \Omega \Big\}.$$

To solve Problem **B** with Boolean variables, we perform its LP relaxation.

Problem C:

$$\min_{(\chi(\cdot), \boldsymbol{\tau}^N) \in \Gamma_2^k \times \hat{\Omega}^N} I\left(\chi(\cdot), \boldsymbol{\tau}^N\right),$$

where

$$\Gamma_2^k = \Big\{ \chi(\cdot) : \chi(\cdot) \in \Gamma_1^k,$$

$$\int_{\Omega} \sum_{l=1}^{L} \gamma_i^l \lambda_i^l \chi_l(x) \rho(x) dx = b_i, \quad i = \overline{1, p},$$

$$\int_{\Omega} \sum_{l=1}^{L} \gamma_i^l \lambda_i^l \chi_l(x) \rho(x) dx \le b_i, \quad i = \overline{p+1, N} \Big\};$$

$$\Gamma_1^k = \Big\{ \chi(\cdot) = \left(\chi_1(\cdot), \ldots, \chi_l(\cdot), \ldots, \chi_L(\cdot)\right) : 0 \le \chi_l(x) \le 1,$$

$$l = \overline{1, L}; \sum_{l=1}^{L} \chi_l(x) = 1 \text{ a.e. for } x \in \Omega \Big\}.$$

Justification of the reduction of Problem **B** to Problem **C.** From the fact that $\Gamma_0^k \subset \Gamma_1^k$, it follows that $\Gamma^k \subset \Gamma_2^k$.

Statement 1. Γ_2^k is a bounded, closed, and convex set in the Hilbert space $L_2^L(\Omega)$ with the norm $\|\chi(\cdot)\| = \sqrt{\int_{\Omega} \sum_{l=1}^{L} \left[\chi_l(x)\right]^2 dx}$.

DOI 10.15588/1607-3274-2025-2-6

Proof. Let $\hat{\chi}(\cdot)$ and $\overline{\chi}(\cdot)$ be arbitrary elements of the set Γ_2^k, and let α be a constant such that $0 \le \alpha \le 1$. We will show that $\alpha\hat{\chi}_l(x) + (1-\alpha)\overline{\chi}_l(x) \in \Gamma_2^k$. Indeed, almost everywhere for $x \in \Omega$

$$\sum_{l=1}^{L}\left(\alpha\hat{\chi}_l(x) + (1-\alpha)\overline{\chi}_l(x)\right) =$$

$$= \alpha\sum_{l=1}^{L}\hat{\chi}_l(x) + (1-\alpha)\sum_{l=1}^{L}\overline{\chi}_l(x) = \alpha + (1-\alpha) = 1.$$

For each $i = 1,\ldots,p$:

$$\int_{\Omega}\sum_{l=1}^{L}\gamma_i^l\lambda_i^l\left(\alpha\hat{\chi}_l(x) + (1-\alpha)\overline{\chi}_l(x)\right)\rho(x)dx =$$

$$= \alpha\int_{\Omega}\sum_{l=1}^{L}\gamma_i^l\lambda_i^l\hat{\chi}_l(x)\rho(x)dx + (1-\alpha)\int_{\Omega}\sum_{l=1}^{L}\gamma_i^l\lambda_i^l\overline{\chi}_l(x)\rho(x)dx =$$

$$= \alpha b_i + (1-\alpha)b_i = b_i.$$

For each $i = p+1,\ldots,N$:

$$\int_{\Omega}\sum_{l=1}^{L}\gamma_i^l\lambda_i^l\left(\alpha\hat{\chi}_l(x) + (1-\alpha)\overline{\chi}_l(x)\right)\rho(x)dx =$$

$$= \alpha\int_{\Omega}\sum_{l=1}^{L}\gamma_i^l\lambda_i^l\hat{\chi}_l(x)\rho(x)dx + (1-\alpha)\int_{\Omega}\sum_{l=1}^{L}\gamma_i^l\lambda_i^l\overline{\chi}_l(x)\rho(x)dx \le$$

$$\le \alpha b_i + (1-\alpha)b_i = b_i.$$

Since for $x \in \Omega$ $0 \le \hat{\chi}_l(x), \overline{\chi}_l(x) \le 1$, it follows that $0 \le \alpha\hat{\chi}_l(x) + (1-\alpha)\overline{\chi}_l(x) \le 1$, $l = \overline{1,L}$. Thus, the convexity of the set Γ_2^k is proven.

Let the sequence $\{\chi^{(m)}(\cdot)\} \in \Gamma_2^k$ converge to some function $\chi(\cdot)$ in the norm of the space $L_2^L(\Omega)$. Consider a subsequence $\{\chi^{(m_r)}(\cdot)\}$, that converges to $\chi(\cdot)$ almost everywhere on Ω. For $\chi^{(m_r)}(\cdot) \in \Gamma_2^k$ the following conditions hold:

$$\int_{\Omega}\sum_{l=1}^{L}\gamma_i^l\lambda_i^l\rho(x)\chi_l^{(m_r)}(x)dx = b_i, \quad i = 1,2,\ldots,p;$$

$$\int_{\Omega}\sum_{l=1}^{L}\gamma_i^l\lambda_i^l\rho(x)\chi_l^{(m_r)}(x)dx \le b_i, \quad i = p+1,\ldots,N;$$

$$0 \le \chi_l^{(m_r)}(x) \le 1, l = \overline{1,L};$$

$$\sum_{l=1}^{L}\chi_l^{(m_r)}(x) = 1, \text{ a.e. for } x \in \Omega.$$

Taking into account that the function $\rho(x)$ is bounded, measurable, and non-negative on the set Ω, according to the Dominated Convergence Theorem [14], the limit transition holds as $m_r \to \infty$

$$\lim_{m_r\to\infty}\int_{\Omega}\sum_{l=1}^{L}\gamma_i^l\lambda_i^l\rho(x)\chi_l^{(m_r)}(x)dx =$$

$$= \int_{\Omega}\lim_{m_r\to\infty}\left(\sum_{l=1}^{L}\gamma_i^l\lambda_i^l\rho(x)\chi_l^{(m_r)}(x)\right)dx =$$

$$= \int_{\Omega}\sum_{l=1}^{L}\gamma_i^l\lambda_i^l\rho(x)\left(\lim_{m_r\to\infty}\chi_l^{(m_r)}(x)\right)dx = \int_{\Omega}\sum_{l=1}^{L}\gamma_i^l\lambda_i^l\rho(x)\chi_l^{(m_r)}(x)dx.$$

Thus, we conclude that all the above conditions are satisfied with the function $\chi(\cdot)$. This means that the set Γ_2^k is closed.

Let $\chi(\cdot) \in \Gamma_2^k$, then $0 \le \chi_l(x) \le 1$ a. e. for $x \in \Omega, l = \overline{1,L}$,

$$\|\chi(\cdot)\| = \sqrt{\int_{\Omega}\sum_{l=1}^{L}\left[\chi_l(x)\right]^2 dx} \le \sqrt{\int_{\Omega}\sum_{l=1}^{L}1^2 dx} = \sqrt{Lmes(\Omega)} = Const.$$

The boundedness of Γ_2^k is proven.

Lemma 2. For each fixed vector $\overline{\boldsymbol{\tau}}^N \in \hat{\Omega}^N$, the functional $\bar{I}(\chi(\cdot)) = I\left(\chi(\cdot), \overline{\boldsymbol{\tau}}^N\right)$ in Problem **A** is linear and continuous on the set Γ_2^k.

Proof. Let $\overline{\boldsymbol{\tau}}^N$ be an arbitrary but fixed vector from $\hat{\Omega}^N$. Define the quantity

$$q = \sup_{x\in\Omega}\max_{i=1,N}\left(c(x,\tau_i)/w_i + a_i\right)\rho(x).$$

The linearity of the functional $\bar{I}\left(\chi(\cdot)\right)$ is obvious because of the linearity of the Lebesgue integral in the functional $I(\chi(\cdot), \overline{\boldsymbol{\tau}}^N)$.

To prove the boundedness of $\bar{I}\left(\chi(\cdot)\right)$, we use Hölder's inequality:

$$\left|\bar{I}(\chi(\cdot))\right| = \left|I\left(\chi(\cdot), \overline{\boldsymbol{\tau}}^N\right)\right| =$$

$$= \left|\frac{1}{k}\int_{\Omega}\sum_{l=1}^{L}\sum_{i=1}^{N}\left(c(x,\tau_i)/w_i + a_i\right)\lambda_i^l\chi_l(x)\rho(x)dx\right| \le$$

$$\le \left|\frac{1}{k}\cdot q\int_{\Omega}\sum_{l=1}^{L}\sum_{i=1}^{N}\lambda_i^l\chi_l(x)dx\right| = \left|q\int_{\Omega}\sum_{l=1}^{L}\chi_l(x)dx\right| \le$$

$$\le q\sqrt{\int_{\Omega}\sum_{l=1}^{L}\left[\chi_l(x)\right]^2 dx} = q\cdot\|\chi(\cdot)\|_{L_2^L(\Omega)}.$$

Thus, the functional $\bar{I}\left(\chi(\cdot)\right)$ is linear, bounded, and, according to [14], continuous with respect to $\chi(\cdot)$.

Statement 2. If the conditions (4) hold for Problem **A**, then for each fixed vector $\boldsymbol{\tau}^N \in \hat{\Omega}^N$ Problem **C** is solvable with respect to $\chi(\cdot)$.

Proof. Let $\boldsymbol{\tau}^N$ be an arbitrary but fixed vector from $\hat{\Omega}^N$ in Problem **A** and let the conditions (4) hold. According to Lemma 1, the set of feasible partitions is non-empty, meaning the set Γ^k of admissible vector-functions

DOI 10.15588/1607-3274-2025-2-6

$\chi(\cdot)$ in Problem **C** is also no-empty. According to Lemma 2, the functional $I(\chi(\cdot),\boldsymbol{\tau}^N)$ is linear (convex) and continuous with respect to $\chi(\cdot)$ on the set Γ_2^k. According to Statement 1, Γ_2^k is convex, closed, and bounded, and therefore, by the generalized Weierstrass theorem [14], the functional $I\left(\chi(\cdot),\boldsymbol{\tau}^N\right)$ attains its exact lower bound on Γ_2^k. Thus, Problem **C** is solvable with respect to $\chi(\cdot)$ for each fixed $\boldsymbol{\tau}^N \in \hat{\Omega}^N$.

Statement 3. Let $\bar{\boldsymbol{\tau}}^N \in \hat{\Omega}^N$ be an arbitrary but fixed vector. Among the set of points in Γ_2^k, where the functional $\bar{I}(\chi(\cdot)) = I\left(\chi(\cdot),\bar{\boldsymbol{\tau}}^N\right)$ attains its minimum, there exists at least one extreme point of Γ_2^k.

Proof. By the generalized Weierstrass theorem, the continuous (see Lemma 2) functional $\bar{I}(\chi(\cdot))$ on the convex, closed, and bounded set Γ_2^k (see Statement 1) attains its exact lower bound, and the set Γ^* of its minimum points is non-empty, convex, and bounded, making it weakly compact in $L_2^L(\Omega)$. According to the Krein-Milman theorem [15], such a set Γ^* has an extreme point, denoted as $\chi^*(\cdot)$. We now show that $\chi^*(\cdot)$ is an extreme point of the set Γ_2^k.

Assume the contrary. Then it can be expressed as a linear combination of two points $u(\cdot),v(\cdot) \in \Gamma_2^k \setminus \Gamma^*, u \neq v$: $\chi^*(\cdot) = \alpha u(\cdot) + (1-\alpha)v(\cdot)$, where $0 < \alpha < 1$. Since $\chi^*(\cdot)$ is a minimum point of the functional, it follows that $\bar{I}(u(\cdot)) \geq \bar{I}(\chi^*(\cdot))$, $\bar{I}(v(\cdot)) \geq \bar{I}(\chi^*(\cdot))$. Due to its linearity

$$\bar{I}(\chi^*(\cdot)) = \alpha\bar{I}(u(\cdot)) + (1-\alpha)\bar{I}(v(\cdot)) =$$
$$= \bar{I}(v(\cdot)) + \alpha(\bar{I}(u(\cdot)) - \bar{I}(v(\cdot))).$$

This is possible only if $\bar{I}(\chi^*(\cdot)) = \bar{I}(u(\cdot)) = \bar{I}(v(\cdot))$. Thus $u(\cdot),v(\cdot) \in \Gamma^*$. This leading to a contradiction. We conclude that $\chi^*(\cdot)$ is an extreme point of Γ^*.

Statement 3 is proven.

Statement 4. Any extreme point of the set Γ_2^k is a characteristic vector-function of some k-th order partition $\bar{\omega} = \left\{\Omega_{\sigma_1},...,\Omega_{\sigma_l},\ldots,\Omega_{\sigma_L}\right\}$ of the set Ω.

Proof. Assume the contrary: let $\chi(\cdot)$ be an extreme point of the set Γ_2^k, but at least one of its components $\chi_s(x), 1 \leq s \leq L$, is not a characteristic function of the corresponding subset Ω_{σ_s} in the *k*-th order partition of the set Ω. Without loss of generality, assume that this is the case for the function $\chi_1(x)$. This means that there exists a subset $\mathrm{P} \subset \Omega$, $mes(\mathrm{P}) > 0$, such that for all $x \in \mathrm{P}$: $\delta < \chi_1(x) < 1-\delta$, $0 < \delta < 1$.

Introduce an auxiliary function $\mu(\cdot)$, that satisfies the following conditions:

1) for all $x \in \Omega \setminus \mathrm{P}$ $\mu(x) = 0$;

2) for all $x \in \mathrm{P}$

$$|\mu(x)| < \delta \tag{7}$$

3) where $x \in \mathrm{P}$ $\mu(\cdot)$ is a nontrivial solution to the system of equations.

$$\int_{\mathrm{P}} \gamma_i^1 \lambda_i^1 \rho(x)\mu(x)dx = 0,\ i = 1,2,\ldots,N \tag{8}$$

$$\int_{\mathrm{P}} \sum_{l=2}^{L} \gamma_i^l \lambda_i^l \rho(x) \frac{\chi_l(x)}{\sum_{j=2}^{L} \chi_j(x)} \mu(x)dx = 0,\ i = 1,2,\ldots,N. \tag{9}$$

The function $\mu(\cdot)$, which satisfies conditions (1)–(3), can be constructed, for example, using the following approach. To partition P into $(2N+1)$ non-overlapping subsets of nonzero measure and define $\mu(\cdot)$ as a piecewise constant function on P, taking a constant value on each subset. The corresponding values can be found as a nontrivial solution to system (8), (9) – a system of $2N$ linear homogeneous algebraic equations with respect to $(2N+1)$ variables. The obtained values are then normalized to satisfy condition (7).

Using the function $\mu(\cdot)$, we construct two vector-functions $\hat{\chi}(\cdot)$ and $\bar{\chi}(\cdot)$ as follows: for all $x \in \Omega$

$$\hat{\chi}_1(x) = \chi_1(x) + \mu(x),$$
$$\hat{\chi}_j(x) = \chi_j(x) - \frac{\chi_j(x)}{\sum_{l=2}^{L} \chi_l(x)} \mu(x),\ j = \overline{2,L};$$
$$\bar{\chi}_1(x) = \chi_1(x) - \mu(x),$$
$$\bar{\chi}_j(x) = \chi_j(x) + \frac{\chi_j(x)}{\sum_{l=2}^{L} \chi_l(x)} \mu(x),\ j = \overline{2,L};$$

We will show that $\hat{\chi}(\cdot)$ and $\bar{\chi}(\cdot) \in \Gamma_2^k$. Indeed, due to conditions (8) and (9), for all $i = 1,2,\ldots,N$:

$$\int_{\Omega} \sum_{l=1}^{L} \gamma_i^l \lambda_i^l \rho(x)\hat{\chi}_l(x)dx = \int_{\Omega\setminus\mathrm{P}} \sum_{l=1}^{L} \gamma_i^l \lambda_i^l \rho(x)\chi_l(x)dx +$$
$$\int_{\mathrm{P}} (\gamma_i^1 \lambda_i^1 (\chi_1(x) + \mu(x))dx +$$
$$+ \int_{\mathrm{P}} \sum_{l=2}^{L} \gamma_i^l \lambda_i^l (\chi_l(x) - \frac{\chi_l(x)}{\sum_{j=2}^{L} \chi_j(x)} \mu(x)))\rho(x)dx =$$

DOI 10.15588/1607-3274-2025-2-6

$$= \int_{\Omega\setminus P}\sum_{l=1}^{L}\gamma_i^l\lambda_i^l\rho(x)\chi_l(x)dx +$$

$$+\int_P\left(\gamma_i^1\lambda_i^1\chi_1(x)+\sum_{l=2}^{L}\gamma_i^l\lambda_i^l\chi_l(x)\right)\rho(x)dx +$$

$$+\int_P\gamma_i^1\lambda_i^1\mu(x)\rho(x)dx-\int_P\sum_{l=2}^{L}\gamma_i^l\lambda_i^l\frac{\chi_l(x)}{\sum_{j=2}^{L}\chi_j(x)}\rho(x)\mu(x)dx=$$

$$=\int_\Omega\sum_{l=1}^{L}\gamma_i^l\lambda_i^l\rho(x)\chi_l(x)dx.$$

Similarly,

$$\int_\Omega\sum_{l=1}^{L}\gamma_i^l\lambda_i^l\rho(x)\overline{\chi}_l(x)dx=\int_\Omega\sum_{l=1}^{L}\gamma_i^l\lambda_i^l\rho(x)\chi_l(x)dx, i=\overline{1,N}.$$

By direct verification, we confirm the validity of the equalities $\sum_{l=1}^{L}\hat{\chi}_l(x)=1, \sum_{l=1}^{L}\overline{\chi}_l(x)=1$. For example, for $\overline{\chi}(\cdot)$ we have:

$$\sum_{l=1}^{L}\overline{\chi}_l(x)=\chi_1(x)-\mu(x)+\sum_{l=2}^{L}(\chi_l(x)+\frac{\chi_j(x)}{\sum_{j=2}^{L}\chi_j(x)}\mu(x))=$$

$$=\sum_{l=1}^{L}\chi_l(x)+\frac{1}{\sum_{j=2}^{L}\chi_j(x)}(-\mu(x)\sum_{j=2}^{L}\chi_j(x)+\mu(x)\sum_{l=2}^{L}\chi_l(x))=$$

$$=\sum_{l=1}^{L}\chi_l(x)=1.$$

By the definition of the functions $\hat{\chi}_1(\cdot)$, $\overline{\chi}_1(\cdot)$ and condition (7), it follows that: $\hat{\chi}_1(\cdot)\ge 0$, $\overline{\chi}_1(\cdot)\ge 0$ for all $x\in\Omega$. The remaining components of the vector-functions $\hat{\chi}_1(\cdot),\overline{\chi}_1(\cdot)$ are also non-negative. Indeed, considering that $\chi(\cdot)\in\Gamma_2^k$, for $j=\overline{2,L}$ we obtain:

$$\hat{\chi}_j(x)=\chi_j(x)-\frac{\chi_j(x)}{\sum_{l=2}^{L}\chi_l(x)}\mu(x)\ge$$

$$\ge\chi_j(x)-\frac{\chi_j(x)}{\delta}|\mu(x)|\ge\chi_j(x)-\frac{\chi_j}{\delta}\cdot\delta=0.$$

Similarly, we verify the inequality $\overline{\chi}_j(x)\ge 0, j=\overline{2,L}$.

By construction and the previously derived relationships, for all $x\in\Omega$: $0\le\hat{\chi}_i(x)\le 1$, $0\le\overline{\chi}_i(x)\le 1, \forall l=\overline{1,L}$.

Thus, it is proven that $\hat{\chi}(\cdot),\overline{\chi}(\cdot)\in\Gamma_2^k$. However, the representation $\chi(\cdot)=\frac{1}{2}\hat{\chi}(\cdot)+\frac{1}{2}\overline{\chi}(\cdot)$ contradicts the statement that $\chi(\cdot)$ is an extreme point of the set Γ_2^k. Therefore $\chi(\cdot)$ must be a characteristic vector-function of some k-th order partition of the set Ω. Statement 4 is proven.

Thus, according to Statement 3, among the points of the set Γ_2^k, where the linear functional $I(\chi(\cdot),\boldsymbol{\tau}^N)$ attains its minimum value for a fixed vector $\boldsymbol{\tau}^N\in\hat{\Omega}^N$ there exists at least one extreme point of Γ_2^k. According to Statement 2, extreme points are characteristic vector-functions of subsets $\Omega_{\sigma_l}, l=\overline{1,L}$, which form a k-th order partition of the set Ω for each fixed vector $\boldsymbol{\tau}^N\in\hat{\Omega}^N$. Thus, the set of optimal solutions to Problem **C** includes the optimal solutions to Problem **B**, which means that Problem **B** can be reduced to Problem **C** by selecting from the solutions of the latter those that are also solutions to Problem **B**. This reduction forms the basis of optimal multiplex partitioning methods, and the necessary and sufficient conditions for optimal multiplex partitioning have been obtained.

Optimality conditions for the solution of Problem **C.** We construct the Lagrange functional for Problem **C**:

$$W((\chi(\cdot),\boldsymbol{\tau}^N),(\psi_0(\cdot),\boldsymbol{\psi}))=$$

$$=\frac{1}{k}\int_\Omega\sum_{l=1}^{L}\sum_{i=1}^{M}(c(x,\tau_i)/w_i+a_i)\lambda_i^l\chi_l(x)\rho(x)dx+$$

$$+\sum_{i=1}^{N}\psi_i(\int_\Omega\sum_{l=1}^{L}\gamma_i^l\lambda_i^l\chi_l(x)\rho(x)dx-b_i)+$$

$$+\int_\Omega\psi_0(x)(\sum_{l=1}^{L}\chi_l(x)-1)dx=$$

$$=\int_\Omega\sum_{l=1}^{L}(\sum_{i=1}^{N}((\frac{c(x,\tau_i)}{w_i}+a_i)/k+\gamma_i^l\psi_i)\lambda_i^l\rho(x)+\psi_0(x))\chi_l(x)dx-$$

$$-\int_\Omega\psi_0(x)dx-\sum_{i=1}^{N}\psi_i b_i.$$

The functional $W\left(\left(\chi(\cdot),\boldsymbol{\tau}^N\right),(\psi_0(\cdot),\boldsymbol{\psi})\right)$ is defined on the Cartesian product $\left(\Lambda\times\hat{\Omega}^N\right)\times\left(\Phi\times\Psi\right)$, where

$$\Lambda=\left\{\chi(\cdot)\in L_2^L(\Omega):0\le\chi_l(x)\le 1\ \forall x\in\Omega, l=\overline{1,L}\right\};$$

$$\Phi=\left\{\psi_0:\psi_0(\cdot)\in L_2(\Omega)\right\};$$

$$\Psi=\left\{\boldsymbol{\psi}\in R^N:\psi_i\ge 0, i=p+1,\ldots,N\right\}.$$

Definition 3. A pair $\left(\left(\hat{\chi}(\cdot),\hat{\boldsymbol{\tau}}^N\right),(\hat{\psi}_0(\cdot),\hat{\boldsymbol{\psi}})\right)$ is called a saddle point of the Lagrange functional $W((\chi(\cdot),\boldsymbol{\tau}^N),(\psi_0(\cdot),\boldsymbol{\psi}))$ on the set $\left(\Lambda\times\hat{\Omega}^N\right)\times\left(\Phi\times\Psi\right)$, if for all $\left(\chi(\cdot),\boldsymbol{\tau}^N\right)\in\Lambda\times\hat{\Omega}^N$ and for all $\left(\psi_0(\cdot),\boldsymbol{\psi}\right)\in\Phi\times\Psi$, the following inequalities hold:

$$W\left(\left(\hat{\chi}(\cdot),\hat{\boldsymbol{\tau}}^N\right),(\psi_0(\cdot),\boldsymbol{\psi})\right)\le W\left(\left(\hat{\chi}(\cdot),\hat{\boldsymbol{\tau}}^N\right),(\hat{\psi}_0(\cdot),\hat{\boldsymbol{\psi}})\right),$$

$$W\left(\left(\hat{\chi}(\cdot),\hat{\boldsymbol{\tau}}^N\right),(\hat{\psi}_0(\cdot),\hat{\boldsymbol{\psi}})\right)\le W\left(\left(\chi(\cdot),\boldsymbol{\tau}^N\right),(\hat{\psi}_0(\cdot),\hat{\boldsymbol{\psi}})\right).$$

DOI 10.15588/1607-3274-2025-2-6

The problem dual to Problem **C** is formulated as follows:

$$H(\psi_0(\cdot),\boldsymbol{\psi}) \to \max_{(\psi_0(\cdot),\boldsymbol{\psi})\in\Phi\times\Psi}$$
$$H(\psi_0(\cdot),\boldsymbol{\psi}) = \min_{(\chi,\boldsymbol{\tau}^N)\in\Lambda\times\hat{\Omega}^N} W((\chi(\cdot),\boldsymbol{\tau}^N),(\psi_0(\cdot),\boldsymbol{\psi})) \quad (10)$$

Theorem 1 (see [16]). For Problem **C** and (10) to be related by the duality relation $I_* = W^*$, and for the supremum in (10) to be attainable, it is necessary and sufficient that a saddle point of the functional $W((\chi(\cdot),\boldsymbol{\tau}^N),(\psi_0(\cdot),\boldsymbol{\psi}))$ exists on the set $(\Lambda\times\hat{\Omega}^N)\times(\Phi\times\Psi)$.

Thus, solving the pair of problems **C** and (10) is equivalent to finding a saddle function of the functional $W((\chi(\cdot),\boldsymbol{\tau}^N),(\psi_0(\cdot),\boldsymbol{\psi}))$ on the set $(\Lambda\times\hat{\Omega}^N)\times(\Phi\times\Psi)$.

Let the vectors $\overline{\boldsymbol{\psi}}\in\Psi$ and $\overline{\boldsymbol{\tau}}^N\in\hat{\Omega}^N$ be arbitrary but fixed in the functional $H(\psi_0(\cdot),\boldsymbol{\psi})$. Consider the problem

$$W\left(\left(\chi(\cdot),\overline{\boldsymbol{\tau}}^N\right),\left(\psi_0(\cdot),\overline{\boldsymbol{\psi}}\right)\right) \to \min_{\chi(\cdot)\in\Lambda}\max_{\psi_0(\cdot)\in\Phi}. \quad (11)$$

Further, for brevity, we will use the following notation: $d_i(x) = \left(c(x,\tau_i)/w_i + a_i\right)/k$, $i=\overline{1,N}$.

The center τ_i may be fixed or not, depending on the context.

For each arbitrarily fixed point $x\in\Omega$ we introduce a function of (L+1) variables:

$$Q\left(\chi(x),\psi_0(x)\right) =$$
$$= \sum_{l=1}^{L}\left[\sum_{i=1}^{N}\left(d_i(x)+\gamma_i^l\psi_i\right)\lambda_i^l\rho(x)+\psi_0(x)\right]\chi_l(x)-\psi_0(x).$$

This function is defined on the Cartesian product $\Lambda_x\times\Phi_x$ of the projections of the sets Λ and Φ for $x\in\Omega$.

Theorem 2. For an admissible pair $\left(\hat{\chi}(\cdot),\hat{\psi}_0(\cdot)\right)\in\Lambda\times\Phi$ to be a solution of problem (11), it is necessary and sufficient that almost everywhere for $x\in\Omega$, the following condition holds:

$$Q\left(\hat{\chi}(x),\hat{\psi}_0(x)\right) = \max_{\psi_0(x)\in\Phi_x}\min_{\chi(x)\in\Lambda_x} Q\left(\chi(x),\psi_0(x)\right). \quad (12)$$

Proof. Necessity. Let $\left(\hat{\chi}(\cdot),\hat{\psi}_0(\cdot)\right)\in\Lambda\times\Phi$ be an optimal solution to problem (11), i.e., $\forall\chi(\cdot)\in\Lambda$, $\psi_0(\cdot)\in\Phi$

$$W\left(\left(\hat{\chi}(\cdot),\overline{\boldsymbol{\tau}}^N\right),\left(\psi_0(\cdot),\overline{\boldsymbol{\psi}}\right)\right) \le W\left(\left(\hat{\chi}(\cdot),\overline{\boldsymbol{\tau}}^N\right),\left(\hat{\psi}_0(\cdot),\overline{\boldsymbol{\psi}}\right)\right) \quad (13)$$
$$W\left(\left(\hat{\chi}(\cdot),\overline{\boldsymbol{\tau}}^N\right),\left(\hat{\psi}_0(\cdot),\overline{\boldsymbol{\psi}}\right)\right) \le W\left(\left(\chi(\cdot),\overline{\boldsymbol{\tau}}^N\right),\left(\hat{\psi}_0(\cdot),\overline{\boldsymbol{\psi}}\right)\right) \quad (14)$$

We will show that almost everywhere for $x\in\Omega$ this pair $\left(\hat{\chi}(\cdot),\hat{\psi}_0(\cdot)\right)$ satisfies condition (12). Assume the contrary: there exists a subset $\tilde{\Omega}$ of the set Ω such that $mes(\tilde{\Omega})>0$ and $\forall x\in\tilde{\Omega}$ condition (12) does not hold, i.e., $\forall x\in\tilde{\Omega}$ there exist $\tilde{\chi}(x)\in\Lambda_x$, for which the following inequality is valid:

$$Q\left(\tilde{\chi}(x),\hat{\psi}_0(x)\right) < Q\left(\hat{\chi}(x),\hat{\psi}_0(x)\right).$$

We construct a new pair of admissible functions for the problem (11):

$$\left(\overline{\chi}(x),\hat{\psi}_0(x)\right) = \begin{cases}\left(\tilde{\chi}(x),\hat{\psi}_0(x)\right)\in\Lambda_x\times\Phi_x, & \forall x\in\tilde{\Omega},\\ \left(\hat{\chi}(x),\hat{\psi}_0(x)\right)\in\Lambda_x\times\Phi_x, & \forall x\in\Omega\setminus\tilde{\Omega}.\end{cases}$$

Integrating $Q\left(\overline{\chi}(x),\hat{\psi}_0(x)\right)$ over the entire region Ω and adding the constant $\left(-\sum_{i=1}^{N}\overline{\psi}_i b_i\right)$, we obtain:

$$W\left(\left(\overline{\chi}(\cdot),\overline{\boldsymbol{\tau}}^N\right),\left(\hat{\psi}_0(\cdot),\overline{\boldsymbol{\psi}}\right)\right) = \int_\Omega Q\left(\overline{\chi}(x),\hat{\psi}_0(x)\right)dx - \sum_{i=1}^{N}\overline{\psi}_i b_i =$$
$$= \int_{\tilde{\Omega}} Q\left(\tilde{\chi}(x),\hat{\psi}_0(x)\right)dx + \int_{\Omega\setminus\tilde{\Omega}} Q\left(\hat{\chi}(x),\hat{\psi}_0(x)\right)dx - \sum_{i=1}^{N}\overline{\psi}_i b_i.$$

Similarly splitting the integral in $W\left(\left(\chi(\cdot),\overline{\boldsymbol{\tau}}^N\right),\left(\psi_0(\cdot),\overline{\boldsymbol{\psi}}\right)\right)$ with $\chi(\cdot)=\hat{\chi}(\cdot),\psi_0(\cdot)=\hat{\psi}_0(\cdot)$ and comparing the right-hand sides of the obtained relations, we conclude:

$$W\left(\left(\overline{\chi}(\cdot),\overline{\boldsymbol{\tau}}^N\right),\left(\hat{\psi}_0(\cdot),\overline{\boldsymbol{\psi}}\right)\right) < W\left(\left(\hat{\chi}(\cdot),\overline{\boldsymbol{\tau}}^N\right),\left(\hat{\psi}_0(\cdot),\overline{\boldsymbol{\psi}}\right)\right),$$

which contradicts (14).

We can also assume the existence of a subset $\breve{\Omega}$ of the set Ω such that $mes(\breve{\Omega})>0$ and $\forall x\in\breve{\Omega}$, there exists $\tilde{\psi}_0(x)\in\Phi_x$ such that the following inequality holds:

$$Q\left(\hat{\chi}(x),\hat{\psi}_0(x)\right) < Q\left(\hat{\chi}(x),\tilde{\psi}_0(x)\right).$$

Then, for the pair $\left(\hat{\chi}(x),\overline{\overline{\psi}}_0(x)\right)$, defined as follows

$$\left(\hat{\chi}(x),\overline{\overline{\psi}}_0(x)\right) = \begin{cases}\left(\hat{\chi}(x),\tilde{\psi}_0(x)\right)\in\Lambda_x\times\Phi_x, & \forall x\in\breve{\Omega}\\ \left(\hat{\chi}(\cdot),\hat{\psi}_0(\cdot)\right)\in\Lambda_x\times\Phi_x, & \forall x\in\Omega\setminus\breve{\Omega}\end{cases}$$

condition (13) will be violated. The resulting contradiction proves the necessity of condition (12) for the pair $\left(\hat{\chi}(\cdot),\hat{\psi}_0(\cdot)\right)$ to be a solution of problem (11).

Sufficiency. Let the pair $\left(\hat{\chi}(\cdot),\hat{\psi}_0(\cdot)\right)$ satisfy condition (12) almost everywhere for $x\in\Omega$. We will show that it is a solution to the problem (12). Let $x\in\Omega$ $\chi(x)\in\Lambda_x,\psi_0(x)\in\Phi_x$. Then, almost everywhere for $x\in\Omega$

$$Q\left(\hat{\chi}(x),\hat{\psi}_0(x)\right) \le Q\left(\chi(x),\hat{\psi}_0(x)\right),$$
$$Q\left(\hat{\chi}(x),\hat{\psi}_0(x)\right) \ge Q\left(\hat{\chi}(x),\psi_0(x)\right).$$

Integrating these inequalities over all $x\in\Omega$ and taking into account that the inequality may fail only on a set of points in Ω, where the values of the integrand do not affect the value of the integral, we obtain:

$$\int_\Omega Q\left(\hat{\chi}(x),\hat{\psi}_0(x)\right)dx \le \int_\Omega Q\left(\chi(x),\hat{\psi}_0(x)\right)dx,$$
$$\int_\Omega Q\left(\hat{\chi}(x),\hat{\psi}_0(x)\right)dx \ge \int_\Omega Q\left(\hat{\chi}(x),\psi_0(x)\right)dx.$$

Adding the constant $-\sum_{i=1}^{N}\overline{\psi}_i b_i$ to both sides of the obtained inequalities, we obtain inequalities (13) and (14). Theorem 2 is proven.

DOI 10.15588/1607-3274-2025-2-6

Theorem 3. The optimal solution of Problem **B** is determined by the following formulas: for all $l=1,\dots,L$, and almost everywhere for $x\in\Omega$

$$\hat{\chi}_l(x)=\begin{cases}1, \quad \text{if } \sum\limits_{i=1}^{N}\Big((c(x,\hat{\tau}_i)/w_i+a_i)/k+\gamma_i^l\hat{\psi}_i\Big)\lambda_i^l= \\ =\min\limits_{s=1,L}\sum\limits_{i=1}^{N}\Big((c(x,\hat{\tau}_i)/w_i+a_i)/k+\gamma_i^s\hat{\psi}_i\Big)\lambda_i^s, \\ 0 \quad \text{otherwise}, \qquad\qquad \forall l=\overline{1,L};\end{cases} \tag{15}$$

where $(\hat{\tau}_1,...,\hat{\tau}_N,\ \hat{\psi}_1,...,\hat{\psi}_N)$ is the solution to the following problem:

$$G(\boldsymbol{\psi})=\min_{\boldsymbol{\tau}^N\in\hat{\Omega}^N} G_1(\boldsymbol{\tau},\boldsymbol{\psi})\to\max \tag{16}$$

subject to the conditions:

$$\psi_i\ge 0,\quad i=p+1,\dots,N, \tag{17}$$

where

$$G_1\left(\boldsymbol{\tau}^N,\boldsymbol{\psi}\right)=-\sum_{i=1}^{N}\psi_i b_i+$$
$$+\int_{\Omega}\min_{\sigma_l\in M(N_s,k)\atop l=\overline{1,L}}\sum_{i\in\sigma_l}\Big[(c(x,\tau_i)/w_i+a_i)/k+\gamma_i^l\psi_i\Big]\rho(x)dx.$$

Proof. The reduction of Problem **B** to Problem **C** was justified above. Theorem 1 reduces the solution of the latter to finding a saddle point of its Lagrange functional. Fix the vectors $\overline{\boldsymbol{\psi}}\in\Psi$ and $\overline{\boldsymbol{\tau}}^N\in\hat{\Omega}^N$ in it. According to Theorem 2, to determine the remaining components of the saddle point of the Lagrange functional, it is necessary to solve problem (12) for each point x from Ω.

Let x be an arbitrarily fixed point from Ω. Due to the separability of the function $Q(\chi(x),\psi_0(x))$ with respect to its variables, the following equality holds:

$$\max_{\psi_0(x)\in\Phi_x}\min_{\chi(x)\in\Lambda_x}Q(\chi(x),\psi_0(x))=$$
$$=\max_{\psi_0\in\Phi_x}\min_{\chi\in\Lambda_x}\sum_{i=1}^{L}(\sum_{i=1}^{N}(d_i+\gamma_i^l\overline{\psi}_i)\lambda_i^l\rho+\psi_0)\chi_l-\psi_0=$$
$$=\max_{\psi_0^l}\left\{\sum_{l=1}^{L}\min_{0\le\chi_l\le 1}\left[\sum_{i=1}^{N}\Big(d_i(x)+\gamma_i^l\overline{\psi}_i\Big)\lambda_i^l\rho(x)+\psi_0\right]\chi_l-\psi_0\right\}.$$

The point $(\hat{\chi}(x),\hat{\psi}_0(x))$ will be a solution to the problem (12) if and only if the following conditions [16] are satisfied:

1. $Q(\hat{\chi}(x),\hat{\psi}_0(x))=\min\limits_{\chi(x)\in\Lambda_x}Q(\chi(x),\hat{\psi}_0(x))$;
2. $\dfrac{\partial Q(\hat{\chi}(x),\hat{\psi}_0(x))}{\partial\psi_0}=0 \quad\Leftrightarrow\quad \sum\limits_{l=1}^{L}\chi_l(x)-1=0$.

For an arbitrary $\psi_0(x)$, the function $Q(\chi(x),\psi_0(x))$ attains its minimum value over all $\chi(x)\in\Lambda_x$, where $\Lambda_x=\{\chi=(\chi_1,...,\chi_l,...,\chi_L):0\le\chi_l\le 1,\ l=1,\dots,L\}$. At the point $\hat{\chi}(x)$, whose components satisfy the conditions: for $l=1,\dots,L$

$$\hat{\chi}_l(x)=\begin{cases}1, \text{ if } \sum\limits_{i=1}^{N}\Big(d_i(x)+\gamma_i^l\overline{\psi}_i\Big)\lambda_i^l\rho(x)+\psi_0(x)<0, \\ 0, \text{ if } \sum\limits_{i=1}^{N}\Big(d_i(x)+\gamma_i^l\overline{\psi}_i\Big)\lambda_i^l\rho(x)+\psi_0(x)>0, \\ \alpha, \text{if } \sum\limits_{i=1}^{N}\Big(d_i(x)+\gamma_i^l\overline{\psi}_i\Big)\lambda_i^l\rho(x)+\psi_0(x)=0,\end{cases} \tag{18}$$

where $\alpha\in[0,1]$.

Among all solutions of Problem **C**, we consider those that are extreme points of the feasible set of its solutions. Due to the arbitrariness of the choice of $\alpha\in[0,1]$ we consider a particular case of formula (18), namely: for $l=1,\dots,L$,

$$\hat{\chi}_l(x)=\begin{cases}1, \quad if \sum\limits_{i=1}^{N}\Big(d_i(x)+\gamma_i^l\overline{\psi}_i\Big)\lambda_i^l\rho(x)+\psi_0(x)<0, \\ 0, \quad if \sum\limits_{i=1}^{N}\Big(d_i(x)+\gamma_i^l\overline{\psi}_i\Big)\lambda_i^l\rho(x)+\psi_0(x)>0, \\ 0\vee 1, if \sum\limits_{i=1}^{N}\Big(d_i(x)+\gamma_i^l\overline{\psi}_i\Big)\lambda_i^l\rho(x)+\psi_0(x)=0.\end{cases} \tag{19}$$

For $\psi_0(x)=\hat{\psi}_0(x)$ in inequality (18), particularly (19), it holds the equality: $\sum\limits_{l=1}^{N}\chi_l(x)-1=0$. Then among the components of the vector $\hat{\chi}(x)$ in (19), there is only one unit component, let its index be l, and this formula can be written as:

$$\hat{\chi}_l(x)=\begin{cases}1, \text{ if } \sum\limits_{i=1}^{N}\Big(d_i(x)+\gamma_i^l\overline{\psi}_i\Big)\lambda_i^l\rho(x)+\hat{\psi}_0(x)= \\ =\min\limits_{s=1,L}\sum\limits_{i=1}^{N}\Big(d_i(x)+\gamma_i^s\overline{\psi}_i\Big)\lambda_i^s\rho(x)+\hat{\psi}_0(x), \\ 0 \quad \text{otherwise}, \qquad\qquad \forall l=\overline{1,L}.\end{cases} \tag{20}$$

Substituting (20) into the function $Q(\chi(x),\psi_0(x))$, we obtain:

$$Q(\hat{\chi}(x),\hat{\psi}_0(x))=\min_{s=1,L}(\sum_{i=1}^{N}(d_i(x)+\gamma_i^s\overline{\psi}_i)\lambda_i^s\rho(x)+\hat{\psi}_0(x))-$$
$$-\hat{\psi}_0(x)=\min_{s=1,L}\left(\sum_{i=1}^{N}\Big(d_i(x)+\gamma_i^s\overline{\psi}_i\Big)\lambda_i^s\right)\rho(x).$$

Due to the arbitrariness of the choice of point x, the optimal value of the functional in problem (11) with fixed vectors $\overline{\boldsymbol{\psi}}\in\Psi$ and $\overline{\boldsymbol{\tau}}^N\in\hat{\Omega}^N$ is expressed as:

DOI 10.15588/1607-3274-2025-2-6

$$G\left(\overline{\boldsymbol{\tau}}^N,\overline{\boldsymbol{\psi}}\right)=W\left(\left(\hat{\chi}(\cdot),\overline{\boldsymbol{\tau}}^N\right),\left(\hat{\psi}_0(\cdot),\overline{\boldsymbol{\psi}}\right)\right)=$$

$$=\int_\Omega \min_{s=1,L}\left(\sum_{i=1}^N\left(d_i(x)+\gamma_i^s\overline{\psi}_i\right)\lambda_i^s\right)\rho(x)dx-\sum_{i=1}^N\psi_i b_i\ ,$$

or, substituting the expression for $d_i(x)$ and avoiding the use of index indicators that form the combination σ_s, $s=\overline{1,L}$:

$$G(\overline{\boldsymbol{\tau}}^N,\overline{\boldsymbol{\psi}})=-\sum_{i=1}^N\psi_i b_i+$$

$$+\int_\Omega \min_{\substack{\sigma_l\in M(N_s,k)\\ l=1,..,L}}\sum_{i\in\sigma_l}((c(x,\overline{\tau}_i)/w_i+a_i)/k+\gamma_i^l\overline{\psi}_i)\rho(x)dx.$$

Due to the arbitrariness of the choice of vectors $\overline{\boldsymbol{\psi}}$ and $\overline{\boldsymbol{\tau}}^N$, and taking into account the obtained expression, we rewrite the functional of problem (10), excluding the function $\psi_0(x)$, in the following form:

$$\overline{H}(\boldsymbol{\psi})=-\sum_{i=1}^N\psi_i b_i+$$

$$+\min_{\tau^N\in\hat{\Omega}^N}\int_\Omega \min_{\substack{\sigma_l\in M(N,k)\\ l=1,..,L}}\sum_{i\in\sigma_l}((\frac{c(x,\tau_i)}{w_i}+a_i)/k+\gamma_i^l\psi_i)\rho(x)dx.$$

According to (19), almost everywhere for $x\in\Omega_{\sigma_l}$ the following system of inequalities holds:

$$\begin{cases}\sum_{i=1}^N\left(d_i(x)+\gamma_i^l\overline{\psi}_i\right)\lambda_i^l\rho(x)+\psi_0(x)\le 0,\\ -\sum_{i=1}^N\left(d_i(x)+\gamma_i^s\overline{\psi}_i\right)\lambda_i^s\rho(x)-\psi_0(x)\le 0,\forall s=\overline{1,L},s\ne l.\end{cases}$$

This system is solvable due to the solvability of Problem **C** (and **B**). Adding each of the remaining inequalities to the *l*-th inequality, we obtain almost everywhere for $x\in\Omega_{\sigma_l}$, $\forall s=\overline{1,L},s\ne l$

$$\sum_{i=1}^N\left(d_i(x)+\gamma_i^l\overline{\psi}_i\right)\lambda_i^l\rho(x)\le\sum_{i=1}^N\left(d_i(x)+\gamma_i^s\overline{\psi}_i\right)\lambda_i^s\rho(x).$$

Recalling that $\rho(x)\ge 0$ for $x\in\Omega$, almost everywhere for $x\in\Omega_{\sigma_l}$ the following system of inequalities will hold: $\forall s=\overline{1,L},\ s\ne l$

$$\sum_{i=1}^N\left(d_i(x)+\gamma_i^l\overline{\psi}_i\right)\lambda_i^l\le\sum_{i=1}^N\left(d_i(x)+\gamma_i^s\overline{\psi}_i\right)\lambda_i^s.$$

Formula (19), considering the above, can be written as follows:

$$\hat{\chi}_l(x)=\begin{cases}1,\text{if }\sum_{i=1}^N(d_i(x)+\gamma_i^l\overline{\psi}_i)\lambda_i^l=\min_{s=1,L}\sum_{i=1}^N(d_i(x)+\gamma_i^s\overline{\psi}_i)\lambda_i^s,\\ 0\quad\text{otherwise},\end{cases}\quad\forall l=\overline{1,L}.$$

For $\hat{\boldsymbol{\psi}}\in\Psi$ and $\hat{\boldsymbol{\tau}}^N\in\hat{\Omega}^N$ to be components of the saddle point of the Lagrange functional of Problem **C**, they must be the optimal solution to the following problem:

$$G(\boldsymbol{\psi})=\min_{\boldsymbol{\tau}^N\in\hat{\Omega}^N}G_1(\boldsymbol{\tau},\boldsymbol{\psi})\to\max,$$
$$\psi_i\ge 0,\quad i=p+1,\dots,N,$$

where

$$G_1(\boldsymbol{\tau}^N,\boldsymbol{\psi})=-\sum_{i=1}^N\psi_i b_i+$$

$$+\int_\Omega\min_{\substack{\sigma_l\in M(N,k)\\ l=1,..,L}}\sum_{i\in\sigma_l}((\frac{c(x,\tau_i)}{w_i}+a_i)/k+\gamma_i^l\psi_i)\rho(x)dx.$$

Thus, the characteristic functions of the subsets $\Omega^*_{\sigma_l},l=\overline{1,L}$, which form the optimal multiplex partition, are found using the following formula: for all $l=1,\dots,L$, and almost everywhere $x\in\Omega$

$$\hat{\chi}_l(x)=\begin{cases}1,\quad\text{if }\sum_{i=1}^N((c(x,\hat{\tau}_i)/w_i+a_i)/k+\gamma_i^l\hat{\psi}_i)\lambda_i^l=\\ =\min_{s=1,L}\sum_{i=1}^N((c(x,\hat{\tau}_i)/w_i+a_i)/k+\gamma_i^s\hat{\psi}_i)\lambda_i^s,\\ 0\quad\text{otherwise},\end{cases}\quad\forall l=\overline{1,L};$$

where $(\hat{\tau}_1,...,\hat{\tau}_N,\ \hat{\psi}_1,...,\hat{\psi}_N)$ is the solution to the problem:

$$G(\boldsymbol{\psi})=\min_{\boldsymbol{\tau}^N\in\hat{\Omega}^N}G_1(\boldsymbol{\tau},\boldsymbol{\psi})\to\max,\ \psi_i\ge 0,\ i=\overline{p+1,N}.$$

Theorem 3 is proven.

Remark. Let $\gamma_j^l=\frac{1}{k}$ for all $j=\overline{1,N}$ and $l=\overline{1,L}$. Then the indices in these parameters can be omitted, and almost everywhere for $x\in\Omega$ in (15), the component $\hat{\chi}_l(x)=1$ when

$$\sum_{i=1}^N\frac{1}{k}(c(x,\hat{\tau}_i)/w_i+a_i+\hat{\psi}_i)\lambda_i^l=$$

$$=\min_{s=1,L}\frac{1}{k}\sum_{i=1}^N(c(x,\hat{\tau}_i)/w_i+a_i+\hat{\psi}_i)\lambda_i^s.$$

Considering that for any $s=\overline{1,L}$ among the N values λ_i^s only k are nonzero, the minimum value of the sum on the right will be achieved at the index *l*, such that

$$\forall i\in\sigma_l,\forall j\in\mathbf{N}\setminus\sigma_l:(\frac{c(x,\hat{\tau}_i)}{w_i}+a_i)+\hat{\psi}_i\le(\frac{c(x,\hat{\tau}_j)}{w_j}+a_j)+\hat{\psi}_j.$$

That is $\hat{\chi}_l(x)=1$ corresponds to the vector $\hat{\lambda}^l$ with the following components:

$$\hat{\lambda}_i^l(x)=\begin{cases}1,\text{if }\frac{c(x,\hat{\tau}_i)}{w_i}+a_i+\hat{\psi}_i\le\frac{c(x,\hat{\tau}_j)}{w_j}+a_j+\hat{\psi}_j,\\ \forall i\in\sigma_l,\ j\in\mathrm{N}\setminus\sigma_l,\\ 0\text{ otherwise.}\end{cases}$$

DOI 10.15588/1607-3274-2025-2-6

Thus, when the demand for services in the Ω_{σ_l}, $l=\overline{1,L}$, is distributed evenly among the centers, the mathematical formulation of the multiplex partition problem can be limited to the characteristic vector-function $\lambda(\cdot)=(\lambda_1(\cdot),...,\lambda_N(\cdot))$, defined on Ω by the following rule: if $x\in\Omega_{\sigma_l}$, then $\lambda_i(x)=1\forall i\in\sigma_l$, and $\lambda_j(x)=1\forall j\in\mathbf{N}\setminus\sigma_l$, $l=\overline{1,L}$. Then, in terms of characteristic functions, Problem **A** is written as follows:

Problem D:

$$\min_{(\lambda(\cdot),\boldsymbol{\tau}^{N-m})\in\hat{\Gamma}^k\times\hat{\Omega}^{N-m}} I\left(\lambda(\cdot),\boldsymbol{\tau}^{N-m}\right),$$

where:

$$I(\lambda(\cdot),\boldsymbol{\tau}^{N-m})=\frac{1}{k}\int_\Omega\sum_{i=1}^{N}\left(c(x,\tau_i)/w_i+a_i\right)\lambda_i(x)\rho(x)dx,$$

$$\hat{\Gamma}^k=\left\{\lambda(\cdot):\lambda(\cdot)\in\hat{\Gamma}_0^k,\right.$$

$$\frac{1}{k}\int_\Omega\rho(x)\lambda_i(x)dx=b_i,\quad i=1,\ldots,p,$$

$$\left.\frac{1}{k}\int_\Omega\rho(x)\lambda_i(x)dx\le b_i,\quad i=p+1,\ldots,N\right\};$$

$$\hat{\Gamma}_0^k=\left\{\lambda(\cdot)=(\lambda_1(\cdot),...,\lambda_N(\cdot)):\lambda_i(x)=0\vee1,\ i=1,\ldots,N,\right.$$

$$\left.\sum_{i=1}^{N}\lambda_i(x)=k,\ l=1,\ldots,L,\ \text{almost everywhere for } x\in\Omega\right\}.$$

The optimal solution to this problem, based on the above material, can also be expressed as follows:

$$\hat{\lambda}_i(x)=\begin{cases}1 if\ \ \forall i\in\sigma(x),\\ 0\ \ j\in\mathrm{N}\setminus\sigma(x),\ i=\overline{1,N},\end{cases}$$

where $\sigma(x)=\left\{j_1,j_2,\ldots,j_k\right\}$ is the set of indices of the first k elements in the array $D_{sorted}(x)=\left\{\hat{d}_{j_1}(x),\hat{d}_{j_2}(x),\ldots,\hat{d}_{j_N}(x)\right\}$ sorted in ascending order, with elements $\hat{d}_i(x)=\dfrac{c(x,\hat{\tau}_i)}{w_i}+a_i+\hat{\psi}_i$, $i=\overline{1,N}$, and $\hat{\tau}_1,...,\hat{\tau}_N$, $\hat{\psi}_1,...,\hat{\psi}_N$ is the solution to the problem:

$$G(\boldsymbol{\psi})=\min_{\boldsymbol{\tau}^N\in\hat{\Omega}^N}G_1(\boldsymbol{\tau},\boldsymbol{\psi})\to\max,\ \psi_i\ge0,\ i=\overline{p+1,N},$$

$$G_1(\boldsymbol{\tau}^N,\boldsymbol{\psi})=\frac{1}{k}\int_\Omega\sum_{i\in\sigma(x)}\left(\frac{c(x,\tau_i)}{w_i}+a_i+\psi_i\right)\rho(x)dx-\sum_{i=1}^{N}\psi_i b_i.$$

4 EXPERIMENTS

Based on the formulas obtained in Theorem 3 and the remark to it, computational methods and algorithms for solving continuous problems of optimal multiplex partitioning of sets have been developed, some variants of which are presented in the works [12, 13]. Computational experiments were conducted to verify the correctness of the algorithms and the adequacy of the mathematical model of optimal location of service centers and multiplex allocation of service demand, continuously spread over a certain territory. The latter can be uniform or proportional to the capacities of the centers.

Specific cases of problem A were solved: 1) optimal multiplex partitioning of a set with fixed centers without restrictions on their capacities; 2) OMPS with fixed centers without restrictions; 3) OMPS with location of centers with unlimited and limited their capabilities.

To illustrate the work of the proposed mathematical model and approaches, we developed a software implementation using C# in Visual Studio. For the experimental environment, we used a Lenovo laptop featuring an 8-core Intel Core i7 CPU, 16 GB of RAM, a 512 GB SSD, and running Windows 10.

5 RESULTS

In the problems presented below, the following data are common: $\Omega=\left\{x\in R^2:0\le x_i\le10,\ i=1,2\right\}$; $\rho(x)=1$ $\forall x\in\Omega$; $a_i=0$, $w_i=1,\forall i=\overline{1,N}$; the distance function is the Minkowski metric with parameter p: $c\left(x,\tau_i\right)=\sqrt[p]{(x_1-\tau_1^i)^p+(x_2-\tau_2^i)^p}$.

Problem 1. Figure 1 shows a duplex ($k=2$) partition of the square for $N=7$ fixed (*a*) and optimally located (*b*) centers.

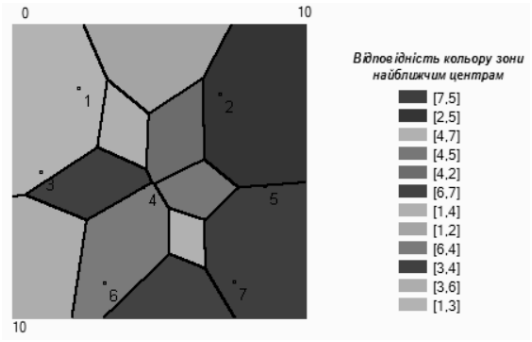

a

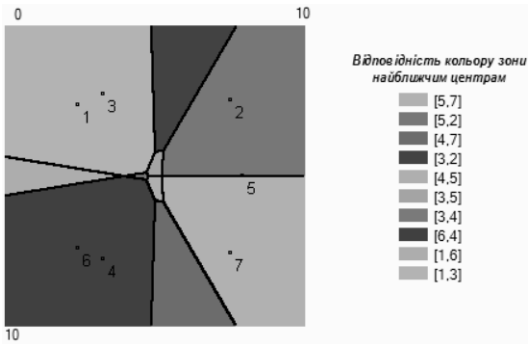

b

Figure 1 – Duplex partition of the square for 7 centers: a – fixed centers, b – optimally located centers

DOI 10.15588/1607-3274-2025-2-6

The case considered is $p = 2$, with unlimited center capacities, and demand for services is evenly distributed in shared areas. On the right side of the partition in the figures, here and further, the color of each zone corresponds to the pair of centers that must serve it. Table 1 provides the corresponding coordinates of the centers and their calculated capacities.

Since the demand for services is evenly distributed over the entire area and equals 1, the computed capacities essentially represent the area that each center must cover. The objective function value in the OMPS problem with fixed centers is: F = 230.2844, execution time = 2 sec., number of obtained subsets (zones) = 12. The same parameters in the OMPS problem with center location are: F = 210.6106, execution time = 32 sec, number of zones = 10. As seen, due to the optimal placement of centers, the objective function value decreased by 8.54%.

Problem 2. Figure 2 shows a 2nd-order partition of the square for the same fixed centers as in Problem 1, but with capacity constraints (see Table 2).

Table 1 – Coordinates and capacities of centers in Problem 1

Center №	Center coordinates				Center capacity, b_i	
	fixed		optimally located		fixed	optimally located
	τ_1^i	τ_2^i	τ_{1*}^i	τ_{2*}^i		
1	2.24	2.16	2.389	2.607	13.844	12.813
2	7.04	2.36	7.471	2.453	16.010	12.426
3	0.96	5	3.221	2.236	14.553	14.966
4	4.44	5.52	3.222	7.724	14.408	14.969
5	8.56	5.48	7.899	4.979	17.477	18.789
6	3.12	8.76	2.389	7.352	12.063	12.812
7	7.52	8.72	7.471	7.506	10.847	12.426

The problem was solved when the demand for services in the shared area of two centers is distributed both evenly (Problem D, Fig. 2a) and proportionally (Problem A, Fig. 2b). The number of non-empty zones was the same in both cases: Number of zones = 11, the solution time was almost the same, about 50 seconds, and the objective function values of the direct problem were 322.34 and 296.896, respectively.

As seen from Table 2 and Figure 2b, in the case when demand in the shared area of two centers is distributed proportionally to their capacities, even low-capacity centers do not fully exhaust their capabilities, although they cover a large area. This is explained by the fact that in these areas, most of the work is taken on by centers whose capacities are significantly larger than others. If the problem of optimal duplex partitioning is solved for the same seven fixed centers with the capacities computed above but changing the form of demand distribution in shared areas, the resulting partition is shown in Figure 3.

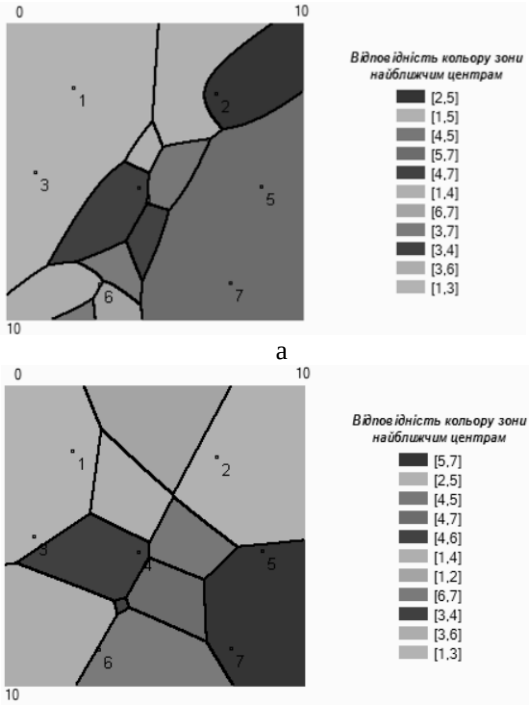

Figure 2 – Duplex service zones in Problem 2 for seven centers. Distribution of customers between centers on their common area is: a – uniform, b – proportional

Table 2 – Load on centers in Problem 2

Center №	Capacity b_i	Real capacity calculated in case of distribution customs between centers on their common area	
		uniform	Proportional
1	100	20.773	21.645
2	4	4.062	1.085
3	100	22.204	26.415
4	6	5.941	1.125
5	100	25.083	30.550
6	3	2.988	0.433
7	100	18.149	17.949

The values of the dual (computed and provided to verify the correctness of the algorithm) and direct problem functionals, solution time, number of zones, and calculated capacities of the centers are provided below according to the figure:

Fig. 3,a – F_{dual} = 421.4912, F_{direct}= 421.4927, time = 53 sec., Number zones = 8; B_{real} = (21.645; 1.085; 26.415; 1.125; 30.550; 0.433; 17.949);

Fig. 3,b – F_{dual} = 293.8833, F_{direct}= 293.8835, time = 58 sec., Number zones = 12: B_{real} = (20.773; 4.062; 22.204; 5.941; 25.083; 2.988; 18.150).

DOI 10.15588/1607-3274-2025-2-6

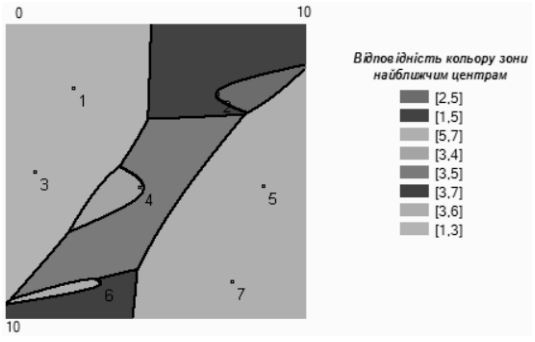

a

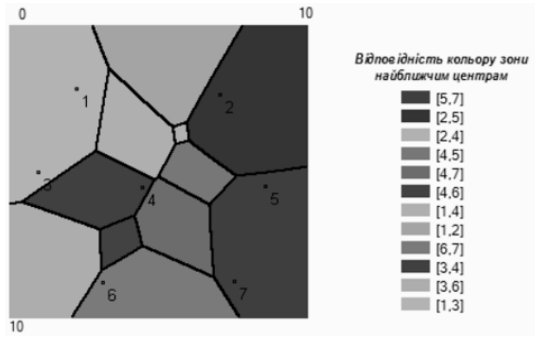

b

Figure 3 – Optimal duplex partition of the square for seven centers with limited capacities. Demand in shared zones is distributed: a – uniform (capacity corresponds to Fig. 2 b), b – proportional (capacity like Fig. 2 a)

Problem 3. Figure 4 a shows the solution to the optimal duplex partition problem of the square with the location of seven centers.

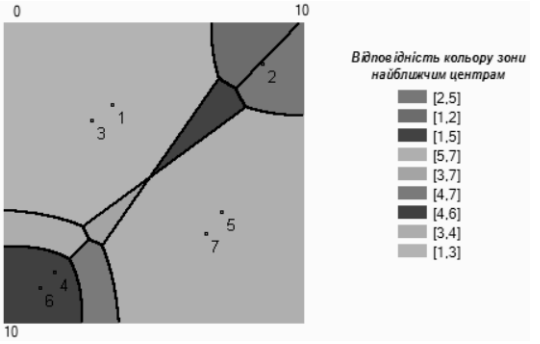

a

	Tx	Ty	wi	ai	Bi	realBi
1	3,594...	2,731...	1	0	30	21,974200
2	8,595...	1,372...	1	0	4	4,0025999
3	2,915...	3,245...	1	0	30	20,949400
4	1,672...	8,294...	1	0	6	5,9873999
5	7,250...	6,276...	1	0	30	22,323200
6	1,207...	8,787...	1	0	3	2,9661999
7	6,731...	7,018...	1	0	30	20,998600

b

Figure 4 – Solution of the optimal duplex partition problem of the square with the location of seven centers with limited capacities: a – partition; b – coordinates of the centers and their capacities

Some of them have limited capacities (in Figure 4b, the grid table shows the coordinates of the placed centers, their limited capacities B_i, and the demand they must cover realB_i). The 2nd-order partition of the square for the same fixed centers as in Problem 1, but with capacity constraints (see Table 2), was solved when the demand for services in the shared area of two centers is distributed evenly. The number of non-empty zones is 9, the solution time is 56 seconds, and the objective function value of the direct problem is 277.76.

We present a few more examples in which solutions of problems are predictable and confirm the correctness of the algorithm.

Problem 4. The problem of optimal duplex partitioning with the location of 8 centers. The Minkowski metric parameter is given. The initial placement of centers is shown in Fig. 5, a; the optimally located centers and the corresponding duplex partition are presented in Fig. 5,b. In Fig. 6, the table provides the coordinates of the placed centers, initial parameter values w_i, a_i, b_i, center capacities calculated according to the obtained partition (last column). At the optimal solution, F_{dual} = 166.602, F_{direct} = 166.678.

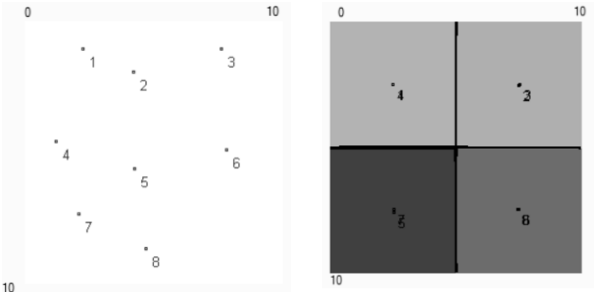

a b

Figure 5 – Optimal duplex partition of the square with the location of eight centers: a – initial placement of centers; b – optimal placement of centers and their corresponding zones

	Tx	Ty	wi	ai	Bi	realBi
1	2,489...	2,480...	1	0	100	12,498
2	7,473...	2,510...	1	0	100	12,400
3	7,501...	2,484...	1	0	100	12,381
4	2,494...	2,464...	1	0	100	12,317
5	2,504...	7,541...	1	0	100	12,297
6	7,464...	7,454...	1	0	100	12,386
7	2,530...	7,442...	1	0	100	12,499
8	7,435...	7,452...	1	0	100	12,418

Figure 6 – Calculation results in Problem 5

The results of computational experiments for solving optimal triplex partitioning problems of the square with fixed and optimally located centers are shown in Figures 7–9. The Manhattan metric (Figures 7, 8) and the Euclidean metric (Figure 9) were used to calculate the distance between points.

DOI 10.15588/1607-3274-2025-2-6

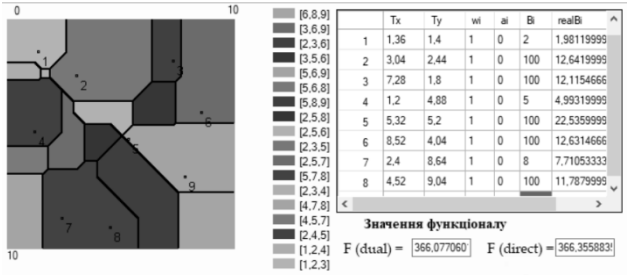

Figure 7 – Optimal triplex partitioning of the square with fixed centers and limited capacities of the 1st, 4th, and 7th centers

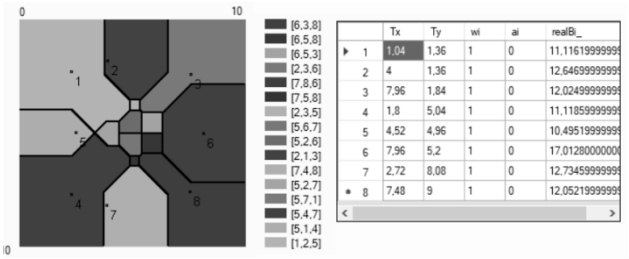

Figure 8 – Optimal triplex partitioning problem of the square with the location of ten centers

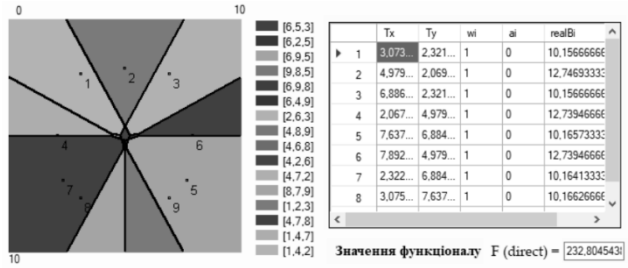

Figure 9 – Optimal triplex partitioning of the square with location of nine centers (Euclidean metric)

6 DISCUSSION

Unlike the OMPS models and problems presented in [4, 5, 12, 13], in this paper, first, the partitioning criterion is refined by considering the average cost of providing a service to a client, calculated for all centers that can serve them. This allows for a more accurate representation of the service provision in the objective function.

Second, the results of multiplex partitioning of sets with constraints on the centers' capacity are presented for different approaches of calculating capacity utilization. Specifically, cases are considered where the demand for a service in the k-th order zone is distributed among the corresponding centers either proportionally to their capacities (as in [12, 13]) or evenly. In both cases, the capacity utilization constraints are met because of optimal partitioning, but the last may differ significantly. Typically, in the first case, the service areas for low-capacity centers are smaller and their capabilities are not fully utilized. The full utilization of the small center capacity is characteristic for an even demand distribution.

Under certain initial conditions, the placement-partitioning results correspond to the properties of the solutions of OMPS problems presented in [12, 13]. When capacity constraints are present, they are always satisfied, and the objective functions of the primal and dual problems converge with acceptable accuracy.

Thus, the obtained results confirm the validity of the developed mathematical model for optimal zoning of territories with the facility location in the form of an optimal multiplex partitioning problem of continuous sets.

CONCLUSIONS

The scientific novelty of this research lies in the theoretical justification of methods and algorithms for optimal multiplex partitioning of sets. This is achieved through the formulation and proof of propositions and theorems that establish the properties of the functional, define the set of feasible solutions, and determine the necessary and sufficient conditions for optimality.

The practical significance of this research lies in the ability to apply the developed methods and algorithms for decision-making in the distribution of structural objects within a logistics system and the determination of their service zones based on specific criteria.

Future research will focus on generalizing these problems by considering the temporal variability of the demand function, the hierarchical structure of logistics systems, and the multi-stage nature of distribution processes. Additionally, efforts will be made to adapt the developed algorithms for practical applications in territorial zoning, taking into account existing infrastructure and interconnections between real-world objects.

ACKNOWLEDGEMENTS

The work is supported by the state budget scientific research project of Dnipro University of Technology "Mathematical and computer modeling of the rational distribution of material resources in multi-level transport and logistics systems" (state registration number 0125U000080).

REFERENCES

1. Stanina O. D., Us S. A., Koriashkina L. S. Modeli ta metody rozv'jazannja zadach opymal'noho rozmishchennja dvoetapnoho vyrobnyctva z neperervno rozpodilenym resursom : monografija. Dnipro : vydets "Svidler A. L.", 2021, 200 p.
2. Marianov V., Eiselt H. A. Fifty Years of Location Theory – A Selective Review, *European Journal of Operational Research*, 2024, Vol. 318, № 3, pp. 701–718. DOI: 10.1016/j.ejor.2024.01.036.
3. Drezner Z., Eiselt H. A. Competitive location models: A review, *European Journal of Operational Research*, 2024, Vol. 316, № 1, pp. 5–18. DOI: 10.1016/j.ejor.2023.10.030.
4. Koriashkina L. S. Rozshyrennja odnogo klasu neskinchenno-vymirnykh optymizacijnykh zadach, *Visn. Cherkas'koho un-tu. Ser. Prykl. matem. Inf.*, 2015, № 18 (351), pp. 28–36.
5. Koriashkina L. S., Lubenets D. Matematychni modeli ta metody mul'typleksnoho rozbyttja i bahatokratnoho pokryttja mnozhyn dlya zadach rozmishchennja-rozpodilu, *Information Technology: Computer Science, Software Engineering and Cyber Security*, 2023, № 4, pp. 12–25.
6. Drezner Z. In: Salhi S., Boylan J. (eds) Continuous Facility Location Problems, *The Palgrave Handbook of Operations*

DOI 10.15588/1607-3274-2025-2-6

Research. Cham, Palgrave Macmillan, 2022. DOI: 10.1007/978-3-030-96935-6_9.
7. Wolf G. W. Solving location-allocation problems with professional optimization software, *Transactions in GIS*, 2022, Vol. 26, № 7, pp. 2741–2775. DOI: 10.1111/tgis.12997.
8. Alumur S. A. Hub location and related models, *Contributions to Location Analysis – In Honor of Zvi Drezner's 75th Birthday*. Switzerland, Springer, 2019, pp. 237–252.
9. Callaghan B., Salhi S., Brimberg J. Optimal solutions for the continuous p-centre problem and related-neighbour and conditional problems: A relaxation-based algorithm, *Journal of the Operational Research Society*, 2019, Vol. 70, № 2, pp. 192–211.
10. Brimberg J., Maier A., Schöbel A. When closest is not always the best: The distributed p-median problem, *Journal of the Operational Research Society*, 2021, Vol. 72, № 2, pp. 200–216.
11. Yao J., Murray A. T. A Spatial Optimization Approach for Solving a Multi-facility Location Problem with Continuously Distributed Demand, 2020. DOI: 10.1007/978-3-030-43694-0_6.
12. Koriashkina L. S., Cherevatenko A. R. Continuous problems of optimal multiplex-partitioning of sets without constraints and solving methods, *Journal of Computational & Applied Mathematics*, 2015, № 2 (119), pp. 15–32.
13. Koriashkina L. S., Cherevatenko A. P. Neperervni linijni zadachi opymal'noho mul'typleksnoho rozbyttja mnozhyn z obmezhenniamy, *Visnyk Har'kivs'koho nacional'noho universytetu imeni V. N. Karazina. Serija «Matematychne modeljuvannja. Informacijni tehnologii. Avtomatyzovani systemy upravlinnja»*, 2015, Vyp. 28, pp. 77–91.
14. Royden H. L., Fitzpatrick P. M. Real analysis. 4th ed. Boston, Pearson, 2010.
15. Rudin W. Functional analysis, 2nd ed. New York, McGraw-Hill, 1991.
16. Boyd S., Vandenberghe L. Convex optimization. Cambridge, Cambridge University Press, 2004.

Received 03.02.2025.
Accepted 27.04.2025.

УДК 519.8

МАТЕМАТИЧНІ ОСНОВИ МЕТОДІВ ОПТИМАЛЬНОГО МУЛЬТИПЛЕКСНОГО РОЗБИТТЯ КОНТИНУАЛЬНИХ МНОЖИН

Коряшкіна Л. С. – д-р техн. наук, доцент кафедри системного аналізу та управління Національного технічного університету «Дніпровська політехніка», Дніпро, Україна.

Лубенець Д. Є. – аспірант кафедри системного аналізу та управління Національного технічного університету «Дніпровська політехніка», Дніпро, Україна.

Мінєєв О. С. – канд. техн. наук, доцент кафедри системного аналізу та управління Національного технічного університету «Дніпровська політехніка», Дніпро, Україна.

Сазонова М. С. – канд. фіз.-мат. наук, дослідник секції оптимізації та теорії систем кафедри математики Королівського технологічного інституту, Стокгольм, Швеція.

АНОТАЦІЯ

Актуальність. Об'єктом дослідження є процес розміщення сервісних центрів (служб соціального захисту, складів аварійного постачання та ін.) і розподілу між ними попиту на послугу у регіоні. Представлено математичні моделі і обґрунтовано методи розв'язання оптимізаційних задач розміщення-розподілу, в яких передбачено перекриття сервісних зон на той випадок, коли найближчий центр не зможе надати послугу. Актуальність дослідження обумовлена необхідністю вирішення завдань, пов'язаних, приміром, з територіальним розподілом об'єктів логістичних систем і завчасним плануванням запобіжних заходів в районах потенційних техногенних аварій, організації евакуаційних процесів або надання первинної гуманітарної допомоги населенню у разі надзвичайних ситуацій.

Мета – забезпечення надання гарантованого сервісу у короткий термін шляхом прикріплення клієнта до декількох найближчих центрів, розроблення відповідного математичного та програмного забезпечення.

Метод. Введено поняття характеристичної вектор-функції розбиття *k*-го порядку множини, теоретично аргументовано використання процедури ЛП-релаксації задачі, записаної у термінах таких характеристичних функцій. Математичне забезпечення розроблено з використанням елементів функціонального аналізу, теорії двоїстості, негладкої оптимізації.

Результати. Представлено і досліджено математичну модель оптимального територіального зонування з розміщенням центрів, при наявності обмежень на їхні потужності у вигляді неперервної задачі оптимального мультиплексного розбиття множин (ОМРМ), яка описує розподільчі процеси в логістичних системах за критеріями мінімізації відстані до декількох найближчих центрів з урахуванням їх можливостей. Доведено ряд тверджень та теорем стосовно властивостей функціоналу і множини допустимих розв'язків задачі. Отримано необхідні та достатні умови оптимальності, на яких базуються розроблені методи і алгоритми оптимального мультиплексного розбиття множин.

Висновки. Теоретичні положення і результати обчислювальних експериментів, наведені у роботі, свідчать про коректність розробленого математичного апарата і легко переносяться на окремі випадки розглянутої задачі. Доведені твердження та теореми лежать в основі обчислювальних методів оптимального зонування територій із розміщенням центрів, які варто використовувати при організації розподілу матеріальних потоків для оцінювання місткості центрів і парку задіяних транспортних засобів.

КЛЮЧОВІ СЛОВА: континуальна множина, мультиплексне розбиття, оптимізація, ЛП-релаксація, умови оптимальності, задачі розміщення-розподілу.

DOI 10.15588/1607-3274-2025-2-6

ЛІТЕРАТУРА

1. Станіна О. Д. Моделі та методи розв'язання задач оптимального розміщення двоетапного виробництва з неперервно розподіленим ресурсом : монографія / О. Д. Станіна, С. А. Ус, Л. С. Коряшкіна. – Дніпро : вид-ць «Свідлер А. Л.», 2021. – 200 с.
2. Marianov V. Fifty Years of Location Theory – A Selective Review / V. Marianov, H. A. Eiselt // European Journal of Operational Research. – 2024. – Vol. 318, № 3. – P. 701–718. – DOI: 10.1016/j.ejor.2024.01.036.
3. Drezner Z. Competitive location models: A review / Z. Drezner, H. A. Eiselt // European Journal of Operational Research. – 2024. – Vol. 316, № 1. – P. 5–18. – DOI: 10.1016/j.ejor.2023.10.030.
4. Коряшкіна Л. С. Розширення одного класу нескінченновимірних оптимізаційних задач / Л. С. Коряшкіна // Вісник Черкаського університету. Серія «Прикладна математика. Інформатика». – 2015. – № 18 (351). – С. 28–36.
5. Коряшкіна Л. С. Математичні моделі та методи мультиплексного розбиття і багатократного покриття множин для задач розміщення-розподілу / Л. С. Коряшкіна, Д. Лубенець // Information Technology: Computer Science, Software Engineering and Cyber Security. – 2023. – № 4. – С. 12–25.
6. Drezner Z. Continuous Facility Location Problems / Z. Drezner // The Palgrave Handbook of Operations Research / ed. by S. Salhi, J. Boylan. – Cham : Palgrave Macmillan, 2022. – DOI: 10.1007/978-3-030-96935-6_9.
7. Wolf G. W. Solving location-allocation problems with professional optimization software / G. W. Wolf // Transactions in GIS. – 2022. – Vol. 26, № 7. – P. 2741–2775. – DOI: 10.1111/tgis.12997.
8. Alumur S. A. Hub location and related models / S. A. Alumur // Contributions to Location Analysis – In Honor of Zvi Drezner's 75th Birthday. – Switzerland : Springer, 2019. – P. 237–252.
9. Callaghan B. Optimal solutions for the continuous p-centre problem and related-neighbour and conditional problems: A relaxation-based algorithm / B. Callaghan, S. Salhi, J. Brimberg // Journal of the Operational Research Society. – 2019. – Vol. 70. – P. 192–211.
10. Brimberg J. When closest is not always the best: The distributed p-median problem / J. Brimberg, A. Maier, A. Schöbel // Journal of the Operational Research Society. – 2021. – Vol. 72. – P. 200–216.
11. Yao J. A Spatial Optimization Approach for Solving a Multi-facility Location Problem with Continuously Distributed Demand / J. Yao, A. T. Murray. – 2020. – DOI: 10.1007/978-3-030-43694-0_6.
12. Koriashkina L. S. Continuous problems of optimal multiplex-partitioning of sets without constraints and solving methods / L. S. Koriashkina, A. P. Cherevatenko // Journal of Computational & Applied Mathematics. – 2015. – № 2 (119). – P. 15–32.
13. Коряшкіна Л. С. Неперервні лінійні задачі оптимального мультиплексного розбиття множин з обмеженнями / Л. С. Коряшкіна, А. П. Череватенко // Вісник Харківського національного університету імені В. Н. Каразіна. Серія «Математичне моделювання. Інформаційні технології. Автоматизовані системи управління». – 2015. – Вип. 28. – С. 77–91.
14. Royden H. L. Real analysis / H. L. Royden, P. M. Fitzpatrick. – 4th ed. – Boston : Pearson, 2010.
15. Rudin W. Functional analysis / W. Rudin. – 2nd ed. – New York : McGraw-Hill, 1991.
16. Boyd S. Convex optimization / S. Boyd, L. Vandenberghe. – Cambridge : Cambridge University Press, 2004.

DOI 10.15588/1607-3274-2025-2-6

НЕЙРОІНФОРМАТИКА ТА ІНТЕЛЕКТУАЛЬНІ СИСТЕМИ

NEUROINFORMATICS AND INTELLIGENT SYSTEMS

UDC 519.1: 004.93

TWO-LAYER GRAPH INVARIANT FOR PATTERN RECOGNITION

Batsamut V. M. – Dr. Sc., Professor, The Head of the Scientific Research Center of the National Academy of the National Guard of Ukraine, Kharkiv, Ukraine.

Batsamut M. V. – Student of Ivan Franko National University of Lviv, Lviv, Ukraine.

Bashkatov Y. H. – PhD, Associate Professor, Head of the Department of Tactics of the National Academy of the National Guard of Ukraine, Kharkiv, Ukraine.

Tolstonosov D. Yu. – PhD, Associate Professor, Intercessor of the Head of the Department of Combat and Logistics Security, Faculty of Service and Combat Activities of the National Guard of Ukraine, Kyiv, Ukraine.

ABSTRACT

Context. The relevance of the article is driven by the need for further development of object recognition (classification) algorithms, reducing computational complexity, and increasing the functional capabilities of such algorithms. The graph invariant proposed in the article can be applied in machine vision systems for recognizing physical objects, which is essential during rescue and monitoring operations in crisis areas of various origins, as well as in delivering firepower to the enemy using swarms of unmanned aerial vehicles.

Objective is to develop a graph invariant with low computational complexity that enables the classification of physical objects with a certain level of confidence in the presence of external interference.

Method. The physical object to be recognized (identified) is modeled by a connected undirected weighted graph. To identify the constant characteristics of different model graphs, the idea of selecting the minimum and maximum weighted spanning trees in the structure of these graphs is applied. For this purpose, the classical and modified Boruvka-Sollin's method are used (modified – for constructing the maximum weighted spanning tree). Such a stratification of the structure of the initial graph into two layers provides a larger information base during image analysis regarding the belonging of a certain implementation to a certain class of objects.

Next, for each of the resulting spanning trees, two numerical characteristics are calculated: the weight of the spanning tree and the Randić index. The first characteristic contains indirect information about the linear dimensions of the object, while the second conveys its structural features. These characteristics are independent of vertex labeling and the graphical representation of the graph, which is a necessary condition for graph isomorphism verification. From these four obtained characteristics, an invariant is formed, which describes the corresponding physical object present in a single scene.

To fully describe one class or subclass of objects in four scenes (top view; front and rear hemispherical views; side view), the pattern recognition system must have four corresponding invariants.

Results. 1) A two-layer invariant of a weighted undirected graph has been developed, enabling the recognition of physical objects with a certain level of confidence; 2) A method for recognizing physical objects has been formalized in graph theory terms, based on hashing the object structure using the weights of the minimum and maximum spanning trees of the model graph, as well as the Randić index of these trees; 3) The two-layer invariant of the weighted undirected graph has been verified on test tasks for graph isomorphism checking.

Conclusions. The conducted theoretical studies and a series of experiments confirm the feasibility of using the proposed graph invariant for real-time pattern recognition and classification tasks. The estimates obtained using the developed method are probabilistic, allowing the system operator to flexibly approach the classification of physical objects within the machine vision system's field of view, depending on the technological process requirements or the operational situation in the system's deployment area.

KEYWORDS: physical object, weighted undirected graph, isomorphism, minimal (maximal) spanning tree of a model graph, graph invariant, pattern recognition, algorithm, method.

ABBREVIATIONS

UMS is an unmanned systems;

EW is an electronic warfare.

NOMENCLATURE

G is an undirected weighted graph modeling an object;

V is a set of vertices of the model graph G;

v is a number of vertices of the graph G;

E is a set of edges of a model graph G;

q is a number of edges of a graph G;

G_* is a model graph of object implementation;

DOI 10.15588/1607-3274-2025-2-7

G' is a minimum spanning tree of a model graph G;

G'' is a maximum spanning tree of a model graph G;

E' is a set of edges that make up a tree G';

E'' is a set of edges that make up a tree G'';

$W(G')$ is a tree weight G';

$W(G'')$ is a tree weight G'';

$r(G')$ is a Randić index for the tree G';

$r(G'')$ is a Randić index for the tree G'';

$B(G)$ is a graph invariant G;

n is a dimension of the invariant;

e_{ij} is an edge of a graph;

$w(e_{ij})$ is a weighting edge e_{ij};

$d(v_i)$, $d(v_j)$ is a degrees of vertices between which there is an edge e_{ij};

X^m is a training sample;

m is a sample size;

Y is a set of object class names;

N is a number of implementations of objects subject to classification;

O is an estimation of the computational complexity of the algorithm;

P is a probability of correct classification of objects.

INTRODUCTION

The experience of combat operations conducted on the territory of Ukraine since 2014 and Russia's large-scale war against Ukraine, which began on February 24, 2022, indicate that increasing the combat effectiveness of means of defeating enemy manpower and equipment, developing new and improving existing types of weapons equipped with elements of artificial intelligence, remains a promising direction of development in the field of developing new models of weapons and military equipment.

The experience gained during the war years confirms that the massive use of both air, surface (underwater), and ground-based unmanned systems (UMS) on the battlefield clearly creates advantages over the enemy [1]. Such advantages can lead to positive changes in favor of their troops even at the operational level. In confirmation of these words, it is enough to recall the change in the operational situation in the Black Sea basin, which occurred as a result of the use of unmanned surface vehicles of the Sea Baby and Magura types by the Ukrainian Defense Forces against the Black Sea Fleet of the Russian Federation over a certain period of time.This influence forced the Russian Federation to relocate the main combat fleet to Novorossiysk.

At the same time, it should be noted that UMSs (ground, air, surface) are equipped with video cameras, which allows the operator of such a complex to control the drone in real time and direct it to the target. One of the effective ways to combat unmanned aerial vehicles is the use of electronic warfare (EW) means.The general principle of operation of EW means is to introduce artificial interference into the radio communication channels of the drone control, which allows such a device to be diverted from the target, and even to disable it at a considerable distance from the target.

Recently, to increase the effectiveness of the use of UMS in conditions of EW, manufacturers have begun to use elements of artificial intelligence, equipping their products with target "capture" systems, the so-called automatic UMS targeting systems.After the operator fixes the target, the drone attacks it in autonomous mode, which makes it invulnerable to enemy EW at the final section of the trajectory.

In the case of using a swarm (large group) of unmanned aerial vehicles, control according to the "operator-drone" scheme becomes ineffective, since it requires an appropriate number of operators, and most importantly, their coordinated work in a group in a rapidly changing environment, which is practically impossible to achieve in practice (this especially applies to aerial drones and is due to their relatively high flight speeds and the complexity of controlling the drone in the air).In order to eliminate this problematic situation, the control of the drone swarm is carried out under the control of artificial intelligence, according to the "launch it and forget it" principle.For this purpose, the next stage in the development of artificial intelligence was the introduction of so-called machine vision systems, equipped with methods and appropriate special mathematical and software for following a set route, recognizing, identifying images (targets) and distributing them between individual swarm agents (its subgroups) for effective destruction of enemy military equipment and other targets (inflicting maximum possible losses).

Upon arrival in the designated area, such a swarm of drones "independently" solves the task of inflicting the most effective fire damage on the enemy [2]. In the face of enemy EW and other obstacles on the battlefield (weather, natural, time of day, smoke, dust, camouflage elements, etc.), the problem arises of detecting enemy targets and correctly recognizing them for further distribution among the group's agents for effective destruction.The essence of distributing targets is to determine their number by category, to determine the degree of importance of each category, to screen out unimportant targets and to directly distribute the group's agents to important (defined) targets for their destruction.

The problematic issue of machine vision in this process remains obtaining a clear image of targets in conditions of external interference, their (targets) correct recognition and classification into certain categories in conditions of image noise.Another problematic issue is the time characteristics of pattern recognition algorithms (their computational complexity), which is caused by the high speed of aerial drones. Of course, these characteristics in machine vision systems tend to be reduced.

Endowing multi-agent systems with certain behavior (intelligence), in particular in matters of pattern recognition in conditions of external battlefield interference, requires the development of certain methods of working with images.

DOI 10.15588/1607-3274-2025-2-7

In general, the task of pattern recognition lies in the plane of checking images for isomorphism of their corresponding model graphs. For this purpose, the calculation of constant characteristics of graphs, the so-called invariants, is carried out. In completely identical images, the invariants of the corresponding model graphs selected for evaluation are the same, which allows us to draw certain conclusions. If the invariants differ, the corresponding images are considered different. This approach is classical and is used in cases where there are no interferences in the process of obtaining the initial image of a physical object (or in conditions where such influence is insignificant), for example: passenger flow at airports and border checkpoints; quality control of products in production; identification of a citizen within the framework of performing various police functions; electronic processing of texts and documents, etc.

In battlefield conditions, the influence of extraneous conditions on the quality of the image of objects is usually significant, which significantly affects the efficiency of machine vision systems. However, even in such conditions, the task of recognizing and classifying images must be performed, even with some loss of recognition reliability. Therefore, the decision rules for classifying images can be probabilistic in nature.

The object of the study is a pattern recognition process.

The subject of the study is the stability of graph invariants for solving pattern recognition problems.

The purpose of the study is to develop a graph invariant with low computational complexity, which will allow classifying physical objects with a certain level of confidence in the presence of external interference.

1 PROBLEM STATEMENT

Pattern recognition problems, among others, can be formalized and solved using graph theory models and methods [3], since graphs best model the structure of a physical object. That is why we will model the implementation of images by some weighted undirected graph $G=(V,E)$, where $V=\{v_1,...,v_v\}$ – a set of graph vertices that model key points in the structure of an object; $E=\{e_1,...,e_q\}$ – the set of graph edges that model the linear elements of an object. Each edge from the set E will have a certain weight coefficient $w(e_{ij})$, which will quantitatively characterize the length of the edge e_{ij}.

Taking into account the features of pattern recognition in conditions of external interference, the formulation of the corresponding problem in general terms will have the following form.

Let X be a set of descriptions of physical objects, and each object $x\in X$ is modeled by a weighted undirected graph G. Let Y is the set of object class names. There is an unknown target dependency – mapping $y^*: X\to Y$, whose values are known only on the objects of the training sample $X^m=\{(x_1,y_1),...,(x_m,y_m)\}$. It is necessary to develop an invariant $B(G)=\{\omega_1,\omega_2,...,\omega_n\}$, and based on such an invariant, construct an algorithm $a: X\to Y$, capable of classifying arbitrary objects $x\in X$.

2 LITERATUREREVIEW

One of the theoretical bases of pattern recognition is graph theory. Within the framework of this theory, pattern recognition usually involves testing different model graphs for isomorphism. It is believed that if the model graphs are isomorphic, then the objects corresponding to them are identical, and vice versa, in the absence of isomorphism, the test objects differ from each other to some extent. Such a simple rule allows for the classification of objects. A sign of graph isomorphism is the identity of their invariants – constant characteristics of the graphs selected for comparison (numerical, structural, geometric, etc. characteristics). In the case of an ordered set of several such characteristics, we speak of a hash function. Typically, hash functions are used to increase the reliability of recognition.

A fairly large number of works are devoted to the problem of detecting isomorphisms of graphs, one of the most characteristic of which is [4–6]. A number of generalizations are also given in such works as [7–10]. In [5] it is shown that such problems are combinatorial and difficult to solve. Algorithms for solving them in asymptotics have factorial computational complexity. In this regard, only heuristic methods remain acceptable for solving such problems [3, 6].

Therefore, neither the branch and bound method nor mathematical programming methods will be effective here, which at best reduce the complexity of the problem from factorial dependence to polynomial (as a rule, relative to the number of vertices of the graph), and this is unacceptable for solving problems of practical dimension. At the same time, existing heuristic methods for solving such problems (or rather, attempts to solve them) have, as a rule, computational complexity $O(|V|^c)$, where $4\le c\le 6$ [5, 6, 11], which also sharply limits the dimensionality of the problems solved in practice. For real-time operation, it is desirable to have the computational complexity of the corresponding methods (algorithms) at the level $c\le 3$ [6].

In [6], the authors presented an interesting approach to determining graph isomorphism, which is based on an invariant in the form of binary trees obtained as a result of the convolution (reduction) of model graphs. The authors of the article claim that the computational complexity of the corresponding algorithm does not exceed the estimate $O(|V|^3)$.

In [12], the author proposed a graph invariant based on calculating the shortest path matrix between all pairs of vertices of the model graph. The corresponding algorithm also has a computational complexity of $O(|V|^3)$, since it is based on the Warshall-Floyd or Bellman algorithm with the appropriate complexity [13, 14, 15].

DOI 10.15588/1607-3274-2025-2-7

However, the problem of reducing the computational complexity of pattern recognition algorithms does not lose its relevance today, and in the military sphere it acquires new, more stringent requirements. Our article is devoted to solving this problem.

3 MATERIALS AND METHODS

Unfortunately, no graph invariant has been discovered yet that would unambiguously indicate graph isomorphism. Attempts to find such an invariant were made by scientists in the 1960s–1980s, but were unsuccessful [16].

However, it is necessary to solve specific problems of pattern recognition, and this forces us to return to the development and study of invariants that would allow us to solve the problem of the existence or absence of isomorphism with a high degree of reliability.

The invariant proposed in this article is based on the definition in the structure of the initial model graph G its minimum and maximum weight of spanning trees G' and G'' respectively, Fig. 1.

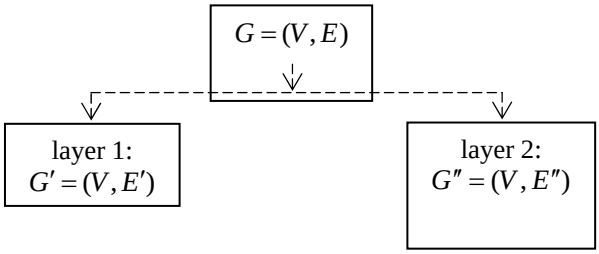

Figure 1 – Model graph layering G

Assertion. Any arbitrary undirected weighted graph $G=(V,E)$ with cycles, if only $\forall w(e_{ij})$ are not the same, has at least two spanning trees G' and G'', moreover $w(G') < w(G'')$, $E' \bigcap E'' \neq \varnothing$.

This splitting of the structure of the initial graph into two layers (hence the title of the article) provides a larger information base during further analysis of the image for the purpose of its reliable classification, since both trees characterize the same physical object. Thus, the spanning tree G' will contain a certain set of minimal, in a certain sense, linear dimensions of a physical object, and the spanning tree G'' – respectively maximum. Therefore, it becomes possible to obtain two numerical characteristics $w(G')$ and $w(G'')$, which will characterize the model graph G:

$$w(G') = \sum_{\forall e_{ij} \in G'} w(e_{ij}), \quad (1)$$

$$w(G'') = \sum_{\forall e_{ij} \in G''} w(e_{ij}). \quad (2)$$

We will also determine the structural features of a physical object by two layers. For this, we will use the Randić index [17], which characterizes the degrees of vertices between which there is an edge:

$$r = \sum_{\forall e_{ij} \in E} \frac{1}{\sqrt{d(v_i) \cdot d(v_j)}}. \quad (3)$$

Thus, for G' and G'' we will obtain the corresponding numerical characteristics $r(G')$ and $r(G'')$.

Therefore, the invariant proposed in this article is a four-dimensional object (hash function) and will be described by the following expression:

$$B(G) = \{w(G'); w(G''); r(G'); r(G'')\}. \quad (4)$$

The general algorithm for pattern recognition will consist of the following steps:

1. Obtain an image of a physical object from video and photo recording devices.
2. Using the Haar feature method, find the key points of an object in its image [18, 19, 20].
3. Based on the resolution of video or photo recording devices, determine the linear dimensions of the object, then proceed to the normalized values of these dimensions. To this end, determine the largest linear dimension in the composition of the physical object and list all the others relative to it. Therefore, all dimensions must be within the interval $(0,1]$. Form a model weighted graph G.
4. Based on the model graph G, construct the trees G' and G''. For this purpose, use one of the well-known algorithms: Boruvka-Sollin's [21] or Kruskal's [22]. To construct a tree G'', modify the specified algorithms in terms of the order of selection of edges of the model graph G – the selection should be made from edges with a larger value of $w(e_{ij})$ in the direction of edges with a smaller value of $w(e_{ij})$.
5. Behind the built trees G' and G'' by expressions (1) and (2) calculate numerical characteristics $w(G')$ and $w(G'')$ in accordance. By expression (3) – characteristics $r(G')$ and $r(G'')$. Using expression (4), construct an invariant of the model graph G – prototype of a physical object.
6. For different classes of objects that are potentially subject to recognition, form appropriate training samples with the most probable characteristics of invariants. One of the known methods is to perform recognition of physical objects on the ground.

4 EXPERIMENTS

In the course of the experiment, we will first of all investigate the stability of the invariant to image distortions (noise). To do this, we will calculate the corresponding characteristics of the invariant for the reference image, then for the image of the same physical

DOI 10.15588/1607-3274-2025-2-7

object, but in a different scene. Then we will determine the degree of deviation of the second invariant from the invariant for the reference image. A tank is chosen as the physical object T-72M, Fig. 2, *a*.

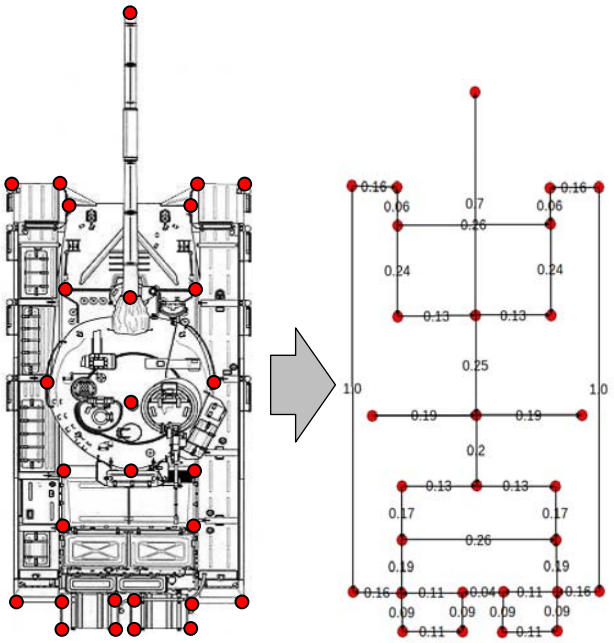

a b

Figure 2 – T-72M tank (top view):
a – key points of the object; b – weighted model graph G

The model graph G and the normalized weights of its edges are presented in Fig. 2, *b*. The length of the object's chassis was chosen as the standard linear dimension.

The constructed trees G' and G'' are presented in Fig. 3.

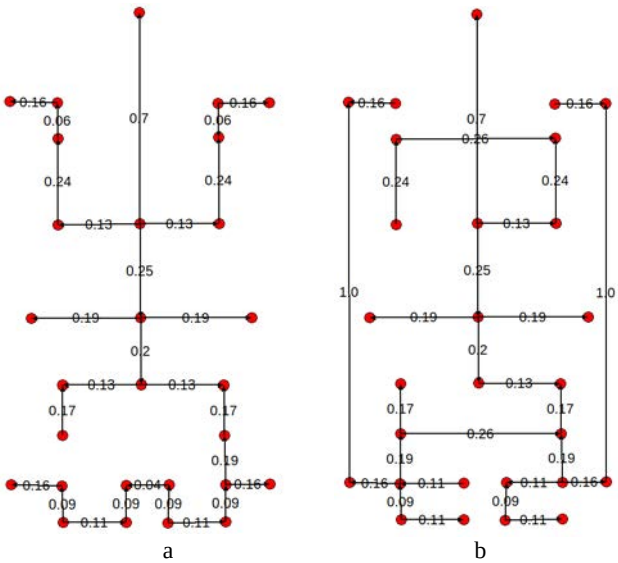

a b

Figure 3 – Weighted Span Trees of a Model Graph G:
a – tree G'; b – tree G''

Based on the edge weights shown in Fig. 3 according to expressions (1) and (2), we obtain $w(G')$ =4,44, $w(G'')$ =6,77.

The calculated Randić indices of the edges of the trees G' and G'' are shown in Fig. 4.

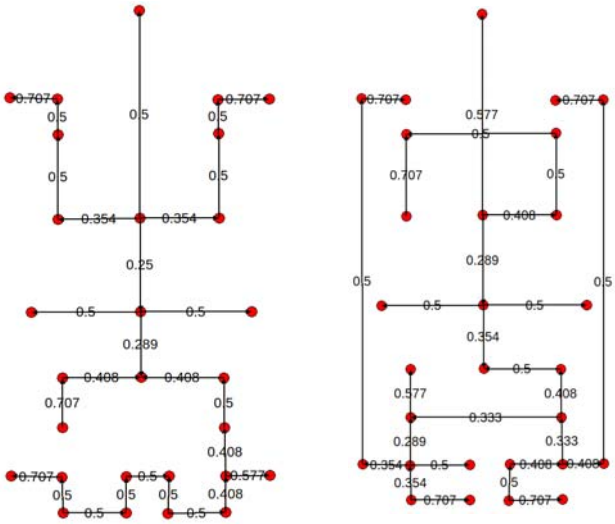

a b

Figure 4 – Randić indices:
a – tree G'; b – tree G''

According to expression (3), we obtain $r(G')$ =13.285 and $r(G'')$ =13.128. Therefore, the invariant for the reference image of a physical object (see Fig. 2, *a*) will have the form $B(G) = \{4.44; 6.44; 13.285; 13.128\}$.

Let us imagine that the observer is in a different position relative to the object (upper hemisphere, side view). The object is represented by a weighted model graph G_*, Fig. 5. As can be seen from the figure, in this position additional elements of the object were opened for viewing, which were not visible in Fig. 2. Such elements are: the front part of the object; its left caterpillar. In addition, thanks to such a scene, some linear dimensions of the object changed, but insignificantly.

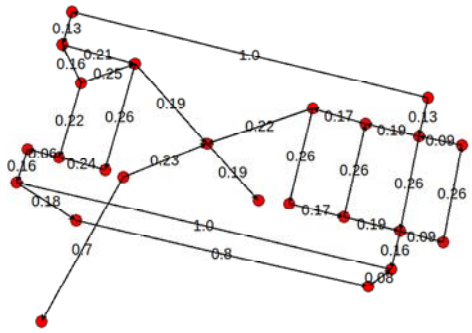

Figure 5 – Weighted Model Graph G_* of the T-72M tank (upper hemisphere, side view)

DOI 10.15588/1607-3274-2025-2-7

Let's build the appropriate trees G'_* and G''_*, see Fig. 6.

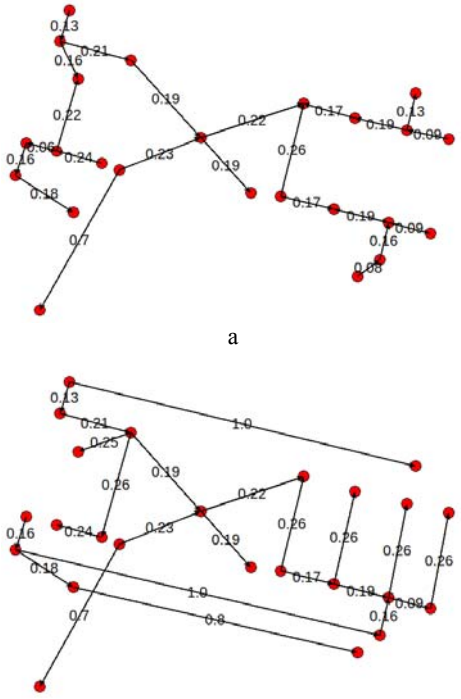

a

b

Figure 6 – Weighted Span Trees of a Model Graph G_*:
a – tree G'_*; b – tree G''_*

Using expressions (1) and (2) for the graph G_*, we obtain its numerical characteristics: $w(G'_*)$ =4.42 and $w(G''_*)$ =7.41. The calculated Randić indices for the edges of the trees G'_* and G''_* are shown in Fig. 7.

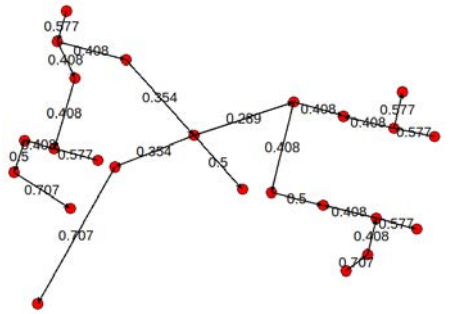

a

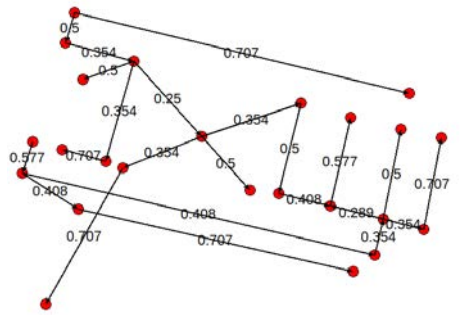

b

Figure 7 – Randić indices:
a – tree G'_*; b – tree G''_*

According to expression (3), we obtain the following numerical characteristics: $r(G'_*)$ =13.178 and $r(G''_*)$ =11.075.

Thus, the invariant for an alternative representation of a physical object (see Fig. 5) will be represented by the expression $B(G_*) = \{4{,}42;\ 7{,}41;\ 11{,}178;\ 11{,}075\}$.

Next, we will evaluate the recognition capabilities of the algorithm based on the proposed invariant. To do this, we will determine the degree of deviation of the images shown in Fig. 2 and Fig. 5. For this purpose, according to expression (5), in four-dimensional space (by the number of elements of the invariant), we calculate the distance (d) between two points corresponding to the invariants $B(G)$ and $B(G_*)$. The expression looks like:

$$d = \sqrt{\sum_{i=1}^{n} (x_i - y_i)^2}\ , \qquad (5)$$

where d – distance between points; x_i and y_i – elements of invariants $B(G)$ and $B(G_*)$ in accordance.

For this, with respect to $r(G')$, which is the maximum numerical characteristic in tuples $B(G)$ and $B(G_*)$, their elements are normalized. As a result of normalization, we obtained:

$\overline{B(G)} = \{0.334;\ 0.485;\ 1;\ 0.988\}$

$\overline{B(G_*)} = \{0.333;\ 0.557;\ 0.841;\ 0.833\}$.

The results of the calculations show that $d = 0.23$. Since Fig. 2 shows a "reference" image of a physical object of the "tank" type, with a probability of $P \approx 0{,}77$ the image presented in Fig. 5 can also be attributed to the class of physical objects of the "tank" type.

The obtained probability value is quite high. However, it should be noted that this probability estimate was obtained based on the results of a single comparison of two images of the same object located in different scenes (only to demonstrate the essence of the approach to pattern recognition using the developed invariant). It is clear that this estimate cannot be extended to all other possible cases and other physical objects. Under other conditions, the probability of assigning a particular physical object to one or another class of objects will be somewhat different.

In order to reveal the actual recognition ability of pattern recognition methods using the developed type of invariant, a well-known method was used – the method of standards [27].

The experiment was built according to the following scheme. The input training matrix had three classes of possible enemy targets: "tank"; "plane"; "truck", (see Fig. 8). The number of subclasses was from two to three. The corresponding training matrices mainly consisted of 4 records of invariants (tuples) characterizing the corresponding objects in four scenes: top view; view of the posterior and anterior hemispheres; side view.

DOI 10.15588/1607-3274-2025-2-7

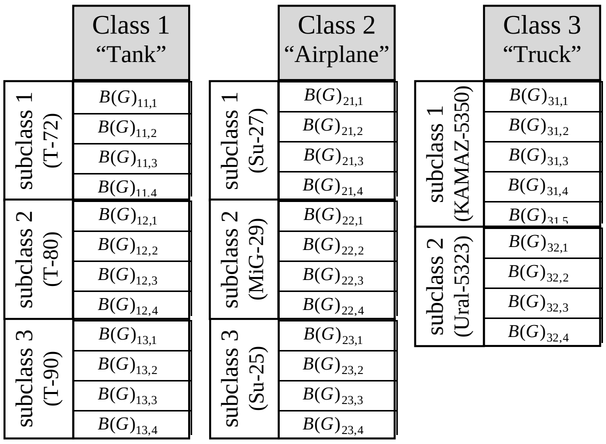

Figure 8 – Structure of the training matrix

For each subclass, 40 different implementations were tested – images of the corresponding physical objects. Therefore, the total number of implementations that were subject to classification according to the training matrix was equal to $N = 320$.

The following results were obtained from the experiment. At the class level, all images were correctly classified. At the subclass level, there were isolated cases of misclassification within one class. Thus, some implementations were classified as belonging to other subclasses. The number of such errors and their nature are given in Table 1.

Table 1 – Number and nature of cases of image misclassification during the experiment

	«Tank»	«Airplane»	«Truck»
subclass 1	(2) ↑	(5) ↑ •	(3) ↑ •
subclass 2	(4) ↑ • •	• ↓ (4)	• ↓ (6)
subclass 3	• ↓ (2)		--
Total images	120	120	80
Error, (%)	~6.6	~7.5	~11.2

Therefore, taking into account the results of the experiment, it can be stated that the proposed invariant provides the correct classification of images: at the class level with probability $P = 1$; at the subclass level with probability up to $0.8 \le P \le 0.9$.

5 RESULTS

The two-layer invariant of the weighted undirected model graph proposed in the article allows:

– due to the individual properties of the two spanning trees into which the initial model graph is stratified, expand the information base for analyzing physical objects during their classification.

– using the numerical characteristics of two spanning trees used in its composition, describe both the linear dimensions of a certain physical object and its structural features, which are the main aspects for classifying objects.

– with a high probability of performing correct pattern recognition.

6 DISCUSSION

The stratification of the object structure into two substructures and the set of numerical characteristics of the model graph proposed in the article allowed us to develop and propose an invariant that allows us to check graphs for isomorphism, and thus, to use this approach for the classification of real physical objects.The numerical characteristics used in the invariant characterize both the linear properties of the object and its structural properties, which is an important point in the process of recognizing enemy military equipment on the battlefield.

The stratification of the initial structure of the model graph into two conditional layers (minimum and maximum weight spanning trees) allowed to increase the recognition capabilities of methods based on graph theory tools. Thus, the probability of correct classification of objects belonging to different classes is equal to $P = 1$, the accuracy of classification of objects of different subclasses approaches $0.8 \le P \le 0.9$.

An important characteristic of various algorithms, including pattern recognition algorithms, is their computational complexity. It is clear that on real structures, and therefore on structures with a larger number of nodes and denser ones, the number of operations for searching for spanning trees will be much higher. Therefore, the computational complexity of the combinatorial algorithm that determines the characteristics of the proposed invariant will be determined by the computational complexity of its "basic element" – the algorithm for finding the spanning tree, which is estimated by $O(E \log V)$ [24]. Since two trees need to be found, the total computational complexity of the combinatorial algorithm can be estimated as $O(2[E \log V])$.

The obtained logarithmic estimate of the computational complexity of the algorithm is quite acceptable for its use in real time.

CONCLUSIONS

The article solves a relevant scientific and applied problem – the development of a graph invariant, using which it is possible, with a high level of probability, to correctly recognize various physical objects.

The scientific novelty of the developed graph invariant is as follows:

1) in the stratification of the initial structure of the model weighted undirected graph into two spanning trees – minimal and maximal in weight, which allows doubling the degree (depth) of verification of linear and structural properties of the same physical object;

2) in proposing an invariant structure containing two linear and two structural properties (characteristics) of objects, which allows checking model graphs for isomorphism and, on this basis, classifying objects.

The practical value of the proposed invariant is due to the fact that its application ensures the probability of

DOI 10.15588/1607-3274-2025-2-7

correct classification of objects $P = 1$ (at the class level), and $0.8 \le P \le 0.9$ (at the subclass level).

The computational complexity of the algorithm for calculating the invariant proposed in the article has a logarithmic dependence on the dimension and density of the model graph, which allows using such an algorithm in real time.

A promising direction for further researchis the development of a complete invariant of a model graph with polynomial computational complexity.

ACKNOWLEDGMENTS

This article highlights one of the results obtained by the authors in 2020–2021 while implementing the research project (state registration number 0120U002173) at the Research Center of the National Academy of the National Guard of Ukraine. The authors are grateful to their colleagues for their support during the research and active participation in the discussion of the results. All authors declare that they have neither financial support nor obligations.

REFERENCES

1. Dotsenko V. Drone Armies. How Drones Are Replacing Artillery, Aviation, and Boats in the War in Ukraine [Electronic resource]. Access mode: https://forbes.ua/war-in-ukraine/armii-droniv-yak-u-viyni-v-ukraini-bpla-zaminyuyut-artileriyu-aviatsiyu-i-kateri-06122022-10273.
2. Girnyk E. Ukraine creates “drone swarm” capable of attacking without human intervention – The Times [Electronic resource]. Access mode: https://unian.net/weapons/voyna-dronov-ukraina-sozdaet-bespilotniki-kotorye-ubivayut-roem-the-times-12674718.html.
3. Christofides N. Theory of graphs. Algorithmic approach. Moscow, Mir, 1978, 432 p.
4. Berge C. Isomorphism problems forhypergraphs, Mathematical centre tracts, 1974, pp. 3–12. DOI: 10.1007/BFb0066174.
5. Corneil D. G., Gotlieb C. C. An efficient algorithm for Graph isomorphism, *J. of A.C.M.*,1970, Vol. 17, No. 1, pp. 51–64. DOI: 10.1145/321556.321562.
6. A’Ggel Al-Zabi Bilal Rady, Kernytsky A. B., Lobur M. V., et al. New invariants for establishing graph isomorphisms, *Academic Journals and Conferences*, 2008, Vol. 626, pp. 90–93.
7. McCarthy M. K., Davida G. J. Invariant features and the graph isomorphism problem, *IEEE Syst. Man and Cybern. Soc. Proc. Int. Conf. Cybern and Soc. Boston, Mass*, 1973, pp. 81–85.
8. Foggia P., Sansone C., Vento M. A performance comparison of five algorithms for graph isomorphism, *In Proc. 3rd IAPR-TC15 Workshop Graph-Based Representations in Pattern Recognition*, 2001, pp. 188–199.
9. Messmer B. T., Bunke H. Efficient subgraphisomorp-hismdetection: a decomposition approach, *IEEE Trans. Knowl. Data Eng*, 2000, Vol. 12, pp. 307–323. DOI: 10.1109/69.842269.
10. Conte D., Foggia P., Sansone C. et al. Thirtyyears of Graph Matching in pattern Recognition, *International Journal of Pattern Recognition and Artificial Intelligence*, 2004, Vol. 18, No. 3, pp. 265–298. DOI:10.1142/S0218001404003228.
11. Automatic generation of graphs and graphs identification problem, *Technical Report, april*, 1974, No. 16.
12. Dunaev A. A. Using Graph Theory for Face Identification, *International Research Journal*, 2017, Vol. 09(63), Issue 3. pp. 31–35. DOI: 10.23670/IRJ.2017.63.089.
13. Floyd R. Algorithm 97: Shortest Path, *Communications of the ACM*, 1961, Vol. 5 (6), 345 p. DOI: 10.1145/367766.368168.
14. Warshall S. Algorithm on Boolean matrices, *Journal of the ACM*, 1962, Vol. 9 (1), pp. 11–12. DOI: 10.1145/321105.321107.
15. Batsamut V., Manzura S., Kosiak O. et al. Fast Algorithm for Calculating Transitive Closures of Binary Relations in the Structure of a Network Object, *International Journal of Computing*, 2021, Vol. 20(4), pp. 560–566. DOI: 10.47839/ijc.20.4.2444.
16. Graph invariant[Electronic resource]. Access mode: https://uk.wikipedia.org/wiki/Інваріант_графа.
17. Delorme C., Favaron O., Rautenbach D. On the Randić index, *Discrete Mathematics, 6 November*, 2002, Vol. 257, Issue 1, pp. 29–38. DOI: 10.1016/S0012-365X(02)00256-X.
18. Messom C. H., Barczak A.L.C. Fast and Efficient Rotated Haar-like Features Using Rotated Integral Images, *Australian Conference on Robotics and Automation (ACRA 2006)*, 2006, pp. 1–6.
19. Lienhart R., Maydt J. An Extended Set of Haar-like Features for Rapid Object Detection, *IEEE ICIP Sep.*, 2002, Vol. 1, pp. 900–903. DOI: 10.1109/ICIP.2002.1038171.
20. Bernardin K., Camp F. V. D., Stiefelhagen R. Automatic person detection and tracking using fuzzy controlled active cameras, *In: Proc. IEEE Computer Society Conference on Computer Vision and Pattern Recognition*, 2007, pp. 1–8. DOI: 10.1109/CVPR.2007.383502.
21. Faridawaty Marpaung, Arnita, Wirdatull Jannah Idris Comperative of Prim’s, Kruskal’s and Boruvka’s algoritma to solve minimum spanning tree problems, *Jurnal Handayani*, 2019, Vol. 10, No. 2, pp. 80–89. DOI:10.24114/jh.v10i2.16053.
22. Kruskal J. On the Shortest Spanning Subtree of a Graph and the Traveling Salesman Problem, *Proc. AMS*, 1956, Vol. 7, No. 1, pp. 48–50. DOI: 10.1090/S0002-9939-1956-0078686-7.
23. Dovbysh A. S., Shelekhov I. V. Fundamentals of Pattern Recognition Theory. Sumy, Sumy State University, 2015, Vol. 1, 109 p.
24. Boruvka’s algorithm [Electronic resource]. Access mode: https://uk.wikipedia.org/wiki/Алгоритм_Борувки.

Received 22.01.2025.
Accepted 20.04.2025.

DOI 10.15588/1607-3274-2025-2-7

УДК 519.1: 004.93

ДВОШАРОВИЙ ІНВАРІАНТ ГРАФА ДЛЯ РОЗПІЗНАВАННЯ ОБРАЗІВ

Бацамут В. М. – д-р військ. наук, професор, начальник науково-дослідного центру службово-бойової діяльності Національної гвардії України Національної академії Національної гвардії України, Харків, Україна.

Бацамут М. В. – студент Львівського національного університету ім. Івана Франка, Львів, Україна.

Башкатов Є. Г. – канд. військ. наук, доцент, начальник кафедри тактики Національної академії Національної гвардії України, Харків, Україна.

Толстоносов Д. Ю. – канд. юрид. наук, доцент, заступник начальника кафедри бойового та логістичного забезпечення факультету службово-бойової діяльності Національної гвардії України Київського інституту Національної гвардії України, Київ, України.

АНОТАЦІЯ

Актуальність. Актуальність статті обумовлюється потребою у подальшому розвитку алгоритмів розпізнавання (класифікації) об’єктів, у зменшенні обчислювальної складності і збільшенні функціональних можливостей таких алгоритмів. Запропонований у статті інваріант графа може бути застосований у системах машинного зору для розпізнавання фізичних об’єктів, що є важливим у ході виконання рятувальних, моніторингових завдань у кризових районах різного характеру походження, а також у ході нанесення противнику вогневого ураження із застосуванням рою безпілотних апаратів.

Мета роботи полягає в розробленні інваріанту графа з низькою обчислювальною складністю, який дозволятиме з певним рівнем довірчої ймовірності класифікувати фізичні об’єкти в умовах зовнішніх завад.

Метод. Фізичний об’єкт, що підлягає розпізнаванню (ідентифікації) моделюється зв’язним неорієнтованим зваженим графом. Для виявлення сталих характеристик різних модельних графів застосовано ідею виділення в структурі цих графів мінімального і максимального за вагою каркасних дерев. З цією метою застосовується класичний і модифікований методи Борувки-Солліна (модифікований – для побудови максимального зваженого каркасного дерева). Таке розшарування структури початкового графа на два шари надає більшої інформаційної бази у ході аналізу зображення щодо приналежності певної реалізації до деякого класу об’єктів.

Далі, для кожного з отриманих таким чином каркасних дерев, відшукуються значення двох числових характеристик: ваги каркасного дерева та індексу Рандіча. Перша характеристика несе в собі опосередковану інформацію про лінійні розміри об’єкту, а друга – про його структурні особливості. Ці характеристики не залежать від способу позначення вершин та графічного зображення графа, що є необхідною умовою для перевірки графів на ізоморфізм.З отриманих таким чином чотирьох характеристик складається інваріант, яким описується відповідний фізичний об’єкт, що перебуває в одній сцені.

Для повного опису одного класу або підкласу об’єктів в чотирьох сценах (вид зверху; вид передньої та задньої полусфер; вид збоку) система розпізнавання образів повинна мати чотири відповідні інваріанти.

Результати. 1) Розроблено двошаровий інваріант зваженого неорієнтованого графу, який дозволяє з певним рівнем довірчої ймовірності розпізнавати фізичні об’єкти; 2) В термінах теорії графів формалізовано метод розпізнавання фізичних об’єктів, що заснований на хешуванні структури об’єкту вагою мінімального і максимального каркасних дерев модельного графу, а також індексом Рандіча цих дерев; 3) Виконано верифікацію двошарового інваріанту зваженого неорієнтованого графу на тестових задачах з перевірки графів на ізоморфізм.

Висновки. Проведені теоретичні дослідження та низка проведених експериментів підтверджують можливість використання пропонованого інваріанту графів в задачах розпізнавання та класифікації образів в масштабі реального часу. Оцінки, що виробляються із використанням розробленого методу, носять ймовірнісний характер, що дозволяє особі, яка налаштовує систему машинного зору, гнучко підходити до класифікації фізичних об’єктів в полі зору такої системи, виходячи з вимог до технологічного процесу або з умов оперативної обстановки в районі застосування системи.

КЛЮЧОВІ СЛОВА: фізичний об’єкт, зважений неорієнтований граф, ізоморфізм, мінімальне (максимальне) каркасне дерево модельного графа, інваріант графа, розпізнавання образів, алгоритм, метод.

ЛІТЕРАТУРА

1. Доценко В. Армії дронів. Як безпілотники замінюють артилерію, авіацію і катери на війні в Україні[Електрон. ресурс]. – Режим доступу: https://forbes.ua/war-in-ukraine/armii-droniv-yak-u-viyni-v-ukraini-bpla-zaminyuyut-artileriyu-aviatsiyu-i-kateri-06122022-10273.
2. Гирнык Є. Украина создает «рой дронов», способный атаковать без вмешательства человека – The Times [Електрон. ресурс]. – Режим доступу: https://unian.net/weapons/voyna-dronov-ukraina-sozdaet-bespilotniki-kotorye-ubivayut-roem-the-times-12674718.html.
3. Кристофидес Н. Теория графов. Алгоритмический поход / Н. Кристофидес. – М. : Мир, 1978. – 432 с.

DOI 10.15588/1607-3274-2025-2-7

4. Berge C. Isomorphism problems for hypergraphs / C. Berge // Mathematical centre tracts. – 1974. – P. 3–12. DOI: 10.1007/BFb0066174.
5. Corneil D. G. An efficient algorithm for Graph isomorphism / D. G. Corneil, C. C. Gotlieb // J. of A.C.M. – 1970. – Vol. 17. – No. 1. – P. 51–64. DOI: 10.1145/321556.321562.
6. New invariants for establishing graph isomorphisms / [Bilal Rady A'Ggel Al-Zabi, A. B. Kernytsky, M. V. Lobur, et al.] // Academic Journals and Conferences. – 2008. – Vol. 626. – P. 90–93.
7. McCarthy M. K. Invariant features and the graph isomorphism problem / M. K. McCarthy, G. J. Davida // IEEE Syst. Man and Cybern. Soc. Proc. Int. Conf. Cybern and Soc. Boston, Mass. – 1973. – P. 81–85.
8. Foggia P. A performance comparison of five algorithms for graph isomorphism / P. Foggia, C. Sansone, M. Vento // In Proc. 3rd IAPR-TC15 Workshop Graph-Based Representations in Pattern Recognition, 2001. – P. 188–199.
9. Messmer B. T. Efficient subgraph isomorphism detection: a decomposition approach / B. T. Messmer, H. Bunke // IEEE Trans. Knowl. Data Eng. – 2000. – Vol. 12. – P. 307–323. DOI: 10.1109/69.842269.
10. Thirty years of Graph Matching in pattern Recognition / [D. Conte, P. Foggia, C. Sansone et al.] // International Journal of Pattern Recognition and Artificial Intelligence. – 2004. – Vol. 18. – No. 3. – P. 265–298. DOI:10.1142/S0218001404003228.
11. Proskurowski A. Automatic generation of graphs and graphs identification problem / A. Proskurowski // Technical Report, april. – 1974. – No. 16.
12. Дунаев А. А. Использование теории графов для идентификации лиц / А. А. Дунаев // Международный научно-исследовательский журнал, 2017. – № 09(63). – ч. 3. – С. 31–35. DOI: 10.23670/IRJ.2017.63.089.
13. Floyd R. Algorithm 97: Shortest Path / R. Floyd // Communications of the ACM. – 1961. – Vol. 5 (6). – 345 p. DOI: 10.1145/367766.368168.
14. Warshall S. Algorithm on Boolean matrices / S. Warshall // Journal of the ACM. – 1962. – Vol. 9 (1). – P. 11–12. DOI: 10.1145/321105.321107.
15. Fast Algorithm for Calculating Transitive Closures of Binary Relations in the Structure of a Network Object / [V. Batsamut, S. Manzura, O. Kosiak et al.] // International Journal of Computing. – 2021. – Vol. 20(4). – P. 560–566. DOI: 10.47839/ijc.20.4.2444.
16. Інваріант графа [Електрон. ресурс]. – Режим доступу: https://uk.wikipedia.org/wiki/Інваріант_графа.
17. Delorme C. On the Randić index / C. Delorme, O. Favaron, D. Rautenbach // Discrete Mathematics, 6 November. – 2002. – Vol. 257, Issue 1. – P. 29–38. DOI: 10.1016/S0012-365X(02)00256-X.
18. Messom C. H. Fast and Efficient Rotated Haar-like Features Using Rotated Integral Images / C. H. Messom, A.L.C. Barczak // Australian Conference on Robotics and Automation (ACRA2006). – 2006. – P. 1–6.
19. Lienhart R. An Extended Set of Haar-like Features for Rapid Object Detection / R. Lienhart, J. Maydt // IEEE ICIP Sep., 2002. – Vol. 1. – P. 900–903. DOI: 10.1109/ICIP.2002.1038171.
20. Bernardin K. Automatic person detection and tracking using fuzzy controlled active cameras / K. Bernardin, V. D. Camp F., R. Stiefelhagen // In: Proc. IEEE Computer Society Conference on Computer Vision and Pattern Recognition. – 2007. – P. 1–8. DOI: 10.1109/CVPR.2007.383502.
21. Faridawaty Marpaung. Comperative of Prim's, Kruskal's and Boruvka's algoritma to solve minimum spanning tree problems / Faridawaty Marpaung, Arnita, Wirdatull Jannah Idris // Jurnal Handayani. – 2019. – Vol. 10, No. 2. – P. 80–89. DOI:10.24114/jh.v10i2.16053.
22. Kruskal J. On the Shortest Spanning Subtree of a Graph and the Traveling Salesman Problem / J. Kruskal // Proc. AMS. – 1956. – Vol. 7, No. 1. – P. 48–50. DOI: 10.1090/S0002-9939-1956-0078686-7.
23. Довбиш А. С. Основи теорії розпізнавання образів: навчальний посібник / А. С. Довбиш, І. В. Шелехов. –Суми : Сумський державний університет, 2015. – ч. 1. – 109 с.
24. Алгоритм Борувки [Електрон. ресурс]. – Режим доступу: https://uk.wikipedia.org/wiki/Алгоритм_Борувки.

DOI 10.15588/1607-3274-2025-2-7

UDC 004.88

SITUATION ANTICIPATION AND PLANNING FRAMEWORK FOR INTELLIGENT ENVIRONMENTS

Burov E. V. – Doctor of Sciences, Professor, Professor of the Department of Information Systems and Networks, Lviv Polytechnic National University, Lviv, Ukraine.

Zhovnir Y. I. – Postgraduate student of the Department of Information Systems and Networks Lviv Polytechnic National University, Lviv, Ukraine.

Zakhariya O. V. – Postgraduate student of the Department of Information Systems and Networks Lviv Polytechnic National University, Lviv, Ukraine.

Kunanets N. E. – Doctor of Sciences, Professor, Professor of the Department of Information Systems and Networks Lviv Polytechnic National University, Lviv, Ukraine.

ABSTRACT

Context. Situation anticipation, prediction and planning play an important role in intelligent environments, allowing to learn and predict the behavior of its users, anticipate maintenance and resource provision needs. The object of study is the process of modeling the situation anticipation and planning in the situation-aware systems.

Objective. The goal of the work is to develop and analyze the ontology-based framework for modeling and predicting the situation changes for intelligent agents, allowing for proactive agent behavior.

Method. This article proposes a framework for anticipation and planning based on GFO ontology. Each task or problem is considered a situoid, having a number of intermediate situations. Each task or problem is considered a situoid, having several intermediate situations. The framework is focused on the analysis of changes between situations, coming from anticipated actions or events. Contextually organized knowledge base of experiential knowledge is used to retrieve information about possible developments scenarios and is used for planning and evaluation. The framework allows to build and compare trajectories of configuration changes for specific objects, situations or situoids. The planning and anticipation process works in conditions of incomplete information and unpredicted external events, because the projections are constantly updated using feedback from sensor data and reconciliating this information with predicted model.

Results. The framework for reasoning and planning situations based on GFO ontology, allowing to model spatial, temporal and structural data dependencies.

Conclusions. The situation anticipation framework allows to represent, model and reason about situation dynamics in the intelligent environment, such as intelligent residential community. Prospects for further research include the elaboration of contextual knowledge storing and processing, reconciliation and learning procedures based on real-world feedback and the application of proposed framework in the real-world system, such as intelligent security systems.

KEYWORDS: GFO, situational awareness, anticipation, situation analysis, situoid.

ABBREVIATIONS

GFO is a General formal Ontology;

ISFO is an Integrated System of Foundational Ontologies;

IFDAO is an Integrated Framework for the Development and Application of Ontologies;

GOL is a General Ontological Language;

DFIG is a Data Fusion Information Group;

UFO is an Unified Foundational Ontology;

DCIM is a Data Collection and Interpretation Module;

SMA is a Situation modeling agent;

GMM is a Goal management module.

NOMENCLATURE

Tsk is a task;

t_{st}, t_{end} is a starting and ending times of task or situoid;

Su is a situoid;

$Sit_{st}^{su}, Sit_{end}^{su}$ are the starting and ending situations in situoid;

Ch is a chronoid;

Cf_{t_1} is a configuration in the time moment t_1;

$Gl_{\text{int},ti}$ is an agent's intention in moment t_i;

Cm is a conceptual model;

$Cm_{env,ti}$ is a conceptual model of environment in moment t_i;

$Cm_{con,ti}$ is a conceptual model of context in the moment t_i;

F_{sim} is a function measuring the distance between two contexts;

Pl is a plan;

Ac is a specification of action;

F_{sel} is a function for selecting the situation trajectory using criteria Cr;

TP is a true positive;

FP is a false positives;

FN is a false negatives;

TN is a true negatives detections;

$T_{responce}$ is a time of response;

$T_{analysis}$ is a time of analysis;

T_{action} is a time of action execution;

$S(t)$ is a current situation at time t, described by the parameters of the environment;

A is a set of available agent actions;

DOI 10.15588/1607-3274-2025-2-8

ε is a set of possible external events that affect the situation;

K is a contextually organized knowledge base that contains data on previous situations and scenarios of their development;

$P(S_i, a, e)$ is a model of transition between situations that determines the probability of transitioning from a situation;

From S_i to S_j for actions $a \in A$ and events $e \in E$;

σ is a set of sensor data updated in real time;

τ is a trajectory of changes in situations $S(t_1), S(t_2), S(t_n)$ for a given period of time;

π is an optimal action plan of the agent $a_1, a_2, ...a_k$ to achieve a given goal;

$S(t)$ is a predicted situation at a given time t_t.

INTRODUCTION

The recent progress in information technology and artificial intelligence fueled by further growth of computation capacities creates many opportunities in all areas of economy and research. The scientific and technological area of intelligent ambience follows the age-old vision of intelligent environments helping humans to live fulfilled lives [1]. It is a recurrent theme in literature on smart homes and ambient intelligence [2, 3]. Situational awareness is a required feature for agents implemented in the intelligent environment, because it permits to discover potentially dangerous situations, guess and follow user's intents and act proactively [4, 5]. Situational awareness, in turn requires the ability to model and reason about situations and actions leading from one situation to another. Such ability is also linked to the implementation of goal-driven behavior of agents. The purpose of this article is the development of a conceptual framework for situation anticipation and planning analysis based on General Formal Ontology (GFO).

The object of study is the process of modeling the situation anticipation and planning in the situation-aware systems.

The implementation of such a process is a necessary condition for the development of fully autonomous intelligent agents. However, existing models, such as DFIG model [6] don't support it.

The subject of study is the frameworks and methods for modeling the situation development in intelligent agents.

The purpose of the work is to develop and analyze the ontology-based framework for modeling and predicting the situation changes for intelligent agents, allowing for proactive agent behavior.

1 PROBLEM STATEMENT

Let us assume that we have:

Input variables: $S(t)$, A, ε, K, $P(S_i, a, e)$, σ.

Output variables: τ, π, $S(t)$.

Optimization criterion:

The task of forecasting and planning is to minimize the loss function $L(\tau, \hat{\tau})$ where $L(\tau, \hat{\tau}) = \sum_{t=1}^{n} d(S(t), \hat{S}(t))$, where $d(S, \hat{S})$ measure of deviation from the real situation $S(t)$, $S(\hat{t})$ from the predicted.

Limitation

$\forall a \in A,\ e \in E \div P(S_i, a, e) \in [0,1]$.

Trajectory τ must be achievable in the situation $S(O)$.

Forecasting and planning must work in conditions of incomplete information $\sigma(t) \neq S(t)$, where $S(t)$ is a complete description of the environment that is not available due to limited sensors

Problem statement:

The task of developing a framework for predicting situations and planning in intelligent environments is to construct an optimal trajectory τ and action plan π based on transition models $P(S_i, a, e)$, knowledge K, current sensor data σ and ensuring proactive agent behavior when fulfilling optimization criteria $L(\tau, \hat{\tau})$ in conditions of uncertainty and limitations.

Knowledge base *Knb* is organized around tasks, which are represented as situoids *Su* and agent's intents, and stores the information about situations dynamics in the form of intermediary situations *Sit* and actions *Ac* leading from one situation to another:

$$(Sit_i, Gl_{int,k}, Ac) \rightarrow Sit_j.$$

The problem is to build a reasoning framework, allowing to represent and model the situational dynamics in the form of a sequence of situations $S(t_1), S(t_2), S(t_n)$, using the knowledge from knowledge base *Knb* and similarity function F_{sim} evaluating the similarity between current context $Cm_{con,tc}$ and contexts from knowledge base.

Suppose given the original sample as a set of precedents (instances) $< x, y >$, where $x = \{x^S\}, x = \{x_j\}, x^S = \{x^S_j\}$, $y = \{y^S\}, s = 1, 2, ..., S, j = 1, 2, ..., N$.

For a given sample of precedents $<x, y>$ the problem of model synthesis can be presented as the problem of finding $< F(), w >: y^{S*} = F(w, x^S), f(F(), w, < x, y >) \rightarrow opt$, where the model structure $F()$ usually specified by the user in practice, and the set of controlled parameters w is adjusted based on the training sample.

In turn, the problem of subsample formation from a given sample $<x, y>$ is to find such a set $of < x', y' >: x' \subset \{x^S\}, y' = \{y^S \mid x^S \in x'\}, S' < S, N' = N$, wherein $f(< x', y' >, < x, y >) \rightarrow opt$.

DOI 10.15588/1607-3274-2025-2-8

2 REVIEW OF THE LITERATURE

The integration of situational awareness into intelligent agents presents a significant challenge within the field of artificial intelligence. The primary factors that contribute to this challenge include:

– The necessity of incorporating both predictive abilities and environmental perception, alongside the reasoning and evaluation of potential actions.

– Being focused on objectives while utilizing goals to empower intelligent agents with agency and autonomy, aiding in the selection of the most crucial goal to pursue at any given moment, and taking actions that align with this goal.

– Concentrating on a specific area of the environment relevant to the chosen goal, emphasizing shifting attention rather than explicitly querying and selecting related information.

– Utilizing contextual knowledge effectively.

The ambiguous nature of knowledge, where ontology concepts may have multiple meanings depending on context.

The ever-changing environment necessitates continual updates and validation of the model.

In the same time the ability to represent situation related information and reason about it remains the major requirement for autonomous intelligent agents [7].

The recent advancements in our comprehension of cognitive mechanisms in the human mind have the potential to offer valuable insights into the realm of artificial intelligence systems. This cognitive process has evolved over millennia and stands as the most effective form of cognition known to us presently [8].

The notion of concept is foundational in our understanding of cognition. Concepts emerge from the act of categorization and identification of patterns within our mental constructs. Once established, concepts are utilized to construct predictive frameworks of the environment. Devoid of concepts, our experiential perception would be limited [9].

Concepts serve to provide meaning to our environment, enabling us to engage in rational thinking through interconnected concepts. The fluid nature of concepts entails that their meanings evolve based on the context and intentions of the user. Prototype theory is used to explain the diverse interpretations of concepts across varying scenarios [10, 11].

Concepts not only mirror tangible entities in the real world, but also extend to abstract and imaginative constructs. The capacity to manipulate abstract concepts showcases the human mind's potent ability, enabling us to transcend constraints imposed by working memory capacity and processing speed.

Hence, conceptual modeling, characterized by the proficiency in developing and reasoning with conceptual frameworks, proves to be an effective method for information representation and processing. This approach holds promise for integration into artificial intelligence systems.

According to contemporary comprehension within cognitive psychology [12], the human brain engages in the navigation and evaluation of the surrounding environment through the utilization of predictive modeling. Formerly, the concept of consciousness was depicted as a sequential progression, commencing with the perception of the environment, followed by the interpretation of data readings, the construction of a model based on said interpretations and existing knowledge, and ultimately, the process of decision-making and subsequent action.

The predictive models derive from recollections of past encounters, serving as a framework of pertinent patterns that are continuously reconstructed (updated) while considering the prevailing objectives and environmental attributes accessible through sensor data. Individuals without prior experiences are essentially deprived of such experiential knowledge and thereby struggle to comprehend their present circumstances.

The external information is perceived as alterations within the environment, which are then reconciled with the predictive model to form a cohesive entirety. Throughout this reconciliation process, the model itself may undergo modifications. Such process occurs across various levels of abstraction, beginning with overarching, fundamental principles and gradually delving into specific details.

The usage of predictive modeling yields multiple benefits, such as enhanced responsiveness to environmental and objective changes, the capacity for logical reasoning and knowledge acquisition, along with the continual adjustment of patterns based on real-world encounters. The mind persistently generates hypotheses regarding the current context and subsequently checks them against sensory input, various communication mediums, and the outcomes of logical deliberation.

The insights derived from the existing comprehension of the human cognitive process of situational awareness, which revolves around predictive modeling, could be leveraged to refine the models pertaining to situational awareness within agents operating in intelligent environments.

Predictive and anticipation computing are integral to enhancing the functionality and user experience of intelligent environments. These technologies leverage data analytics, machine learning, and artificial intelligence to create smart environments that respond proactively to user needs.

However, there's a difference between predictive and anticipatory computing [13]. Anticipatory computing involves awareness of past, present, and future, enabling proactive responses to changing conditions. This approach allows for a more dynamic and responsive intelligent environment, where systems can anticipate and adapt to various scenarios. In contrast, predictive computing focuses more on forecasting future events based on historical data. Both predictive and anticipatory computing are used in resolving multiple problems and accomplishing tasks in intelligent environments. They are integral to enhancing the functionality and user experience of intelli-

DOI 10.15588/1607-3274-2025-2-8

gent homes. These technologies use data analytics, machine learning, and artificial intelligence to create smart environments that respond proactively to user needs.

The analysis of literature shows that the application of predictive computing in intelligent environments, such as intelligent homes is happening in such areas:

– Personalized user experience involves analyzing user behavior and preferences, and smart home systems can adapt their operation to individual needs. For example, artificial intelligence algorithms can learn a user's daily routine and adjust lighting, heating, and entertainment systems accordingly. This personalization increases comfort and convenience, making homes more intuitive and responsive to the lifestyle of their residents [14–17];

– Energy management is predictive analytics and can optimize energy consumption by analyzing usage patterns. Smart devices can adjust heating and cooling systems in real time, resulting in significant energy savings and cost reductions. For example, systems can adjust settings in advance based on predicted occupancy or weather changes [17, 18];

– Predictive maintenance involves performing predictive calculations that can predict potential failures in devices and systems, allowing for proactive maintenance. By monitoring device performance and usage data, smart home systems can alert users to problems before they lead to breakdowns, thus extending the life of devices and minimizing downtime [17, 19];

– Improved security, as smart security systems use predictive analytics to detect unusual patterns that may indicate security threats. For example, AI-powered cameras can recognize familiar faces and alert homeowners to strangers, providing real-time security updates and automated responses to potential breaches [20]. Another application of machine learning and predictive analytics is risk assessment using AI. AI can analyze historical security data to identify patterns and predict future risks. This allows for more robust security protocols tailored to the specific threats a household faces [21];

– IoT integration provides predictive computing that enables seamless integration of a variety of smart devices in the home. This interconnection allows devices to exchange data and information, creating a cohesive intelligent environment that enhances user experience. For example, a smart thermostat can communicate with security systems to adjust heating when the home is empty, optimizing both comfort and energy efficiency [22].

3 MATERIALS AND METHODS

The important precondition to building knowledge-based system for intelligent agents is selecting the underlying conceptual constructs used to build the framework model. This task is crucial to the research, because on its result depend such properties of framework as expressibility, the ability to communicate and process knowledge. In our research is used the method of ontological modeling, based on formal foundational ontology.

Such an ontology provides the logically non-contradictory set of interrelated conceptual constructs which are well-grounded in reality. Foundational ontologies, such as Unified Foundational Ontology (UFO) [23], General Formal Ontology (GFO) [24] supply the basic sets of elements, the vocabulary and syntax rules to build the anticipation framework upon them. Both UFO and GFO are rich in details and are well developed.

However, the important additional requirement for a framework working with anticipated situations is the support of spatial and temporal conceptual constructs. As a foundation of our modeling framework, we have selected GFO (General Formal Ontology) which is 4d ontology [25], supporting spatial and temporal conceptualizations.

GFO is a foundational ontology that provides a systematic framework for describing forms, modes, and views of existence across different levels of abstraction and granularity. It combines methods from mathematical logic, philosophy, artificial intelligence, and linguistics.

GFO is a component of ISFO (Integrated System of Foundational Ontologies). ISFO is a part of an Integrated Framework for the Development and Application of Ontologies (IFDAO). Besides ISFO the system IFDAO includes the subsequently developed modules: a Library of Ontology Languages, and a System of Development Tools. This system of tools supports the development of domain oriented and generic ontologies.

One of the main philosophical principles of GFO is foundational ontology should allow for different, even logically inconsistent conceptualizations, reflecting the variety of perspectives in different contexts. Foundational ontology is represented as partial order if logical theories, some of which may be inconsistent with theories not situated on the same partial ordering path [26, 27]. Therefore, ISFO represents an integrated and evolutionary system of foundational ontologies.

The important part of ISFO is GOL (General Ontological Language) used to express ontological concepts and relationships [28]. It provides a formal means for defining and structuring knowledge within ontologies. GOL allows otologists to create axiomatic theories and specify the semantics of concepts. While GFO represents the foundational principles, GOL serves as the linguistic vehicle for expressing those principles. GOL enables the development of domain-specific ontologies by providing a standardized way to describe entities, properties, and their interconnections.

Let's consider the components of GFO related to the representation of changes in the state of the world, being important for modeling predictions. The existence of an object in time is described with three interrelated concepts: presential, persistent and perpetuant. Presentials are individuals which are fully present in time-point. Presential is a state of an individual in specific time moment. Persistent is a universal, which instantiates presentials. This instantiation comes in every time moment. Persistant

DOI 10.15588/1607-3274-2025-2-8

corresponds to an individual that can change and preserve its identity (it is a collection of presentials in multiple time moments. Perpetuant is an individual, instantiated by persistant and describes a specific individual which changes over time. For example, a Person is a Persistant; John is Perpetuant; John in specific time moment is Presential.

Topoid is a basic ontological category in GFO that represents a connected, bounded region of space. It is used to model spatial locations and can be thought of as a generalized spatial region that can vary in its dimensionality (e.g., points, lines, surfaces, volumes). Each topoid is characterized by its spatial extent, dimensionality and boundaries. Spatial Extent describes where entities are located.

The concept of topoid is flexible in terms of dimensionality, allowing for the representation of different kinds of spatial entities:

– 0D Topoid: a point;

– 1D Topoid: a line or curve;

– 2D Topoid: a surface or area;

– 3D Topoid: a volume or solid region.

Topoids are characterized by having clear boundaries, making them distinct from other spatial regions. Topoids play a crucial role in GFO's spatial ontology [29], providing a foundational element for representing spatial aspects of reality. They can participate in various spatial relations such as containment, adjacency, overlap, and separation. Topoids are integrated with other ontological categories in GFO, such as objects and processes, to provide a comprehensive model of reality. For example, in the case of intelligent residence topoid can represent its location and territory, the locations of specific buildings, the trajectories of moving objects.

The concept of chronoid is central to how GFO models the temporal dimension of reality. A chronoid is an ontological category that represents a connected, bounded region of time. It is used to model temporal intervals and periods, providing a way to describe when events and processes occur. A chronoid is characterized by its temporal extent and boundaries. Temporal Extent means that each chronoid occupies a definite duration in time. Boundaries allows to distinguish between different chronoids and temporal regions.

Chronoids are important in GFO's temporal ontology, allowing for the representation of time-related aspects of reality [30]. They can participate in various temporal relations such as precedence, overlap, containment, and succession. Chronoids are integrated with other ontological categories in GFO, such as objects and processes. In the context of intelligent residence chronoid, for example, could be used to represent a schedule for cleaning and maintenance.

A configuroid is an ontological category that represents structured configurations or arrangements of entities. It is used to model the specific way in which entities are organized or related to one another within a particular structure.

Configuroids have such key characteristics: Structural arrangement, Composite nature and relational properties, identifying connections between parts in the structure. Configuroids can participate in various structural relations, such as part-whole relationships, adjacency, and connectivity. In the context of intelligent home configuroid could be used to represent the structure of computer network.

However, it is important to differentiate between terms "configuration" and "configuroid". A "configuration" refers to a particular arrangement or setup of components within a system. It emphasizes the state or condition of being arranged or structured in a specific way. Configuration is state-oriented and describes the specific structure state in specific time moment. Configuration is contextual, often implying the context or circumstances under which entities are arranged. For instance, the configuration of a machine might refer to how its parts are assembled and how it operates under specific conditions. Configurations can change over time as entities are rearranged or modified.

A configuroid is an ontological category used to represent structured configurations or patterns in a more formal and abstract manner. It serves as a higher-level concept that captures the essence of structured arrangements.

In the GFO, a situoid is a concept used to represent situations or contexts [31]. It is an essential component for modeling the contextual and situational aspects of reality within ontology.

Situoids exhibit following characteristics:

– Contextual complex due to situationoids are used to capture the entire context or situation, including all relevant entities and their relationships;

– Temporal and spatial boundaries are the constraints on the situationoid in both time and space, i.e. it exists within a specific time range and spatial region;

– The dynamic nature of situationoids, as they can change over time as entities and their relationships evolve within the context.

Situoid is a unit of comprehension. Comprehension here refers to the act of understanding or grasping the meaning of something, whether it is the experience, the formation of concepts, or the recognition of objects.

In the context of situoids, comprehension plays a crucial role in making sense of the events or elements that make up a situoid. It involves considering these events or elements together in a single mental act before they can bear any meaning. Comprehension in situoids comes before inference or judgment and involves considering the events or elements as a whole, rather than focusing on individual steps or relations. Theoretical comprehension of a situoid involves being able to find a universal category that the situoid is an instance of which includes the finding of similar situoids in experiential knowledge.

DOI 10.15588/1607-3274-2025-2-8

Situoid can be defined by the goal or task and considered as a movement between two bounding situations, current and the target one. Situoids integrate with other ontological categories in GFO, such as objects, processes, topoids (spatial regions), and chronoids (temporal regions), to provide a comprehensive model of reality. Each situoid has associated topoid, chronoid and configuroid. It means that it happens in space and time and the world is undergoing structural change during its existence.

Situations are situoid configuration in specific time moments. We can consider them as slices of situoids in the time points. Situoid is bounded with situations and can have a number of situations inside. Each situation, like a situoid can be considered as a whole, but also analyzed structurally.

For example, a medical emergency in a hospital can be represented as a situoid. This situoid would include patients, doctors, nurses, medical equipment, and their relationships and interactions during the emergency. It captures the specific spatial region (e.g., an emergency room) and the temporal duration (e.g., the time during which the emergency unfolds).

The proposed framework model explores the situational dynamics with ontological models of situoids and situations using topoids, chronoids and configuroids to specify spatial, temporal and structural aspects of situations and allow to model each situation development process as a whole.

4 EXPERIMENTS

Intelligent residential community systems need predictive mechanisms and anticipative analysis to deduce and follow user needs and behavior, make decisions and plan, look for possible issues and understand their consequences. On the other hand, the software agent working in intelligent residence has a limited set of tasks and problems; its activity is constrained both in time and space, which makes the implementation and functioning of such agent less resource intensive.

We consider the anticipatory and planning framework from the perspective of intelligent agent with situational awareness, which uses it. In [32] is shown that prediction and modeling feature constitute the central function of intelligent agent. This article also proposes the structure of such an agent as a set of interacting functional modules.

Let's define the core assumptions and requirements for the anticipation and planning framework:

– The basic building blocks of this framework are provided by GFO ontology;

– The planning and modeling will be represented as situational dynamics within situoids;

– The predictions and models in framework will use experiential knowledge about situational dynamics in similar situations and situoids;

– Knowledge and modeling are organized contextually, a context being defined as specific task/goal being achieved in specific environment;

– Therefore, only relevant to context elements will be included in situation specification;

– The framework should support planning for the execution of tasks and reaching goals. But it should also allow us to model the development of situations when an agent is idle;

– Knowledge models are updated from comparison of predicted situations with real ones. The information about parameters of real state comes from the sensors;

– Framework will support different levels of granularity and specificity in planning. This will allow us to counteract the lack of information and incremental self-correcting movement towards the goal;

– It will also allow for multivariate modeling, considering different scenarios of situations development in the future;

– Historical information about past situations will be used to detect patterns and make decisions.

To understand the functioning of the proposed anticipation framework we need first to describe its place within the larger system of intelligent residential community. For the purpose of this article, we will use the simplified version of agent architecture from [32] (Fig. 1).

Sensors are in the agents, local to specific devices, placed in different parts of intelligent residential community. A separate functional module, Data Collection and Interpretation Module (DCIM) collects data from devices, interprets it according to agent's ontology and stores them in database. Using data obtained from sensors DCIM builds the Environment model which contains data about found objects and their parameters dynamics. DCIM also uses the Environment model to detect patterns in data indicating known or threatening developments to timely counteract them. Environment model is a conceptual model, storing the dynamics of objects tracked in intelligent community over time. It is represented as a temporal knowledge graph [33].

DCIM interacts with Situation modeling agent (SMA) populating the models of situations with relevant objects information. Situation modeling-agent may ask DCIM for additional information and formulate the data collection task. DCIM also performs searches in the external databases and web upon the request of SMA. Goal management module (GMM) provides the current task and intent for intelligent agent. SMA uses experiential knowledge from knowledge base and updates it in the process of learning. Contextual model is used to constrain the situation model taking into consideration the current goal and agent's environment.

DOI 10.15588/1607-3274-2025-2-8

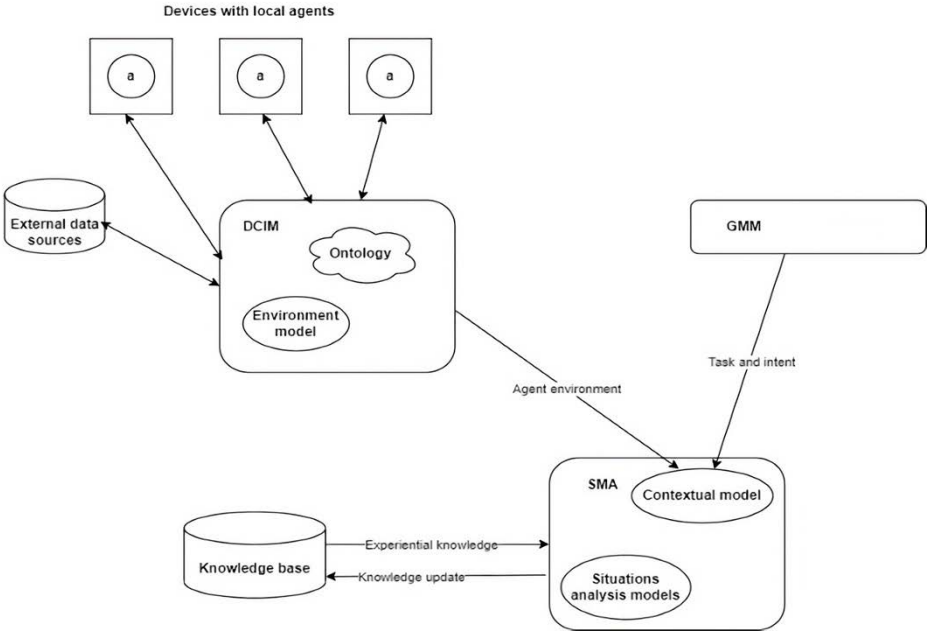

Figure 1 – The structure of intelligent residence system

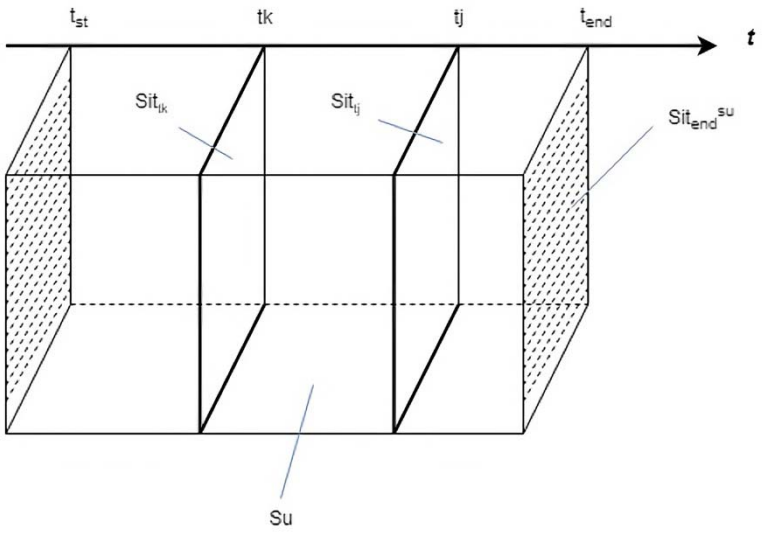

Figure 2 – The representation of situational dynamics in a situoid

5 RESULTS

Intelligent agent in every moment of time executes a task T_{sk}. This task is done in time and space, and therefore has a start t_{st} and completion moments t_{end}. Even if such an agent is doing nothing, it is aware of this and performs the observation of environment, predicting the natural changes happening in the observed environment.

Since the purpose of this article is to describe the planning and anticipation framework, we will omit the analysis of space dimension changes, described by corresponding topoid, unless it is involved in the detection of behavioral patterns in the intelligent community.

SMA can work with multiple tasks and problems in parallel. However, for the sake of simplicity we will exclude from our analysis the coordination of different tasks and focus on the predictions and planning within a single task.

Situoid GFO object is suitable for the representation of such task, because the dynamics of task execution and the prediction of future states can be represented as a sequence of situations inside the situoid. Each situoid Su is bounded by situations. The starting situation Sit_{st}^{su} corresponds to the state when the task was issued. The ending situation Sit_{end}^{su} corresponds to the state when the task is completed or abandoned. Starting and ending situations are projected onto chronoid *Ch*, in this case – a timeline, where situations are placed. Between the starting and ending situations in situoid exist a number of intermediate situations $(Sit_{t1}, Sit_{t2}, ..., Sit_{tk})$, which are also attached to the timeline (Fig. 2). Only the situations which represent

DOI 10.15588/1607-3274-2025-2-8

some interest in anticipation or planning process are considered.

Apart from task, situoid can be created to reach the specific goal or resolve the detected problem. The process of modeling situations in all cases is similar. Each situoid created is considered as a whole within the context of task execution in the current environment.

Context for the situations is provided by the current state of environment and current intent $Gl_{int,tc}$ in task executed in it. The agent's environment model $Cm_{env.tc}$ is provided by DCIM as a part of *Environment model* $Cm_{env.tc} \supseteq Cm'_{env.tc}$ for the current time t_c. Context constrains and limits the number of elements included in the model of situation to only relevant to the intention in current time moment

$$Cm_{con.tc} = (Cm'_{env.tc}, Cl_{\text{int}.tc}, t_c). \quad (1)$$

The process of task execution is modeled as a sequence of situations ($Sit_{t1,}$ $Sit_{t2,}$ …. Sit_{tn}), and corresponding sequence of configurations ($Cf_{t1,}$ $Cf_{t2,..}$ Cf_{tk}), . Each configuration in sequence is represented as knowledge graph:

$$Cf_{li} = (SV_{con}, SE_{rel}, t_i), \quad (2)$$

where SV_{con} is a set of nodes, corresponding to objects and SE_{rel} is a set of relationships used in situation specification. Both objects and relationships are classified according to the system's ontology. Specific configurations in (2) can be different, which reflects the situation configurations dynamics in the process of task execution.

Each situoid created is considered as a whole within the context of task execution. In each situoid we can specify the current situation, past situations, and the number of projected situations. All those situations are taken into account in making decisions for task execution.

Past situations are stored sparingly. They are usually linked to important events or changes in the process of task execution. Everything else in between is restored/approximated at need using available situational knowledge. The reason to preserve historical information is to be able to detect patterns in historical data, which can influence decisions and projections.

System creates only one version of the current situation. It is formed as an update of projected situation with *Environment model* data. This data introduces corrections into projected model, obtained from experiential knowledge.

However, there are multiple projected future situations. One of them describes the task completion (ending situation Sit^{su}_{end}). There are situations, specifying milestones or intermediary states placed between current and end situation. And there's the projection of the next situation, which is seen as a result of the implementation of agent intention in the dynamic environment.

As a basis for projections the experiential knowledge is used. This knowledge is stored contextually, that is a key for retrieval is context similarity. When a system looks for information in knowledge base it looks for the knowledge about the execution of similar task in similar environment. When similarity is established, the system makes a mapping between situation and knowledge pattern. In this way access to knowledge represented by patterns is provided.

Therefore, a function F_{sim} measuring the distance between the current context (1) and the key-context $(Cm^{kb}_{env}, Gl^{kb}_{\text{int}})$ from the knowledge base should be implemented. In the process of searching the value of this function should be minimized:

$$F_{sim} : ((Cm'_{env,tc}, Gl_{\text{int},tc}), (Cm^{kb}_{env}, Gl^{kb}_{\text{int}})) \to \min \quad (3)$$

Knowledge is stored in the form of loosely organized patterns. For each pattern the information about its usage conditions is provided, including exceptions, variations depending on environmental conditions. Patterns are organized as Pattern Language, where patterns are linked in larger configurations of patterns or clusters. That allows them to be used together. Patterns are formulated on higher abstraction level, so one pattern could be used for a host of similar situations with the variation of parameters.

Knowledge patterns are represented as conceptual models in the form of weighted temporal knowledge graphs. The weights in knowledge graph are used to manage importance/relevance of specific parts of graph in specific situation. The temporal dimension of graphs will help to project the application of knowledge in future and place them on the situoid's timeline.

Modeling the transitions between the situations is an essential part of predicting future situations. These transitions involve changes in parameters, produced by different causes. Transitions could be natural and happen without the agent's intervention or they can be planned, including the proactive agent actions.

We model the basic anticipation of change as two situations and change leading from one to another (Fig. 3).

The source situation $Sit_{src,ti}$ is considered as a starting point for change, the target situation $Sit_{tg,tj}$ is the ending point of change. There's no limitation on how far in time the target state is located. The sole constraint is that it should be after the source situation $t_j > t_i$. After the specification of source and target situation, the system specifies the action, process or event from its experiential knowledge which can change the source state to the target state. This action or process we will summarily designate as a plan *Pl*. This anticipation of change could be considered as a situoid *Su`* fully contained within the initial situoid $Su : Su \supseteq Su'$ It is represented as a tuple

DOI 10.15588/1607-3274-2025-2-8

$$Su' = (Sit_{src,ti}, Sit_{tg.tj}, Pl, Cm_{con}) \quad (4)$$

where Pl is a plan. In case of a situoid Su' representing the atomic change reflecting the current intention, instead of plan we specify the action Ac. Contextual information, reflecting the dependency from the environment and goal is represented by Cm_{con}.

At task creation the anticipation operation is first done between the starting and ending boundaries of situioids. The modeling system looks for processes executing similar tasks in the past. Such knowledge provides the plan, intermediary states and the confirmation of the task feasibility. Next, the situoid is split by intermediary situations using the available knowledge. In this way a plan Pl for reaching the goal, specified by the ending situation is built. This plan can be represented by a complex graph, like Gantt chart, including multiple intermediary situations.

Alternatively, a system could specify only starting and ending situations, and mark some intermediary states, without the detailed plan elaboration. This could be required in conditions of limited computational resources or reaction time, or if there are too many unknowns and random factors influencing the reaching of the goal. This is not unlike the flexible development process.

However, every time the anticipation includes consideration of basic transition between the current situation and the next situations. Such change can be envisioned as the result of the natural course of events (all changes are produced by natural causes, no action from agent is done) or some specific set of external events, or some actions performed by intelligent agent. A modeling system can create and analyze several future situations, compare them and select the most appropriate course of actions for agent.

The changes between the situations can be represented as transitions between points in multi-dimensional space of object parameters in conceptual space [34]. They can be also specified as changes in configurations between situations, highlighting the configurational dynamics. In the process of projecting and planning it could be useful to track trajectories of parameter changes. In the proposed framework we envisage such trajectories:

– A trajectory for a specific object or its parameters involves changing the parameters (configurations) of the object or its connections between several intermediate situations. For example, such a trajectory can reflect the movement of a person on a campus;

– A situation trajectory considers the situation as a single whole, as a holistic model. A situation trajectory tracks changes between situations and is used to predict multivariate development of situations within a single situationoid. It is necessary to develop several situation trajectories in order to adapt to possible external events that occur and to create contingency plans. Another use case for multivariate situation analysis is to predict and compare the consequences of the actions of different agents (Fig. 4);

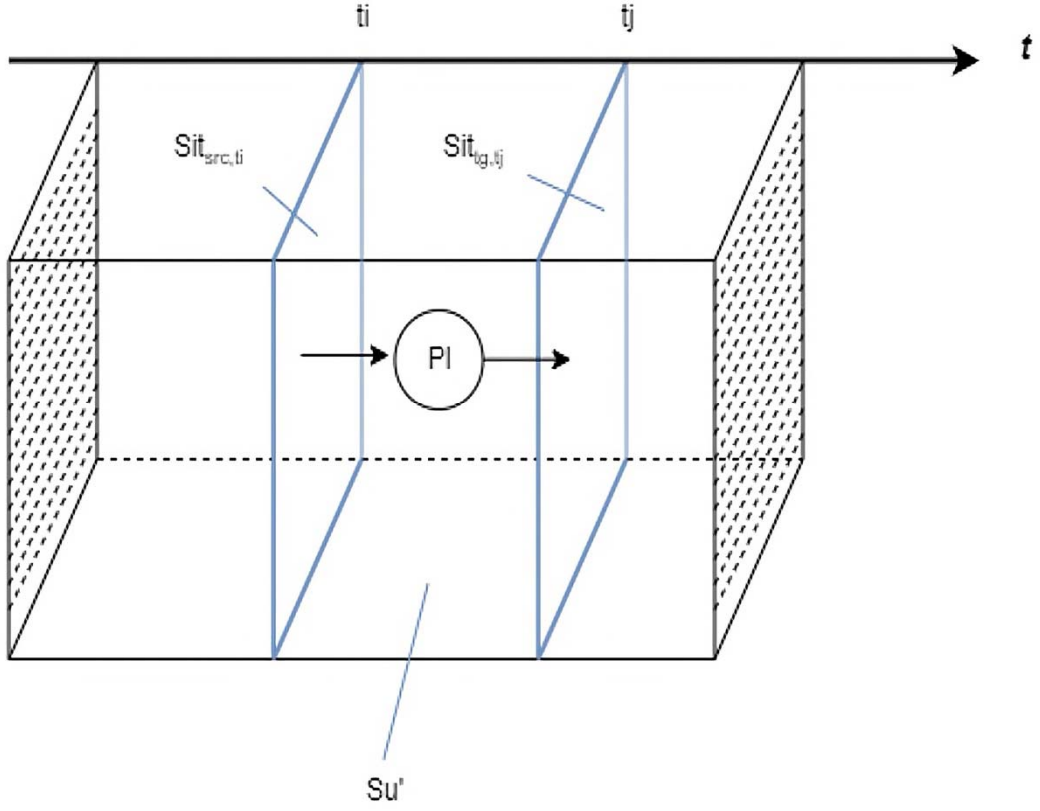

Figure 3 – Modeling changes between situations

DOI 10.15588/1607-3274-2025-2-8

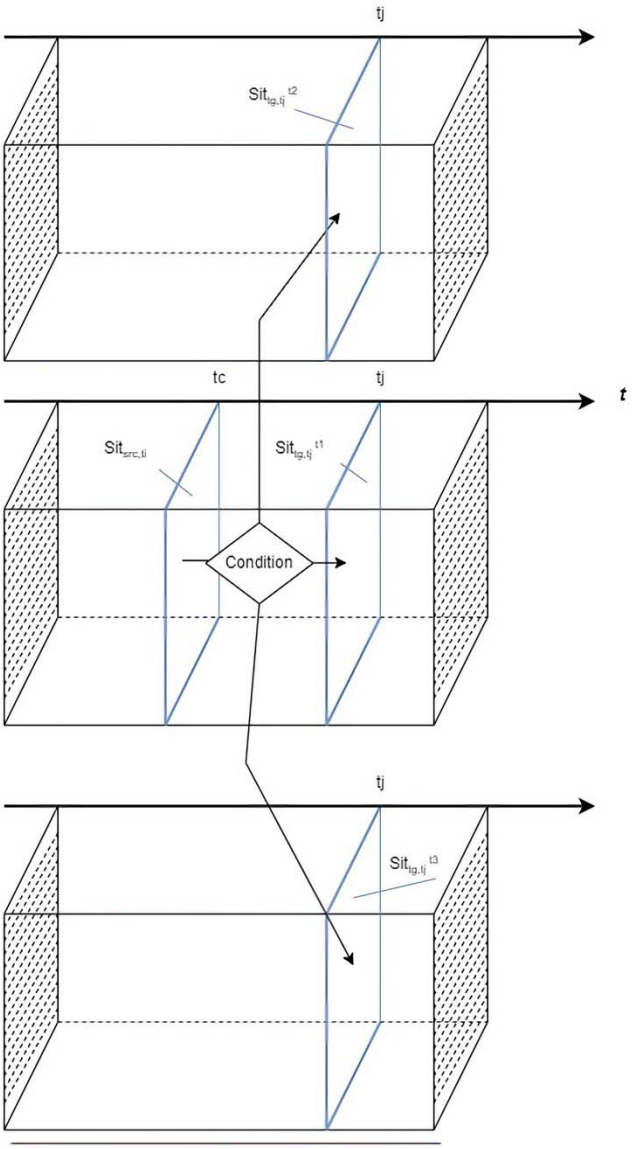

Figure 4 – Multivariate situation analysis with situation trajectories

– A situationoid trajectory is used when the execution of a task generates other tasks that are not related to or are not contained in the parent task and situationoid. In this case, the agent operates on dependent projects and tasks, each represented in its own situationoid.

The system builds several anticipation models and gains useful information when comparing them. The first such model is the Observer model. It implies no actions from the intelligent agent, just following the natural flow of events. What will happen if nothing is done. Another model is the Intention model, representing the result of immediate agent's action. What will be the expected result of such an action? Intention models are always built before an actual action is done, to anticipate the action's consequences and outcomes. Long-term planning models have intermediary situations and goals. They are often not specified in detail at start and are modified during the task execution.

The current situation model is built based on the anticipated model. This model is updated using data from Environment model provided by DCIM. In this operation only differences between anticipated configuration and real configuration are passed from DCIM. This allows us to reduce data traffic and increase performance (Fig. 5).

Next, the system defines the Intention model Sit_{tg} for the next situation and looks in knowledge base for possible actions leading to this situation. In this stage several models $SSit_{tg} = \{Sit_{tg}\}$ can be built including the *Observer model* or different variants of Intention models using different actions. The consequences of such actions are projected in the form of situation trajectories. Next, the most effective and efficient action variant is chosen and implemented using selection function F_{sel} and selection criteria Cr:

$$F_{sel} : (SSit_{tg}, Cr) \rightarrow \min \qquad (5)$$

DOI 10.15588/1607-3274-2025-2-8

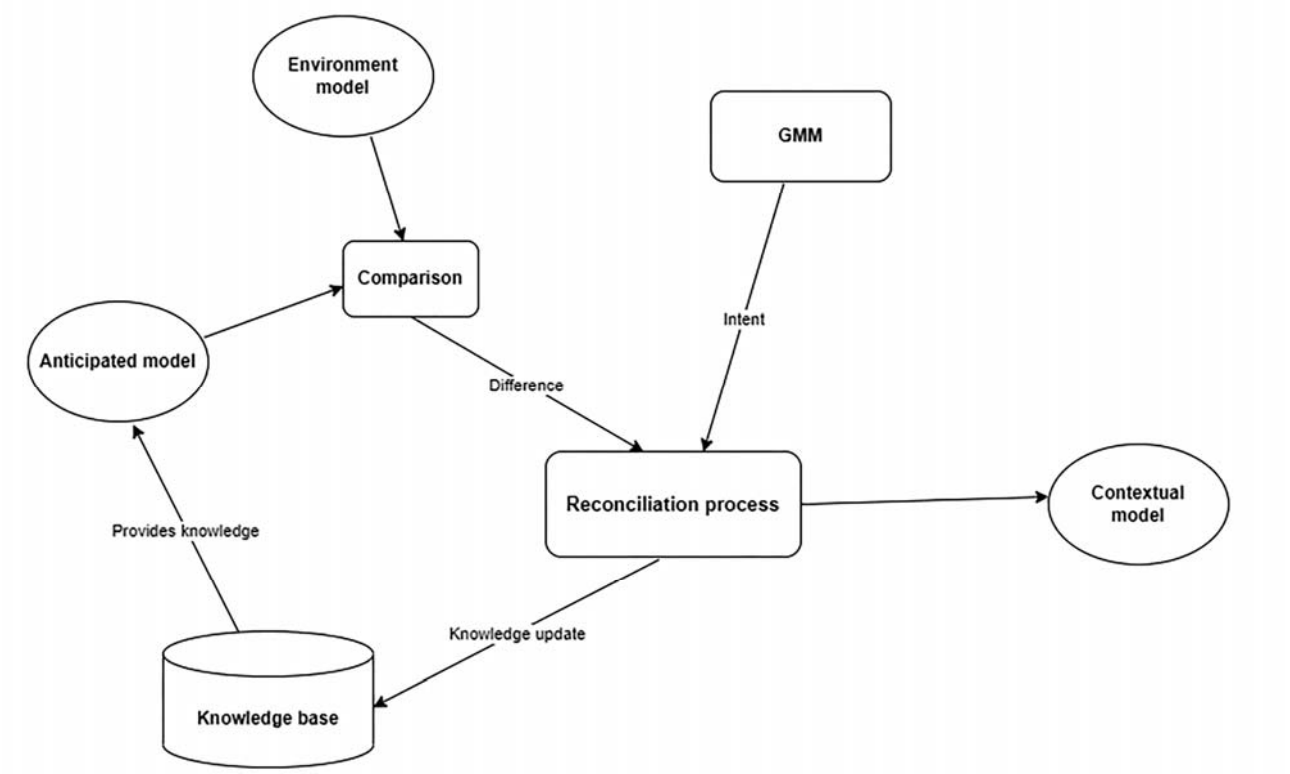

Figure 5 – Updating model with feedback from real-world data

The result of actions is tested observing the changes in Environment model. Errors and deviations from the expected results are noted and corresponding corrective actions are planned, changing the future situation projections.

The differences between the built projections and the real-world data are evaluated and, in case if they cannot be compensated by simple change of parameters of patterns used for anticipation, the patterns are updated, or new pattern is created in knowledge base for the current context. Thus, the intelligent system constantly reconciliates its knowledge base patterns with the real-world feedback and updates its knowledge (Fig. 5).

Let's consider an example of real-world efficiency evaluation for the application of proposed framework for the reasoning about security in larger residential community. The environment is monitored using a variety of sensors, embedded in surveillance cameras, movement detectors, temperature sensors. System should detect and generate the sequence of actions for intruder detection, device malfunction or fire.

Let current context $Cm_{con,tc}$ in time moment t_c, obtained from the sensor supplied data be:

– Movement sensors: detected movement in parking area;

– Survellance cameras: unrecognized person detected;

– Temperature sensors: data are within the normal range.

Knowledge base Knb contains previously detected situations:

– Sit_1 – usual activity (community members are in the parking);

– Sit_2 – anomaly (intruder detected in the parking);

– Sit_3 – fire (detected by abnormal rise of temperature);

– Sit_4 – sensor malfunction.

Similarity function F_{sim} compares the current context to the situations in the knowledge base. Prior to using this function current context specification $Cm_{con,tc}$ should be transformed into vector form (using numerical encoding of parameters). Next, F_{sim} is calculated using the selected similarity metric (such as cosine similarity (6) or Euclidean distance).

$$F_{sim} = \frac{\sum_{i=1}^{n} Cm_i \; Sit_i}{\sqrt{\sum_{i=1}^{n} Cm_i^2} \; \sqrt{\sum_{i=1}^{n} Sit_i^2}}. \qquad (6)$$

The results of similarity function calculations are:

– $F_{sim}\left(Cm_{con,tc},\ Sit_1\right) = 0.45$ (low similarity);

– $F_{sim}\left(Cm_{con,tc},\ Sit_2\right) = 0.85$ (high similarity);

– $F_{sim}\left(Cm_{con,tc},\ Sit_3\right) = 0.25$;

– $F_{sim}\left(Cm_{con,tc},\ Sit_4\right) = 0.30$.

DOI 10.15588/1607-3274-2025-2-8

Selecting the situation with the highest similarity function value, the system concludes that intruder is detected. As a result, system activates the security protocol for situation Sit_2, consisting of such actions as security personnel alerting, focusing additional cameras on the intruder and tracking his movement, switching on additional movement sensors.

The system anticipates several possible developments of the situation. For example, if security staff arrives current context reverts to usual activity (Sit_1). After the end of incident situoid, the system stores the data about the incident in knowledge base and updates the parameters of similarity function for better detection in the future.

For the evaluation of efficiency of research problem solutions following metrics are used:

1. The accuracy of situation detection is calculated by comparing the number of correctly identified situations TP to all possible situations:

$$Accuracy = \frac{TP + TN}{TP + TN + FP + FN}. \quad (7)$$

For example, if $TP = 85, FP = 5, FN = 10$, the accuracy is 0.85.

2. Response time. Average time for detecting the situation and implementing a corresponding security protocol.

$$T_{responce} = T_{analysis} + T_{action}. \quad (8)$$

For example, if $T_{analysis}$ is 0.5 s and T_{action} is 2.5s. $T_{responce} = 3s$.

Similarity of contexts measure is calculated using formula (6). For example, if current context $Cm_{con,tc}$ is represented by vector [0.8, 0.6,0.9], and Sit_2 – by vector [0.7,0.6,1.0], then using (6) we obtain $F_{sim}\left(Cm_{con,tc}, Sit_2\right) = 0.91$ which reflects a high similarity level.

3. Precision – the probability of making correct actions after the situation detection.

$$P_{recision} = \frac{TP}{TP + FP}. \quad (9)$$

For example, if $TP = 85$ and $FP = 5$, then $P_{recision} = 0.944$. With those quantitative metrics the user can reveal the strengths and weaknesses of proposed framework implementation and specify areas for improvement.

6 DISCUSSION

The ability to anticipate the future based on previous experience is one of the main features of intelligence. Humans are proficient in building multiple models of future events, comparing and analyzing them to select the best course of action. In the process of such modeling the results are compared to real-world data, experiential models and patterns are updated and learning occurs.

Intelligent agents should also implement the ability of anticipation and planning to become fully autonomous and capable of rational decision-making in real-world situations. For example, intelligent security systems can use predictions and experiential knowledge analysis to detect unusual behavior patterns of visitors, responding in real time to threats and learning new threats patterns.

The intended usage of the proposed framework is in combination with knowledge graph based reasoning and ontological modeling.

Compared to other methods and frameworks which can be used to build goal-driven intelligent agents the proposed framework offers several substantial advantages.

Classical STRIPS (Stanford Research Institute Problem Solver) [35] method is working in deterministic environments and does not implement learning. It also lacks an ontological foundation.

BDI (Beliefs, Desires, Intentions) framework [36], which is used to model goal-driven behavior of intelligent agents, is general, it does not focus on situational dynamics.

In recent years intelligent agents are increasingly using a variety of neuronal networks methods to acquire and process knowledge. The proposed network offers the explainability advantage when compared to them.

Situational calculus [37] is modeling the situations and transitions between them. However, it lacks modeling support for temporal, configurational and spatial data and ontological foundation. The usage of topoid, chronoid, configuroid constructs in proposed framework enhances the expressivity of the developed model.

The proposed framework operates with situations as basic units of analysis and predictions tracking and anticipating changes between situations. Situations are represented as knowledge graphs with elements relevant to current context. This context is defined by the current state of environment and intention of intelligent agent. Situations are anticipated using experiential knowledge about changes in similar context in the past, stored in the form of patterns in knowledge base. Knowledge patterns are updated in the process of reconciliation with real-world data, collected from sensors and external knowledge providers.

Situations are described using GFO which is a rich 4d ontology providing the ability to model the temporal, spatial and configurational evolutions of situations. Situoid element from GFO was chosen to represent the bounded situation evolution corresponding to the process of accomplishment of a task or a goal or just modeling the natural course of events. Situoid represents the unit of comprehension and is considered as a whole. The basic anticipation is represented by two consecutive situations and the specification of event/actions leading to change from one situation to another. The framework allows to track and analyze the change trajectories for specific ob-

DOI 10.15588/1607-3274-2025-2-8

jects, situations or situoids over time or contingent to specific conditions.

The proposed framework has the following advantages:

– It is based on the GFO ontology, which provides a logically coherent set of concepts and allows modeling spatial, temporal, and structural data.

– Supports predictions with different levels of specificity. They range from a very detailed specification of the implementation of an intention leading to the next situation to a high-level description of the future situation with a small set of conditions. This allows us to work with incomplete information in an unstable environment, when the exact path leading to the expected situation is not yet known. For example, in the security domain, a situation can be defined in general terms as an unauthorized access of a person to a restricted area, without specifying how exactly this is done.

– Prediction and modeling of change trajectories allows the system to build and compare the impact of several courses of action, which forms the basis for making a decision on the desired course of action. In addition, typical trajectories can become templates stored in a knowledge base, and the system will be able to justify these templates at a higher level of abstraction.

– The system uses knowledge from experience, which can be obtained and improved by studying real data. In the learning process, the system finds typical configurations – templates and their dependencies, abstracting from a lot of irrelevant details and finding the most important properties of situations. For example, the system can find typical behavior of end users in intelligent communities. In addition, it can identify dangerous behavior and take timely measures.

Among the drawbacks of proposed framework, we can cite the high level of generality and abstraction, which on one hand can lead to difficulties of building real-world systems based on it, but on the other makes it applicable to the large set of intelligent systems. Moreover, the representation and management of experiential, contextual knowledge requires further research and is a separate complex problem. Also, knowledge reconciliation with real-world data process is described only conceptually and requires development in future research.

Nevertheless, the authors hope that proposed framework will be useful in modeling anticipation functionality in intelligent environment and can form the basis for future research, leading to the implementation of intelligent environments capable of situation anticipation and analysis using experiential knowledge.

CONCLUSIONS

Representing and modeling the situation dynamics and anticipating the changes is an important feature of autonomous intelligent agent and a challenging task to implement.

The scientific novelty of obtained results is in the development of framework allowing to represent, model and reason about situation dynamics in the intelligent environment, such as intelligent residential community. The proposed framework is based on GFO ontology, which provides a coherent set of conceptual constructs and logical tools to reason about them. Framework allows to model different trajectories of situation development, compare and reason about them. It is also suitable for representing situations with different levels of specificity.

The practical significance of obtained results is that the proposed framework can be applied in intelligent environments, such as intelligent homes, communities, surveillance systems, built using autonomous intelligent agents to represent, anticipate and model the situation dynamics, select the preferred course of actions.

Prospects for further research include the elaboration of contextual knowledge storing and processing, reconciliation and learning procedures based on real-world feedback and the application of proposed framework in the real-world system, such as intelligent security systems.

ACKNOWLEDGEMENTS

The research was conducted in the Information Systems and Network department of Lviv Polytechnic National University. The practical implementation aspects or the research become possible with the support of internet and security solutions company Astra-Lviv (https://astra.in.ua/) .

REFERENCES

1. Augusto J., Callaghan V., Cook D, Kameas A., Satoh I. Intelligent Environments: A Manifesto, *Human-Centric Computing and Information Sciences*, 2013, Vol. 3, pp. 1–18. DOI: 10.1186/2192-1962-3-12.
2. Burzagli L., Pier L., Antona M, Stephanidis C. Intelligent Environments for All: A Path towards Technology-Enhanced Human Well-Being, *Universal Access in the Information Society*, 2022, pp. 1–20.
3. Deshmukh A, Patil D, Pawar P., Kumari S., Muthulakshmi P. Recent Trends for Smart Environments With AI and IoT-Based Technologies: A Comprehensive Review, *Handbook of Research on Quantum Computing for Smart Environments*, 2023, pp. 435–452. DOI: 10.4018/978-1-6684-6697-1.ch023.
4. Machado Pernas A., Augustin, L., Thom, L., Oliveira J. Situation-awareness as a key for proactive actions in ambient assisted living, *Proceedings of the 15th International Conference on Enterprise Information Systems, Angers, France, 4–7 July, 2013.* Angers, 2013, Vol. 2, pp. 418–426.
5. Wang P., Yuan Y., Jia L., Guan X. Intelligent situation awareness based on the fractal dimension and multidimensional reconstruction, *Advanced Theory and Simulations*, 2024, Vol. 7, No. 4, P. 2300949. DOI: 10.1002/adts.202300949.
6. Blasch E. Data fusion information group (DFIG) model meets AI+ ML, P*roceedings of the International Conference on Signal Processing, Sensor: Information Fusion, and Target Recognition XXXI, SPIE, 3–7 April 2022, Orlando, Florida, USA and 6–12 June 202*2. Orlando, 2022, Vol. 12122, pp. 162–171.

DOI 10.15588/1607-3274-2025-2-8

7. Kwok K., Virdi S. Ai-based situation awareness assessment, *Journal of Physics: Conference Series, IOP Publishing*, 2022, P. 012011.
8. Ye F. Concepts and Conceptual Representation. *Studies in No-Self Physicalism*. Singapore, Springer, 2023, pp. 103–188. DOI:10.1007/978-981-19-8143-2_3.
9. Barrett L. How Emotions Are Made: The Secret Life of the Brain, Mar. 2017. [Online]. Available: https://www.semanticscholar.org/paper/How-Emotions-Are-Made%3A-The-Secret-Life-of-the-Brain-Barrett/b54f2fd56ec084aa8e1a3b05dd24d93 ecd5c94 5a
10. Marika C., Inhoff L., Libby A, Noguchi T, Bradley L., Ranganath C. Dynamic integration of conceptual information during learning, *PLOS ONE*, 2018, Vol. 13, No. 11, pp. 152–161. DOI: 10.1371/JOURNAL.PONE.0207357.
11. Cuper A., Cuper-Ferrigno M. A. Few Remarks on Prototype Theory in Cognitive Linguistics, *Language Culture Politics International Journal*, 2021, Vol. 1, pp. 57–67. DOI: 10.54515/lcp.2021.1.57-67.
12. Clark A. Whatever next? Predictive brains, situated agents, and the future of cognitive science, *Behavioral and brain sciences*, 2013, Vol. 36, No. 3, pp. 181–204. DOI: 10.1017/S0140525X12000477.
13. Nadin M. Anticipation and computation: Is anticipatory computing possible?, *Anticipation across disciplines*, 2016, pp. 283–339. DOI: 10.1007/978-3-319-22599-9_18.
14. Vieira A. Predicting online user behaviour using deep learning algorithms, *arXiv*, 2015. URL: https://www.preprint arXiv:1511.06247.
15. Martín A., Fernández-Isabel A., Martín de Diego I., Beltrán M. A survey for user behavior analysis based on machine learning techniques: current models and applications, *Applied Intelligence*, 2021, Vol. 51, No. 8, pp. 6029–6055. DOI: 10.1007/s10489-020-02160-x.
16. Ranjan R., Kumar S. User behaviour analysis using data analytics and machine learning to predict malicious user versus legitimate user, *High-Confidence Computing*, 2022, Vol. 2, No. 1, P. 100034. DOI: 10.1016/j.hcc.2021.100034.
17. Sarker I., Furhad M., Nowrozy R. Ai-driven cybersecurity: an overview, security intelligence modeling and research directions, *SN Computer Science*, 2021, Vol. 2, No. 3, P. 173. DOI: 10.1007/s42979-021-00557-0.
18. Saini J., Arora A., Kamboj S. Prediction of smart building and smart city resources using AI-techniques, *2nd International Conference for Innovation in Technology (INOCON), IEEE*, 2023, pp. 1–5.
19. Carneiro D., Amaral A., Carvalho M., Barreto L. An anthropocentric and enhanced predictive approach to smart city management, *Smart Cities*, 2021, Vol. 4, No. 4, pp. 1366–1390. DOI: 10.3390/smartcities4040072.
20. Pech M., Vrchota J., Bednář J. Predictive maintenance and intelligent sensors in smart factory, *Sensors*, 2021, Vol. 21, No. 4, P. 1470. DOI: 10.3390/s21041470.
21. Rahim A, Zhong Y., Ahmad S., Pławiak P., Hammad M. Enhancing smart home security: anomaly detection and face recognition in smart home IoT devices using logit-boosted CNN models, *Sensors*, 2023, Vol. 23, No. 15, pp. 69–79. DOI: 10.3390/s23156979.
22. Kalogiannidis S., Kalfas D., Papaevangelou O., Giannarakis G., Chatzitheodoridis F. The Role of Artificial Intelligence Technology in Predictive Risk Assessment for Business Continuity: A Case Study of Greece, *Risks*, 2024, Vol. 12, No. 2, P. 19. DOI: 10.3390/risks12020019.
23. UFO community portal. – https://ontouml.org/ufo/
24. Herre H. General Formal Ontology (GFO): A foundational ontology for conceptual modeling, *Theory and applications of ontology: computer applications*. Leipzig, Springer, 2010, pp. 297–345.
25. Loebe F., Burek P., Herre H. GFO: The General Formal Ontology, *Applied Ontology*, 2022, Vol. 17, No. 1, pp. 71–106. DOI: 10.3233/AO-220264.
26. Niles I., Pease A. Towards a standard upper ontology, *Formal Ontology in Information Systems: Collected Papers from the Second International Conference*. New York, ACM Press, 2001, pp. 2–9.
27. Burek P., Loebe F., Herre H. Towards GFO 2.0: Architecture, Modules and Applications. Amsterdam, IOS Press, 2020, pp. 32–45
28. Degen W., Heller B., Herre H., Smith B. Gol: A General Ontological Language, *Formal Ontology in Information Systems (FOIS)*. New York: ACM Press, 2001, pp. 34–46.
29. Baumann R., Loebe F, Herre H. Towards an Ontology of Space for GFO. Amsterdam, IOS Press, 2016, pp. 53–66.
30. Baumann R., Loebe F., Herre H. Axiomatic Theories of the Ontology of Time in GFO, *Applied Ontology*, 2014, Vol. 9, No. 3–4, pp. 171–215. DOI:10.3233/AO-140136
31. Hoehndorf R. Situoid Theory, *Proceedings of the International Conference on Ontologies and Semantic Technologies*, 2005, pp. 23–34. DOI: 10.1234/ontologies.st.2005.0123..
32. Burov Y. Goal-driven Situation Awareness Process Based on Predictive Modeling, *COLINS-2024: 8th International Conference on Computational Linguistics and Intelligent Systems, April 12–13, 2024*. Lviv, 2024, pp. 157–168.
33. Pan S., Cambria E., Marttinen P. Pan S, Cambria E, Marttinen P, Philip S., Philip S. A survey on knowledge graphs: Representation, acquisition, and applications, *IEEE transactions on neural networks and learning systems*, 2021, Vol. 33, No. 2, pp. 494–514. DOI: 10.1109/TNNLS.2021.3070843.
34. Gärdenfors P., Warglien M. Using conceptual spaces to model actions and events, *Journal of semantics*, 2012, Vol. 29, No. 4, pp. 487–519. DOI: 10.1093/jos/ffs007.
35. Artificial Intelligence Planning with STRIPS, A Gentle Introduction | Primary Objects. [Online]. Available: https://www.primaryobjects.com/2015/11/06/artificial-intelligence-planning-with-strips-a-gentle-introduction/
36. Stringer, P., Cardoso R, Huang X, Dennis L. Adaptable and Verifiable BDI Reasoning, *Electronic Proceedings in Theoretical Computer Science*, 2020, 319, pp. 117–25, DOI:doi.org/10.4204/EPTCS.319.9.
37. Paraskevas, A. A Note on Situation Calculus, *Uncertainty Discourse and Applications 1*, 2024, No. 1, pp. 66–72.

Received 10.10.2024.
Accepted 19.04.2025.

DOI 10.15588/1607-3274-2025-2-8

УДК 004.88

ФРЕЙМВОРК ДЛЯ ПЕРЕДБАЧЕННЯ СИТУАЦІЙ ТА ПЛАНУВАННЯ В ІНТЕЛЕКТУАЛЬНИХ СЕРЕДОВИЩАХ

Буров Є. В. – д-р техн. наук, професор, професор кафедри інформаційних систем та мереж Національний університет «Львівська політехніка», Львів, Україна.
Жовнір Ю. І. – аспірант кафедри інформаційних систем і мереж НУ «Львівська політехніка», Львів, Україна.
Захарія О. В. – аспірант кафедри інформаційних систем і мереж НУ «Львівська політехніка», Львів, Україна.
Кунанець Н. Е. – д-р наук із соціальних комунікацій, професор, професор кафедри інформаційних систем та мереж НУ «Львівська політехніка», Львів, Україна.

АНОТАЦІЯ

Актуальність. Передбачення, прогнозування та планування ситуації відіграють важливу роль у інтелектуальних середовищах, дозволяючи вивчати та прогнозувати поведінку своїх користувачів, передбачати потреби в обслуговуванні та забезпеченні ресурсами. Об'єктом дослідження є процес моделювання ситуації, передбачення і планування в ситуаційно-обізнаних системах.

Мета роботи. Метою роботи є розробка та аналіз онтологічного фреймворку для моделювання та прогнозування динаміки змін ситуації для інтелектуальних агентів, що дозволяє реалізувати проактивну поведінку агентів.

Метод. У цій статті запропонована основа для передбачення та планування на основі онтології GFO. Кожна задача або задача розглядається як ситуоїд, що має ряд проміжних ситуацій. Фреймворк орієнтований на аналіз змін між ситуаціями, спричинених передбаченими діями або подіями. Контекстуально організована база знань використовується для отримання інформації про можливі сценарії розвитку подій і використовується для планування та оцінки. Фреймворк дозволяє будувати і порівнювати траєкторії зміни конфігурацій для конкретних об'єктів, ситуацій або ситуоїдів. Процес планування і передбачення працює в умовах неповної інформації і непередбачуваних зовнішніх подій, тому що прогнози постійно оновлюються за допомогою зворотного зв'язку від даних сенсорів і звірки цієї інформації з прогнозованою моделлю.

Результати. Фреймворк для міркування та планування ситуацій на основі онтології GFO, що дозволяє моделювати просторові, часові та структурні залежності даних.

Висновки. Фреймворк передбачення ситуації дозволяє подавати, моделювати та обґрунтовувати динаміку ситуації в інтелектуальному середовищі, наприклад, у розумному житловому будинку. Перспективи подальших досліджень включають розробку процедур зберігання та опрацювання контекстних знань, узгодження та навчання на основі зворотного зв'язку в реальних умовах та застосування запропонованого фреймворку реальних системах, таких як інтелектуальні системи безпеки.

КЛЮЧОВІ СЛОВА: GFO, ситуаційна обізнаність, передбачення, ситуаційний аналіз, ситуоїд.

ЛІТЕРАТУРА

1. Intelligent Environments: A Manifesto / [J. Augusto, V. Callaghan, D. Cook et al.] // Human-Centric Computing and Information Sciences. – 2013. – Vol. 3. – P. 1–18. DOI: 10.1186/2192-1962-3-12.
2. Intelligent Environments for All: A Path towards Technology-Enhanced Human Well-Being / [L. Burzagli, L. Pier, M. Antona, C. Stephanidis] // Universal Access in the Information Society. – 2022. –P. 1–20.
3. Trends for Smart Environments With AI and IoT-Based Technologies: A Comprehensive Review / [A. Deshmukh, D. Patil, P. Pawar et al.] // Handbook of Research on Quantum Computing for Smart Environments. – 2023. – P. 435–452. DOI: 10.4018/978-1-6684-6697-1.ch023.
4. Situation-awareness as a key for proactive actions in ambient assisted living / [A. Machado Pernas, L. Augustin, L. Thom, J. Oliveira] // Proceedings of the 15th International Conference on Enterprise Information Systems, Angers, France, 4–7 July, 2013. – Angers, 2013. – Vol. 2. – P. 418–426.
5. Intelligent situation awareness based on the fractal dimension and multidimensional reconstruction / [P. Wang, Y. Yuan, L. Jia, X. Guan] // Advanced Theory and Simulations. – 2024. – Vol. 7, No. 4. – P. 2300949. DOI: 10.1002/adts.202300949.
6. Blasch E. Data fusion information group (DFIG) model meets AI+ ML / E. Blasch // Proceedings of the International Conference on Signal Processing, Sensor: Information Fusion, and Target Recognition XXXI, SPIE, 3–7 April 2022, Orlando, Florida, USA and 6–12 June 2022. – Orlando, 2022. – Vol. 12122. – P. 162–171.
7. Kwok K. Ai-based situation awareness assessment / K. Kwok, S. Virdi // Journal of Physics: Conference Series, IOP Publishing. – 2022. – P. 012011.
8. Ye F. Concepts and Conceptual Representation / F. Ye // Studies in No-Self Physicalism. – Singapore: Springer, 2023. – P. 103–188. DOI:10.1007/978-981-19-8143-2_3.
9. Barrett L. How Emotions Are Made: The Secret Life of the Brain, Mar. 2017. [Online] / L. Barrett. – Available: https://www.semanticscholar.org/paper/How-Emotions-Are-Made%3A-The-Secret-Life-of-the-Brain-Barrett/b54f2fd56ec084aa8e1a3b05dd24d93 ecd5c94 5a
10. Dynamic integration of conceptual information during learning / [C. Marika, L. Inhoff, A. Libby] // PLOS ONE. – 2018. – Vol. 13, No. 11. – P. 152–161. DOI: 10.1371/JOURNAL.PONE.0207357.
11. Cuper A. Few Remarks on Prototype Theory in Cognitive Linguistics / A. Cuper, M. A. Cuper-Ferrigno // Language Culture Politics International Journal. – 2021. – Vol. 1. – P. 57–67. DOI: 10.54515/lcp.2021.1.57-67.

DOI 10.15588/1607-3274-2025-2-8

12. Clark A. Whatever next? Predictive brains, situated agents, and the future of cognitive science / A. Clark // Behavioral and brain sciences. – 2013. – Vol. 36, No. 3. – P. 181–204. DOI: 10.1017/S0140525X12000477.
13. Nadin M. Anticipation and computation: Is anticipatory computing possible? / M. Nadin // Anticipation across disciplines. – 2016. – P. 283–339. DOI: 10.1007/978-3-319-22599-9_18.
14. Vieira A. Predicting online user behaviour using deep learning algorithms / A. Vieira // arXiv. – 2015. – URL: https://www.preprint arXiv:1511.06247.
15. A survey for user behavior analysis based on machine learning techniques: current models and applications / [A. Martín, A. Fernández-Isabel, I. Martín de Diego, M. Beltrán] // Applied Intelligence. – 2021. – Vol. 51, No. 8. – P. 6029–6055. DOI: 10.1007/s10489-020-02160-x.
16. Ranjan R. User behaviour analysis using data analytics and machine learning to predict malicious user versus legitimate user / R. Ranjan, S. Kumar //High-Confidence Computing. – 2022. – Vol. 2, No. 1. – P. 100034. DOI: 10.1016/j.hcc.2021.100034.
17. Sarker I. Ai-driven cybersecurity: an overview, security intelligence modeling and research directions / I. Sarker, M. Furhad, R. Nowrozy // SN Computer Science. – 2021. – vol. 2, No. 3. – P. 173. DOI: 10.1007/s42979-021-00557-0.
18. Saini J. Prediction of smart building and smart city resources using AI-techniques / J. Saini, A. Arora, S. Kamboj // 2nd International Conference for Innovation in Technology (INOCON), IEEE. – 2023. – P. 1–5.
19. An anthropocentric and enhanced predictive approach to smart city management / [D. Carneiro, A. Amaral, M. Carvalho, L. Barreto] // Smart Cities. – 2021. – Vol. 4, No. 4. – P. 1366–1390. DOI: 10.3390/smartcities4040072.
20. Pech M. Predictive maintenance and intelligent sensors in smart factory / M. Pech, J. Vrchota, J. Bednář // Sensors. – 2021. – Vol. 21, No. 4. – P. 1470. DOI: 10.3390/s21041470.
21. Enhancing smart home security: anomaly detection and face recognition in smart home IoT devices using logit-boosted CNN models / [A. Rahim, Y. Zhong, S. Ahmad et al.] // Sensors. – 2023. – Vol. 23, No. 15. – P. 69–79. – DOI: 10.3390/s23156979.
22. The Role of Artificial Intelligence Technology in Predictive Risk Assessment for Business Continuity: A Case Study of Greece / [S. Kalogiannidis, D. Kalfas, O. Papaevangelou et al.] // Risks. – 2024. – Vol. 12, No. 2. – P. 19. DOI: 10.3390/risks12020019.
23. UFO community portal. – https://ontouml.org/ufo/
24. Herre H. General Formal Ontology (GFO): A foundational ontology for conceptual modelling / H. Herre // Theory and applications of ontology: computer applications. – Leipzig : Springer. – 2010. –P. 297–345.
25. Loebe F. GFO: The General Formal Ontology / F. Loebe, P. Burek, H. Herre // Applied Ontology. – 2022. – Vol. 17, No. 1. – P. 71–106. DOI: 10.3233/AO-220264.
26. Niles I. Towards a standard upper ontology / I. Niles, A. Pease // Formal Ontology in Information Systems: Collected Papers from the Second International Conference. – New York : ACM Press, 2001. – P. 2–9.
27. Burek P. Towards GFO 2.0: Architecture, Modules and Applications / P. Burek, F. Loebe, H. Herre. – Amsterdam : IOS Press, 2020. – P. 32–45
28. Gol: A General Ontological Language / [W. Degen, B. Heller, H. Herre, B. Smith] // Formal Ontology in Information Systems (FOIS). – New York : ACM Press, 2001. – P. 34–46.
29. Baumann R. Towards an Ontology of Space for GFO / R. Baumann, F. Loebe, H. Herre. – Amsterdam : IOS Press, 2016. – P. 53–66.
30. Baumann R. Axiomatic Theories of the Ontology of Time in GFO / R. Baumann, F. Loebe, H. Herre // Applied Ontology. – 2014. – Vol. 9, No. 3–4. – P. 171–215. DOI:10.3233/AO-140136
31. Hoehndorf, R. Situoid Theory / R. Hoehndorf // Proceedings of the International Conference on Ontologies and Semantic Technologies. – 2005. – P. 23–34. DOI: 10.1234/ontologies.st.2005.0123..
32. Burov Y. Goal-driven Situation Awareness Process Based on Predictive Modeling / Y. Burov // COLINS-2024: 8th International Conference on Computational Linguistics and Intelligent Systems, April 12–13, 2024, Lviv. – 2024. – P. 157–168.
33. A survey on knowledge graphs: Representation, acquisition, and applications / [S. Pan, E. Cambria, P. Marttinen et al.] // IEEE transactions on neural networks and learning systems. –2021. – Vol. 33, No. 2. – P. 494–514. DOI: 10.1109/TNNLS.2021.3070843.
34. Gärdenfors P. Using conceptual spaces to model actions and events / P. Gärdenfors, M. Warglien // Journal of semantics. – 2012. – Vol. 29, No. 4. – P. 487–519. DOI: 10.1093/jos/ffs007.
35. Artificial Intelligence Planning with STRIPS, A Gentle Introduction | Primary Objects. [Online]. – Available: https://www.primaryobjects.com/2015/11/06/artificial-intelligence-planning-with-strips-a-gentle-introduction/
36. Adaptable and Verifiable BDI Reasoning / [P. Stringer, R. Cardoso, X. Huang, L. Dennis] //Electronic Proceedings in Theoretical Computer Science. – 2020. – 319. – P. 117–25. DOI:doi.org/10.4204/EPTCS.319.9.
37. Paraskevas A. A Note on Situation Calculus / A. Paraskevas // Uncertainty Discourse and Applications 1. – 2024. – No. 1. – P. 66–72.

DOI 10.15588/1607-3274-2025-2-8

UDC 004.942, 004.89

A STUDY ON THE USE OF NORMALIZED L_2-METRIC IN CLASSIFICATION TASKS

Kondruk N. E. – PhD, Associate Professor, Associate Professor of Department of Cybernetics and Applied Mathematics, Uzhhorod National University, Uzhhorod, Ukraine.

ABSTRACT

Context. In machine learning, similarity measures, and distance metrics are pivotal in tasks like classification, clustering, and dimensionality reduction. The effectiveness of traditional metrics, such as Euclidean distance, can be limited when applied to complex datasets. The object of the study is the processes of data classification and dimensionality reduction in machine learning tasks, in particular, the use of metric methods to assess the similarity between objects.

Objective. The study aims to evaluate the feasibility and performance of a normalized L_2-metric (Normalized Euclidean Distance, NED) for improving the accuracy of machine learning algorithms, specifically in classification and dimensionality reduction.

Method. We prove mathematically that the normalized L_2-metric satisfies the properties of boundedness, scale invariance, and monotonicity. It is shown that NED can be interpreted as a measure of dissimilarity of feature vectors. Its integration into *k*-nearest neighbors and *t*-SNE algorithms is investigated using a high-dimensional Alzheimer's disease dataset. The study implemented four models combining different approaches to classification and dimensionality reduction. Model M1 utilized the *k*-nearest neighbors method with Euclidean distance without dimensionality reduction, serving as a baseline; Model M2 employed the normalized L_2-metric in *k*NN; Model M3 integrated *t*-SNE for dimensionality reduction followed by kNN based on Euclidean distance; and Model M4 combined *t*-SNE and the normalized L_2-metric for both reduction and classification stages. A hyperparameter optimization procedure was implemented for all models, including the number of neighbors, voting type, and the perplexity parameter for *t*-SNE. Cross-validation was conducted on five folds to evaluate classification quality objectively. Additionally, the impact of data normalization on model accuracy was examined.

Results. Models using NED consistently outperformed models based on Euclidean distance, with the highest classification accuracy of 91.4% achieved when it was used in *t*-SNE and the nearest neighbor method (Model M4). This emphasizes the adaptability of NED to complex data structures and its advantage in preserving key features in high and low-dimensional spaces.

Conclusions. The normalized L_2-metric shows potential as an effective measure of dissimilarity for machine learning tasks. It improves the performance of algorithms while maintaining scalability and robustness, which indicates its suitability for various applications in high-dimensional data contexts.

KEYWORDS: normalized Euclidean distance, machine learning, classification, *t*-SNE, similarity measures, *k*-Nearest Neighbors.

ABBREVIATIONS

*k*NN is the *k*-Nearest Neighbors algorithm;

NED is the Normalized Euclidean Distance;

t-SNE is a *t*-distributed Stochastic Neighbor Embedding.

NOMENCLATURE

$|\cdot|$ is a Euclidean norm;

R^n is a *n*-dimensional vector space;

$\boldsymbol{u}$ is a non-zero *n*-dimensional feature vector;

$\boldsymbol{v}$ is a non-zero *n*-dimensional feature vector;

α is a scalar.

INTRODUCTION

In machine learning and data analysis, one key task is finding and using effective ways to measure the similarity between objects. Distance metrics and similarity measures serve as mathematical tools for this purpose. They are the basis for many algorithms, including classification, clustering, dimensionality reduction, and recommender systems. Traditional metrics, such as Euclidean, cosine, and Manhattan distances, are widely used because of their simplicity and efficiency. However, their use can limit the effectiveness of algorithms in the context of specific data. In particular, standard metrics cannot always adequately assess the similarity between objects when the data have different measurement scales when there is a complex correlation between features, etc.

Accordingly, there is a need to find new, more flexible, and accurate tools that can take into account the specifics of different types of data and tasks and not only more accurately reflect the similarity between objects but also ensure correctness in the context of different metric spaces for some applied tasks. On the other hand, it is necessary to investigate whether these new tools can be easily integrated into existing machine learning algorithms and ensure their efficiency.

The object of the study is the process of data classification and dimensionality reduction in machine learning tasks, in particular, the use of metric methods to assess the similarity between objects.

Any function that satisfies the basic properties of non-negativity and reflexivity can be considered a similarity measure. If it satisfies the triangle inequality, it can be considered a distance metric, so the number of such functions is infinite. There are many well-known distance measures in the literature, which, although they have a common goal, differ significantly in focus and formulation. Choosing the optimal measure for a particular task should consider additional properties that may affect the effectiveness of its application. This leads to the need not only to develop measures but also to study their properties.

DOI 10.15588/1607-3274-2025-2-9

The subject of this study is the normalized L_2-metric as a means of assessing the similarity between objects and its impact on the efficiency of algorithms.

This paper aims to investigate the feasibility of using normalized L_2-metric in classification and reduction algorithms to improve their efficiency.

1 PROBLEM STATEMENT

Let $\boldsymbol{u}$ and $\boldsymbol{v}$ from R^n be vectors, in particular, describing the numerical values of some features of objects.

The normalized L_2-metric between two vectors $\boldsymbol{u}$ and $\boldsymbol{v}$ can be defined using the formula (1):

$$\mathrm{NED}(\boldsymbol{u},\boldsymbol{v}) = \frac{|\boldsymbol{u}-\boldsymbol{v}|}{|\boldsymbol{u}|+|\boldsymbol{v}|}. \quad (1)$$

Here, $|\cdot|$ denotes the Euclidean norm of the vector. This distance finds the ratio of the norm of the difference between the vectors to the sum of their norms, which ensures the normalization of the result. Note that (1) is defined only for non-zero vectors $\boldsymbol{u}$, $\boldsymbol{v}$. In the case of zero vectors, NED can be redefined to be zero.

As is known [1], of all the normalized L_p-distances, only when p=2 is a metric, i.e., it satisfies the triangle inequality. We will study and generalize other mathematical properties of the metric NED and evaluate the effectiveness of its integration into distance-based algorithms: k-nearest neighbors and t-distributed stochastic proximity embedding for high-dimensional data.

2 REVIEW OF THE LITERATURE

Since many real-world problems are based on finding similarities between groups of objects or populations, the list of fields of knowledge that use similarity measures is quite broad: biology, physics, chemistry, geography, ecology, social sciences, anthropology, algebra, statistical mathematics, engineering, and computer science [1].

Distance and similarity measures play a critical role in many machine learning tasks, including case-based reasoning, clustering, and classification [2–6], often impacting model performance more than the choice of algorithm [1]. However, this aspect receives insufficient attention in the literature, as it requires deep knowledge of the subject area and is difficult to generalize.

Modern studies on assessing the predictive capabilities of various similarity metrics for different datasets and conditions were conducted, particularly in [7–11]. Researchers have studied the relationship between commonly used distance measures, their performance in various machine learning tasks, and their robustness to noise [9]. The article [8] investigates the predictive capabilities of various similarity metrics (Euclidean, Pearson's correlation, Spearman's rank correlation coefficient, Kendall's coefficient) based on their application to data sets of different dimensions and properties, as well as the evaluation of the results obtained. Some metrics have been shown to be better suited for large datasets, while others are more reliable when applied to smaller outlier datasets. Data quality, correlation, and data types also play a role. Thus, research in this area emphasizes carefully selecting similarity measures depending on the application and data.

Selecting an effective tool for measuring the similarity between objects is critical in distance-based machine learning algorithms such as the k-nearest neighbors method [10, 11], clustering [4–6], and reduction. For example, in clustering tasks, using different similarity measures allows to obtain more clearly interpreted groups and apply a systematic approach to identifying different types of relationships between data [5, 6].

The effectiveness of various normalized L_1-metrics has been studied in [9–11], but the use of normalized Euclidean distance (1) in machine learning tasks has hardly been investigated. Again, It should be emphasized that among all normalized L_p-metrics, only NED is a distance metric.

This article is devoted to analyzing and summarizing the properties of the normalized L_2-metric (1) and evaluating its effectiveness in distance-based algorithms and high-dimensional data.

3 MATERIALS AND METHODS

Let's explore the properties of the NED metric.

1. Boundedness: $0 \le \mathrm{NED}(\boldsymbol{u}, \boldsymbol{v}) \le 1$.

Proof. The lower bound follows from the fact that NED is a distance metric [1]. Let us prove the upper bound using the triangle property.

For any vectors $\boldsymbol{u}, \boldsymbol{v} \in R^n$, it holds: $|\boldsymbol{u}-\boldsymbol{v}| \le |\boldsymbol{u}| + |\boldsymbol{v}|$.

This inequality reflects that the length of a side of a triangle (the difference of two vectors) is always less than or equal to the sum of the lengths of the other two sides.

$$\mathrm{NED}(\boldsymbol{u},\boldsymbol{v}) = \frac{|\boldsymbol{u}-\boldsymbol{v}|}{|\boldsymbol{u}|+|\boldsymbol{v}|} \le \frac{|\boldsymbol{u}|+|\boldsymbol{v}|}{|\boldsymbol{u}|+|\boldsymbol{v}|} = 1.$$

Proven.

Consequence. If $\boldsymbol{u}$, $\boldsymbol{v}$ are antiparallel, then NED $(\boldsymbol{u}, \boldsymbol{v}) = 1$.

Proof. Two vectors are called antiparallel if they are collinear and oppositely directed.

So, $\boldsymbol{v} = -\alpha\cdot\boldsymbol{u}$, $\alpha > 0$, then

$$\mathrm{NED}(\boldsymbol{u},\boldsymbol{v}) = \frac{|\boldsymbol{u}-(-\alpha\boldsymbol{u})|}{|\boldsymbol{u}|+|-\alpha\boldsymbol{u}|}.$$

In the numerator:

$$|\boldsymbol{u}-(-\alpha\cdot\boldsymbol{u})| = |\boldsymbol{u}+\alpha\cdot\boldsymbol{u}| = (1+\alpha)\cdot|\boldsymbol{u}|.$$

In the denominator:

$$|\boldsymbol{u}|+|-\alpha\cdot\boldsymbol{u}| = |\boldsymbol{u}|+|\alpha|\cdot|\boldsymbol{u}| = |\boldsymbol{u}|+\alpha\cdot|\boldsymbol{u}| = (1+\alpha)\cdot|\boldsymbol{u}|.$$

So,

DOI 10.15588/1607-3274-2025-2-9

$$\mathrm{NED}(\boldsymbol{u},\boldsymbol{v}) = \frac{1+\alpha}{1+\alpha} = 1.$$

Proven.

Remarks. Based on the boundedness property and the consequence, we can conclude that this distance metric (1) is also a similarity measure. That is, the more similar the feature vectors of objects are, the closer the NED value will be to zero. On the other hand, if the feature vectors are as dissimilar as possible, the closer the NED value will approach one.

Therefore, it is proposed to interpret NED as a measure of dissimilarity.

2. Invariance to scale: NED($\alpha\boldsymbol{u}$, $\alpha\boldsymbol{v}$) = NED($\boldsymbol{u}$, $\boldsymbol{v}$), where α is some number.

Proof.

$$\mathrm{NED}(\alpha\boldsymbol{u},\alpha\boldsymbol{v}) = \frac{|\alpha\boldsymbol{u}-\alpha\boldsymbol{v}|}{|\alpha\boldsymbol{u}|+|\alpha\boldsymbol{v}|} = \frac{|\alpha(\boldsymbol{u}-\boldsymbol{v})|}{|\alpha|\|\boldsymbol{u}|+|\alpha|\|\boldsymbol{v}|} =$$
$$= \frac{|\alpha|\|(\boldsymbol{u}-\boldsymbol{v})|}{|\alpha|(|\boldsymbol{u}|+|\boldsymbol{v}|)} = \mathrm{NED}(\boldsymbol{u},\boldsymbol{v}).$$

Proven.

3. The monotonicity property.

If $\boldsymbol{u}$, $\boldsymbol{v}$, $\boldsymbol{w}$ are non-zero vectors, $|\boldsymbol{w}| \le |\boldsymbol{v}|$ and $|\boldsymbol{u}-\boldsymbol{v}| \le |\boldsymbol{u}-\boldsymbol{w}|$, then NED ($\boldsymbol{u}$, $\boldsymbol{v}$) ≤ NED ($\boldsymbol{u}$, $\boldsymbol{w}$).

Proof. Consider the difference:

$$\mathrm{NED}(\boldsymbol{u},\boldsymbol{v}) - \mathrm{NED}(\boldsymbol{u},\boldsymbol{w}) = \frac{|\boldsymbol{u}-\boldsymbol{v}|}{|\boldsymbol{u}|+|\boldsymbol{v}|} - \frac{|\boldsymbol{u}-\boldsymbol{w}|}{|\boldsymbol{u}|+|\boldsymbol{w}|} =$$
$$= \frac{|\boldsymbol{u}-\boldsymbol{v}|\cdot(|\boldsymbol{u}|+|\boldsymbol{w}|)-|\boldsymbol{u}-\boldsymbol{w}|\cdot(|\boldsymbol{u}|+|\boldsymbol{v}|)}{(|\boldsymbol{u}|+|\boldsymbol{v}|)\cdot(|\boldsymbol{u}|+|\boldsymbol{w}|)} \le$$
$$\le \frac{|\boldsymbol{u}-\boldsymbol{w}|\cdot(|\boldsymbol{u}|+|\boldsymbol{w}|)-|\boldsymbol{u}-\boldsymbol{w}|\cdot(|\boldsymbol{u}|+|\boldsymbol{v}|)}{(|\boldsymbol{u}|+|\boldsymbol{v}|)\cdot(|\boldsymbol{u}|+|\boldsymbol{w}|)} =$$
$$= \frac{|\boldsymbol{u}-\boldsymbol{w}|\cdot(|\boldsymbol{u}|+|\boldsymbol{w}|-|\boldsymbol{u}|-|\boldsymbol{v}|)}{(|\boldsymbol{u}|+|\boldsymbol{v}|)\cdot(|\boldsymbol{u}|+|\boldsymbol{w}|)} =$$
$$= \frac{|\boldsymbol{u}-\boldsymbol{w}|\cdot(|\boldsymbol{w}|-|\boldsymbol{v}|)}{(|\boldsymbol{u}|+|\boldsymbol{v}|)\cdot(|\boldsymbol{u}|+|\boldsymbol{w}|)} \le 0.$$

Given that all Euclidean norms are positive values and $|\boldsymbol{w}| \le |\boldsymbol{v}|$, the difference in the numerator will take on non-positive values. Consequently, the expression will also be non-positive.

Proven.

4 EXPERIMENTS

The DARWIN dataset [12], which contains data on Alzheimer's disease based on handwriting analysis (452 features about 174 respondents), was selected for the experiments. As a result of data pre-processing, 450 predictor features and one target feature, which is binary, were retained. This made it possible to train models in high-dimensional data. The *k*-nearest neighbors algorithm and the Euclidean distance metric were used as a benchmark to evaluate the effectiveness of the dissimilarity measure (1). The index for assessing the quality of classification is a metric that determines the proportion of correct predictions of the model, i.e., the ratio of the number of correct predictions to the total number of observations.

Next, a procedure was implemented to find the optimal hyperparameters of the kNN algorithm adapted to use the Euclidean metric and the dissimilarity measure (1). The classifiers were trained on unstandardized and standardized data using standard normalization and different approaches to neighbor voting.

The approach of reducing the high-dimensional data space to two dimensions based on the *t*-SNE method was also used. The perplexity parameter was varied in the range from 5 to 40 in increments of 5 to study the effect of this parameter on classification accuracy.

We optimized the kNN hyperparameters using a grid search, which included the number of neighbors in the range from 2 to 15 and the type of voting – simple (uniform) and weighted (distance). During each iteration, the value of the *t*-SNE perplexity parameter was updated, and the classifier was optimized for the reduced data. The dimensionality of the feature space was reduced using Euclidean distance and NED.

Cross-validation was used to evaluate the classification quality on five blocks, corresponding to 20% of all data, to form the test sample. The best results of classification accuracy were recorded, and for each combination of parameters, it was determined whether they outperformed the previous results. As a result, the optimal hyperparameters of the models were determined, including the *t*-SNE perplexity parameters, the number of neighbors, the type of voting, and the accuracy achieved for these settings.

5 RESULTS

Table 1 show the results of the experiments for non-standardized and standardized data: the optimal hyperparameters of the four models, including the value of the *t*-SNE perplexity parameter, the number of kNN neighbors, the type of voting, and the achieved accuracy of the classifiers.

Fig. 1 graphically illustrates the comparison of the dependence of the accuracy of classifiers built based on M1–M4 models under optimally tuned hyperparameters (Table 1) and the number of kNN neighbors with and without using data standardization approaches.

In Fig. 1, the solid line represents the performance of models based on the NED dissimilarity measure (M2, M4), while the dashed line represents models based on Euclidean distance (M1, M3). Bold points indicate where the highest accuracy is achieved. Fig. 1a and 1c illustrate the comparison of model performance for non-standardized data, while Fig. 1b and 1d show the performance for standardized data. Fig. 1a and 1b show the accuracies of the M1 and M2 models, while Fig. 1c and 1d illustrate the accuracies of the M3 and M4 models.

DOI 10.15588/1607-3274-2025-2-9

Table 1 – Experimental results on optimal hyperparameters and model accuracy

Model		M1: model without *t*-SNE reduction; the distance metric in *k*NN is Euclidean.	M2: model without *t*-SNE reduction; the distance metric in kNN is NED.	M3: model with *t*-SNE using Euclidean distance; the distance metric in kNN is Euclidean.	M4: model with *t*-SNE using NED distance; the distance metric in *k*NN is NED.
Non-standardized data	Optimal Hyperparameters	Number of neighbors – 4, weighted voting.	Number of neighbors – 4, weighted voting.	Perplexity – 30, number of neighbors – 4, weighted voting.	Perplexity – 10, number of neighbors – 10, weighted voting.
	Accuracy	75%	81 %	80 %	87 %
Standardized data	Optimal Hyperparameters	Number of neighbors – 2, weighted voting.	Number of neighbors – 6, weighted voting.	Perplexity – 25, number of neighbors – 3, simple voting.	Perplexity – 25, number of neighbors – 9, weighted voting.
	Accuracy	73 %	89 %	87 %	91.4 %

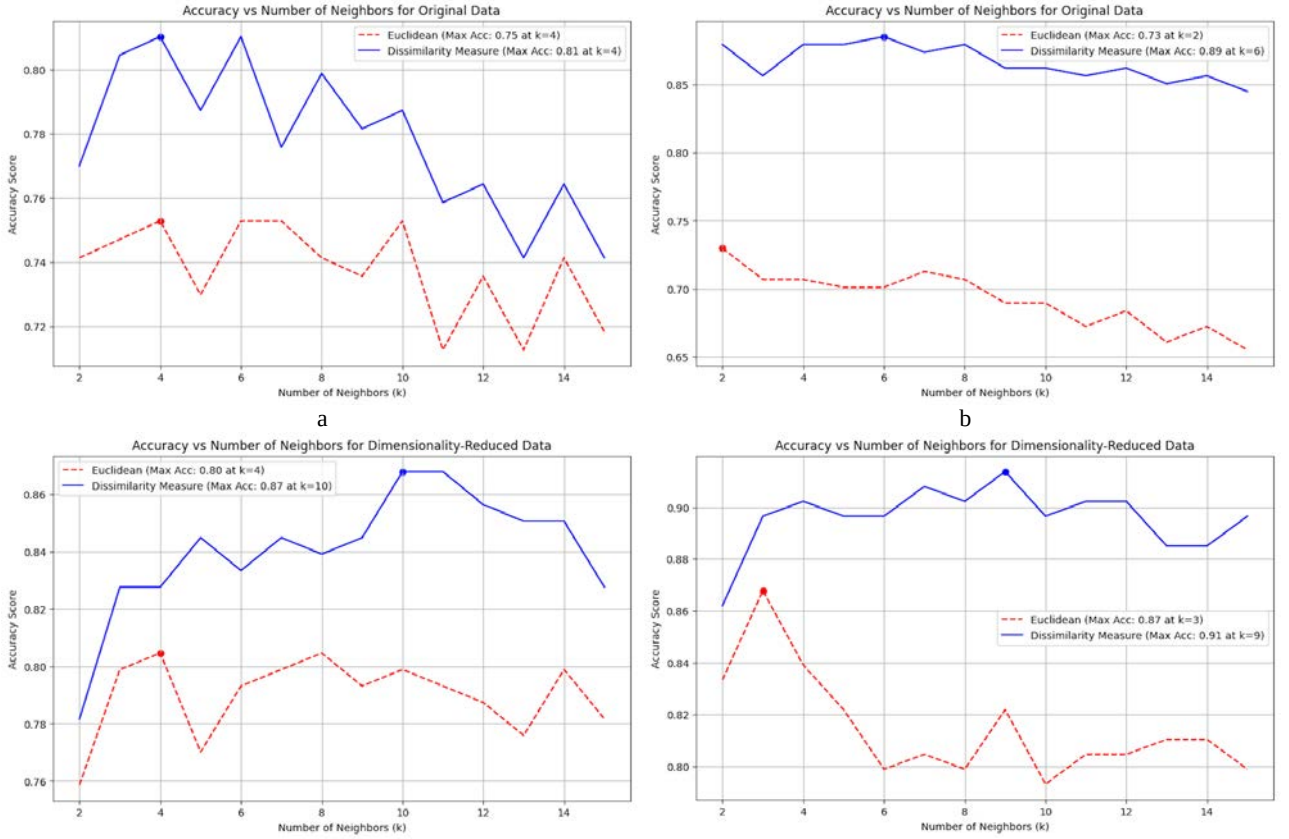

Figure 1 – Comparison of predictive accuracy of the models M1–M4

6 DISCUSSION

The results presented in Table 1 demonstrate the effectiveness of using the *t*-SNE dimensionality reduction technique to enhance model kNN performance. Specifically, models based on Euclidean distance (M1, M3) achieved a 5% improvement in accuracy for non-standardized data and a 14% improvement for standardized data. For models using the NED dissimilarity measure (M2, M4), performance gains were 6% for non-standardized data and 2% for standardized data.

When comparing models based on NED (M2, M4) and Euclidean distance (M1, M3), the NED-based models consistently showed higher accuracy across various values of the nearest neighbors parameter (Fig. 1). For non-standardized data, the highest accuracy of 87% was achieved with the NED measure, exceeding the corresponding result of 80% for the Euclidean metric by 7%. Similarly, for standardized data, the use of NED improved accuracy by 4%, with the best performance reaching 91.4% (model M4). These findings highlight the competitiveness of the proposed dissimilarity measure (1), which demonstrates greater adaptability to complex data structures compared to the Euclidean metric.

The experiments combining *t*-SNE for dimensionality reduction and *k*NN for classification emphasize the significant influence of the choice of distance measure and model parameters on classification outcomes. The NED measure (1) proved particularly effective when applied in combination with *t*-SNE, where it was also used to compute distances between points during data compression. This approach, implemented in model M4, outperformed all other configurations, achieving an accuracy of 91.4%.

DOI 10.15588/1607-3274-2025-2-9

This result indicates that the proposed measure (1) can better capture data structures in high-dimensional spaces and after dimensionality reduction.

As shown in Section 3 of this article, the normalized Euclidean distance (NED) metric simultaneously acts as a distance metric and a similarity measure and satisfies the important properties for algorithms: scale invariance, monotonicity, and boundedness. It has been experimentally shown that the use of NED consistently allows models to achieve higher accuracy than the traditional Euclidean metric. These characteristics emphasize the adaptability of NED to work with complex datasets and its ability to preserve key properties even in spaces with reduced dimensionality.

CONCLUSIONS

The problem of developing a mathematical framework to enhance the efficiency of existing machine learning algorithms is addressed. One of the central elements of distance-based methods is the approach to distance measurement.

The scientific novelty of the results lies in demonstrating that the normalized L_2 distance metric (1) can be interpreted as a measure of dissimilarity between feature vectors, making it valuable for comparing relative differences between vectors. It is proven that the NED satisfies the properties of boundedness, monotonicity, and scale invariance.

The practical significance of the results is reflected in the developed software that implements the dissimilarity measure (1) within the *k*-nearest neighbors method and *t*-SNE feature space reduction. A comparative analysis of the accuracy of four models was conducted using applied high-dimensional data. The highest accuracy achieved through cross-validation was 91.4%, obtained by Model M4, which integrates NED into the classifier and feature space reduction. It is worth noting that the experiments demonstrated the ability of measure (1) to significantly improve the efficiency of distance-based algorithms in solving specific classes of applied classification problems under standardized and non-standardized, high-dimensional, and reduced data conditions.

Future research prospects include studying the efficiency of applying the normalized Euclidean metric to other applied problems.

ACKNOWLEDGEMENTS

The work is supported by the state budget scientific research project of Uzhhorod National University, “Computational Intelligence Methods for Data Processing and Analysis” (state registration number 0121U109279).

REFERENCES

1. Deza M. M., Deza E. Encyclopedia of Distances, *Encyclopedia of Distances*. Berlin, Heidelberg, Springer, 2009. DOI: 10.1007/978-3-642-00234-2_1.
2. Mathisen B. M., Aamodt A., Bach K., Langseth H. Learning similarity measures from data, *Progress in Artificial Intelligence*, 2019, Vol. 9, pp. 129–143. DOI: 10.1007/s13748-019-00201-2.
3. Vangipuram S. K., Appusamy R. A survey on similarity measures and machine learning algorithms for classification and prediction, *International Conference on Data Science, E-learning and Information Systems 2021 (DATA'21): Proceedings. – Association for Computing Machinery*, 2021, pp. 198–204. DOI: 10.1145/3460620.3460755.
4. Kondruk N. E. Methods for determining similarity of categorical ordered data, *Radio Electronics, Computer Science, Control*, 2023, Vol. 65, No. 2, pp. 31–36. DOI: 10.15588/1607-3274-2023-2-4.
5. Kondruk N. E. Use of length-based similarity measure in clustering problems, *Radio Electronics, Computer Science, Control*, 2018, Vol. 46, No. 3, pp. 98–105. DOI: 10.15588/1607-3274-2018-3-11.
6. Kondruk N. E., Malyar M. M. Analysis of Cluster Structures by Different Similarity Measures, *Cybernetics and Systems Analysis*, 2021, Vol. 57, pp. 436–441. DOI: 10.1007/s10559-021-00368-4.
7. Vital A., Amancio D. R. A comparative analysis of local similarity metrics and machine learning approaches: application to link prediction in author citation networks, *Scientometrics*, 2022, Vol. 127, pp. 6011–6028. DOI: 10.1007/s11192-022-04484-6.
8. Radisic I., Lazarevic S., Antović I., Stanojevic V. Evaluation of Predictive Capabilities of Similarity Metrics in Machine Learning, *2020 24th International Conference on Information Technology (IT)*, 2020, pp. 1–4. DOI: 10.1109/IT48810.2020.9070437.
9. Blanco-Mallo E., Morán-Fernández L., Remeseiro B., Bolón-Canedo V. Do all roads lead to Rome? Studying distance measures in the context of machine learning, *Pattern Recognition*, 2023, Vol. 141. Article ID: 109646. DOI: 10.1016/j.patcog.2023.109646.
10. Pulungan A. F., Zarlis M., Suwilo S. Analysis of Braycurtis, Canberra and Euclidean Distance in KNN Algorithm, *Sinkron: Jurnal dan Penelitian Teknik Informatika*, 2019, Vol. 4, № 1, pp. 74–77. DOI: 10.33395/sinkron.v4i1.10207.
11. Sandhu G., Singh A., Lamba P. S., Virmani D., Chaudhary G. Modified Euclidean-Canberra blend distance metric for kNN classifier, *Intelligent Decision Technologies*, 2023. Vol. 17, № 2, pp. 527–541. DOI: 10.3233/IDT-220233.
12. Cilia N. D., De Stefano C., Fontanella F., Di Freca A. S. An experimental protocol to support cognitive impairment diagnosis by using handwriting analysis, *Procedia Computer Science*, 2018, Vol. 141, pp. 466–471. DOI: 10.24432/C55D0K.

Received 05.02.2025.
Accepted 20.04.2025.

DOI 10.15588/1607-3274-2025-2-9

УДК 004.942, 004.89

ДОСЛІДЖЕННЯ ВИКОРИСТАННЯ НОРМАЛІЗОВАНОЇ L_2-МЕТРИКИ В ЗАДАЧАХ КЛАСИФІКАЦІЇ

Кондрук Н. Е. – канд. техн. наук, доцент, доцент кафедри кібернетики і прикладної математики Ужгородського національного університету, Ужгород, Україна.

АНОТАЦІЯ

Актуальність. У машинному навчанні міри подібності та метрики відстані відіграють ключову роль у задачах класифікація, кластеризація та зменшення розмірності. Ефективність традиційних метрик, зокрема евклідової відстані, може бути обмеженою при застосуванні до складних наборів даних. Об'єктом дослідження є процеси класифікації та зменшення розмірності у задачах машинного навчання, зокрема використання метричних методів для визначення подібності між об'єктами.

Мета роботи – оцінка доцільності та ефективності нормалізованої L_2-метрики (нормалізованої евклідової метрики, NED) для підвищення точності алгоритмів машинного навчання, зокрема в задачах класифікації та зменшення розмірності.

Метод. Математично доведено, що нормалізована L_2-метрика задовольняє властивості обмеженості, масштабної інваріантності та монотонності. Показано, що NED можна інтерпретувати як міру несхожості векторів ознак. Її інтеграція в алгоритми *k*-найближчих сусідів і *t*-SNE досліджується на основі даних про хворобу Альцгеймера високої розмірності. У дослідженні реалізовано чотири моделі, що поєднують різні підходи до класифікації та зменшення розмірності. Модель M1 використовувала метод *k*-найближчих сусідів з евклідовою відстанню без зменшення розмірності, як базова; модель M2 використовувала нормалізовану L_2-метрику в *k*NN; модель M3 інтегрувала *t*-SNE для зменшення розмірності, а потім *k*NN на основі евклідової відстані; модель M4 поєднувала *t*-SNE і нормалізовану L_2-метрику як для зменшення розмірності, так і класифікації. Для всіх моделей було застосовано процедуру оптимізації гіперпараметрів, включаючи кількість сусідів, тип голосування та параметр перплексії в *t*-SNE. Для об'єктивної оцінки якості класифікації було проведено перехресну перевірку на п'яти фолдах. Крім того, було досліджено вплив нормалізації даних на точність моделі.

Результати. Моделі, що використовували NED, стабільно перевершували моделі на основі евклідової відстані, причому найвища точність класифікації (91,4%) була досягнута при інтегруванні NED у *t*-SNE та методі найближчих сусідів (модель M4). Це підкреслює адаптивність NED до складних структур даних та її перевагу у збереженні ключових ознак як у високорозмірному, так і в низькорозмірному просторах.

Висновки. Нормалізована метрика L_2 демонструє потенціал як ефективна міра несхожості для задач машинного навчання. Вона покращує продуктивність алгоритмів, зберігаючи при цьому масштабованість і надійність, що вказує на її придатність для різних застосувань у контексті даних високої розмірності.

КЛЮЧОВІ СЛОВА: нормалізована евклідова відстань, машинне навчання, класифікація, *t*-SNE, міри подібності, *k*-найближчих сусідів.

ЛІТЕРАТУРА

1. Deza M. M. Encyclopedia of Distances / M. M. Deza, E. Deza // Encyclopedia of Distances. – Berlin, Heidelberg : Springer, 2009. DOI: 10.1007/978-3-642-00234-2_1.
2. Learning similarity measures from data / [B. M. Mathisen, A. Aamodt, K. Bach, H. Langseth] // Progress in Artificial Intelligence. – 2019. – Vol. 9. – P. 129–143. DOI: 10.1007/s13748-019-00201-2.
3. Vangipuram S. K. A survey on similarity measures and machine learning algorithms for classification and prediction / S. K. Vangipuram, R. Appusamy // International Conference on Data Science, E-learning and Information Systems 2021 (DATA'21): Proceedings. – Association for Computing Machinery, 2021. – P. 198–204. DOI: 10.1145/3460620.3460755.
4. Кондрук Н. Е. Способи визначення подібності категоріальних впорядкованих даних / Н. Е. Кондрук // Радіоелектроніка, інформатика, управління. – 2023. – № 2 (65). – С. 31–36. DOI: 10.15588/1607-3274-2023-2-4.
5. Кондрук Н. Е. Використання довжинної міри подібності в задачах кластеризації / Н. Е. Кондрук // Радіоелектроніка, інформатика, управління. – 2018. – № 3 (46). – С. 98–105. DOI: 10.15588/1607-3274-2018-3-11.
6. Kondruk N. E. Analysis of Cluster Structures by Different Similarity Measures / N. E. Kondruk, M. M. Malyar // Cybernetics and Systems Analysis. – 2021. – Vol. 57. – P. 436–441. DOI: 10.1007/s10559-021-00368-4.
7. Vital A. A comparative analysis of local similarity metrics and machine learning approaches: application to link prediction in author citation networks / A. Vital, D. R. Amancio // Scientometrics. – 2022. – Vol. 127. – P. 6011–6028. DOI: 10.1007/s11192-022-04484-6.
8. Evaluation of Predictive Capabilities of Similarity Metrics in Machine Learning / [I. Radisic, S. Lazarevic, I. Antović, V. Stanojevic] // 2020 24th International Conference on Information Technology (IT). – 2020. – P. 1–4. DOI: 10.1109/IT48810.2020.9070437.
9. Do all roads lead to Rome? Studying distance measures in the context of machine learning / [E. Blanco-Mallo, L. Morán-Fernández, B. Remeseiro, V. Bolón-Canedo] // Pattern Recognition. – 2023. – Vol. 141. – Article ID: 109646. DOI: 10.1016/j.patcog.2023.109646.
10. Pulungan A. F. Analysis of Braycurtis, Canberra and Euclidean Distance in KNN Algorithm / A. F. Pulungan, M. Zarlis, S. Suwilo // Sinkron: Jurnal dan Penelitian Teknik Informatika. – 2019. – Vol. 4, № 1. – P. 74–77. DOI: 10.33395/sinkron.v4i1.10207.
11. Modified Euclidean-Canberra blend distance metric for *k*NN classifier / [G. Sandhu, A. Singh, P. S. Lamba, D. Virmani, G. Chaudhary] // Intelligent Decision Technologies. – 2023. – Vol. 17, № 2. – P. 527–541. DOI: 10.3233/IDT-220233.
12. An experimental protocol to support cognitive impairment diagnosis by using handwriting analysis / [N. D. Cilia, C. De Stefano, F. Fontanella, A. S. Di Freca] // Procedia Computer Science. – 2018. – Vol. 141. – P. 466–471. DOI: 10.24432/C55D0K.

DOI 10.15588/1607-3274-2025-2-9

UDC 004.93

BEARING FAULT DETECTION BY USING AUTOENCODER CONVOLUTIONAL NEURAL NETWORK

Kysarin M. K. – Student of the Faculty of Information Technologies, State University of Trade and Economics, Kyiv, Ukraine.

ABSTRACT

Context. Bearings are an important part for the functioning of various means of transportation. They have the property of wear and failure, which requires high-quality and timely detection of faults. Failures are not always easy to detect, so the use of traditional detection methods may not be effective enough. The use of machine learning methods well-suited to the task can effectively solve the problem of detecting bearing faults. The object of study is the process of non-destructive diagnosis of bearings. The subject of study is methods of selecting hyperparameters and other optimization for building a diagnostic model based on a neural network according to observations.

Objective. The goal of the work is to create a model based on a neural network for detecting bearing faults based on the ZSL.

Method. A proposed filter smooths the data, preserving key characteristics such as peaks and slopes, and eliminates noise without significantly distorting the signal. A normalization method vibration data is proposed, which consists of centering the data and distributing the amplitude within optimal limits, contributing to the correct processing of this data by the model architecture. A model based on a neural network is proposed to detect bearing faults by data processing and subsequent binary classification of their vibrations. The proposed model works by compressing the vibration data into a latent representation and its subsequent recovery, calculating the error between the recovered and original data, and determining the difference between the errors of healthy and faulty bearing vibration data. The Zero-Shot Learning machine learning method involves training, validating the model only on healthy vibration data, and testing the model only on faulty vibration data. Due to the proposed machine learning method, the model based on a neural network is able to detect faulty bearings present in the investigated fault class and theoretically new fault classes, that is, the model can detect different classes of data that it did not see during training. The architecture of the model is built on the convolutional and max-pooling layers of the encoder, and the reverse convolutional layers for the decoder. The best hyperparameters of the model are selected using a special method.

Results. Using the Pytorch library, a model capable of binary classification of healthy and faulty bearings was obtained through training, validation, and testing in the Kaggle software environment.

Conclusions. Testing of the constructed model architecture confirmed the model's ability to classify healthy and fault bearings binaryly, allowing it to be recommended for use in practice to detect bearing faults. Prospects for further research may include testing the model through integration into predictive maintenance systems for timely fault detection.

KEYWORDS: bearing fault, autoencoder, convolutional neural network, zero-shot learning, binary classification.

ABBREVIATIONS

AE is an autoencoder;

AE-CNN is an autoencoder convolutional neural network;

CWRU is a Case Western Reserve University;

CNN is a convolutional neural network;

DAE is a deep autoencoder;

DNN is a deep neural network;

FFT is a fast Fourier transform;

GAE is a graph autoencoder;

GAF is a Gramian angular field algorithm;

GCN is a model that specializes in learning the node characteristics of graph data;

GPMS is a Green Power Monitoring Systems company;

LSTM is a long short-term memory;

MMN is a min-max normalization data method;

MSE is a mean squared error;

PCA is a principal component analysis method;

SGF is a Savitzky-Golay filter;

SSAE is a stacked sparse autoencoder;

STFT is a technology that has been developed to overcome the limitations of FFT;

TPE is a Tree-structured Parzen Estimator method;

VAE is a variational autoencoder;

XG is a Xavier Glotor initialization;

ZSL is a zero-shot learning machine learning scenario.

NOMENCLATURE

α is a hyperparameter of the learning rate of the AE-CNN model;

a is a minimum data value for the MMN;

b is a maximum data value for the MMN;

b_k are the coefficients of the polynomials for the SGF;

B_1 is a exponential smoothing coefficient of the first momentum for the Adam optimization algorithm;

B_2 is a exponential smoothing factor for the second momentum for the Adam optimization algorithm;

c_b is a probability distribution for bad combinations of hyperparameters of the AE-CNN model;

c_g is a probability distribution for good combinations of hyperparameters of the AE-CNN model;

c_{in} is a number of filters at the input to the convolutional layer;

c_{out} is a number of filters at the output of the convolutional layer;

d is a data provided by the AE-CNN model;

ε is a small value in the Adam optimization algorithm to prevent division by zero;

E is a MSE;

DOI 10.15588/1607-3274-2025-2-10

E_{test} is a set of test error values;
E_{train} is a set of training error values;
E_{val} is a set of validation error values;
f is a samples of bad vibration data with faults;
g is a samples of good vibration data;
γ is a threshold separating good and bad values of E;
h is a set of hyperparameters of the AE-CNN model;
k is a shift index of the smoothing window for the SGF;
k_c is a size of the one-dimensional convolutional layer filter;
l is a shift parameter for the AE-CNN convolutional one-dimensional layer;
L_{train} is a training loss value;
L_{val} is a validation loss value;
m is a width of the window for the SGF;
$M()$ is an AE-CNN model structure;
n is a sample of vibration data;
n_{in} is a number of input connections (neurons) included in the layer;
n_{out} is a number of output connections (neurons) coming out of the layer;
N is a number of samples of vibration data;
p is a max-pooling filter size;
$P()$ is a probability distribution;
t is a number of time points in the vibration data sample;
U is an uniform distribution;
W is a set of controlled (adjusted) weights of the AE-CNN model;
x is an one point in the original sample;
$\hat{x}$ is an one point in a recovered sample;
x_{index} is an index of one point in the original sample;
X_{test} is a test samples of bad vibration data with faults;
X_{train} is a training samples of good vibration data;
X_{val} is a validation samples of good vibration data;
y is an optimization iteration number, the current step of the Adam optimization algorithm;
z is a MSE threshold.

INTRODUCTION

The study deals with the development of a special neural network to detect faults in bearings that affect their reliability and safety. The problem is that bearings can wear or break over time, and these failures are often accompanied by vibrations that are not always easy to detect. Depending on different situations, different methods of detecting bearing faults may be effective [16]. Detection of such faults using traditional methods can be difficult and not always effective [1], [15], especially if the faults are still at an early stage. Therefore, it is necessary to develop an automated system capable of analyzing the vibration signals and determining whether the bearing is good or bad.

One of the powerful options for detecting the fault features is AE-CNN, which can be trained only on healthy vibration samples, ensuring their generalization and extracting knowledge from data, without losing the ability to further classify faulty data samples.

The object of study is the process of non-destructive diagnosis of bearings.

Vibration data are used to diagnose the condition of these bearings and identify possible faults.

The process of pre-processing the vibration data to be suitable for AE-CNN is very careful. This is caused by the fact that the initial vibration data is very noisy due to the influence of other sound factors from the environment. Therefore, to realize the classification ability of AE-CNN, a filter and normalization must be applied to the vibration data. The size and quality of the training sample used can significantly affect the training and accuracy of the AE-CNN model. Therefore, reducing the size of the samples, and ensuring the preservation of its main properties, is necessary to improve the quality of AE-CNN and the speed of its construction.

The subject of study is methods of selecting hyperparameters and other optimization for building a diagnostic model based on a neural network according to observations.

The purpose of the work is to create a model based on a neural network for detecting bearing faults based on the ZSL.

1 PROBLEM STATEMENT

Suppose $g_N(t)$ and $f_N(t)$ are given. Training, validation, and test samples are formed from data prepared for model processing: X_{train}, X_{val}, X_{test}.

For given, respectively, good and bad bearing classes {0,1}, the task of detecting the difference between bearing classes through the AE-CNN model can be represented as (if $M(h, W, d)$ with $d \in \{X_{train}, X_{val}, X_{test}\}$ then class($M(h, W, d) \in \{0,1\}$)) $\rightarrow$ opt. h of the best model $M()$ is determined by a special selection method, and W is adjusted through the optimizer of the learning process.

2 REVIEW OF THE LITERATURE

Aiming to address the issue of strong background noise in bearing failures and the lack of evident fault features, this paper [2] proposes a fault diagnosis method that combines Savitzky-Golay Gram angle field feature enhancement with ResNet18. The acquired signal is segmented, and the segmented signal is subjected to Butterworth high-pass filtering to extract the high-frequency component of the signal containing fault information.

The optimized SGF and adaptive spectrum editing are proposed to detect the fault feature of the rolling element bearing under low-speed and variable-speed conditions [3].

This manuscript elaborates on the development of a VAE-CNN model, designed for the fault diagnosis of rolling bearings. By amalgamating the CNN model's superior capacity for representing vibration signal data with the VAE model's robustness to data noise, the proposed VAE-CNN model excels in scenarios where only a limited amount of observational data is available at the initial stages of rolling bearing operation. The VAE-

DOI 10.15588/1607-3274-2025-2-10

CNN model achieves over 90% accuracy in diagnosing different fault types at various speeds [4].

This study [5] proposes a GAE-based approach for fusing node features in an Euclidean dataset. The primary advantage of the proposed approach lies in its adaptive ability to capture the complex structure of the dataset and fuse node features using a GAE, effectively extracting the latent features. Normalization is a vital pre-processing step as it addresses the issue of varying magnitudes among different base detectors, which makes direct comparison and combination challenging. To enhance the convergence speed of the algorithm, in the proposed approach normalized the output of the base detectors.

This approach [6] uses both an unsupervised and a supervised model. First, the current signal in the time domain is segmented with respect to the fundamental frequency, and then a DAE is trained with the normal state data to estimate the approximation of the system function. The residual signal is then calculated from the difference between the raw and estimated signals produced by the AE for all conditions, which helps to extract discriminative features from the current signal data without any labels. Finally, a two-layer CNN is built with the residual signals to identify bearing faults. The experiments were performed 100 times by randomly selecting the training/testing dataset, and the result showed good stable convergence with high accuracy.

This study [7] proposes a novelty detection and fault diagnosis method for bearing fault recognition and diagnosis based on a hybrid DAE. The method uses one model to accomplish two tasks, detecting new faults and classifying known faults. To address the challenge of requiring a large number of training samples in existing deep learning methods, this study combines the unsupervised training characteristics of AEs with the powerful feature extraction ability of CNNs, adopting a semi-supervised training method that can learn fault features from both labeled and unlabeled samples, reducing the required sample size for training.

The proposed method [8] incorporates a GAF-based image generation technique from a 1-dimensional current signal for a 2-layer CNN model to construct a data-driven intelligent fault-diagnosis approach for bearings. As the current signal is affected by surrounding noises, it becomes very difficult to extract the fault signatures manually. When the data are converted into the polar coordinates for image transformation, the different bearing-condition data create distinctive patterns, which helps the CNN model to easily extract the necessary high-level features. In all considering operating conditions, this proposed GAF and 2-dimensional CNN-based approach can attain good accuracy.

This study [9] is based on deep learning methods for bearing fault diagnosis. Firstly, a CNN model is designed for end-to-end bearing fault diagnosis. Then, considering the presence of strong noise in actual working conditions, a bearing fault diagnosis model based on AE-CNN is proposed to achieve bearing fault diagnosis under noisy conditions. The experiment results on the CWRU demonstrate the effectiveness of the proposed model. The method proposed in this study can be used for fault diagnosis of bearings under noise conditions and has engineering practical value.

This article [10] highlights the advantages of deep learning models, particularly AE and CNNs, for fault diagnosis in bearing systems. Unlike traditional machine learning algorithms, which require extensive manual feature design, AE and CNN can automatically extract high-level features from large-scale, unlabeled data. AE, though simple, benefits from enhancements such as stacking layers and adding noise. CNN excels in feature extraction due to its unique architecture and translation invariance.

This study [11] indicates that experimental results show that VAE is a more competent and promising dimensionality reduction tool than PCA.

This work presents SSAE-DNN, which in combination with a complex envelope spectrum for inputs performs fault diagnosis of rotary machines when there are fluctuations of the shaft speed. In the proposed scheme, vibration signals related to different health conditions of a motor bearing are preprocessed using the complex envelope signal. In the proposed method, information obtained by the stacked autoencoders from the defect frequency, as well as its principle harmonics present in the complex envelope spectrum for a given fault, makes it possible to classify faults with varying speeds. The efficiency of the proposed scheme was validated using rotating machine bearing data for four different shaft speeds. The minimum average classification accuracy for every experiment was 90%, which demonstrates that the proposed scheme can also classify faults when fluctuations of the shaft speed exist.

3 MATERIALS AND METHODS

Let's divide all vibration data into good and bad, respectively, as follows: $g_N(t)$ and $f_N(t)$. To reduce the noise in the data arising from environmental factors, the SGF is applied to the data, which is defined by the following formulas:

$$g'_N(t) = \sum_{k=-\frac{m}{2}}^{\frac{m}{2}} b_k g_N(t+k),$$

$$f'_N(t) = \sum_{k=-\frac{m}{2}}^{\frac{m}{2}} b_k f_N(t+k),$$

where

$$k = \frac{m-1}{2}. \quad (1)$$

The filtered data must have one dimension because if the data is submitted to AE-CNN at different scales of variation, it can complicate the data processing of the

DOI 10.15588/1607-3274-2025-2-10

model and significantly degrade the classification results. Taking into account this feature, MMN is used, which is determined by the formulas:

$$s_g = \frac{g'_N(t) - \min(g'_N(t))}{\max(g'_N(t)) - \min(g'_N(t))}(b-a) + a,$$

$$s_f = \frac{f'_N(t) - \min(f'_N(t))}{\max(f'_N(t)) - \min(f'_N(t))}(b-a) + a.$$

where b and a are determined according to research requirements.

Normalized data ready for submission to AE-CNN is divided into training, validation, and test samples: X_{train}, $X_{val} = \{s_g\}$; $X_{test} = \{s_f\}$.

Following the ZSL principle, the training and validation data consists only of the working vibration samples, and the test data consists only of the faulty vibration samples.

Given the periodicity of the vibration data, the healthy data samples have stable healthy features along their entire length, as well as the fault features in the corresponding faulty samples are observed consistently along their entire length. Taking these data properties into account, the data is reduced to an optimal size to optimize the data processing speed of the AE-CNN model.

The architecture of the AE-CNN model is divided into an encoder, a latent space, and a decoder.

The encoder architecture is proposed in four stages. Each stage has a convolutional one-dimensional layer and a maximum pooling layer. A convolutional one-dimensional layer performs a convolution operation where filters are moved over d and compute scalar products.

The data in each stage of the encoder is processed according to the formulas:

$$c = \max_{i=0,\ldots,p-1}(Wd + l),$$

where

$$d = \{n_s \mid s \in [x_{index}, x_{index} + k_c - 1]\}.$$

l is initially initialized to zero. This is a standard approach, as the offset value can be adjusted quickly during training without much damage to the result, so zero initialization works well.

W in AE-CNN models from the beginning of processing are initialized through XG according to the defined formula:

$$W = U\left(-\sqrt{\frac{6}{n_{in} + n_{out}}}, \sqrt{\frac{6}{n_{in} + n_{out}}}\right),$$

where

$$n_{in} = c_{in} k_c,$$

$$n_{out} = c_{out} k_c.$$

To reduce the dimensionality of the data to the state of the latent representation, a linear layer is used, which has one matrix of weights, which determines the connections between input and output neurons. Each output neuron is connected to all input neurons.

The decoder uses similar formulas as the encoder, but in reverse order, since the main purpose of the decoder is to recover or reconstruct the input data from the latent representation.

To optimize W and α of the model, the Adam optimization algorithm is used, which is determined by the following formulas:

$$W_{y+1} = W_y - \alpha \frac{\hat{m}_y}{\sqrt{\hat{v}_y} + \varepsilon},$$

$$\hat{m}_y = \frac{m_y}{1 - \beta_1^y},$$

$$\hat{v}_y = \frac{v_y}{1 - \beta_2^y},$$

$$m_y = \beta_1 m_{y-1} + (1 - \beta_1)\nabla W_y,$$

$$v_y = \beta_2 v_{y-1} + (1 - \beta_2)(\nabla W_y)^2,$$

$$\nabla W_y = \frac{\partial E}{\partial W_y}.$$

The initial values of m_{y-1} and v_{y-1} are initialized with zeros.

The research uses the method of TPE hyperparameter selection, which works according to the following formulas:

$$h_{new} = \arg\max \frac{c_g(h)}{c_b(h)},$$

$$c_g(h) = P(h \mid E \le \gamma),$$

$$c_b(h) = P(h \mid E > \gamma).$$

This method divides h into good and bad groups using a certain γ, and builds models to estimate the probability of each group. This makes it possible to find new h that have a higher probability of belonging to good values, thus optimizing the choice of h. γ is usually chosen as a certain quantile.

In this case, E is the last validation error at the end of the current trial h through TPE.

The AE-CNN model goes through the processes of training, validation, and updating W and is tested on X_{test}.

DOI 10.15588/1607-3274-2025-2-10

At all stages, E determined by the following formulas is used:

$$e_{train} = \frac{\sum_{n=1}^{t}(x_{train} - \hat{x}_{train})^2}{t},$$

$$e_{val} = \frac{\sum_{n=1}^{t}(x_{val} - \hat{x}_{val})^2}{t},$$

$$e_{test} = \frac{\sum_{n=1}^{t}(x_{test} - \hat{x}_{test})^2}{t}.$$

Let the sets of errors be defined as E_{train}, E_{val}, E_{test}={e_1, e_2, …, e_N} which is calculated on the last epoch of the final trained AE-CNN model. To obtain the difference between the signs of good and bad bearings, the difference between E_{val} and E_{test} was used. z is determined by the formula:

$$z = \max(E_{val}).$$

All samples with E>z are considered faulty.

In the final step, E_{test} is compared with z, and if e_{test}>z, then the corresponding sample is considered faulty.

4 EXPERIMENTS

The data for the study supplied by GMPS owner Eric Bechhoefer has 1158 samples of vibration data, of which 865 are good and 293 are bad. Each sample has 93752 values recorded over 5 minutes.

Experimentally, m was selected with a value of 24, b_k with a value of 13, and k was calculated with a value of 11 according to formula (1).

Based on the periodicity in the samples, in each SGF-treated faulty sample, pulses with increased amplitude of the fault-determining signal are observed. The research recorded that the first pulse appears on average at 513 values of the faulty sample, the period during which each subsequent pulse is recorded is 935 values.

In the process of normalization of vibration data according to formula (2), b with a value of 0.3 and a with a value of –0.3 were used, these values were selected taking into account that after normalization of healthy samples and normalization of faulty samples based on the calculated metrics of healthy samples, the maximum module values of faulty samples will not exceed the range from –1 to 1.

Based on the signs of periodicity of both healthy and faulty vibration samples, it was decided to reduce the samples to the first 1500 values to optimize the duration of data processing in the AE-CNN model.

Empirical studies show that the best results are obtained if the authors use 20–30% of the data for testing, and the remaining 70–80% ofThe data for training [12].

Adhering to the ZSL principle, good samples in the amount of 605 and 260, 70% and 30% of g_N, respectively, were selected for the training and validation processes, and all 293 faulty samples were selected for the testing process.

In the best encoder architecture selected through TPE, the parameters c_{in}=1, c_{out}=13 were used on the first one-dimensional convolutional layer; on the second layer c_{in}=13, c_{out}=22; on the third layer c_{in}=22, c_{out}=57; on the fourth layer c_{in}=57, c_{out}=94. Each one-dimensional convolutional layer used k_c=3, p=2, and a padding parameter equal to 1 to preserve dimensionality and include zero values at the edges, allowing the filters to better treat edge values that would otherwise be treated less than other values in the center. Output padding with one extra value, without significantly affecting learning, was added to control the decoder layers' output sizes.

A linear layer is used to provide an initial size for the data supplied to the decoder. An unflatten layer is used to ensure the corresponding data size expected by the reverse convolutional layers of the decoder.

The best reverse convolutional layers of the decoder selected through TPE have the parameters of the first layer c_{in}=94, c_{out}=57; on the second layer c_{in}=57, c_{out}=22; on the third layer c_{in}=22, c_{out}=13; on the fourth layer c_{in}=13, c_{out}=1. 18 epochs selected through TPE were used for training and validation processes. The best α of the AE-CNN model determined through TPE was set to 0.0004. It should be noted that TPE determines the initial possible α, after which the Adam optimizer adjusts the determined α. The batch size for simultaneous sample processing by the AE-CNN model was determined to be 16.

5 RESULTS

The results of the AE-CNN model training and validation processes are shown in Table 1. The table shows L_{train} and L_{val} for 18 epochs. z and mean of E_{test} values are also represented.

Table 1 shows the satisfactory reduction of L_{train} and L_{val} over epochs. It can be seen that the mean E_{test}>z, so the method of detecting faults by comparing E of the AE-CNN model of the reproduced samples with z works in practice.

Table 1 – Results of training and validation of the AE-CNN model

Epochs	L_{train}	L_{val}
1	0.0097	0.0092
2	0.0091	0.0091
3	0.0091	0.0090
4	0.0089	0.0086
5	0.0078	0.0076
6	0.0064	0.0064
7	0.0052	0.0056
8	0.0045	0.0052
9	0.0041	0.0050
10	0.0039	0.0048
11	0.0037	0.0048
12	0.0036	0.0047
13	0.0035	0.0047
14	0.0034	0.0046
15	0.0033	0.0046
16	0.0033	0.0046
17	0.0032	0.0046
18	0.0032	0.0046
z	0.00467195	
Mean of E_{test}	0.007458317	

DOI 10.15588/1607-3274-2025-2-10

L_{train} and L_{val} are calculated at the end of each epoch and are dynamic during all epochs due to changes in the performance of the AE-CNN model.

Table 2 shows the mean values of E_{val} and E_{test} calculated from groups of 16 samples with the corresponding number to batch size showing a clear difference between them. The last row of Table 2 represents the mean values for the E_{val} and E_{test} columns.

Table 2 – The results of calculating the mean values of E_{val} and E_{test} for each batch group

Batch group	E_{val}	E_{test}
1	0.0045924	0.00741719
2	0.00449713	0.00747784
3	0.00457025	0.00725762
4	0.00458623	0.00775483
5	0.00447544	0.00727971
6	0.00461615	0.00741939
7	0.00446275	0.00729698
8	0.00461744	0.00755094
9	0.00463127	0.00701465
10	0.00448145	0.00788275
11	0.00452703	0.00733029
12	0.00454546	0.00676255
13	0.0046516	0.0077562
14	0.00459267	0.00735691
15	0.00456514	0.00795846
16	0.00467195	0.00786724
17	0.00454972	0.00778848
18		0.00705316
19		0.00748284
Mean of E	0.0045667106	0.0074583173

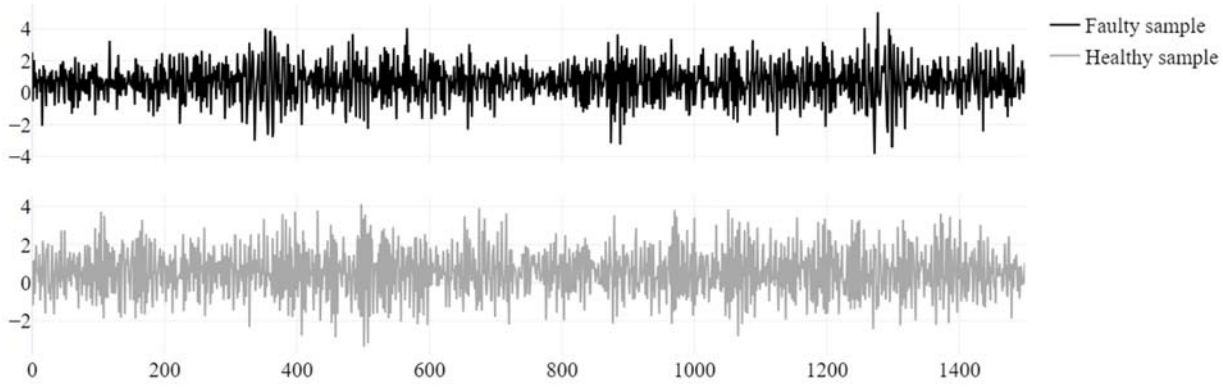

Figure 1 – The example of two faulty and healthy samples without SGF-MMN treatment

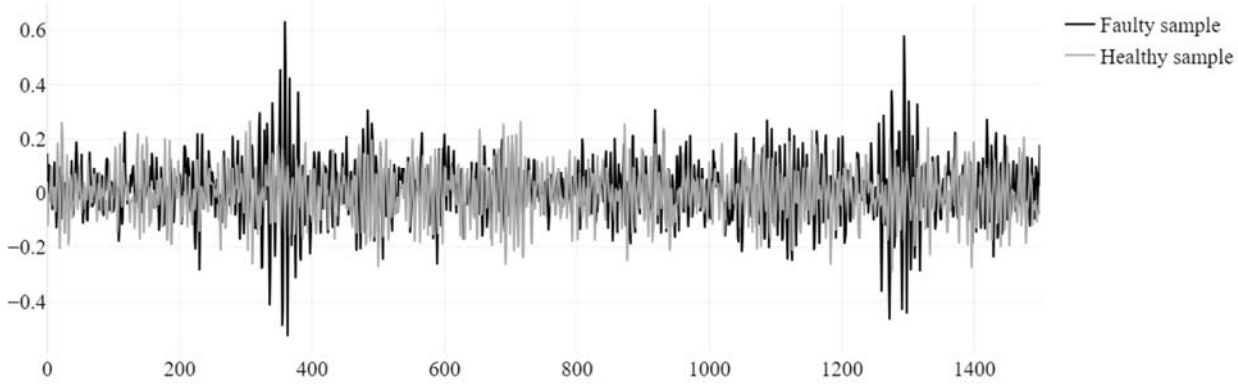

Figure 2 – The example of two SGF-MMN-treated faulty and healthy samples

DOI 10.15588/1607-3274-2025-2-10

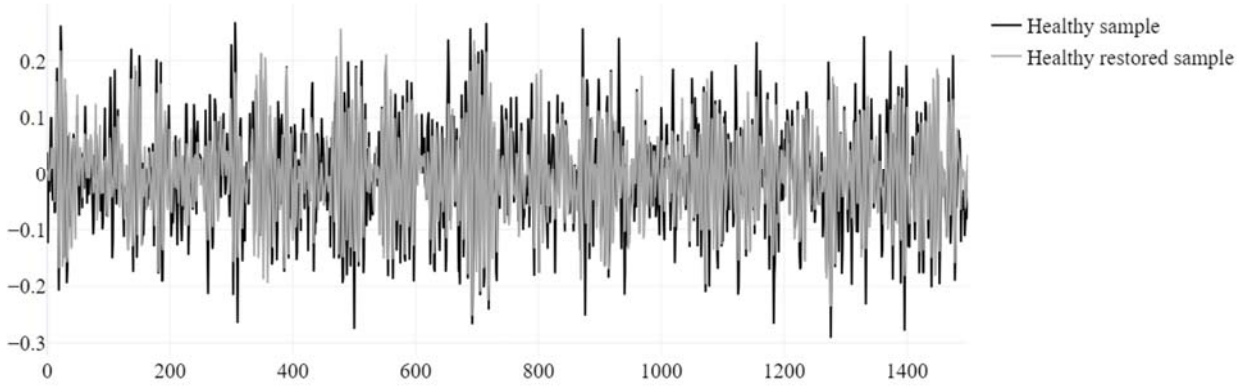

Figure 3 – The example of a healthy SGF-MMN-treated sample and its recovery from the AE-CNN model

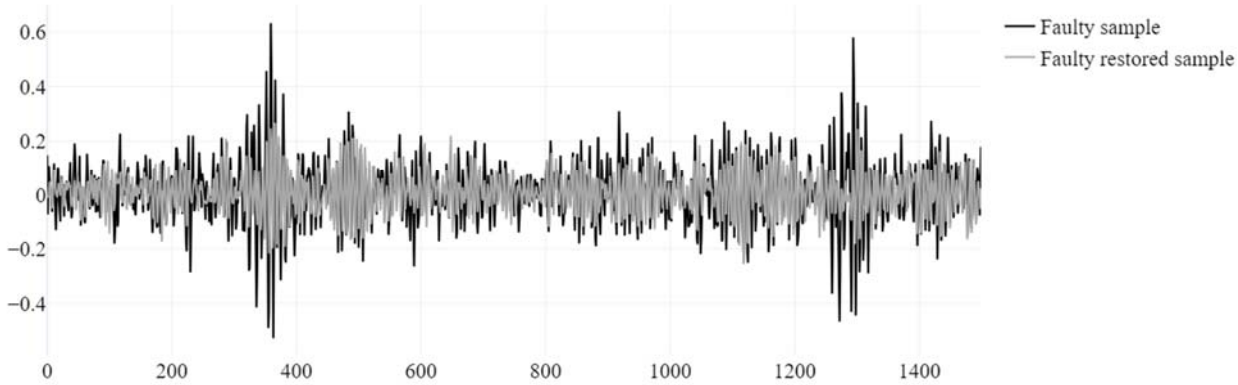

Figure 4 – The example of a faulty SGF-MMN-treated sample and its recovery from the AE-CNN model

Fig. 1 shows that the faulty and healthy samples without proper data pre-processing have blurred class characteristics, which can complicate the perception of the AE-CNN model and worsen its classification ability.

Fig. 2 shows that the SGF-MMN-treated vibrations of healthy and faulty samples mainly differ only in the characteristic pulses that are present in the faulty sample and absent in the healthy sample.

Fig. 3 shows that the AE-CNN model restores the healthy sample with satisfactory accuracy, highlighting the main details of the healthy sample, which confirms the qualitative performance of the AE-CNN model.

Fig. 4 shows that the AE-CNN model recovers a faulty sample without characteristic pulses due to the fact that the AE-CNN model learned to recover only healthy data features, which is why there is a clear difference between E_{val} and E_{test} in Table 2.

6 DISCUSSION

The dimensionality of the vibration samples was reduced to 1500 values, but still, the AE-CNN model showed good performance results in sample recovery and classification of faulty samples through the comparison of E_{val} and E_{test}. It is assumed that if the AE-CNN model will handle full-size samples, with proper tuning of $M()$ and corresponding h, the AE-CNN model will do well in the classification task. The difference when processing full-size samples will be that the difference between E_{val} and E_{test} will be much larger because the reduced faulty samples have a much smaller number of characteristic pulses than the full-size faulty samples.

It is worth noting that if the bearing faults have small amplitude and low intensity of the characteristic signals [5], that is, if the vibrations of the faulty samples are very similar to the vibrations of the healthy samples and have barely noticeable signs of the fault, the AE-CNN model constructed in this study is likely to be much more difficult to track the characteristics of faulty samples and distinguish them from healthy samples by a slight difference in class features, in this case, the E comparison method may be less effective.

The proposed combinatorial method in the study [5] solves the given problem. The method transforms the original dataset into a graph dataset and uses the feature aggregation module to aggregate the features of neighboring nodes.

Considering that during the SGF processing of the data provided for this study, only the features of the classes shown in Fig. 2 were detected, the AE-CNN model was built for the task of binary classification based on these features of the classes of healthy and faulty samples. It is also worth noting that the SGF parameters selected for processing the data provided in this study are appropriate only for this data and may vary when properly applied to other data.

DOI 10.15588/1607-3274-2025-2-10

In the study [7], the hyperparameters of the DAE hybrid network are mainly set based on common experience and are constantly adjusted by trial and error to achieve higher diagnostic accuracy. In this study, this feature was taken into account and the TPE method was used to select *h* in the AE-CNN model. Also, the method proposed in the study [7] can only detect new faults and cannot distinguish between different new faults, it is not able to represent and distinguish faults in more detail. In this research, the AE-CNN model can detect new faults if they have specific characteristics that are significantly different from the healthy characteristics of the samples. Still, it can also not distinguish between classes of possible faulty samples.

The method proposed in the study [9] is also based on the AE-CNN model and can be used to diagnose bearing faults under noise conditions. The AE-CNN model in this study uses data processed by SGF and MMN, however, in the case of using noisy data processed through MMN only, it is not known what the classification ability of the AE-CNN model will be, but assumed that it will be lower due to the presence of noise in the data, which can distort the characteristics of classes important for classification.

Research [10] mentions the integrated use of different deep learning models, such as LSTM network and CNN, the advantages of each model can be complementary. It is assumed that adding layers of LSTM to the AE-CNN model, given its ability to remember well the short-term and long-term features of the data, can indeed if correctly implemented, help to better capture the dependencies between successive pulses and long-term trends in vibration data, especially if the AE-CNN model processes samples of the full-size of 93752 values.

In the paper [13], a GCN-based LSTM autoencoder with a self-attention model for bearing fault diagnosis was proposed and evaluated using multivariate time series data. The proposed model was found to increase the accuracy of fault diagnosis by combining the GCN layer and the LSTM layer to extract important features from the frequency domain. In the data pre-processing step, data including various fault states and steady states were standardized, while features in the frequency domain were extracted through STFT conversion. A competent implementation of STFT can likely help improve the efficiency of AE-CNN in detecting faulty samples by taking into account frequency components and observing the change in frequency over time.

CONCLUSIONS

The task of detecting bearing faults when applying the machine learning method based on the ZSL principle has been solved.

The scientific novelty of the obtained results is that, for the first time, a machine learning method with the selection of hyperparameters was proposed for building the AE-CNN model based on the best-selected hyperparameters. The hyperparameter selection method divides the combinations of hyperparameters into good and bad using a certain threshold value of the objective function and builds models to estimate the probability of each group. This makes it possible to find new combinations of hyperparameters that have a higher probability of being good, thereby optimizing the choice of hyperparameters.

The practical significance of the obtained results is that, following the ZSL principle, a model based on a neural network was built that detects bearing faults and successfully performs binary classification of healthy and faulty samples of vibration data. The results of the experiment make it possible to recommend the proposed data pre-processing methods and the built model for practical application, as well as to determine the effective conditions for applying the data pre-processing methods and the built model based on a neural network.

Prospects for further research consist of testing the built model based on a neural network on other vibration data of bearings and its implementation in practical operations to detect bearing faults.

ACKNOWLEDGMENTS

Acknowledgments go to GPMS owner Eric Bechhoefer for providing the data.

REFERENCES

1. Mao W., He J., Li Y. et al. Bearing fault diagnosis with auto-encoder extreme learning machine: a comparative study [Electronic resource], *Journal of Mechanical Engineering Science*, 2017, Vol. 231, № 8, pp. 1560–1578. Mode of access: https://journals.sagepub.com/doi/10.1177/0954406216675896
2. Huang Z., Song X., Liao Z. et al. Bearing fault feature enhancement and diagnosis based on Savitzky-Golay filtering Gramian angular field [Electronic resource], *IEEE Access*, 2024, Vol. 12, pp. 87991–88005. Mode of access: https://ieeexplore.ieee.org/document/10570176
3. Chen X., Guo Y., Na J. Encoder signal-based optimized Savitzky-Golay and adaptive spectrum editing for feature extraction of rolling element bearing under low-speed and variable-speed conditions [Electronic resource], *ISA Transactions*, 2024, Vol. 154, pp. 371–388. Mode of access: https://www.sciencedirect.com/science/article/abs/pii/S0019057824003677?via%3Dihub
4. Wang Y., Li D., Li L. et al. A novel deep learning framework for rolling bearing fault diagnosis enhancement using VAE-augmented CNN model [Electronic resource], *Heliyon*, 2024, Vol. 10, № 15. Mode of access: https://doi.org/10.1016/j.heliyon.2024.e35407
5. Wang M., Yu J., Leng H.et al. Bearing fault detection by using graph autoencoder and ensemble learning [Electronic resource], *Scientific Reports*, 2024, Vol. 14, № 1, pp. 1–15. Mode of access: https://www.nature.com/articles/s41598-024-55620-6#citeas
6. Toma R. N., Piltan F., Kim J.-M. A deep autoencoder-based convolution neural network framework for bearing fault classification in induction motors [Electronic resource], *Sensors*, 2021, Vol. 21, № 24. Mode of access: https://www.mdpi.com/1424-8220/21/24/8453
7. Zhao Y., Hao H., Chen Y. et al. Novelty detection and fault diagnosis method for bearing faults based on the hybrid deep autoencoder network [Electronic resource],

DOI 10.15588/1607-3274-2025-2-10

Electronics, 2023,Vol. 12, № 13. Mode of access: https://www.mdpi.com/2079–9292/12/13/2826
8. Toma R. N., Piltan F., Im K. et al. A bearing fault classification framework based on image encoding techniques and a convolutional neural network under different operating conditions [Electronic resource], *Sensors*, 2022, Vol. 22, № 13. Mode of access: https://www.mdpi.com/1424-8220/22/13/4881
9. Yuan F., Xun P., Wang W. et al. Bearing fault diagnosis based on auto-encoder combined with CNN [Electronic resource], *Fuzzy Systems and Data Mining IX : Proceedings of the Fuzzy Systems and Data Mining Conference, 18–20 November 2023 : proceedings*. Xiamen, IOS Press, 2023, Vol. 354, pp. 334–344. Mode of access: https://ebooks.iospress.nl/doi/10.3233/FAIA231039
10. Rao C. A survey of autoencoder and convolutional neural network based methods for fault diagnosis [Electronic resource], *Advances in Engineering Technology Research*, 2024, Vol. 11, № 1, pp. 516–528. Mode of access: https://madison–proceedings.com/index.php/aetr/article/view/2529
11. Zhang S., Zhang S., Wang B.et al. Deep learning algorithms for bearing fault diagnostics – a comprehensive review [Electronic resource], *IEEE Access*, 2020, Vol. 8, pp. 29857–29881. Mode of access: https://ieeexplore.ieee.org/document/8988271
12. Gholamy A., V. Kreinovich, O. Kosheleva Why 70/30 or 80/20 relation between training and testing sets: a pedagogical explanation [Electronic resource], Mode of access: https://api.semanticscholar.org/CorpusID:7467506
13. Lee D. H. Choo, J. Jeong GCN-based LSTM Autoencoder with self-attention for bearing fault diagnosis [Electronic resource], *Sensors*, 2024, Vol. 24, № 15. Mode of access: https://www.mdpi.com/1424-8220/24/15/4855
14. Sohaib M., Kim J.-M. Reliable fault diagnosis of rotary machine bearings using a stacked sparse autoencoder-based deep neural network [Electronic resource], *Shock and Vibration*, 2018, Vol. 2018, № 1. Mode of access: https://onlinelibrary.wiley.com/doi/10.1155/2018/2919637
15. Gu Y., Cao J., Song X.et al. A denoising autoencoder-based bearing fault diagnosis system for time-domain vibration signals [Electronic resource], *Wireless Communications and Mobile Computing*, 2021, Vol. 2021, № 1. Mode of access: https://onlinelibrary.wiley.com/doi/10.1155/2021/9790053
16. Althubaiti A., Elasha F., Teixeira J. A. Fault diagnosis and health management of bearings in rotating equipment based on vibration analysis – a review [Electronic resource], *Journal of Vibroengineering*, 2021, Vol. 24, № 1, pp. 46–74. Mode of access: https://www.extrica.com/article/22100

Received 30.01.2025.
Accepted 10.04.2025.

УДК 004.93

ВИЯВЛЕННЯ НЕСПРАВНОСТІ ПІДШИПНИКА ЗА ДОПОМОГОЮ ЗГОРТКОВОЇ НЕЙРОННОЇ МЕРЕЖІ АВТОКОДУВАЛЬНИКА

Кисарін М. К. – студент факультету інформаційних технологій Державного торговельно-економічного університету, Київ, Україна.

АНОТАЦІЯ

Актуальність. Підшипники є важливою частиною для функціонування різних засобів пересування. Вони мають властивість зношуватися і виходити з ладу, що вимагає якісного і своєчасного виявлення несправностей. Збої не завжди легко виявити, тому використання традиційних методів виявлення може бути недостатньо ефективним. Використання методів машинного навчання, які добре підходять для завдання, може ефективно вирішити проблему виявлення несправностей підшипників. Об'єктом дослідження є процес неруйнівної діагностики підшипників. Предметом дослідження є методи підбору гіперпараметрів та іншої оптимізації для побудови діагностичної моделі на основі нейронної мережі за даними спостережень.

Мета роботи – створення моделі на основі нейронної мережі для виявлення несправностей підшипників на основі ZSL.

Метод. Запропонований фільтр згладжує дані, зберігаючи ключові характеристики, такі як піки та нахили, і усуває шум без істотного спотворення сигналу. Запропоновано метод нормалізації вібраційних даних, який полягає в центруванні даних і розподілі амплітуди в оптимальних межах, що сприяє коректній обробці цих даних архітектурою моделі. Запропоновано модель на основі нейронної мережі для виявлення несправностей підшипників шляхом обробки даних і подальшої двійкової класифікації їх коливань. Запропонована модель працює шляхом стиснення даних про вібрацію в приховане представлення та їх подальшого відновлення, обчислення похибки між відновленими та вихідними даними та визначення різниці між похибками даних про вібрацію справного та несправного підшипників. Метод машинного навчання Zero-Shot Learning передбачає навчання, перевірку моделі лише на справних даних про вібрацію та тестування моделі лише на несправних даних про вібрацію. Завдяки запропонованому методу машинного навчання модель на основі нейронної мережі здатна виявляти несправні підшипники, наявні в досліджуваному класі несправностей і теоретично нові класи несправностей, тобто модель може виявляти різні класи даних, які вона не бачила під час навчання. Архітектура моделі побудована на згорткових рівнях і рівнях максимального об'єднання кодера, а також на зворотних згорткових рівнях для декодера. Спеціальним методом вибираються найкращі гіперпараметри моделі.

Результати. Використовуючи бібліотеку PyTorch, було отримано модель, здатну до бінарної класифікації справних і несправних підшипників, шляхом навчання, валідації та тестування в програмному середовищі Kaggle.

Висновки. Тестування побудованої архітектури моделі підтвердило здатність моделі класифікувати справні та несправні підшипники двійково, що дозволяє рекомендувати її для використання на практиці для виявлення несправностей підшипників. Перспективи подальших досліджень можуть включати тестування моделі шляхом інтеграції в системи прогнозного обслуговування для своєчасного виявлення несправностей.

КЛЮЧОВІ СЛОВА: несправність підшипника, автокодувальник, згорткова нейронна мережа, навчання з нуля, бінарна класифікація.

DOI 10.15588/1607-3274-2025-2-10

ЛІТЕРАТУРА

1. Bearing fault diagnosis with auto-encoder extreme learning machine: a comparative study [Electronic resource] / [W. Mao, J. He, Y. Li et al.] // Journal of Mechanical Engineering Science. – 2017. – Vol. 231, № 8. – P. 1560–1578. – Mode of access: https://journals.sagepub.com/doi/10.1177/0954406216675896
2. Bearing fault feature enhancement and diagnosis based on Savitzky-Golay filtering Gramian angular field [Electronic resource] / [Z. Huang, X. Song, Z. Liao et al.] // IEEE Access. – 2024. – Vol. 12. – P. 87991–88005. – Mode of access: https://ieeexplore.ieee.org/document/10570176
3. Chen X. Encoder signal-based optimized Savitzky-Golay and adaptive spectrum editing for feature extraction of rolling element bearing under low-speed and variable-speed conditions [Electronic resource] / X. Chen, Y. Guo, J. Na // ISA Transactions. – 2024. – Vol. 154. – P. 371–388. – Mode of access: https://www.sciencedirect.com/science/article/abs/pii/S0019057824003677?via%3Dihub
4. A novel deep learning framework for rolling bearing fault diagnosis enhancement using VAE-augmented CNN model [Electronic resource] / [Y. Wang, D. Li, L. Li et al.] // Heliyon. – 2024. – Vol. 10, № 15. – Mode of access: https://doi.org/10.1016/j.heliyon.2024.e35407
5. Wang M. Bearing fault detection by using graph autoencoder and ensemble learning [Electronic resource] / [M. Wang, J. Yu, H. Leng et al.] // Scientific Reports. – 2024. – Vol. 14, № 1. – P. 1–15. – Mode of access: https://www.nature.com/articles/s41598-024-55620-6#citeas
6. Toma R. N. A deep autoencoder-based convolution neural network framework for bearing fault classification in induction motors [Electronic resource] / R. N. Toma, F. Piltan, J.-M. Kim // Sensors. – 2021. – Vol. 21, № 24. – Mode of access: https://www.mdpi.com/1424-8220/21/24/8453
7. Novelty detection and fault diagnosis method for bearing faults based on the hybrid deep autoencoder network [Electronic resource] / [Y. Zhao, H. Hao, Y. Chen et al.] // Electronics. – 2023. – Vol. 12, № 13. – Mode of access: https://www.mdpi.com/2079-9292/12/13/2826
8. A bearing fault classification framework based on image encoding techniques and a convolutional neural network under different operating conditions [Electronic resource] / [R. N. Toma, F. Piltan, K. Im et al.] // Sensors. – 2022. – Vol. 22, № 13. – Mode of access: https://www.mdpi.com/1424-8220/22/13/4881
9. Bearing fault diagnosis based on auto-encoder combined with CNN [Electronic resource] / [F. Yuan, P. Xun, W. Wang et al.] Fuzzy Systems and Data Mining IX : Proceedings of the Fuzzy Systems and Data Mining Conference, 18–20 November 2023 : proceedings. – Xiamen : IOS Press, 2023. – Vol. 354. – P. 334–344. – Mode of access: https://ebooks.iospress.nl/doi/10.3233/FAIA231039
10. Rao C. A survey of autoencoder and convolutional neural network based methods for fault diagnosis [Electronic resource] / C. Rao // Advances in Engineering Technology Research. – 2024. – Vol. 11, № 1. – P. 516–528. – Mode of access: https://madison-proceedings.com/index.php/aetr/article/view/2529
11. Zhang S. Deep learning algorithms for bearing fault diagnostics – a comprehensive review [Electronic resource] / [S. Zhang, S. Zhang, B. Wang et al.] // IEEE Access. – 2020. – Vol. 8. – P. 29857–29881. – Mode of access: https://ieeexplore.ieee.org/document/8988271
12. Gholamy A. Why 70/30 or 80/20 relation between training and testing sets: a pedagogical explanation [Electronic resource] / A. Gholamy, V. Kreinovich, O. Kosheleva // Mode of access: https://api.semanticscholar.org/CorpusID:7467506
13. Lee D. GCN-based LSTM Autoencoder with self-attention for bearing fault diagnosis [Electronic resource] / D. Lee, H. Choo, J. Jeong // Sensors. – 2024. – Vol. 24, № 15. – Mode of access: https://www.mdpi.com/1424-8220/24/15/4855
14. Sohaib M. Reliable fault diagnosis of rotary machine bearings using a stacked sparse autoencoder-based deep neural network [Electronic resource] / M. Sohaib, J.-M. Kim // Shock and Vibration. – 2018. – Vol. 2018, № 1. – Mode of access: https://onlinelibrary.wiley.com/doi/10.1155/2018/2919637
15. Gu Y. A denoising autoencoder-based bearing fault diagnosis system for time-domain vibration signals [Electronic resource] / [Y. Gu, J. Cao, X. Song et al.] // Wireless Communications and Mobile Computing. – 2021. – Vol. 2021, № 1. – Mode of access: https://onlinelibrary.wiley.com/doi/10.1155/2021/9790053
16. Althubaiti A. Fault diagnosis and health management of bearings in rotating equipment based on vibration analysis – a review [Electronic resource] / A. Althubaiti, F. Elasha, J. A. Teixeira // Journal of Vibroengineering. – 2021. – Vol. 24, № 1. – P. 46–74. – Mode of access: https://www.extrica.com/article/22100

DOI 10.15588/1607-3274-2025-2-10

UDC 004.896

SYNTHESIS OF NEURAL NETWORK MODELS FOR TECHNICAL DIAGNOSTICS OF NONLINEAR SYSTEMS

Leoshchenko S. D. – PhD, Associate Professor of the Department of Software Tools, National University "Zaporizhzhia Polytechnic", Zaporizhzhia, Ukraine.

Oliinyk A. O. – Dr. Sc., Professor, Professor of the Department of Software Tools, National University "Zaporizhzhia Polytechnic", Zaporizhzhia, Ukraine.

Subbotin S. A. – Dr. Sc., Professor, Head of the Department of Software Tools, National University "Zaporizhzhia Polytechnic", Zaporizhzhia, Ukraine.

Morklyanyk B. V. – Dr. Sc., Professor, Professor of the Department of Information Technology, Military Academy, Kyiv, Ukraine.

ABSTRACT

Context. The problem of synthesizing a diagnostic model of complex technical processes in nonlinear systems, which should be characterized by a high level of accuracy, is considered. The object of research is the process of synthesizing a neural network model for technical diagnostics of nonlinear systems.

Objective of the work is to synthesize a high-precision neural network model based on previously accumulated historical data about the system.

Method. It is proposed to use artificial neural networks for modeling nonlinear technical systems. First, you need to perform an overall assessment of the complexity of the task. Based on the assessment, a decision can be made on the best approach to organizing neuromodel synthesis. So, for the task, the level of 'random complexity' was chosen, because despite the relative structure of the data, their total array is quite large in volume and requires careful study in order to ensure high quality of the solution. Therefore, in the future, it was proposed to use a neuromodel based on recurrent networks of the GRU topology and use swarm intelligence methods for neurosynthesis, in particular the A3C method. The results obtained showed a high level of solution obtained, but due to the high level of resource intensity, the proposed approach requires further modifications.

Results. A diagnostic model of complex technical processes in nonlinear systems of optimal topology, characterized by a high level of accuracy, is obtained. The built neuromodel reduces the risks associated with ensuring human safety.

Conclusions. The conducted experiments confirmed the operability of the proposed approach and allow us to recommend it for further refinement in order to implement technical, industrial and operational process control systems in practice in automation systems. Prospects for further research may lie in optimizing the resource intensity of synthesis processes.

KEYWORDS: technical diagnostics, nonlinear systems, machine learning, neural network synthesis, indicator system, neuromodel, sampling, learning, error.

ABBREVIATIONS

A3C is an Asynchronous Advantage Actor-Critic method;

AdaGrad is an adaptive gradient algorithm;

ANN is an artificial neural net;

BTTT is a backpropagation throw the time method;

DNN is a deep neural network;

GBO is a gradient-based optimization method;

GRU is a gated recurrent unit;

ML is machine learning;

LSTM is a long short-term memory network;

RC is random complexity;

RL is a reinforcement learning;

RNN is recurrent neural network.

NOMENCLATURE

Inf_{Sample} is a general information of input data (data set);

K_{input} is a number of element types in the neural network;

K_{corrY} is a number of independent variables that strongly correlate with the original features;

K_{imp} is a number of the most significant independent variables among factors4

$K_{ntcorrX}$ is a number of independent variables that are weakly dependent on others or do not correlate with each other;

n is a number of input features that characterize sample instances;

N_i is a multiple neurons at the network input;

N_{i_l} is a neuron at the network input;

N_o is a multiple neurons at the network output;

N_{o_p} is a neuron at the network output;

N_h is a multiple neurons of the hidden network layer;

N_{h_r} is a hidden network layer neuron;

$Num_{elemtype}$ is a number of element types in the neural network;

NN is a neural network;

NN_{struct} is a structure of neural network;

l is a number of neurons at the network input;

$Lev_{accmeas}$ is a measurement accuracy level;

Lev_{fctr} is a level of significant and less significant and/or non-significant factors4

Lev_{manag} is a level of possible control and management;

Lev_{task} is a conditional difficulty level of the task;

DOI 10.15588/1607-3274-2025-2-11

$Lev_{smplfctn}$ is a level of possible simplification of the structure;

m is a number of dependent (categorical) features of sample instances;

p is a number of neurons at the network output;

$Param_T$ is additional and specificity parameters of task;

q is a number of connections between neurons in the network;

r is number of neurons in the hidden network layer;

RC is random complexity;

$Sample$ is a data set;

$Task$ is general represent of the modeling task;

w is a multiple of connections between neurons;

w_q is a connection between neurons in the network;

x_n is a independent attribute of the sample instance;

X is a set of independent attribute (variables);

y_m is a value of the dependent variable (attribute) of the sample instance;

Y is a set of values of dependent variables.

INTRODUCTION

ML is widely used for diagnostics of complex technical processes, as it provides a number of advantages that are not available in classical approaches using manual control, rule systems, and the like. Today, ML is a powerful tool for solving such problems [1]–[4].

In nonlinear technical systems, there are quite complex patterns in the data received from Sensor Systems. Such data contains nonlinear relationships, i.e. technical processes often involve nonlinear interactions between several variables (for example, temperature, pressure, vibration). ML models can automatically recognize these patterns. In addition, most systems generate large amounts of sensor or operational data. ML can efficiently process large data sets and identify mission-critical functions [1]–[4].

The main further goal of using ML models is to automate diagnostics. ML-based models will allow you to perform real-time analysis. ML models can analyze data in real time, allowing instant fault detection and diagnostics. Moreover, the use of ML will reduce human intervention. Unlike manual diagnostics, ML systems can process data independently, reducing reliance on industry experts [1]–[4].

Processing noise in data and uncertainty. Complex systems often operate in environments where data is noisy or incomplete. ML models are designed to summarize imperfect data. In addition, ML models can estimate the probability of various failures or technological anomalies, providing probabilistic results that help with decision-making [1]–[4].

ML-based models are characterized by a high level of adaptability to new conditions. Technical processes often develop due to changes in operating conditions or system configuration. ML models can be retrained or modified to adapt to these changes. Pre-trained ML models can be adapted to new but similar processes with minimal additional training.

In industries such as manufacturing, power plants, or transportation, ML can perform diagnostic tasks for thousands of sensors and subsystems simultaneously. ML can be deployed on peripherals or in centralized systems to scale diagnostics in multiple locations [4].

ML models analyze patterns in historical data to predict when components might fail, preventing unplanned downtime. Uncontrolled ML models can detect deviations from normal operating conditions, warning of potential problems at an early stage.

ML models allow you to determine which variables or functions are most important for fault diagnosis, providing valuable information for system optimization. By studying patterns in misclassification or anomalies, ML can help pinpoint the root causes of problems [1].

Summing up, we should note the main advantages in terms of costs and efficiency, namely:

– reduced downtime: early detection of malfunctions minimizes production shutdowns and repair costs;

– reduced labor costs: automated diagnostics reduces the need for constant monitoring by operators;

– by providing accurate and timely information, ML allows you to make more informed decisions.

The object of study is synthesizing a high-precision neural network model based on previously accumulated historical data about the system.

The subject of the study is a neural network model of complex technical processes in nonlinear systems, which should be characterized by a high level of accuracy.

The purpose of the work is to construct and study neuromodels of complex technical processes in nonlinear systems, which should be characterized by a high level of accuracy with a preliminary definition of structural features based on the use of a system of indicators.

1 PROBLEM STATEMENT

Let it be that a data set $Sample$, containing data on mechanical parameters (e.g., vibration) recorded by specialized sensors and obtained during an operational study of a complex nonlinear technical system (e.g., helicopter transmission, car, or engine) is given. Then, $Sample = \langle X, Y \rangle$, where $X = \{x_1, x_2, x_3, ..., x_i\}$, where $i = \overline{1;1158}$, and $Y = \{y\}$ is the key output variable.

Then, it is necessary to determine such a set of $X*$, to ensure Y that the diagnostic error is minimized by a diagnostic model based on such a data set: $Error\left(Model_{diag}\left(X*\right)\right) \to \min$.

Most of the tasks, for which is planning to use ML models, have a different nature and a high level of specificity ($Param_T$) [5]. However, when using the apparatus of neural networks, it is sufficient to have a comprehensive assessment of the complexity of the task: $Task = \{Param_T, Lev_{Task}\}$ [5]. Such a comprehensive assessment can be obtained on the basis of information about the input data of the task (a sample of data) and a group of criteria for evaluating the accuracy of the data

DOI 10.15588/1607-3274-2025-2-11

and the requirements for the model: $Lev_{Task} = \{Inf_{sample}, Lev_{smplfctm}, Lev_{fctr}, Lev_{accmeas}, Lev_{manag}\}$.

It was noted in [5] that a complex neuromodel based on a RNN and DNN topologies will be sufficient for tasks belonging to the RC category. Then such a model (NN) will consist of: a set of neurons $N = \{N_i, N_o, N_h\}$ consisting of subsets of input $N_i = \{N_{i_1}, N_{i_2}, ..., N_{i_l}\}, l = 1,2,...,|N_i|$, output $N_o = \{N_{o_1}, N_{o_2}, ..., N_{o_p}\}, p = 1,2,...,|N_o|$, and hidden neurons $N_h = \{N_{h_1}, N_{h_2}, ..., N_{h_r}\}, r = 1,2,...,|N_h|$. The number of neurons in the hidden layer ($N_h = \{N_{h_1}, N_{h_2}, ..., N_{h_r}\}, r = 1,2,...,|N_h|$) can be calculated based on analytical estimates of the input data [5].

After that, it can proceed to determining the weights of connections between neurons $w = \{w_q\}$, in other words, to parametric synthesis. Having determined the values of the elements of sets, we can consider the synthesis of ANN: complete [5].

Therefore, the first subtask will be to determine the exact category of complexity of the problem based on the values of the criteria $Lev_{Task} = \{Inf_{sample}, Lev_{smplfctm}, Lev_{fctr}, Lev_{accmeas}, Lev_{manag}\}$ and data about the data sample. The next subtask will be the calculation of the number of neurons in the hidden layer of the network $|N_h| = K_{input} - K_{corrY} - K_{imp} - K_{ntcorrX}$ [5].

2 REVIEW OF THE LITERATURE

GRU is a type of RNN designed for processing sequential data. GRUs are particularly effective for tasks related to time series or sequential data, where dependencies need to be fixed over time. Presented in [6], GRUs are a simplified version of LSTM, but retain comparable performance while reducing computational complexity.

The GRU consists of two main gateways [6], [7]:

a) update gate:

– decides how much past information should be saved;

– helps the network focus on up-to-date past information, while forgetting unnecessary details;

b) reset gate:

– manages how much past information should be deleted for the current time step;

– allows the network to reload its memory when new patterns or states appear [6], [7].

GRUs do an excellent job of fixing time dependencies in sequential data, such as sensor readings during technical processes. They can detect patterns or anomalies in time-dependent data, which is crucial for diagnosing failures in dynamic systems.

GRUs have fewer parameters compared to LSTM, which reduces computing costs. This speeds up GRU training and deployment, especially for large data sets or systems with real-time constraints [6], [7].

GRUs can study long-term dependencies in sequences, avoiding problems such as vanishing gradients faced by Standard RNNs. This is very important for diagnosing processes in which the consequences of past events (for example, earlier anomalies) affect the current state [8].

Complex technical processes often lead to noisy data. GRUs are resistant to such noise due to their closed mechanisms that selectively filter out irrelevant information [9].

GRU can efficiently process multidimensional time series of data. For example, power plant operation Diagnostics may include simultaneous analysis of temperature, pressure, and vibration data [7].

GRUs are computationally efficient and can be deployed for real-time fault detection and diagnostics, which is vital in mission-critical systems such as production lines or power grids [7].

GRUs adapt well to a variety of technical processes, making them versatile for applications in various industries, from Automotive to aerospace.

GRU in diagnostics is recommended to be used for:

a) fault detection:

– detection of anomalies in machine behavior by analyzing time series of sensor data

– example: detection of unusual vibrations in turbines or engines;

b) preventive maintenance:

– predict possible system failures by analyzing historical data;

– example: industrial equipment wear monitoring for maintenance planning;

c) process optimization:

– analysis of time dependencies to optimize operating parameters;

– example: configure the input data of a chemical enterprise based on sensor feedback to maximize performance;

d) root cause analysis:

– tracking patterns in time series data to identify the underlying cause of the malfunction;

– example: diagnostics of pressure fluctuations in pipelines.

Thus, GRUs are ideal for diagnosing complex technical processes, as they provide an optimal balance of computational efficiency, resistance to encrypted data, and the ability to capture complex time patterns. Their real-time capabilities and adaptability make them a one-stop solution for dynamic applications with large amounts of data [8].

A3C is an advanced RL method that can become an effective method for synthesizing GRU-based networks, especially for tasks that require high accuracy, such as diagnosing complex technical processes. The benefits of A3C are in good agreement with the requirements for GRU training networks to perform these tasks [9], [10].

A3C is a reinforcement learning system in which:

– many agents work asynchronously in parallel environments, collecting data and learning from different experiences;

– it uses two networks:

DOI 10.15588/1607-3274-2025-2-11

– actor: determines what actions should be taken (network of policies);

– critic: evaluates the quality of actions taken by evaluating the value function;

– the method optimizes performance by combining policy-based methods (learning policies) and value-based methods (evaluating the value of states or actions);

– for GRU networks: GRU can serve as a basic architecture for participating and / or critical networks to process sequential or temporary data.

A3C uses the term entropy-based regularization to encourage research, allowing GRU to learn from less common but important patterns [9], [10].

GRUs, combined with A3C, perfectly captures these dependencies, focusing on sequences that maximize benefits while effectively identifying the most significant patterns in the data.

A3C stabilizes the learning process by asynchronous updating of weighting factors by multiple agents. This asynchronous process smooths out gradients, resulting in faster convergence and a reduced risk of overtraining.

3 MATERIALS AND METHODS

As it was given in the previous section, the modeling task can be unified for a specific task after a certain comprehensive assessment of its complexity. Given that the structure of ANN ($NN = (struct, param)$) allows to most subtly encode the relationships between the input data ($X = \{x_1, x_2, ...x_n\}$) [5], it is necessary to accurately select the synthesis option for such a non-network model. Based on the values of the indicators to assess the complexity of the task ($Lev_{Task} = \{Inf_{sample}, Lev_{smplfctm}, Lev_{fctr}, Lev_{accmeas}, Lev_{manag}\}$), it can be chosen a way to synthesize the most acceptable structure [5].

The general scheme of chosen the category of complicity using indicators prepared as a formula (1).

$$Lev_{Task} = \begin{cases} Lev_{smplfctn} \le 0, Lev_{fctr} \le 0, Lev_{accmeas} = 0, Lev_{manag} = 0 \to OS \\ Lev_{smplfctn} > 0, Lev_{fctr} \le 0, Lev_{accmeas} = 0, Lev_{manag} = 0 \to OC \\ Lev_{smplfctn} \le 0 \,||\, Lev_{smplfctn} \ge 0, Lev_{fctr} > 0, Lev_{accmeas} > 0, Lev_{manag} = 0 \to CAwP \\ Lev_{smplfctn} > 0, Lev_{fctr} > 0, Lev_{accmeas} \ge 0, Lev_{manag} \ge 0 \to RC \end{cases}. \quad (1)$$

Therefore, we can conclude that it has a level of complexity of the RC category, that is why we will be using combine of GRU model and A3C method for training (Fig. 1).

A3C directly optimizes the expected reward (or a surrogate) by combining [11], [12]:

Actor Loss: Encourages the GRU to make better predictions for diagnosis.

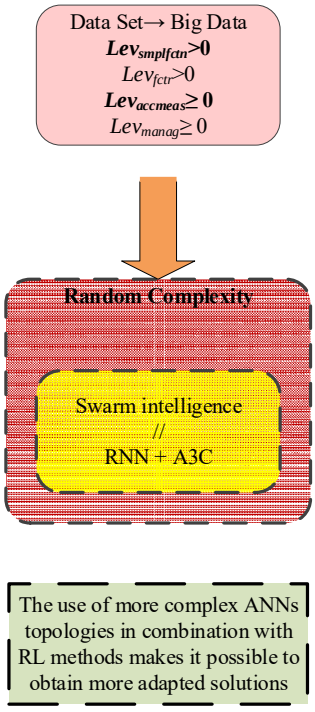

Figure 1 – Organized simplicity category of modeling task

Critic Loss: Ensures the network evaluates the quality of predictions accurately [13], [14].

This joint optimization ensures that the GRU learns both what actions to take and how good those actions are, leading to a more accurate and robust model.

In diagnosing complex processes, data is often noisy or changes over time.

A3C's parallel agents, combined with GRU's gating mechanisms, allow the system to:

– focus on relevant patterns;

– adapt to dynamic data distributions;

– improve robustness to outliers and transient conditions.

A3C utilizes multiple agents working independently, which reduces bottlenecks in learning long-term dependencies in GRUs.

This enables better model performance on large-scale problems with time-series data, where capturing subtle temporal patterns is essential [8]–[13].

GRUs already excel at modeling sequences, but A3C reinforces this by focusing on rewarded patterns:

– fault patterns that result in high rewards (accurate predictions) are emphasized;

– unimportant or noisy patterns are downplayed.

A3C agents experience diverse states and collect varied trajectories, effectively regularizing the training process. This diversity improves the GRU network's generalization, avoiding overfitting to specific fault scenarios.

Collect multivariate time-series data (in next section it will be noticed that this is vibration) from sensors.

A3C Setup:

– use GRUs for both the Actor and Critic networks:

– input: sequential sensor data;

DOI 10.15588/1607-3274-2025-2-11

– actor output: predicted fault class or action;

– critic output: value of the current sequence.

Training:

– deploy multiple agents in parallel, each exploring different sensor sequences and learning asynchronously.

Train GRUs to:

– recognize normal and fault patterns$

– predict future states or faults based on sequential dependencies.

Optimization:

– use the A3C loss function to refine GRU parameters:

– minimize actor loss for better fault classification.

– minimize critic loss to improve evaluation of prediction quality.

Deployment:

– the resulting GRU model can diagnose faults with high accuracy in real-time.

4 EXPERIMENTS

For testing was perpetrate next data set:

– 1158 Vibration Data Sets

– roughly 2/3s of the files are nominal data, while 1/3 have a gear fault.

Scoring: Percent Correct, total correct / 1158

Generally, for experimental comparing different strategies of ML approaches was using list of Python libraries and packages, as:

– TensorFlow Agents for RL methods;

– Keras for different ANNs models [15] (as DNN, RNN, CNN, etc.).

Table 1 – Model results based on test data

Model + method combination	Synthesis time, s	Accuracy on training part of data set	Accuracy on test part of data set
Perceptron + Backpropagation	5236	92.77	92.04
DNN + GBO	6286	96.52	95.72
DNN + AdaGrad	4632	97.24	96.25
GRU + Backpropagation Through Time	5965	96.39	95.76
GRU + A3C	7045	98.58	98.37
GRU + MGA	8906	98.73	98.66

5 RESULTS

Table 1 shows the results of models based on test data. During compression special attention was concentrated on accuracy of models for different depended features.

Accuracy was calculated as:

$$E = \frac{error_{class}}{Number_{sampl}} \cdot 100\% .$$

In multiclass classification, accuracy is a standard metric that measures the proportion of correctly predicted labels out of the total predictions made. It is particularly straightforward when each instance belongs to one of multiple classes, and only one label is correct.

For different ML models was using different training methods.

6 DISCUSSION

From the test results, it can be seen that the GRU-based approach in combination with RL is one of the slowest approaches. Therefore, the difference in comparison even with DNN sometimes almost 2 times indicates a high resource intensity in terms of time, because RL methods do not differ in high speed. Moreover, setting up GRU metaparameters requires additional processing of the gate value, which also slows down the synthesis time. On the other hand, when using the more classical BPTT, the time has been reduced, but this approach to training, firstly, is quite difficult to parallelize, which significantly slows it down for working on high-performance computing systems, and secondly, despite the more optimized synthesis time, the accuracy of work is still not high.

In addition, despite the large number of computing nodes, DNN also does not provide an acceptable level of accuracy. And given the importance of ensuring the safety of people during technical processes, it is not possible to compromise accuracy. Also, it is worth noting that despite the optimization of the synthesis time, when working with such a model, the load on computing resources is also high.

An ordinary Perceptron was taken for analysis simply to ensure that even the simplest neural network models show a high level of accuracy (more than 90%), but still do not fully allow abstracting complex data connections.

The use of MGA [16] for GRU synthesis was also considered separately as a stochastic approach. Despite the highest time indicators, this particular solution demonstrated the highest accuracy, but the synthesis process itself, in addition to high time requirements, also imposes high requirements on computing power.

CONCLUSIONS

The urgent scientific and applied problem of synthesizing a diagnostic model of complex technical processes in nonlinear systems, which should be characterized by a high level of accuracy, is considered is solved.

The scientific novelty lies in the study of the use of a system of criteria for determining the structural features of a neural network model. Based on the assessment of the complexity of the task and the system of indicators, it was possible to obtain neuromodel with a high level of accuracy of work.

The practical significance lies in the fact that the developed neural network models can be used during the implementation of real technical processes in production facilities. Their use will significantly reduce production costs and automate the modeling process.

Prospects for further research and development are mechanisms of optimization of computing resources using.

DOI 10.15588/1607-3274-2025-2-11

ACKNOWLEDGEMENTS

The work was carried out with the support of the state budget research project of the state budget of the National University "Zaporozhzhia Polytechnic": "Intelligent information processing methods and tools for decision-making in the military and civilian industries" (state registration number 0124U000250).

REFERENCES

1. Ameisen E. Building Machine Learning Powered Applications, Going from Idea to Product. California, O'Reilly Media, 2020, 260 p.
2. Bonaccorso G. Mastering Machine Learning Algorithms, Expert techniques to implement popular machine learning algorithms and fine-tune your models. Birmingham, Packt Publishing, 2018, 576 p.
3. Patan K. Artificial Neural Networks for the Modelling and Fault Diagnosis of Technical Process. Berlin, Springer, 2008, 112 p. DOI: 10.1007/978-3-540-79872-9
4. Leoshchenko S., Oliinyk A., Subbotin S., Zaiko T. Using Modern Architectures of Recurrent Neural Networks for Technical Diagnosis of Complex Systems, *2018 International Scientific-Practical Conference Problems of Info-communications. Science and Technology (PIC S&T), Kharkiv, 9–12 October 2018, proceedings*. Kharkiv, IEEE, 2018, pp. 411–416. DOI: 10.1109/INFOCOMMST.2018.8632015
5. Leoshchenko S., Subbotin S., Oliinyk A., Narivs'kiy O. Implementation of the indicator system in modeling complex technical systems. *Radio Electronics, Computer Science, Control*, 2021, Vol. 1, pp. 117–126. DOI: 10.15588/1607-3274-2021-1-12
6. Learning Phrase Representations using RNN Encoder-Decoder for Statistical Machine Translation, URL: https://arxiv.org/abs/1406.1078
7. Ahmadian A., Salahshour S. Soft Computing Approach for Mathematical Modeling of Engineering. London, Chapman and Hall (CRC Press), 2021, 222 p.
8. Sayyaadi H. Modeling, Assessment, and Optimization of Energy Systems. Cambridge, Academic Press, 2020, 558 p.
9. Koulamas C., Lazarescu M.T. Real-Time Sensor Networks and Systems for the Industrial IoT. Basel, Mdpi AG, 2020, 242 p. DOI: 10.3390/books978-3-03943-431-2
10. Senge P. M. The Fifth Discipline, The Art & Practice of The Learning Organization. New York, Doubleday, 2006, 445 p.
11. Bruce P., Bruce A. Practical Statistics for Data Scientists, 50 Essential Concepts. California, O'Reilly Media, 2017, 318 p.
12. Finch W.H. Exploratory Factor Analysis. California, SAGE Publications, 2019, 144 p.
13. Rencher A. C., Christensen W. F. Methods of Multivariate Analysis. New Jersey, John Wiley & Sons, 2012, 800 p.
14. Dean A., Voss D., Draguljić D. Design and Analysis of Experiments (Springer Texts in Statistics), 2nd Edition. Berlin, Springer, 2017, 865 p. DOI: 10.1007/978-3-319-52250-0
15. Sewak M. Deep Reinforcement Learning, Frontiers of Artificial Intelligence. Berlin, Springer, 2020, 220 p. DOI: 10.1007/978-981-13-8285-7
16. Leoshchenko S., Oliinyk A., Subbotin S., Lytvyn V., V. Shkarupylo V. Modification and parallelization of genetic algorithm for synthesis of artificial neural networks. *Radio Electronics, Computer Science, Control*, 2019, Vol. 4, pp. 68–82. DOI: 10.15588/1607-3274-2019-4-7.

Received 26.01.2025.
Accepted 04.04.2025.

УДК 004.896

СИНТЕЗ НЕЙРОМЕРЕЖЕВИХ МОДЕЛЕЙ ДЛЯ ТЕХНІЧНОГО ДІАГНОСТУВАННЯ НЕЛІНІЙНИХ СИСТЕМ

Леощенко С. Д. – д-р філософ., доцент кафедри програмних засобів Національного університету «Запорізька політехніка», Запоріжжя Україна.

Олійник А. О. – д-р техн. наук, доцент, професор кафедри програмних засобів Національного університету «Запорізька політехніка», Запоріжжя, Україна.

Субботін С. О. – д-р техн. наук, професор, завідувач кафедри програмних засобів Національного університету «Запорізька політехніка», Запоріжжя, Україна.

Морклянник Б. В. – д-р техн. наук, професор, професор кафедри інформаційних технологій, Воєнна академія, м. Київ, Україна

АНОТАЦІЯ

Актуальність. Розглянуто задачу синтезу діагностичної моделі складних технічних процесів у нелінійних системах, що має відрізнятися високим рівнем точності. Об'єктом дослідження є процес синтезу нейромережевої моделі для технічного діагностування нелінійних систем.

Мета роботи полягає у синтезі нейромережевої моделі високої точності, на основі попередньо накопичених історичних даних про систему.

Метод. Запропоновано використовувати штучні нейронні мережі для моделювання нелінійних технічних систем. По-перше, необхідно виконати загальну оцінку складності задачі. На основі оцінки можна прийняти рішення про подальший підхід до організації синтезу нейромоделі. Від так, для поставленої задачі було обрано рівень складності безладна складність, адже не зважаючи на відносну структурованість даних, їх загальний масив є досить великим за об'ємом та вимагає ретельного опрацювання з метою забезпечення високої якості рішення. Тому в подальшому було запропоновано використовувати нейромодель на основі рекурентних мереж топології GRU та використати для нейросинтезу методи ройового інтелекту, зокрема метод АЗС. Отримані результати засвідчили високий рівень отриманого рішення, проте через високий рівень ресурсоємності запропонований підхід вимагає подальших модифікацій.

Результати. Отримано діагностичну модель складних технічних процесів у нелінійних системах оптимальної топології, що відрізняється високим рівнем точності. Побудована нейромодель знижує ризики пов'язані зі забезпеченням людської безпеки.

Висновки. Проведені експерименти підтвердили працездатність запропонованого підходу і дозволяють рекомендувати його для подальшого допрацювання з метою імплементації на практиці в системи автоматизації систем контролю технічних, промислових та експлуатаційних процесів. Перспективи подальших досліджень можуть полягати в оптимізації ресурсоємності процесів синтезу.

КЛЮЧОВІ СЛОВА: технічне діагностування, нелінійні системи, машинне навчання, синтез нейронних мереж, система індикаторів, нейромодель, вибірка, навчання, помилка.

DOI 10.15588/1607-3274-2025-2-11

ЛІТЕРАТУРА

1. Ameisen E. Building Machine Learning Powered Applications: Going from Idea to Product / E. Ameisen. – California: O'Reilly Media, 2020. – 260 p.
2. Bonaccorso G. Mastering Machine Learning Algorithms: Expert techniques to implement popular machine learning algorithms and fine-tune your models / G. Bonaccorso. – Birmingham : Packt Publishing, 2018. – 576 p.
3. Patan K. Artificial Neural Networks for the Modelling and Fault Diagnosis of Technical Processe / K. Patan. – Berlin : Springer, 2008. – 112 p. DOI: 10.1007/978-3-540-79872-9
4. Using Modern Architectures of Recurrent Neural Networks for Technical Diagnosis of Complex Systems / [S. Leoshchenko, A. Oliinyk, S. Subbotin, T. Zaiko] // 2018 International Scientific-Practical Conference Problems of Infocommunications. Science and Technology (PIC S&T), Kharkiv, 9–12 October 2018 : proceedings. – Kharkiv: IEEE, 2018. – P. 411–416. DOI: 10.1109/INFOCOMMST.2018.8632015
5. Implementation of the indicator system in modeling complex technical systems / [S. Leoshchenko, S. Subbotin, A. Oliinyk, O. Narivs'kiy] // Radio Electronics, Computer Science, Control. – 2021. – Vol. 1. – P. 117–126. DOI: 10.15588/1607-3274-2021-1-12
6. Learning Phrase Representations using RNN Encoder-Decoder for Statistical Machine Translation [Electronic resource]. – Access mode: https://arxiv.org/abs/1406.1078
7. Ahmadian A. Soft Computing Approach for Mathematical Modeling of Engineering / A. Ahmadian, S. Salahshour . – London: Chapman and Hall (CRC Press), 2021. – 222 p.
8. Sayyaadi H. Modeling, Assessment, and Optimization of Energy Systems / H. Sayyaadi. – Cambridge : Academic Press, 2020. – 558 p.
9. Koulamas C. Real-Time Sensor Networks and Systems for the Industrial IoT / C. Koulamas, M. T Lazarescu. – Basel: Mdpi AG, 2020. – 242 p. DOI: 10.3390/books978-3-03943-431-2
10. Senge P. M. The Fifth Discipline: The Art & Practice of The Learning Organization / P. M. Senge. – New York : Doubleday, 2006. – 445 p.
11. Bruce P. Practical Statistics for Data Scientists: 50 Essential Concepts / P. Bruce, A. Bruce. – California : O'Reilly Media, 2017. – 318 p.
12. Finch W. H. Exploratory Factor Analysis: 1st Edition / W. Holmes Finch. – California : SAGE Publications, 2019. – 144 p.
13. Rencher A. C. Methods of Multivariate Analysis / A. C. Rencher, W. F. Christensen. – New Jersey : John Wiley & Sons, 2012. – 800 p.
14. Dean A. Design and Analysis of Experiments (Springer Texts in Statistics) / A. Dean, D. Voss, D. Draguljić. – Berlin : Springer, 2017. – 865 p. DOI: 10.1007/978-3-319-52250-0
15. Sewak M. Deep Reinforcement Learning: Frontiers of Artificial Intelligence / M. Sewak. – Berlin : Springer, 2020. – 220 p. DOI: 10.1007/978-981-13-8285-7
16. Modification and parallelization of genetic algorithm for synthesis of artificial neural networks / [S. Leoshchenko, A. Oliinyk, S. Subbotin et al.] // Radio Electronics, Computer Science, Control. – 2019. – № 4. – P. 68–82. DOI: 10.15588/1607-3274-2019-4-7

DOI 10.15588/1607-3274-2025-2-11

UDC 004.8, 519.816

EVALUATION OF QUANTIZED LARGE LANGUAGE MODELS IN THE TEXT SUMMARIZATION PROBLEM

Nedashkovskaya N. I. – Dr. Sc., Associate Professor at the Department of Mathematical Methods of System Analysis, Institute for Applied Systems Analysis at National Technical University of Ukraine "Igor Sikorsky Kyiv Polytechnic Institute", Kyiv, Ukraine.

Yeremichuk R. I. – Bachelor of Systems Analysis, Kyiv, Ukraine.

ABSTRACT

Context. The problem of increasing the efficiency of deep artificial neural networks in terms of memory and energy consumption, and the multi-criteria evaluation of the quality of the results of large language models (LLM) taking into account the judgments of users in the task of summarizing texts, are considered. The object of the study is the process of automated text summarization based on LLMs.

Objective. The goal of the work is to find a compromise between the complexity of the LLM, its performance and operational efficiency in text summarization problem.

Method. An LLM evaluation algorithm based on multiple criteria is proposed, which allows choosing the most appropriate LLM model for text summarization, finding an acceptable compromise between the complexity of the LLM model, its performance and the quality of text summarization. A significant improvement in the accuracy of results based on neural networks in natural language processing tasks is often achieved by using models that are too deep and over-parameterized, which significantly limits the ability of the models to be used in real-time inference tasks, where high accuracy is required under conditions of limited resources. The proposed algorithm selects an acceptable LLM model based on multiple criteria, such as accuracy metrics BLEU, Rouge-1, 2, Rouge-L, BERT-scores, speed of text generalization, or other criteria defined by the user in a specific practical task of intellectual analysis. The algorithm includes analysis and improvement of consistency of user judgments, evaluation of LLM models in terms of each criterion.

Results. Software is developed for automatically extracting texts from online articles and summarizing these texts. Nineteen quantized and non-quantized LLM models of various sizes were evaluated, including LLaMa-3-8B-4bit, Gemma-2B-4bit, Gemma-1.1-7B-4bit, Qwen-1.5-4B-4bit, Stable LM-2-1.6B-4bit, Phi-2-4bit, Mistal-7B-4bit, GPT-3.5 Turbo and other LLMs in terms of BLEU, Rouge-1, Rouge-2, Rouge-L and BERT-scores on two different datasets: XSum and CNN/ Daily Mail 3.0.0.

Conclusions. The conducted experiments have confirmed the functionality of the proposed software, and allow to recommend it for practical use for solving the problems of text summarizing. Prospects for further research may include deeper analysis of metrics and criteria for evaluating quality of generated texts, experimental research of the proposed algorithm on a larger number of practical tasks of natural language processing.

KEYWORDS: limited resources, natural language processing, text summarization, large language models, quantization, multi-criteria analysis.

ABBREVIATIONS

NN is a neural network;
LLM is a large language model;
LLaMA is a large language model by Meta AI;
NLP is a natural language processing;
PLM is a pretrained transformer language model;
BERT is a bidirectional encoder representations by transformer;
BNN is a binary neural network;
STE is a straight-through estimator;
QAT is a quantization aware training;
PTQ is a post-training quantization;
ROUGE is a recall-oriented understudy for gisting evaluation – a set of metrics;
BLEU is a bilingual evaluation understudy algorithm;
PCM is a pairwise comparison matrix.

NOMENCLATURE

r is a real-valued input;
$[\alpha, \beta]$ is a cutoff range;
b is a quantization bit width;
r^q is a result of quantization of r;
S is a real-valued scaling coefficient;
Z is a integer zero point;
$f(r)$ is a transformation operation for quantization;
int is a rounding operation;
clip is a clipping function;
$\hat{r}$ is a result of dequantization;
Δ_i is a quantization threshold;
y_i is a quantization level;
$Q(\beta, b)$ is a set of quantization levels;
$\prod(\cdot)$ is an operation of projecting;
w is a weight;
w^b is a binarized weight;
$\sigma(w)$ is a "hard sigmoid" function;
a, b, c are weighting coefficients;
λ is a coefficient of regularization;
Q_a is a learnable quantization function;
L_{CE} is a traditional cross-entropy loss function;
L_{DL} is a distribution loss;
$H(\cdot,\cdot)$ is a loss function between the teacher model and the apprentice model;
w^{FP} is a full-precision weight of the teacher model;

DOI 10.15588/1607-3274-2025-2-12

p^T, p^S are predictions based on the teacher and student models.

INTRODUCTION

The importance of text summarization has increased with the information explosion in the digital age. Today, a huge amount of data is generated every second from various sources such as news, scientific reports, emails and social media posts. For both private individuals and businesses, it is almost impossible to consume available information without spending significant time. Text summarization tools offer a practical solution, quickly represent the essence of voluminous documents, and thus allow efficient information consumption.

Large language models (LLMs) have fundamentally changed the process of text summarization, providing opportunities that surpass traditional statistical methods [1, 2]. Trained on vast amounts of textual data from various sources, the LLMs develop a comprehensive understanding of linguistic nuances, idiomatic expressions and complex sentence structures. As a result, they can create summaries that not only capture the essential information from the texts, but also preserve the style and tone of original text [1, 3].

One of the most significant effects of LLMs is their ability to perform text summarization at extremely large scales and at extremely high speeds, quickly extracting key points from large volumes of text. This capability allows businesses, researchers, and policymakers to stay informed and make data-driven decisions without having to manually sift through extensive documents.

LLMs can work with various types and formats of texts: books, news articles, blog posts, technical reports and other [1]. These models support many languages and offer the possibility of summarization in different languages [4, 5].

LLMs are now very accessible to users, not even requiring authorization to use the latest updated version of the GPT 3.5 Turbo model [4]. In addition, LLMs offer a recommendation service and a personalized summarization experience: the user, for example, may indicate his/her interests or the most relevant text's aspects, and the models adjust their summarization strategies accordingly. Such personalization allows to create individual resumes which are more relevant and useful for individual users, increasing their interest and satisfaction.

However, summarization using LLMs also faces a number of problems [6]. The first and the most important of them is to ensure a high level of accuracy of the generated summaries and a contextual understanding of input text documents. While LLMs can create coherent resumes, the complexity of human language and the subtleties of textual nuance often present challenges. The problem is that the LLMs sometimes try to capture irony, sarcasm, and implicit meaning in text documents, which can lead to summaries that distort the original content. In addition, LLMs may omit important information or emphasize less important details, especially in texts of high information density or complex structure.

The second challenge is the bias of summaries generated by LLMs. The reason for this problem lies in the fact that the extremely large training data sets are usually created by humans and, as a result, are already characterized by a certain level of bias. Texts generated by LLMs can further reinforce these biases, leading to a distorted or partial representation of the original texts. This problem is particularly relevant in such sensitive areas as news distribution, legal document processing and educational content, where impartiality and fairness are of paramount importance.

At last, the use of LLMs requires powerful processors and large amounts of memory. To run, for example, a model of the GPT-4 level, which has at least 70 billion parameters, you need at least 48 GB of video memory [5].

In the end of 2023 and the beginning of 2024, the focus of the LLM community has shifted to the release of open-source and quantized models. In April 2024, Meta AI introduced LLaMA-3 70B and quantized LLaMA-3 8B models, which are improved versions of the LLaMA-2 [7]. The release of LLaMA-3 has once again raised the bar of quality for models of their size. For instance, the LLaMa-3 8B model aims to perform better than the LLaMa-3 70B in some tasks, while having 8.75 times fewer parameters.

The object of study is the process of automated text summarization using LLMs.

The subject of study is the analysis of quantization techniques and several different LLMs, which were proposed in 2023 and the beginning of 2024, depending on a set of multiple criteria.

The purpose of the work is to develop an algorithm of LLMs' evaluation in terms of multiple quantitative and qualitative criteria.

1 PROBLEM STATEMENT

Suppose $a_1, a_2, ..., a_n$ are alternative LLMs, such as LLaMa-3, Gemma, Qwen, Stable LM-2, Phi-2, Mistal, and their quantized versions, GPT-3.5 Turbo and other LLMs (decision alternatives), and $c_1, c_2, ..., c_m$ are the following decision criteria:

– metrics ROUGE, BLEU and BERT-score, which are used for evaluation of generated texts;

– speed of text summarization;

– convenience of using the LLM.

It is necessary:

– to evaluate decision alternatives (modern LLMs of various sizes) in a text summarization problem in terms of above decision criteria, using different data sets: CNN/ Daily Mail 3.0.0, and Extreme Summarization (XSum);

– to integrate modern LLMs of various sizes: LLaMa-3, Gemma, Qwen, Stable LM-2, Phi-2, Mistal, GPT-3.5 Turbo into a summarization service.

DOI 10.15588/1607-3274-2025-2-12

2 REVIEW OF THE LITERATURE

Several approaches are considered to improve the efficiency of NN models in terms of memory size, power consumption and others, while simultaneously providing an acceptable compromise between accuracy and generalization property of the models:

– designing efficient architectures for NN models; adaptation and co-design of NN architectures for a specific target hardware;

– quantization;

– pruning;

– model distillation.

The issue of quantization of NNs is partly related to works in the field of neuroscience [8–10], according to which the human brain stores information in discrete and quantized rather than continuous form.

One reason for the need for quantization is that the information, which is stored in continuous format, is exposed to noise (external, thermal, synaptic and other), and such noise is always present in small quantities in the physical environment, including the human brain [11]. Signals in discrete form may be more robust to such low-level noise. In addition, discrete representations have a higher generalization ability [12] and higher efficiency in resource-constrained applications [13].

Model distillation consists of first training a large model, and then using it as a teacher to train a more compact model [14 – 16]. The main challenge is to obtain accurate results with a high degree of data compression as a result of distillation. Strong compression for knowledge distillation methods usually leads to a significant decrease in the accuracy of the results. Accuracy can be improved by combining knowledge distillation with quantization and pruning techniques [16].

In recent years, there has been a trend to use pre-trained language representations in natural language processing systems, which are applied more flexibly and independently of the task. Single-layer representations based on word-to-vector models were first explored and transferred to task-specific architectures [17, 18]. After that, the recurrent neural networks with contextual state, multiple representation layers [19–22] and sequence-to-sequence model with copy mechanism [23] were used to form stronger representations.

Recently, pretrained transformer language models (PLMs) have developed [24], which are directly fine-tuned, completely eliminating the need for task-specific architectures [25–27].

The Bidirectional Encoder Representations by Transformer (BERT) model [25] marked a significant advance in NLP tasks. BERT is extended to the sequence generation task in [26], where a two-stage decoding process is designed for efficient usage of BERT's context modeling ability. Firstly, the summary is generated using a left context-only-decoder. After that, each word of the summary is masked, the refined word is predicted, and the reinforcement objective is cooperated with the refined decoder for further improvement of the naturalness of the generated sequence [26]. A self-supervised pre-training objective for abstractive summarization, a gap-sentences generation and study strategies for selecting those sentences are proposed in PEGASUS model [27]. The PEGASUS is able to be adapted very quickly, and fine-tune with small numbers of supervised pairs.

The T5 (Text-to-Text Transfer Transformer) model had 11 billion parameters and used a transfer learning approach, outperforming its predecessors BERT and GPT2 in a wide range of NLP applications, including text classification, question answering, and especially text summarization [28]. The GPT-3 model proposed in 2020 already had 175 billion parameters and could be zero-short transferred to downstream tasks without fine-tuning [1]. In 2020, a new learning method known as replaced token detection was introduced in the ELECTRA model. In a pre-training task, this model learns to distinguish real input tokens from plausible but synthetically generated replacements [29]. ELECTRA is effective in extractive note-taking, where identifying and summarizing the most important sentences in a text is critical.

The DeBERTa (Decoding-enhanced BERT with Disentangled Attention) model, released in 2020 as an improvement to BERT, separated the representation of words from their positions in the text, which allowed the model to more clearly understand contextual relationships, create contextually deeper and more coherent summarizations, generalize different types of texts [30].

GPT-3.5, also known as ChatGPT, introduced in 2022 provides enhanced interactivity, allowing users to interact with the model directly by refining the summarization results [4]. Dynamically responding to user input and adjusting its responses, GPT-3.5 became not just a tool for passive data processing, but also an active participant in information analysis and decision-making processes.

Further advances in this area have been made by fine-tuning LLMs for a set of tasks formulated as instructions, allowing the models to better respond to instructions and reducing the need for labeled data. It is emphasized in [31] that fine-tuning on instructions can improve performance across a range of models, prompting setups, and evaluation tasks. As a result, Flan-T5 model with 11 billion parameters [31] achieves strong few-shot performance compared to much larger models, such as PaLM 62B.

An open-source LLaMA (Large Language Model Meta AI) model was proposed by Meta AI in February 2023 and marked a significant evolution in NLP for deploying advanced NLP tools in resource-constrained environments by optimizing performance in various computing environments [32]. The LLaMA model has an ability to produce high output quality with less training data, which optimizes use of this model for real-time text summarization problems, where fast and accurate compression of information is very important. Also, the release of the LLaMA model greatly improved the position of open-source models, since there were and still are a lot of big players hiding detailed information about the architecture, number of parameters, training

DOI 10.15588/1607-3274-2025-2-12

configurations, data sets, etc. This has prompted many of the big players in AI to release even more open-source models of the GPT-level from OpenAI.

In the Gemini model proposed by Google in May 2023, two-context processing of texts and integration of information from different sources were introduced [33]. In this regard, the Gemini model is effective for dynamic content such as news streams.

The Mistral open-source model [34], developed by an independent research group from France and released in July 2023, aimed to solve the problem of generating resume texts of better quality in many different languages that were previously unavailable. The Mistral model became more powerful than the similar LLaMa model by 7 billion parameters, actually taking first place among open-source models at that time according to expert evaluations [34]. Anyone can download the Mistral model weights for free and run it locally having the appropriate computing resources, unlike GPT-4 and GPT-3.5 models, which are only available as an application programming interface service.

In 2023 and 2024, there is also a trend to reduce the dimensions of LLMs, so that they can effectively work on devices with limited computing resources. Examples of such models are Qwen1.5 – 0.5B, 1.8B, 4B, Stable LM – 1.6B, Phi-2 – 2.7B, Phi-3 – 3.8B and TinyLlama - 1.1B. Recently, 8-bit and 4-bit quantization opens up an opportunity of running LLMs on consumer hardware [35 – 37].

Non-uniform quantization, binarized weights and activations, extreme and mixed precision quantization, quantization aware training (QAT) and post-training quantization (PTQ) are used in modern LLMs [37].

In order to choose the best models for text summarization based on user preferences and multiple quality criteria, and to increase the speed and quality of text summarization based on LLMs, it is necessary to evaluate modern quantized LLMs of different sizes in a text summarization problem using several data sets and metrics BLEU, Rouge-n, Rouge-L and BERT-score.

3 MATERIALS AND METHODS

Uniform quantization. The basic quantization operation performs uniform quantization using the following steps [38, 39]:

1. Specify the range of a real-valued quantity to be quantized, and to clip values outside this range.

2. Map real values to integer values which are represented by the required bit-width of the quantized representation. This is often performed by rounding each real value to the nearest integer.

Let r be a real-valued input, [α, β] be the range of r chosen for quantization (the cutoff range), and b is the quantization bit-width. Uniform quantization represents the full-precision input value $r \in [\alpha, \beta]$ as the low-precision integer within the range $[-2^{b-1}, 2^{b-1}-1]$. Inputs outside the range are cut to the nearest boundary.

Asymmetric uniform or affine quantization represents a real value $r \in \mathbb{R}$ as a signed b-bit integer $r^q \in \{-2^{b-1}, -2^{b-1}+1, ..., 2^{b-1}-1\}$. The following transformation operation is defined by

$$f(r) = S \cdot r + Z,$$

$$S = \frac{2^b - 1}{\beta - \alpha},\ Z = -\text{int}(\alpha \cdot S) - 2^{b-1},$$

where S is a real-valued scaling coefficient, Z is the zero point – the integer, to which the real-valued zero is mapped, and int is a rounding operation, which displays a real value to an integer. The scaling coefficient S divides the range of the real-valued r into several partitions. In the 8-bit case, $S = \frac{255}{\beta - \alpha}$ and $Z = -\text{int}(\alpha \cdot S) - 128$.

The uniform quantization operation, also called asymmetric, is defined as follows [39]:

$$r^q = \text{quantize}(r, b, S, Z) =$$
$$= \text{clip}(\text{int}(S \cdot r + Z), -2^{b-1}, 2^{b-1} - 1),$$

where $\text{clip}(r,l,u) = l$ if $r < l$, $\text{clip}(r,l,u) = u$ if $r > u$ and $\text{clip}(r,l,u) = r$ if $l \le r \le u$.

The corresponding dequantization operation, which computes an approximation of the original real-valued input $\hat{r} \approx r$, is defined by

$$\hat{r} = \text{dequantize}(r^q, S, Z) = \frac{1}{S}(r^q - Z).$$

In the symmetric uniform quantization, the cutoff range and integer range are symmetric around zero, that is α = − β, and the zero-point Z=0. For example, the integer range [−127, 127] is used for 8-bit quantization, and we do not use the –128 value in favor of symmetry. For int8, the loss of one out of 256 representable values is minor. However, for lower bit quantization we have to re-evaluate the trade-off between representable values and symmetry of quantization.

Symmetric uniform quantization represents a real value $r \in \mathbb{R}$ as a signed b-bit integer $r^q \in \{-2^{b-1}+1, -2^{b-1}+2, ..., 2^{b-1}-1\}$. The following transformation operation is defined by

$$f(r) = S \cdot r,$$
$$S = \frac{2^{b-1} - 1}{\beta},$$

and the result of quantization is as follows:

$$r^q = \text{quantize}(r, b, S) =$$
$$= \text{clip}(\text{int}(S \cdot r), -2^{b-1} + 1, 2^{b-1} - 1).$$

Uniform quantization operations are shown on Fig. 1.

DOI 10.15588/1607-3274-2025-2-12

Calibration is the process of selecting the cutoff range [α, β] [38, 39]. A popular method is to set $\alpha = r_{\min}$ and $\beta = r_{\max}$ for asymmetric uniform quantization. In this case, S is specified as $S = \frac{\max(|r|)}{2^{b-1}-1}$. In a case of symmetric quantization method, the maximum of absolute values is used: $\beta = \max(|r_{\min}|, |r_{\max}|)$. Then S is given as $S = \frac{2\max(|r|)}{2^b - 1}$.

A percentile of the distribution of absolute values observed during calibration also can be set [40]. For example, the 99% percentile would cut off 1% of the largest values. The Kullback-Leibler divergence can be used for calibration, which minimizes the loss of information between the quantized values and the original floating-point values.

Asymmetric uniform quantization is often applied in practice, as it results in a wider and therefore more accurate range, however, leading to more computationally expensive inference compared to symmetric quantization.

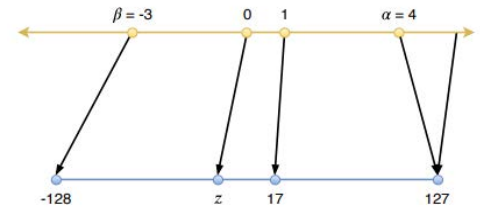

a

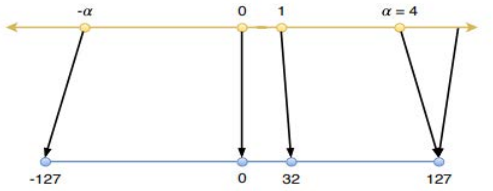

b

Figure 1 – Quantization of real values to int8: a – asymmetric, b – symmetric [39]

Non-uniform quantization methods provide higher accuracy for a fixed bit width, and these methods allow more attention to be focused on important regions of weight or activation values, such as in the case of bell-shaped distributions with long tails, and also support dynamic definition of cutoff ranges [41–43].

The non-uniform quantization operation is specified as

$$f(r) = y_i \text{ if } r \in [\Delta_i, \Delta_{i+1}),$$

where Δ_i are quantization thresholds, and y_i are quantization levels.

The quantization of a real-valued input r can be presented as

$$r^q = \prod_{Q(\beta,b)} \text{clip}(r, \beta),$$

where $Q(\beta, b)$ is a set of quantization levels, β is the cutoff threshold, the cutting function $\text{clip}(\cdot, \beta)$ clips values of r into range [– β, β], and b is the bit-width. Operation $\prod(\cdot)$ projects clipped r value onto the quantization level.

In a case of uniform quantization, the quantization levels are defined as

$$Q(\beta, b) = \beta \times \left\{0, \frac{\pm 1}{2^{b-1}-1}, \frac{\pm 2}{2^{b-1}-1}, \frac{\pm 3}{2^{b-1}-1}, ..., \pm 1\right\}.$$

For non-uniform "powers-of-two" quantization method, the quantization levels are constrained to be powers-of-two values or zero (Fig. 2) [42]:

$$Q^{PoT}(\beta, b) = \beta \times \left\{0, \pm 2^{-2^{b-1}+1}, \pm 2^{-2^{b-1}+2}, ..., \pm 2^{-1}, \pm 1\right\}.$$

Multiplication between a number 2^x, that is a power of two, and other number q can be implemented by bitwise shifting as follows:

$$2^x \cdot u = \begin{cases} u, & \text{if } x = 0 \\ u << x, & \text{if } x > 0 \\ u >> x, & \text{if } x < 0 \end{cases},$$

where ≫ is the right shift operation, which accelerates the computation and takes only one clock cycle in modern CPU architectures [42].

Quantization layers can also be trained along with model parameters using gradient descent methods [44].

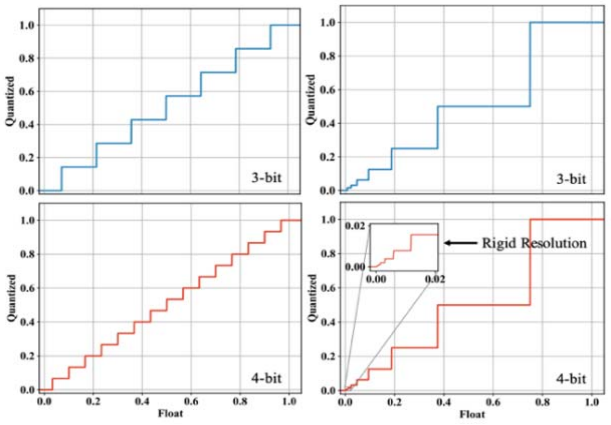

a b

Figure 2 – Quantization of unsigned data to 3-bit or 4-bit: a – uniform, b – Powers-of-Two (PoT) quantization [42]

In binary networks (BNNs) – networks with binary weights and activations – most arithmetic operations are replaced with bit-wise operations, which potentially lead to a substantial increase in power-efficiency. BNNs and a method for their training are proposed in [45]. Experiments in [45] show that binarization cardinally reduces memory consumption, namely number of accesses and memory size during the forward pass at run-time and train-time.

DOI 10.15588/1607-3274-2025-2-12

When training a BNN, the weights and the activations are both constrained to +1 or −1. The binarization function can be either deterministic:

$$w^b = \text{sign}(w) = \begin{cases} +1, & \text{if } w \geq 0 \\ -1, & \text{otherwise} \end{cases}$$

or stochastic:

$$w^b = \text{sign}(w) = \begin{cases} +1, & \text{with probability } p = \sigma(w) \\ -1, & \text{with probability } 1-p \end{cases},$$

where σ is the "hard sigmoid" function:

$$\sigma(x) = \text{clip}\left(\tfrac{w+1}{2}, 0, 1\right) = \max\left(0, \min\left(1, \tfrac{w+1}{2}\right)\right).$$

A significant benefit of joint binarization of weights and activations in BNNs is that the floating-point matrix multiplication is replaced by lightweight operations

$$\text{XnorDotProduct}\left(a_{k-1}^b W_k^b\right), \quad k = 1, \ldots, L,$$

followed by bit counting.

This operation is based on a following trick: it is relatively easy to handle continuous-valued inputs as fixed-point numbers, with *m* bits of precision [45]. For example, in the common case of 8-bit fixed point inputs:

$$sum = x \cdot w^b, \; sum = \sum_{n=1}^{8} 2^{n-1}(x^n \cdot w^b),$$

where *x* is a vector of 1024 8-bit inputs, w^b is a vector of 1024 1-bit weights, and *sum* is the resulting weighted sum.

Binarization, which limits quantized values to a 1-bit representation is considered as the most extreme quantization method. Binary operations can be computed efficiently using bitwise arithmetic and achieve significant speedup compared to higher precisions such as FP32 and INT8. Peak binary arithmetic performance on NVIDIA V100 GPUs is 8 times faster than INT8 [46].

Also, binarization can radically reduce memory requirements by 32 times. For many complex problems, however, simple binarization methods usually result in a serious decrease in accuracy.

Several methods were proposed to reduce decrease in accuracy in extreme quantization [47]:

1. Minimize the quantization error. The floating-point parameters are approximated by introducing a scaling factor $a \in \mathbb{R}$ for the binary parameter. Then, the quantization of weight *w* is formulated as $w \approx a \cdot w^b$, where w^b is the binarized weight. Optimal scaling factor and binary weights are found minimizing the quantization error

$$\min_{a, w^b} \| w - a \cdot w^b \|^2.$$

Thus, $w^b \in \{-a, a\}$ and lead to less quantization error than directly using values $\{-1, 1\}$. This method increases the inference accuracy of the network, and still have the benefits of fast computation.

A two-step quantization method is proposed to overcome shortcomings of the previous method [48]:

– All activations are low-bit quantized using a learnable quantization function Q_a. All weights are considered as full-precision values.

– Q_a is fixed, and scaling factor $a \in \mathbb{R}$ and the low-bit quantized weight vector w^b are learned as follows:

$$\min_{a, w^b} \| z - Q_a(a(x \odot w^b)) \|_2^2,$$

where the minimization problem can be solved iteratively.

2. Improve the network loss function. Additional quantization-aware loss item is proved to be practical and is introduced as regularizer [49]:

$$L = L_{CE} + \lambda \cdot L_{DL},$$

where L_{CE} is the traditional cross-entropy loss function, L_{DL} is the distribution loss to learn the binarization property, and λ is the coefficient of regularization.

Another approach uses the distillation technique, training a low-precision student network using a full-precision, well-trained, and large-scale teacher network. The loss function in this approach is as follows [15]

$$L(x; w^{FP}, w^b) = a \cdot H(y, p^T) + b \cdot H(y, p^S) + c \cdot H(p^T, p^S),$$

where $H(\cdot,\cdot)$ is the loss function between the teacher model and the apprentice model; w^{FP} is the full-precision weights of the teacher model, w^b is the binary weights of the apprentice (student) model; p^T, p^S are predictions based on the teacher and student models; *y* is the label for sample *x*; *a*, *b*, *c* are weighting coefficients.

3. Improved Training Method. The training method of BNNs, proposed in [45], uses the shift-based AdaMax algorithm and is a variant of the dropout method, but instead of randomly setting half of the activations to zero while computing the gradients, the binarization of activation and weight values is performed. A version of the straight-through estimator (STE) is applied with additional saturation effect to propagate gradients through a non-differentiable signed function while using the standard back-propagation algorithm.

When using a pre-trained model, quantization can lead to distortion of parameters of the trained model and, as a result, to convergence to a non-optimal value of the loss function. To deal with this problem, a NN model may be retrained using the quantized parameters to minimize the decrease in accuracy after quantization. The method is called QAT and consists of the following steps (Fig.3, a) [47, 50]:

DOI 10.15588/1607-3274-2025-2-12

1. Pretraining the base NN model without taking into account quantization. Model accuracy assessment.

2. Apply quantization to all layers of the pre-trained model. The resulting model supports quantization, but is not quantized. For example, the weights are float32 instead of int8. Only individual layers of the pre-trained model can be quantized to increase the accuracy of the model.

3. Fine-tuning (retraining) the model obtained in the previous step, which is quantization aware, on a subset of training data. Assessing the accuracy of the model and comparing it with the accuracy of the base model.

4. Building an actually quantized model with int8 weights and uint8 activations. Evaluating the accuracy of this model and comparing it with the accuracy of the base model.

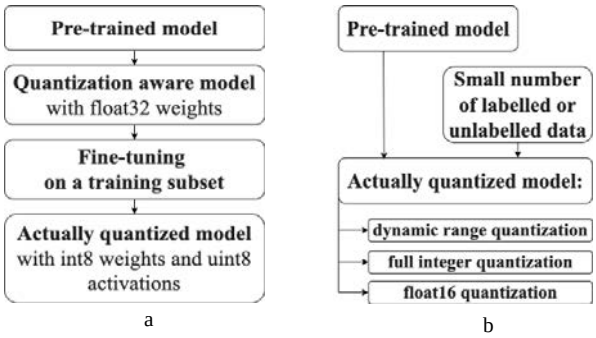

a b

Figure 3 – QAT (a) and PTQ (b) methods of quantization

The process of fine-tuning the quantization aware model in above step 3 is as follows:

– the usual forward and backward pass, as well as the gradient step for updating the weight, are performed with floating point,

– model parameters are quantized after gradient update,

– the non-differentiable quantization operator is approximated by the identity function called the STE [51]. Later, instead of the rounding operation, a *W*-shaped non-smooth regularization function was proposed [52].

The QAT method helps to minimize the decrease of accuracy after quantization, despite the use of a rough approximation STE. The main limitation of QAT is the computational cost of retraining the NN. For example, low-bit precision quantization models may require several hundred epochs of the retraining. Also, the QAT method requires sufficient training data to retrain.

Post-training quantization (PTQ) performs quantization of weights and activations of a pre-trained model without additional fine-tuning (Fig.3b) [47, 50, 53]. Thus, PTQ is very fast method for quantizing NN models.

The evaluation of modern LLMs aims to answer the question whether model's size, architecture, quantization, and features of architecture significantly affect the summarization efficiency. Efficiency of texts generated in a process of summarization is estimated in terms of metrics ROUGE [54], BLEU [55] and BERT-score [56]. Additionally, speed of text summarization and convenience of using the LLM are analyzed. Qualitative decision criterion "convenience of using" requires, in its turn, expert or user evaluation. Weights of decision criteria are also calculated based on expert (user) preferences or judgements about relative importance of the criteria in a given problem.

The proposed algorithm for multiple-criteria evaluation of LLMs has several stages (Fig. 4).

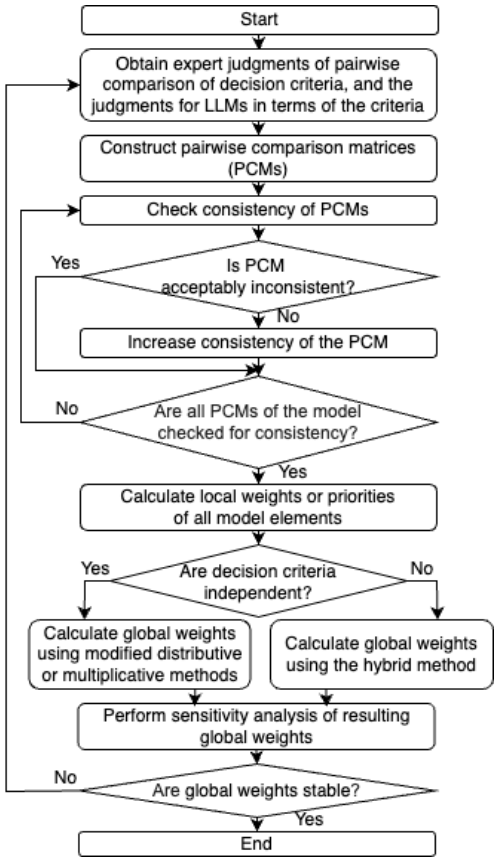

Figure 4 – An algorithm for LLMs multiple-criteria evaluation

At the first stage, expert compare importance of decision criteria using special scale, and his/her judgements are presented as pairwise comparison matrices (PCMs) [57]. Expert also estimates LLMs in terms of the criteria based on previously calculated metrics ROUGE, BLEU and BERT-score. Consistency of expert judgments is analyzed, using method of assessment and increasing of consistency [57]. This method is based on the property of weak inconsistency of PCM, finds undesirable cycles in a PCM and the most inconsistent elements of PCM. The method can be applied to various types of PCMs, such as multiplicative, additive, fuzzy and other [58]. As a result, we obtain PCMs of acceptable quality (inconsistency).

At next stage, the fuzzy preference method [59] is used for calculating local weights or priorities of model elements (LLMs and decision criteria). After that, local weights of model elements are aggregated using modified distributive, multiplicative or proposed hybrid

DOI 10.15588/1607-3274-2025-2-12

aggregation methods depending on the mutual dependence of the criteria. At the last stage, a sensitivity analysis of results is performed, and stability of results is assessed.

4 EXPERIMENTS

Experiments to evaluate the quality of text summarization by various LLMs were conducted on two different data sets: CNN/Daily Mail 3.0.0 [60] and Extreme Summarization (XSum) [61].

The CNN/Daily Mail 3.0.0 dataset includes over 300,000 unique English language news articles written by CNN and Daily Mail journalists. Initially, the set was developed for tasks of machine reading and understanding of texts, and subsequently for tasks of extractive and abstract summarization. Each entry in this set is represented by the following three key fields: the “id” field contains the SHA1 hash of the URL in hexadecimal format from which the text was retrieved; the “article” field is the text of the news article itself; and “highlights” of the article written by the author.

The XSum dataset was designed specifically to address complex summarization problems. The set entries are represented by the following fields: “id”, “document”, which is the text of the news article itself, “summary”, which contains a one-sentence summary of the article.

Using two different data sets helps to increase the validity of obtained results for evaluation of the quality of text summarization by various LLMs.

Experiments were conducted using a temperature value of 0.1 and a maximum token length of 100 for each LLM, as proposed in [3]. The summation of 25 test samples of each data set was carried out.

5 RESULTS

Various LLMs in both standard and quantized form were tested on the ROUGE, BERT-score and BLEU metrics, in order to assess the impact of quantization on the performance of the models (Tables 1 and 2).

LLMs of different configurations and sizes were compared with each other, and it was analyzed how the number of model parameters affects the quality of summarization and processing speed.

Values of performance metrics for different LLMs depending on the size and quantization level of the models are shown in Tables 1 and 2 for the CNN/Daily Mail 3.0.0 and the XSUM datasets, respectively.

An example of expert pairwise comparison judgements of decision criteria made in fundamental scale and the corresponding PCM are shown in Figs. 5 and 6. These judgements (and PCM) have no cycles, are acceptably inconsistent and can be used for calculation of reliable local weights, shown on the right parts of Figs. 5 and 6.

An example of unacceptable PCM is shown in Fig. 7. In this case, the system finds the most inconsistent element of PCM and offers a new value for it, which ensures an increase of consistency level of the entire PCM (Fig. 7).

Table 1 – Metric values for different LLMs on the CNN/Daily Mail 3.0.0 dataset

LL model	Number of parameters (in billions)	Rouge-1	Rouge-2	ROUGE-L	BLEU	BERT-precision	BERT-recall	BERT-F1
LLaMa-3-8B-4bit	8	0.288	0.094	0.261	0.044719	0.858	**0.881**	**0.869**
Gemma-2B	2	0.263	0.08	0.245	0.039777	0.858	0.871	0.864
Gemma-2B-4bit	2	0.269	0.078	0.247	0.036853	**0.861**	0.873	0.867
Gemma-7B-4bit	7	0.271	0.082	0.245	0.036121	0.857	0.875	0.866
Gemma-1.1-2B	2	0.256	0.069	0.223	0.032376	0.858	0.874	0.866
Gemma-1.1-2B-4bit	2	0.251	0.067	0.227	0.031926	0.856	0.874	0.865
Gemma-1.1-7B-4bit	7	0.259	0.082	0.238	0.035257	0.858	0.876	0.867
Qwen-1.5-0.5B	0.5	0.286	0.097	0.248	0.045120	0.84	0.867	0.853
Qwen-1.5-0.5B-4bit	0.5	0.268	0.08	0.237	0.039331	0.844	0.867	0.855
Qwen-1.5-1.8B	1.8	0.283	0.083	0.253	0.040930	0.852	0.873	0.862
Qwen-1.5-4B	4	**0.295**	0.109	0.266	0.057609	0.85	0.876	0.863
Qwen-1.5-4B-4bit	4	0.294	**0.111**	**0.267**	**0.066049**	0.848	0.874	0.861
Qwen-1.5-7B-4bit	7	0.284	0.079	0.245	0.039231	0.855	0.88	0.868
Stable LM-2-1.6B	1.6	0.27	0.072	0.241	0.034851	0.853	0.872	0.862
Stable LM-2-1.6B-4bit	1.6	0.271	0.086	0.241	0.044366	0.852	0.877	0.864
Phi-2	2.7	0.283	0.097	0.259	0.051176	0.857	0.878	0.867
Phi-2-4bit	2.7	0.277	0.09	0.253	0.045895	0.858	0.876	0.867
Mistal-7B-4bit	7	0.26	0.071	0.229	0.028532	0.853	0.873	0.863
GPT-3.5 Turbo	175	0.275	0.078	0.25	0.035723	0.858	0.878	0.868

DOI 10.15588/1607-3274-2025-2-12

Table 2 – Metric values for different LLMs on the XSum dataset

LL model	Number of parameters (in billions)	Rouge-1	Rouge-2	ROUGE-L	BLEU	BERT-precision	BERT-recall	BERT-F1
LLaMa-3-8B-4bit	8	0.179	0.031	0.137	0.012043	0.842	0.886	0.864
Gemma-2B	2	0.175	0.031	0.141	0.007783	0.842	0.881	0.861
Gemma-2B-4bit	2	0.182	0.032	0.149	0.009392	0.843	0.882	0.862
Gemma-7B-4bit	7	0.173	0.03	0.149	0	0.844	0.884	0.863
Gemma-1.1-2B	2	0.167	0.023	0.139	0	0.844	0.881	0.862
Gemma-1.1-2B-4bit	2	0.167	0.025	0.134	0	0.845	0.882	0.863
Gemma-1.1-7B-4bit	7	0.18	0.035	0.153	0.013915	**0.846**	0.887	**0.866**
Qwen-1.5-0.5B	0.5	0.146	0.019	0.116	0.007328	0.819	0.864	0.841
Qwen-1.5-0.5B-4bit	0.5	0.151	0.021	0.115	0.007367	0.825	0.868	0.846
Qwen-1.5-1.8B	1.8	0.181	0.029	0.142	0.007655	0.839	0.881	0.859
Qwen-1.5-4B	4	0.178	0.024	0.146	0.006867	0.837	0.878	0.857
Qwen-1.5-4B-4bit	4	0.175	0.031	0.144	0.011973	0.83	0.873	0.851
Qwen-1.5-7B-4bit	7	0.185	0.035	0.155	**0.014836**	0.843	**0.891**	**0.866**
Stable LM-2-1.6B	1.6	0.174	0.028	0.149	0.008054	0.839	0.878	0.858
Stable LM-2-1.6B-4bit	1.6	0.165	0.026	0.136	0.006938	0.837	0.88	0.858
Phi-2	2.7	0.185	**0.036**	**0.165**	0.011087	0.841	0.883	0.861
Phi-2-4bit	2.7	**0.186**	0.034	0.159	0.010903	0.843	0.882	0.862
Mistal-7B-4bit	7	0.185	0.03	0.159	0.012617	0.843	0.888	0.865
GPT-3.5 Turbo	175	0.179	**0.036**	0.15	0.011358	0.845	0.888	**0.866**

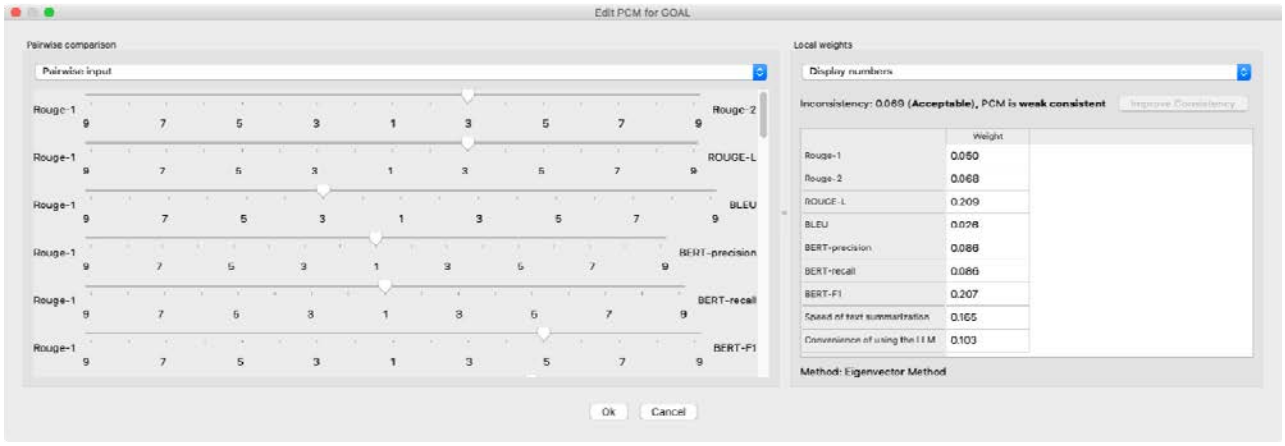

Figure 5 – An example of expert pairwise comparison judgements of decision criteria made in fundamental scale

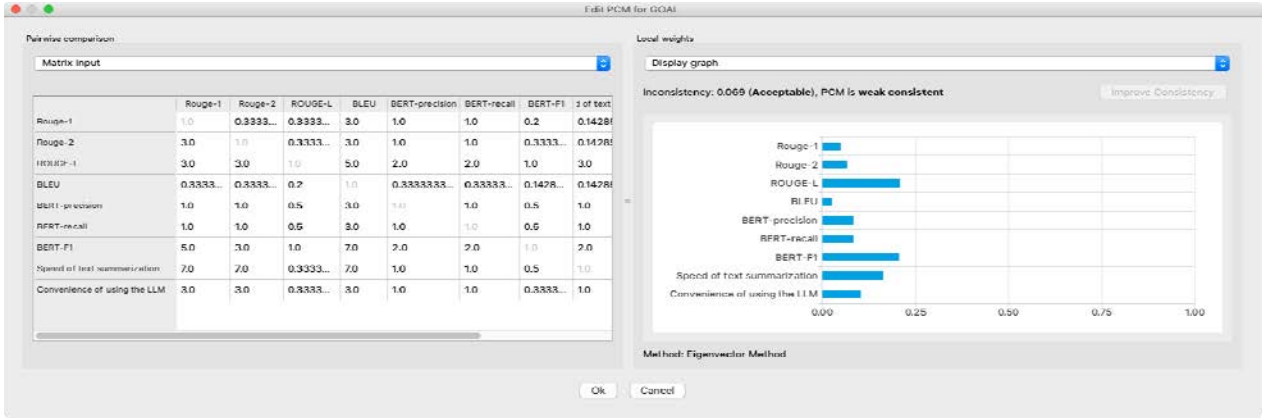

Figure 6 – An example of PCM and calculated weights of decision criteria

DOI 10.15588/1607-3274-2025-2-12

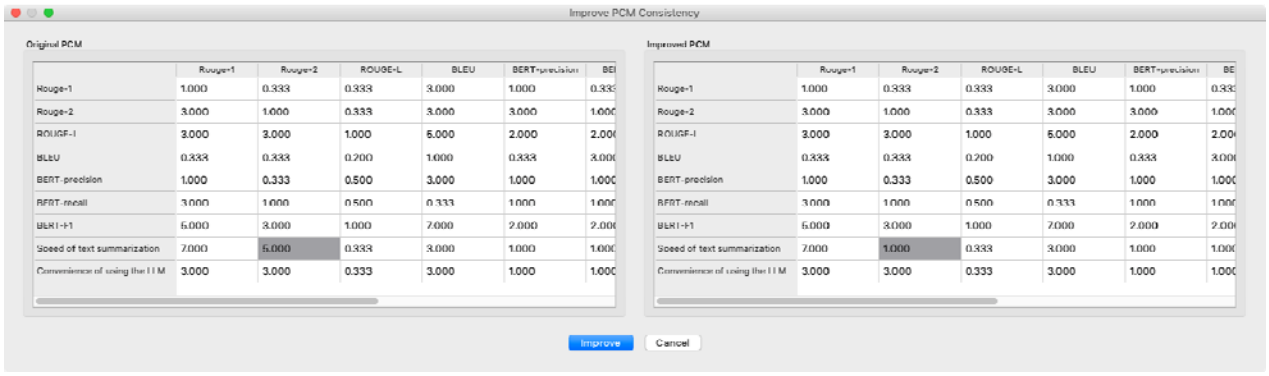

Figure 7 –The most inconsistent element of PCM (marked in gray) and its correction without the participation of an expert

The web interface for the text summarization service is developed using FastAPI, providing fast response to user actions during summarization processes which are computationally intensive.

The interface includes elements necessary for the summarization process (Fig. 8):

1. Drop-down menus to select language, model type and voice for audio feedback.
2. A text field for entering the URL of the article for which you want to generate a summary.
3. Button to start the process.
4. Areas displaying the initial text, summarized text, the area displaying the progress of the operation and the reproduced audio of the summarized text.

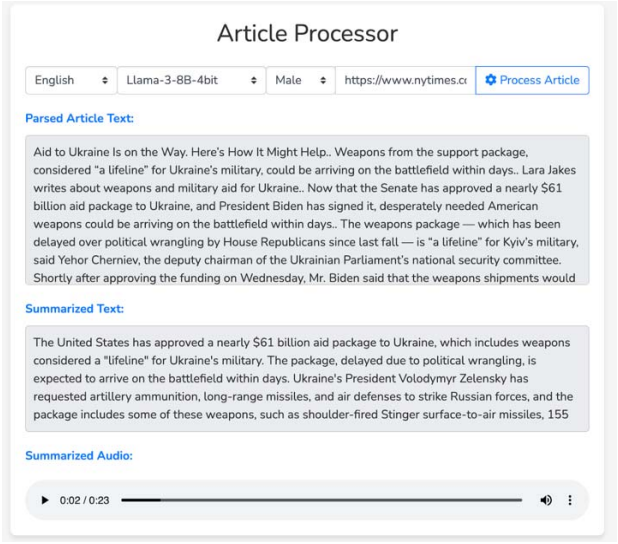

Figure 8 – Visualization of the service Web-interface after completion of all stages of summarization on the example of an arbitrary article from the New York Times

A WebSocket connection is used for real-time communication between the client and the server, allowing dynamically display updates, task progress, intermediate and final results without the need to reload the page.

To generate summarized text, the user first selects desired LLM model, text language, voice type, and specifies the URL of the article. After clicking the “Process Article” button, the request is sent to the backend, where the appropriate model is loaded based on the parameters selected by the user. The article is then downloaded, processed and summarized.

The system in real time informs the user about the status of their request with the help of a progress indicator and a direct display of the analyzed and summarized text.

A separate area of the interface displays the original text so that users can compare it with the summarized one. The summarized text is displayed together with the possibility to listen to the audio of the summarized text. Progress indicators visually show the current state of processing stages, increasing user engagement and ensuring clarity of system operation.

6 DISCUSSION

A comparative analysis of the obtained values of the metrics (Tables 1 and 2) shows that the model’s size, architecture, quantization, and features of architecture significantly affect the summarization efficiency. Thus, models with more parameters tend to be capable of better understanding of context and more complex patterns in texts. However, the GPT-3.5 Turbo model with 175 billion parameters did not outperform the other considered in this study models on the ROUGE, BERT, and BLEU metrics on either the CNN/Daily Mail 3.0.0 set or the XSum dataset.

Well-structured LLMs with fewer parameters outperformed larger LLMs by some metrics in this study. Thus, the LLaMa-3 quantized model with 8 billion parameters showed the best performance in BERT metrics, and the Qwen-1.5 quantized model with 4 billion parameters was the best in ROUGE and BLEU metrics on the CNN/Daily Mail 3.0.0 set.

On the XSum set, the quantized models Gemma-1.1 and Qwen-1.5, both with 7 billion parameters, showed the highest performance in BERT metrics, and the quantized model Qwen-1.5-7B-4bit was the best among the considered models in terms of BLEU. The Phi-2 model with 2.7 billion parameters was the best according to the ROUGE metrics, showing the highest values of this metric among the other considered models.

Quantization of all considered models increased the speed of inferences based on these models. In some cases, the performance of quantized models decreased on considered metrics, but the decrease was minor compared to the significant advantages of quantized models in speed and resource utilization.

DOI 10.15588/1607-3274-2025-2-12

The obtained results indicate that quantization is a viable strategy for the LLMs that leads to a significant increase in the speed of the model inferences while maintaining acceptable levels of accuracy and consistency of summarization results.

Asymmetric uniform quantization is often used in practice, as it results in a wider and therefore more accurate range compared to symmetric quantization [39]. Asymmetric quantization, however, leads to more computationally expensive inference in comparison with the symmetric variant.

In discussed quantization methods, we need to know the range of change of the real-valued activation or weight value so that we can determine the correct scaling coefficients. This requires access to all training data. In cases where there is no access to the original training data during the quantization procedure (for example, the training data set is too large), the zero-shot quantization methods should be used.

An additional task is the integration of LLMs into existing information systems at enterprises and optimization of the dynamics of interaction with users. Users need intuitive interfaces and the ability to customize results, which requires continuous improvement in the human-machine interaction aspects of LLM applications. Having a service with LLM, which can host a large number of users at the same time, can be afforded by companies with a large budget, since this requires a large number of servers to run large language models.

CONCLUSIONS

The large size of the NN models significantly limits their ability to be deployed and used by many applications that require real-time output, low power consumption and high accuracy in conditions of limited resources. Quantization is an extremely important technology for further improving the efficiency of NLP models in conditions of limited computing resources.

The scientific novelty of obtained results is that the algorithm for LLMs' evaluation in terms of multiple criteria (metrics) is proposed, and estimates of quality for nineteen different quantized and unquantized LLMs of various sizes, including LLaMa-3-8B-4bit, Gemma-2B-4bit, Qwen-1.5-4B-4bit, Stable LM-2-1.6B-4bit, Phi-2-4bit, Mistal-7B-4bit, GPT-3.5 Turbo are obtained in terms of metrics Rouge-1,2, Rouge-L, BLEU and BERT-scores. To the best of our knowledge, such estimates of quality of the considered open-source LLMs have been obtained for the first time. The proposed algorithm for multi-criteria model's evaluation allows to choose the most appropriate model for summarizing the text, to find a compromise between the complexity of the model, its performance and operational efficiency.

The practical significance of obtained results is that the software for multiple criteria LLMs evaluation and choosing the most appropriate model for text summarization has been developed. Also a service has been developed that automatically receives text from an online article, summarizes and speaks it. The web interface for the text summarization service has been created using FastAPI, providing fast response to user actions during summarization processes which are computationally intensive.

Prospects for further research are to study the proposed algorithm for a broad class of practical problems.

ACKNOWLEDGEMENTS

This study was funded and supported by National Technical University of Ukraine "Igor Sikorsky Kyiv Polytechnic Institute" (NTUU KPI) in Kyiv (Ukraine), and also financed in part of the NTUU KPI Science-Research Work by the Ministry of Education and Science of Ukraine "Development of the theoretical foundations of scenario analysis based on large volumes of semi-structured information" (State Reg. No. 0117U002150).

REFERENCES

1. Brown T., Mann B., Ryder N. et al. Language models are few-shot learners, *Advances in neural information processing systems*, 2020, Vol. 33, pp. 1877–1901. DOI: arXiv:2005.14165
2. Xie, Q. Bishop J. A., Tiwari P. et al. Pre-trained language models with domain knowledge for biomedical extractive summarization, *Knowledge-Based Systems*, 2022, Vol. 252. DOI: 10.1016/j.knosys.2022.109460
3. Basyal L., Sanghvi M. Text summarization using large language models, *ArXiv*, 2023. DOI: 2310.10449
4. OpenAI GPT 3.5 Turbo [Electronic resource]. Access mode: https://platform.openai.com/docs/models/gpt-3-5-turbo
5. OpenAI GPT-4 [Electronic resource]. Access mode: https://openai.com/index/gpt-4
6. Xu J., Ju D., Li M. et al. Recipes for safety in open-domain chatbots, *ArXiv*, 2021. DOI: 2010.07079
7. Meta LLaMa 3 [Electronic resource]. Access mode: https://llama.meta.com/llama3
8. McCulloch W. S., Pitts W. A logical calculus of the ideas immanent in nervous activity, *Bulletin of Mathematical Biophysics*, 1943, Vol. 5, № 4, pp. 115– 133. DOI: 10.1007/BF02478259
9. VanRullen R. Is perception discrete or continuous? / R. VanRullen, C. Koch // Trends in cognitive sciences. – 2003. – Vol. 7, № 5. – P. 207–213. DOI: 10.1016/S1364-6613(03)00095-0
10. Tee J., Taylor D. P. Is information in the brain represented in continuous or discrete form?, *IEEE Transactions on Molecular, Biological and Multi-Scale Communications*, 2020, Vol. 6, № 3, pp. 199–209. DOI: 1805.01631
11. Faisal A. A., Selen L. P. J., Wolpert D. M. Noise in the nervous system, *Nature reviews neuroscience*, 2008, Vol. 9, № 4, pp. 292–303. DOI: 10.1038/nrn2258
12. Varshney L. R., Varshney K. R. Decision making with quantized priors leads to discrimination, *Proceedings of the IEEE*, 2016, Vol. 105, № 2, pp. 241–255. DOI:10.1109/JPROC.2016.2608741
13. Varshney L. R., Sjöström P. J., Chklovskii D. B. Optimal information storage in noisy synapses under resource constraints, *Neuron*, 2006, Vol. 52, № 3, pp. 409–423. DOI: 10.1016/j.neuron.2006.10.017
14. Hinton G., Dean J., Vinyals O. Distilling the knowledge in a neural network, *NIPS 2014 Deep Learning Workshop*, 2015, pp. 1–9. DOI: 1503.02531

DOI 10.15588/1607-3274-2025-2-12

15. Mishra A. D. Marr Apprentice: using knowledge distillation techniques to improve low-precision network accuracy, *ArXiv*, 2017. DOI: 1711.05852
16. Polino A., Pascanu R., Alistarh D. Model compression via distillation and quantization, *Proceedings of the Workshop at ICLR*, 2018. DOI: 1802.05668
17. Mikolov T., Chen K., Corrado G. et al. Efficient estimation of word representations in vector space, *Proceedings of the Workshop at ICLR, Scottsdale*, 2013, pp. 1–12. DOI: 1301.3781
18. Pennington J., Socher R., Manning C. GloVe: global vectors for word representation, *Proceedings of the 2014 Conference on Empirical Methods in Natural Language Processing, Doha, Qatar. Association for Computational Linguistics*, 2014, pp. 1532–1543.
19. Dai A. M., Le Q. V. Semi-supervised sequence learning, *Advances in neural information processing systems*, 2015. DOI: 1511.01432
20. McCann B., Bradbury J., Xiong C. et al. Learned in translation: contextualized word vectors, *Advances in neural information processing systems.* – 2017. – P. 6297–6308. DOI: 1708.00107
21. Peters M. E., Neumann M., Zettlemoyer L. et al. Dissecting contextual word embeddings: architecture and representation, *Proceedings of the 2018 Conference on Empirical Methods in Natural Language Processing. Association for Computational Linguistics*. Brussels, Belgium, 2018, pp. 1499–1509. DOI: 10.18653/v1/D18–1179
22. Gehrmann S., Deng Y., Rush A. M. Bottom-up abstractive summarization, *Proceedings of the 2018 Conference on Empirical Methods in Natural Language Processing*. Brussels, Belgium, 2018, pp. 4098–4109.
23. See A., Liu P. J., Manning C. D. Get to the point: summarization with pointer-generator networks, P*roceedings of the 55th Annual Meeting of the Association for Computational Linguistics*. Canada, 2017, pp. 1073–1083.
24. Vaswani A., Shazeer N., Parmar N. et al. Attention is all you need, *31st Conference on Neural Information Processing Systems (NIPS 2017)*. Long Beach, CA, USA, 2017, pp. 6000–6010.
25. Devlin J., Chang M.-W., Lee K. et al. BERT: Pre-training of deep bidirectional transformers for language understanding, *Proceedings of the 2019 Conference of the North American Chapter of the Association for Computational Linguistics: Human Language Technologies*. Minnesota, 2019, pp. 4171–4186.
26. Zhang H., Cai J., Xu J., Wang J. Pretraining-based natural language generation for text summarization, *Computational natural language learning, Hong Kong*. China, 2019, pp. 789–797. DOI: 10.18653/v1/K19–1074
27. Zhang J., Zhao Y., Saleh M. et al. PEGASUS: Pre-training with extracted gap-sentences for abstractive summarization, *Proceedings of the 37th International Conference on Machine Learning*, 2020, pp. 11328–11339.
28. Raffel C., Shazeer N., Roberts A.et al. Exploring the limits of transfer learning with a unified text-to-text transformer, *The Journal of Machine Learning Researc*, 2020, Vol. 21, № 1, pp. 5485–5551.
29. Clark K., Luong M.-T., Le Q. V. et al. ELECTRA: Pre–training Text Encoders as Discriminators Rather Than Generators, *8th International Conference on Learning Representations, 2020 [Electronic resource]*. Access mode: https://iclr.cc/virtual_2020/poster_r1xMH1BtvB.html
30. He P., Liu X., Gao J., Chen W. DeBERTa: decoding-enhanced BERT with disentangled attention, *ArXiv*, 2021, DOI: 2006.03654
31. Chung H. W., Hou L., Longpre S. et al. Scaling instruction-finetuned language models, *Journal of Machine Learning Research*, 2024, Vol. 25, pp. 1–53.
32. Touvron H., Lavril T., Izacard G. et al. LLaMA: open and efficient foundation language models, *ArXiv*, 2023. DOI: 2302.13971
33. Gemini [Electronic resource]. Access mode: https://gemini.google.com/
34. Jiang A. Q., Sablayrolles A., Mensch A. et al. Mistral 7B, *ArXiv*, 2023. DOI: 2310.06825
35. Labonne M. Quantize LLaMa with GGUF and llama.cpp [Electronic resource], 2023. Access mode: https://towardsdatascience.com/quantize-llama-models-with-ggml-and-llama-cpp-3612dfbcc172
36. Zmora N., Wu H., Rodge J. Achieving FP32 accuracy for INT8 inference using quantization aware training with NVIDIA TensorRT, *NVIDIA Technical Blog.* [Electronic resource]. Access mode: https://developer.nvidia.com/blog/achieving-fp32-accuracy-for-int8-inference-using-quantization-aware-training-with-tensorrt/
37. Dettmers T., Lewis M., Belkada Y. et al. LLM.int8(): 8-bit matrix multiplication for transformers at scale, *Proceedings of the 36th International Conference on Neural Information Processing Systems*, 2022, pp. 30318–30332. DOI: 2208.07339
38. Jacob B., Kligys S., Chen B. et al. Quantization and training of neural networks for efficient integer-arithmetic-only inference, *Proceedings of the IEEE Conference on Computer Vision and Pattern Recognition*, 2018, pp. 2704–2713. DOI: 1712.05877
39. Wu H., Judd P., Zhang X. et al. Integer quantization for deep learning inference: Principles and empirical evaluation, *ArXiv*, 2020. DOI: 2004.09602
40. McKinstry J. L., Esser S. K., Appuswamy R. et al. Discovering low-precision networks close to full-precision networks for efficient embedded inference, *ArXiv*, 2019. DOI: 1809.04191
41. Baskin C., Schwartz E., Zheltonozhskii E. et al. Uniq: Uniform noise injection for non–uniform quantization of neural networks, *ACM Transactions on Computer Systems*, 2021, Vol. 37, № 1–4, pp. 1–15. DOI: 10.1145/3444943
42. Li Y. Dong X., Wang W. Additive powers-of-two quantization: an efficient nonuniform discretization for neural networks, *ArXiv*, 2020. DOI: 1909.13144
43. Fang J., Shafiee A., Abdel-Aziz H. et al. Post-training piecewise linear quantization for deep neural networks, *Proceedings of the European Conference on Computer Vision*, 2020, pp. 69–86. DOI: 2002.00104v2
44. Jung S., Son C., Lee S. et al. Learning to quantize deep networks by optimizing quantization intervals with task loss, *Proceedings of IEEE/CVF Conference on Computer Vision and Pattern Recognition*, 2019, pp. 4350–4359. DOI: 1808.05779
45. Hubara I., Courbariaux M., Soudry D. et al. Binarized neural networks, *Proceedings of the 30th Conference on Neural Information Processing Systems (NIPS)*, 2016, pp. 4114–4122.
46. NVIDIA V100 TENSOR CORE GPU [Electronic resource]. Access mode: https://www.nvidia.com/en-us/data-center/v100

DOI 10.15588/1607-3274-2025-2-12

47. Qin H., Gong R., Liu X. et al. Binary neural networks: a survey, *Pattern Recognition*, 2020, Vol. 105. DOI: 10.1016/j.patcog.2020.107281
48. Wang P., Hu Q., Zhang Y. et al. Two-step quantization for low-bit neural networks, *IEEE/CVF Conference on Computer Vision and Pattern Recognition*, 2018. DOI:10.1109/CVPR.2018.00460
49. Ding R., Chin T.-W., Liu Z. et al. Regularizing activation distribution for training binarized deep networks, *IEEE/CVF Conference on Computer Vision and Pattern Recognition*. – 2019. DOI:10.1109/CVPR.2019.01167
50. Quantization aware training. Post-training quantization [Electronic resource], Access mode: https://www.tensorflow.org/model_optimization/guide/
51. Bengio Y., Léonard N., Courville A. Estimating or propagating gradients through stochastic neurons for conditional computation, *ArXiv*, 2013. DOI: 1308.3432
52. Bai Y., Wang Y.-X., Liberty E. Proxquant: Quantized neural networks via proximal operators, *ArXiv*, 2019. DOI: 1810.00861
53. Hubara I., Nahshan Y., Hanani Y. et al. Improving post training neural quantization: layer-wise calibration and integer programming, *ArXiv*, 2020. DOI: 2006.10518
54. Lin C.-Y. ROUGE: A package for automatic evaluation of summaries, *Proceedings of the Workshop on Text Summarization Branches Out*. Spain, Association for Computational Linguistics, 2004, pp. 74–81.
55. [Papineni K., Roukos S., Ward T. et al. bBleu: a method for automatic evaluation of machine translation, *Proceedings of the 40th Annual Meeting of the Association for Computational Linguistics. Pennsylvania*, USA, 2002, pp. 311–318.
56. Zhang T., Kishore V., Wu F. et al. BERTScore: evaluating text generation with BERT, *International Conference on Learning Representations*, 2020, pp. 1–43. DOI: 1904.0967
57. Nedashkovskaya N. I. Investigation of methods for improving consistency of a pairwise comparison matrix, *Journal of the Operational Research Society*, 2018, Vol. 69, № 12, pp. 1947–1956. DOI: 10.1080/01605682.2017.1415640
58. Nedashkovskaya N. I. Estimation of the accuracy of methods for calculating interval weight vectors based on interval multiplicative preference relations, *IEEE 3rd Internatioal Conference on System Analysis & Intelligent Computing (SAIC)*, 2022. DOI: 10.1109/SAIC57818.2022.9922977
59. Nedashkovskaya N. I. Method for weights calculation based on interval multiplicative pairwise comparison matrix in decision-making models, *Radio Electronics, Computer Science, Control*, 2022, №3, pp. 155–167. DOI: 10.15588/1607-3274-2022-3-15
60. CNN/DailyMail 3.0.0 dataset [Electronic resource]. Access mode: https://huggingface.co/datasets/cnn dailymail.
61. XSum dataset [Electronic resource]. https://huggingface.co/datasets/xsum.

Received 22.01.2025.
Accepted 21.04.2025.

УДК 004.8, 519.816

ОЦІНЮВАННЯ КВАНТОВАНИХ ВЕЛИКИХ МОВНИХ МОДЕЛЕЙ В ЗАДАЧІ УЗАГАЛЬНЕННЯ ТЕКСТІВ

Недашківська Н. І. – д-р техн. наук, доцент, доцент кафедри математичних методів системного аналізу Національного технічного університету України «Київський політехнічний інститут імені Ігоря Сікорського», Інститут прикладного системного аналізу, Київ, Україна.

Єремічук Р. І. – бакалавр системного аналізу, Київ, Україна.

АНОТАЦІЯ

Актуальність. Розглянуто задачу підвищення ефективності глибоких штучних нейронних мереж щодо обсягу пам'яті та енергоспоживання, та багатокритеріальне оцінювання якості результатів великих мовних моделей (LLM) з урахуванням суджень користувачів в задачі сумаризації текстів. Об’єктом дослідження є процес автоматизації сумаризації текстів на основі LLM.

Мета роботи – знайти компроміс між складністю моделі LLM, її точністю та ефективністю в задачі сумаризації або узагальнення текстів.

Метод. Запропоновано алгоритм оцінювання моделей LLM за багатьма критеріями (метриками), який дозволяє обрати найбільш підходящу модель LLM для сумаризації тексту, знайти прийнятний компроміс між складністю моделі LLM, її продуктивністю та якістю узагальнення тексту. Значне підвищення точності результатів на основі нейронних мереж у задачах обробки природної мови часто досягається використанням занадто глибоких і надмірно параметризованих моделей, що суттєво обмежує здатність моделей використовуватися у задачах виводу в реальному часі, за потреби високої точності в умовах обмежених ресурсів. Пропонований алгоритм обирає прийнятну модель LLM за багатьма критеріями, такими як показники точності BLEU, Rouge-1, 2, Rouge-L, BERT-оцінки, швидкість сумаризації або іншими критеріями, які визначаються користувачем в конкретній практичній задачі інтелектуального аналізу тексту. Алгоритм включає аналіз і підвищення узгодженості суджень користувачів, оцінювання моделей LLM за кожним критерієм, агрегування локальних ваг моделей, аналіз чутливості отриманих глобальних ваг моделей.

Результати. Розроблено програмне забезпечення для автоматичного отримання текстів з онлайн-статей і сумаризації цих текстів, та для оцінювання якості моделей LLM. Отримано оцінки якості дев’ятнадцяти квантованих і неквантованих моделей LLM різних розмірів, серед яких LLaMa-3-8B-4bit, Gemma-2B-4bit, Gemma-1.1-7B-4bit, Qwen-1.5-4B-4bit, Stable LM-2-1.6B-4bit, Phi-2-4bit, Mistal-7B-4bit, GPT-3.5 Turbo за показниками BLEU, Rouge-1, Rouge-2, Rouge-L і BERT-оцінок на двох різних наборах текстів XSum та CNN/Daily Mail 3.0.0.

Висновки. Проведені експерименти підтвердили працездатність пропонованого математичного забезпечення, дозволяють рекомендувати його для використання при вирішенні задач сумаризації текстів на практиці. Перспективи подальших досліджень можуть полягати у більш глибокому аналізі метрик та критеріїв оцінювання якості сгенерованих текстів, а також експериментальному дослідженні пропонованого алгоритму на більшій кількості практичних задач обробки природної мови.

КЛЮЧОВІ СЛОВА: обмеженість ресурсів, обробка природної мови, сумаризація або узагальнення тексту, великі мовні моделі, квантизація, багатокритеріальний аналіз.

DOI 10.15588/1607-3274-2025-2-12

ЛІТЕРАТУРА

1. Language models are few–shot learners / [T. Brown, B. Mann, N. Ryder et al.] // Advances in neural information processing systems. – 2020. – Vol. 33. – P. 1877–1901. DOI: arXiv:2005.14165
2. Pre-trained language models with domain knowledge for biomedical extractive summarization / [Q. Xie, J. A. Bishop, P. Tiwari et al.] // Knowledge-Based Systems. – 2022. – Vol. 252. DOI: 10.1016/j.knosys.2022.109460
3. Basyal L. Text summarization using large language models / L. Basyal, M. Sanghvi // ArXiv. – 2023. DOI: 2310.10449
4. OpenAI GPT 3.5 Turbo [Electronic resource]. – Access mode: https://platform.openai.com/docs/models/gpt-3-5-turbo
5. OpenAI GPT-4 [Electronic resource]. – Access mode: https://openai.com/index/gpt-4
6. Recipes for safety in open–domain chatbots / [J. Xu, D. Ju, M. Li et al.] // ArXiv. – 2021. DOI: 2010.07079
7. Meta LLaMa 3 [Electronic resource]. – Access mode: https://llama.meta.com/llama3
8. McCulloch W. S. A logical calculus of the ideas immanent in nervous activity / W. S. McCulloch, W. Pitts // Bulletin of Mathematical Biophysics. –1943. –Vol. 5, № 4. – P. 115–133. DOI: 10.1007/BF02478259
9. VanRullen R. Is perception discrete or continuous? / R. VanRullen, C. Koch // Trends in cognitive sciences. – 2003. – Vol. 7, № 5. – P. 207–213. DOI: 10.1016/S1364-6613(03)00095-0
10. Tee J. Is information in the brain represented in continuous or discrete form? / J. Tee, D. P. Taylor // IEEE Transactions on Molecular, Biological and Multi-Scale Communications. – 2020. – Vol. 6, № 3. – P. 199–209. DOI: 1805.01631
11. Faisal A. A. Noise in the nervous system / A. A. Faisal, L. P. J. Selen, D. M. Wolpert // Nature reviews neuroscience. – 2008. – Vol. 9, № 4. – P. 292–303. DOI: 10.1038/nrn2258
12. Varshney L. R. Decision making with quantized priors leads to discrimination / L. R. Varshney, K. R. Varshney // Proceedings of the IEEE. – 2016. – Vol. 105, № 2. – P. 241–255. DOI:10.1109/JPROC.2016.2608741
13. Varshney L. R. Optimal information storage in noisy synapses under resource constraints / L. R. Varshney, P. J. Sjöström, D. B. Chklovskii // Neuron. – 2006. – Vol. 52, № 3. – P. 409–423. DOI: 10.1016/j.neuron.2006.10.017
14. Hinton G. Distilling the knowledge in a neural network / G. Hinton, J. Dean, O. Vinyals // NIPS 2014 Deep Learning Workshop. – 2015. – P. 1–9. DOI: 1503.02531
15. Mishra A. Apprentice: using knowledge distillation techniques to improve low-precision network accuracy / A. Mishra, D. Marr // ArXiv. – 2017. DOI: 1711.05852
16. Polino A. Model compression via distillation and quantization / A. Polino, R. Pascanu, D. Alistarh // Proceedings of the Workshop at ICLR. – 2018. DOI: 1802.05668
17. Efficient estimation of word representations in vector space / [T. Mikolov, K. Chen, G. Corrado et al.] // Proceedings of the Workshop at ICLR, Scottsdale. – 2013. – P. 1–12. DOI: 1301.3781
18. Pennington J. GloVe: global vectors for word representation / J. Pennington, R. Socher, C. Manning // Proceedings of the 2014 Conference on Empirical Methods in Natural Language Processing, Doha, Qatar. Association for Computational Linguistics. – 2014. – P. 1532–1543.
19. Dai A. M. Semi-supervised sequence learning / A. M. Dai, Q. V. Le // Advances in neural information processing systems. – 2015. DOI: 1511.01432
20. Learned in translation: contextualized word vectors / [B. McCann, J. Bradbury, C. Xiong et al.] // Advances in neural information processing systems. – 2017. – P. 6297–6308. DOI: 1708.00107
21. Dissecting contextual word embeddings: architecture and representation / [M. E. Peters, M. Neumann, L. Zettlemoyer et al.] // Proceedings of the 2018 Conference on Empirical Methods in Natural Language Processing. Association for Computational Linguistics, Brussels, Belgium. – 2018. – P. 1499–1509. DOI: 10.18653/v1/D18–1179
22. Gehrmann S. Bottom-up abstractive summarization / S. Gehrmann, Y. Deng, A. M. Rush // Proceedings of the 2018 Conference on Empirical Methods in Natural Language Processing, Brussels, Belgium. – 2018. – P. 4098–4109.
23. See A. Get to the point: summarization with pointer-generator networks / A. See, P. J. Liu, C. D. Manning // Proceedings of the 55th Annual Meeting of the Association for Computational Linguistics, Canada. – 2017. – P. 1073–1083.
24. Attention is all you need / [A. Vaswani, N. Shazeer, N. Parmar et al.] // 31st Conference on Neural Information Processing Systems (NIPS 2017), Long Beach, CA, USA. – 2017. – P. 6000 – 6010.
25. BERT: Pre-training of deep bidirectional transformers for language understanding / [J. Devlin, M.-W. Chang, K. Lee et al.] // Proceedings of the 2019 Conference of the North American Chapter of the Association for Computational Linguistics: Human Language Technologies, Minnesota. 2019. – P. 4171–4186.
26. Pretraining-based natural language generation for text summarization / [H. Zhang, J. Cai, J. Xu, J. Wang] // Computational natural language learning, Hong Kong, China. – 2019. – P. 789–797. DOI: 10.18653/v1/K19–1074
27. PEGASUS: Pre-training with extracted gap-sentences for abstractive summarization / [J. Zhang, Y. Zhao, M. Saleh et al.] // Proceedings of the 37th International Conference on Machine Learning. – 2020. – P. 11328–11339.
28. Exploring the limits of transfer learning with a unified text–to–text transformer / [C. Raffel, N. Shazeer, A. Roberts et al.] // The Journal of Machine Learning Research. – 2020. – Vol. 21, № 1. – P. 5485–5551.
29. ELECTRA: Pre-training Text Encoders as Discriminators Rather Than Generators / [K. Clark, M.-T. Luong, Q. V. Le et al.] // 8th International Conference on Learning Representations, 2020 [Electronic resource]. – Access mode: https://iclr.cc/virtual_2020/poster_r1xMH1BtvB.html
30. DeBERTa: decoding-enhanced BERT with disentangled attention / [P. He, X. Liu, J. Gao, W. Chen] // ArXiv. – 2021. DOI: 2006.03654
31. Scaling instruction-finetuned language models / [H. W. Chung, L. Hou. S. Longpre et al.] // Journal of Machine Learning Research. – 2024. – Vol. 25. – P. 1–53.
32. LLaMA: open and efficient foundation language models / [H. Touvron, T. Lavril, G. Izacard et al.] // ArXiv. – 2023. DOI: 2302.13971
33. Gemini [Electronic resource]. – Access mode: https://gemini.google.com/
34. Mistral 7B / [A. Q. Jiang, A. Sablayrolles, A. Mensch et al.] // ArXiv. – 2023. DOI: 2310.06825
35. Labonne M. Quantize LLaMa with GGUF and llama.cpp [Electronic resource] / M. Labonne. – 2023. – Access mode:

DOI 10.15588/1607-3274-2025-2-12

https://towardsdatascience.com/quantize-llama-models-with-ggml-and-llama-cpp-3612dfbcc172
36. Zmora N. Achieving FP32 accuracy for INT8 inference using quantization aware training with NVIDIA TensorRT / N. Zmora, H. Wu, J. Rodge // NVIDIA Technical Blog. [Electronic resource]. – Access mode: https://developer.nvidia.com/blog/achieving-fp32-accuracy-for-int8-inference-using-quantization-aware-training-with-tensorrt/
37. LLM.int8(): 8-bit matrix multiplication for transformers at scale / [T. Dettmers, M. Lewis, Y. Belkada et al.] // Proceedings of the 36th International Conference on Neural Information Processing Systems. – 2022. – P. 30318–30332. DOI: 2208.07339
38. Quantization and training of neural networks for efficient integer-arithmetic-only inference / [B. Jacob, S. Kligys, B. Chen et al.] // Proceedings of the IEEE Conference on Computer Vision and Pattern Recognition. – 2018. – P. 2704–2713. DOI: 1712.05877
39. Integer quantization for deep learning inference: Principles and empirical evaluation / [H. Wu, P. Judd, X. Zhang et al.] // ArXiv. – 2020. DOI: 2004.09602
40. Discovering low-precision networks close to full-precision networks for efficient embedded inference / [J. L. McKinstry, S. K. Esser, R. Appuswamy et al.] // ArXiv. – 2019. DOI: 1809.04191
41. Uniq: Uniform noise injection for non–uniform quantization of neural networks / [C. Baskin, E. Schwartz, E. Zheltonozhskii et al.] // ACM Transactions on Computer Systems. – 2021. – Vol. 37, № 1–4. – P. 1–15. DOI: 10.1145/3444943
42. Li Y. Additive powers–of–two quantization: an efficient nonuniform discretization for neural networks / Y. Li, X. Dong, W. Wang // ArXiv. – 2020. DOI: 1909.13144
43. Post-training piecewise linear quantization for deep neural networks / [J. Fang, A. Shafiee, H. Abdel-Aziz et al.] // Proceedings of the European Conference on Computer Vision. – 2020. – P. 69–86. DOI: 2002.00104v2
44. Learning to quantize deep networks by optimizing quantization intervals with task loss / [S. Jung, C. Son, S. Lee et al.] // Proceedings of IEEE/CVF Conference on Computer Vision and Pattern Recognition. – 2019. – P. 4350–4359. DOI: 1808.05779
45. Binarized neural networks / [I. Hubara, M. Courbariaux, D. Soudry et al.] // Proceedings of the 30th Conference on Neural Information Processing Systems (NIPS). – 2016. – P. 4114–4122.
46. NVIDIA V100 TENSOR CORE GPU [Electronic resource]. – Access mode: https://www.nvidia.com/en-us/data-center/v100
47. Binary neural networks: a survey / [H. Qin, R. Gong, X. Liu et al.] // Pattern Recognition. – 2020. – Vol. 105. DOI: 10.1016/j.patcog.2020.107281
48. Two-step quantization for low-bit neural networks / [P. Wang, Q. Hu, Y. Zhang et al.] // IEEE/CVF Conference on Computer Vision and Pattern Recognition. – 2018. DOI:10.1109/CVPR.2018.00460
49. Regularizing activation distribution for training binarized deep networks / [R. Ding, T.-W. Chin, Z. Liu et al.] // IEEE/CVF Conference on Computer Vision and Pattern Recognition. – 2019. DOI:10.1109/CVPR.2019.01167
50. Quantization aware training. Post-training quantization [Electronic resource]. – Access mode: https://www.tensorflow.org/model_optimization/guide/
51. Bengio Y. Estimating or propagating gradients through stochastic neurons for conditional computation / Y. Bengio, N. Léonard, A. Courville // ArXiv. – 2013. DOI: 1308.3432
52. Bai Y. Proxquant: Quantized neural networks via proximal operators / Y. Bai, Y.-X. Wang, E. Liberty // ArXiv. – 2019. DOI: 1810.00861
53. Improving post training neural quantization: layer-wise calibration and integer programming / [I. Hubara, Y. Nahshan, Y. Hanani et al.] // ArXiv. – 2020. DOI: 2006.10518
54. Lin C.-Y. ROUGE: A package for automatic evaluation of summaries / C.-Y. Lin // Proceedings of the Workshop on Text Summarization Branches Out, Spain. Association for Computational Linguistics. – 2004. – P. 74–81.
55. Bleu: a method for automatic evaluation of machine translation / [K. Papineni, S. Roukos, T. Ward et al.] // Proceedings of the 40th Annual Meeting of the Association for Computational Linguistics, Pennsylvania, USA. – 2002. – P. 311–318.
56. BERTScore: evaluating text generation with BERT / [T.Zhang, V. Kishore, F. Wu et al.] // International Conference on Learning Representations. – 2020. – P. 1–43. DOI: 1904.0967
57. Nedashkovskaya N. I. Investigation of methods for improving consistency of a pairwise comparison matrix / N. I. Nedashkovskaya // Journal of the Operational Research Society. – 2018. – Vol. 69, № 12, P. 1947–1956. DOI: 10.1080/01605682.2017.1415640
58. Nedashkovskaya N. I. Estimation of the accuracy of methods for calculating interval weight vectors based on interval multiplicative preference relations / N. I. Nedashkovskaya // IEEE 3rd Internatioal Conference on System Analysis & Intelligent Computing (SAIC). – 2022. DOI: 10.1109/SAIC57818.2022.9922977
59. Nedashkovskaya N. I. Method for weights calculation based on interval multiplicative pairwise comparison matrix in decision-making models / N. I. Nedashkovskaya // Radio Electronics, Computer Science, Control. – 2022. – №3. – P. 155–167. DOI: 10.15588/1607-3274-2022-3-15
60. CNN/DailyMail 3.0.0 dataset [Electronic resource]. – Access mode: https://huggingface.co/datasets/cnn dailymail.
61. XSum dataset [Electronic resource]. – https://huggingface.co/datasets/xsum.

DOI 10.15588/1607-3274-2025-2-12

UDC 621.43, 004.032.26

METHOD FOR ANALYZING INPUT DATA FROM GEAR VIBRATIONS

Shalimov O. Y. – Student of the Department of Automation and control in technical systems, National Technical University "Kharkiv Polytechnic Institute", Kharkiv, Ukraine.

Moskalchuk O. O. – Student of the Department of Automation and control in technical systems, National Technical University "Kharkiv Polytechnic Institute", Kharkiv, Ukraine.

Yevseienko O. M. – PhD, Associate Professor, Associate Professor of the Department of Automation and control in technical systems, National Technical University "Kharkiv Polytechnic Institute", Kharkiv, Ukraine.

ABSTRACT

Context. The paper considers the problem of analyzing large data vectors for analyzing helicopter engine performance. This issue is crucial for improving the reliability and efficiency of modern aviation technologies.

Objective. To create a method for analyzing engine vibration data to achieve accurate classification of engine states based on vibration signals**.**

Method. The input data is analyzed, and a decision is made to create a neural network that is trained to recognize the class of the input vector. The neural network can work immediately and be configured for further training based on similar data. The program was implemented using a classical neural network method. The optimal weights and offsets are calculated with derivatives to minimize the loss function. The stochastic gradient descent (SGD) algorithm was used for optimization, and different activation functions were tested to find the best configuration. Choosing the right activation functions ensured maximum performance.

Results. The graphs of the input vectors show that vectors from the first class had more peaks, which helped facilitate classification. After applying this method, the accuracy was about 70–75%, which was insufficient for the task. To improve this, we enhanced the model structure and reconfigured the activation functions. With the new method, the neural network can classify the input vector with 100% accuracy.

Conclusions. This study presents an approach to analyzing engine vibration data for assessing performance. The scientific novelty lies in adapting a multilayer perceptron (MLP) for classifying vibration signals. The research shows that high accuracy can be achieved without deep architectures by optimizing the MLP. This method is universally applicable, eliminating additional model adaptation costs, which is crucial for industrial use. The practical significance is demonstrated through software and experiments, proving the effectiveness of the MLP for performance monitoring when model parameters and activation functions are properly adjusted.

KEYWORDS: 1D convolutional neural networks**,** multilayer perceptron, stochastic gradient descent, loss function, engine vibration analysis, helicopter performance, signal classification, neural network, machine learning.

ABBREVIATIONS

CNN is a convolutional neural network
FCNN is a fully connected neural network;
ICA is an independent component analysis;
MLP is a multilayer perceptron;
NN is a neural network;
PCA is a principal component analysis;
RAM is a random-access memory;
SGD is a stochastic gradient descent;
ZSL is a zero-shoot learning.

NOMENCLATURE

$a^{(l)}$ is an activation of the previous layer (or the input vector if it is the first layer);
$b^{(l)}$ is an offset vector for the l-th layer;
f is an filter size;
i is an iteration index;
L is a number of the layer on which the calculation is performed;
R is a set of numbers in a single vector;
s is a step size;
$W^{(l)}$ is a matrix of weights for the l-th layer;
X a set of vectors with input data;
x a value of the input layer;
y this is an outer layer;
$Z^{(l)}$ is an intermediate layer;
Δ is a gradient of a function;
δ is an error for layer l;
Θ is an extracted feature set
λ is a regularization hyperparameter;
$\sigma(x)$ is a sigmoid function.

INTRODUCTION

Any working component has a so-called 'service life'. After a certain amount of time or a specific period of operation, the component requires a mandatory technical inspection to ensure continued reliability. For instance, in the context of a helicopter flight, safety is paramount. To guarantee flight safety, we must implement a robust method of training a neural network, which should ultimately provide accurate assessments of engine conditions.

Predicting whether an inspection is truly necessary before examining a component is a significant challenge. Vibrations can be read and analyzed, but interpreting them is not straightforward. This task is inherently complex, making it difficult to achieve reliable results through traditional methods. Therefore, we need an alternative approach to analyze vibration data in a way that is both efficient and accessible.

Modern technology offers such an alternative in the form of neural networks. Neural networks can process large volumes of data at high speeds and handle multitasking beyond the capabilities of human or traditional computer algorithms. However, we cannot simply use any

DOI 10.15588/1607-3274-2025-2-13

neural network and expect it to perform the task effectively. A neural network must be carefully trained to understand the specifics of the problem it is intended to solve. Only with appropriate training can it provide the accurate and reliable results we need.

The object of study is the process of training a neural network using the Zero Shot method. ZSL for neural networks allows models to classify objects they have not seen during training. This is achieved by using semantic information such as object descriptions or attributes to generalize knowledge into new classes.

The purpose of the work is to use the available methods to classify vectors into two classes and automate this process. This is necessary because you have to work with large amounts of data, so you need to work with methods that are suitable for working with big data. The goal is to implement a method for classifying data samples.

Given a large set of data, namely 1158 sets, and a file that stores shortcuts (classes) for each of the vectors, it is necessary to develop a tool that, using the given data, will learn to diagnose which files are good and which have a damaged component within a given data sample. Class 1 represents the correct operation of the engine, while Class 0 indicates that the engine has a malfunction.

1 PROBLEM STATEMENT

We have a dataset of 1158 vectors taken from the helicopter gear and a file containing information about the class of each vector. Construct an algorithm that determines the corresponding label Y (class 1 or 0) for a new vector $x \in R$. It will calculate the necessary parameters for the vector classification algorithm. Increase the classification accuracy and minimize the loss function.

2 REVIEW OF THE LITERATURE

Traditional fault detection contains three main steps: data acquisition, features extraction, fault detection and classification [1]. As a common practice the data is collected with the help of numerous sensors. Feature extraction is typically implemented through linear or nonlinear transformations and data decomposition. Linear methods include PCA [2] and ICA [3]. Nonlinear techniques, such as kernel-based methods, have been shown to perform better than their linear counterpart, PCA [4]. Reducing the size or dimensionality of input data is also useful, as it is difficult to work with large signals or images and because training time increases. Straightforward methods, such as max pooling, have been actively used to address this problem [5].

In recent years, 1D convolutional neural network has been actively used to extract the most significant features from raw data for vibration-based fault detection. For example, Hsueh et al. [6] proposed a method in which they used a wavelet transform to convert a signal into a two-dimensional grayscale image and then trained a deep CNN on it to extract robust features. This data is then used to train a classification neural network that determines the health status of the system.

Another example of sophisticated feature extraction is presented in [7], where 1D vibration signals are transformed into 2D time-frequency images. While this transformation adds an additional layer of computation and complexity, the classification results are significantly better than those obtained from simple max pooling.

An uncommon solution for fault detection can be a simple MLP [8] or FCNN. However, it is important to note that the training time can be unacceptable, as an FCNN must be able to process large amounts of data [9]. As mentioned previously, many data extraction and decomposition techniques exist that help reduce these limitations.

3 MATERIALS AND METHODS

The method has been designed and tailored to address the problem. The first step was to accept signals and distribute them into vectors according to the peaks. The second step is feature extraction. Feature extraction helps reduce the dimensionality of input data while retaining the information that has the most significant impact on solving the task. A large data vector is compressed into a smaller one to save resources and speed up the process using the formulas below in this section [9]:

$$X[k] = \sum_{n=0}^{N-1} x[n] \cdot \exp(-2\pi i \frac{kn}{N}), k = 0,1,2,\ldots,N-1, \quad (1)$$

$$\theta : R^n \to R^m, m = 469, \quad (2)$$

$$\text{MaxPool}(x \mid f,s)_i = \max(x_{is:is+f}), \quad (3)$$

$$\text{MaxPool}(x \mid 100,100)_i = \max(x_{i\cdot 100:i\cdot 100+100}). \quad (4)$$

In the third step, we start training our neural network. For the sake of simplicity and clarity, we provide an algorithm for one vector. However, in the problem, we use it for 100 files and divide them into 10 mini-batches. We run the neural network once with randomly set parameters for weights and offsets. In general, it looks like this: For each hidden layer, activation is performed using the sigmoid function according to the formula:

$$a^{(l+1)} = \sigma(W^{(l)} a^{(l)} + b^{(l)}). \quad (5)$$

For the layer, denoted L, softmax is used to calculate the probabilities using the following formulas:

$$z(L) = (W^{(l)} a^{(l)} + b^{(l)}), \quad (6)$$

$$y = soft\max z(L), \quad (7)$$

where the function softmax is determined by the formula:

$$soft\max(z(L)) = \frac{e^{z_i}}{\sum_j e^{z_i} j}. \quad (8)$$

Backward pass: we calculate an error of the output layer using the cross-entropy loss function [13] with softmax by the formula:

$$\sigma^{(l)} = a^{(l)} - y. \quad (9)$$

DOI 10.15588/1607-3274-2025-2-13

Gradients for the displacement weights of the output layer L are calculated using the formulas:

$$\nabla b(L) = \sigma(L), \quad (10)$$

$$\nabla w^{(L)} = \delta^{(L)} \cdot (a^{(L-1)})^T. \quad (11)$$

Neural network regularization helps to avoid over-training, in this case, adding a penalty for large values of model weights [11]. This prevents the model from "re-learning" [12] on training data.

$$L = L_0 + \lambda \|W\|^2. \quad (12)$$

Recursive calculation of errors for previous layers:

For each layer l (moving from the original layer to the first layer):

Define the derivative of the sigmoid function by the formula:

$$\sigma`(z) = \sigma(z)(1 - \sigma(z)). \quad (13)$$

The error for layer l is calculated through the error of the next layer and the derivative of the activation function by the formula:

$$\delta^{(L)} = ((W^{(L+1)})^T \circ \sigma`(z^{(L)}), \quad (14)$$

where $\circ$ denotes an elementary multiplication (Adamar multiplication)

Gradients for weights and offsets in hidden layers: For each layer l by the formulas:

$$\nabla b^{(1)} = \sigma^{(l)}, \quad (15)$$

$$\nabla w^{(L)} = \delta^{(L)} \cdot (a^{(L-1)})^T. \quad (16)$$

Formulas 15 and 16 will be implemented later within this function, named **_backprop**. This function **_backprop** calculates the gradients of weights and biases for each layer, as well as the value of the loss function for the current example.

4 EXPERIMENTS

After analyzing the data, it was clear that using full vectors for learning would not be completely appropriate. The file that stored the data had weight while the program was running, and this amount of information was stored in RAM, making the training of such a neural network very resource-intensive and inefficient for performance.

To gain a better understanding, we built graphs and noticed that the graphs for different classes were distinct. This is shown in Figure 1.

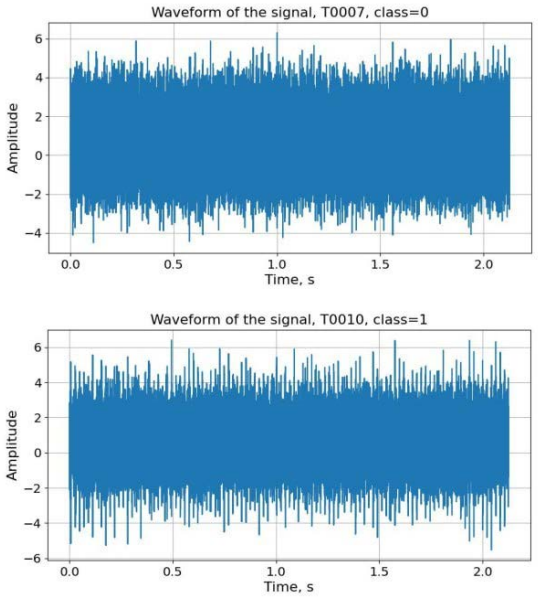

Figure 1 – Example of peaks for different classes

The graphs corresponding to class = "1" had more peaks, which were used to try to classify the vectors. First, using the discrete Fourier transform [10] with the formula (1), we converted the signal into its amplitude. We also noticed a difference in the amplitude graphs, which is shown in Figure 2.

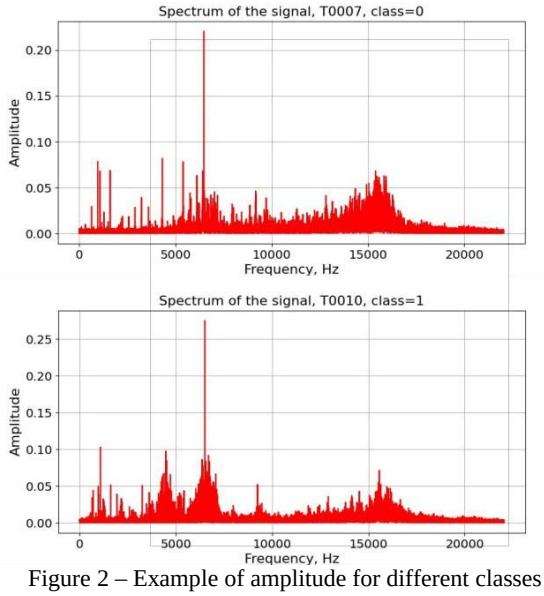

Figure 2 – Example of amplitude for different classes

It was decided to take the modulus of the amplitude vector, shift it by 0.1 values down to account for values less than zero, and retain only the maximum peaks. This is shown in Figure 3.

DOI 10.15588/1607-3274-2025-2-13

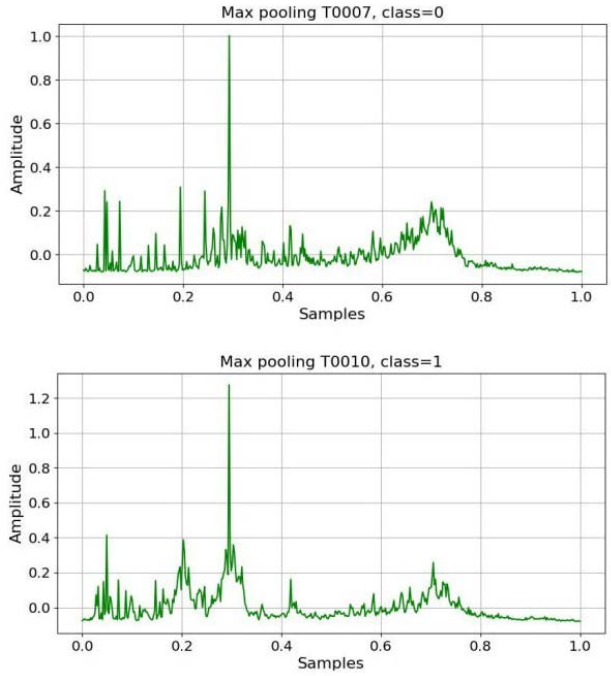

Figure 3 – Example of modulus of the amplitude for different classes

We clarified that it is possible to classify vectors by peaks. To facilitate the process, we decided to compress the data. Such manipulations with the input data allowed the input vector to have not 93.752 values, but 469 by formulas (2–4). This did not affect the training of the neural network but helped reduce the time and resources needed for training. Next, the multilayer perceptron method was used, which is a common instance of the error propagation algorithm.

The input data is permuted by the Hadamard multiplication, using a randomly generated weight vector, which is combined with the input vector using a specific displacement vector (also randomly generated). This process is repeated a specific number of times, producing an output value, which is compared with the standard (given to us by class 1 or 0). We then calculate the error, and from this error, we proceed in reverse order, gradually calibrating weights and biases. Repeating this over a certain number of files generates specific weight and bias vectors. This dataset will be used to train the neural network, which, using these vectors and the multilayer perceptron method, will be able to classify a vector with a certain probability.

5 RESULTS

The results obtained from the analysis of engine vibration data using the proposed multilayer perceptron method show promising improvements in classification accuracy. The accuracy of the initial model was 70–75%, but after further adjustments to the model structure and optimization of the activation functions, the accuracy reached nearly 100%. This significant enhancement underscores the effectiveness of the chosen approach in classifying vibration signals, which is essential for performance monitoring in helicopter engines.

DOI 10.15588/1607-3274-2025-2-13

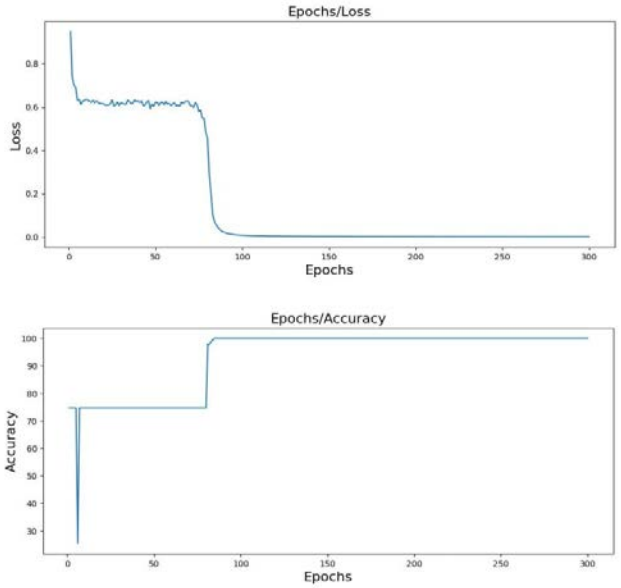

Figure 4 – Results of the learning neural network

The graphs presented in the study clearly illustrate the improvement in model accuracy after optimization. One graph shows a comparison of the accuracy between the initial and optimized models, highlighting a significant increase in accuracy after adjusting the network structure and selecting optimal activation functions. Another graph visualizes the learning process, where the reduction in error on both the training and test datasets signals good model consistency. Additionally, when comparing with other approaches, such as convolutional neural networks, it is evident that our model, despite its simplicity, yields competitive results with lower computational costs. These visualizations help to better understand the effectiveness of the applied method and emphasize its potential for real-world applications, where processing speed and resource efficiency are critical.

The comparison with similar studies reveals both similarities and differences in the methodology and results. For example, Hsueh et al. [6] used a wavelet transform followed by a CNN for fault detection. While this approach also provided robust feature extraction, it added complexity and computational overhead. In contrast, our approach using MLPs, despite its simplicity, demonstrated high accuracy without requiring deep architectures. This is particularly beneficial for real-time applications where computational resources and processing speed are critical.

6 DISCUSSION

As is evident from Figure 4, increasing the number of epochs in the formed sample improves classification accuracy. The time spent on learning is optimized. Even an increase in input data has almost no effect on the speed of diagnosis, maintains acceptable accuracy, and does not significantly increase the training time.

There is an increase in speed compared to similar methods, such as 1D Convolutional Neural Networks. Compared to the original model, the accuracy improve-

ment is nearly 100%. This confirms the feasibility of using the proposed method.

It should also be noted that the training method qualitatively affects the speed and effectiveness of training compared to similar methods. This has made it possible to improve the training process itself.

The limitations of the study primarily stem from the necessity of adjusting model parameters (e.g., weights and activation functions), which can introduce challenges in scaling the model to larger datasets. However, the proposed method's ability to work with a limited number of layers without compromising accuracy is a key advantage in real-world applications, where training time and computational efficiency are often constrained.

Practical applications of this method are significant. The approach demonstrated here could be directly applied to performance monitoring and predictive maintenance in aviation systems, where it could reduce downtime and prevent potential failures. This has important implications for both safety and cost-effectiveness in the aviation industry.

While the study provides a solid foundation for vibration-based fault detection, further research is required to enhance the model's adaptability to varying conditions and sensor configurations. Exploring hybrid models that combine the strengths of both convolutional networks and fully connected networks could lead to even more robust solutions. Additionally, the integration of real-time data collection and analysis in the model would make the method more dynamic and responsive to operational changes.

CONCLUSIONS

The problem of providing automation for vibration analysis is an urgent one. One of the most effective ways to address this is by using a neural network. Neural networks come in different types and functionalities, which allows them to be applied to various tasks. In our case, we decided to develop and train an MLP-based neural network. The use of a neural network developed based on the MLP method and SGD training is a clear and universal solution for solving similar classification problems.

Due to the combination of methods and their high-quality implementation, we obtained satisfactory results. Unfortunately, the results may vary slightly depending on the number of epochs and initial conditions. However, this should not be considered a flaw, and this method can be regarded as a correct solution for similar problems. Compared to methods that use convolution, our method is more accurate and efficient. This allows for a more accurate understanding of vibrations and the data derived from them.

The prospects for further research involve studying the capabilities of the neural network to learn from and analyze similar data. Pilot testing with similar methods and further analysis are also planned. Practical application will aim to improve and adjust the neural network.

ACKNOWLEDGEMENTS

We would like to thank Oleksiy Tielnov for his help and support throughout the project, his suggestions and links to articles were very useful and essential for our work.

REFERENCES

1. Pan J. et al. LiftingNet: a novel deep learning network with layerwise feature learning from noisy mechanical data for fault classification, *IEEE Transactions on Industrial Electronics*, 2017, Vol. 65, Iss. 6, pp. 4973–4982.
2. Abdi H., Williams L. J. Principal component analysis, *Wiley Interdisciplinary Reviews Computational Statistics*, 2010, Vol. 2, Iss. 4, pp. 433–459.
3. Lee T. W. Independent Component Analysis, Independent Component Analysis : Theory and Applications. Boston, MA, 1998, pp. 27–66.
4. Lee J-M. et al. Nonlinear process monitoring using kernel principal component analysis, *Chemical Engineering Science*, 2004, Vol. 59, Iss. 1, pp. 223–234.
5. Lin M., Chen Q., Yan S. Network in Network, *Proceedings of the 2nd International Conference on Learning Representations, ICLR, 2014, 14–16 Apr.* Banff, Canada, 2014. Access mode: https://www.semanticscholar.org/reader/5e83ab70d0cbc003471e87ec306d27d9c80ecb16.
6. Hsueh Yu-Min et al. Fault diagnosis system for induction motors by CNN using empirical wavelet transform, *Symmetry*, 2019, Vol. 11, Iss. 10, pp. 1–15.
7. Xu Juan et al. Zero-shot learning for compound fault diagnosis of bearings [Electronic resource], *Expert Systems with Applications*, 2022, Vol. 190. Access mode: https://doi.org/10.1016/j.eswa.2021.116197.
8. Lichtner-Bajjaoui A. Neural Networks and Applications [Electronic resource] : Advanced Mathematics Master Program, Universitat de Barcelona. Barcelona, 2020, 51 p. Access mode: https://diposit.ub.edu/dspace/bitstream/2445/180441/2/tfm_lichtner_bajjaoui_aisha.pdf/.
9. Nielsen M. Neural Networks and Deep Learning [Electronic resource] : textbook. Access mode: http://neuralnetworksanddeeplearning.com/.
10. Scornet E. Convolutional Neural Networks [Electronic resource]. Access mode: https://erwanscornet.github.io/teaching/CNN.pdf.
11. Kriesel D. A Brief Introduction to Neural Networks [Electronic resource]. Access mode: https://www.dkriesel.com/_media/science/neuronalenetze-en-zeta2-2col-dkrieselcom.pdf .
12. Haykin S. Neural Networks and Learning Machines [Electronic resource]. 3-rd ed. New York [et al.], 2009, 938 p. Access mode: https://dai.fmph.uniba.sk/courses/NN/haykin.neural-networks.3ed.2009.pdf..
13. Roch S. Mathematical methods in data science (with Python) [Electronic resource]. Access mode: https://mmids-textbook.github.io/index.html.

Received 30.01.2025.
Accepted 04.04.2025.

DOI 10.15588/1607-3274-2025-2-13

УДК 621.43, 004.032.26

МЕТОД АНАЛІЗУ ВХІДНИХ ДАНИХ З ВІБРАЦІЙ ЗУБЧАСТИХ МЕХАНІЗМІВ

Шалімов О. Є. – студент кафедри Автоматики та управління в технічних системах, Національний технічний університет «Харківський політехнічний інститут».

Москальчук О. О. – студент кафедри Автоматики та управління в технічних системах, Національний технічний університет «Харківський політехнічний інститут».

Євсеєнко О. М. – канд. техн. наук, доцент, доцент кафедри Автоматики та управління в технічних системах, Національний технічний університет «Харківський політехнічний інститут».

АНОТАЦІЯ

Актуальність. Розглянуто задачу аналізу векторів даних великого обсягу для аналізу працездатності двигуна гелікоптерів. Ця проблема є критично важливою для покращення надійності та ефективності сучасних авіаційних технологій.

Мета роботи. Створити метод для аналізу вібраційних даних двигуна з метою точного класифікування станів двигуна на основі вібраційних сигналів.

Метод. Проаналізовано вхідні дані, після чого було прийнято рішення створити нейромережу для розпізнавання класу вхідного вектора. Нейромережа може працювати одразу або бути налаштованою для подальшого навчання на подібних даних. Програма була реалізована з використанням класичного методу нейромереж. Оптимальні ваги та зміщення обчислюються за допомогою похідних для мінімізації функції втрат. Для оптимізації було використано алгоритм стохастичного градієнтного спуску (SGD), а також було протестовано різні функції активації для вибору найкращої конфігурації. Вибір правильних функцій активації забезпечив максимальну ефективність.

Результати. На графіках вхідних векторів видно, що вектори з першого класу мали більше піків, що полегшило процес класифікації. Після застосування цього методу точність досягла 70–75%, що було недостатньо для задачі. Для покращення результатів була змінена структура моделі та переналаштовані функції активації. З новим методом нейромережа здатна класифікувати вхідні вектори з точністю 100%.

Висновки. У цьому дослідженні представлено підхід до аналізу вібраційних даних двигуна для оцінки його працездатності. Наукова новизна методу полягає в адаптації багатошарового перцептрону (MLP) для класифікації вібраційних сигналів. Дослідження показало, що навіть без глибоких архітектур можна досягти високої точності, оптимізувавши MLP. Цей метод є універсальним, що дозволяє уникнути додаткових витрат на адаптацію моделі, що важливо для промислового використання. Практичне значення підтверджується програмним забезпеченням та експериментами, що доводять ефективність MLP для моніторингу працездатності, коли параметри моделі та функції активації налаштовані належним чином.

Перспективи подальших досліджень полягають у вивченні можливостей нейромережі для навчання та аналізу подібних даних, а також у пілотних тестуваннях із використанням схожих методів і подальшому аналізі.

КЛЮЧОВІ СЛОВА: 1D Convolutional Neural Networks, Multilayer Perceptron, Stochastic Gradient Descent, Loss Function, аналіз вібрацій двигуна, класифікація сигналів, нейромережа, машинне навчання.

ЛІТЕРАТУРА

1. LiftingNet: a novel deep learning network with layerwise feature learning from noisy mechanical data for fault classification / J. Pan [et al.] // IEEE Transactions on Industrial Electronics. – 2017. – Vol. 65, Iss. 6. – P. 4973–4982.
2. Abdi H. Principal component analysis / H. Abdi, L. J. Williams // Wiley Interdisciplinary Reviews Computational Statistics. – 2010. – Vol. 2, Iss. 4. – P. 433–459.
3. Lee T. W. Independent Component Analysis / T. W. Lee // Independent Component Analysis : Theory and Applications / Lee T. W. – Boston, MA, 1998. – P. 27–66.
4. Nonlinear process monitoring using kernel principal component analysis / J-M. Lee [et al.] // Chemical Engineering Science. – 2004. – Vol. 59, Iss. 1. – P. 223–234.
5. Lin M. Network in Network / Min Lin, Qiang Chen, Shuicheng Yan // Proceedings of the 2nd International Conference on Learning Representations, ICLR, 2014, 14–16 Apr. – Banff, Canada, 2014. – Access mode: https://www.semanticscholar.org/reader/5e83ab70d0cbc003471e87ec306d27d9c80ecb16.
6. Fault diagnosis system for induction motors by CNN using empirical wavelet transform / Yu-Min Hsueh [et al.] // Symmetry. – 2019. – Vol. 11, Iss. 10. – P. 1–15.
7. Zero-shot learning for compound fault diagnosis of bearings [Electronic resource] / Juan Xu [et al.] // Expert Systems with Applications. – 2022. – Vol. 190. – Access mode: https://doi.org/10.1016/j.eswa.2021.116197.
8. Lichtner-Bajjaoui A. Neural Networks and Applications [Electronic resource] : Advanced Mathematics Master Program / Aisha Lichtner-Bajjaoui ; Universitat de Barcelona. – Barcelona, 2020. – 51 p. – Access mode: https://diposit.ub.edu/dspace/bitstream/2445/180441/2/tfm_lichtner_bajjaoui_aisha.pdf.
9. Nielsen M. Neural Networks and Deep Learning [Electronic resource] : textbook / Michael Nielsen. – Access mode: http://neuralnetworksanddeeplearning.com/.
10. Scornet E. Convolutional Neural Networks [Electronic resource] / E. Scornet. – Access mode: https://erwanscornet.github.io/teaching/CNN.pdf.
11. Kriesel D. A Brief Introduction to Neural Networks [Electronic resource] / David Kriesel. – Access mode: https://www.dkriesel.com/_media/science/neuronalenetze-en-zeta2-2col-dkrieselcom.pdf.
12. Haykin S. Neural Networks and Learning Machines [Electronic resource] / Simon Haykin. – 3-rd ed. – New York [et al.], 2009. – 938 p. – Access mode: https://dai.fmph.uniba.sk/courses/NN/haykin.neural-networks.3ed.2009.pdf.
13. Roch S. Mathematical methods in data science (with Python) [Electronic resource] / Sebastien Roch. – Access mode: https://mmids-textbook.github.io/index.html.

DOI 10.15588/1607-3274-2025-2-13

ПРОГРЕСИВНІ ІНФОРМАЦІЙНІ ТЕХНОЛОГІЇ

PROGRESSIVE INFORMATION TECHNOLOGIES

УДК 004.9

ОБРОБКА ТЕКСТОВИХ ДАНИХ СОЦІАЛЬНИХ МЕДІА НА ПРИРОДНІЙ МОВІ ЗА ДОПОМОГОЮ BERT ТА XGBOOST

Батюк Т. М. – аспірант кафедри «Інформаційні системи та мережі», Національний університет «Львівська політехніка», Львів, Україна.

Досин Д. Г. – д-р техн. наук, старший науковий співробітник, професор кафедри «Інформаційні системи та мережі», Національний університет «Львівська політехніка», Львів, Україна.

АНОТАЦІЯ

Актуальність. Зростання обсягу текстових даних у соціальних мережах вимагає розробки ефективних методів аналізу настроїв, здатних враховувати як лексичні, так і контекстуальні залежності. Традиційні підходи до обробки тексту мають обмеження у розумінні семантичних зв'язків між словами, що впливає на точність класифікації. Інтеграція глибоких нейронних мереж для векторизації тексту з ансамблевими алгоритмами машинного навчання та методами інтерпретації результатів дозволяє покращити якість аналізу настроїв.

Метою дослідження є розробка та оцінка нового підходу до класифікації настроїв текстових повідомлень, що поєднує Sentence-BERT для глибокої семантичної векторизації, XGBoost для високоточної класифікації, SHAP для пояснення внеску ознак, sentence embedding similarity для оцінки семантичної подібності та λ-регуляризацію для покращення узагальнюючої здатності моделі. Дослідження спрямоване на аналіз впливу цих методів на якість класифікації, визначення найбільш значущих ознак та оптимізацію параметрів для забезпечення балансу між точністю та інтерпретованістю моделі.

Метод. У дослідженні використовується Sentence-BERT для перетворення текстових даних у векторний простір із глибокими семантичними зв'язками. Для класифікації настроїв застосовується XGBoost, який забезпечує високу точність та стабільність навіть на нерівномірно розподілених наборах даних. Для пояснення внеску ознак використано метод SHAP, що дозволяє визначити, які фактори найбільше впливають на прогноз. Додатково використовується sentence embedding similarity для порівняння текстів за семантичною подібністю, а λ-регуляризація оптимізує баланс між узагальненням та точністю моделі.

Результати. Запропонований підхід демонструє високу ефективність у задачах класифікації настроїв. Значення ROC-AUC підтверджує здатність моделі точно розрізняти класи емоційного забарвлення тексту. Використання SHAP забезпечує інтерпретованість результатів, дозволяючи пояснити вплив кожної ознаки на класифікацію. Sentence embedding similarity підтверджує ефективність Sentence-BERT у виявленні семантично подібних текстів, а λ-регуляризація покращує узагальнюючу здатність моделі.

Висновки. Дослідження демонструє наукову новизну через комплексне поєднання Sentence-BERT, XGBoost, SHAP, sentence embedding similarity та λ-регуляризації для покращення точності та інтерпретованості аналізу настроїв. Отримані результати підтверджують ефективність запропонованого підходу, що робить його перспективним для застосування у моніторингу громадської думки, автоматизованій модерації контенту та персоналізованих рекомендаційних системах. Подальші дослідження можуть бути спрямовані на адаптацію моделі до специфічних доменів, розширення джерел текстових даних та вдосконалення методів інтерпретації для покращення довіри до автоматизованого аналізу настроїв.

КЛЮЧОВІ СЛОВА: Машинне навчання, нормалізація ознак, трансформери, матриця плутанини, Sentence-BERT, класифікація текстових даних.

АБРЕВІАТУРИ

SB – sentence-BERT;
CB – XGBoost;
ВП – векторний простір;
ВТ – векторизація тексту;
НФ – нормалізація функції;
ПО – поєднання ознак;
ПГ – посилення градієнта;
ОМ – оцінка моделі;
SNS – Sentence Embedding Similarity.

НОМЕНКЛАТУРА

$\cos(\theta)$ – косинусна схожість;
A – вектор першого значення;
B – вектор другого значення;
A_i – компоненти вектору A;
B_i – компоненти вектору B;
$|D|$ – кількість даних у поточній колекції;
f_{BERT} – функція трансформера S-BERT;
v – вектор фіксованої довжини;
T – текстовий вхід;
ε – фактор нульового вектора;
λ – коефіцієнт семантичної подібності;
μ – середнє значення ознаки;
σ – стандартне відхилення ознаки;
n_i – загальна кількість повторень слова;

DOI 10.15588/1607-3274-2025-2-14

$\sum_k n_k$ – загальна кількість слів у документі;
$\sum A_j B_j$ – скалярний добуток векторів A та B;
$\sum \lambda |A_j||B_j|$ – компонент, що враховує вплив модулів елементів;
$\sum (A_j^2)^{1\backslash 2}$ – нормалізація вектора A;
$\sum (B_j^2)^{1\backslash 2}$ – нормалізація вектора B;
n_j – середня кількість повторень слова;
F_μ – підхід, який описує оцінку ознак;
F_σ – підхід, що описує стандартне відхилення оцінки ознаки;
n – розмірність векторів A і B;
μ_1 – вектори, що представляють два документи;
μ_2 – скалярний добуток векторів;
S_i – об'єкт описаний векторним набором значень;
i – індекс компоненту модулів елементів вектора;
j – індекс векторного елементу;
N – множина повторень елементів вектора;
M – множина параметрів моделі даних;
Σ – множина стандартних відхилень ознак;
Θ – множина коефіцієнтів векторних перетворень;
X – система аналізу текстових даних;
n_k – кількість слів в розподіленому документі;
k – індекс векторного розподілу;

ВСТУП

У сучасну епоху цифровізації стрімке зростання обсягу текстових даних у соціальних мережах створює нові виклики для їх обробки та аналізу. Соціальні платформи, такі як Twitter, є важливим джерелом інформації для вивчення громадської думки, прогнозування поведінкових трендів і моніторингу соціальних процесів. Однак, аналіз цих даних ускладнюється їх неструктурованим характером, варіативністю мовних конструкцій та високою швидкістю оновлення контенту. Традиційні методи обробки тексту часто виявляються недостатньо ефективними для розв'язання цих задач, що обумовлює необхідність розробки нових підходів.

Актуальність дослідження зумовлена потребою у вдосконалених методах аналізу текстових даних, які здатні точно визначати емоційний тон повідомлень та забезпечувати їх ефективну класифікацію. Сучасні трансформерні моделі, зокрема Sentence-BERT, дозволяють отримати якісні векторні представлення тексту, що враховують як лексичний, так і контекстуальний рівні аналізу. Однак, застосування стандартного Sentence-BERT до аналізу настроїв у соціальних мережах потребує адаптації та вдосконалення його механізмів, оскільки класичні підходи не враховують специфічні особливості коротких текстових повідомлень, таких як лексичні скорочення, емодзі та багатозначність виразів.

Предметом дослідження є методи аналізу текстових даних соціальних мереж, а об'єктом – процес векторизації тексту та його подальша класифікація за допомогою алгоритмів машинного навчання. У межах дослідження розглядаються сучасні методи обробки природної мови, що включають застосування глибоких нейронних мереж для створення числових представлень тексту та використання алгоритмів градієнтного бустингу для їх аналізу. Особливу увагу приділено удосконаленню методів векторизації тексту, які дають змогу отримати більш точне представлення семантичного змісту повідомлень.

Для цього Sentence-BERT проходить додаткове навчання на текстових даних соціальних мереж, що дозволяє враховувати їх специфіку та покращує якість отриманих векторних ознак. Розробка нової стратегії агрегованого пулінгу дозволяє підвищити точність обчислення семантичної близькості між текстами, оскільки враховує не лише середнє значення вихідних представлень слів, а й локальні особливості їх використання в контексті.

Додатково здійснюється адаптація алгоритму XGBoost до роботи з текстовими ознаками, що включає розширення набору вхідних характеристик, а також використання методів балансування класів для підвищення стійкості моделі до нерівномірного розподілу даних у навчальному наборі. Завдяки комплексному підходу, що включає поєднання трансформерних моделей та градієнтного бустингу, запропоноване рішення сприяє підвищенню якості класифікації настроїв у текстах соціальних мереж.

Основною метою роботи є розробка вдосконаленого підходу до класифікації настроїв текстових повідомлень шляхом модифікації Sentence-BERT та адаптації XGBoost для обробки векторизованих текстових даних. Для досягнення цієї мети необхідно вирішити кілька ключових задач. По-перше, необхідно здійснити додаткове навчання Sentence-BERT на текстах соціальних мереж, що дозволить покращити його здатність враховувати контекстуальні особливості коротких повідомлень. По-друге, слід розробити ефективну стратегію агрегованого пулінгу, яка забезпечить більш точне представлення текстових ознак та сприятиме кращому захопленню семантичних залежностей між словами. По-третє, потрібно адаптувати алгоритм XGBoost для роботи із текстовими ознаками, що передбачає розширення його можливостей щодо обробки категоріальних даних та підвищення його стійкості до можливих аномалій у текстових представленнях. Нарешті, необхідно впровадити методи балансування класів, які допоможуть усунути проблему нерівномірного розподілу даних.

Наукова новизна дослідження полягає у розробці адаптивного підходу до аналізу текстових даних, що поєднує вдосконалену архітектуру Sentence-BERT із глибоким навчанням на текстах соціальних мереж та адаптований механізм обробки ознак у XGBoost. Додавання механізму контрастного навчання дозволяє підвищити чутливість моделі до контекстних особливостей повідомлень. Крім того, адаптація XGBoost до обробки текстових ознак шляхом оптимізації вхідних характеристик та введення додаткових регуляційних стратегій забезпечує стабільну роботу моделі.

DOI 10.15588/1607-3274-2025-2-14

Запропоновані вдосконалення дозволяють підвищити точність класифікації настроїв у коротких текстах, мінімізувати вплив дисбалансу класів та забезпечити стійкість моделі до шумових факторів у даних. Практична суть дослідження полягає в потенційному застосуванні в системах автоматизованого моніторингу громадської думки та аналізу клієнтських відгуків що є важливим аспектом для розвитку сучасних інформаційно-аналітичних систем.

Внесок роботи полягає у розробці нових підходів до вдосконалення трансформерних моделей у сфері аналізу текстових даних соціальних мереж та оптимізації алгоритмів градієнтного бустингу для задач текстової класифікації.

1 ПОСТАНОВКА ПРОБЛЕМИ

Інформаційна система аналізу текстових даних з використанням алгоритмів векторизації Sentence-BERT представлена імітаційною моделлю кортежу:

$$X = <\cos(\theta), A, B, |D|, \sum_k n_k, N, F\mu, F\sigma >,$$

де $N = \{n_1, n_2, n_3, n_4\}$, $M = \{\mu_1, \mu_2, \mu_3, \mu_4\}$, $\Sigma = \{\sigma_1, \sigma_2, \sigma_3, \sigma_4\}$, $\Theta = \{\theta_1, \theta_2, \theta_3, \theta_4\}$.

XGBoost – це потужна техніка машинного навчання, яка використовується для задач регресії та класифікації. Його основна ідея полягає в побудові моделі шляхом поступового додавання нових моделей, які виправляють помилки попередніх:

$$\cos(\theta) = A_i \circ B_i \circ n_i,$$
$$|D| = n_i(n_j (n (\mu_1, \mu_2, \mu_3), \sigma_1, \sigma_2), \mu_4),$$
$$n = n_i \circ n_j \circ n_k.$$

Кількість дійсних текстових даних у остаточній векторній колекції: $S_i = i \circ j \circ k$, тому

$$A_iB_i = \theta_1(n_1(\mu_1(S_i, n_4, \sigma_4, \mu_4), \theta_2, \mu_3), \theta_3).$$

Загальна кількість слів у документі та зовнішні нормалізовані дані:

$$\sum_k n_k = \mu \circ \sigma \circ \lambda \circ \Sigma,$$
$$N = n_3(n_4(\mu_4(\theta_4(\mu_2,\theta_2),n_1), \mu_1), \mu_3).$$

Підходи, які описують поточну оцінку функції та стандартне відхилення оцінки функції:

$$F\mu = N \circ M \circ \Sigma \circ \Theta,$$
$$F\sigma = \theta_4(\mu_4(\theta_3(\mu_3(A_iB_i, \sum_k n_k), |D|), n_4), n_3).$$

2 АНАЛІЗ ЛІТЕРАТУРНИХ ДЖЕРЕЛ

У статті [1] авторами досліджується ефективність застосування моделей глибокого навчання, таких як BERT, для векторизації текстів у задачах класифікації настроїв. Основна увага приділяється порівнянню BERT із класичними підходами, зокрема TF-IDF і Word2Vec. Автори підкреслюють переваги BERT у врахуванні контекстуальних зв'язків між словами, що дозволяє значно покращити точність класифікації. Крім того, дослідження включає оцінку впливу різних параметрів векторизації на результати моделювання, таких як розмір словникового запасу та кількість шарів трансформера.

У роботі [2] акцентується увага на інтеграції XGBoost як основної моделі класифікації в задачах аналізу настроїв. Автори зосереджуються на оптимізації гіперпараметрів моделі та її здатності працювати з векторними представленнями текстів, створеними за допомогою BERT. У статті також розглядається вплив дисбалансу класів на результати моделювання, а для його компенсації застосовуються методи збалансування даних, такі як oversampling і undersampling. Отримані результати демонструють високу точність моделі, особливо у випадках, коли використовуються додаткові категоріальні ознаки, такі як час публікації повідомлення або місце користувачів.

Стаття [3] представляє новаторський підхід до оцінки схожості текстів на основі Sentence Embedding Similarity. Автори використовують косинусну схожість між векторами, створеними Sentence-BERT, для аналізу семантичної близькості між повідомленнями. Це дозволяє виявляти схожі за змістом повідомлення та групувати їх у кластеризовані теми. Основний внесок роботи полягає в демонстрації, як подібність між текстами може бути використана для покращення класифікації настроїв, зокрема, для вирішення неоднозначних випадків, де текст містить змішані емоції.

Дослідження [4] зосереджене на вивченні впливу специфічної лексики на результати класифікації настроїв. Автори досліджують, як окремі ключові слова або фрази, такі як «щасливий», «злий» чи «розчарований», впливають на ймовірність передбачень моделі. Використовуючи аналіз важливості ознак у моделі XGBoost, вони показують, що специфічна лексика має суттєвий вплив на результати класифікації. Робота також включає експерименти з вилученням високочастотних слів і аналізом того, як це змінює точність моделі.

У статті [5] розглядається важливість візуалізації результатів класифікації настроїв. Автори пропонують використовувати різні типи графіків, такі як ROC-криві, матриці плутанини, Precision-Recall криві та теплові карти косинусної схожості, для оцінки продуктивності моделі та інтерпретації результатів. Особливу увагу приділено інтерактивним інструментам візуалізації, які дозволяють аналізувати зв'язки між семантично подібними текстами та їх вплив на результати класифікації.

Дослідження [6] підкреслює важливість комбінування моделей, таких як BERT і XGBoost, у задачах аналізу настроїв. У статті представлено експерименти, де ці моделі використовуються у зв'язці для отримання точніших результатів. Автори доводять, що використання гібридних підходів дозволяє краще враховувати як лексичні, так і контекстуальні особливості текстів, що позитивно впливає на загальну продуктивність наведених в статті моделей.

DOI 10.15588/1607-3274-2025-2-14

Стаття [7] демонструє використання Sentence Embedding Similarity для створення кластерів текстів у реальних наборах даних із соціальних мереж. Автори доводять, що цей підхід може бути корисним для зменшення розмірності даних і виділення ключових тем, які потім використовуються для уточнення передбачень настроїв.

У роботі [8] проводиться порівняльний аналіз різних типів векторних представлень, таких як Sentence-BERT, FastText та GloVe, у контексті класифікації настроїв. Автори роблять висновок, що Sentence-BERT забезпечує найвищу точність, особливо у поєднанні з алгоритмами градієнтного бустингу, такими як XGBoost.

У статті [9] автори пропонують застосування моделі XGBoost для автоматичної класифікації настроїв у соціальних мережах, таких як Twitter.

Основна увага приділяється аналізу факторів, які впливають на продуктивність моделі, зокрема, впливу різних підходів до векторизації текстів. Автори використовують Sentence-BERT для створення текстових векторів, а також досліджують, як різні розміри векторів та методи нормалізації впливають на точність передбачень. Робота підкреслює, що інтеграція векторів із додатковими ознаками, такими як час публікації чи кількість лайків, суттєво підвищує точність класифікації.

У статті [10] акцентується увага на застосуванні Sentence Embedding Similarity для групування текстів за темами. Автори досліджують, як використання косинусної схожості між векторами повідомлень може допомогти в аналізі настроїв у великих наборах даних. Основний внесок цієї роботи полягає у демонстрації ефективності кластеризації повідомлень за допомогою схожості їх текстових представлень. Наприклад, у статті представлено результати експериментів, де повідомлення, які містять однакові ключові слова або фрази, автоматично групуються в кластери для подальшого аналізу. Це дозволяє ефективно зменшувати розмірність даних і зосереджувати увагу на ключових темах, які обговорюються у соціальних мережах.

У статті [11] розглядається питання візуалізації результатів аналізу настроїв за допомогою інтерактивних графічних інструментів. Автори пропонують використовувати теплові карти, які показують косинусну схожість між текстовими векторами, створеними Sentence-BERT, для кращого розуміння зв’язків між повідомленнями. Також у роботі представлено інші типи візуалізацій, зокрема ROC-криві, Precision-Recall криві та бар-чарти, що дозволяють оцінювати точність і повноту моделей класифікації.

Основна увага приділяється інтерактивності таких графіків, які дозволяють дослідникам глибше аналізувати зв’язки між даними, а також виявляти патерни у поведінці користувачів соціальних мереж. Крім того, у статті наводяться приклади використання таких інструментів для ідентифікації фейкових новин або виявлення токсичних коментарів. Результат аналізу наявних наукових робіт демонструє значний прогрес у використанні сучасних методів обробки тексту, таких як BERT, XGBoost і Sentence Embedding Similarity, для класифікації настроїв у соціальних мережах. Ці дослідження показують важливість інтеграції трансформерних моделей для врахування контексту текстів, ансамблевих методів для підвищення точності передбачень та візуалізацій для кращого розуміння результатів. Особливо цінними є підходи до вирішення проблеми дисбалансу класів, аналізу семантичної схожості текстів, впливу специфічної лексики та кластеризації даних. Водночас залишаються відкритими питання щодо подальшого вдосконалення цих методів. Зокрема, потребує уваги оптимізація процесу навчання моделей на великих наборах даних, врахування мовних і культурних відмінностей у текстах.

Крім того, важливим напрямом є дослідження методів пояснення результатів моделей для кращого розуміння, чому модель приймає ті чи інші рішення, що може значно підвищити довіру до автоматизованих систем аналізу настроїв.

3 МАТЕРІАЛИ ТА МЕТОДИ

Це дослідження спрямоване на аналіз настроїв у текстових повідомленнях із соціальних мереж, використовуючи передові методи обробки тексту та глибинного навчання. Для аналізу використано датасет Kaggle Dataset: Sentiment140, що містить повідомлення, помічені як негативні, нейтральні або позитивні, що дозволяє ефективно класифікувати настрій повідомлень за допомогою машинного навчання. Основним завданням є створення моделі, здатної не тільки класифікувати настрій, але й оцінювати семантичну схожість між текстами. Для досягнення цієї мети були використані методи Sentence-BERT та Sentence Embedding Similarity [12]. Було запропоновано удосконалений підхід до оцінки семантичної схожості між текстами, застосовуючи нові методи агрегації векторів, що дозволяють більш точно відображати зміст текстів у порівнянні з класичними методами.

У дослідженні ми використовуємо метод косинусної схожості [13] для вимірювання подібності між текстами, де кожен текст спочатку перетворюється у вектор фіксованої довжини за допомогою моделі Sentence-BERT. Це дозволяє забезпечити точну оцінку схожості текстів не тільки за допомогою наявних слів, але й через семантичні зв’язки та контекстуальну подібність. Моделі трансформерів, такі як BERT [14], використовуються для отримання числових векторних уявлень, що зберігають контекстуальні властивості слів. Після перетворення тексту в таку форму, для оцінки схожості використовується вдосконалена версія Sentence Embedding Similarity. Удосконалена формула для обчислення Sentence Embedding Similarity заснована на врахуванні не тільки косинусної

DOI 10.15588/1607-3274-2025-2-14

схожості між векторами, але й додаткових факторів, таких як контекстуальна інформація та семантична вагомість [15] окремих компонентів векторів. Це дозволяє отримати більш точні результати для порівняння текстів, зокрема в задачах, пов'язаних із класифікацією настроїв та виявленням схожості між повідомленнями у соціальних мережах.

Удосконалена формула для обчислення схожості між двома реченнями, наведена в формулі 1, де A і B – це вектори, що представляють два речення S_1 та S_2 , отримані через модель, таку як Sentence-BERT. A_i та B_i це компоненти векторів A і B, що відображають значення на відповідних позиціях, n – кількість елементів у векторі (розмірність векторів), λ – коефіцієнт, який визначає важливість різниці між величинами компонентів векторів для покращення семантичної подібності, ε – маленьке значення для уникнення ділення на нуль у випадку нульового вектора

$$ses(S_1, S_2) = \frac{\sum_{i=1}^{n} A_j B_j + \lambda \times \sum_{i=1}^{n} |A_j| \times |B_j|}{\sqrt{\sum_{i=1}^{n} A_j^2 + \varepsilon} \times \sqrt{\sum_{i=1}^{n} B_j^2 + \varepsilon}}. \quad (1)$$

Моделі на основі трансформерів, зокрема Sentence-BERT, набули значної популярності завдяки своїй здатності ефективно перетворювати текст у числовий формат, що враховує семантичний контекст слів у реченнях. Застосування таких моделей відкриває нові можливості для використання текстових даних в алгоритмах машинного навчання, зокрема для класифікації, кластеризації та інших задач аналізу тексту. Sentence-BERT [16] є модифікацією BERT, оптимізованою для обчислення семантичної схожості між текстами, що робить його надзвичайно ефективним для вирішення задач парного порівняння текстів та визначення схожості між ними. Основною метою S-BERT, що наведений в формулі 2, де T – текстовий вхід, f_{BERT} – функція трансформера S-BERT та v – результат у вигляді вектора фіксованої довжини, що відображає зміст текстів. S-BERT використовує додатковий шар агрегації (наприклад, середнє або максимальне значення) для отримання одного вектора на рівні всього тексту. Це дозволяє швидко та ефективно обчислювати семантичну схожість між текстами.

$$v = f_{BERT}(T). \quad (2)$$

Однією з основних характеристик S-BERT є його здатність працювати із завданнями парного порівняння текстів, що важливо для задач, де потрібно оцінити схожість або відмінності між двома текстами. Завдяки можливості використовувати метрики, такі як косинусна схожість, S-BERT може оцінювати не тільки наявність однакових слів, а й їх контекстуальні зв'язки в реченні. Це дозволяє моделі ефективно застосовуватися для завдань, таких як класифікація настроїв або пошук схожих повідомлень в текстових даних. Крім того, S-BERT є надзвичайно корисним для задач кластеризації, оскільки створює векторні репрезентації, що зберігають семантичні зв'язки між різними елементами тексту.

Для того, щоб максимізувати ефективність роботи з текстами, S-BERT поєднує передтреновані моделі трансформерів, такі як BERT чи DistilBERT, з операцією агрегації, що дозволяє скоротити розмір вихідних векторів, не втрачаючи важливих семантичних особливостей тексту.

Це створює потужний інструмент для аналізу тексту, який забезпечує високу точність при розв'язанні задач класифікації настроїв або пошуку подібних текстів. У той же час, обраний підхід дозволяє зберегти точність обробки текстів при зниженні обсягу необхідних для обробки даних, що робить S-BERT практичним та ефективним у багатьох реальних застосунках.

Удосконалення моделі S-BERT полягає в оптимізації її здатності до обробки великих обсягів текстових даних, зокрема завдяки адаптації агрегаційних функцій для отримання більш точних та репрезентативних векторних характеристик.

У результаті, застосування цієї моделі дозволяє не тільки значно покращити точність класифікації або кластеризації, а й суттєво знизити вимоги до обчислювальних ресурсів при виконанні великих обсягів аналізу текстових даних.

Таким чином, запропонований підхід із використанням моделі S-BERT вносить значний внесок, удосконалюючи методи семантичного аналізу текстів, зокрема через покращення якості та ефективності побудови векторних представлень текстових даних. Важливими аспектами цієї роботи є як теоретичні, так і практичні новації, що сприяють підвищенню точності та зниженню витрат ресурсів при обробці великих обсягів тексту в реальних умовах.. Блок-схему роботи моделі S-BERT зображено на рисунку 1.

Рисунок 1 – Блок-схема роботи моделі S-BERT

DOI 10.15588/1607-3274-2025-2-14

Отримавши векторизований текст з семантичним контекстом наступним кроком буде здійснення машинного навчання з використанням XGBoost, потужної бібліотеки для машинного навчання, яка використовується для вирішення завдань класифікації та регресії. Основною перевагою XGBoost є її здатність ефективно працювати з категоріальними ознаками без необхідності попереднього перетворення або кодування, що значно спрощує підготовку даних і прискорює процес навчання.

Крім того, вона використовує передову технологію градієнтного бустінгу, яка забезпечує високу точність і стабільність моделі. XGBoost базується на методі градієнтного бустінгу на деревах рішень (Gradient Boosting on Decision Trees), який є ефективним і популярним підходом для побудови моделей. Цей метод передбачає побудову послідовності дерев рішень, де кожне наступне дерево коригує помилки попереднього.

Категоріальні ознаки в XGBoost обробляються без необхідності їх явного перетворення в числові значення, що зменшує ймовірність втрати інформації і покращує загальну ефективність. XGBoost є особливо ефективним для задач, де потрібно здійснити класифікацію текстів, в тому числі в задачах аналізу настроїв, спаму, класифікації тематики текстів тощо.

Враховуючи можливість інтеграції з іншими техніками обробки природної мови, такими як Sentence-BERT, XGBoost може отримувати високоточні векторні представлення текстів і ефективно використовувати їх для класифікації.

За допомогою моделей, таких як Sentence-BERT, текстові дані перетворюються у високоякісні вектори, що зберігають семантичну інформацію. Ці вектори [16] передаються до моделі XGBoost для подальшої класифікації. У цьому дослідженні запропоновано удосконалений підхід до класифікації текстових даних, що інтегрує потужний метод машинного навчання – XGBoost, з передовими техніками обробки природної мови.

Особливістю цього підходу стало вдосконалення можливостей моделі XGBoost через додавання методів інтерпретації, таких як SHAP (Shapley Additive Explanations), що дозволяє не лише підвищити точність моделі, а й забезпечити глибоке розуміння її рішень.

Ключовим удосконаленням є інтеграція технології SHAP, яка дозволяє з'ясувати, як окремі ознаки впливають на результати класифікації. Це дає можливість моделі не лише генерувати точні прогнози, але й відкривати внутрішню структуру прийняття рішень, що є важливим для задач, де інтерпретованість результатів є критично важливою. Завдяки використанню SHAP, модель стає прозорою і її результати можна пояснити з точки зору вкладу кожної ознаки в кінцеве рішення, що значно підвищує її надійність та застосовність у реальних умовах.

Зокрема, застосування SHAP дає можливість детально проаналізувати, чому певні текстові характеристики (наприклад, настрій, тональність або конкретні ключові слова) відіграють важливу роль у класифікації. Це дозволяє не лише підвищити точність класифікації, але й зменшити ймовірність помилок або непередбачених результатів, адже кожен етап прийняття рішення моделі стає більш зрозумілим.

Це удосконалення дозволяє зберігати високу продуктивність навіть при роботі з великими обсягами даних. Вдосконалена модель XGBoost демонструє значну стійкість до змін у даних та забезпечує високу точність класифікації навіть у складних ситуаціях, що дозволяє значно розширити сферу її застосування, зокрема в аналітиці текстів, прогнозуванні емоційного стану, або в інших дослідженнях, що потребують детального аналізу текстових даних.

Інтеграція SHAP в модель XGBoost забезпечує не тільки високу точність класифікації, але й ефективну інтерпретацію результатів, що дозволяє користувачам та дослідникам більш глибоко розуміти механізми роботи моделі та адаптувати її до специфічних вимог. Також модель показує високу продуктивність навіть при роботі з великими даними, роботу моделі зображено на рисунку 2.

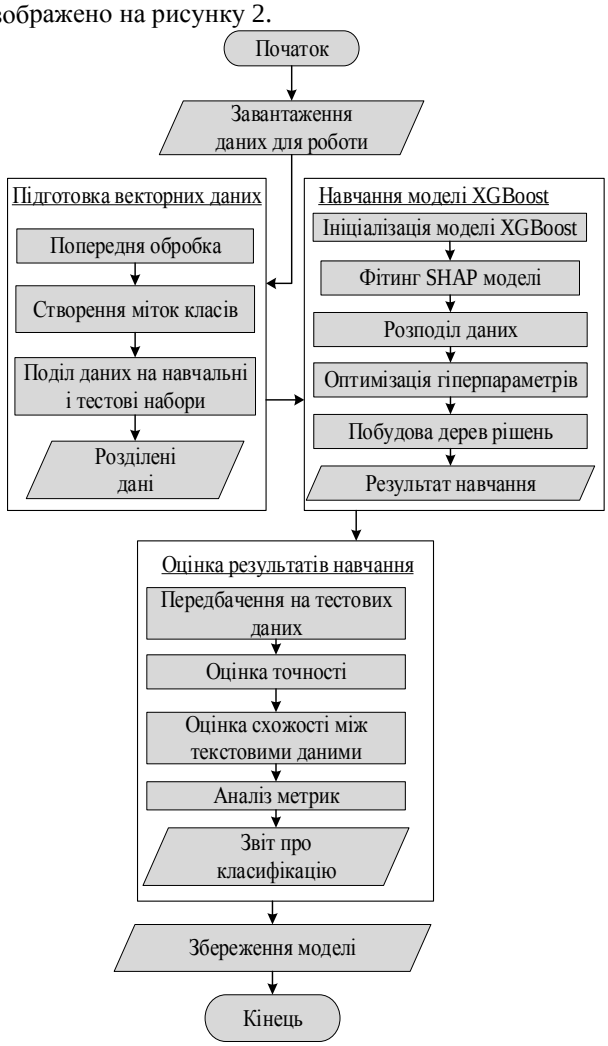

Рисунок 2 – Алгоритм роботи моделі XGBoost

DOI 10.15588/1607-3274-2025-2-14

Після тренування моделі необхідно оцінити її продуктивність на тестовому наборі. Для цього використовуються такі метрики, як точність, матриця плутанини, звіт про класифікацію.

Ці метрики дозволяють оцінити, наскільки добре модель класифікує повідомлення за їхнім настроєм, і визначити, чи модель може правильно передбачити позитивний, негативний або нейтральний настрій.

Для більш детального аналізу результатів використовується метрика Sentence Embedding Similarity, яка дозволяє вимірювати схожість між векторами повідомлень. Це корисно для задач, що вимагають не тільки класифікації, а й виявлення подібності між текстами, що можуть бути схожими за змістом, але мати різні настрої.

Такий підхід дозволяє здійснювати більш глибокий аналіз текстів і покращити якість класифікації. Блок-схема алгоритму роботи інтелектуальної системи зображена на рисунку 3.

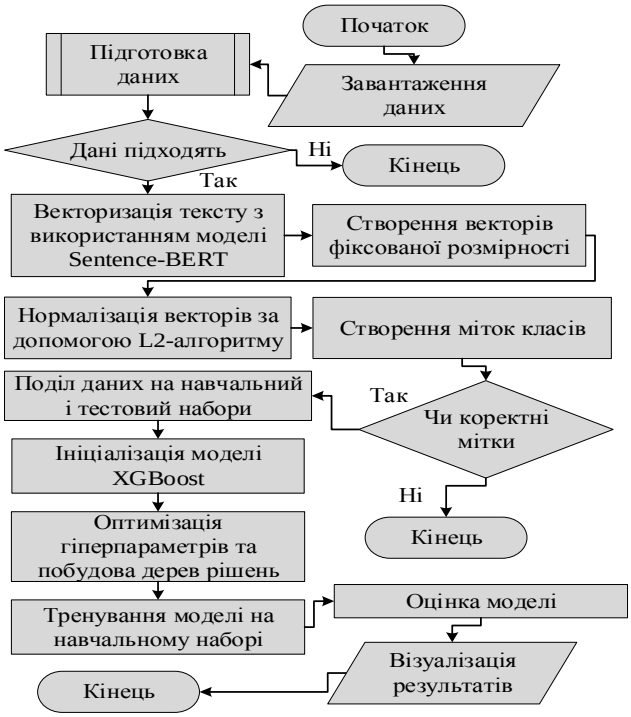

Рисунок 3 – Схема алгоритму інтелектуальної системи

Дослідження датасету Sentiment140 з використанням методів Sentence-BERT, XGBoost та Sentence Embedding Similarity дозволяє створити ефективну інформаційну систему для класифікації повідомлень за настроєм. Ключовими етапами є попередня обробка текстових даних, векторизація та нормалізація, навчання моделі на числових ознаках і подальша оцінка продуктивності за допомогою різних метрик. Важливою частиною є також аналіз схожості між повідомленнями, що дає можливість покращити якість класифікації і забезпечити високу точність моделі.

4 ЕКСПЕРИМЕНТИ

Для дослідження датасету Sentiment140 було обрано мову програмування Python 3.12 та інтегроване середовище розробки PyCharm. Початковим етапом є завантаження необхідного датасету, що містить дані з Twitter, де кожне користувацьке повідомлення супроводжується міткою, що вказує на його емоційний настрій. Датасет Sentiment140 включає такі характеристики: текст повідомлення (текстова ознака – повідомлення залишене в соціальній мережі в певний момент часу розміром до 280 символів), емоційний настрій повідомлення (цільова ознака), а також додаткові параметри, зокрема час публікації та інші метадані. Метою дослідження є вивчення взаємозв'язків між текстовими ознаками та емоційним настроєм в контексті соціальних медіа. Основною метою аналізу цих даних є побудова моделі машинного навчання, здатної класифікувати повідомлення за настроєм (позитивний, негативний або нейтральний) на основі текстового змісту.

Аналіз даних дозволить оцінити ефективність побудованої моделі та її здатність до точного передбачення емоційного настрою користувачів на основі текстових даних, що в свою чергу може бути корисним для аналізу настроїв у великих обсягах текстів в реальному часі. Завантажений датасет зображено на рисунку 4.

Рисунок 4 – Завантажений датасет

Оцінка точності моделі після навчання показала високі результати, що свідчить про її здатність ефективно класифікувати текстові дані. Модель досягла загальної точності 90% на тестовому наборі. Аналіз окремих метрик для кожного класу свідчить про збалансовану продуктивність.

Для класу negative модель продемонструвала точність 91%, повноту 87% та F1-метрику 89%. Це вказує на те, що модель добре ідентифікує негативні приклади, хоча частина з них була класифікована неправильно.

Для класу positive результати показали точність 89%, повноту 92% та F1-метрику 91%. Модель демонструє дещо кращу здатність виявляти позитивні класи, при цьому зберігаючи високу збалансованість між точністю та повнотою.

Зведені метрики показали середню макро-оцінку (macro avg) для точності, повноти та F1-метрики на рівні 90%, що свідчить про рівномірну продуктивність моделі для кожного класу та зважену середню оцінку (weighted avg), яка враховує частоту кожного класу в даних, також становила 90%,

DOI 10.15588/1607-3274-2025-2-14

підкреслюючи стабільну роботу моделі незалежно від кількості зразків кожного класу, дані про точність навчання, повноту та F1-метрику зображено на рисунку 5.

Точність навчання: 0.90

	precision	recall	f1-score	support
negative	0.90	0.90	0.90	239611
positive	0.90	0.90	0.90	240389
accuracy			0.90	480000
macro avg	0.90	0.90	0.90	480000
weighted avg	0.90	0.90	0.90	480000

Рисунок 5 – Інформація про створену модель нейронної мережі

Результати моделі класифікації продемонстрували високу точність і збалансованість у прогнозуванні класів negative і positive. AUC значення для ROC-кривої становить 0,90, що свідчить про високий рівень розділення між класами.

ROC-криві показують стабільну продуктивність моделі при зміні порогу класифікації. Precision-Recall аналіз демонструє для класу negative зростання точності (precision) при зменшенні повноти (recall), досягаючи максимуму в 1,0 для високих порогів.

Повнота зменшується із зниженням порогу, демонструючи стабільність на початкових рівнях і поступове зниження для менш релевантних зразків. Відповідно для класу positive, максимальна точність досягнута на рівні 1,0, що вказує на відмінне виявлення цього класу в певних умовах.

Повнота показує стабільне зменшення, залишаючись значною на середніх рівнях. Числові значення матриці плутанини та результати Precision-Recall аналізу зображено на рисунку 6, матрицю плутанини зображено на рисунку 7.

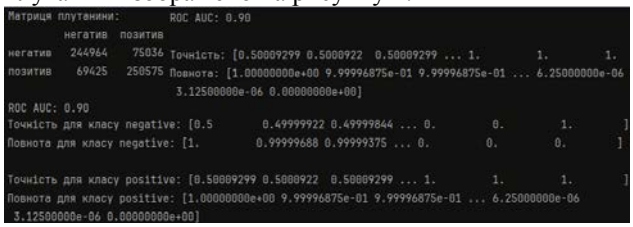

Рисунок 6 – Матриця плутанини та результати Precision-Recall аналізу

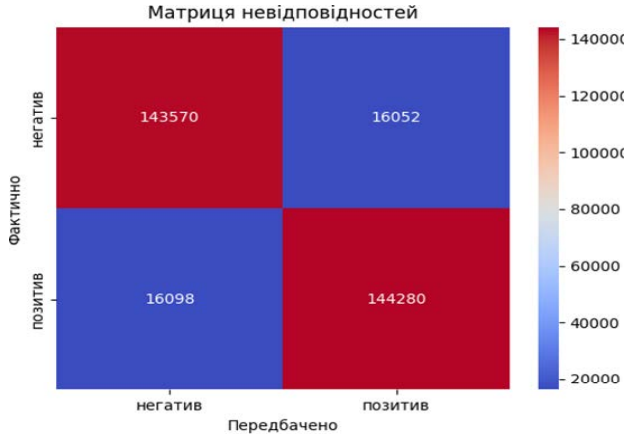

Рисунок 7 – Графічне відображення отриманої матриці плутанини

Ці результати підкреслюють високий рівень точності моделі при класифікації текстових даних, що особливо важливо для завдань аналізу настроїв, де правильна ідентифікація позитивних і негативних висловлювань має критичне значення. Модель показала здатність ефективно працювати з збалансованими наборами даних, що свідчить про її здатність обробляти різноманітні текстові дані без переваги одного класу над іншим, що є важливим для реальних застосувань. Візуалізація ROC-кривої на рисунку 8 чітко демонструє, як добре модель розрізняє твіти з різними настроями, що дозволяє швидко оцінити її ефективність.

Високе значення AUC (0,90) підтверджує, що модель володіє відмінною здатністю до класифікації з мінімальними хибними позитивними та негативними помилками. Площа під ROC-кривою є індикатором того, як добре модель розрізняє класи, і велика площа означає, що кількість хибних рішень значно зменшена.

ROC-крива на рисунку 8 ілюструє, наскільки добре модель розрізняє твіти з негативним і позитивним настроєм.

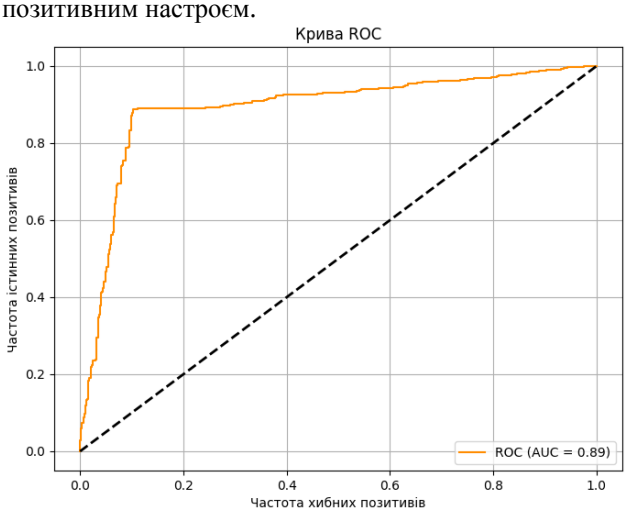

Рисунок 8 – ROC-крива поділу позитивних та негативних класів повідомлень користувачів

Precision-Recall крива на рисунку 9 демонструє, як змінюється співвідношення між точністю і повнотою для класифікації позитивних і негативних твітів залежно від порогового значення. Висока точність свідчить про те, що більшість твітів, які модель класифікує як позитивні або негативні, дійсно належать до відповідного класу. Це важливо для уникнення хибно-позитивних висновків. Висока повнота вказує, що модель здатна знайти всі твіти відповідного настрою в тестовій вибірці, що мінімізує хибно-негативні прогнози. Датасет Sentiment140 складається з коротких текстів (користувацьких повідомлень у Twitter). Такі дані часто містять емоційно насичені слова, скорочення, емодзі або інші нелінійні мовні конструкції, що ускладнює класифікацію. У цьому випадку Precision-Recall крива

DOI 10.15588/1607-3274-2025-2-14

демонструє, що модель ефективно працює навіть у таких умовах, забезпечуючи надійні прогнози.

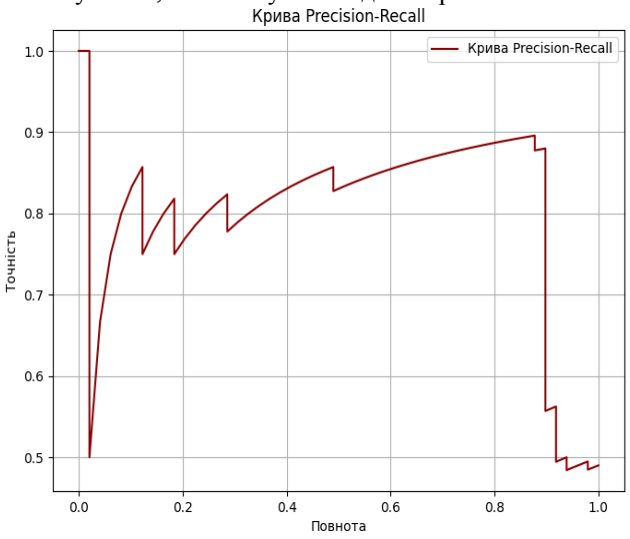

Рисунок 9 – Precision-Recall крива

Калібрувальна крива зображена на рисунку 10 є важливим інструментом для оцінки узгодженості між передбаченими ймовірностями моделі та фактичною часткою позитивних результатів у тестовій вибірці.

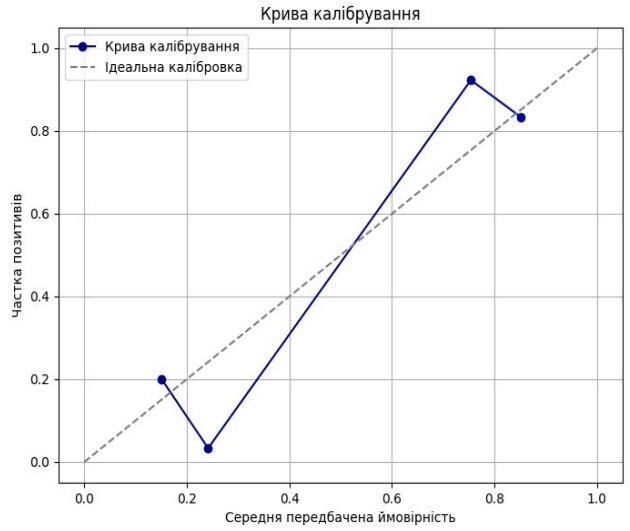

Рисунок 10 – Калібрувальна крива для оцінки узгодженості

5 РЕЗУЛЬТАТИ

Модель демонструє високу точність для передбачених ймовірностей у діапазоні [0,7579–0,8490], де фактична частка позитивних тісно корелює з передбаченнями 0,9286 і 0,8519 відповідно. Це вказує на надійність моделі для впевнених прогнозів.

У нижніх інтервалах ([0,1449–0,2499]) спостерігається недооцінка частки позитивних результатів, що може вказувати на необхідність подальшого калібрування моделі для покращення її продуктивності в цих діапазонах.

Косинусна схожість є одним із ключових інструментів для кількісного оцінювання семантичної подібності між текстовими даними. У даному дослідженні ми обчислили матрицю косинусної схожості між п’ятьма твітами з використанням векторизації Sentence-BERT. Значення косинусної схожості варіюються від 0,636 до 1,000, це зображено на рисунках 11 та 12.

Найвищі показники свідчать про високу семантичну схожість між відповідними текстами, що може вказувати на схожість тематики або ключових виразів у цих твітах.

Результати матриці косинусної схожості підтверджують ефективність Sentence-BERT у виявленні семантичної подібності між текстами. Високі значення для певних пар твітів (наприклад, Твіт 3 і Твіт 4) свідчать про те, що модель правильно ідентифікує близькість змісту, навіть якщо тексти мають відмінності на рівні синтаксису або поверхневої структури.

```
Матриця косинусної схожості між першими 5 твітами:
          Твіт 1    Твіт 2    Твіт 3    Твіт 4    Твіт 5
Твіт 1  1.000000  0.760375  0.772464  0.720631  0.655470
Твіт 2  0.760375  1.000000  0.726243  0.760966  0.748869
Твіт 3  0.772464  0.726243  1.000000  0.650697  0.690497
Твіт 4  0.720631  0.760966  0.650697  1.000000  0.697242
Твіт 5  0.655470  0.748869  0.690497  0.697242  1.000000
Дані калібрувальної кривої:
Середні передбачені ймовірності: [0.15001779 0.2499676  0.75009756 0.85007704]
Частка позитивних: [0.10068988 0.09972455 0.89976803 0.89893478]
```

Рисунок 11 – Матриця косинусної схожості між першими 5 твітами

Нижчі значення (наприклад, Твіт 2 і Твіт 5) можуть вказувати на тексти, які менш пов’язані тематично або мають суттєві відмінності у виразах, що є важливим для аналізу різноманітності даних.

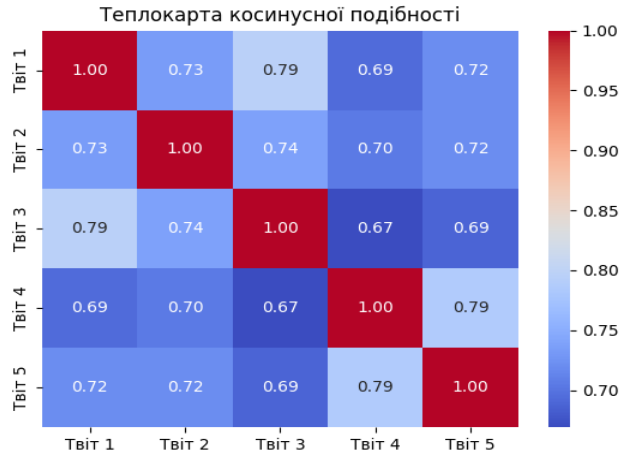

Рисунок 12 – Теплова карта косинусної схожості між першими 5 твітами

F1-міра є важливим показником у задачах класифікації, що об’єднує як точність, так і повноту у єдину метрику, забезпечуючи комплексне розуміння продуктивності моделі, що зображено на рисунку 13. У цьому дослідженні було оцінено F1-міру для різних порогових значень у діапазоні від 0 до 1 з кроком 0,0204. Найвища F1-міра, 0,9074, досягнута для порогів від 0,306 до 0,673, вказує на ефективну продуктивність моделі в цьому діапазоні. Це

DOI 10.15588/1607-3274-2025-2-14

підтверджує здатність моделі точно ідентифікувати як позитивні, так і негативні класи в умовах збалансованого співвідношення точності й повноти. Збереження високого значення F1-міри у середньому діапазоні порогів (0,306–0,673) свідчить про високу стійкість моделі до змін порогових значень, що є важливим аспектом її надійності.

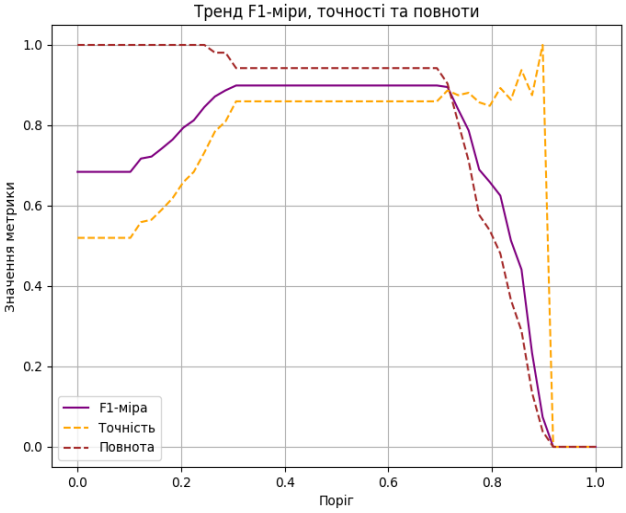

Рисунок 13 – Тренди F1-міри, точності та повноти

Кумулятивний приріст є ключовою характеристикою, що дозволяє оцінити прогресивну зміну продуктивності моделі при аналізі класифікаційних задач.

У цьому дослідженні на рисунку 14 було розглянуто послідовне накопичення правильно класифікованих прикладів для визначення динаміки ефективності моделі.

Стабільний лінійний ріст у середньому діапазоні підкреслює послідовність та надійність моделі, а формування плато у верхньому діапазоні сигналізує про досягнення межі можливостей моделі, що є типовим для задач із високим ступенем складності.

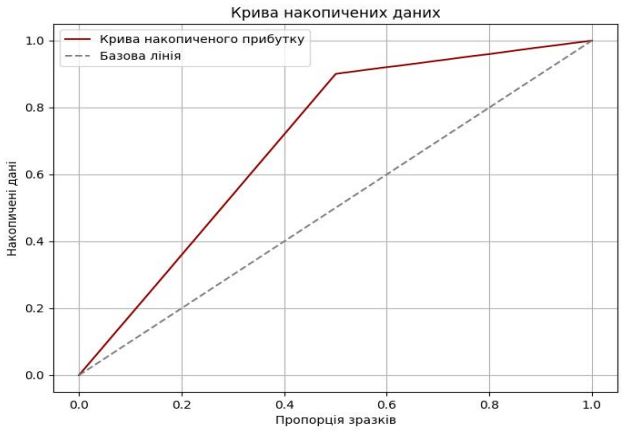

Рисунок 14 – Кумулятивна крива приросту

Отримані результати свідчать про високу продуктивність моделі на основі аналізу різних метрик: матриця плутанини демонструє точність класифікації між класами, ROC-крива підтверджує баланс між чутливістю та специфічністю, а Precision-Recall крива вказує на здатність моделі ефективно працювати з незбалансованими даними.

Калібрувальна крива відображає відповідність передбачених ймовірностей фактичним результатам, тоді як матриця косинусної схожості ілюструє семантичну близькість текстів. Тренди F1-міри, точності та повноти підкреслюють стабільність моделі на різних етапах роботи, що робить її придатною для широкого спектра завдань класифікації.

6 ОБГОВОРЕННЯ

Було здійснено порівняння трьох різних підходів до аналізу текстових даних, кожен з яких використовує комбінації різних методів обробки та моделювання: TF-IDF + onehotencoding + cosine similarity, BERT + XGBoost + sentence embedding similarity, та S-BERT + XGBoost + SHAP + sentence embedding similarity + lambda.

Перший підхід, TF-IDF + onehotencoding + cosine similarity, є класичним методом для текстової класифікації, який на основі частоти термінів в документі створює прості векторні представлення слів, що дозволяє оцінити подібність між текстами за допомогою косинусної міри.

Незважаючи на свою простоту і ефективність для невеликих наборів даних, цей підхід має значні обмеження, оскільки не враховує контексту слів та їх взаємозв'язків у тексті.

Крім того, методи onehotencoding та TF-IDF створюють великі векторні простори для великих наборів даних, що може призвести до зниження продуктивності моделі, особливо коли йдеться про обробку складніших мовних конструкцій.

Другий підхід, який включає BERT + XGBoost + sentence embedding similarity, використовує передові методи трансформерів для представлення текстів у вигляді векторів, що зберігають контекстуальну інформацію слів. BERT значно покращує результат, оскільки здатен усувати багато недоліків класичних методів векторизації, таких як TF-IDF, враховуючи семантичні зв'язки між словами та їхніми контекстами. Використання XGBoost як моделі для класифікації дозволяє ефективно обробляти дані, знижуючи ризик перенавчання завдяки вбудованим методам регуляризації. Проте, цей підхід все ще має певні обмеження при обробці великих обсягів даних, оскільки використання BERT для генерації векторів потребує значних обчислювальних ресурсів, що може бути проблематичним при масштабуванні. На рисунку 15 зображено порівняння часу виконання моделей, на рисунку 16 зображено порівняння використання пам'яті моделей.

DOI 10.15588/1607-3274-2025-2-14

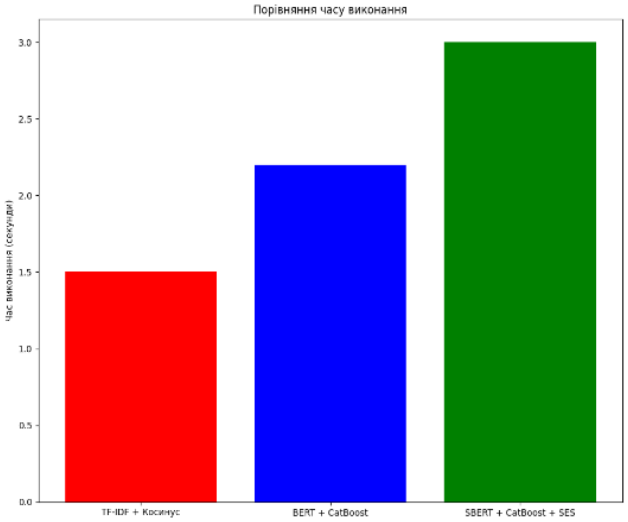

Рисунок 15 – Порівняння часу виконання

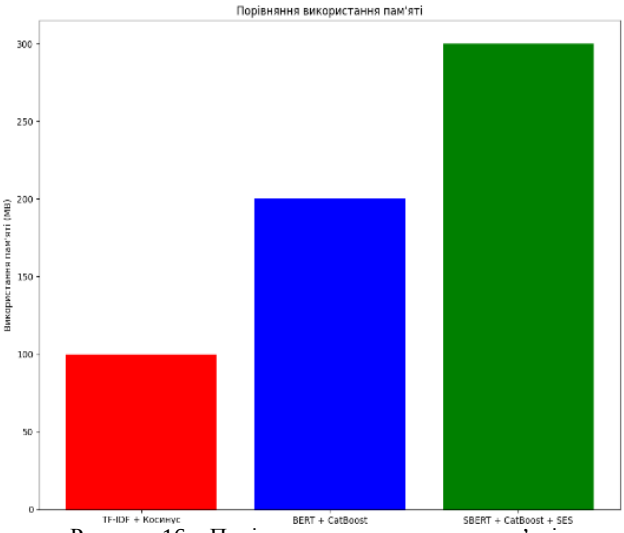

Рисунок 16 – Порівняння використання пам’яті

Останній підхід, S-BERT + XGBoost + SHAP + sentence embedding similarity + lambda, представляє собою більш складну та адаптовану до реальних умов модель. S-BERT (Sentence-BERT) використовує модифікацію BERT, яка дозволяє ефективно працювати з парами текстів, що дає змогу швидше обробляти дані та генерувати високоякісні векторні представлення для задач порівняння текстів. Використання XGBoost з доповненням SHAP дозволяє отримати прозорість моделі через оцінку важливості ознак, що є важливим для розуміння, як модель приймає свої рішення.

Крім того, інтеграція методу lambda допомагає в адаптації до великих обсягів даних і підвищує загальну продуктивність моделі за рахунок вдосконаленого налаштування параметрів та гнучкості в обробці текстів. Цей підхід дає значно кращу точність порівняно з іншими через його здатність ефективно працювати з великими обсягами даних, мінімізуючи час обробки та зберігаючи високу точність класифікації. На рисунку 17 зображено порівняння часу розміру моделей, на рисунку 18 зображено порівняння точності моделей.

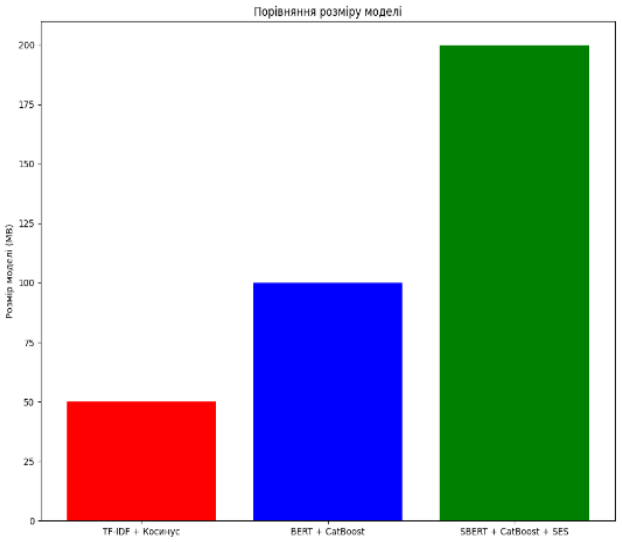

Рисунок 17 – Порівняння розміру моделі

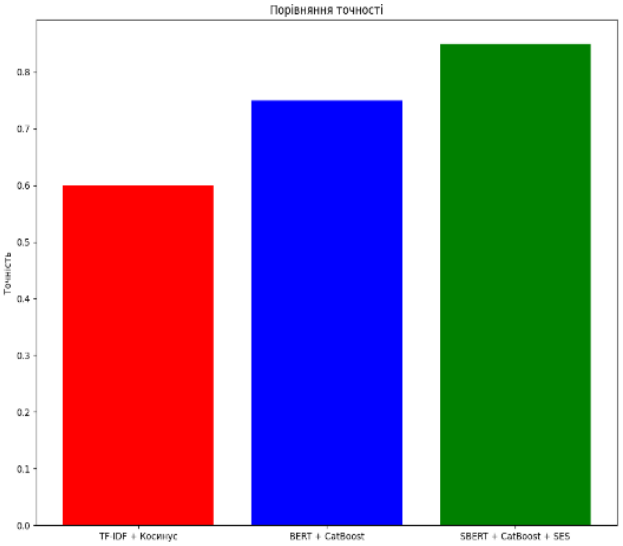

Рисунок 18 – Порівняння точності

Основною перевагою підходу S-BERT + XGBoost + SHAP + sentence embedding similarity + lambda є його здатність до масштабування і гнучкості. Завдяки використанню S-BERT, який є швидшою модифікацією BERT для задач порівняння текстів, і SHAP для інтерпретації результатів, цей підхід може бути використаний для обробки великих наборів даних без втрати точності. Це робить його ідеальним для застосувань, де потрібно обробляти великий обсяг текстової інформації та забезпечувати не тільки високу точність, але й прозорість роботи моделі.

Отже, S-BERT + XGBoost + SHAP + sentence embedding similarity + lambda є найефективнішим підходом серед трьох, здатним забезпечити найкращу точність на великих наборах даних. Це свідчить про важливість використання глибших і більш адаптованих до специфічних задач моделей у

DOI 10.15588/1607-3274-2025-2-14

поєднанні з методами інтерпретації результатів для забезпечення надійних і точних результатів.

ВИСНОВКИ

У даному дослідженні вирішено проблему ефективного аналізу текстових даних у задачах класифікації емоційного забарвлення текстів, що є критично важливим у сучасних умовах постійного зростання обсягу інформації в соціальних мережах. Запропонована методологія поєднує можливості трансформерної архітектури Sentence-BERT для отримання контекстуально збагачених векторних представлень текстів із потужністю градієнтного бустингу XGBoost, що забезпечує високу точність та узагальнюючу здатність класифікації.

Додатково було застосовано метод SHAP для пояснення прийнятих модельних рішень, що дозволяє оцінити вплив окремих ознак на результати передбачень та підвищити довіру до моделі у практичних застосуваннях. Крім того, використання метрики Sentence Embedding Similarity дозволило ефективно виявляти приховані семантичні зв'язки між текстами, що відкриває можливості для глибшого аналізу контенту.

Наукова новизна отриманих результатів полягає в удосконаленні методів текстової класифікації шляхом комбінування методів глибокого навчання та ансамблевих алгоритмів. Вперше продемонстровано, що інтеграція Sentence-BERT та XGBoost із застосуванням інтерпретаційних методів дозволяє не лише підвищити точність класифікації текстів за емоційним забарвленням, але й зробити модель більш прозорою для користувачів. Це особливо важливо для критичних застосувань, таких як аналіз громадської думки, автоматизована модерація контенту та системи підтримки ухвалення рішень, де автоматичне пояснення моделі є ключовим фактором.

Використання Sentence-BERT у поєднанні з класифікатором XGBoost також є перспективним для побудови інтелектуальних систем рекомендацій, де аналіз емоційного забарвлення відгуків може допомагати у формуванні персоналізованих пропозицій.

Запропонований підхід продемонстрував високу точність і стабільність результатів навіть при аналізі великих масивів даних, що свідчить про його масштабованість та придатність для використання в реальних умовах. Одним із важливих аспектів дослідження є оцінка роботи моделі на різних порогових значеннях класифікації, що дало змогу досягти оптимального балансу між точністю та повнотою, забезпечуючи гнучкість у налаштуванні моделі залежно від конкретних завдань.

Практична цінність роботи полягає у можливості використання запропонованої методології для широкого спектра задач, що вимагають аналізу тональності текстів. Зокрема, вона може бути ефективно застосована у сфері аналізу соціальних мереж для оцінки настроїв користувачів та виявлення тенденцій у суспільних дискусіях. Важливим напрямком подальших досліджень є також адаптація моделі до роботи з незбалансованими наборами даних, що є поширеною проблемою у багатьох реальних сценаріях аналізу текстової інформації.

ЛІТЕРАТУРА

1. Data oversampling and imbalanced datasets: an investigation of performance for machine learning and feature engineering / [M. Mujahid, E. Kına, F. Rustam et al.] // Journal of Big Data. – 2024. – Vol. 11, No. 1. – P. 1–32. DOI: 10.1186/s40537-024-00943-4
2. Neural network signal integration from thermogas-dynamic parameter sensors for helicopters turboshaft engines at flight operation conditions / [S. Vladov, L. Scislo, V. Sokurenko et al.] // Sensors. – 2024. – Vol. 24, No. 13. – P. 4246. DOI: 10.3390/s24134246
3. Batiuk T. Intellectual system for clustering users of social networks derived from the message sentiment analysis / T. Batiuk, D. Dosyn // Journal of Lviv Polytechnic National University "Information Systems and Networks". – 2023. – Vol. 13. – P. 121–138. DOI: 10.23939/sisn2023.13.121
4. Ensemble learning with pre-trained transformers for crash severity classification: a deep N.L.P. approach / [S. Jaradat, R. Nayak, A. Paz, M. Elhenawy] // Algorithms. – 2024. – Vol. 17, No. 7. – P. 284. DOI: 10.3390/a17070284
5. The method of restoring lost information from sensors based on auto-associative neural networks / S. Vladov, R. Yakovliev, V. Vysotska et al.] // Applied System Innovation. – 2024. – Vol. 7, no. 3. – P. 53. DOI: 10.3390/asi7030053
6. Core technology topic identification and evolution analysis based on patent text mining – a case study of unmanned ship / [Y. Lin, X. Wang, J. Yang, S. Wang] // Applied Sciences. – 2024. – Vol. 14, No. 11. – P. 4661. DOI: 10.3390/app14114661
7. The impact of input types on smart contract vulnerability detection performance based on deep learning: a preliminary study / [I. M. Aldyaflah, W. Zhao, S. Yang, X. Luo] // Information. – 2024. – Vol. 15, no. 6. – P. 302. DOI: 10.3390/info15060302
8. Batiuk T. A realization of visual biometric validation to enhance guarded and efficient authorization for intellectual systems / T. Batiuk, D. Dosyn // CEUR Workshop Proceedings, 8th Intern. Conf. on Computational Linguistics and Intelligent Systems COLINS 2024. – 2024. – Vol. 3668. – P. 247–268.
9. Ivokhin E. Restructuring of the model "State–Probability of Choice" based on products of stochastic rectangular matrices / E. Ivokhin, O. Oletsky // Cybernetics and Systems Analysis. – 2022. – Vol. 58, No. 2. – P. 242–250. DOI: 10.1007/s10559-022-00456-z
10. Information technology for the operational processing of military content for commanders of tactical army units / [V. Danylyk, V. Vysotska, V. Andrunyk et al.] // International Journal of Computer Network and

DOI 10.15588/1607-3274-2025-2-14

Information Security. – 2024. – Vol. 16, No. 3. – P. 115–143. DOI: 10.5815/ijcnis.2024.03.09
11. Batiuk T. Realization of the decision-making support system for Twitter users' publications analysis / T. Batiuk, D. Dosyn // Radio Electronics Computer Science Control. – 2024. – Vol. 1, No. 24. – P. 175–187. DOI: 10.15588/1607-3274-2024-1-16
12. Oletsky O. Exploring dynamic equilibrium of alternatives on the base of rectangular stochastic matrices / O. Oletsky // CEUR Workshop Proceedings, Modern Machine Learning Technologies and Data Science Workshop MoMLeT&DS 2021. – 2021. – Vol. 2917. – P. 151–160.
13. Oletsky O. On constructing adjustable procedures for enhancing consistency of pairwise comparisons on the base of linear equations / O. Oletsky // CEUR Workshop Proceedings. – 2021. – Vol. 3106. – P. 177–185.
14. Lin Y. Enhanced Transformer-BLSTM model for classifying sentiment of user comments on movies and books / Y. Lin, T. Liu // IEEE Access. – 2024. – P. 1–1. DOI: 10.1109/access.2024.3416755
15. Intellectual system for socialization of individuals with contributed interests derived from NLP, machine learning, and SEO algorithms / [T. Batiuk, V. Vysotska, R. Holoshchuk, S. Holoshchuk] // CEUR Workshop Proceedings, 6th Intern. Conf. on Computational Linguistics and Intellectual Systems COLINS 2022. – 2022. – Vol. 3171. – P. 572–631.
16. Oletsky O. A model of information influences on the base of rectangular stochastic matrices in chains of reasoning with possible contradictions / O. Oletsky // CEUR Workshop Proceedings, IT&I Workshops 2021. – 2021. – Vol. 3179. – P. 354–361.

Accepted 05.02.2025.
Received 29.04.2025.

UDC 004.9

NATURAL LANGUAGE PROCESSING OF SOCIAL MEDIA TEXT DATA USING BERT AND XGBOOST

Batiuk T. – Post-graduate student of Information Systems and Networks Department, Lviv Polytechnic National University, Lviv, Ukraine.

Dosyn D. – Doctor of Sciences, Professor of Information Systems and Networks Department, Lviv Polytechnic National University, Lviv, Ukraine.

ABSTRACT

Context The growth of text data in social networks requires the development of effective methods for sentiment analysis that can take into account both lexical and contextual dependencies. Traditional approaches to text processing have limitations in understanding semantic relationships between words, which affects the accuracy of classification. The integration of deep neural networks for text vectorization with ensemble machine learning algorithms and methods for interpreting results allows improving the quality of sentiment analysis.

Objective. The aim of the study is to develop and evaluate a new approach to text message sentiment classification that combines Sentence-BERT for deep semantic vectorization, XGBoost for high-accuracy classification, SHAP for explaining the contribution of features, sentence embedding similarity for assessing semantic similarity, and λ-regularization to improve the generalization ability of the model. The study is aimed at analyzing the impact of these methods on the quality of classification, identifying the most significant features and optimizing parameters.

Method. The study uses Sentence-BERT to transform text data into a vector space with deep semantic connections. XGBoost is used for sentiment classification, which provides high accuracy and stability even on unevenly distributed datasets. The SHAP method is used to explain the contribution of features, which allows us to determine which factors have the greatest impact on the prediction. Additionally, sentence embedding similarity is used to compare texts.

Results. The proposed approach demonstrates high efficiency in mood classification tasks. The ROC-AUC value confirms the ability of the model to accurately distinguish between classes of emotional coloring of the text. The use of SHAP ensures the interpretability of the results, allowing us to explain the influence of each feature on the classification. Sentence embedding similarity confirms the efficiency of Sentence-BERT in detecting semantically similar texts, and λ-regularization improves the generalization ability of the model.

Conclusions. The study demonstrates scientific novelty through a comprehensive combination of Sentence-BERT, XGBoost, SHAP, sentence embedding similarity, and λ-regularization to improve the accuracy and interpretability of sentiment analysis. The results obtained confirm the effectiveness of the proposed approach, which makes it promising for application in public opinion monitoring, automated content moderation, and personalized recommendation systems. Further research can be aimed at adapting the model to specific domains and improving interpretation methods.

KEYWORDS: Machine learning, feature normalization, Transformers, confusion matrix, Sentence-BERT, text data classification.

REFERENCES

1. Mujahid M. Kına E., Rustam F., Villar M. G., Alvarado E. S., Diez I. D. L. T., Ashraf I. Data oversampling and imbalanced datasets: an investigation of performance for machine learning and feature engineering, *Journal of Big Data*, 2024,

DOI 10.15588/1607-3274-2025-2-14

Vol. 11, No. 1, pp. 1–32. DOI: 10.1186/s40537-024-00943-4
2. Vladov S., Scislo L., Sokurenko V., Muzychuk O., Vysotska V., Osadchy S., Sachenko A. Neural network signal integration from thermogas-dynamic parameter sensors for helicopters turboshaft engines at flight operation conditions, *Sensors*, 2024, Vol. 24, No. 13, P. 4246. DOI: 10.3390/s24134246
3. Batiuk T., Dosyn D. Intellectual system for clustering users of social networks derived from the message sentiment analysis, *Journal of Lviv Polytechnic National University* "Information Systems and Networks", 2023, Vol. 13, pp. 121–138. DOI: 10.23939/sisn2023.13.121
4. Jaradat S., Nayak R., Paz A., Elhenawy M. Ensemble learning with pre-trained transformers for crash severity classification: a deep N.L.P. approach, *Algorithms*, 2024, Vol. 17, No. 7, P. 284. DOI: 10.3390/a17070284
5. Vladov S., Yakovliev R., Vysotska V., Nazarkevych M., Lytvyn V. The method of restoring lost information from sensors based on auto-associative neural networks, *Applied System Innovation*, 2024, Vol. 7, No. 3, P. 53. DOI: 10.3390/asi7030053
6. Lin Y., Wang X., Yang J., Wang S. Core technology topic identification and evolution analysis based on patent text mining – a case study of unmanned ship, A*pplied Sciences*, 2024, Vol. 14, No. 11, P. 4661. DOI: 10.3390/app14114661
7. Aldyaflah I., Zhao W., Yang S., Luo X. The impact of input types on smart contract vulnerability detection performance based on deep learning: a preliminary study, *Information*, 2024, Vol. 15, No. 6, P. 302. DOI: 10.3390/info15060302
8. Batiuk T., Dosyn D. A realization of visual biometric validation to enhance guarded and efficient authorization for intellectual systems, *CEUR Workshop Proceedings, 8th Intern. Conf. on Computational Linguistics and Intelligent Systems COLINS 2024*, 2024, Vol. 3668, pp. 247–268.
9. Ivokhin E., Oletsky O. Restructuring of the model "State–Probability of Choice" based on products of stochastic rectangular matrices, *Cybernetics and Systems Analysis*, 2022, Vol. 58, No. 2, pp. 242–250. DOI: 10.1007/s10559-022-00456-z
10. Danylyk V., Vysotska V., Andrunyk V., Uhryn D., Ushenko Y. Information technology for the operational processing of military content for commanders of tactical army units, *International Journal of Computer Network and Information Security*, 2024, Vol. 16, No. 3, pp. 115–143. DOI: 10.5815/ijcnis.2024.03.09
11. Batiuk T., Dosyn D. Realization of the decision-making support system for Twitter users' publications analysis, *Radio Electronics Computer Science Control*, 2024, Vol. 1, No. 24, pp. 175–187. DOI: 10.15588/1607-3274-2024-1-16
12. Oletsky O. Exploring dynamic equilibrium of alternatives on the base of rectangular stochastic matrices, *CEUR Workshop Proceedings, Modern Machine Learning Technologies and Data Science Workshop MoMLeT&DS* 2021, 2021, Vol. 2917, pp. 151–160.
13. Oletsky O. On constructing adjustable procedures for enhancing consistency of pairwise comparisons on the base of linear equations, *CEUR Workshop Proceedings*, 2021, Vol. 3106, pp. 177–185.
14. Lin Y., Liu T. Enhanced Transformer-BLSTM model for classifying sentiment of user comments on movies and books, *IEEE Access*, 2024, pp. 1–1. DOI: 10.1109/access.2024.3416755
15. Batiuk T., Vysotska V., Holoshchuk R., Holoshchuk S. Intellectual system for socialization of individuals with contributed interests derived from NLP, machine learning, and SEO algorithms, *CEUR Workshop Proceedings, 6th Intern. Conf. on Computational Linguistics and Intellectual Systems COLINS* 2022, 2022, Vol. 3171, pp. 572–631.
16. Oletsky O. A model of information influences on the base of rectangular stochastic matrices in chains of reasoning with possible contradictions, *CEUR Workshop Proceedings, IT&I Workshops 2021*, 2021, Vol. 3179, pp. 354–361.

DOI 10.15588/1607-3274-2025-2-14

UDC 004.932

COMBINED METRIC FOR EVALUATING THE QUALITY OF SYNTHESIZED BIOMEDICAL IMAGES

Berezsky O. M. – Dr. Sc., Professor, Professor of the Department of Computer Engineering, West Ukrainian National University, Ternopil, Ukraine.

Berezkyi M. O. – Post-graduate student of the Department of Computer Engineering, West Ukrainian National University, Ternopil, Ukraine.

Dombrovskyi M. O. – Master of Computer Engineering, West Ukrainian National University, Ternopil, Ukraine.

Liashchynskyi P. B. – PhD, Lecturer of the Department of Computer Engineering, West Ukrainian National University, Ternopil, Ukraine.

Melnyk G. M. – PhD, Associate Professor of the Department of Computer Engineering, West Ukrainian National University, Ternopil, Ukraine.

ABSTRACT

Context. This study addresses the problem of developing a new metric for evaluating the quality of synthesized images. The relevance of this problem is explained by the need for assessing the quality of artificially generated images. Additionally, the study highlights the potential of biomedical image synthesis based on diffusion models. The research results can be applied for biomedical image generation and quantitative quality assessment of synthesized images.

Objective. The aim of this study is to develop a combined metric and an algorithm for biomedical image synthesis to assess the quality of synthesized images.

Method. A combined metric M_C for evaluating the quality of synthesized images is proposed. This metric is based on two existing metrics: M_{IS} and M_{FID}. Additionally, an algorithm for histopathological image synthesis using diffusion models has been developed.

Results. To study the M_{IS}, M_{FID}, and M_C metrics, histopathological images available on the Zenodo platform were used. This dataset contains three classes of histopathological images G1, G2, and G3, representing pathological conditions of breast tissue. Based on the developed image synthesis algorithm, three classes of artificial histopathological images were generated.

Using the M_{IS}, M_{FID}, and M_C metrics, quality assessments of the synthesized histopathological images were obtained. The developed metric will form the basis of a software module for image quality assessment using metrics. This software module will be integrated into CAD systems.

Conclusions. A combined metric for evaluating the quality of synthesized images has been developed, along with a proposed algorithm for biomedical image synthesis. The software implementation of the combined metric and image synthesis algorithm has been integrated into an image quality assessment module.

KEYWORDS: metric, IS metric, FID metric, histopathological images, deep neural networks, diffusion models, Stable Diffusion.

ABBREVIATIONS

GAN is a generative adversarial network;

CNN is a convolutional neural network;

VT is a Vision-Transformer;

Zenodo is a general-purpose open repository developed under the European OpenAIRE program and operated by CERN;

G1 is a class of images of non-proliferative mastopathy;

G2 is a class of images of proliferative mastopathy;

G3 is a class of images of fibrocystic mastopathy;

IS is a distance based on the Google Inception V3 image classification model;

FID is a Fréchet inception distance;

HD is a Hausdorff Distance;

HI is a histopathological image;

U-Net is a network with U-shaped structure;

UF is an uncertainty Fréchet metric;

CIVIs is a clustering internal validity Indices;

VQ-VAE is a vector Quantized-variational autoencoder;

FAED is a Fréchet AutoEncoder distance;

MMD is a maximum mean discrepancy;

MMD GAN is a Maximum Mean Discrepancy for generative adversarial network;

KID is a Kernel Inception Distance;

QMC Quasi-Monte Carlo method;

PyTorch is an open-source machine learning framework Python Torch;

TensorFlow is an open-source platform and framework for machine learning, which includes libraries and tools based on Python and Java;

Clean-FID is a metrics with pre-processing of images;

CLIP is a Contrastive Language-Image Pre-training

CLIP-MMD is a Maximum Mean Discrepancy metric based on CLIP model;

CMMD is a metric based on CLIP embeddings and the maximum mean discrepancy distance with the Gaussian kernel;

ACCURACY is a metric that determines the proportion of correct predictions made by a model out of the total number of predictions.

NotImageNet32 is a synthetic dataset;

CIS is a Conditional Inception Score;

CFID is a Conditional Fréchet Inception Distance;

Wasserstein-1 is an improved of Wasserstein metric;

DOI 10.15588/1607-3274-2025-2-15

SSIM is a structural similarity index measure;

PSNR is a peak signal-to-noise ratio is ratio between the maximum possible power of a signal and the power of corrupting noise;

AUC is an area under the curve;

MS-SSIM is a Multi-Scale SSIM;

PRECISION is an accuracy of a model in predicting the positive class.

RECALL is a metric, that reflects the model's ability to identify all actual positive cases.

F1-score is an average of precision and recall;

LPIPS is a Learned Perceptual Image Patch Similarity;

GMM-GAN is a Graph-based Manifold Matching GAN;

MAE is a Mean Absolute Error;

UMMC is a University Malaya Medical Centre;

WSI is a whole slide image;

H&E is a hematoxylin and eosin;

IHC is an immunohistochemistry;

ER-IHC is an Estrogen Receptor Immunohistochemistry;

ER is an estrogen receptor;

PGR is a progesterone receptor;

HER2 is a human epidermal growth factor receptor 2;

PR is a progesterone receptor;

KI67 is a marker of proliferation Ki-67;

TIFF is a file format for storing raster graphics images;

JPG is a joint photographic experts' group;

MIRAX is a Carl Zeiss MIRAX slide scanner system file format;

CPU is a central processing unit

GPU is a graphics processing unit;

CUDA is a Compute Unified Device Architecture;

CAD stands for Computer-Aided Diagnosis;

RAM is a Random Access Memory;

VRAM is a Virtual Random Access Memory;

GB is a gigabyte;

GOOGLE COLAB is a free cloud-based platform provided by GOOGLE that allows users to write and execute Python code directly in their browser.

NOMENCLATURE

I_r is a set of real histopathological images;

I_l is a training set of histopathological images;

I_{test} is a test set of histopathological images;

I_c is a set of images based on diffusion models,

M_{IS} is a metric based on inception score;

M_{FID} is a metric based on Fréchet inception distance;

M_C is a a combined metric;

t is a time step index; t is selected from the range $t \in [0,T]$;

Z_{0C} is a set of histopathological images into the latent space at timestep t=0;

α_t is a coefficient that determines the noise rate at timestep t;

T is a total number of timesteps;

ε_t is a value of random Gaussian noise at timestep t;

$\hat{\varepsilon}_t$ is an estimated noise value at timestep t;

$\bar{\alpha}_t$ is a coefficient that determines the noise level at the previous timestep t;

β_t is a coefficient controlling the rate of noise reduction at timestep t;

Z_{1C} set of histopathological images into a latent space at timestep $t = T$;

I_{CD} is a set of images after encoder transforms Z_{1C};

$M_1, \ldots, M_n$ are metrics;

$X_1, \ldots, X_n$ are sets;

$N(E, D)$ is a normal distribution;

E is a mean;

D is a variance;

$M(x, y)$ is a given metric that measures the distance or dissimilarity between points x and y in a certain space;

s is a scaling factor applied to the metric;

m is a truncation parameter that limits the metric values;

a is a constant;

v is a translation parameter;

p is a fixed element from the set X;

μ and β are scaling coefficients;

μ_r, μ_G are mean feature vectors for real and generated images;

Σ_r, Σ_G are covariance matrixs for real and generated images.

Tr is a trace of the matrix;

E_x is an expected value over the distribution of x;

$p(x \mid y)$ is a probability distribution of class y for image x;

$p(y)$ is a marginal probability distribution over all classes;

D_{KL} is a Kullback-Leibler divergence.

$M_{FID_{\min}}$ is a minimum value of the M_{FID} metric;

$M_{FID_{\max}}$ is a maximum value of the M_{FID} metric;

$M_{IS_{\min}}$ is a minimum value of the M_{IS} metric;

$M_{IS_{\max}}$ is a maximum value of the M_{IS} metric;

M_{IS}^{N} is a normalized value of the M_{IS};

M_{FID}^{N} is a normalized value of the M_{FID};

α is a weight of a metric, with $\alpha \in [0,1]$.

INTRODUCTION

Biomedical images are structural and functional representations of human and animal organs designed for disease diagnosis and the study of the anatomical and physiological state of the body. Medical images used for disease diagnosis are obtained from digital radiology, computed tomography, nuclear magnetic resonance, ultrasound, microscopy, etc. For the diagnosis of oncological diseases, microscopic color images are used, including cytological, histopathological, and immunohistochemical images. Oncological diseases are a global issue, signifi-

DOI 10.15588/1607-3274-2025-2-15

cantly affecting countries such as the European Union, the United States, and Ukraine [1].

This article examines HIs of breast cancer, which has the highest mortality rate among women [2].

Existing datasets of HIs are limited due to objective reasons. Currently, deep neural networks of the CNN (Convolutional Neural Network) type are used for diagnosis [3]. Training neural networks requires large datasets. A solution to this problem is the synthesis of artificial HIs. The synthesis of artificial images is based on real HIs.

In a short period, the following approaches have been used for medical image synthesis:

1. Autoencoders and fully convolutional networks [4].
2. U-Net and GANs architectures [5].
3. VT architectures.
4. Diffusion models [6].

Thus, at present, the use of diffusion models is a relevant direction in medical image synthesis.

The generated images must be quantitatively evaluated. For this purpose, metrics are used to assess the similarity between the generated image and the real one. Another important task is to evaluate the diversity of the generated images. The most widely used metrics for these tasks are Inception Score (IS) and Fréchet Inception Distance (FID) [8, 9].

The subject of the research is the process of HI generation and quality assessment based on metrics.

The object of the research is metrics for evaluating the quality of synthesized images.

The purpose of the research is to develop a combined metric for assessing the quality of synthesized HIs.

1 PROBLEM STATEMENT

Let a set of real HIs I_r be given. We divide this set into two subsets: I_l and I_{test}, and

$$I_r = I_l \cup I_{test} .$$

To expand the training set I_l, we generate a set of images I_c based on diffusion models, such that:

$$I_c \gg I_l .$$

For image quality assessment, two metrics are used: M_{IS}, M_{FID}.

Each of these metrics has its own advantages and disadvantages. Therefore, it is necessary to develop a combined metric M_C that incorporates both M_{IS} and M_{FID}.

Thus, the objectives of this study are:

1. Development of the combined metric M_C.
2. Development of an algorithm for synthesizing HIs based-on diffusion models.
3. Conducting computational experiments to evaluate the quality of generated images using M_{IS} and M_{FID} metrics and comparing the experimental results with the M_C metric.

2 REVIEW OF THE LITERATURE

The study [9] addresses the problem of evaluating CIVIs for synthetic and real datasets. The novel UF index enables the assessment of clustering quality while considering uncertainty. The authors improved the accuracy and adaptability of clustering metrics, particularly for datasets with non-convex structures or high noise levels.

The authors of [10] focus on evaluating the quality of generated images in GANs. They point out that existing metrics, which are trained on ImageNet for feature extraction, may be inadequate for other data domains. Additionally, these metrics can be sensitive to noise and image distortions and do not always reflect human perception of image quality. To address these issues, the researchers proposed the FAED method, which incorporates VQ-VAE to achieve better clustering and local feature representation compared to traditional evaluation methods.

In [11], the authors introduce the FID metric as an alternative to the IS, arguing its advantages in measuring the similarity between the distributions of real and generated images. The study demonstrates that FID correlates better with human perception and is more sensitive to changes in image quality than IS.

The study [12] examines the training and performance of GANs using the MMD metric, leading to the development of MMD-GAN. The authors compare IS, FID, and their newly proposed KID. They acknowledge that FID is widely used as the primary evaluation tool, as it better captures the distribution of real and generated images compared to IS. However, they highlight FID's bias in small sample sizes, which can lead to inaccurate model comparisons. As an alternative, they propose KID, which serves as an unbiased estimator and is less dependent on feature distribution shifts.

The researchers [13] demonstrate that the IS and FID are biased metrics. The values of these metrics, when computed on finite sample sizes, differ from their true values, which can only be obtained with an infinite sample size. To address this issue, the authors propose the use of the QMC method to improve the estimation of FID and IS on finite datasets.

The study [14] investigates the impact of low-level image processing on the evaluation of generative models, particularly the influence of image resizing and compression techniques on the calculation of FID and IS metrics. The authors show that standard FID implementations in PyTorch and TensorFlow introduce artifacts due to incorrect smoothing during downscaling, affecting the accuracy of the metric. As a solution, the authors propose the Clean-FID evaluation, which eliminates these artifacts by ensuring consistent pre-smoothing and avoiding quantization errors, leading to more reliable quality assessments of generated images.

The authors of [15] argue that the FID metric has significant limitations, including incorrect assumptions about the normality of feature distributions, low efficiency with small sample sizes, and poor alignment with human perception of image quality. As an alternative, they propose

DOI 10.15588/1607-3274-2025-2-15

the CMMD metric, which is based on CLIP embeddings and the MMD method.

The key issue addressed in [16] is the volatility of FID and IS metrics and their limited ability to accurately compare similar generative models. The authors introduce a new evaluation protocol that relies on the creation of a synthetic dataset NotImageNet32 and the use of KL divergence for more objective model comparisons.

The study [17] focuses on the evaluation of generative models in the case of conditional image generation. The authors propose two new metrics: CIS and CFID, which decompose the evaluation into within-class and between-class components, allowing for a more refined assessment of generative models.

The research conducted by [18] examines the training of generative models for unsupervised learning, specifically the challenges in measuring the closeness between real and generated data distributions. The authors introduce a new metric, Wasserstein-1, which addresses training instability and mode collapse issues in GANs, providing a more stable and theoretically grounded approach to generative model evaluation.

The study [19] analyzes various deep learning-based generative models, including CNNs, GANs, Transformers, and Diffusion models, highlighting their applications, architectural differences, and effectiveness in medical image synthesis. The performance evaluation focuses on medical image quality metrics, such as SSIM, PSNR, and segmentation accuracy in downstream tasks.

The article [20] investigates the problem of automatic metastasis detection in breast HIs, examining the impact of color variation on CNN performance. The study's primary objective is to minimize the effect of staining variability and improve classification accuracy through ensemble learning and color normalization techniques. The evaluation metrics used include Accuracy, AUC, Sensitivity, Specificity, and Kappa coefficient.

The research [21] aims to address the insufficient and imbalanced volume of medical data for breast tumor classification using ultrasound and mammography. The use of GANs allows for the generation of synthetic images, which helps reduce overfitting and enhance the performance of deep neural networks in diagnostic tasks. The evaluation of synthetic images is conducted using metrics such as KID, SSIM, and MS-SSIM.

The article [22] focuses on automated classification of histopathological medical images for early breast cancer diagnosis using deep learning. The primary evaluation metrics utilized by the authors include Accuracy, Sensitivity, Specificity, F1-score, and AUC.

The authors of [23] investigate the limited availability of large-scale annotated medical image datasets, which is a critical factor in training deep models for medical imaging. They propose a method for generating ultrasound images using semantic information to enhance realism. In addition to FID, the authors apply PSNR, MS-SSIM, and LPIPS to more accurately measure the similarity of texture features between synthetic and real images.

The study [24] addresses the challenge of cross-modality medical image generation, which is crucial for diagnostics when certain image types are unavailable. The authors introduce the GMM-GAN, which leverages graph neural networks to improve the quality of synthetic images and ensure their alignment with real medical data. The evaluation is conducted using MAE, PSNR, SSIM, and MS-SSIM.

The article [25] focuses on the automated synthesis of medical images in the absence of paired data, which is critical when obtaining multimodal images is restricted. Besides FID, the authors utilize Dice Score, HD, MAE, PSNR, and SSIM to assess the quality of the generated images.

The review study [26] analyzes the application of GANs in digital pathology and HI processing. The article discusses key challenges such as color normalization, resolution enhancement, and artifact removal. Additionally, the study highlights the need to improve consistency across images obtained from different laboratories. The evaluation is based on SSIM, PSNR, Dice Score, and HD, focusing on the quality assessment of synthetic images used by pathologists.

The study [27] applies CNNs and pre-trained models for the classification of oral cancer images. The authors evaluate the performance of their models using standard classification metrics, including Accuracy, Recall, Precision, F1-score, and AUC.

The study [28] explores various methods for evaluating image segmentation quality. The authors review traditional and modern approaches to segmentation assessment, emphasizing objective and subjective evaluation criteria. The paper highlights the importance of quantitative metrics such as Precision, Recall, and SSIM, which are commonly used to validate the performance of segmentation algorithms. The study contributes to the ongoing development of reliable evaluation techniques in image processing, particularly in medical imaging applications.

The article [29] investigates GANs for biomedical image synthesis, proposing a method for automatically searching for optimal GAN architectures. The authors discuss the challenges associated with GAN architecture selection and present an approach that optimizes models for high-quality image generation. The study also evaluates the performance of different architectures using FID, SSIM, and IS to ensure the realism and diversity of the generated images.

The research [30] introduces a deep learning-based method and software for biomedical image generation and classification in small sample settings. The authors address the data scarcity problem in medical imaging by developing a model that enhances image synthesis and classification accuracy. The paper focuses on GAN-based data augmentation, improving classification performance using CNNs and Transformer models. The evaluation is conducted using Accuracy, F1-score, AUC and SSIM to measure the effectiveness of both synthetic image generation and classification accuracy. The results demonstrate

DOI 10.15588/1607-3274-2025-2-15

significant improvements in small-sample learning scenarios, making the approach highly relevant for biomedical applications.

3 MATERIALS AND METHODS

The development of the combined metric and the evaluation of generated HIs consist of the following stages:

1. Preparation of the dataset of HIs of breast pathology.

2. Development of an algorithm for generating HIs based-on diffusion models.

3. Design of a combined metric based on FID and IS metrics.

4. Conducting computational experiments using HIs.

This section describes steps 1, 2, and 3.

For machine learning purposes, researchers utilize public biomedical image datasets.

The ACROBAT dataset [31] consists of 4212 WSI from 1153 patients diagnosed with primary breast cancer. The images were obtained from tissue samples stained with H&E, as well IHC staining for ER, PGR, HER2, and KI67 markers. Each patient has one H&E image and between one to four IHC images. The images were digitized at 10x magnification using Hamamatsu NanoZoomer S360 scanners.

The dataset was collected as part of the "Cancer Histopathology Image Epidemiology Project" (Sweden) and is used for the development of computational pathology methods. It is divided into: training set: 3,406 images, validation set: 200 images, test set: 606 images. The dataset is available in TIFF format and includes metadata with detailed information about each image.

The UMMC ER-IHC Breast Histopathology Whole Slide Image and Allred Score dataset [32] contains 37 whole-slide histological images, obtained in collaboration with the UMMC. The images were stained using IHC for ER and digitized using a 3DHistech Pannoramic Desk scanner at 20x magnification, with a resolution of 80000 × 200000 pixels.

Each image was annotated by pathologists, and the dataset is available in MIRAX format, accompanied by thumbnail images with annotation overlays.

For machine learning in image classification, the authors have created and published a dataset of cytological and histological images [33]. This dataset consists of: 73 cytological images, 68 histological images.

The images were obtained from tissue samples stained with H&E. Additionally, IHC images for ER, HER2, KI67, and PR markers were acquired. Each patient has one H&E image and between one to two IHC images.

The images were digitized at 10x and 20x magnification using a Nikon Eclipse Si laboratory-grade microscope. The dataset, along with diagnostic information, was collected at the Interdepartmental Educational and Research Laboratory of Ternopil National Medical University named after I.Y. Horbachevsky (Ukraine, Ternopil). The dataset is available in JPG format, with metadata including: patient age, cancer stage. The cytological images are categorized into three classes: melanoma, non-proliferative fibrous mastopathy, cystic mastopathy. The histological images belong to the class of invasive ductal carcinoma.

Mastopathy is one of the most common pathologies of the mammary glands in women of reproductive age. While this condition is generally benign, in certain cases, it is associated with an increased risk of malignant tumor development. This characteristic makes mastopathy a critical subject for early diagnosis and regular monitoring.

The dataset contains histological images with a resolution of 3664 × 2748 pixels, stained with H&E. The total number of images is 369. The images in the dataset (Fig. 1) belong to three classes: non-proliferative mastopathy, proliferative mastopathy, fibrocystic mastopathy.

The number of images in each class:

– non-proliferative mastopathy: 37;

– proliferative mastopathy: 45;

– fibrocystic mastopathy: 23.

The preprocessing of HIs is aimed at enhancing image quality, reducing variations, and removing artifacts, thereby improving the accuracy and reliability of analysis results.

Initially, color normalization was performed to minimize variations caused by different staining and scanning conditions. This was achieved through color standardization and intensity normalization methods. Next, noise filtering was applied, specifically using a median filter to reduce unwanted artifacts.

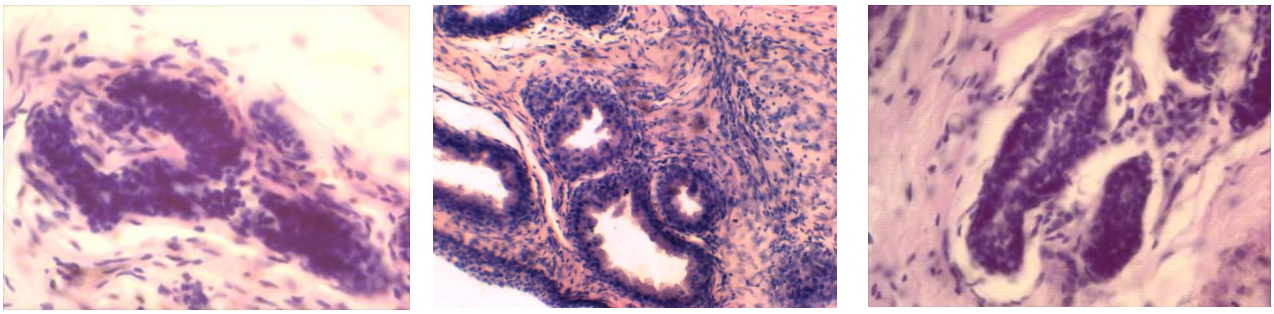

a b c

Figure 1 – Image Types in the Dataset: a – non-proliferative mastopathy; b – proliferative mastopathy; c – fibrocystic mastopathy

DOI 10.15588/1607-3274-2025-2-15

Since the initial dataset is relatively small, the next step involves expanding the sample for all three classes using the Stable Diffusion model.

For the synthesis of HIs, diffusion models were utilized within the Stable Diffusion environment [34]. The Stable Diffusion framework consists of two deep neural networks: Primary Network and Hypernetwork.

The Primary Network is trained on a large dataset of images and stores the parameters (weights) for the general dataset. The training process using HI datasets takes place within the Hypernetwork environment, which adjusts the weights of the base model.

The image generation algorithm in both networks is based on diffusion models and consists of the following steps:

1) training on the HI dataset within the Hypernetwork environment;

2) noise addition process (diffusion) applied to the initial dataset I_c;

3) denoising process (reverse diffusion) to generate high-quality synthetic images.

Let's detail the steps. We perform the transformation of the set of HIs into the latent space:

$$I_c \rightarrow Z_{0C}.$$

Based on Z_{0C}, the noise value is computed at each timestep t as follows:

$$Z_t = \sqrt{\alpha_t} Z_{0C} + \sqrt{1-\alpha_t}\,\varepsilon_t,$$

where: $\varepsilon_t \sim N(0, 1)$, $N(0, 1)$ is the normal distribution with mean $E = 0$ and variance $D = 1$.

The denoising value is computed as follows:

$$Z_{t-1} = \frac{1}{\sqrt{\alpha_t}}\left(Z_t - \frac{\beta_t}{\sqrt{1-\bar{\alpha}_t}}\hat{\varepsilon}_t\right).$$

After completing the denoising process (after $t = T$ timesteps), the vector Z_{1C} is formed in the latent space. Then, the encoder transforms Z_{1C} into the set of images I_{CD}, where $I_{CD} \gg I_C$. The quality of the generated images is evaluated using M_{IS} and M_{FID} metrics.

There are various ways to derive a new metric from an existing one. Let M_1 be a given metric on a set X. Then, a new metric can be constructed based on M_1 through transformations.

Alternatively, given multiple metrics $M_1, \ldots, M_n$, defined on sets $X_1, \ldots, X_n$, we can obtain a new metric on the extended set $X_1, \ldots, X_n$.

Consider two metrics M_1 and M_2 on the set X.

A metric transformation is a new metric obtained as a function of the existing metrics M_1 and M_2 on X.

The general matrix transformations are as follows [35]:

1) Scaled metric:

$$s\,M(x, y),\ s > 0.$$

2) Truncated metric:

$$\min\{mM(x, y)\}.$$

3) Discrete metric transformation:

$$\max\{a, M(x, y)\},\ x \neq y.$$

4) Translation metric:

$$M(x, y) + v.$$

5) Normalized metric transformation:

$$\frac{M(x, y)}{1 + M(x, y)}.$$

6) Biotope metric:

$$M_p(x, y) = \frac{M(x, y)}{M(x, p) + M(y, p) + M(x, y)}.$$

7) Maximum metric transformation:

$$\max\{M_1(x, y), M_2(x, y)\}.$$

8) Metric cone transformation:

$$\mu M_1(x, y) + \beta M_2(x, y).$$

In the article, the 8th transformation is used.

To evaluate the quality of generated images, two common metrics are utilized: M_{FID} and M_{IS}.

The distance calculation between real and generated images is performed using the following formula:

$$M_{FID} = \|\mu_r - \mu_G\|^2 + Tr\left(\Sigma_r + \Sigma_G - 2\left(\Sigma_r\Sigma_G\right)^{\frac{1}{2}}\right).$$

The M_{IS} metric is defined by the following formula:

$$M_{IS} = \exp\left(E_x\left(D_{KL}\left(p(x\,|y) \,\|\, p(y)\right)\right)\right).$$

The Kullback-Leibler divergence D_{KL} is calculated as follows:

$$D_{KL}\left(p(x\,|y) \,\|\, p(y)\right) = \sum_y p(y\,|x) \log \frac{p(y\,|x)}{p(y)}.$$

The goal is to combine these two metrics.

The M_{FID} and M_{IS} metrics have different ranges and interpretations. A lower M_{FID} value indicates that the gen-

DOI 10.15588/1607-3274-2025-2-15

erated image is more similar to the real one. A higher M_{IS} value suggests that the generated images are better represented across different classes.

To combine these metrics, normalization must be performed.

The normalized value of the M_{FID} metric is computed as follows:

$$M_{FID}^{N} = \frac{M_{FID} - M_{FID_{\min}}}{M_{FID_{\max}} - M_{FID_{\min}}}.$$

For the M_{IS} metric, the normalization formula is:

$$M_{IS}^{N} = \frac{M_{IS} - M_{IS_{\min}}}{M_{IS_{\max}} - M_{IS_{\min}}}.$$

Thus, the combined metric is defined as:

$$M_{C} = (1-\alpha)M_{FID}^{N} + \alpha M_{IS}^{N}.$$

4 EXPERIMENTS

In this paper, two types of experiments were conducted: 1. Synthesis of HIs of three classes based on real images in the Stable Diffusion environment. 2. Evaluation of the quality of the generated images using the IS, FID metrics and the combined metric.

For conducting computer experiments on HI synthesis, the Stable Diffusion Web UI software tool by Jarvis Labs was used. The computational resources utilized for this process were: GPU: 1 x A6000 Ampere (CUDA 12.3), CPU: 7 cores, RAM: 32 GB, VRAM: 48 GB.

This configuration ensures high performance for generating synthetic images.

Stable Diffusion version specifications: version: v1.9.4; python: 3.10.14; torch: 2.1.2+cu121; xformers: 0.0.23; post1; gradio: 3.41.2; checkpoint: 5493a0ec49; model: v1-5-pruned-emaonly.safetensors.

Before starting the experiment, small real datasets were expanded using affine transformation algorithms, implemented via the Rudi library [36] in Python.

The Rudi library is used for automated augmentation (generating variations) of cropped images. The following augmentation operations were performed: transformation probability, rotations, scaling, distortion intensity.

During the experiment, three extended datasets representing different image classes were used: histo_fibrocystic_cystic_mastopathy, non-proliferative, proliferative. After expansion, the number of images per class ranged from 119 to 165.

Training was conducted for 10000 steps per dataset, corresponding to 60 to 84 epochs, depending on the number of images in the dataset. Total training time per class: 43 minutes. Time per step: 0.26 seconds. Epoch duration: 31 to 42.9 seconds, varying due to dataset size differences.

The generation of synthetic images was performed using a specialized sampling approach, ensuring high detail and realism in the results. Synthesis of 4000 images per class took approximately 3 hours and 20 minutes.

Figure 2 presents original and generated images for the first class (histo_fibrocystic_cystic_mastopathy), demonstrating the quality of the obtained results.

Figure 3 presents examples of real and generated images for the class (proliferative).

Figure 4 presents examples of real and generated images for the class (non-proliferative).

Original	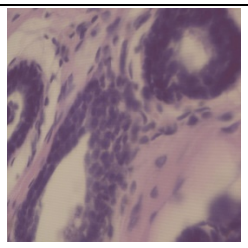	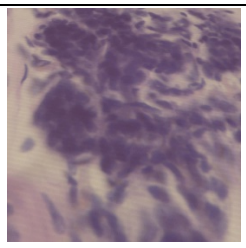	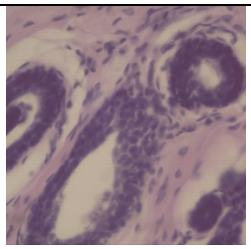	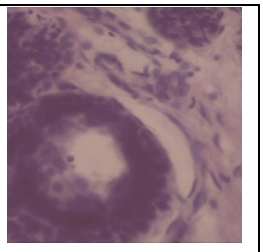
Steps	2500	5000	7500	10000
Generated	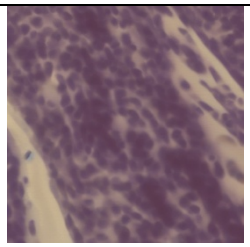	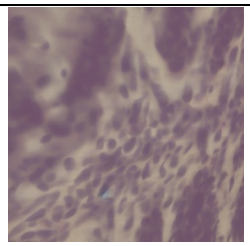	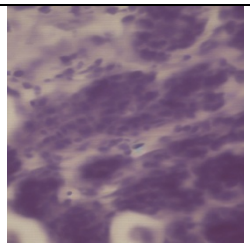	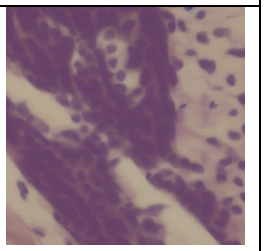

Figure 2 – Examples of real and generated images for the class (histo_fibrocystic_cystic_mastopathy)

DOI 10.15588/1607-3274-2025-2-15

Original	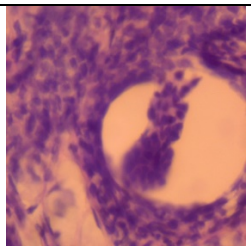	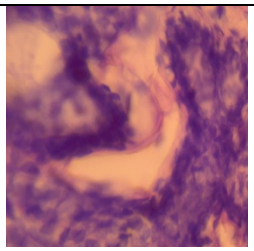	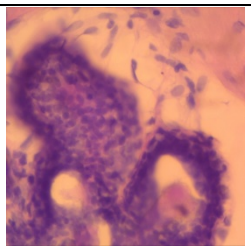	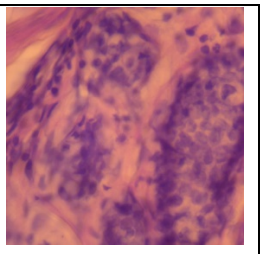
Steps	2500	5000	7500	10000
Generated	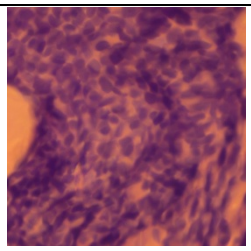	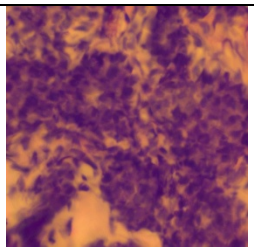	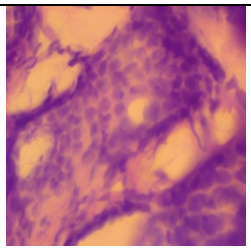	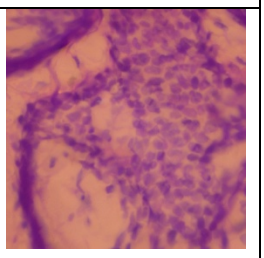

Figure 3 – Example of real and generated images for the class (proliferative)

Original	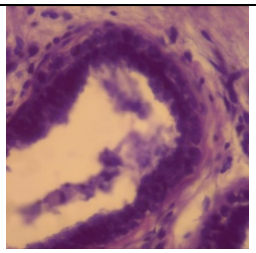	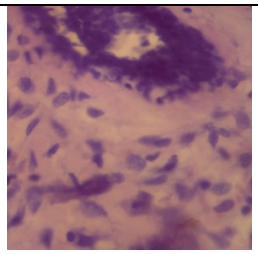	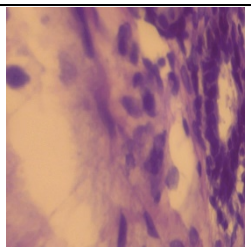	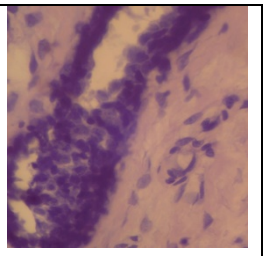
Steps	2500	5000	7500	10000
Generateed	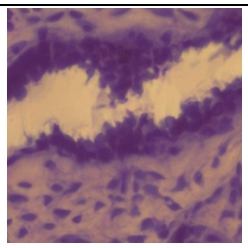	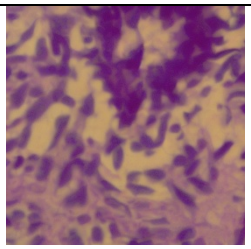	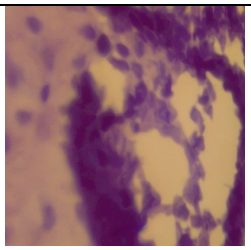	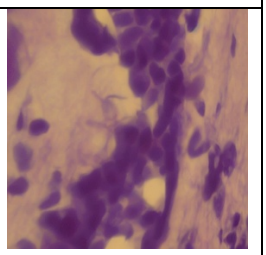

Figure 4 – Example of real and generated images for the class (non-proliferative)

After generation, the synthesized images were compared with the training images based on metrics calculated in Google Colab.

The data was stored in tables containing information on the number of iterations, metric values, and normalized indicators.

Based on the conducted experiments, the following were constructed:

1. Graphs of metric value changes during training (M_{FID}^{N}, M_{IS}^{N}, M_C as a function of iterations).

2. 3D graphs showing the relationship between M_C, M_{FID}^{N}, and M_{IS}^{N} for different values of the parameter α.

The graphs were plotted in the Google Colab environment. Figures 5a and 5b present the graphs of the IS and FID metric dependencies on the number of iterations for three classes: G1, G2 and G3.

Figures 6a and 6b present the dependencies of M_{FID}^{N} and M_{IS}^{N} on the number of iterations for the three classes: G1, G2 and G3.

Figure 7 presents the graph of the dependence of M_C on the number of iterations for class G1. Similarly, graphs of the dependence of M_C on the number of iterations for classes G2 and G3 are provided.

DOI 10.15588/1607-3274-2025-2-15

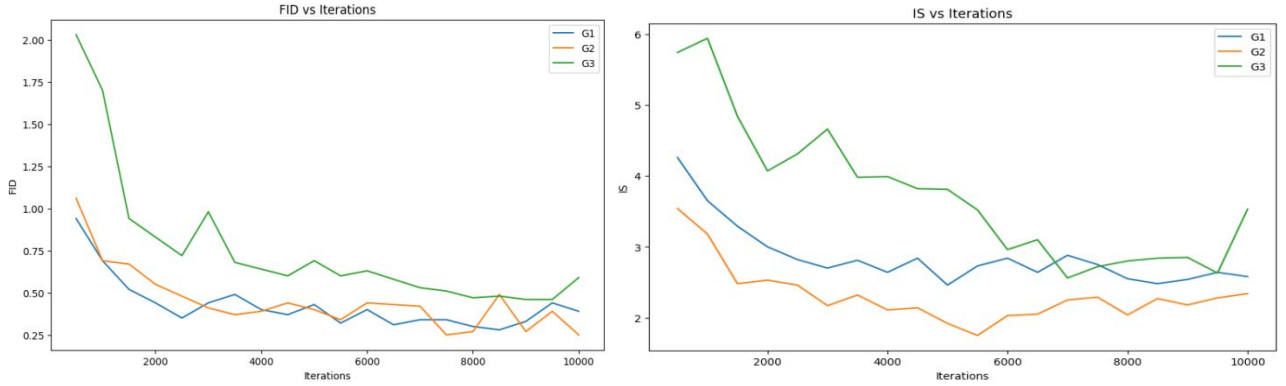

a b

Figure 5 – a – Dependence of IS on the number of iterations; b – Dependence of FID on the number of iterations

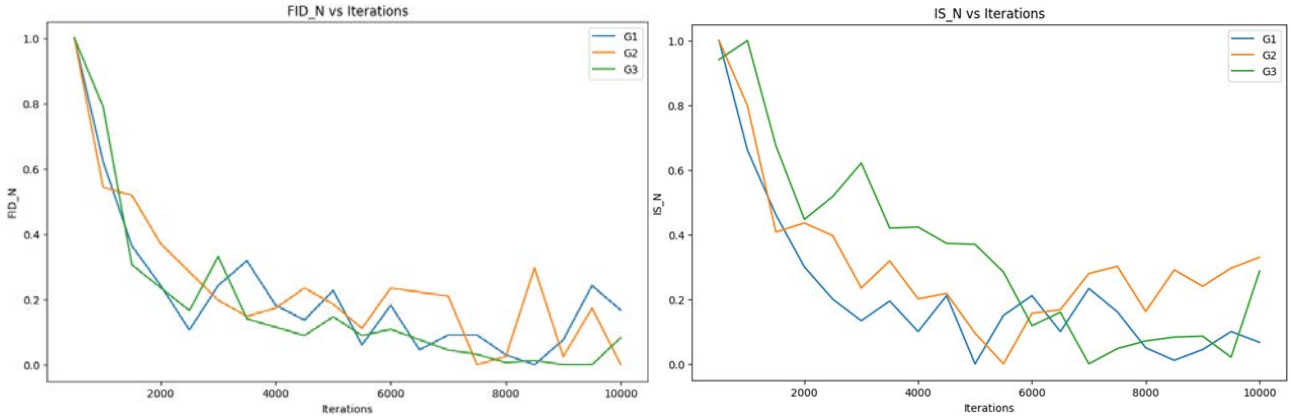

a b

Figure 6 – a – Dependence of M_{FID}^{N} on the number of iterations; b – Dependence of M_{IS}^{N} on the number of iterations

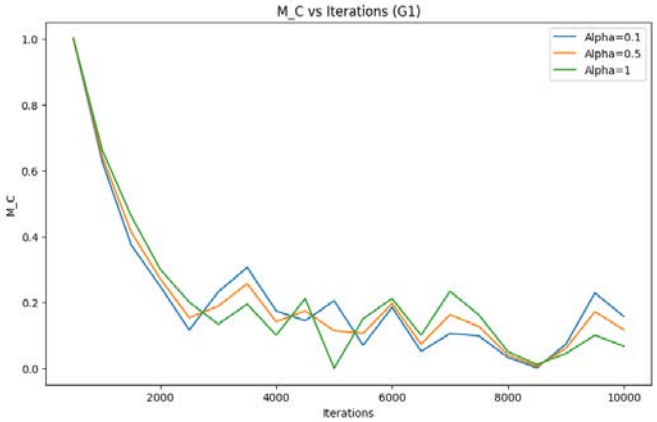

Figure 7 – Dependence of M_C on the number of iterations

Figure 8 presents a 3D graph of the dependence of M_C on the number of iterations for class G3. Similar dependencies are shown for other classes.

DOI 10.15588/1607-3274-2025-2-15

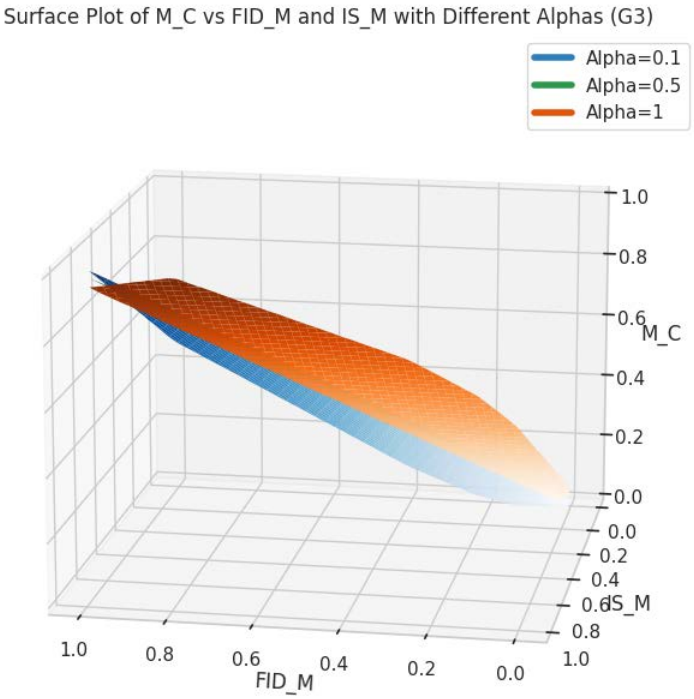

Figure 8 – Dependence of M_C on the number of iterations (class G3)

5 DISCUSSION

Modern classifiers are built on deep neural networks. The required classification accuracy is achieved through a large dataset of input images and prolonged neural network training. However, biomedical image datasets are limited due to objective constraints in obtaining biomedical images. Therefore, an urgent task is the generation of synthetic biomedical images based on real ones. The study [34] demonstrates that a promising approach for biomedical image generation is the use of diffusion models and modern generative tools such as Stable Diffusion. In this work, diffusion models are utilized for generating HIs.

The second crucial task is the evaluation of the generated images. Typically, artificial image evaluation relies on metrics and their modifications. The M_{FID} metric computes the similarity between real and generated images, while the M_{IS} metric measures the diversity of images in the generated dataset. Ideally, the M_{FID} metric should indicate minimal distance between real and generated images, whereas the M_{IS} metric should reflect maximum diversity in the synthesized dataset. This necessitates the combination of these metrics, leading to the development of the combined metric M_C, which allows for adjusting the influence of M_{IS} and M_{FID} on the quality assessment of generated images.

The initial biomedical image dataset consisted of three classes: G1 –37 images, G2 – 45 images, and G3 – 23 images. Using affine transformations, the dataset was expanded to 165 images in each class. Based on Stable Diffusion, 4000 images were generated for each class.

The total training time was 43 minutes per class. The synthesis of 4000 images took approximately 3 hours and 20 minutes for each class. The numerical parameters of the conducted experiments are as follows:

1. For class G1: $M_{FID_{\min}} = 0.28$, $M_{IS_{\min}} = 2.46$; $M_{FID_{\max}} = 0.94$, $M_{IS_{\max}} = 4.26$.
2. For class G2: $M_{FID_{\min}} = 0.25$, $M_{IS_{\min}} = 1.75$; $M_{FID_{\max}} = 1.06$, $M_{IS_{\max}} = 3.54$.
3. For class G3: $M_{FID_{\min}} = 0.46$, $M_{IS_{\min}} = 2.56$; $M_{FID_{\max}} = 2.03$, $M_{IS_{\max}} = 5.94$.

As shown in Figures 5a, 5b, 6a, 6b, and 7, approximately 2500 iterations are sufficient to achieve the required quality of generated images. This trend is observed for the M_{IS}, M_{FID}, and M_C metrics.

The developed combined metric will be integrated into the image quality assessment module based on metric evaluation. The metric module will be one of the components of the CAD software system.

CONCLUSIONS

This paper addresses the problem of evaluating the quality of synthesized images. To this end, a combined metric M_C was developed, based on the M_{IS} and M_{FID} metrics. Additionally, an algorithm for biomedical image synthesis using diffusion models was proposed. The synthesized biomedical images of three breast pathology classes were evaluated using the M_{IS}, M_{FID}, and M_C metrics.

The training and generation time for HIs using diffusion models was reduced by an order of magnitude compared to GANs. High-quality synthetic images were obtained for each histopathological class (G1, G2 and G3),

DOI 10.15588/1607-3274-2025-2-15

demonstrating good performance in terms of the M_{IS}, M_{FID}, and M_C metrics.

The **scientific novelty** of this study lies in the development of a combined metric for evaluating the quality of synthesized images.

The **practical significance** of this research includes the development of a HI synthesis algorithm, generation of HIs for three classes, and the execution of computational experiments to assess the quality of the synthesized images.

Future research directions involve exploring new biomedical image synthesis algorithms based on diffusion models and fuzzy metrics for quality assessment of synthesized images.

ACKNOWLEDGEMENTS

The authors of the article express their gratitude to the Department of Pathological Anatomy with a Sectional Course and Forensic Medicine of I. Ya. Horbachevsky Ternopil National Medical University (Ternopil, Ukraine) for providing histopathological images of breast cancer and personally to Doctor of Medical Sciences, Professor, and Head of the Department Petro Romanovych Selskyi.

REFERENCES

1. Cancer Facts for Women. American Cancer Society. [Electronic resource]. Access mode: https://www.cancer.org/cancer/risk-prevention/understanding-cancer-risk/cancer-facts/cancer-facts-for-women.html
2. Cancer in Ukraine 2021–2022: Incidence, mortality, prevalence and other relevant statistics. Bulletin of the National Cancer Registry of Ukraine № 24, 2021–2022. [Electronic resource]. Access mode: http://www.ncru.inf.ua/publications/BULL_24/PDF_E/bull_eng_24.pdf
3. Berezsky O., Liashchynskyi P., Pitsun O., Izonin I. Synthesis of Convolutional Neural Network architectures for biomedical image classification, *Biomedical Signal Processing and Control*, 2024, №95, P. 106325. DOI: 10.1016/j.bspc.2024.106325
4. Nie D., Cao X., Gao Y., Wang L., Shen D. Estimating CT image from MRI data using 3d fully convolutional networks *In: Deep Learning and Data Labeling for Medical Applications*. Springer International Publishing, 2016, pp. 170–178. DOI: 10.1007/978-3-319-46976-8_18
5. Nie D., Trullo R., Lian J., Petitjean C., Ruan S., Wang Q., Shen D. Medical image synthesis with context-aware generative adversarial networks, *In: Medical Image Computing and Computer Assisted Intervention – MICCAI 2017*. Springer International Publishing, 2017, pp. 417–425. DOI: 10.1007/978-3-319-66179-7_48
6. Khader F., Müller-Franzes G., Arasteh S. T., Han T., Haarburger C., Schulze Hagen M., Schad P., Engelhardt S., Baeßler B., Foersch S., Stegmaier J., Kuhl C., Nebelung S., Kather J. N., Truhn D. Denoising diffusion probabilistic models for 3d medical image generation, *Sci. Rep. 2023 May 5*, Vol. 13, № 1, P. 7303. DOI: 10.1038/s41598-023-34341-2
7. Xu Q., Huang G., Yuan Y., Guo C., Sun Y., Wu F., Weinberger K. An empirical study on evaluation metrics of generative adversarial networks, *ArXiv1806.07755 Cs Stat*, 2018. DOI: 10.48550/arXiv.1806.07755
8. Borji A. Pros and cons of GAN evaluation measures, *Computer Vision and Image Understanding*, 2019, Vol. 179, pp. 41–65. DOI: 10.1016/j.cviu.2018.10.009
9. Rendon N., Giraldo J. H., Bouwmans T., Rodríguez-Buritica S., E. Ramirez, Isaza C. Uncertainty clustering internal validity assessment using Fréchet distance for unsupervised learning, *Engineering Applications of Artificial Intelligence*, 2023, Vol. 124, P. 106635. DOI: 10.1016/j.engappai.2023.106635
10. Buzuti L. F., Thomaz C. E. Fréchet AutoEncoder Distance: A new approach for evaluation of Generative Adversarial Networks, *Computer Vision and Image Understanding*, 2023, Vol. 235, P. 103768. DOI: 10.1016/j.cviu.2023.103768
11. Heusel M., Ramsauer H., Unterthiner T., Nessler B., Hochreiter S. GANs Trained by a Two Time-Scale Update Rule Converge to a Local Nash Equilibrium [Electronic resource]. Access mode: https://arxiv.org/abs/1801.01401. DOI:10.48550/arXiv.1801.01401
12. Bińkowski M., Sutherland Danica J., Arbel Michael, Gretton Arthur Demystifying MMD GANs [Electronic resource], Access mode: https://arxiv.org/abs/1801.01401. DOI:10.48550/arXiv.1801.01401
13. Chong M. J., Forsyth D. Effectively Unbiased FID and Inception Score and where to find them [Electronic resource]. Access mode: https://arxiv.org/abs/1911.07023v3. DOI: 10.48550/arXiv.1911.07023
14. Parmar G. Zhang R., Zhu J.-Y. On Aliased Resizing and Surprising Subtleties in GAN Evaluation [Electronic resource]. Access mode: https://arxiv.org/abs/2104.11222v3. DOI: 10.48550/arXiv.2104.11222
15. Jayasumana S., Ramalingam S., Veit A., Glasner D., Chakrabarti A., Kumar S. Rethinking FID: Towards a Better Evaluation Metric for Image Generation [Electronic resource]. Access mode: https://arxiv.org/abs/2401.09603v2. DOI: 10.48550/arXiv.2401.09603
16. Betzalel E., Penso C., Fetaya E. Evaluation Metrics for Generative Models: An Empirical Study, *Machine Learning and Knowledge Extraction*, 2024, Vol. 6, № 3, pp. 1531–1544. DOI: 10.3390/make6030073
17. Benny Y., Galanti T., Benaim S., Wolf L. Wolf Evaluation Metrics for Conditional Image Generation, *International Journal of Computer Vision*, 2021, Vol. 129, № 5, pp. 1712–1731. DOI: 10.1007/s11263-020-01424-w
18. Arjovsky M., Chintala S., Bottou L. Wasserstein GAN [Electronic resource]. Access mode: https://arxiv.org/abs/1701.07875. DOI: 10.48550/ARXIV.1701.07875
19. Dayarathna S., Islam K. T., Uribe S., Yang G., Hayat M., Chen Z. Deep learning based synthesis of MRI, CT and PET: Review and analysis, *Medical Image Analysis*, 2024, Vol. 92, P. 103046. DOI: 10.1016/j.media.2023.103046

DOI 10.15588/1607-3274-2025-2-15

20. Luz D. S., Lima T. J. B., Silva R. R. V., Magalhães D. M. V., Araujo F. H. D. Automatic detection metastasis in breast histopathological images based on ensemble learning and color adjustment, *Biomedical Signal Processing and Control*, 2022, Vol. 75, P. 103564. DOI: 10.1016/j.bspc.2022.103564
21. Jiménez-Gaona Y., Carrión-Figueroa D., Lakshminarayanan V., Rodríguez-Álvarez M. José GAN-based data augmentation to improve breast ultrasound and mammography mass classification, *Biomedical Signal Processing and Control*, 2024, Vol. 94, P. 106255. DOI: 10.1016/j.bspc.2024.106255
22. Ukwuoma C. C., Cai D., Eziefuna E. O., Oluwasanmi A., Abdi Sabirin F., Muoka G. W., Thomas D., Sarpong K. Enhancing histopathological medical image classification for Early cancer diagnosis using deep learning and explainable AI – LIME & SHAP, *Biomedical Signal Processing and Control*, 2025, Vol. 100, P. 107014. DOI: 10.1016/j.bspc.2024.107014
23. Shi S., Li H., Zhang Y., Wang X. Semantic information-guided attentional GAN-based ultrasound image synthesis method, *Biomedical Signal Processing and Control*, 2025, Vol. 102, P. 107273. DOI: 10.1016/j.bspc.2024.107273
24. Zeng X., Lu B., Zhang J. Medical image synthesis algorithm based on vision graph neural network with manifold matching, *Biomedical Signal Processing and Control*, 2025, Vol. 103, P. 107381. DOI: 10.1016/j.bspc.2024.107381
25. Hu Y., Zhang S., Li W., Sun J., Xu L. X. Unsupervised medical image synthesis based on multi-branch attention structure, *Biomedical Signal Processing and Control*, 2025, Vol. 104, P. 107495. DOI: 10.1016/j.bspc.2025.107495
26. Jose L., Liu S., Russo C., Nadort A., Di Ieva Antonio Generative Adversarial Networks in Digital Pathology and Histopathological Image Processing: A Review, *Journal of Pathology Informatics*, 2021, Vol. 12, № 1, P. 43. DOI: 10.4103/jpi.jpi_103_20
27. Giri S. K., Dash S. Synthesis of clinical images for oral cancer detection and prediction using deep learning, *Mining Biomedical Text, Images and Visual Features for Information Retrieval*, 2025, pp. 339–356. DOI: 10.1016/b978-0-443-15452-2.00017-0
28. Berezsky O. M., Pitsun O. Y. Evaluation methods of image segmentation quality, *Radio Electronics, Computer Science, Control*, 2018, №1, pp. 119–128. DOI: 10.15588/1607-3274-2018-1-14
29. Berezsky O. M., Liashchynskyi P. B. Method of generative-adversarial networks searching architectures for biomedical images synthesis, *Radio Electronics, Computer Science, Control*, 2024, № 1, pp. 104–117. DOI https://doi.org/10.15588/1607-3274-2024-1-10
30. Berezsky O. M., Liashchynskyi P. B., Pitsun O. Y., Melnyk G. M. Deep network-based method and software for small sample biomedical image generation and classification, *Radio Electronics, Computer Science, Control*, 2023, №4,P. 76. DOI: 10.15588/1607-3274-2023-4-8
31. Rantalainen M., Hartman J. ACROBAT – a multi-stain breast cancer histological whole-slide-image data set from routine diagnostics for computational pathology. Karolinska Institutet. [Electronic resource]. Access mode: https://doi.org/10.48723/w728-p041. DOI:10.48723/w728-p041
32. Wan Siti Halimatul Munirah Wan Ahmad, Mohammad Faizal Ahmad Fauzi, Md Jahid Hasan, Zaka Ur Rehman, Jenny Tung Hiong Lee, See Yee Khor, Lai Meng Looi, Fazly Salleh Abas, Afzan Adam, Elaine Wan Ling Chan, Sei-ichiro Kamata UMMC ER-IHC Breast Histopathology Whole Slide Image and Allred Score IEEE Dataport, 2023. [Electronic resource]. Access mode: https://dx.doi.org/10.21227/9gbq-gz50. DOI: 10.21227/9gbq-gz50
33. Berezsky O., Datsko T., Melnyk G. Cytological and histological images of breast cancer [Electronic resource]. Access mode: https://zenodo.org/records/7890874. DOI: 10.5281/zenodo.7890873
34. Berezsky O., Liashchynskyi P., Melnyk G., Dombrovskyi M., Berezkyi M. Synthesis of biomedical images based on generative intelligence tools, *Informatics & Data-Driven Medicine (IDDM 2024): 7th International Conference, Birmingham, UK, November 14–16, 2024, CEUR Workshop Proceedings*, 2024, Vol. 3892, pp. 349–362. DOI: CEUR_WS.org/Vol-3892/paper23.pdf
35. Deza M. M., Deza E. Encyclopedia of Distances. Springer-Verlag Berlin Heidelberg, 2013, 583 p.
36. GitHub – liashchynskyi_rudi_ Lightweight image converter and dataset augmentor, 2024. [Electronic resource]. Access mode: https://github.com/liashchynskyi/rudi

Received 29.01.2025.
Accepted 25.04.2025.

DOI 10.15588/1607-3274-2025-2-15

УДК 004.932

КОМБІНОВАНА МЕТРИКА ДЛЯ ОЦІНКИ ЯКОСТІ СИНТЕЗОВАНИХ БІОМЕДИЧНИХ ЗОБРАЖЕНЬ

Березький О. М. – д-р техн. наук, професор, професор кафедри комп'ютерної інженерії Західноукраїнського національного університету, Тернопіль, Україна.

Березький М. О. – аспірант кафедри комп'ютерної інженерії Західноукраїнського національного університету, Тернопіль, Україна.

Домбровський М. О. – магістр з комп'ютерної інженерії Західноукраїнського національного університету, Тернопіль, Україна.

Лящинський П. Б. – д-р філософії з комп'ютерних наук, викладач кафедри комп'ютерної інженерії Західноукраїнського національного університету, Тернопіль, Україна.

Мельник Г. М. – канд. техн. наук, доцент кафедри комп'ютерної інженерії Західноукраїнського національного університету, Тернопіль, Україна.

АНОТАЦІЯ

Актуальність. У статті досліджено проблему розробки нової метрики для оцінки якості синтезованих зображень. Актуальність проблеми пояснюється необхідністю оцінки якості штучних зображень. Крім цього у роботі показано перспективність синтезу біомедичних зображень на основі дифузійних моделей. Результати дослідження можуть бути використані для синтезу біомедичних зображень та кількісної оцінки якості синтезованих зображень.

Мета роботи – розробка комбінованої метрики та алгоритму синтезу біомедичних зображень для оцінки якості синтезованих зображень.

Метод. У статті розроблено комбіновану метрику M_C для оцінки якості синтезованих зображень. Ця метрика базується на основі двох метрик M_{IS}, M_{FID}. Також розроблено алгоритм синтезу гістопатологічних зображень на основі дифузійних моделей.

Результати. Для дослідження метрик M_{IS}, M_{FID} і M_C використано гістопатологічні зображення, які знаходяться на платформі Zenodo. Цей dataset містить три класи G1, G2, G3 гістопатологічних зображень патологічних станів молочної залози. На основі розробленого алгоритму синтезу зображень отримано три класи штучних гістопатологічних зображень.

На основі метрик M_{IS}, M_{FID} і M_C отримано оцінки якості синтезованих гістопатологічних зображень: Розроблена метрика війде в основу програмного модуля для оцінки якості зображень на основі метрик. Цей програмний модуль буде інтегрований у CAD.

Висновки. Розроблена комбінована метрика для оцінки якості синтезованих зображень і запропонований алгоритм синтезу біомедичних зображень. Програмна реалізація комбінованої метрики і алгоритму синтезу зображень інтегровані у модуль оцінки якості зображень.

КЛЮЧОВІ СЛОВА: метрика, метрики IS, FID, гістопатологічні зображення, глибокі нейронні мережі, дифузійні моделі, Stable Diffusion.

ЛІТЕРАТУРА

1. Cancer Facts for Women. American Cancer Society. [Electronic resource]. – Access mode: https://www.cancer.org/cancer/risk-prevention/understanding-cancer-risk/cancer-facts/cancer-facts-for-women.html
2. Cancer in Ukraine 2021–2022: Incidence, mortality, prevalence and other relevant statistics. Bulletin of the National Cancer Registry of Ukraine № 24, 2021–2022. [Electronic resource]. – Access mode: http://www.ncru.inf.ua/publications/BULL_24/PDF_E/bull_eng_24.pdf
3. Synthesis of Convolutional Neural Network architectures for biomedical image classification / [O. Berezsky, P. Liashchynskyi, O. Pitsun, I. Izonin] // Biomedical Signal Processing and Control. – 2024. – №95. – P. 106325. DOI: 10.1016/j.bspc.2024.106325
4. Estimating CT image from MRI data using 3d fully convolutional networks / [D. Nie, X. Cao, Y. Gao et al.] // In: Deep Learning and Data Labeling for Medical Applications. Springer International Publishing, 2016. – P. 170–178. DOI: 10.1007/978-3-319-46976-8_18
5. Medical image synthesis with context-aware generative adversarial networks / [D. Nie, R. Trullo, J. Lian et al.] // In: Medical Image Computing and Computer Assisted Intervention – MICCAI 2017. Springer International Publishing, 2017. – P. 417–425. DOI: 10.1007/978-3-319-66179-7_48
6. Denoising diffusion probabilistic models for 3d medical image generation / [F. Khader, G. Müller-Franzes, S. T. Arasteh et al.] // Sci. Rep. 2023 May 5. – Vol. 13, №1. – P. 7303. DOI: 10.1038/s41598-023-34341-2
7. An empirical study on evaluation metrics of generative adversarial networks / [Q. Xu, G. Huang, Y. Yuan et al.] // ArXiv1806.07755 Cs Stat, 2018. DOI: 10.48550/arXiv.1806.07755
8. Borji A. Pros and cons of GAN evaluation measures / A. Borji // Computer Vision and Image Understanding. – 2019. – Vol. 179. – P. 41–65. DOI: 10.1016/j.cviu.2018.10.009
9. Uncertainty clustering internal validity assessment using Fréchet distance for unsupervised learning / [N. Rendon, J. H. Giraldo, T. Bouwmans et al.] // Engineering Applications of Artificial Intelligence. – 2023. – Vol. 124. – P. 106635. DOI: 10.1016/j.engappai.2023.106635
10. Buzuti L. F. Fréchet AutoEncoder Distance: A new approach for evaluation of Generative Adversarial Networks / L. F. Buzuti, C. E. Thomaz // Computer Vision and Image Understanding. – 2023. – Vol. 235 – P. 103768. DOI: 10.1016/j.cviu.2023.103768
11. GANs Trained by a Two Time-Scale Update Rule Converge to a Local Nash Equilibrium [Electronic resource] / [M. Heusel, H. Ramsauer, T. Unterthiner et al.] – Access mode: https://arxiv.org/abs/1801.01401. DOI:10.48550/arXiv.1801.01401

DOI 10.15588/1607-3274-2025-2-15

12. Demystifying MMD GANs [Electronic resource] / [M. Bińkowski, Danica J. Sutherland, Michael Arbel, Arthur Gretton] – Access mode: https://arxiv.org/abs/1801.01401. DOI:10.48550/arXiv.1801.01401
13. Chong M. J. Effectively Unbiased FID and Inception Score and where to find them [Electronic resource] / M. J. Chong, D. Forsyth. – Access mode: https://arxiv.org/abs/1911.07023v3. DOI: 10.48550/arXiv.1911.07023
14. Parmar G. On Aliased Resizing and Surprising Subtleties in GAN Evaluation [Electronic resource] / G. Parmar, R. Zhang, J.-Y. Zhu. – Access mode: https://arxiv.org/abs/2104.11222v3. DOI: 10.48550/arXiv.2104.11222
15. Rethinking FID: Towards a Better Evaluation Metric for Image Generation [Electronic resource] / [S. Jayasumana, S. Ramalingam, A. Veit et al.]. – Access mode: https://arxiv.org/abs/2401.09603v2. DOI: 10.48550/arXiv.2401.09603
16. Betzalel E. Evaluation Metrics for Generative Models: An Empirical Study / E. Betzalel, C. Penso, E. Fetaya // Machine Learning and Knowledge Extraction. – 2024. – Vol. 6, № 3. – P. 1531–1544. DOI: 10.3390/make6030073
17. Wolf Evaluation Metrics for Conditional Image Generation / [Y. Benny, T. Galanti, S. Benaim, L. Wolf] // International Journal of Computer Vision. – 2021. – Vol. 129, № 5. – P. 1712–1731. DOI: 10.1007/s11263-020-01424-w
18. Arjovsky M. Wasserstein GAN [Electronic resource] / M. Arjovsky, S. Chintala, L. Bottou. – Access mode: https://arxiv.org/abs/1701.07875. DOI: 10.48550/ARXIV.1701.07875
19. Deep learning based synthesis of MRI, CT and PET: Review and analysis / [S. Dayarathna, K. T. Islam, S. Uribe et al.] // Medical Image Analysis. – 2024. – Vol. 92. – P. 103046. DOI: 10.1016/j.media.2023.103046
20. Automatic detection metastasis in breast histopathological images based on ensemble learning and color adjustment / [D. S. Luz, T. J. B. Lima, R. R.V. Silva et al.] // Biomedical Signal Processing and Control. – 2022. – Vol. 75. – P. 103564. DOI: 10.1016/j.bspc.2022.103564
21. GAN-based data augmentation to improve breast ultrasound and mammography mass classification / [Y. Jiménez-Gaona, D. Carrión-Figueroa, V. Lakshminarayanan, M. José Rodríguez-Álvarez] // Biomedical Signal Processing and Control. – 2024. – Vol. 94. – P. 106255. DOI: 10.1016/j.bspc.2024.106255
22. Enhancing histopathological medical image classification for Early cancer diagnosis using deep learning and explainable AI – LIME & SHAP / [C. C. Ukwuoma, D. Cai, E. O. Eziefuna et al.] // Biomedical Signal Processing and Control. – 2025. – Vol. 100. – P. 107014. DOI: 10.1016/j.bspc.2024.107014
23. Semantic information-guided attentional GAN-based ultrasound image synthesis method / [S. Shi, H. Li, Y. Zhang, X. Wang] // Biomedical Signal Processing and Control. – 2025. – Vol. 102. – P. 107273. DOI: 10.1016/j.bspc.2024.107273
24. Zeng X. Medical image synthesis algorithm based on vision graph neural network with manifold matching / X. Zeng, B. Lu, J. Zhang // Biomedical Signal Processing and Control. – 2025. – Vol. 103. – P. 107381. DOI: 10.1016/j.bspc.2024.107381
25. Unsupervised medical image synthesis based on multi-branch attention structure / [Y. Hu, S. Zhang, W. Li et al.] // Biomedical Signal Processing and Control. –2025. – Vol. 104 – P. 107495. DOI: 10.1016/j.bspc.2025.107495
26. Generative Adversarial Networks in Digital Pathology and Histopathological Image Processing: A Review / [L. Jose, S. Liu, C. Russo et al.] // Journal of Pathology Informatics. – 2021. – Vol. 12, № 1. – P. 43. DOI: 10.4103/jpi.jpi_103_20
27. Giri S. K. Synthesis of clinical images for oral cancer detection and prediction using deep learning / S. K. Giri, S. Dash // Mining Biomedical Text, Images and Visual Features for Information Retrieval. – 2025. – P. 339–356. DOI: 10.1016/b978-0-443-15452-2.00017-0
28. Berezsky O. M. Evaluation methods of image segmentation quality / O. M. Berezsky, O. Y. Pitsun // Radio Electronics, Computer Science, Control. – 2018. – №1. – P. 119–128. DOI: 10.15588/1607-3274-2018-1-14
29. Berezsky O. M. Method of generative-adversarial networks searching architectures for biomedical images synthesis / O. M. Berezsky, P. B. Liashchynskyi // Radio Electronics, Computer Science, Control. – 2024. – № 1. – P. 104–117. DOI https://doi.org/10.15588/1607-3274-2024-1-10
30. Deep network-based method and software for small sample biomedical image generation and classification / [O. M. Berezsky, P. B. Liashchynskyi, O. Y. Pitsun, G. M. Melnyk] // Radio Electronics, Computer Science, Control. – 2023. – №4. – P. 76. DOI: 10.15588/1607-3274-2023-4-8
31. Rantalainen M. ACROBAT – a multi-stain breast cancer histological whole-slide-image data set from routine diagnostics for computational pathology. Karolinska Institutet. [Electronic resource] / M. Rantalainen, J. Hartman. – Access mode: https://doi.org/10.48723/w728-p041. DOI:10.48723/w728-p041
32. UMMC ER-IHC Breast Histopathology Whole Slide Image and Allred Score IEEE Dataport, 2023. [Electronic resource] / [Wan Siti Halimatul Munirah Wan Ahmad, Mohammad Faizal Ahmad Fauzi, Md Jahid Hasan et al.] – Access mode: https://dx.doi.org/10.21227/9gbq-gz50. DOI: 10.21227/9gbq-gz50
33. Berezsky O. Cytological and histological images of breast cancer [Electronic resource] / O. Berezsky, T. Datsko, G. Melnyk – Access mode: https://zenodo.org/records/7890874. DOI: 10.5281/zenodo.7890873
34. Synthesis of biomedical images based on generative intelligence tools / [O. Berezsky, P. Liashchynskyi, G. Melnyk et al.] // Informatics & Data-Driven Medicine (IDDM 2024): 7th International Conference, Birmingham, UK, November 14–16, 2024, CEUR Workshop Proceedings, 2024. – Vol. 3892. – P. 349–362. DOI: CEUR_WS.org/Vol-3892/paper23.pdf
35. Deza M. M. Encyclopedia of Distances / M. M. Deza, E. Deza. – Springer-Verlag Berlin Heidelberg, 2013. – 583 p.
36. GitHub – liashchynskyi_rudi_ Lightweight image converter and dataset augmentor, 2024. [Electronic resource]. – Access mode: https://github.com/liashchynskyi/rudi

DOI 10.15588/1607-3274-2025-2-15

UDC 004.94

DEVELOPMENT OF INNOVATIVE APPROACHES FOR NETWORK OPTIMIZATION USING GEOSPATIAL MULTI-COMPONENT SYSTEMS

Boyko N. I. – PhD, Associate Professor, Associate Professor of the Department of Artificial Intelligence Systems, Lviv Polytechnic National University, Lviv, Ukraine.

Salanchii T. O. – Student, Department of Artificial Intelligence Systems, Lviv Polytechnic National University, Lviv, Ukraine.

ABSTRACT

Context. Developing a geospatial multi-agent system for optimizing transportation networks is crucial for enhancing efficiency and reducing travel time. This involves employing optimization algorithms and simulating agent behavior within the network.

Objective. The aim of this study is to develop a geospatial multi-agent system for optimizing transportation networks, focusing on improving network efficiency and minimizing travel time through the application of advanced optimization algorithms and agent-based modeling.

Method. The proposed method for optimizing transportation networks combines foundational structure with advanced refinement in two stages: pre-processing and evolutionary strategy optimization. In the first stage, a Minimum Spanning Tree is constructed using Kruskal's algorithm to establish the shortest, loop-free network that connects all key points, accounting for natural obstacles and existing routes. This provides a cost-effective and realistic baseline. The second stage refines the network through an evolutionary strategy, where agents representing MST variations are optimized using a fitness function balancing total path length, average node distances, and penalties for excessive edges. Optimization employs crossover to combine solutions and mutation to introduce diversity through edge modifications. Repeated over multiple epochs, this process incrementally improves the network, resulting in an optimized design that minimizes costs, enhances connectivity, and respects real-world constraints.

Results. The results of applying the evolutionary strategy and minimum spanning tree methods were analyzed in detail. Comparing these methods to benchmarks like Tokyo's railway network and the Slime Mold algorithm revealed the advantage of using the evolutionary approach in generating optimal paths. The findings emphasize the need for integrating advanced algorithms to further refine path optimization and network design.

Conclusions. The research successfully developed a geospatial multi-agent system for optimizing transportation networks, achieving its objectives by addressing key challenges in transport network planning. A detailed analysis of existing solutions revealed the dynamic and complex nature of transportation systems and underscored the need for adaptability to environmental changes, such as new routes or obstacles. The proposed approach enhanced the minimum spanning tree with an evolutionary strategy, enabling flexibility and rapid adaptation. Results demonstrated the system's effectiveness in planning optimal intercity transport networks. Future work could refine environmental assessments, improve route cost evaluations, expand metrics, define new performance criteria, and integrate neural network models to further enhance optimization capabilities, particularly for urban networks.

KEYWORDS: geospatial multi-agent system, optimization of transportation networks, evolution strategy.

ABBREVIATIONS

MST is a minimum spanning tree;
CS is a capital particle;
TF is a target food;
ES is an Evolution Strategies.

NOMENCLATURE

$E' \subseteq E$ is the condition for satisfying the goal

$dG'(u,v)$ is the shortest path distance between nodes u and v in G';

λ is a penalty weight;

$d(e)$ is the length of the edge;

$l(p_i, p_j)$ is the shortest route between points p_i and p_j within the network;

S is the set of all shortest paths between all points;

w is the weighting factor that controls the importance;

L is the total graph distance;

D_{avr} is the average value of the minimum distances between any pair of points in the network;

S is the penalty;

$T(v)$ is the number of triangles that include the vertex v;

k_v is the number of neighbors of the vertex;

$N_{triangles}$ is the number of triangles in the graph;

N_{groups} is the number of groups of size 3.

INTRODUCTION

The optimization of transportation networks is increasingly crucial as cities grow and demand for efficient systems rises. A geospatial multi-agent system offers a promising solution to streamline these networks, improving efficiency and reducing travel times. Research has made progress in optimizing transportation, but challenges remain. Traditional methods struggle with the complexity of real-world systems, where factors like traffic density, geography, and transport types interact. Data preprocessing is another hurdle. Integrating geospatial information from various sources requires significant effort, delaying implementation and reducing effectiveness. Another key issue is adaptability. Transportation networks are dynamic, constantly influenced by infrastructure changes and shifting traffic

DOI 10.15588/1607-3274-2025-2-16

patterns. An effective system must adapt quickly to these changes. However, many theoretical models fail to translate into practical, operational systems, limiting their real-world application. This work proposes an evolutionary strategy to transform the MST into an optimized network. The algorithm's effectiveness was tested against the Slime Mold algorithm [23] and Tokyo's railway system, showing promising results. Though the approach holds potential, more research is needed to refine the system's adaptability, streamline data processing, and enhance scalability for broader use.

Object of the study: interaction process and dynamics of vehicle movement within transportation networks, considering the topology of urban areas and optimal routes.

Subject of the study: algorithms for analyzing and optimizing resource allocation in geospatial multi-agent systems aimed at improving the efficiency of transportation networks in cities.

The aim of this study is to develop a geospatial multi-agent system that optimizes transportation networks by addressing key challenges such as data preprocessing, adaptability, and complexity. By applying evolutionary strategies to transform the minimum spanning tree into an optimal network, this research seeks to improve transportation efficiency and flexibility. The findings aim to contribute to the development of more effective and scalable solutions for real-world transportation systems.

Tasks of the research:

– Analyze existing methods for optimizing transportation networks and geospatial systems.

– Develop a new multi-agent system algorithm that accounts for the geospatial features of transportation networks and agent capabilities for movement optimization.

– Model and simulate the system using test data to assess its effectiveness and reliability.

– Analyze the results and compare them with existing transportation optimization methods to confirm the advantages of the developed system.

The advantages of modeling transportation network optimization lie in the ability to predict traffic flow, identify critical congestion points, and propose effective strategies to improve overall system efficiency. Such models can account for various factors, including traffic density, infrastructure, and agent behavior, allowing for a deeper understanding of the dynamic interactions within transportation systems. They are invaluable tools for decision-making, offering insights that can guide the design and implementation of smarter, more efficient transport solutions.

The relevance of this study is explained in the growing need to optimize transportation networks due to increasing urbanization, traffic congestion, and environmental concerns. As transportation systems evolve, traditional methods of management become less effective, highlighting the importance of developing innovative approaches like geospatial multi-agent systems. This research is timely, as it addresses both the practical need for improved traffic management and the scientific challenge of simulating complex, real-world transportation dynamics.

Understanding and optimizing transportation networks is critical not only for reducing travel time but also for minimizing environmental impact and for enhancing public well-being. The outcomes of this research will have direct implications for urban planning, traffic management, and sustainability efforts, contributing to the development of smarter cities with more efficient, adaptive, and environmentally friendly transportation systems.

The focus of the research is on identifying the relationships between various elements of urban transportation networks, such as traffic patterns, infrastructure, and agent behavior, as well as determining the factors that contribute to inefficiencies or congestion in these systems. The object and subject of the research reflect the core aspects investigated within this study to optimize transportation networks and enhance their efficiency in urban environments.

This research is significant as it aims to enhance the optimization of transportation networks, a vital element of modern infrastructure that facilitates the efficient movement of people and goods. Addressing the challenges associated with these networks is essential for promoting economic growth and safeguarding public health. This study proposes the development of a geospatial multi-agent system as a new solution for transportation network optimization. Such systems enable the modeling of complex agent interactions while accounting for the unique characteristics of each network.

Transport networks are inherently dynamic and complex, making traditional management methods increasingly ineffective. The application of geospatial multi-agent systems is particularly relevant in this context, as they offer the ability to simulate and analyze multiple factors simultaneously. For instance, traffic density, diverse modes of transportation, and geographic constraints can all be incorporated into the system's framework.

Despite notable progress in the field, as highlighted in recent studies [5, 7], significant challenges remain. One major issue is the high complexity involved in system development, stemming from the need to integrate numerous variables and adapt to real-world conditions. Additionally, substantial efforts are required for data preprocessing, including the aggregation and transformation of geospatial data from various sources. This often results in inefficiencies and complicates the practical implementation of these systems.

Another key challenge is the adaptability of the system. Transportation networks are constantly evolving - new roads are built, traffic patterns change, and weather affects old roads. Thus, the system must be flexible enough to respond swiftly to these changes. Furthermore, many studies tend to focus on theoretical frameworks

DOI 10.15588/1607-3274-2025-2-16

without addressing practical considerations, which limits their applicability in real-world scenarios.

To address these challenges, this research introduces an evolutionary strategy to transform a minimal spanning tree into an optimized transportation system. The proposed approach is evaluated by comparing its performance to the Slime Mold algorithm [23] and Tokyo's railway network, demonstrating its potential as an effective and innovative solution. While the development of such systems presents several hurdles, it holds immense promise for creating adaptable, efficient, and practical transportation networks.

1 PROBLEM STATEMENT

The problem of optimizing a transportation network can be described using graph theory, where the network is represented as a graph $G=(V,E)$. Here, V denotes the set of nodes (e.g., cities or junctions), and E represents the set of edges (e.g., potential routes) with weights $w(e)$, which correspond to costs such as distance, time, or construction expenses.

The goal is to determine a subgraph $G'=(V,E')$ that satisfies several objectives:

1. Minimizing Total Path Length: the network should have the lowest possible total cost, calculated as the sum of weights of all selected edges in E.

$$\min(\sum_{e\in E'} w(e)).$$

2. Ensure Connectivity: G' must form a connected subgraph such that every pair of nodes $(u,v)\in V$ is reachable.

3. Optimize Average Shortest Path Length: Minimize the average shortest path length between all pairs of nodes:

$$\min(\frac{1}{|V|(|V|-1)}\sum_{(u,v)\in V} dG'(u,v)).$$

4. Restrict Excessive Edge Addition: Impose a penalty P for adding extra edges beyond a defined threshold k:

$$P(E')=\lambda * \max(0,|E'|-|V|+k).$$

These goals are expressed in a single optimization function that balances the total path length, connectivity efficiency, and penalties for excessive edges. Additionally, constraints are applied to ensure the network respects real-world factors such as geographical obstacles, infrastructural limitations, and dynamic changes in environmental conditions.

This formulation allows for the adaptive and efficient design of transportation networks under dynamic and real-world constraints.

2 LITERATURE REVIEW

Optimization methods are critical in addressing modern challenges in network systems, transportation, and urban planning. This summary highlights the most relevant recent studies on optimal transport and network optimization, focusing on their practical applications, advancements, and limitations.

In research [2], "Imitation-regularized optimal transport on networks: provable robustness and application to logistics planning", the authors address disruptions in network systems with a method called Simulation-Regularized Optimal Transport (I-OT). This approach enhances system resilience and provides practical applications in logistics planning using real-world data. However, the study assumes that networks are Markovian, a simplification that might not always hold true. Additionally, it does not examine the stability of I-OT solutions concerning Schrödinger's bridge problems, nor does it compare I-OT with other transport planning methods, leaving questions about its relative performance unanswered.

Study [3], "Heuristic Optimal Transport in Branching Networks" introduces an efficient heuristic algorithm for large-scale transport problems. This algorithm reduces computation time significantly, adapts well to various network topologies, including those with multiple sources, and sinks. Nonetheless, the reliance on heuristic approximations can compromise solution accuracy, creating a trade-off between speed and precision. Furthermore, the method may struggle with transport tasks involving nonlinear cost functions or complex constraints, limiting its applicability.

Research [4], "Optimal intervention in traffic networks" proposes a topological optimization-based method for route planning in construction projects, focusing on reducing congestion and improving real-time infrastructure planning. The study demonstrates its efficiency through use cases but highlights a critical limitation: the high computational resources required for the optimization process. This drawback could result in complicated practical adoption, especially in scenarios with limited computational infrastructure.

In article [5], "Network centrality guided multi-objective particle swarm optimization for transport optimization on networks", the authors present a multi-objective particle swarm optimization algorithm incorporating Gaussian mutation to balance exploration and exploitation effectively. The algorithm performs well in achieving convergence to Pareto fronts and identifying optimal solutions. However, its high computational complexity raises concerns for large-scale applications. Additionally, the lack of comprehensive comparisons with other state-of-the-art methods and real-world validations limits its generalizability and practical relevance.

These studies illustrate the advancements and trade-offs in applying optimization techniques to real-world problems. While promising, future research must address

DOI 10.15588/1607-3274-2025-2-16

scalability, robustness, and broader applicability to realize their full potential.

Table 1 provides research analysis of related publications that were selected from few sources: Scopus and ArXiv.

Table 1 – Review of related papers

Link	Methodology	Pros of the methodology	Cons of the methodology
[2]	Simulation-regularized optimal transport	Enhances resilience of network systems; practical in logistics planning with real-world data	Assumes Markovian networks (not always valid); lacks comparative analysis with other methods; limited stability insights
[3]	Heuristic algorithm for branching networks	Efficient for large-scale applications; adaptable to varied topologies	Compromises accuracy for speed; less effective for nonlinear costs or complex constraints
[4]	Topological optimization for real-time planning	Reduces congestion; effective in infrastructure development	Requires significant computational resources, limiting practicality in resource-constrained scenarios
[5]	Particle swarm with Gaussian mutation	Balances exploration and exploitation; efficient Pareto convergence	High computational complexity; lacks broader comparisons and real-world validation

Summing up the results presented in Table 1, the analysis highlights the significance of optimizing transportation networks and logistics systems using innovative methodologies. The reviewed studies emphasize the relevance of resilient and efficient approaches to address modern challenges in network planning. While the methodologies demonstrate notable advancements in efficiency, adaptability, and real-world applicability, certain limitations persist, such as computational complexity, reliance on specific assumptions, and the need for comprehensive comparative analyses. These findings underscore the importance of further research to refine these methods and enhance their scalability and robustness for practical applications.

3 MATERIALS AND METHODS

This study explores a promising approach to optimizing transportation networks using bio-inspired algorithms and geospatial data. The focus is on developing efficient, resilient, and adaptive systems capable of addressing the complexities of urban environments. To evaluate the proposed method, the Slime Mold Algorithm [23] was employed as a benchmark due to its ability to model self-organizing network behavior.

To test these methodologies, we used a modified dataset derived from the open-source Slime Mould project [23]. This dataset includes geographic coordinates (latitude and longitude) and Cartesian coordinates (x, y) of Tokyo subway stations, formatted in GeoJSON. For convenience, the data was converted into a pandas DataFrame, facilitating integration with analytical tools and evolutionary algorithms. Converted dataset contains the geographic coordinates (latitude, longitude) and coordinates (x, y) of subway stations, enabling efficient modeling and analysis of Tokyo's transportation infrastructure. An example of the transformed data is displayed on Table 2.

Table 2 – Example of a modified data set

node	lon	lat	x	y
0	118, 86	32, 04	201	163
1	118, 78	32, 05	116	174
2	118, 98	32, 09	320	208
4	118, 79	32, 04	127	166

A map of the subway system, with stations marked as nodes and connections represented as edges is provided on Figure 1.

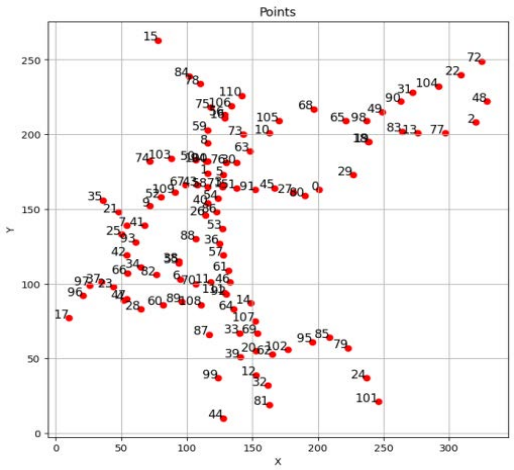

Figure 1 – Map of subway station locations in Tokyo

The slime mold algorithm is inspired by the natural behavior of Physarum polycephalum and simulates the organic growth of transport networks. This method mimics how slime molds optimize paths to connect resources efficiently. By balancing efficiency and resilience, the algorithm generates adaptive road networks capable of withstanding environmental or infrastructural changes.

The networks designed using the slime algorithm are characterized by their speed and cost-effectiveness, as well as their ability to self-regulate. This makes them particularly well-suited for dynamic environments that require ongoing optimization.

When it comes to road network design, the slime algorithm excels in achieving a balance between efficiency and resilience. It prioritizes minimizing distances while also ensuring that the network can withstand failures and adapt to shifts in the environment or infrastructure.

As a result, these networks are not just fast and economical; they also possess the capability to self-regulate, even in adverse conditions. This unique combination of features makes the slime algorithm a powerful tool for creating robust road networks.

DOI 10.15588/1607-3274-2025-2-16

Utilizing the self-organizing principles found in slime mold, this algorithm facilitates the development of transportation networks that can adjust to evolving conditions, such as rising traffic levels or new construction initiatives. This adaptability makes it particularly suitable for dynamic environments that require ongoing enhancement and optimization of transport infrastructure [17].

In this study, the slime algorithm [23] was employed to assess and compare the effectiveness of the proposed method. Therefore, it is pertinent to provide a brief overview of how the algorithm operates.

Slime simulation involves several factors. According to the literature, when Physarum is placed in a medium, such as a petri dish filled with nutrients like oatmeal, it creates a network of protoplasmic tubes to link all available food sources. In this context, the slime sample, its environment, and the nutrients present are the primary elements to consider when modeling the nutrient transport system. The slime model presented in [23] utilizes agent-based modeling to replicate the decision-making processes involved in the movement of the slime sample. This model consists of four essential components: the grid, the food sources, the slime itself, and the slime particles or agents.

A grid serves as the foundational structure that represents the environment for slime modeling. Each element of the grid is initialized as a cell, creating a comprehensive framework for the simulation. This grid consists of two distinct informational layers: the first layer is dedicated to nutrients and slime, while the second layer is composed of pheromones that play a crucial role in guiding the movement of the slime.

In this modeling approach, nutrients are represented as food sources (FS). Each food source is initialized with the highest constant pheromone value in the second layer of the grid, ensuring that the slime can effectively locate and connect to these resources. The primary objective of the slime is to cover and connect all food sources throughout the entire grid, thereby optimizing nutrient transport.

The slime is represented as a “population” of Physarum cells or agents. It maintains various global states that assist each agent, or slime particle, in making movement decisions based on the second layer of the grid. A key component in this process is the capital particle (CS), which designates the target food (TF) for all agents. The CS is randomly chosen from slime particles positioned at the four corners of the slime’s “covered area”. Once the CS is selected, it seeks out the nearest unconnected food source, which becomes the TF until it is linked.

Since the slime’s ultimate aim is to capture and connect all food sources on the grid, the CS is dynamically updated in real-time. Additionally, the slime continuously replicates agents (slime particles) to move toward the TF. This ongoing adaptation is referred to as the evolutionary process. To illustrate this process clearly, a map of food sources (FS) is provided, along with a pheromone map that reflects the number of epochs, as shown in Figure 2.

Figure 2 – Pheromone distribution map across epochs

Each slime particle functions as an individual “agent” within the structure of the slime mold. These particles possess local states that enable them to make decisions regarding their movement. To navigate their environment effectively, a slime particle typically goes through two primary phases: the sensory phase and the diffusion phase. During the sensory phase, a slime particle identifies a food path (FP), which represents the shortest route from the nearest connected food source to the target food (TF). Each food source along this path is referred to as a step food (SF) leading to the TF. Once the FP is established, the agent transitions into the diffusion phase. In this stage, it expands its reach while assessing the conditions of adjacent cells. A schematic illustration of this process can be found in Figure 3.

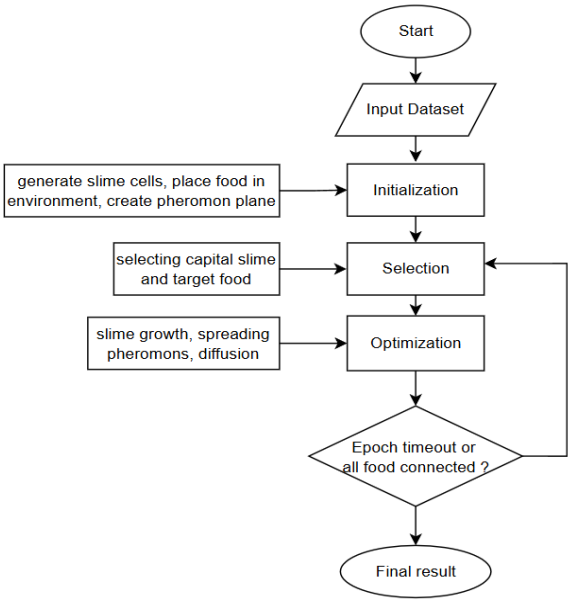

Figure 3 – Schematic representation of Slime Mould algorithm

The diffusion process contains six key features:

1. The pheromone level of a slime particle decreases with each diffusion step.

2. Diffusion is directed toward the nearest step food (SF).

3. If sufficient pheromone is present, diffusion can extend to other neighboring cells.

4. A slime particle will refrain from spreading if it is too distant from the nearest connected food source.

5. During the diffusion stage, a new replicated slime particle may be generated, potentially exhibiting mutated traits such as altered movement direction or pheromone emission.

6. Different conditions of neighboring cells will influence how the pheromone level of the slime particle changes.

DOI 10.15588/1607-3274-2025-2-16

As a conclusion – at each stage, the algorithm improves the system using the physical properties of slime. Pheromones allow the algorithm to estimate the value of each segment: the higher the value of pheromones, the higher the probability that the segment will remain in the final decision. Diffusion, on the other hand, helps to "dry out" suboptimal segments, eliminating routes that do not contribute to efficient communication between stations.

Evolution Strategies represent a method for addressing optimization problems, drawing inspiration from the principles of natural selection and evolution. Similar to other evolutionary computation techniques, this approach utilizes a population of potential solutions that are iteratively improved through mutation, selection, and crossover processes. In this context, each decision is represented as an "individual" or "agent" characterized by a specific set of parameters that define its attributes. The primary goal of evolutionary strategies is to refine these parameters, ultimately identifying the most effective options through continuous improvement.

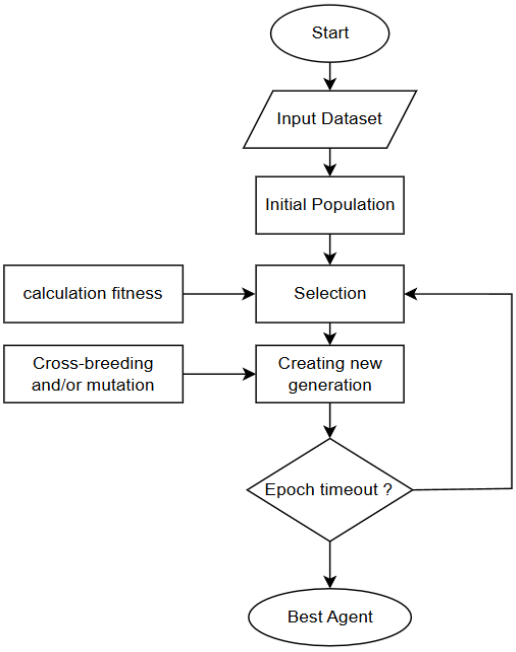

Figure 4 – Schematic representation of Evolution Strategy

One notable characteristic of evolutionary strategies is their capacity to adjust to intricate, multidimensional settings that involve numerous variables. These strategies can be utilized across various fields, particularly in optimization tasks related to technical systems, economics, and biological applications.

A fundamental component of evolutionary strategies is the mutation process, which creates new potential solutions by altering the parameters of existing individuals. Additionally, the selection process plays a crucial role, as it guarantees that only the most effective individuals contribute their traits to the subsequent generation. This combination of mutation and selection fosters continuous improvement in the search for optimal solutions.

This approach is widely used in designing complex systems, such as road networks and communication infrastructures, where maintaining a balance between efficiency and sustainability is essential. In such systems, changes in the environment, resource constraints, and unpredictable disruptions often pose significant challenges. Evolutionary strategies are particularly valuable in these cases, as they can generate solutions that remain effective despite fluctuating conditions. Their adaptability makes them well suited for optimizing dynamic systems that require resilience and long-term viability.

The developed transport network optimization method consists of two stages:

1. Input data is pre-processed: using the Kruskal algorithm, a minimum spanning tree (MST) is created, which forms a basic network with the minimum total length of paths between key points (for example, cities).

2. Using evolution strategy to improve MST by adding "usefull" segments to enhance connectivity, reduce travel time, and increase network resilience while maintaining cost efficiency.

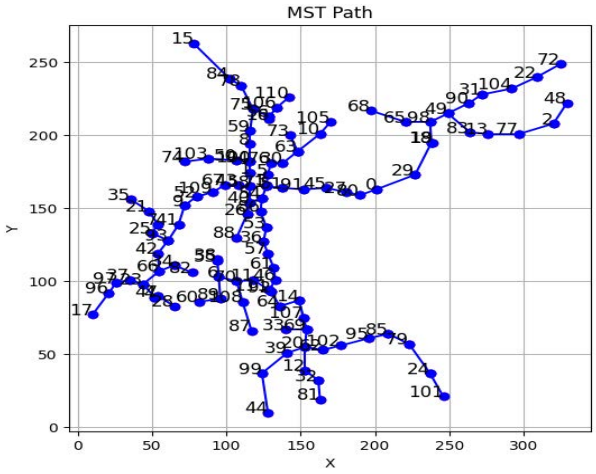

Figure 5 – Example of MST using Kruskal's method

Kruskal's algorithm is a well-known greedy algorithm designed to find a minimum spanning tree (MST) within a weighted graph. This algorithm operates on the principle of incrementally adding edges that possess the least weight, all while ensuring that no loops are formed. The process continues until every nodes in the graph is connected, resulting in a robust structure. Schematic representation of algorithm is on Fig. 6.

By utilizing the minimum spanning tree, we can establish a network that guarantees the connectivity of all points at the lowest possible cost. This foundational network serves as a solid base for future additions to the transport infrastructure. As new edges are added, the efficiency of the network can be significantly improved, paving the way for a more effective and responsive transportation system. In essence, Kruskal's algorithm not only provides a solution to the problem of connectivity but also lays the foundation for ongoing development in the next stage.

DOI 10.15588/1607-3274-2025-2-16

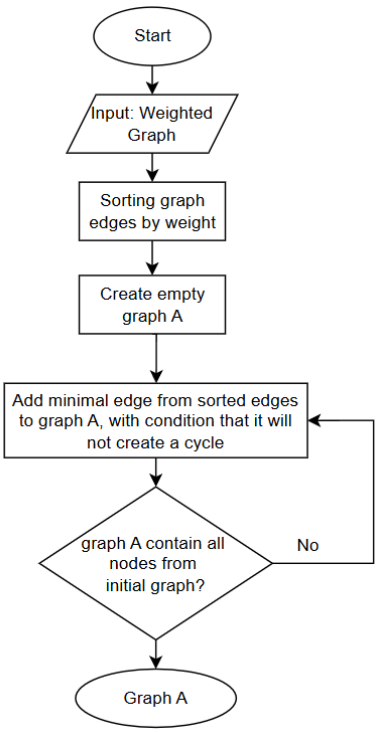

Figure 6 – Schematic representation of Kruskal algorithm

The second stage of the method uses an evolutionary strategy to gradually improve the network structure. It begins with forming an initial population of agents, where each agent represents a set of additional edges added to the minimal spanning tree. These extra edges help refine the network, making it more efficient.

Next, each agent is scored using a fitness function that considers several factors. Let us have a set of vertices $P = \{p_1, p_2, p_3 ... p_n\}$, representing key nodes in the network, and a list of edges E, representing the paths between points in the agent. To form an optimal network, we can set the following fitness function f, that considers listed metrics:

1. Total Graph Length: Total sum of edges, used to reduce the cost of building new roads.

For instance, let $L(E)$ be the total length of all edges in the set E. This metric can be represented into the fitness function (1):

$$L = \sum_{e \in E} d(e), \tag{1}$$

the goal is to find a combination E that L is minimal while fulfilling other conditions.

Average distance between any pair of points: Minimizing this value ensures that the points in the network are not too far apart, improving overall efficiency. Let D_{avr} represent the average of the minimum distances between any pair of points in the network (2):

$$D_{avr} = \frac{1}{|S|} \sum_{p_i, p_j \in P} l(p_i, p_j), \tag{2}$$

is a formalized representation of the definition of the set of all shortest paths between all points.

2. Extra Edge Penalty: To prevent excessive network complexity, the algorithm imposes a penalty when the number of extra edges surpasses a predefined threshold. This threshold is set as a permissible ratio of the total number of points—for instance, 1.1, which allows up to 10% additional edges. When this limit is exceeded, a penalty is introduced (3):

$$S = \begin{cases} \lambda * (|E| - \alpha * |P|), if \ |E| > \alpha * |P| \\ 0 \end{cases}, \tag{3}$$

in the experiments performed $\lambda = 0.01$.

Then the final fitness function can be expressed as (4):

$$F = w * L + D_{avg} + S \ . \tag{4}$$

During the third step, agents undergo changes via crossover and mutation. Crossover in this method is performed by selecting common additional edges that are present in two parent agents. This strategic choice is designed to preserve the fundamental structure of each solution, ensuring that the strengths of both parents are retained in the child.

Following this, the algorithm introduces an element of diversity and potential for further optimization. This is achieved by randomly selecting unique edges from each parent and incorporating them into the shared edges. To illustrate, consider a scenario where one agent possesses four extra edges while another has six, with three of those edges being common to both. In this case, the new agent will inherit the three common edges, but it will also receive three randomly chosen unique edges from each parent. This approach guarantees that the total number of additional segments in the offspring matches the maximum number found in either parent. This process is visually represented in Figure 7.

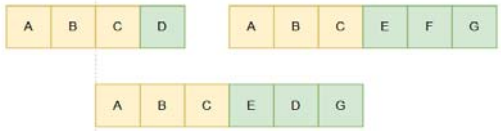

Figure 7 – Crossover operation

By employing this method, the algorithm effectively maintains a stable foundation derived from both parent agents. At the same time, it explores new possibilities by integrating unique elements. This dual approach not only preserves the valuable characteristics of the parent solutions but also enhances the search for optimal solutions, making the overall process efficient and robust.

Despite the effectiveness of this approach, a complete mutation remains essential. Without it, there is a risk that parents sharing the same genome may stagnate in their evolutionary journey. In this method, mutation is executed through a random selection among three distinct actions: removing, replacing, or adding an edge.

DOI 10.15588/1607-3274-2025-2-16

In cases where addition is the chosen action, a new edge is introduced to the list of additional edges. This new edge is selected from those that have not yet been utilized. However, it is important to note that this addition can only occur if the total number of additional edges does not surpass the predetermined maximum limit.

When the deletion option is chosen, one edge is randomly eliminated from the agent's set of additional edges. This action not only simplifies the path but also encourages the exploration of more streamlined solutions.

On the other hand, if the replacement option is selected, a randomly chosen additional edge is substituted with a new one. This new edge is drawn from the pool of available edges, deliberately excluding those already incorporated into the agent's structure. This strategy ensures variability while maintaining a constant total number of additional edges.

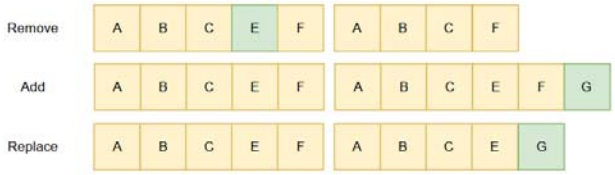

Figure 8 – Visualization of mutation types

This implementation of mutation strategy is designed to maintain balance of solution stability and exploration, ensuring that the agent maintains path connectivity and optimality while simultaneously discovering new possible solutions.

The fourth step of the algorithm involves iterative improving through evaluation, crossover. This process is repeated for a predetermined number of epochs, allowing the system to gradually enhance the quality of solutions.

With each iteration, the population of agents undergoes continuous improvement, driven by the selection of the most promising candidates. Over time, this iterative process minimizes the gap between the best and worst performing agents, moving toward an optimal solution.

As the algorithm progresses (See Fig. 9), weaker solutions are gradually eliminated, while stronger ones propagate, ensuring that each generation is more refined than the last. By the final epoch, the selection process has filtered the population to its most effective configuration. Ultimately, the agent exhibiting the highest performance is chosen as the best solution.

The clustering coefficient is a metric that measures the likelihood that neighbors of a node in a graph are also connected to each other, forming a triangle. This coefficient indicates the local density of connections for each node and helps to understand the structure of the graph at a local level. Figures 10 (a) and 10 (b) illustrate the differences in the structure of graphs with different clustering coefficients: in a graph with high clustering.

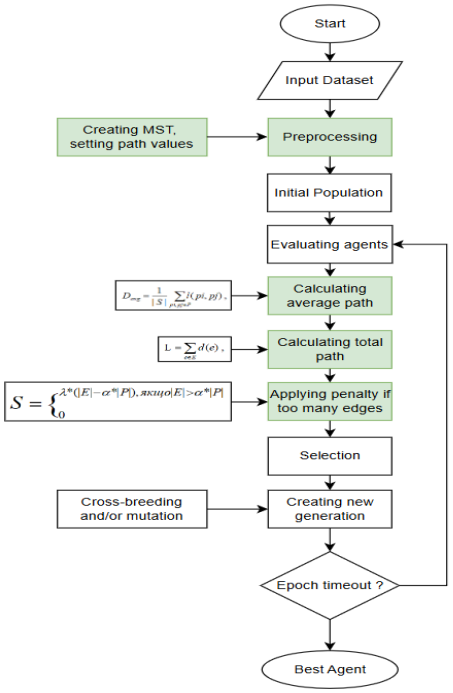

Figure 9 – Schematic representation of proposed algorithm

a b

Figure 10 – Example of graphs with different clustering coefficient

The clustering coefficient for an individual node is defined as the ratio of the number of existing connections between its neighbors to the maximum possible number of such connections. The local clustering coefficient for a vertex indicates how much its neighbors are also neighbors with each other. It is defined as follows (5):

$$C_{local}(V) = \frac{2T(v)}{k_v(k_v - 1)} \cdot \quad (5)$$

The higher the clustering coefficient, the more the node is part of a tightly connected group where its neighbors also interact closely with one another.

High values of the clustering coefficient indicate that the graph tends to form strongly connected local groups, or "clusters". The clustering coefficient for a graph (global) is given by (6):

$$C_{global} = \frac{3N_{triangles}}{N_{groups}}, \quad (6)$$

a triangle in a graph is a group of three vertices where each one is connected to the other two, while groups of three vertices are simply all possible triplets of vertices, regardless of whether they are connected.

The clustering coefficient for the entire graph allows for the assessment of the overall tendency to form such

DOI 10.15588/1607-3274-2025-2-16

local clusters. For a random graph, this coefficient is always equal to 0, as nodes are only connected to nodes with which they have the shortest paths, without forming triangles, which are the basis for clustering. For an agent, the clustering coefficient is equal to 0, meaning that the agent maintains separate lines of communication but does not engage in close connections with other nodes.

In the process of solving optimization problems, it is important to consider and compare several approaches to achieve effective results. This study examines two methods: the slime mold method, which simulates the behavior of slime mold in finding the optimal path between food sources, and the evolutionary strategy, which is based on improving the MST. Both methods have distinct mechanisms for search, self-organization, and adaptation, which define their unique advantages and limitations. Comparative Tables 3–6 presents an analysis of the stages of these methods, from initialization to optimization. The goal of this comparison is to identify the most suitable method for solving optimization problems under the given conditions.

Table 3 – Initialization stage comparison

Initialization	
Slime Mould	Slime particles are created, and a grid of food and pheromones is generated
Evolution Strategy	Combinations of all possible paths between vertices are created, and an initial population of agents is formed, where each agent is a list of paths.
Evolution strategy based on MST improvement (Proposed method)	MST is generated, combinations of all possible paths between vertices are created, and an initial population of agents is formed, where each agent is an addition to the MST.

Table 4 – Search stage comparison

Search	
Slime Mould	A leader particle is selected to indicate the general direction for others; agents move and leave pheromone hints for other particles.
Evolution Strategy	Each agent is evaluated through a fitness function.
Evolution strategy based on MST improvement (Proposed method)	Each agent is evaluated through a fitness function; the average path, total path is calculated, and a penalty is added if the number of paths exceeds the allowed limit.

Table 5 – Self organizing stage comparison

Self-organizing	
Slime Mould	Using the diffusion process, the slime improves the system.
Evolution Strategy	Agents are sorted by fitness value (agents that could not build a connected path/graph are excluded).
Evolution strategy based on MST improvement (Proposed method)	Agents are sorted by fitness value.

Table 6 – Information processing stage comparison

Information Processing	
Slime Mould	Due to the physical properties of pheromones, non-optimal segments are “dried up” and important segments remain.
Evolution Strategy	The top 50% of the best-fitted agents are selected. Agents randomly form pairs that undergo classical crossover (with the preservation of graph connectivity) with a chance of random mutation.
Evolution strategy based on MST improvement (Proposed method)	The top 50% of the best-fitted agents are selected. Agents randomly form pairs that undergo crossover with a chance of random mutation. This allows for the reproduction of the initial population size while maintaining fitness and diversity.

Based on the analysis of the stages of work of each method, certain conclusions can be drawn regarding their effectiveness. The evolutionary strategy based on improving the MST has proven to be more adaptable for situations where flexibility and the ability to adapt are important, as its mechanisms of crossover and mutation allow for the preservation of a diversity of solutions within the population of agents. This strategy promotes a higher adaptability of agents to changing conditions, which positively affects the effectiveness of optimization in complex networks.

The slime method also has advantages in terms of the speed of self-organization due to the physical properties of pheromones, which allow for the identification of important segments and the “drying out” of non-optimal ones. Therefore, for tasks that require a quick convergence to an optimal solution, the slime method is also appropriate. Given the advantages of the evolutionary strategy for adaptive environments, it is advisable to use it as the primary method for further experiments.

4 EXPERIMENTS

Conducting experiments is of great importance, as it allows us to evaluate how effectively the system improves transportation efficiency and reduces travel time. These experiments measure the performance of the optimization algorithms and assess their ability to handle real-world challenges such as congestion and disruptions. Moreover, the results help validate the evolutionary strategy’s transformation of minimum cost distance into optimal paths while extending the minimal spanning tree for practical applications, offering valuable insights into network optimization.

To implement the evolutionary algorithm system, Python was chosen as the primary programming language due to its versatility, readability, and extensive ecosystem of libraries. Python is widely recognized for its simplicity and cross-platform compatibility, making it an ideal choice for developing diverse software solutions. In particular, the following libraries and tools were used to develop the application:

– NetworkX: This library specializes in analyzing and visualizing complex networks and graphs. It was used for constructing minimum spanning trees, checking graph connectivity, and visualizing transportation networks.

DOI 10.15588/1607-3274-2025-2-16

– NumPy is a library for scientific computing in Python. Essential for numerical computations, NumPy excels at handling large, multi-dimensional arrays with performance optimizations through C-based implementation.

– Pandas: Known for its robust data manipulation capabilities, Pandas offers the DataFrame structure, which facilitates efficient data cleaning, filtering, grouping, and aggregation.

– Matplotlib & Seaborn: These libraries provided tools for creating high-quality visualizations, from basic plots to more advanced data representations.

This section focuses on identifying the optimal parameters for an evolutionary strategy, which are critical for ensuring the algorithm's efficiency and performance. Specifically, we examine key parameters such as the number of epochs and population size. These parameters significantly influence both the quality of the solutions obtained and the convergence speed of the algorithm.

The number of epochs determines the iterations of the optimization process. A higher number of epochs allows the algorithm to fine-tune its search for the best solutions. However, it also increases the execution time. Striking a balance between learning efficiency and execution speed is essential for parameter optimization.

Population Size Population size directly impacts the diversity of solutions explored during optimization. Larger populations offer more options for evolutionary selection, increasing the likelihood of finding a global optimum. On the other hand, excessively large populations can complicate the optimization process and increase computational costs.

To identify the optimal algorithm parameters, a series of experiments were conducted. Two primary metrics were used for evaluation:

– Execution time: How long the method takes to complete.

– Fitness of the best agent: Calculated using the objective function described earlier.

The goal was to balance execution speed and result accuracy, maximizing system resource efficiency.

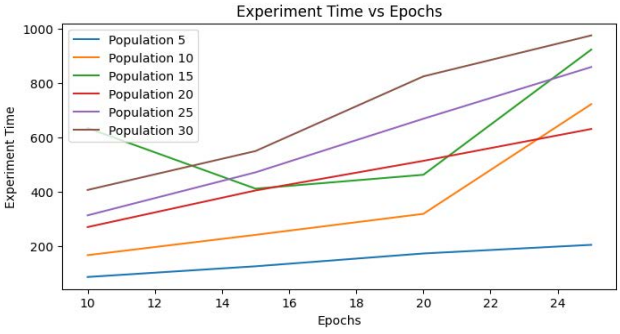

Figure 11 – Relationship between execution time and the number of epochs for different population sizes

Analysis reveals that increasing both population size and the number of epochs gradually extends the execution time. This is because larger populations require more processing time.

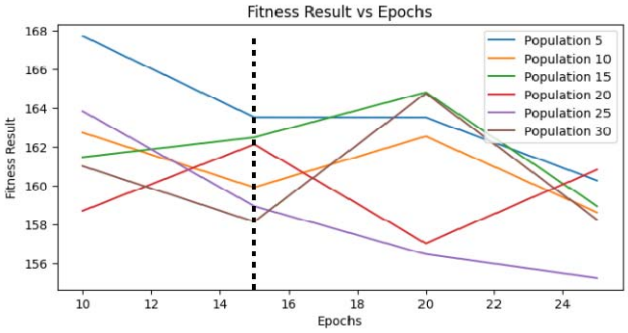

Figure 12 – Relationship between fitness results and the number of epochs for different population sizes

The Fig. 11–12 shows that increasing epochs does not always lead to consistent fitness improvements. For example, populations of 15 and 20 exhibit instability in later stages.

Based on the experiments, the optimal parameter combination is a population size of 25 agents and 15 epochs. This choice is supported by a clear trend of fitness improvement with increasing epochs, as observed in the fitness-epochs graph. This balance ensures efficient resource utilization while maintaining high solution quality.

Using the optimal parameters (25 agents and 15 epochs), a comparison was conducted to evaluate the efficiency of the developed method against the slime mold algorithm. For the slime mold algorithm, 350 epochs were used, as this provided sufficient time for the agents to grow and form optimal paths. The Tokyo subway system was also included as a benchmark example for comparison.

The evaluation was based on the criterion of the average distance between each pair of points (2).

This approach allowed us to determine how well the optimal paths identified by the algorithms align with real-world transportation routes and whether they could provide more efficient connections between stations compared to the existing subway network. MST is displayed on Figure 13. The calculations and results are presented in Tables 7–9. For better visualization, each table includes comparison between MST and generated system (red edges are common for MST and generated system, green are present only in generated system).

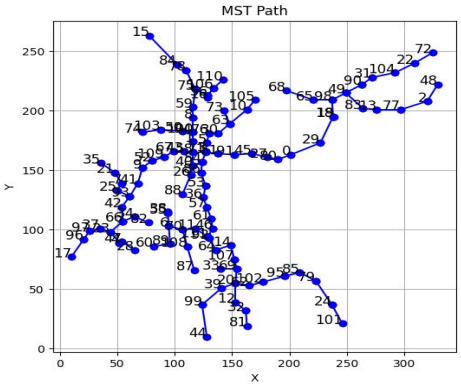

Figure 13 – Generated MST

DOI 10.15588/1607-3274-2025-2-16

Table 7 – Calculation and analysis of Tokyo railway system

Tokyo railway	
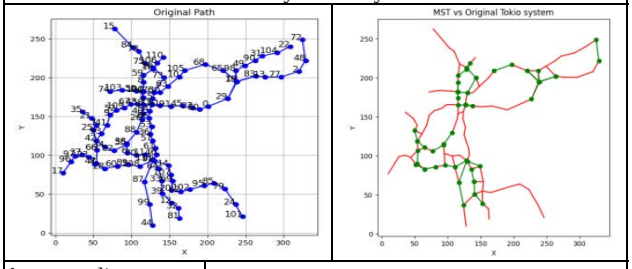	
Average distance	$AVG = \frac{1}{\lvert S \rvert}\sum_{a\in S} a = \frac{1971289.6}{12544} = 157.15$
Total distance	$L = \sum_{t\in E} t = 1738.6$
Clustering coefficient	$C_{global} = \frac{3N_{triangles}}{N_{groups}} = 0$ as there is no triangle in the system

Table 8 – Calculation and analysis of Slime Mould system

Slime Mould method	
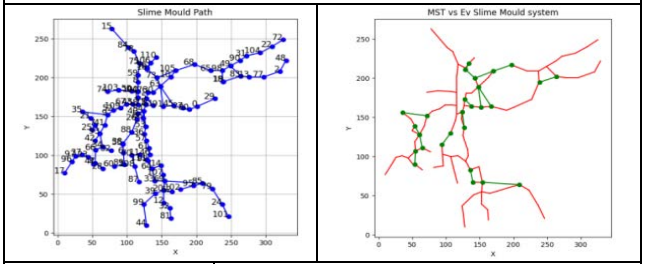	
Average distance	$AVG = \frac{1}{\lvert S \rvert}\sum_{a\in S} a = \frac{2488781.6}{12544} = 198.40$
Total distance	$L = \sum_{t\in E} t = 1676.67$
Clustering coefficient	$C_{global} = \frac{3N_{triangles}}{N_{groups}} = \frac{3}{75} = 0.04$

Table 9 – Calculation and analysis of system generated by proposed method

Proposed method	
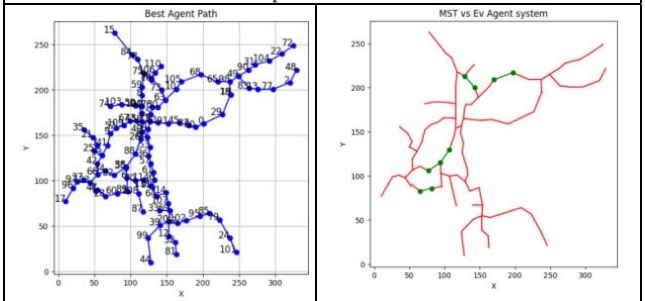	
Average distance	$AVG = \frac{1}{\lvert S \rvert}\sum_{a\in S} a = \frac{1930396.16}{12544} = 153.89$
Total distance	$L = \sum_{t\in E} t = 1527.66$
Clustering coefficient	$C_{global} = \frac{3N_{triangles}}{N_{groups}} = 0$ as there is no triangle in the system

5 RESULTS

In this chapter, we will evaluate the performance of the various algorithms employed to optimize transportation networks. It is crucial to assess not only the visual representations of the results but also to quantify those using relevant metrics. As described in the previous section, the average distance, total distance, and clustering coefficient were estimated for each algorithm. The results of the calculations are given in Table 10.

Table 10 – Comparison of each system

	Tokyo system	Slime Mould	Proposed method
Average distance	157.15	198.40	153.88
Total distance	1738.65	1676.667	1527.66
Clustering coefficient	0	0.04	0

Let us compare the effectiveness of the systems: each algorithm demonstrates different results regarding the average distance between pairs of points. The actual Tokyo railway system, which served as the benchmark, showed a score of 157.15. The slime algorithm, while it identified some optimal paths, had a worse score of 198.40, indicating lower efficiency compared to the benchmark. The developed method achieved the best result of 153.88.

Based on the comparative studies conducted, the developed method (using optimal parameters: 25 agents and 15 epochs) demonstrated the highest efficiency. It provided a shorter average distance between stations compared to the actual Tokyo railway system and achieved this improvement alongside a reduction in the overall path length, indicating its potential for further use in optimizing transportation networks.

Moreover, the total distance metric further emphasizes the advantages of the proposed method. With a total distance of 1527.66, it outperformed both the Tokyo system and the Slime Mould algorithm, which recorded total distances of 1738.65 and 1676.67, respectively. This reduction in total distance not only signifies a more efficient routing of transportation but also suggests potential cost savings and reduced travel times for users.

The clustering coefficient, while not as critical in this context, also provides insight into the connectivity of the network. The proposed method maintained a clustering coefficient of 0, similar to the Tokyo system, while the Slime Mould algorithm achieved a coefficient of 0.04. This indicates that the proposed method retains a level of simplicity in its structure, which can be beneficial for implementation and scalability.

In conclusion, the results indicate that the proposed method is not only effective in optimizing transportation networks but also demonstrates a significant improvement over existing systems. Future work should focus on refining the algorithm further, potentially incorporating more complex models or hybrid approaches that could enhance performance even more. By exploring advanced techniques such as machine learning or multi-agent systems, we can continue to push the boundaries of transportation network optimization.

DOI 10.15588/1607-3274-2025-2-16

6 DISCUSSION

Conducted research aimed at developing a geospatial multi-agent system for optimizing transportation networks. A comprehensive analysis of the subject area was performed, focusing on existing solutions and identifying promising research directions.

The study revealed several critical challenges in planning optimal transportation systems, particularly the dynamic nature and complexity of transportation networks. An additional issue is the necessity for the system to adapt to environmental changes, which is vital due to the constant evolution of routes and the emergence of obstacles. To address these challenges, a novel approach was proposed that enhances the minimum spanning tree (MST) using evolutionary strategies.

The results indicate that the developed system can effectively plan optimal transportation connections between cities. This system has the potential to significantly reduce travel time and costs, benefiting both passengers and transportation operators. Further research should aim to refine the methods for assessing environmental factors and the costs associated with selected routes, as well as improve existing metrics and develop new criteria for evaluating efficiency.

Additionally, integrating the system with neural network models could lead to a more in-depth analysis and optimization of transportation routes, particularly in complex urban environments where traditional methods may be inadequate. By utilizing neural networks to process geographical maps and spatial data, the system can generate structured input data that enhances route planning and urban development strategies. This integration has the potential to revolutionize our approach to urban transportation planning, making it more adaptive and efficient in response to ever-changing conditions.

CONCLUSIONS

The conducted research on developing a geospatial multi-agent system for optimizing transportation networks has yielded significant insights into the complexities and dynamic nature of transportation planning. The study's findings underscore the practical significance of the proposed system, which demonstrates the capability to effectively plan optimal transportation connections between cities. This advancement has the potential to substantially reduce travel time and costs, providing tangible benefits for both passengers and transportation operators.

Scientific Novelty: The research contributes to the scientific community by introducing a novel approach that combines evolutionary strategies with traditional transportation planning methods. This innovative perspective not only addresses existing challenges but also opens new avenues for exploration in the field of transportation optimization.

Practical Significance: The results of this research are particularly relevant for urban planners and transportation authorities, as they offer a novel solution to the pressing challenges of optimizing transportation networks. By enhancing the minimum spanning tree (MST) with evolutionary strategies, the system can adapt to environmental changes and evolving routes, thereby improving the overall efficiency of transportation systems.

Prospects for Further Research: The prospects for further research are promising, particularly in the areas of algorithm refinement and the development of new evaluation metrics for transportation efficiency. Investigating the application of the proposed system across various practical scenarios, including urban and rural settings, could yield valuable insights. Additionally, exploring the potential of machine learning and artificial intelligence in conjunction with the multi-agent system may lead to breakthroughs in adaptive transportation planning, ultimately revolutionizing how we approach urban mobility in response to changing demands.

Recommendations for Further Research: To build upon the findings of this study, it is recommended that future research focus on refining methods for assessing environmental factors and the associated costs of selected routes. Additionally, exploring the integration of neural network models into the system could provide deeper insights into route optimization, especially in complex urban environments. This integration could facilitate the processing of geographical maps and spatial data, leading to more structured input data that enhances route planning and urban development strategies.

ACKNOWLEDGEMENTS

The study was created within research topic "Methods and means of artificial intelligence to prevent the spread of tuberculosis in wartime" (№0124U000660), which is carried out at the Department of Artificial Intelligence Systems of the Institute of Computer Sciences and Information of technologies of the National University "Lviv Polytechnic".

REFERENCES

1. Moher D., Liberati A., Tetzlaff J. Preferred Reporting Items for Systematic Reviews and Meta-Analyses, *The PRISMA Statement. PLoS Medicine*, 2020, Vol. 6(7), P. e1000097, Mode of access: https://doi.org/10.1371/journal.pmed.1000097.
2. Oishi K., Hashizume Y., Jimbo T., Kaji H., Kashima K. Imitation-regularized optimal transport on networks: provable robustness and application to logistics planning, *arXiv preprint arXiv*, 2024, P. 1906.07114, Mode of access: https://doi.org/10.48550/arXiv.2402.17967.
3. Andrecut M. Heuristic Optimal Transport in Branching Networks, *arXiv preprint arXiv*, 2021, P. 1906.07115, Mode of access: https://doi.org/10.48550/arXiv.2311.06650.
4. Cominetti L., Como G., Ozdaglar A., Parise F. Optimal intervention in traffic networks, *arXiv preprint arXiv*, 2021, P. 1906.07116, Mode of access: https://doi.org/10.48550/arXiv.2102.08441.
5. Wu J., Pu C., Ding S., Cao G., Pardalos P. M. NC-MOPSO: Network centrality guided multi-objective particle swarm optimization for transport optimization on networks, *arXiv preprint arXiv*, 2021, P. 906.07117, Mode of access: https://doi.org/10.48550/arXiv.2009.03575.
6. Aslani B., Mohebbi S. Learn to decompose multiobjective optimization models for large-scale networks, *arXiv preprint arXiv*, 2021, P. 1906.07118, Mode of access: https://doi.org/10.1111/itor.13169.

DOI 10.15588/1607-3274-2025-2-16

7. Sbayti O., Housni K., Hicham Hanin M., El Makrani A. Comparative analysis of proactive and reactive routing protocols in VANET environment, *International Journal of Electrical and Computer Engineering (IJECE)*, 2023, Vol. 13(5), P. 5374–5387, Mode of access: https://doi.org/10.11591/ijece.v13i5.pp5374-5387.
8. Rafael H., Pereira M., Herszenhut D., Saraiva M., Farber S. Ride-hailing and transit accessibility considering the trade-off between time and money, *Cities*, 2024, Vol. 144, P. 104663, Mode of access: https://doi.org/10.1016/j.cities.2023.104663
9. Baptista D., De Bacco C. Convergence properties of optimal transport-based temporal networks, *arXiv preprint arXiv*, 2021, Mode of access: https://doi.org/10.1007/978-3-030-93409-5_48
10. Wen W., Zhang W., Deng H. Research on Urban Road Network Evaluation Based on Fractal Analysis, *Journal of Advanced Transportation*, 2023, P. 1–8, Mode of access: https://doi.org/10.1155/2023/9938001.
11. Choi J., Kang M. Analyzing and Improving Optimal-Transport-based Adversarial Networks, *arXiv:2310.02611*, 2023, Mode of access: https://doi.org/10.48550/arXiv.2310.02611.
12. VANET (Vehicular Ad-hoc Network) [Electronic resource]. Access mode: https://en.wikipedia.org/wiki/Vehicular_ad-hoc_network (access date: 11.12.2024). Title from the screen.
13. AODV (Ad-hoc On-Demand Distance Vector routing) [Electronic resource]. Access mode: https://en.wikipedia.org/wiki/Ad-hoc_On-Demand_Distance_Vector_routing (access date: 11.12.2024). Title from the screen.
14. DSDV (Destination-Sequenced Distance Vector routing) [Electronic resource]. Access mode: https://en.wikipedia.org/wiki/Destination-Sequenced_Distance_Vector_routing (access date: 11.12.2024). Title from the screen.
15. OLSR (Optimized Link State Routing) [Electronic resource]. Access mode: https://en.wikipedia.org/wiki/Optimized_Link_State_Routing_Protocol (access date: 11.12.2024). Title from the screen.
16. Yang X.-S. Nature-Inspired Algorithms in Optimization: Introduction, Hybridization and Insights, *arXiv:2401.00976*, 2023, Mode of access: https://doi.org/10.1007/978-981-99-3970-1.
17. Wei Y., Othman Z., Mohd Daud K., Luo Q., Zhou Y. Advances in Slime Mould Algorithm: A Comprehensive Survey, *Biomimetics*, 2024, Vol. 9, P. 31, Mode of access: https://doi.org/10.3390/biomimetics9010031.
18. Bellman-Ford Algorithm [Electronic resource]. Access mode: https://brilliant.org/wiki/bellman-ford-algorithm (access date: 11.12.2024). Title from the screen.
19. A* Algorithm [Electronic resource]. Access mode: https://en.wikipedia.org/wiki/A*_search_algorithm (access date: 11.12.2024). Title from the screen.
20. Network flow problem [Electronic resource]. Access mode: https://en.wikipedia.org/wiki/Network_flow_problem (access date: 11.12.2024). Title from the screen.
21. Network flow problem, Ford–Fulkerson algorithm [Electronic resource]. Access mode: https://www.networkflowalgs.com/book.pdf (access date: 11.12.2024). Title from the screen.
22. Wagdy A., Hadi A. A, Khater A. Gaining-sharing knowledge based algorithm for solving optimization problems: a novel nature-inspired algorithm, *International Journal of Machine Learning and Cybernetics*, 2023, Mode of access: https://doi.org/10.1007/s13042-019-01053-x.
23. SlimeMould [Electronic resource]. Access mode: https://github.com/MoeBuTa/SlimeMould (access date: 11.12.2024). Title from the screen.
24. Boyko N., Pytel A. Aspects of the study of genetic algorithms and mechanisms for their optimization for the travelling salesman problem, *International Journal of Computing*, 2021, Vol. 20(4), P. 543–550, Mode of access: https://doi.org/10.47839/ijc.20.4.2442.
25. Vyklyuk Ya., Nevinskyi D., Boyko N. GeoCity – a New Dynamic-Spatial Model of Urban Ecosystem, *J. Geogr. Inst. Cvijic*, 2023, Vol. 73(2), P. 187–203, Mode of access: https://doi.org/10.2298/IJGI2302187V.

Received 16.01.2025.
Accepted 29.04.2025.

УДК 004.94

РОЗРОБКА ІННОВАЦІЙНИХ ПІДХОДІВ ДЛЯ ОПТИМІЗАЦІЇ МЕРЕЖ ЗА ДОПОМОГОЮ ГЕОПРОСТОРОВИХ БАГАТОКОМПОНЕНТНИХ СИСТЕМ

Бойко Н. І. – канд. економ. наук, доцент, доцент кафедри Систем штучного інтелекту, Національний університет «Львівська політехніка», Львів, Україна.

Саланчій Т. О. – студент кафедри Систем штучного інтелекту, Національний університет «Львівська політехніка», Львів, Україна.

АНОТАЦІЯ

Актуальність. Розробка геопросторової багатагентної системи для оптимізації транспортних мереж є важливою для підвищення ефективності та зменшення часу подорожі. Це передбачає використання алгоритмів оптимізації та моделювання поведінки агентів у межах мережі.

Мета роботи є розробка геопросторової багатагентної системи для оптимізації транспортних мереж, зосереджуючи увагу на покращенні ефективності мережі та мінімізації часу подорожі шляхом застосування передових алгоритмів оптимізації та моделювання на основі агентів.

Метод. Запропонований метод оптимізації транспортних мереж поєднує базову структуру з розширеним уточненням у два етапи: попередня обробка та оптимізація еволюційної стратегії. На першому етапі будується мінімальне остовне дерево за допомогою алгоритму Крускала для встановлення найкоротшої мережі без петель, яка з'єднує всі ключові точки, враховуючи природні перешкоди та існуючі маршрути. Це забезпечує економічно ефективну та реалістичну базову лінію. Другий етап удосконалює мережу за допомогою еволюційної стратегії, де агенти, що представляють варіації мінімального остового дерева, оптимізуються за допомогою функції пристосування, яка балансує загальну довжину шляху, середню відстань до вузлів і штрафи за надмірні краї. Оптимізація використовує кросовер для поєднання рішень і мутацію для введення різноманітності через модифікації країв. Цей процес, повторюється протягом багатьох епох, поступово покращує мережу, в результаті чого створюється оптимізований шлях, який мінімізує витрати, покращує підключення та поважає обмеження подані в режимі реального часу.

Результати. Результати застосування еволюційної стратегії та методів мінімальної вартості відстані були детально проаналізовані. Для еволюційної стратегії були оцінені такі метрики, як ефективність шляхів і обчислювальні витрати, що

DOI 10.15588/1607-3274-2025-2-16

продемонструвало значні покращення в оптимізації мережі. У випадку MST, хоча метод надав базову структуру для вибору шляхів, візуальні та числові оцінки підкреслили обмеження в розв'язанні складних реальних обмежень. Порівняння цих методів з еталонами, такими як залізнична мережа Токіо та алгоритм слизової цвілі, виявило перевагу еволюційного підходу в генерації оптимальних шляхів. Висновки підкреслюють необхідність інтеграції передових алгоритмів для подальшого вдосконалення оптимізації шляхів і проектування мереж.

Висновки. Дослідження успішно розробило геопросторову багатоагентну систему для оптимізації транспортних мереж, досягнувши поставлених цілей шляхом вирішення ключових проблем у плануванні транспортної мережі. Детальний аналіз існуючих рішень виявив динамічний і складний характер транспортних систем і підкреслив необхідність адаптації до змін навколишнього середовища, таких як нові маршрути або перешкоди. Запропонований підхід розширив мінімальне охоплююче дерево за допомогою еволюційної стратегії, забезпечивши гнучкість і швидку адаптацію. Результати продемонстрували ефективність системи в плануванні оптимальних міжміських транспортних мереж. Майбутня робота може вдосконалити екологічні оцінки, покращити оцінку вартості маршруту, розширити показники, визначити нові критерії продуктивності та інтегрувати моделі нейронних мереж для подальшого підвищення можливостей оптимізації, особливо для міських мереж.

КЛЮЧОВІ СЛОВА: геопросторова мультиагентна система, оптимізація транспортних мереж, еволюційна стратегія.

ЛІТЕРАТУРА

1. Moher D. Preferred Reporting Items for Systematic Reviews and Meta-Analyses / D. Moher, A. Liberati, J. Tetzlaff // The PRISMA Statement. PLoS Medicine. – 2020. – Vol. 6(7). – P. e1000097. – Mode of access: https://doi.org/10.1371/journal.pmed.1000097.
2. Imitation-regularized optimal transport on networks: provable robustness and application to logistics planning / [K. Oishi, Y. Hashizume, T. Jimbo et al.] // arXiv preprint arXiv. – 2024. – P. 1906.07114. – Mode of access: https://doi.org/10.48550/arXiv.2402.17967.
3. Andrecut M. Heuristic Optimal Transport in Branching Networks / M. Andrecut // arXiv preprint arXiv. – 2021. – P. 1906.07115. – Mode of access: https://doi.org/10.48550/arXiv.2311.06650.
4. Optimal intervention in traffic networks / [L. Cianfanelli, G. Como, A. Ozdaglar, F. Parise] // arXiv preprint arXiv. – 2021. – P. 1906.07116. – Mode of access: https://doi.org/10.48550/arXiv.2102.08441.
5. NC-MOPSO: Network centrality guided multi-objective particle swarm optimization for transport optimization on networks / [J. Wu, C. Pu, S. Ding et al.] // arXiv preprint arXiv. – 2021. – P. 906.07117. – Mode of access: https://doi.org/10.48550/arXiv.2009.03575.
6. Aslani B. Learn to decompose multiobjective optimization models for large-scale networks / B. Aslani, S. Mohebbi // arXiv preprint arXiv. – 2021. – P. 1906.07118. – Mode of access: https://doi.org/10.1111/itor.13169.
7. Comparative analysis of proactive and reactive routing protocols in VANET environment / [O. Sbayti, K. Housni, M. Hicham Hanin, A. El Makrani] // International Journal of Electrical and Computer Engineering (IJECE). – 2023. – Vol. 13(5). – P. 5374–5387. Mode of access: https://doi.org/10.11591/ijece.v13i5.pp5374-5387.
8. Ride-hailing and transit accessibility considering the trade-off between time and money / [H. Rafael, M. Pereira, D. Herszenhut et al.] // Cities. – 2024. – Vol. 144. – P. 104663. – Mode of access: https://doi.org/10.1016/j.cities.2023.104663
9. Baptista D. Convergence properties of optimal transport-based temporal networks / D. Baptista, C. De Bacco // arXiv preprint arXiv. – 2021. – Mode of access: https://doi.org/10.1007/978-3-030-93409-5_48
10. Wen W. Research on Urban Road Network Evaluation Based on Fractal Analysis / W. Wen, W. Zhang, H. Deng // Journal of Advanced Transportation. – 2023. – P. 1–8. – Mode of access: https://doi.org/10.1155/2023/9938001.
11. Choi J. Analyzing and Improving Optimal-Transport-based Adversarial Networks / J. Choi, M. Kang // arXiv:2310.02611. – 2023. – Mode of access: https://doi.org/10.48550/arXiv.2310.02611.
12. VANET (Vehicular Ad-hoc Network) [Electronic resource]. – Access mode: https://en.wikipedia.org/wiki/Vehicular_ad-hoc_network (access date: 11.12.2024). – Title from the screen.
13. AODV (Ad-hoc On-Demand Distance Vector routing) [Electronic resource]. – Access mode: https://en.wikipedia.org/wiki/Ad-hoc_On-Demand_Distance_Vector_routing (access date: 11.12.2024). – Title from the screen.
14. DSDV (Destination-Sequenced Distance Vector routing) [Electronic resource]. – Access mode: https://en.wikipedia.org/wiki/Destination-Sequenced_Distance_Vector_routing (access date: 11.12.2024). – Title from the screen.
15. OLSR (Optimized Link State Routing) [Electronic resource]. – Access mode: https://en.wikipedia.org/wiki/Optimized_Link_State_Routing_Protocol (access date: 11.12.2024). – Title from the screen.
16. Yang X.-S. Nature-Inspired Algorithms in Optimization: Introduction, Hybridization and Insights / X.-S. Yang // arXiv:2401.00976. – 2023. – Mode of access: https://doi.org/10.1007/978-981-99-3970-1.
17. Advances in Slime Mould Algorithm: A Comprehensive Survey / [Y. Wei, Z. Othman, K. Mohd Daud et al.], // Biomimetics. – 2024. – Vol. 9. – P. 31. – Mode of access: https://doi.org/10.3390/biomimetics9010031.
18. Bellman-Ford Algorithm [Electronic resource]. – Access mode: https://brilliant.org/wiki/bellman-ford-algorithm (access date: 11.12.2024). – Title from the screen.
19. A* Algorithm [Electronic resource]. – Access mode: https://en.wikipedia.org/wiki/A*_search_algorithm (access date: 11.12.2024). – Title from the screen.
20. Network flow problem [Electronic resource]. – Access mode: https://en.wikipedia.org/wiki/Network_flow_problem (access date: 11.12.2024). – Title from the screen.
21. Network flow problem, Ford–Fulkerson algorithm [Electronic resource]. – Access mode: https://www.networkflowalgs.com/book.pdf (access date: 11.12.2024). – Title from the screen.
22. Wagdy A. Gaining-sharing knowledge based algorithm for solving optimization problems: a novel nature-inspired algorithm / A. Wagdy, A. A Hadi, A. Khater // International Journal of Machine Learning and Cybernetics. – 2023. – Mode of access: https://doi.org/10.1007/s13042-019-01053-x.
23. SlimeMould [Electronic resource]. – Access mode: https://github.com/MoeBuTa/SlimeMould (access date: 11.12.2024). – Title from the screen.
24. Boyko N. Aspects of the study of genetic algorithms and mechanisms for their optimization for the travelling salesman problem / N. Boyko, A. Pytel // International Journal of Computing. – 2021. – Vol. 20(4). – P. 543–550. – Mode of access: https://doi.org/10.47839/ijc.20.4.2442.
25. Vyklyuk Ya. GeoCity – a New Dynamic-Spatial Model of Urban Ecosystem / Ya. Vyklyuk, D. Nevinskyi, N. Boyko // J. Geogr. Inst. Cvijic. – 2023. – Vol. 73(2). – P. 187–203. – Mode of access: https://doi.org/10.2298/IJGI2302187V

DOI 10.15588/1607-3274-2025-2-16

UDC 004.023

OPTIMIZATION BASED ON FLOWER CUTTING HEURISTICS FOR SPACE ALLOCATION PROBLEM

Czerniachowska K. S. – PhD, Lecturer, Department of Process Management, Wroclaw University of Economics and Business, Wroclaw, Poland.

Subbotin S. A. – Dr. Sc., Professor, Head of the Department of Software Tools, National University "Zaporizhzhia Polytechnic", Zaporizhzhia, Ukraine.

ABSTRACT

Context. This research discusses the shelf space allocation problem with vertical and horizontal product categorization, which also includes the products of general and brand assortment as well as products with different storage conditions stored on different shelves and incompatible products stored on the same shelf but no nearby.

Objective. The goal is to maximize the profit, product movement, or sales after allocating products on store shelves, defining the shelf for the product and the number of stock-keeping units it has.

Method. The research proposes the two variants of heuristics with different sorting rules inside utilized as an approach to solving the retail shelf space allocation problem with horizontal and vertical product categorization. It also covers the application of 13 developed steering parameters dedicated to instances of different sizes, which allows to obtain cost-effective solutions of high quality.

Results. The results obtained by heuristics were compared to the optimal solutions given by the commercial CPLEX solver. The effectiveness of the proposed heuristics and the suitability of the control settings were demonstrated by their ability to significantly reduce the number of possible solutions while still achieving the desired outcomes. Both heuristics consistently produced solutions with a quality surpassing 99.80% for heuristic H1 and 99.98% for heuristic H2. Heuristics H1 found 12 optimal solutions, and heuristics H2 found 14 optimal solutions among 15 test instances – highlighting their reliability and efficiency.

Conclusions. The specifics of the investigated model can be used by supermarkets, apparel stores, and electronics retailers. By following the explained heuristics stages and the methods of parameter adjustments, the distributor can systematically develop, refine, and deploy a heuristic algorithm that effectively addresses the shelf space allocation problems at hand while being robust and scalable.

KEYWORDS: heuristics, shelf space allocation, knapsack problem, decision-making/process.

ABBREVIATIONS

SSAP is a shelf space allocation problem;
SKU is a stock-keeping unit.

NOMENCLATURE

S is a total number of shelves;
P is a total number of products;
K is a total number of categories;
T is a total number of tags;
i, a, b are shelf indexes;
j, c, d are product indexes;
k is a category index;
t is a tag index;
r is an orientation index.

Parameters of the shelf i:

s_i^l is a shelf length;

s_i^h is a shelf height;

s_i^d is a shelf depth;

s_{ti}^g is a shelf binary tag t.

Parameters of the product j:

p_j^w is a product width;

p_j^h is a product height;

p_j^d is a product depth;

p_j^u is a product unit movement/profit;

p_{tj}^t is a product tag t;

p_j^k is a product category;

p_j^s is a group of products for separate storage (not on the same shelf);

p_j^n is a group of incompatible products (must be allocated on the same shelf but not side by side);

p_{jr}^o is a product orientation binary parameter;

$f_j^{\min}$, $f_j^{\max}$ are minimum and maximum numbers of SKUs;

$s_j^{\min}$, $s_j^{\max}$ are minimum and maximum numbers of shelves for allocation of the product;

p_j^l is a limitation of the product in the warehouse;

Additional product parameters expressions:

p_{jr}^w is a product width considering orientation;

p_{jr}^d is a product depth considering orientation;

p_{jr}^h is a product height considering orientation;

Parameters of the category k:

c_k^m is a minimum category size as a percentage of the shelf length;

c_k^t is a category size tolerance between shelves in the category as a percentage of the shelf length.

Parameters of the tag t:

b_t^n is a tag type;

DOI 10.15588/1607-3274-2025-2-17

b_{ij}^{t} is a product to shelf compatibility tag;

x_{ijr} is a product placement binary variable;

f_{ijr} is a number of SKUs of the product j on the shelf i on orientation r.

INTRODUCTION

The retailer SSAP involves determining how to optimally distribute available shelf space across different products in a retail environment. The problem is often critical to improving product visibility, sales, and customer satisfaction, as shelf space directly influences purchase behaviour. When considering vertical and horizontal product categorization, this problem becomes more complex and requires strategic decision-making. In this research, we investigate the SSAP with simultaneous vertical and horizontal categorization.

Vertical categorization refers to how products are arranged within each category (i.e., the layout of products in a column or row vertically on the shelf). This could involve stacking products on shelves based on brand, price range, size, or sales frequency, where products within the same category are placed in a vertical alignment. Example: On a shelf dedicated to soft drinks, Coca-Cola might be placed above Pepsi, with smaller bottles at the top and larger ones at the bottom.

Horizontal categorization refers to how different product categories are distributed across the entire shelf space, where each category (such as beverages, snacks, cleaning products, etc.) gets a designated portion of the shelf. Products within each category are then placed horizontally within their allotted space. Example: One horizontal section of the shelf could be dedicated to beverages, another to snacks, and another to cleaning supplies.

Both the retailer and the consumer can gain a number of important advantages from the obvious horizontal and vertical grouping of general assortment and high-end brands on store shelves. The purchasing experience is more efficient, well-organized, and straightforward thanks to these classifications. These are the main advantages:

1. Enhanced shopping experience.

Effortless navigation: Based on their requirements, tastes, or budgets, customers can find products with ease. Customers can more easily locate particular product classes, including “general” or “luxury” items, thanks to horizontal and vertical categorization, without becoming overwhelmed by a sloppy display.

Clear product segmentation: Grouping products logically helps shoppers understand what’s available and where to look for what they need, making their shopping experience more enjoyable and less stressful.

2. Helpful comparison.

Fast price and feature comparison: Customers may quickly compare various goods based on features, quality, or price by grouping premium brands and general selection into areas that are clearly defined. Customers can compare similar products within their price range, for example, by distinguishing brands with lower and higher prices.

Evident visual indications for decision-making: By placing premium brands at eye level or on higher shelves, for example, visual cues can gently nudge consumers toward more expensive items, while more accessible displays of less expensive items can aid in their decision-making.

3. Increased sales and conversion rates.

Up-selling and cross-selling opportunities: Clear distinctions between general assortment and expensive brands enable upselling opportunities. Shoppers interested in a mid-tier product might be persuaded to consider a more expensive version once they see the differences in product quality or features.

Impulse purchases: When expensive brands are clearly separated but still prominently displayed, customers may be enticed to make purchases they hadn’t initially planned for, especially if they perceive the products to be of higher quality or status.

4. A higher level of brand awareness.

Premium brand setting up: Clearly positioned vertically or horizontally at eye level or in high-traffic locations is advantageous for premium or luxury companies. This raises its profile and strengthens the brand’s exclusivity and prestige, setting it apart from the more generic collection items.

Tactical shelf placement: Brands may make sure that their items are positioned in high-visibility areas where they are more likely to be discovered and, consequently, increase the likelihood of purchase by employing vertical or horizontal categorization.

5. Better stock management.

Streamlined inventory control: Categorizing products into clear sections makes it easier for retailers to manage stock levels and ensure that shelves are adequately stocked. Retailers can identify popular price segments and adjust their inventory accordingly, reducing the chances of stockouts or overstocking.

Efficient restocking and display management: With a categorized system, store employees can quickly identify which products need to be restocked or repositioned, improving operational efficiency and ensuring a consistently appealing display.

6. Optimized space utilization.

Effective shelf management: Categorizing products effectively maximizes shelf space by ensuring products are grouped logically based on their characteristics. It reduces clutter and prevents overcrowding of certain product types, making the best use of available retail space.

Customized layouts: Retailers can experiment with different layouts of horizontal and vertical categorization to optimize space based on customer traffic flow and product demand.

7. Better customer targeting.

Appealing to different demographics: By clearly categorizing products, retailers can cater to a broader range of

DOI 10.15588/1607-3274-2025-2-17

customers, from budget-conscious shoppers to those looking for luxury items. The layout helps customers quickly identify products that match their buying intentions and budget, which can lead to higher satisfaction and loyalty.

Tailored marketing and promotions: Retailers can use shelf categorization to target specific customer segments with tailored promotions or discounts for specific product groups. For example, a store could highlight premium brands with exclusive offers or bundle general assortment items together to offer value deals.

8. Consistent branding and store identity.

Clear brand identity: Categorization ensures that each brand or product category is consistently presented in alignment with its image. For example, expensive brands might be placed in more elegant, sophisticated sections, while more budget-friendly brands could be organized in straightforward, no-frills sections. This enhances the overall atmosphere of the store and reinforces the store's identity.

Brand loyalty: Over time, customers will associate specific areas of the store with their favourite products or brands, leading to stronger brand loyalty. A consistent categorization system helps reinforce this connection by making it easier for customers to find their preferred brands quickly.

9. Competitive advantage.

Differentiation in the marketplace: A well-organized store with clear categorization of general assortment and premium products can set a retailer apart from competitors. It creates a more seamless and pleasant shopping experience, which can attract customers and positive word-of-mouth referrals.

Customer satisfaction: By providing customers with a clear, organized, and easy-to-navigate shopping environment, retailers can increase customer satisfaction, which ultimately drives higher retention rates and repeat business.

The main goal in solving the retailer SSAP is to optimize profits, sales or product movement while maintaining a balanced and accessible store layout. Retailers aim to:

– maximize product visibility: products that drive sales should be easily visible and accessible, which can lead to strategic vertical and horizontal placement;

– increase sales efficiency: allocating more shelf space to high-demand or high-margin items can increase the sales of those products while avoiding overstocking less popular items;

– enhance customer experience: a well-organized shelf helps customers find what they need quickly, increasing the likelihood of a purchase. Clear categorization and logical product positioning are keys to a satisfying shopping experience;

– minimize space wastage: proper categorization can avoid the underuse of space (e.g., leaving gaps on a shelf that could be used for additional products).

The object of study is the retailer shelf space allocation problem with simultaneous horizontal and vertical product categorization on the shelves. This problem can be framed as a linear programming or integer programming optimization problem. The objective function typically seeks to maximize sales, product movement or profit, subject to constraints related to shelf space availability, product demand, product compatibility (i.e., products that should be grouped together), product size and packaging.

The subject of study is the heuristics algorithms for maximizing profits or product movement when allocating products on the shelves and specifying the number of SKUs for each one. Some approaches to solving the problem include heuristic algorithms (such as genetic algorithms, simulated annealing, or greedy methods) for approximating optimal solutions and data-driven methods, where historical sales data and customer behaviour are used to inform decisions about product placement and space allocation.

The purpose of the work is to increase the speed and quality of solution generation by developing heuristics and introducing the tuning parameters which significantly reduce the solution space without violating the quality of the solution obtained.

1 PROBLEM STATEMENT

The model proposed in this study contrasts with the vertical product categorization models outlined in [1–3], which emphasize the need for separate storage of products on different shelves and the allocation of incompatible items on either the same or different shelves. Unlike these previous models [1–3], the current approach integrates a more flexible method of product arrangement, allowing for better optimization of shelf space. This model also considers the dynamic relationships between products, such as complementary separate storage and incompatible goods, to enhance sales and customer satisfaction. By refining how products are grouped and allocated, retailers can improve operational efficiency and increase consumer purchase behaviour.

The criteria function of the SSAP can be formulated as follows:

$$\max \sum_{i=1}^{S} \sum_{j=1}^{P} \sum_{r=0}^{2} p_j^u f_{ijr}, \quad (1)$$

Subject to:

$$\forall (i)[\sum_{j=1}^{P} \sum_{r=0}^{2} p_{jr}^w f_{ijr} \le s_i^w], \quad (2)$$

$$\forall (i,r,j : p_{jr}^h > s_i^h)[f_{ijr} = 0], \quad (3)$$

$$\forall (i,r,j : p_{jr}^d > s_i^d)[f_{ijr} = 0], \quad (4)$$

$$\forall (i,j,r)[x_{ijr} \le f_{ijr} \le f_j^{\max}], \quad (5)$$

$$\forall (i,j)[f_j^{\min} x_{ijr} \le \sum_{r=0}^{2} f_{ijr} \le f_j^{\max} x_{ijr}], \quad (6)$$

$$\forall (i,j,r)[x_{ijr} \le p_j^o], \quad (7)$$

$$\forall (i,j)[\sum_{r=0}^{2} x_{ijr} \le 1], \quad (8)$$

DOI 10.15588/1607-3274-2025-2-17

$$\forall(i)\forall(c,d: p_c^S = p_d^S, \quad c \neq d, \quad c,d = 1,...,P) \quad , \quad [\sum_{r=0}^{2} x_{icr} + \sum_{r=0}^{2} x_{idr} \leq 1] \tag{9}$$

$$\forall(i)\forall(a,b: p_a^n = p_b^n, \quad a,b = 1,...,P) \quad , \quad [\sum_{r=0}^{2} x_{iar} = \sum_{r=0}^{2} x_{ibr}] \tag{10}$$

$$\forall(k,i,c) \quad [\sum_{\substack{j=1,\\ p_j^k = k}}^{P} \sum_{r=0}^{2} x_{ijr} - \sum_{\substack{j=1,\\ p_j^n = c,\\ p_j^k = k}}^{P} \sum_{r=0}^{2} x_{ijr} \geq , \quad \geq \sum_{\substack{j=1,\\ p_j^n = c,\\ p_j^k = k}}^{P} \sum_{r=0}^{2} x_{ijr} - 1] \tag{11}$$

$$\forall(i,j,r)[\frac{s_i^w x_{ijr}}{p_{jr}^w} \geq f_{ijr}], \tag{12}$$

$$\forall(j)[s_j^{\min} \leq \sum_{i=1}^{S} \sum_{r=0}^{2} x_{ijr} \leq s_j^{\max}], \tag{13}$$

$$\forall(j)[\sum_{i=1}^{S} \sum_{r=0}^{2} f_{ijr} \leq p_j^l], \tag{14}$$

$$\forall(j)\forall(a,b: |a-b| \neq 1 \wedge a < b, \quad a,b = 1,...,S)\forall(r)[x_{ajr} + x_{bjr} \leq 1], \tag{15}$$

$$\forall(i,j)[\prod_{t=1}^{T} b_{tij}^t \geq \sum_{r=0}^{2} x_{ijr}], \tag{16}$$

$$\forall(i,k)[(\sum_{\substack{j=1,\\ p_j^k = k}}^{P} \sum_{r=0}^{2} p_{jr}^w f_{ijr} \geq \left\lceil s_i^l \cdot c_k^m \right\rceil) \vee (\sum_{\substack{j=1,\\ p_j^k = k}}^{P} \sum_{r=0}^{2} f_{ijr} = 0)] \quad , \tag{17}$$

$$\forall(k)[\max_{i=1,...,S} (\sum_{\substack{j=1,\\ p_j^k = k}}^{P} \sum_{r=0}^{2} p_{jr}^w f_{ijr}) - \min_{i=1,...,S} (\sum_{\substack{j=1,\\ p_j^k = k}}^{P} \sum_{r=0}^{2} p_{jr}^w f_{ijr}) \leq \left\lceil \max_{i=1,...,S} (s_i^l) \cdot c_k^t \right\rceil] \quad , \tag{18}$$

Decision variables:

$$\forall(i,j,r)[x_{ijr} \in \{0,1\}], \tag{19}$$

$$\forall(i,j,r)[f_{ijr} = \{f_j^{\min} ... f_j^{\max}\}], \tag{20}$$

The constraints signify the following. (2) – the total product width is within the shelf length. (3) – the product height must fit the shelf height. (4) – the product depth must fit the shelf depth. (5) – the product is placed on the shelf. (6) – minimum and maximum number of product SKUs must be within the limits. (7) – specific orientation (front, side, top) is possible for the product. (8) – only one specific orientation is possible is possible for the product. (9) –if products are required to be stored separately, they must be placed on different shelves. (10) – if products are marked as incompatible, they must be placed on the same shelf. (11) – if products are marked as incompatible products, they must not be placed nearby. (12) – product on-the-shelf placement and SKU relationships. (13) – minimum and maximum number of shelves on which the product may be placed. (14) – product storage limit if the product is placed on multiple shelves. (15) – if the product is placed on multiple shelves, the shelves must be allocated nearby. (16) – tags compatibility for the shelves and products must be satisfied. (17) – minimum category size if the products from the category are placed on the shelf must be satisfied. (18) – category size tolerance, i.e., products from the category, must possibly be evenly distributed on the shelves within the category.

There are two decision variables. (19) – the product is placed on the shelf. (20) – the number of product SKUs.

Binary variables could have the following values.

$$r = \begin{cases} 0, \text{ for front orientation} \\ 1, \text{ for side orientation} \\ 2, \text{ for top orientation} \end{cases};$$

$$s_{ti}^g = \begin{cases} 1, \text{ if shelf } i \text{ is tagged} \\ 0, \quad \text{otherwise} \end{cases};$$

$$p_{jr}^o = \begin{cases} 1, \text{ if specific orientation is available} \\ 0, \quad \text{otherwise} \end{cases};$$

$$p_{jr}^w = \begin{cases} p_j^w, \text{ if } r = 0, \text{ width for front orientation} \\ p_j^d, \text{ if } r = 1, \text{ depth for side orientation} \\ p_j^h, \text{ if } r = 2, \text{ height for top orientation} \end{cases};$$

$$p_{jr}^d = \begin{cases} p_j^d, \text{ if } r = 0, \text{ depth for front orientation} \\ p_j^w, \text{ if } r = 1, \text{ width for side orientation} \\ p_j^w, \text{ if } r = 2, \text{ width for top orientation} \end{cases};$$

$$p_{jr}^h = \begin{cases} p_j^h, \text{ if } r = 0, \text{ height for front orientation} \\ p_j^h, \text{ if } r = 1, \text{ height for side orientation} \\ p_j^d, \text{ if } r = 2, \text{ depth for top orientation} \end{cases};$$

$$b_{tij}^t = \begin{cases} 1, \text{ if } s_{ti}^t = p_{tj}^t \wedge b_t^n = \{H\} \\ 0, \quad \text{otherwise} \end{cases}, \text{ – for the horizontal,}$$

e.g. brand products level shelves;

$$b_{tij}^t = \begin{cases} \min(p_{tj}^t; 1) \wedge b_t^n = \{V^+\} \\ 1, \text{ if } p_{tj}^t = 1 \wedge s_{ti}^t = p_{tj}^t \wedge b_t^n = \{H^+\} \\ 0, \text{ if } p_{tj}^t = 1 \wedge s_{ti}^t \neq p_{tj}^t \wedge b_t^n = \{H^+\} \\ 1, \text{ if } p_{tj}^t = 0 \wedge b_t^n = \{H^+\} \end{cases}, \text{ – for the}$$

horizontal and vertical, e.g. general assortment shelves.

DOI 10.15588/1607-3274-2025-2-17

Binary product placement decision variable could have the following values.

$$x_{ijr} = \begin{cases} 1, \text{ if product } j \text{ is placed on shelf } i \\ \quad \text{on orientation } r \\ 0, \text{ otherwise} \end{cases}$$

2 REVIEW OF THE LITERATURE

Merchandising and retail literature discussed retail layout by shelf space management, which aims to identify the most profitable range of products and their resulting placement and space distribution on shelves. By analyzing consumer behaviour and purchasing patterns, researchers have identified that the strategic placement of products, considering factors such as visibility and accessibility, can significantly influence consumer decisions and ultimately drive higher revenue. Empirical research, such as [4] and [5] demonstrated that product exposure has a major impact on revenue and is contingent on the shelf location. The placement of products within prime shelf locations, such as eye-level or end-cap displays, can increase product exposure and lead to higher purchase rates, underscoring the critical role of shelf space allocation in retail profitability. Nevertheless, most models neglect to account for position visibility instead of focusing on product demand, space elasticity and cross-elasticity, and inventory management [6–10].

Some retailing research focuses on maximizing the visibility of products on shelves to encourage impulse buying, recognizing that consumer purchases can be strongly influenced by immediate, unplanned decisions [4–5, 11–13]. By strategically placing high-margin or attention-grabbing items in easily accessible and highly visible areas, retailers can create environments that prompt spontaneous purchases. This approach often involves techniques such as placing products near checkout counters, at eye level, or within frequent customer pathways to trigger impulse buying behaviours, ultimately boosting sales and enhancing store profitability.

There are some principles for marketing managers regarding the impulse purchase likelihood among different product categories with different customers' adjacency preferences. Locating the fish aisle next to the fruit and vegetables aisle would allow consumers to spend much time in the fruit aisle during the planning of their fish orders. The garment aisle and the cosmetics aisle should lay close together for female customers. Complementary packaged food aisles and lentils/oil aisles should lie next to each other [14].

A product's value has always been determined by the direct revenues it generates. However, rather than existing in isolation, products impact one another's sales. A large-scale product network is formed when products are frequently provided as a group of web pages connected by suggestion hyperlinks in e-commerce environments [15]. This relationship can be particularly seen in retail shelf space allocation, where products are often placed together based on complementary purchasing behaviour or category relevance. For instance, in brick-and-mortar stores, similar or complementary products are grouped to increase the likelihood of impulse buying and cross-selling, while in e-commerce environments, a product's value can also be influenced by its proximity to related items, as seen through suggestion hyperlinks or "customers also bought" recommendations. The dynamic nature of product networks, where products influence each other's visibility and purchase probability, emphasizes the importance of strategically allocating shelf space, both in physical stores and online, to maximize overall sales and optimize consumer purchasing patterns.

The goal for every retail store is to identify the most significant differences between substitutable and complementary products which will influence customers' buying behaviour or purchase decisions. Substitutable products are those that can be easily replaced by alternatives, and their placement on shelves should be strategically positioned to highlight price or quality comparisons, driving consumers toward their preferred choice. In contrast, complementary products are those that are often purchased together, and their placement near each other encourages bundling or cross-selling, which can increase the overall value of the transaction. By carefully analyzing these differences, retailers can make informed decisions about shelf space allocation, ultimately enhancing the shopping experience and maximizing sales opportunities.

Under the overall store layout, it is important to decide which types of products can be positioned next to each other. This is where the concepts of space distribution and space layout are interconnected. A store layout would provide the buyer with logic while allowing the retailer to accomplish his/her own goals in terms of introducing the store to customers to as much of the merchandise variety as possible and increasing the importance of each customer's purchase [16].

In [17] the authors conducted research that examined the relationship between consumer preferences for specific product brands and future product demand. They focused on how these preferences influenced decisions regarding the allocation of shelf space in retail stores. Their study suggested that retailers should consider consumer brand choice as a key factor when determining the optimal amount of shelf space for different products. This was critical for ensuring that high-demand products were readily available and visible to consumers, potentially leading to increased sales [17]. Later, another authors in [18] introduced an improved model that built upon work in [17] by incorporating the cost effect. Their model addressed the need for a more balanced approach, taking into account not only consumer demand but also the costs associated with stocking and displaying various products on store shelves [18].

However, for the buying association between items, customer behaviours/patterns for product-to-shelf assignment issues should be considered. When shopping in a supermarket, the customer walks through the store's aisles, pauses at some locations, explores his or her considerations, and selects the best choices. This process continues until the entire shopping trip is completed [19].

DOI 10.15588/1607-3274-2025-2-17

Merchandising and retail shelf space studies emphasize the importance of efficient shelf space management to enhance product visibility and optimize sales performance [20–23].

3 MATERIALS AND METHODS

In the given research, we introduce novel flower-cutting heuristics aimed at addressing the difficulties identified in the retail SSAP studies we analyzed. Our approach includes two distinct heuristic variants, each characterized by a particular sorting sequence for allocation. These variants offer different methods for prioritizing the allocation process, allowing for greater flexibility in handling various problem scenarios. By incorporating these innovative sorting strategies, our methodology enhances the efficiency and effectiveness of flower-cutting heuristics solutions, contributing to improved outcomes in SSAP-related challenges. The two heuristics present alternative ways to optimize the process based on differing allocation priorities, ensuring better adaptability to different sets of constraints.

A series of numbers, which we call in the research as the shelf allocation, indicates whether a product is put on the shelf or not. One can arrange items on the shelf in one of three ways: top-facing (0/3), side-facing (0/2) or front-facing (0/1). Products are oriented on the shelf according to the coding system. When the value is zero, the product is not put on the shelf. A series of numbers, which we call in the research as the product allocation, indicates how many SKUs are placed on the shelf.

The following step-by-step instructions outline the general structure of the new flower-cutting heuristic, highlighting how tuning and sorting strategies can influence the shelf and product allocation process and lead to an efficient solution for the investigated SSAP problem.

Stage 1. Problem initialization. Define the SSAP by categorization, including the number of shelves, products, and product categories to which these products belong. Set up any constraints and requirements for the allocation on the shelves. Establish success indicators.

Stage 2. Allocation principles. Preparing the garden: set up the necessary input parameters to define the garden, which represents a complex solution space. In this metaphor, flowers of varying heights and bud sizes, along with different flower densities in different areas, symbolize diverse solutions to explore. Each flower represents a potential solution, and the gardener must prepare to navigate this environment for effective problem-solving. Identifying flower clearings: create solutions focusing on specific areas of the garden. It selects clearings that are most likely to yield optimal results based on predefined criteria. By narrowing the search area, the heuristic improves efficiency. Inside the selected clearing, many flowers may grow, so the gardener must establish rules to focus only on certain flowers, further narrowing the solution space. Picking the flowers: Solutions are generated using specific criteria, sorting order, and interval parameters for a systematic approach. The proposed method, like a gardener, selects flowers from the chosen clearings, leaving others to grow according to defined parameters to improve accuracy and efficiency.

Stage 3. Allocation parameters. The Gardener's movement path length optimizes the distance travelled by the gardener, aiming to gather the most high-quality flowers while reducing unnecessary movement. Target flower height sets the minimum height for flowers to be picked, focusing on taller, more profitable blooms. Target flower spacing interval controls the distance between cut flowers in a patch, ensuring the gardener skips some flowers to avoid cutting too many in the same area, optimizing the selection of high-value flowers. Gardener's basket size limits the number of flowers picked in one trip, emphasizing quality over quantity by prioritizing the largest, most valuable flowers.

Stage 4. Parameters of performance tuning.

Parameters of flower clearing cultivation. Parameter 1 – the minimum number of products that can be allocated on the shelf while generating product allocations. Parameter 2 – the maximum number of products that can be allocated on the shelf while generating product allocations. Parameter 3 – the set of profitable groups of products to be allocated on the shelf.

Parameters for travelling through the chosen flower clearings. Parameter 4 – the minimum category width after forming product allocations. Parameter 5 – the maximum category width after forming product allocations. Parameter 6 – if the grouping option (for each total width, only 1 product allocation with the maximum total profit) is generated. Parameter 7 – the maximum number of product allocations on the shelf according to the sorting order. Parameter 8 – the maximum number of product allocations of the category prioritized according to the variant of profitability.

For these paremeters we define sortung rules.

Sorting rule 7.1: category width ↑, category profit ↓ – this prioritizes narrower product allocations that give high profit.

Sorting rule 7.2: category profit ↓, category width ↑ – this prioritizes profitable product allocations that allocate less shelf space.

Sorting rule 8.1: profit ↓, profit ratio ↓. Sorting rule 8.2: profit ratio ↓, profit ↓.

Parameters for the interval between cut flowers on the chosen clearings. Parameter 9 – the interval of taking the product allocations on the shelf after taking all product allocations according to parameter 7. Parameter 10 – the maximum number of product allocations on the shelf created with the interval parameter 9, the sorting rule is the same as in parameter 7. Parameter 11 – the interval of taking the product allocations of the category after taking all product allocations according to parameter 8. Parameter 12 – the maximum number of product allocations of the category created with the interval parameter 11; the sorting rule is the same as in parameter 8.

Parameter of the flowers to be selected to the gardener's basket. Parameter 13 – the minimum profit for each category.

DOI 10.15588/1607-3274-2025-2-17

Stage 5. Constraint checking and adjustment. After each allocation step, verify if the allocation adheres to all provided constraints. Do not generate allocations with violation of constraints required to be re-allocated or adjusted to maintain feasibility (generate only appropriate product allocations checking constraints in earlier steps).

Stage 6. Optimization step. The selection approach continuously refines solutions by not focusing on similar ones and cutting only the flowers that meet the value criteria. It maximizes profitability while optimizing resource use, reducing the gardener's time and preventing the basket from being overfilled. If applicable, apply a tuning or improvement of input parameters to fine-tune the generation of product allocations and re-run the solution-obtaining procedure from the beginning.

Stage 7. Termination criteria. The algorithm terminates once all products have been allocated on the shelves, all constraints have been satisfied and the gardener basket is filled up with a set of high-quality flowers (solutions).

Stage 8. Final allocation output. Return the final allocation plan – the biggest flower from the gardener's basket – which includes the optimal or near-optimal allocation of products along the shelves based on the chosen heuristic variant.

The flower garden scenario is depicted in Figure 1, with particular attention paid to the flower clearing where flowers – which stand in for possible solutions – are growing. In the actual solution space, there could be more than one number of the garden's chosen parts of the garden to be explored. Above a certain initial height threshold, flowers are cut and arranged in the basket, defining the flower clearing. Like in the actual world, not all of the flowers in this particular clearing have been cut; instead, there is some space between them. Depending on the clearing, there may be variations in the height thresholds, widths, and flower intervals. Even if flowers in other clearings are higher than the thresholds of the chosen clearing, they are not taken into consideration. Therefore, the selection of appropriate clearings steered by the tuning parameters is needed. Finding and choosing the clearings with the largest blooms is the goal, making sure that no lucrative clearing is missed. The gardener's duty is unaffected by the distances between the chosen flower clearings. Only the chosen clearings where the gardener cuts flowers are used to determine how long it takes the algorithm to generate and choose solutions to be verified.

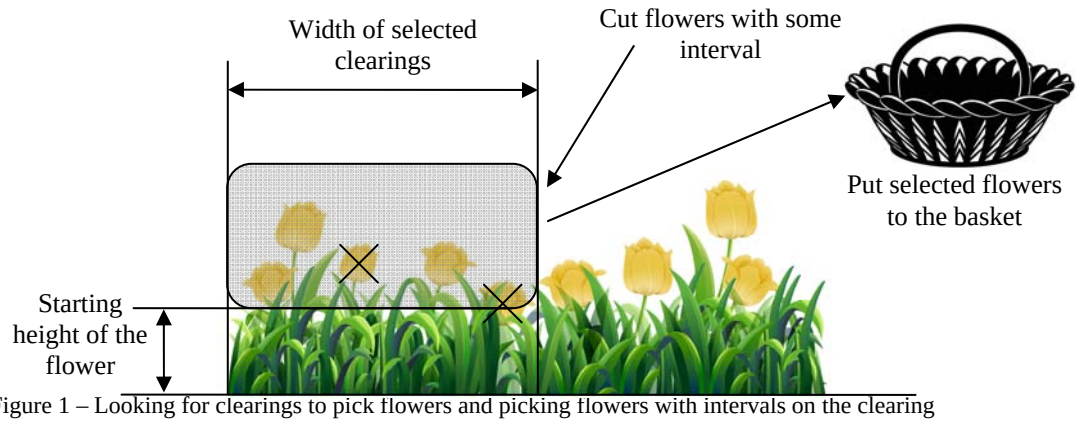

Figure 1 – Looking for clearings to pick flowers and picking flowers with intervals on the clearing

4 EXPERIMENTS

The computer program implementing the proposed heuristics was developed. The experiment was conducted on a personal computer with the following technical characteristics. Processor: AMD Ryzen 5 1600 Six-Core Processor 3.20 GHz. System type: 64-bit Operation System, x64-based processor. RAM: 16 GB. Operation system: Windows 10

There were three sets of products prepared. In each set, there were 10, 15, 20 products that needed to be placed on four shelf racks measured by different lengths of shelf: 250, 375, 500, 625, and 750 cm. The products in each set differed with the range of parameters such as dimensions, including height, depth, width, and movement/profit.

In order to define distinct category areas for product distribution on the rack, two vertical category partitions were made for product sets. Making the best use of shelf space by efficiently arranging the products within the categories in the rack was the aim of this problem.

The experimental design incorporated a range of retail constraints, allowing for a comprehensive analysis of the heuristics' performance under varied conditions. Through the use of different testing scenarios, the study highlighted the adaptability of the heuristics when dealing with fluctuating parameters and complex problem settings. By varying the input data across multiple test cases, the experiments provided critical data on the heuristics' efficiency, shedding light on their strengths and areas for improvement.

The testing methodology was meticulously crafted to ensure that the heuristics could be evaluated against both small-scale and large-scale problems, providing a well-rounded assessment. The integration of diverse configurations into the experiment enabled a deep dive into the heuristics' behaviour, ensuring their relevance and applicability to a wide range of practical shelf space allocation problems.

Table 1 illustrates the heuristic settings used in the test examples experiment. For small instances with 10 prod-

DOI 10.15588/1607-3274-2025-2-17

ucts, one parameter was applied. To reduce the solution space, all 13 parameters were used for larger instances (20 products). Medium instances with 15 products utilized 10 parameters. Both heuristic strategies employed the same input parameters to minimize the solution space.

Table 1 – The set of parameters used in the test instances

Tuning parameter	Number of products		
	10	15	20
Parameter 1	–	–	●
Parameter 2	–	–	●
Parameter 3	–	–	●
Parameter 4	–	●	●
Parameter 5	–	●	●
Parameter 6	–	●	●
Parameter 7	–	●	●
Parameter 8	–	●	●
Parameter 9	–	●	●
Parameter 10	–	●	●
Parameter 11	–	●	●
Parameter 12	–	●	●
Parameter 13	●	●	●

5 RESULTS

Table 2 compares the performance of two newly introduced heuristics, H1 and H2, with the best results achieved by the commercial CPLEX solver. This comparison spans multiple test cases and focuses on the profit ratio, which indicates the proportion of profit generated by the heuristics relative to the optimal profit determined by CPLEX. For each heuristic and test case, the profit ratio was calculated to assess how closely the heuristics approximated the optimal solutions.

The analysis provides valuable insights into the effectiveness of the heuristics in solving the problem. By examining the profit ratio across different test cases, the evaluation shows how well H1 and H2 perform compared to the commercial solver. This approach offers a clear measure of the heuristics' performance in real-world applications. Additionally, the table presents the solution time for each heuristic test case, offering a comprehensive view of both the efficiency and accuracy of the methods.

Table 3 illustrates the impact of adding parameters 7–12 to reduce the solution space. For the smallest example (a set of 10 products), an assessment of product allocations without parameters, these parameters were provided and all produced product allocations were evaluated. Therefore, there is no information about them in this table. The percentages in Table 2 illustrate the ratio between the evaluated solutions and those that were obtained following the application of the prior reduction parameters. This implies that just a portion of the solutions were evaluated even after the solution space reduction parameters were applied.

Parameter 6 (the grouping option) was applied to 15 and 20 product sets instances except for the smallest 10 products one, after which parameter 7 was applied also to these two product sets. After all product allocations on the shelf specified by parameter 7 were taken, the interval of taking the product allocations on the shelf (parameter 9) was set to 2, and a number of product allocations specified by parameter 10 were taken. The number of product allocations taken with interval (parameter 10) was significantly less compared to the previous number of product allocations (parameter 7) because the quality of them is lower.

Table 3 also illustrates the impact of reducing the solution space by utilizing category parameters 8, 12. After all product allocations generated for the category specified by parameter 8 were taken, the interval of taking the product allocations for the category (parameter 11) was set to 2, and a number of product allocations specified by parameter 12 were taken. The number of product allocations taken with interval (parameter 12) was significantly less compared to the previous number of product allocations (parameter 8) because the quality of them is lower.

Table 4 describes the values chosen for reduction parameters 4 and 5, which represent the minimum and maximum category widths once product allocations are formed.

After determining the potential product allocations on each shelf, the average category width may be calculated. Even though the precise product allocations that will be selected for the final solution are unknown, they still enable the estimation of category width and profit.

Parameter 4, which determines the minimum category width after product allocations are formed, has one value set. This value is compared to the average category width of the product allocations and the shelf width to ensure accuracy.

A percentage of the shelf width is used to represent parameter 5, or the maximum category width. Additionally, it contrasted with the average shelf width and category width of the product allocations. The mentioned parameters were not applied to the 10-product instances, therefore there is no information about them in Table 4.

Table 4 also shows the results of determining values for the category profit parameter 13. All instances used this parameter for reducing the solution space.

Table 5 displays the number of product allocations and solutions generated by heuristics H1 and H2. These allocations yielded solutions or product allocations that satisfy all criteria.

Constraint violations, however, can make it impossible to develop a solution if insufficient product allocations are looked at. When the option with the largest overall profit was selected from the group of possibilities, the main goal was accomplished. Because of the specific criteria used in each heuristic, heuristics H1 and H2 yield different numbers of solutions even though they use the same steering settings. The number of product allocations employed in both techniques was the same.

The total number of shelf allocations in a general case is $(r+1)^{PS} = 4^{PS}$.

The number 4 signifies the various ways a product can be allocated: (1) not displayed on the shelf, (2) displayed on the shelf facing forward, (3) displayed on the shelf sideways, and (4) displayed on the shelf from the top.

DOI 10.15588/1607-3274-2025-2-17

Table 2 – Performance of the developed heuristics

Products	Shelf width	Profit ratio of H1	Profit ratio of H2	Time of H1, minutes	Time of H2, minutes	Time of CPLEX, s
10	250	100.00%	100.00%	0.06	0.08	0.44
	375	100.00%	100.00%	0.11	0.17	0.59
	500	100.00%	100.00%	1.51	1.49	0.45
	625	100.00%	100.00%	0.60	0.56	0.78
	750	100.00%	100.00%	0.58	0.60	0.36
15	250	100.00%	99.98%	0.48	3.28	0.56
	375	99.80%	100.00%	1.15	18.74	0.75
	500	100.00%	100.00%	1.01	17.74	0.86
	625	100.00%	100.00%	1.57	1.40	0.78
	750	100.00%	100.00%	1.65	1.65	0.81
20	250	99.94%	100.00%	0.67	0.66	1.08
	375	100.00%	100.00%	1.85	1.86	1.38
	500	100.00%	100.00%	1.33	1.54	0.84
	625	99.88%	100.00%	1.27	1.27	1.20
	750	100.00%	100.00%	2.93	4.36	0.86
Minimum		99.80%	99.98%	0.06	0.08	0.36
Average		99.97%	100.00%	1.12	3.69	0.78
Maximum		100.00%	100.00%	2.93	18.74	1.38

Table 3 – The usage of the maximum number of product allocations on the shelf (Parameters 7, 10) and for the category (Parameters 8, 12) for heuristics H1 and H2

		Checked allocations on shelves (parameter 7)			Checked allocations on shelves with intervals (parameter 10)			Checked allocations for categories (parameter 8)		Checked allocations for categories with interval (parameter 12)	
Products	Shelf width	Shelf 2	Shelf 3	Shelf 4	Shelf 2	Shelf 3	Shelf 4	Category 1	Category 2	Category 1	Category 2
15	250	57.37%	100.00%	100.00%	1.25%	10.03%	2.58%	2.74%	22.59%	0.34%	2.82%
	375	10.00%	80.24%	20.67%	0.42%	3.66%	0.81%	6.37%	21.26%	0.29%	0.97%
	500	3.76%	32.97%	7.25%	0.18%	1.65%	0.34%	6.12%	37.71%	0.51%	3.14%
	625	2.75%	24.82%	5.10%	0.09%	0.85%	0.17%	13.18%	100.00%	0.94%	
	750	1.88%	16.92%	3.36%	1.02%	1.67%	3.08%	7.11%	37.03%	0.51%	2.64%
20	250	10.25%	13.35%	27.73%	0.16%	0.26%	0.36%	100.00%	46.60%		1.94%
	375	1.57%	1.85%	2.55%	0.40%	0.69%	1.16%	100.00%	100.00%		
	500	3.98%	6.88%	11.63%	0.07%	0.17%	0.09%	20.06%	67.04%	1.43%	2.79%
	625	0.72%	1.71%	0.90%	0.01%	0.03%	0.01%	100.00%	31.80%		1.77%
	750	0.11%	0.31%	0.14%	1.25%	10.03%	2.58%	100.00%	74.37%		7.44%
Minimum		0.11%	0.31%	0.14%	0.01%	0.03%	0.01%	2.74%	21.26%	0.29%	0.97%
Average		39.49%	51.94%	45.29%	0.93%	2.11%	0.96%	63.71%	69.23%	0.67%	2.94%
Maximum		100.00%	100.00%	100.00%	5.74%	10.03%	3.08%	100.00%	100.00%	1.43%	7.44%

Table 4 – The usage of the minimum and maximum width after forming product allocations (parameters 4 and 5) and usage of the minimum category profit (parameter 13)

Products	Shelf width	Minimum width of the category compared to the average category width of product allocations (parameter 4)		Minimum width of the category compared to the shelf width (parameter 4)		Maximum width of the category compared to the average category width of product allocations (parameter 5)		Maximum width of the category compared to the shelf width (parameter 5)		Minimum profit of the category compared to the average category profit of product allocations (parameter 13)	
		Cat. 1	Cat. 2	Cat. 1	Cat. 2	Cat. 1	Cat. 2	Cat. 1	Cat. 2	Cat. 1	Cat. 2
10	250	–	–	–	–	–	–	–	–	107%	31%
	375	–	–	–	–	–	–	–	–	87%	108%
	500	–	–	–	–	–	–	–	–	80%	80%
	625	–	–	–	–	–	–	–	–	73%	108%
	750	–	–	–	–	–	–	–	–	98%	92%
15	250	80%	47%	44%	26%	124%	95%	68%	52%	141%	61%
	375	83%	63%	45%	35%	112%	107%	61%	59%	131%	87%
	500	78%	73%	43%	40%	93%	106%	51%	58%	112%	102%
	625	111%	44%	61%	24%	138%	70%	75%	38%	149%	73%
	750	110%	61%	60%	33%	125%	77%	68%	42%	143%	74%
20	250	96%	46%	54%	26%	129%	79%	72%	44%	165%	24%
	375	106%	53%	59%	29%	135%	70%	75%	39%	158%	31%
	500	116%	52%	62%	28%	134%	75%	72%	40%	164%	37%
	625	119%	58%	62%	30%	138%	76%	72%	40%	165%	43%
	750	102%	83%	52%	43%	117%	92%	60%	47%	150%	62%
Minimum		78%	44%	43%	24%	93%	70%	51%	38%	73%	24%
Average		100%	58%	54%	31%	150%	124%	78%	64%	128%	67%
Maximum		119%	83%	62%	43%	212%	212%	100%	100%	165%	108%

DOI 10.15588/1607-3274-2025-2-17

Table 5 – Numbers of generated product allocations and solutions in heuristics H1, H2

Products	Shelf width	Number of generated product allocations to be checked	Number of solutions H1	Number of solutions H2
10	250	$6.17 \cdot 10^5$	$5.96 \cdot 10^4$	$5.96 \cdot 10^4$
	375	$3.67 \cdot 10^6$	$9.31 \cdot 10^4$	$9.31 \cdot 10^4$
	500	$9.59 \cdot 10^6$	$1.31 \cdot 10^6$	$1.31 \cdot 10^6$
	625	$2.51 \cdot 10^6$	$5.18 \cdot 10^5$	$5.18 \cdot 10^5$
	750	$5.27 \cdot 10^5$	$5.20 \cdot 10^5$	$5.20 \cdot 10^5$
15	250	$2.58 \cdot 10^9$	$2.10 \cdot 10^2$	$1.49 \cdot 10^6$
	375	$8.93 \cdot 10^9$	$6.64 \cdot 10^2$	$1.06 \cdot 10^7$
	500	$1.56 \cdot 10^9$	$3.51 \cdot 10^5$	$1.02 \cdot 10^7$
	625	$3.10 \cdot 10^8$	$7.31 \cdot 10^4$	$7.70 \cdot 10^4$
	750	$1.86 \cdot 10^9$	$1.15 \cdot 10^4$	$4.81 \cdot 10^4$
20	250	$2.12 \cdot 10^7$	$1.80 \cdot 10^1$	$3.05 \cdot 10^2$
	375	$2.86 \cdot 10^7$	$1.00 \cdot 10^2$	$1.00 \cdot 10^2$
	500	$6.25 \cdot 10^8$	$3.60 \cdot 10^3$	$1.14 \cdot 10^5$
	625	$2.23 \cdot 10^7$	$2.00 \cdot 10^0$	$2.70 \cdot 10^3$
	750	$2.71 \cdot 10^6$	$9.29 \cdot 10^4$	$1.20 \cdot 10^5$
Minimum		$5.27 \cdot 10^5$	$2.00 \cdot 10^0$	$1.00 \cdot 10^2$
Average		$1.06 \cdot 10^9$	$2.02 \cdot 10^5$	$1.67 \cdot 10^6$
Maximum		$8.93 \cdot 10^9$	$1.31 \cdot 10^6$	$1.06 \cdot 10^7$

Each product has the option to be placed in only one among the available orientations based on the product package. The total number of product allocation possibilities for any set of products can be determined using formula

$$\prod_{j=1}^{P} (f_j^{\max} - f_j^{\min} + 1)^S .$$

Additionally, this calculation accounts for every potential positioning choice for each product. Therefore, as the number of products increases, the number of possible allocations grows.

Table 6 displays the number of possible shelf and product allocations in the general scenario, which corresponds to the entire solution space as calculated by the previously given equations. However, Table 5 shows a significant difference between the number of shelf and product allocations produced by heuristics H1 and H2.

Table 6 – Numbers of all possible shelf and product allocations in the general case

Products	Number of shelf allocations	Number of product allocations
10	$1.21 \cdot 10^{24}$	$1.10 \cdot 10^{52}$
15	$1.33 \cdot 10^{36}$	$1.15 \cdot 10^{78}$
20	$1.46 \cdot 10^{48}$	$1.21 \cdot 10^{104}$

This illustrates how employing heuristic rules with steering parameters is both very valid and useful. These instinctive rules are very logical and useful for directing decision-making. They are strong problem-solving tools that use logical thinking and real-world insights to successfully negotiate challenging situations. They are effective problem-solving tools that successfully navigate difficult circumstances by applying reasoned reasoning and practical insights.

6 DISCUSSION

The proposed flower-picking heuristics provides the following key advantages.

– enhanced problem handling. The heuristic's category-based approach enables it to tackle complex problems more efficiently by focusing on relevant groups of items, reducing the complexity compared to individual item processing. This method allows for better optimization of space and resources in retail stores or other structured environments;

– customizable parameter settings. The pre-solution investigation allows the heuristic to customize its parameter settings based on the problem's specific characteristics. This adaptability ensures that the heuristic can perform well across a variety of problem types, improving its generalization potential;

– adaptive input parameters improving through iteration. The iterative tuning of parameters means that the heuristic can evolve and improve as it interacts with the problem. This dynamic changing of input parameters process helps it better navigate the solution space or changes in the problem's structure, making it more robust and flexible in the long term;

– optimization of termination logic. The heuristic's termination condition is tailored to the problem's needs rather than being based on arbitrary iteration limits. Integrating various tuning parameters ensures that the algorithm concludes only when a sufficient number of viable solutions have been identified, preventing unnecessary computations and promoting more efficient problem-solving;

– cost-effectiveness. Due to its ability to focus only on the most relevant parts of the solution space and its flexibility in parameter adjustment, the heuristic reduces the need for extensive computational resources, making it a more cost-effective solution for large-scale problems;

– increased accuracy. By refining parameters through iteration and pre-solution investigation, the heuristic is able to deliver more accurate and effective solutions. This increases its reliability, especially in complex scenarios with multiple interacting variables;

– greater adaptability to real-world problems. The combination of category-based optimization, iterative adjustments, and flexible termination criteria allows the heuristic to adapt to real-world scenarios where problems may evolve or require a more tailored solution approach over time. This makes the method particularly suitable for dynamic environments like inventory management, logistics, or warehouse design;

– efficient resource utilization. By intelligently narrowing down the solution space and stopping once a satisfactory set of solutions has been found, the heuristic optimizes the use of computational and time resources, ensuring that solutions are reached in a timely and resource-efficient manner.

DOI 10.15588/1607-3274-2025-2-17

CONCLUSIONS

In this study, we investigate a model for the retail SSAP that incorporates both vertical and horizontal product categorization on the shelves. The model accounts for key constraints such as the need to store certain products on different shelves due to safety concerns, odour issues, or potential chemical reactions. Additionally, it considers the importance of not placing products from the same category side by side if they could cause confusion for customers or pickers. The model allows for flexibility in the division between vertical categories, which can be either rigid or more adaptable based on the store's specific layout and product types. Furthermore, it designates specific shelf levels for both brand-specific and general assortment products, ensuring efficient space usage and product organization. This approach optimizes both accessibility and safety, ultimately enhancing the customer experience while maintaining effective inventory management.

The retailer SSAP with vertical and horizontal categorization is commonly used in supermarkets (managing aisles with multiple product categories such as fresh food, canned goods, cleaning products, etc), apparel stores (Allocating space across different clothing categories, sizes, and brands), and electronics retailers (organizing shelves for various gadgets, accessories, and brands).

The retailer SSAP, with vertical and horizontal categorization, focuses on optimizing the arrangement of products on the shelves in a way that maximizes sales, ensures product visibility, improves the shopping experience, and minimizes space wastage. It involves balancing product demand, accessibility, and the overall store layout strategy.

The scientific novelty of the obtained results lies in the development of two variants of new heuristics called flower-cutting heuristics that provide innovative solutions to complex problems within the retail store. These heuristics introduce novel approaches for optimizing products on the shelves. Unlike previous methods, the new heuristics take into account multiple dynamic factors and could be steered by the set of parameters appropriate for instances of different sizes. Additionally, the heuristics offer greater flexibility and adaptability, allowing for adjustments based on real-time data and changing store conditions. This advancement represents a significant step forward in improving the efficiency of product placement strategies in retail environments. Furthermore, the heuristics demonstrate improved performance in terms of both operational efficiency and customer satisfaction, offering a valuable contribution to the field of retail optimization.

The practical significance of the results lies in the development of heuristics called the flower-cutting heuristics and 13 steering parameters, which allow a quick search of the solution space and obtain high-quality results, along with the execution of experiments to assess the properties of the modelled SSAP. These experimental findings provide valuable insights, making it possible to recommend the proposed indicators for practical use in real-world scenarios.

Prospects for further research are to study the applicability of the SSAP model and the heuristics for various store sizes and product types, accommodating future growth and changes in the retail environment. In other words, future research in this area could explore several promising directions to further enhance the efficiency and effectiveness of retail store SSAP models. One potential direction is the integration of advanced machine learning and artificial intelligence techniques to dynamically adjust product categorization and shelf allocation based on real-time data, such as customer purchasing behaviour, stock levels, and demand patterns. Another area of exploration could be the development of more sophisticated algorithms for optimizing product placement that consider not only physical constraints but also factors such as shelf visibility, accessibility, and customer preferences.

REFERENCES

1. Czerniachowska K. A genetic algorithm for the retail shelf space allocation problem with virtual segments, *OPSEARCH*, 2022, Vol. 59, № 1, pp. 364–412. DOI: 10.1007/s12597-021-00551-3.
2. Czerniachowska K., Lutoslawski K., Fojcik M. Heuristics for shelf space allocation problem with vertical and horizontal product categorization, *Procedia Computer Science*, 2022, Vol. 207, pp. 195–204. DOI: 10.1016/j.procs.2022.09.052.
3. Czerniachowska K. The Method of Finding High-Runner Products in the Assortment, *Informatyka w zarządzaniu*, 2023, pp. 52–65. DOI: 10.15611/2023.51.0.03.
4. Drèze X., Hoch S. J., Purk M. E. Shelf management and space elasticity, *Journal of Retailing*, 1994, Vol. 70, № 4, pp. 301–326. DOI: 10.1016/0022-4359(94)90002-7.
5. Chandon P., Hutchinson J. W., Bradlow E. T. et al. Does in-store marketing work? Effects of the number and position of shelf facings on brand attention and evaluation at the point of purchase, *Journal of Marketing*, 2009, Vol. 73, № 6, pp. 1–17. DOI: 10.1509/jmkg.73.6.1.
6. Hwang H., Choi B., Lee M. J. A model for shelf space allocation and inventory control considering location and inventory level effects on demand, *International Journal of Production Economics*, 2005, Vol. 97, № 2, pp. 185–195. DOI: 10.1016/j.ijpe.2004.07.003.
7. Hariga M. A. Al-Ahmari A., Mohamed A. R. A. A joint optimisation model for inventory replenishment, product assortment, shelf space and display area allocation decisions, *European Journal of Operational Research*, 2007,Vol. 181, № 1, pp. 239–251. DOI: 10.1016/j.ejor.2006.06.025.
8. Hwang H., Choi B., Lee G. A genetic algorithm approach to an integrated problem of shelf space design and item allocation, *Computers and Industrial Engineering*, 2009, Vol. 56, № 3, pp. 809–820. DOI: 10.1016/j.cie.2008.09.012.
9. Hübner A. H., Kuhn H. Retail category management: State-of-the-art review of quantitative research and software applications in assortment and shelf space management, *Omega*, 2012, Vol. 40, № 2, pp. 199–209. DOI: 10.1016/j.omega.2011.05.008.
10. Irion J., Lu J. C., Al-Khayyal F. et al. //A piecewise linearization framework for retail shelf space management models, *European Journal of Operational Research*, 2012, Vol. 222, № 1. DOI: 10.1016/j.ejor.2012.04.021.

DOI 10.15588/1607-3274-2025-2-17

11. Botsali A. R., Peters B. A. A network based layout design model for retail stores, *Industrial Engineering Conference*, Atlanta, GA, 2005.
12. Zhang W., Rajaram K. Managing limited retail space for basic products: Space sharing vs. space dedication, *European Journal of Operational Research*, 2017, Vol. 263, № 3, pp. 768–781. DOI: 10.1016/j.ejor.2017.05.045.
13. Flamand T., Ghoniem A., Maddah B. Promoting impulse buying by allocating retail shelf space to grouped product categories, *Journal of the Operational Research Society*, 2016, Vol. 67, № 7, pp. 953–969. DOI: 10.1057/jors.2015.120.
14. Ozcan T., Esnaf S. A Discrete Constrained Optimization Using Genetic Algorithms for A Bookstore Layout, *International Journal of Computational Intelligence Systems*, 2013, Vol. 6, № 2. DOI: 10.1080/18756891.2013.768447.
15. Oestreicher-Singer G., Libai B., Sivan L. et al. The network value of products, *Journal of Marketing*, 2013, Vol. 77, № 3, pp. 1–14. DOI: 10.1509/jm.11.0400.
16. Varley R. Retail product management: Buying and merchandising.Routledge, 2005, Second edition. DOI: 10.4324/9780203358603.
17. Anderson E. E., Amato H. N. Mathematical model for simultaneously determining the optimal brand-collection and display-area allocation, *Operations Research*, 1974, Vol. 22, № 1. DOI: 10.1287/opre.22.1.13.
18. Hansen P., Heinsbroek H. Product selection and space allocation in supermarkets, *European Journal of Operational Research*, 1979, Vol. 3, № 6, pp. 474–484. DOI: 10.1016/0377-2217(79)90030-4.
19. Tsai C.-Y., Huang S.-H. Integrating Product Association Rules and Customer Moving Sequential Patterns for Product-to-Shelf Optimization, *International Journal of Machine Learning and Computing*, 2015, Vol. 5, № 5, pp. 344–352. DOI: 10.7763/ijmlc.2015.v5.532.
20. Czerniachowska K., Subbotin S. Merchandising rules for shelf space allocation with product categorization and vertical positioning, *Informatyka Ekonomiczna*, 2021, Vol. 2021, № 4, pp. 34–59. DOI: 10.15611/ie.2021.1.02.
21. Kpossa M. R., Lick E. Visual merchandising of pastries in foodscapes: The influence of plate colours on consumers' flavour expectations and perceptions, *Journal of Retailing and Consumer Services*, 2020, Vol. 52. DOI: 10.1016/j.jretconser.2018.10.001.
22. Czerniachowska K. Merchandising rules for shelf space allocation with horizontal and vertical positions, *Informatyka Ekonomiczna*, 2021, Vol. 2021, № 4, pp. 9–33. DOI: 10.15611/ie.2021.1.01.
23. Ali Soomro D. Y., Abbas Kaimkhani S., Iqbal J. Effect of Visual Merchandising Elements of Retail Store on Consumer Attention, *Journal of Business Strategies*, 2017, Vol. 11, № 1. DOI: 10.29270/jbs.11.1(17).002.

Received 07.03.2025.
Accepted 05.05.2025.

УДК 004.023

ОПТИМІЗАЦІЯ НА ОСНОВІ ЕВРИСТИКИ ЗБИРАННЯ КВІТІВ ДЛЯ ПРОБЛЕМИ РОЗПОДІЛУ ПРОСТОРУ

Черняховська К. С. – доктор філософії, викладач кафедри управління процесами Вроцлавського університету економіки і бізнесу, Вроцлав, Польща.
Субботін С. О. – д-р техн. наук, професор, завідувач кафедри програмних засобів Національного університету «Запорізька політехніка», Запоріжжя, Україна.

АНОТАЦІЯ

Актуальність. Досліджується проблема розподілу простору на полицях з наявною вертикальною та горизонтальною категоризацією продуктів, які також включають продукти загального асортименту та брендового асортименту. Окрім того, в моделі наявні також продукти з різними вимаганнями щодо умов зберігання, котрі повинні зберігатися на різних полицях, а також несумісні продукти, котрі повинні зберігаються на одній полиці, але не поруч.

Мета роботи полягає в тому, щоб максимізувати прибуток, товарний рух або продажі після розміщення продуктів на полицях магазину, визначивши полицю для продукту та кількість його складських одиниць.

Метод. У дослідженні запропоновано два варіанти евристики з різними правилами сортування всередині, які використовуються як підхід до вирішення проблеми розподілу простору на полицях я наявною видимою горизонтальною та вертикальною категоризацією продуктів. Дослідження також охоплює застосування 13 розроблених параметрів управління евристиками, призначених для екземплярів різних розмірів, що дозволяє отримати економічно ефективне рішення високої якості.

Результати отримані за допомогою евристик, порівнювали з оптимальними рішеннями, опрацьованими комерційним вирішувачем CPLEX. Ефективність запропонованих евристик і придатність параметрів управління було продемонстровано їхньою здатністю значно зменшити простір пошукувань, при цьому досягаючи бажаних результатів. Обидві евристики послідовно створювали рішення з якістю, що перевищувала 99.80% для евристики H1 і 99.98% для евристики H2. Евристика H1 знайшла 12 оптимальних рішень, а евристика H2 знайшла аж 14 оптимальних рішень з 15 екземплярів тестування, підкреслюючи їх надійність і ефективність.

Висновки. Особливості досліджуваної моделі можуть використовувати супермаркети, магазини одягу, роздрібні торговці електроніки. Дотримуючись описаних етапів створення евристики та методів коригування параметрів, дистриб'ютор може систематично розробляти, уточнювати та розгортати евристичний алгоритм, який ефективно вирішує поточні проблеми розподілу на полицях, будучи надійним і масштабованим.

КЛЮЧОВІ СЛОВА: евристика, розподіл місця на полицях, проблема рюкзака, процес прийняття рішень.

DOI 10.15588/1607-3274-2025-2-17

ЛІТЕРАТУРА

1. Czerniachowska K. A genetic algorithm for the retail shelf space allocation problem with virtual segments / K. Czerniachowska // OPSEARCH. – 2022. – Vol. 59, № 1. – P. 364–412. DOI: 10.1007/s12597-021-00551-3.
2. Czerniachowska K. Heuristics for shelf space allocation problem with vertical and horizontal product categorization / K. Czerniachowska, K. Lutoslawski, M. Fojcik // Procedia Computer Science. – 2022. – Vol. 207. – P. 195–204. DOI: 10.1016/j.procs.2022.09.052.
3. Czerniachowska K. The Method of Finding High-Runner Products in the Assortment / K. Czerniachowska // Informatyka w zarządzaniu. – 2023. – P. 52–65. DOI: 10.15611/2023.51.0.03.
4. Drèze X. Shelf management and space elasticity / X. Drèze, S. J. Hoch, M. E. Purk // Journal of Retailing. – 1994. – Vol. 70, № 4. – P. 301–326. DOI: 10.1016/0022-4359(94)90002-7.
5. Does in-store marketing work? Effects of the number and position of shelf facings on brand attention and evaluation at the point of purchase / [P. Chandon, J. W. Hutchinson, E. T. Bradlow et al.] // Journal of Marketing. – 2009. – Vol. 73, № 6. – P. 1–17. DOI: 10.1509/jmkg.73.6.1.
6. Hwang H. A model for shelf space allocation and inventory control considering location and inventory level effects on demand / H. Hwang, B. Choi, M. J. Lee // International Journal of Production Economics. – 2005. – Vol. 97, № 2. – P. 185–195. DOI: 10.1016/j.ijpe.2004.07.003.
7. Hariga M. A. A joint optimisation model for inventory replenishment, product assortment, shelf space and display area allocation decisions / M. A. Hariga, A. Al-Ahmari, A. R. A. Mohamed // European Journal of Operational Research. – 2007. – Vol. 181, № 1. – P. 239–251. DOI: 10.1016/j.ejor.2006.06.025.
8. Hwang H. A genetic algorithm approach to an integrated problem of shelf space design and item allocation / H. Hwang, B. Choi, G. Lee // Computers and Industrial Engineering. – 2009. – Vol. 56, № 3. – P. 809–820. DOI: 10.1016/j.cie.2008.09.012.
9. Hübner A. H. Retail category management: State-of-the-art review of quantitative research and software applications in assortment and shelf space management / A. H. Hübner, H. Kuhn // Omega. – 2012. – Vol. 40, № 2. – P. 199–209. DOI: 10.1016/j.omega.2011.05.008.
10. A piecewise linearization framework for retail shelf space management models / [J. Irion, J. C. Lu, F. Al-Khayyal et al.] // European Journal of Operational Research. – 2012. – Vol. 222, № 1. DOI: 10.1016/j.ejor.2012.04.021.
11. Botsali A. R. A network based layout design model for retail stores / A. R. Botsali, B. A. Peters // Industrial Engineering Conference, Atlanta, GA. – 2005.
12. Zhang W. Managing limited retail space for basic products: Space sharing vs. space dedication / W. Zhang, K. Rajaram // European Journal of Operational Research. – 2017. – Vol. 263, № 3. – P. 768–781. DOI: 10.1016/j.ejor.2017.05.045.
13. Flamand T. Promoting impulse buying by allocating retail shelf space to grouped product categories / T. Flamand, A. Ghoniem, B. Maddah // Journal of the Operational Research Society. – 2016. – Vol. 67, № 7. – P. 953–969. DOI: 10.1057/jors.2015.120.
14. Ozcan T. A Discrete Constrained Optimization Using Genetic Algorithms for A Bookstore Layout / T. Ozcan, S. Esnaf // International Journal of Computational Intelligence Systems. – 2013. – Vol. 6, № 2. DOI: 10.1080/18756891.2013.768447.
15. The network value of products / [G. Oestreicher-Singer, B. Libai, L. Sivan et al.] // Journal of Marketing. – 2013. – Vol. 77, № 3. – P. 1–14. DOI: 10.1509/jm.11.0400.
16. Varley R. Retail product management: Buying and merchandising. / R. Varley. – Routledge, 2005. – Second edition. DOI: 10.4324/9780203358603.
17. Anderson E. E. Mathematical model for simultaneously determining the optimal brand-collection and display-area allocation / E. E. Anderson, H. N. Amato // Operations Research. – 1974. – Vol. 22, № 1. DOI: 10.1287/opre.22.1.13.
18. Hansen P. Product selection and space allocation in supermarkets / P. Hansen, H. Heinsbroek // European Journal of Operational Research. – 1979. – Vol. 3, № 6. – P. 474–484. DOI: 10.1016/0377-2217(79)90030-4.
19. Tsai C.-Y. Integrating Product Association Rules and Customer Moving Sequential Patterns for Product-to-Shelf Optimization / C.-Y. Tsai, S.-H. Huang // International Journal of Machine Learning and Computing. – 2015. – Vol. 5, № 5. – P. 344–352. DOI: 10.7763/ijmlc.2015.v5.532.
20. Czerniachowska K. Merchandising rules for shelf space allocation with product categorization and vertical positioning / K. Czerniachowska, S. Subbotin // Informatyka Ekonomiczna. – 2021. – Vol. 2021, № 4. – P. 34–59. DOI: 10.15611/ie.2021.1.02.
21. Kpossa M. R. Visual merchandising of pastries in foodscapes: The influence of plate colours on consumers' flavour expectations and perceptions / M. R. Kpossa, E. Lick // Journal of Retailing and Consumer Services. – 2020. – Vol. 52. DOI: 10.1016/j.jretconser.2018.10.001.
22. Czerniachowska K. Merchandising rules for shelf space allocation with horizontal and vertical positions / K. Czerniachowska // Informatyka Ekonomiczna. – 2021. – Vol. 2021, № 4. – P. 9–33. DOI: 10.15611/ie.2021.1.01.
23. Ali Soomro D. Y. Effect of Visual Merchandising Elements of Retail Store on Consumer Attention / D. Y. Ali Soomro, S. Abbas Kaimkhani, J. Iqbal // Journal of Business Strategies. – 2017. – Vol. 11, № 1. DOI: 10.29270/jbs.11.1(17).002.

DOI 10.15588/1607-3274-2025-2-17

УДК 004.2

ОПТИМАЛЬНИЙ РОЗПОДІЛ ОБМЕЖЕНИХ РЕСУРСІВ В МУЛЬТИПРОЦЕСОРНИХ СИСТЕМАХ

Косолап А. І. – д-р фіз.-мат. наук, професор, професор кафедри комп'ютерних наук та інформаційних технологій Дніпровського національного університету ім. Олеся Гончара, Дніпро, Україна.

АНОТАЦІЯ

Актуальність. В роботі розглядаються мультипроцесорні системи, які складаються з безлічі процесорів з загальною оперативною пам'яттю. Ефективність функціонування таких систем залежить від операційної системи. Вона повинна забезпечити рівномірне завантаження процесорів завданнями, при якому пікове навантаження на оперативну пам'ять буде мінімальним. Це досить складна проблема. В даній роботі вона розв'язується шляхом побудови оптимізаційних моделей та розробкою ефективних евристичних алгоритмів. Дана проблема розв'язується в два етапи. На першому етапі знаходиться оптимальне завантаження процесорів завданнями, а на другому – мінімізація пікового навантаження оперативної пам'яті. Побудовано декілька оптимізаційних моделей цієї задачі, для розв'язування яких ефективним є метод точної квадратичної регуляризації. Розроблені також ефективні евристичні алгоритми. Проведені порівняльні обчислювальні експерименти, які підтверджують ефективність запропонованої технології розв'язування даної проблеми.

Мета роботи. Розробка математичних оптимізаційних моделей, методів та алгоритмів оптимального розподілу ресурсів в мультипроцесорних системах.

Метод. Ефективним є двоетапний розв'язок даної проблеми. Запропоновано декілька оптимізаційних моделей, які містять булеві змінні. Такі моделі досить складні для знаходження оптимальних розв'язків. Для їх розв'язування пропонується використовувати метод точної квадратичної регуляризації. Цей метод оптимізації використовується вперше для даного класу задач, тому він потребував розробки відповідного алгоритмічного забезпечення. В операційних системах, як правило, реалізуються евристичні алгоритми. Тому пропонуються ефективні евристичні алгоритми, які використовують фінальний принцип, що значно покращує розв'язок задачі.

Результати. Побудовані нові оптимізаційні моделі розподілу обмежених ресурсів в мультипроцесорних системах. Розроблені ефективні евристичні алгоритми, які реалізовані програмно засобами VBA в пакеті Excel. Розроблене також програмне забезпечення для введення початкових даних оптимізаційних моделей, що спрощує їх розв'язування. Приведені результати обчислюваних експериментів.

Висновки. Розроблена нова ефективна технологія оптимального розподілу ресурсів в мультипроцесорних системах. Розроблені евристичні алгоритми, які реалізовані програмно. Проведені обчислювальні експерименти підтверджують ефективність запропонованої технології розв'язування задачі.

КЛЮЧОВІ СЛОВА: мультипроцесорні системи, оптимізаційні моделі, задачі з булевими змінними, евристичні алгоритми, метод точної квадратичної регуляризації, фінальний принцип.

АБРЕВІАТУРИ

Solver – надбудова Excel;

OpenSolver – надбудова Excel з відкритим кодом;

EQR – точна квадратична регуляризація.

НОМЕНКЛАТУРА

t_i – надбудова Excel з відкритим кодом;

t_{ij} – час виконання i-го завдання на j-му процесорі;

v_i – обсяг оперативної пам'яті для i-го завдання;

T – мінімальний час виконання всіх завдань;

V – пікове навантаження на оперативну пам'ять;

s, r – параметри квадратичної регуляризації;

d – змінна методу EQR;

x_{ij} – булева змінна, яка дорівнює одиниці, якщо i-те завдання виконується j-м процесором;

$||x||^2$ – квадрат Евклідової норма вектору x;

t_{ik} – булева змінна, яка дорівнює одиниці, якщо i-те завдання виконується в момент часу k;

x_i – час початку виконання i-го завдання;

n – кількість завдань мультипроцесорної системи;

m – кількість процесорів мультипроцесорної системи;

i – змінна індексів сум, параметрів та змінних;

j – змінна індексів сум, параметрів та змінних;

k – змінна індексів сум, параметрів та змінних;

$g_i(t, x_i, v_i)$ – кусково-постійна функція графіку i-го завдання;

I_j – множина завдань j-го процесора.

ВСТУП

Сьогодні існує безліч важливих задач в різних галузях людської діяльності, які ще не можуть бути ефективно розв'язані за допомогою сучасних комп'ютерних систем. Такі задачі відносяться до класу NP-складних. Потужності сучасних комп'ютерних систем недостатньо для розв'язування таких задач. Ці задачі можуть бути розв'язані за рахунок вдосконалення математичних моделей, розробки нових та ефективних методів та алгоритмів, а також за рахунок збільшення потужності обчислювальних систем. В наш час збільшення потужності обчислювальних систем відбувається шляхом розробки мультипроцесорних систем. З'являються багатоядерні процесори, будуються мультипроцесори, які можуть містити сотні і тисячі процесорів. Відповідно такі системи будуть працювати ефективно, якщо всі процесори будуть завантажені рівномірно, а ресурси оперативної пам'яті будуть розподілятися оптимально. За ефективність роботи мультипроцесорних систем відповідає

DOI 10.15588/1607-3274-2025-2-18

їх операційна система. В наш час мультипроцесорні операційні системи знаходяться в процесі розвитку.

В мультипроцесорних системах операційна система визначає, які завдання будуть виконуватися на яких процесорах і в якому порядку, щоб пікове навантаження на загальну оперативну пам'ять було мінімальним. Ця задача може розв'язуватися шляхом побудови оптимізаційних моделей, або розробкою ефективних евристичних алгоритмів. Оптимізаційні моделі будуть містити булеві змінні і можуть бути лінійними або квадратичними. Для розв'язування таких задач, як правило, використовуються методи розгалужень та границь. Це точні методи, але для знаходження оптимальних розв'язків вони потребують досить багато часу. Такі методи реалізовані програмно, зокрема в надбудовах Solver, OpenSolver пакету Excel. Надбудова OpenSolver з відкритим кодом більш ефективна та дозволяє розв'язувати задачі великої розмірності. Але обчислювальні експерименти показали, що ці програми часто передчасно завершують розрахунки і не знаходять оптимальні розв'язки. Показано, що кращою альтернативою цим програмам є метод точної квадратичної регуляризації [1], який використовує теж програму OpenSolver, але для перетвореної задачі. Цей метод потребує для розв'язування задачі досить мало часу і знаходить кращі розв'язки задачі.

Альтернативою оптимізаційним моделям є розробка ефективних евристичних алгоритмів. Такі алгоритми можуть розв'язувати задачі, навіть великої розмірності, за долі секунди. Показано, що такі алгоритми можуть бути вдосконалені шляхом використання фінального принципу. Цей принцип полягає в тому, що для розв'язування задачі використовується два алгоритму. Після завершення роботи першого алгоритму запускається наступний алгоритм, який покращує розв'язок задачі. Як показали обчислювальні експерименти такий принцип дозволяє майже завжди знаходити оптимальні розв'язки в задачі розподілу навантаження мультипроцесорних систем.

Об'єктом дослідження даної роботи є мультипроцесорні системи, операційні системи таких систем та їх оптимальне функціонування.

Предметом дослідження є оптимізаційні моделі мультипроцесорних систем та ефективні евристичні алгоритми оптимального розподілу ресурсів в таких системах.

Метою даного дослідження є розробка оптимізаційних моделей мультипроцесорних систем з розподілом обмежених ресурсів та побудова відповідних ефективних евристичних алгоритмів.

1 ПОСТАНОВКА ЗАДАЧІ

Розглядається мультипроцесорна система, яка містить m процесорів рівної потужності та n завдань, які необхідно виконати ($n > m$). Для кожного i-го завдання відомий час виконання t_i та обсяг оперативної пам'яті v_i. Необхідно виконати всі завдання за мінімальний час так, щоб пікове навантаження на оперативну пам'ять було мінімальним. Таким чином, вхідними даними задачі є набір параметрів (n, m, t_i, v_i, i =1,…,n). Вихідними даними задачі є x_{ij} – час початку виконання i-го завдання на j-му процесорі, або послідовність їх виконання на кожному процесорі, мінімальний час T виконання всіх завдань та мінімальне пікове навантаження V на оперативну пам'ять мультипроцесорної системи.

Критерієм оптимізації буде мінімальне значення V при мінімальному T. Задача має декілька обмежень. Зокрема, кожне завдання повинно бути виконано, одночасно кожен процесор може виконувати тільки одне завдання, що означає $x_{ij} + t_i \le x_{kj}$ або $x_{kj} + t_k \le x_{ij}$, тобто або i-те завдання передує виконанню k-го завдання, або навпаки для кожного процесору. Ці умови рівнозначні квадратичним обмеженням $(x_{ij} + t_i - x_{kj})(x_{kj} + t_k - x_{ij}) \le 0$. Термін виконання кожного завдання буде менше T, тобто $x_{ij} + t_i \le T$, $\forall ij$, а обсяг оперативної пам'яті в кожний момент часу не перевищує значення V. Виконання останнього обмеження достатньо перевірити в момент початку виконання кожного завдання. Таку умову задати досить складно і вона буде визначена при побудові математичної моделі шляхом введення додаткових булевих змінних. Крім того, необхідно врахувати технічні обмеження, зокрема, в момент початку виконання i-го завдання на j-му процесорі може виконуватися не більше $m - 1$ завдань на інших процесорах. Таким чином, вихідними даними задачі є набір (x_{ij}, $\forall ij$, T, V).

Дана задача розглядається, коли кожне завдання виконується без переривань або з перериваннями. Для задачі з перериваннями задається квант часу q. Тоді кожне завдання виконується не більше кванту часу, після чого виконання завдання переривається і процесор починає виконувати наступне завдання та згодом повертається на виконання перерваного завдання. Кожну частину перерваного завдання можна розглядати як окреме завдання, що призводить до збільшення кількості завдань в задачі з перериваннями.

Дана задача розв'язується в два етапи. На першому етапі всі завдання розподіляються по процесорам системи так, щоб час виконання всіх завдань був мінімальним. Якщо всі t_i є цілими і час роботи процесорів відрізняється не більше ніж на одиницю, то такий розподіл завдань буде оптимальним.

На другому етапі, після розподілу завдань, розв'язується задача мінімізації пікового навантаження оперативної пам'яті мультипроцесорної системи. Це досягається шляхом переупорядкування виконання завдань на кожному процесорі.

Розглянута задача допускає різні узагальнення. Зокрема завдання можуть поступати в реальному часі, термін їх виконання може бути невідомий, також такі завдання можуть бути взаємопов'язані, що накладає додаткові лінійні умови на порядок виконання завдань, наприклад, $x_{ij} + t_i \le x_{kj}$. Задачі з цими узагальненнями можуть бути ефективно розв'язані, якщо знайдені ефективні алгоритми розв'язування поставленої задачі.

DOI 10.15588/1607-3274-2025-2-18

2 ОГЛЯД ЛІТЕРАТУРИ

Перші публікації присвячені балансуванню навантаження мультипроцесорних систем розпочалися ще в 70-х роках минулого століття [2–3]. В роботі [4] було показано, що майже всі задачі, пов'язані з мультипроцесорними системами, відносяться до класу NP-складних. В той час побудовані математичні моделі даного класу задач мали переважно теоретичний характер. Складність проблеми спонукала розробку безлічі евристичних алгоритмів рівномірного завантаження процесорів [5–11], що важливо для ефективної паралельної обробки даних. Такі дослідження актуальні до нашого часу [12]. Значна увага була приділена розробці ефективних алгоритмів балансування навантаження мультипроцесорних систем для різних умов їх функціонування. Такі алгоритми можна знайти в монографії [13], де також приведені оптимізаційні квадратичні моделі, але без урахуванням пам'яті. Зауважимо, що задачу оптимального завантаження мультипроцесорної системи можна перетворити до мультимодальної задачі про рюкзак [13–14], але така задача теж не враховує завантаженість оперативної пам'яті мультипроцесорної системи.

3 МАТЕРІАЛИ І МЕТОДИ

Досить просто побудувати оптимізаційну модель оптимального розподілу завдань в мультипроцесорній системі по критерію мінімізації часу завершення виконання всіх завдань. Така модель має наступний вигляд

$$\min\{T \mid \sum_{i=1}^{n} t_i x_{ij} \le T,\ j=1,...,m,\ \sum_{j=1}^{m} x_{ij} = 1, i=1,...,n,\ x_{ij} = 0 \vee 1, \forall ij\}, \quad (1)$$

де T – час виконання завдань, x_{ij} – булеві змінні. Змінна $x_{ij} = 1$, якщо i-те завдання виконується на j-му процесорі, інакше така змінна дорівнює нулю. Дану модель легко розширити на випадок, коли деякі завдання повинні виконуватися в заданому порядку. Тоді модель (1) необхідно доповнити лінійними обмеженнями вигляду $x_{ij} + t_i \le x_{kj}$, яке означає, що k-те завдання буде виконуватися після i-го завдання на j-му процесорі. Таких обмежень може бути декілька.

Якщо процесори різної потужності, то задача оптимального розподілу завдань буде мати вигляд

$$\min\{T \mid \sum_{i=1}^{n} t_{ij} x_{ij} \le T,\ j=1,...,m,\ \sum_{j=1}^{m} x_{ij} = 1, i=1,...,n,\ x_{ij} = 0 \vee 1, \forall ij\}, \quad (2)$$

Задачі (1)–(2) є лінійними з булевими змінними. Кількість змінних дорівнює $nm+1$, а кількість обмежень $n + m + 1$. Ці задачі можна розв'язати в пакеті Excel надбудовою OpenSolver. Для задач малої розмірності ця програма дозволяє отримати оптимальні розв'язки. Але вже для 24 завдань і чотирьох процесорів ця програма не знайшла оптимальний розв'язок. Наведемо дані цієї задачі. Час виконання завдань дорівнює (3, 49, 11, 41, 14, 38, 3, 16, 21, 16, 38, 17, 25, 11, 26, 28, 17, 12, 32, 45, 32, 24, 38, 29). Програма OpenSolver знайшла наступний час роботи кожного процесору (148, 153, 153, 152) в той час, як оптимальним часом роботи кожного процесору є (152, 151, 151, 152), що на одну одиницю часу краще. Зі зростанням розмірності задачі ця різниця буде збільшуватися, крім того, час розв'язування задачі (1) програмою OpenSolver буде швидко зростати.

Квадратична регуляризація задачі (1) зводить її до наступної

$$\max\{\|x\|^2 \mid T + s + (r-1)\|x\|^2 \le d, \sum_{i=1}^{n} t_{ij} x_{ij} \le T, j=1,..m,\ \sum_{j=1}^{m} x_{ij} = 1, i=1,...,n, \sum_{i=1}^{n}\sum_{j=1}^{m} x_{ij}(1-x_{ij}) + r\|x\|^2 \le d, 0 \le x \le 1\}. \quad (3)$$

Задача (3) не містить булевих змінних, тому її розв'язування програмою OpenSolver займає долі секунди. Для отримання оптимального розв'язку задачі (1) метод EQR потребує 10–20 розв'язувань задачі (3) програмою OpenSolver, для зростаючих значень d доти не виконається умова $r\|x\|^2 = d$ з заданою точністю.

Після розподілу завдань кожен процесор може виконувати свої завдання в довільній послідовності. Але, якщо кожне завдання потребує заданий обсяг оперативної пам'яті, то послідовність виконання завдань кожним процесором буде впливати на пікове навантаження оперативної пам'яті. Побудуємо модель мінімізації пікового навантаження оперативної пам'яті.

Представимо виконання завдань у вигляді графіка, де кожне завдання зображено відрізком, довжина якого дорівнює часу виконання завдання, а по осі ординат такий відрізок співпадає з обсягом оперативної пам'яті v_i. Тоді сума всіх відрізків буде графіком завантаження оперативної пам'яті. Представимо кожний відрізок кусково-постійною функцією $g_i(t, x_i, v_i)$. Отримаємо наступну модель задачі

$$\min\{V \mid x_i + t_i \le T, i=1,...,n, (x_i + t_i - x_j)(x_j + t_j - x_i) \le 0,\ \forall i \ne j, \sum_{i=1}^{n} g_i(x_j, x_i, v_i) \le V, j=1,...,n\}. \quad (4)$$

Задача (4) містить нелінійні квадратичні обмеження, які задають умову послідовного виконання завдань на кожному процесорі. Або i-те завдання передує виконанні j-го завдання, або навпаки. Обмеження задачі (4) неопуклі і тому породжують її мультимодальність. Ускладнює задачу і обмеження на оперативну

DOI 10.15588/1607-3274-2025-2-18

пам'ять, яке містить кусково-постійні функції. Задача (4) містить мінімальну кількість змінних n+1 та кількість обмежень $\frac{n}{2}(\frac{n}{m}-1)+2n$ Не дивлячись на невелику розмірність задачі (4), її складно розв'язати, що пов'язано з розривністю функцій $g_i(t, x_i, v_i)$.

Розглянемо альтернативну модель задачі (4). Будемо допускати, що час виконання кожного завдання є цілим числом. Поставимо у відповідність кожному i-му завданню послідовність бінарних чисел t_{ik}. Число чисел такої послідовності дорівнює T. Якщо завдання обробляється процесором, то відповідні числа послідовності дорівнюють одиниці, інакше вони дорівнюють нулю. Тоді задача мінімізації пікового навантаження оперативної пам'яті буде мати вигляд

$$\min\{V \mid \sum_{i=1}^{n} v_i t_{ik} \le V, k=1,...,T, \sum_{k=1}^{T} t_{ik} = t_i, i=1,...,n, \sum_{i\in I_j} t_{ik} \le 1, \forall jk, t_{ik} = 0 \vee 1, \forall ik\}, \quad (5)$$

де I_j – множина завдань, що виконуються j-м процесором. Задача (5) є лінійною з булевими змінними. Кількість змінних дорівнює nT+1, а кількість обмежень $T(n+1)+n$. Наприклад, для розглянутої вище задачі з 4-ма процесорами і 24 завданнями будемо мати 3648 булевих змінних і 5824 обмеження. Задача (5) допускає виконання завдань з перериваннями. Для виконання завдань без переривань необхідно добавити наступні обмеження

$$\sum_{k=1}^{T-1} (t_{ik} + t_{ik+1})^2 \ge 4(t_i - 1) + 1, i = 1,...,n. \quad (6)$$

Обмеження (6) зводить задачу (5) до квадратичної. Враховуючи велику розмірність задачі (5) її досить складно розв'язати навіть для задач невеликої розмірності.

Будемо вдосконалювати модель (4). Для цього введемо булеві змінні z_{ij} = 1, якщо i-те завдання виконується в момент початку виконання j-го завдання і z_{ij} = 0 інакше. Тоді повинні виконуватися обмеження

$$(x_i + t_i - x_j)(x_j - x_i) \ge 0, \forall i \ne j,$$

які виконується тільки тоді, коли в момент початку j-го завдання виконується i-те завдання. Але перший множник повинен бути більше нуля, тому

$$(x_i + t_i - x_j - \varepsilon)(x_j - x_i) \ge 0, \forall i \ne j, \quad (9)$$

де ε –мале додатне число. Це квадратичне обмеження замінимо лінійними обмеженнями

$$Q(z_{ij} - 1) \le (x_i + t_i - x_j - \varepsilon), \forall i \ne j, \quad (10)$$

$$Q(z_{ij} - 1) \le (x_j - x_i), \forall i \ne j, \quad (11)$$

де $Q = \sum_{i=1}^{n} t_i$ (велике додатне число). Тоді обмеження на оперативну пам'ять будуть мати вигляд

$$v_i + \sum_{j\ne i} z_{ji} \le V, i = 1,...,n. \quad (12)$$

Заміна останнього обмеження в задачі (4) на обмеження (9)–(12) призводить до нової моделі

$$\begin{gathered} \min\{V \mid x_i + t_i \le T, i = 1,...,n, \\ (x_i + t_i - x_j)(x_j + t_j - x_i) \le 0, \forall i \ne j, \\ Q(z_{ij} - 1) \le (x_i + t_i - x_j - \varepsilon), \forall i \ne j, \\ Q(z_{ij} - 1) \le (x_j - x_i), \forall i \ne j, \\ v_i + \sum_{j\ne i} z_{ji} \le V, i = 1,...,n\}. \end{gathered} \quad (13)$$

Квадратичні обмеження задачі (13) теж можна замінити лінійними

$$(x_i + t_i - x_j) \le Q(1 - y_{ij}), \forall i \ne j, \quad (14)$$

$$(x_j + t_j - x_i) \le Q y_{ij}, \forall i \ne j, \quad (15)$$

де y_{ij} = 1, якщо i-те завдання виконується раніше j-го завдання і y_{ij} = 0, якщо навпаки. Задача (13) після заміни квадратичних обмежень на (14)–(15) стає лінійною.

Кількість додатних значень z_{ij} буде дорівнювати $n(m-1)$, тому додаємо ще обмеження

$$\sum_{i=1}^{n} \sum_{j=1}^{m} z_{ij} = n(m-1). \quad (16)$$

Зауважимо, що якщо на множині завдань задано часткове упорядкування, то дані моделі необхідно доповнити відповідними лінійними обмеженнями.

Альтернативою розробленим оптимізаційним моделям можуть бути евристичні алгоритми. Ми пропонуємо два таких алгоритму. Перший алгоритм буде розподіляти завдання по процесорам, а другий – мінімізувати пікове навантаження оперативної пам'яті.

Алгоритм 1.

Крок 1. Упорядкуємо всі завдання в порядку спадання часу їх виконання.

Крок 2. Будемо роздавати послідовно (в порядку черги) завдання тим процесорам, які перші закінчують обробку завдань.

Крок 3. Перевіряємо, чи можна обміняти завдання двох процесорів з найбільшим та найменшим часом роботи при якому різниця часів роботи по модулю

DOI 10.15588/1607-3274-2025-2-18

цих процесорів буде мінімальною. Далі цей процес повторюємо до тих пір, доти така заміна можлива, інакше робота алгоритму закінчується.

Існуючі алгоритми включають тільки перші два кроки. Але, як показали експерименти, ці два кроки не дають оптимальний розподіл завдань. Крок 3 реалізує фінальний принцип і може бути окремим алгоритмом.

Алгоритм 2.

Крок 1. Використовуємо розглянутий вище алгоритм 1 для розподілу завдань по процесорам.

Крок 2. Для непарних номерів процесорів упорядкуємо завдання по спаданню обсягів оперативної пам'яті, а для парних – по зростанню обсягів оперативної пам'яті.

Крок 3. Шляхом попарної перестановки завдань на кожному процесорі знайдемо перестановку, яка максимально зменшить пікове навантаження оперативної пам'яті. Цей процес продовжується доти така перестановка можлива.

В цьому алгоритмі на кроці 3 теж реалізується фінальний принцип.

Розглянуті алгоритми реалізовані програмно засобами VBA для Excel 10. На вході цієї програми маємо терміни виконання завдань та їх обсяги оперативної пам'яті, які заносяться на аркуш Excel в дві колонки. Подвійним клацанням миші викликається діалогове вікно в яке вноситься кількість завдань та кількість процесорів. Результат розрахунку (завдання кожного процесору та порядок їх виконання) виносяться на аркуш Excel разом з піковим навантаженням оперативної пам'яті. Для задач великої розмірності програма знаходить розв'язок задачі за долі секунди. В діалогове вікно програми можна ввести квант часу і тоді програма розіб'є кожне завдання квантом часу та знайде пікове навантаження оперативної пам'яті з перериваннями виконання завдань.

4 ЕКСПЕРИМЕНТИ

Експерименти проводились в пакеті Excel 10. Для розв'язування запропонованих оптимізаційних моделей використовувалась надбудова OpenSolver, а для розв'язування задач за алгоритмами була написана програма. Дані для часу виконання завдань та обсягів оперативної пам'яті обиралися цілі числа датчиком випадкових чисел в заданих межах. Для розв'язування задачі по запропонованим моделям надбудовою OpenSolver необхідно на аркуш Excel ввести початкові дані. Це час виконання кожного завдання, обсяг їх оперативної пам'яті та початкові змінні задачі. Крім того необхідно ввести формули цільових функцій та обмежень задачі. Для задач (1), (5) ввести формули досить просто, враховуючи те, що Excel дозволяє копіювати формули. Але для задач (4), (13) ввести формули досить складно. Наприклад, для задачі з $n = 24$ і $m = 4$ тільки одна формула (всього 24 таких формул) має вигляд

=H5+IF(AND(C14>=D14;C14<I14);I5;0)+IF(AND(C14>=D15;C14<I15);I6;0)+IF(AND(C14>=D16;C14<I16);I7;0)+IF(AND(C14>=D17;C14<I17);I8;0)+IF(AND(C14>=D18;C14<I18); I9; 0)+IF(AND(C14>=D19; C14<I19); I10;0)+IF(AND(C14>=E14;C14<J14);J5;0)+IF(AND(C14>=E15;C14<J15);J6;0)+IF(AND(C14>=E16; C14<J16); J7;0)+IF(AND(C14>=E17;C14<J17);J8;0)+IF(AND(C14>=E18;C14<J18);J9;0)+IF(AND(C14>=E19;C14<J19);J10;0)+IF(AND(C14>=F14;C14<K14);K5;0)+IF(AND(C14>=F15;C14<K15);K6;0)+IF(AND(C14>=F16;C14<K16); K7;0)+IF(AND(C14>=F17;C14<K17);K8;0)+IF(AND(C14>=F18;C14<K18);K9;0)+IF(AND(C14>=F19;C14<K19); K10; 0)

Щоб не допустити помилок, була розроблена програма, яка вводить формули для цих задач.

Проведені експерименти показали, що алгоритм 1 майже завжди знаходить оптимальний розв'язок задачі (1). Розглянемо приклад з трьома процесорами та 15 завданнями t = (5, 9, 1, 3, 7, 6, 2, 2, 6, 9, 4, 1, 8, 8, 4). Програма OpenSolver і алгоритм 1 знайшли оптимальний розв'язок даної задачі, який показаний в табл. 1. Але ці розв'язки різні.

Таблиця 1 – Розв'язок задачі (1)

OpenSolver			Алгоритм 1		
P_1	P_2	P_3	P_1	P_2	P_3
5	9	3	5	6	4
6	1	7	9	2	1
2	6	2	1	2	8
4	1	9	3	6	8
8	8	4	7	9	4

Якщо враховувати обсяг оперативної пам'яті для даної задачі, наприклад, v = (38, 31, 30, 24, 12, 11, 12, 17, 28, 30, 31, 26, 21, 15, 3) для кожного завдання, то розв'язування задачі (5) програмою OpenSolver протягом трьох годин не дало результату. Розмірність приведеної задачі: 375 булевих змінних і 415 обмежень. Алгоритм 2 знайшов розв'язок цієї задачі (табл. 2) з піковим навантаженням на оперативну пам'ять 80.

Таблиця 2 – Розв'язок задачі алгоритмом 2

t			v		
P_1	P_2	P_3	P_1	P_2	P_3
5	6	4	38	11	31
9	2	1	31	12	26
1	2	8	30	17	21
3	6	8	24	28	15
7	9	4	12	30	3

Далі задача (5) для даного прикладу розв'язувалась методом EQR з використанням надбудови OpenSolver. За одну хвилину було знайдено розв'язок цієї задачі з піковим навантаженням на оперативну пам'ять рівним 72, при цьому завдання виконувалися з перериваннями.

DOI 10.15588/1607-3274-2025-2-18

Задачі розміром $n = 9$ і $m = 3$ розв'язувались також по моделі (13)–(16) програмою OpenSolver. Такі задачі були розв'язані за 30 сек. Але задача розміром $n = 12$ і $m = 3$ не була розв'язана програмою OpenSolver за 3 години.

Таким чином, для розв'язування задач малих розмірностей по запропонованим моделям може бути використана програма OpenSolver. Для більших розмірностей необхідно використовувати метод EQR, складовою частиною якого є програма OpenSolver.

Порівняння результатів розрахунків по моделям і алгоритмам показали, що розв'язки майже завжди співпадають. Це свідчить про високу ефективність запропонованих евристичних алгоритмів.

5 РЕЗУЛЬТАТИ

Для задачі оптимального навантаження мультипроцесорної системи та мінімізації пікового навантаження на її оперативну пам'ять розроблено декілька оптимізаційних моделей, а також два евристичних алгоритми. Для розв'язування задачі використовується потужна надбудова OpenSolver, а алгоритми реалізовані у вигляді програми. Як показали обчислювальні експерименти, розроблена програма часто знаходить оптимальні розв'язки задачі. Пропонується уточнювати результати, отримані евристичними алгоритмами, за допомогою запропонованих моделей. Безпосереднє розв'язування задачі по приведеним моделям програмою OpenSolver можливе тільки для задач малої розмірності. Для задач великої розмірності пропонується використовувати метод EQR.

6 ОБГОВОРЕННЯ

На відміну від однопроцесорних систем, мультипроцесорні системи є значно складнішими у плані їх оптимального функціонування. В сучасних операційних системах мультипроцесорних систем уже реалізовані алгоритми рівномірного завантаження процесорів завданнями. Над їх вдосконаленням розробники операційних систем ще працюють. Більш складною задачею в таких системах є оптимальний розподіл ресурсів. В першу чергу це оперативна чи кеш пам'ять. Не дивлячись на стрімке зростання її обсягів, вона залишається дефіцитним ресурсом. Оптимальне навантаження оперативної пам'яті мультипроцесорної системи є досить складною задачею. Для її розв'язування необхідні прості оптимізаційні моделі, а також ефективні евристичні алгоритми. Евристичні алгоритми, як правило, реалізуються в операційних системах. Оптимізаційні моделі необхідні для перевірки ефективності евристичних алгоритмів та проведення досліджень в галузі мультипроцесорних систем.

Складність задачі оптимального розподілу ресурсів в мультипроцесорних системах призводить до мультимодальних моделей. Такі моделі носять комбінаторний характер та містять булеві змінні. Існуючі програми для розв'язування таких задач, як правило, використовують методи розгалужень та границь. Такі методи будують бінарне дерево розв'язків підзадач і кількість таких підзадач до отримання точного розв'язку задачі може бути досить значною, навіть для задач малої розмірності. Це залежить від структури обмежень. Програма OpenSolver легко знаходить розв'язки в задачах про рюкзак з 1000 і більше булевими змінними, але стикається зі значними обчислювальними проблемами при розв'язуванні поставленої в даній роботі задачі оптимального розподілу ресурсів в мультипроцесорних системах.

Використання методу EQR значно спрощує розв'язування поставленої задачі. Це пов'язано з тим, що модель з булевими змінними перетворюється до моделі з неперервними змінними. Такі задачі програма OpenSolver досить швидко розв'язує для тисяч змінних. Крім того, метод EQR використовує квадратичну регуляризацію, яка спрощую структуру задачі.

На даний час проведено достатньо обчислювальних експериментів, які підтверджують ефективність обраної технології розв'язування складної задачі оптимального розподілу ресурсів в мультипроцесорних системах.

ВИСНОВКИ

В роботі розглянута актуальна задача оптимального розподілу ресурсів в мультипроцесорних системах. Зокрема, задача оптимального навантаження таких систем з мінімізацією пікового навантаження оперативної пам'яті. Задача розглядається як без переривань у виконанні завдань, так і з перериваннями. Для даної задачі побудовано декілька оптимізаційних моделей та евристичні алгоритми.

Дана задача може бути узагальнена для взаємопов'язаних завдань. Для таких завдань моделі необхідно доповнити мережевими графіками, які визначають взаємозалежність завдань. Для цього необхідно доповнити моделі задачі лінійними обмеженнями, які визначають порядок виконання завдань.

Наукова новизна роботи полягає в тому, що двоетапна постановка задачі з мінімізацією пікового навантаження оперативної пам'яті є новою. Новими є також запропоновані оптимізаційні моделі, крім задачі (1). Ці моделі містять мінімальну кількість змінних та обмежень у порівнянні з існуючими моделями для подібного класу задач. Евристичні алгоритми використовують, запропонований автором, фінальний принцип, який значно покращує розв'язки задачі. Для приведених моделей вперше використано розроблений автором метод EQR.

Практична цінність роботи полягає в тому, що її результати можуть бути використані для вдосконалення сучасних мультипроцесорних операційних систем. Отримані результати можуть бути використані також для подальших досліджень в мультипроцесорних системах.

Майбутні напрями дослідження та розробки будуть включати наступні узагальнення даної задачі. Зокрема, розгляд гетерогенних мультипроцесорних

DOI 10.15588/1607-3274-2025-2-18

систем, врахування інших обмежених ресурсів та зниження електроспоживання в таких системах.

ПОДЯКА

Робота виконана за кошти державного бюджету НДР ДНУ ім. О. Гончара «Інтелектуальна обробка даних в комп'ютерних інформаційних системах» (державний регістраційний номер 0122U001397), яка виконувалась з 01.01.2022 по 31.12.2024 роки.

ЛІТЕРАТУРА

1. Kosolap A. A new method for global optimization / A. Kosolap // ESAIM: Proceedings and surveys. – 2021. – Vol. 71. – P. 121–130. DOI 10.1051/proc/202171121.
2. Ramamoorthy C. V. Optimal Scheduling Strategies in a Multiprocessor System/ C. V. Ramamoorthy, K. M. Chandy and M. J. Gonzalez // IEEE Transactions on Computers. – 1972. – Vol. C-21, No. 2. – P. 137–146. DOI: 10.1109/TC. 1972.5008918.
3. Coffman E. G. An Application of Bin-Packing to Multiprocessor Scheduling/ E. G. Coffman, Jr., M. R. Garey, and D. S. Johnson //SIAM Journal of Computing.– 1978.– Vol. 7, Iss. 1. – P. 1–17. DOI: 10.1137/0207001.
4. Garey M. R. Complexity Results for Multiprocessor Scheduling under Resource Constraints/ M. R. Garey and D. S. Johnson // SIAM Journal on Computing. – 1975. – Vol. 4, Iss. 4. – P. 397–411. DOI: 10.1137/0204035.
5. Dilawar N. A Review of Power Efficient Load Balancing Algorithms for Multicore Systems / N. Dilawar, M. Zakarya and I. Ur Rahman// World Applied Sciences Journal. – 2013. – Vol. 27(9). – P. 1175–1182. DOI: 10.5829/idosi. wasj. 2013.27.09.1627.
6. Scheduling in Distributed Computing Systems Analysis, Design & Models / [D. P. Vidyarthi, D. K. Sarker, A. K. Tripathi, L. T. Yang]. – Springer Science+Business Media, LLC, 2009. – 300 p.
7. Khawatreh S. A. An Efficient Algorithm for Load Balancing in Multiprocessor Systems / S. A. Khawatreh // International Journal of Advanced Computer Science and Applications. – 2018. – Vol. 9, No. 3. – P. 160–164. DOI: 10.14569/ IJACSA.2018.090324.
8. Kermia O. Load Balancing and Efficient Memory Usage for Homogeneous Distributed Real-Time Embedded Systems / O. Kermia and Y. Sorel // International Conference on Parallel Processing – Workshops, Portland, OR, USA. – 2008. – P. 39–46. DOI: 10.1109/ICPP-W.2008.20.
9. Teixeira R. B. Shared resources in multiprocessor real-time systems scheduled by RUN / R. B. Teixeira, G. Lima // Real-Time Syst. – 2022. – No. 58. – P. 153–188. DOI 10.1007/ s11241-021-09374-3.
10. Walter R. A characterization of optimal multiprocessor schedules and new dominance rules / R. Walter, A. Lawrinenko // Journal of Combinatorial Optimization. – 2020. – Vol. 40. – P. 876–900. DOI 1007/s10878-020-00634-9.
11. Mehrabi A. An Adaptive Genetic Algorithm for Multiprocessor Task Assignment Problem with Limited Memory / A. Mehrabi, S. Mehrabi, Ali D. Mehrabi [Electronic resource]. – Access mode: Access mode: https://www.oalib.com/research/2169214
12. Revilla-Duarte U. Proactive Load Balancing to Reduce Unnecessary Thread Migrations on Chip Multi-Processor (CMP) System / [U. Revilla-Duarte, M. A. Ramırez-Salinas, L. A. Villa-Vargas, A. Tchernykh] // Computación y Sistemas. – 2024. – Vol. 28, No. 2. – P. 623–645. DOI: 10.13053/CyS-28-2-4403.
13. Kellerer H. Knapsack Problems / H. Kellerer, U. Pferschy, D. Pisinger. – Springer-Verlag Berlin Heidelberg, 2004. – 554 p. DOI l0.I007/978-3-540-24777-7.
14. Hill R. R. Generation Methods for Multidimensional Knapsack Problems and their Implications / R. R. Hill, C. S. Hiremath // Systemics, Cybernetics and Informatics. – 2007. – Vol. 5, № 5. – P. 59–64. DOI: 10.54808/JSCI.21.04.42

Стаття надійшла до редакції 14.01.2025.
Після доробки 18.04.2025.

UDC 004.2

OPTIMAL ALLOCATION OF LIMITED RESOURCES IN MULTIPROCESSOR SYSTEMS

Kosolap A. I. – Doctor of Physical and Mathematical Sciences, Professor, Professor of the Department of Computer Science and Information Technologies, Oles Honchar Dnipro National University, Dnipro, Ukraine.

ABSTRACT

Context. The paper considers multiprocessor systems consisting of many processors with a common RAM. The efficiency of such systems depends on the operating system. It must ensure a uniform loading of processors with tasks, in which the peak load on RAM will be minimal. This is a rather complex problem. In this paper, it is solved by building optimization models and developing effective heuristic algorithms. This problem is solved in two stages. The first stage is the optimal loading of processors with tasks, and the second is the minimization of the peak load on RAM. Several optimization models of this problem have been built, for the solution of which the exact quadratic regularization method is effective. Effective heuristic algorithms have also been developed. Comparative computational experiments have been conducted, which confirm the effectiveness of the proposed technology for solving this problem.

Objective. Development of mathematical optimization models, methods, and algorithms for optimal resource allocation in multiprocessor systems.

Method. A two-stage solution to this problem is effective. Several optimization models containing Boolean variables are proposed. Such models are quite complex for finding optimal solutions. To solve them, it is proposed to use the method of exact quadratic regularization. This optimization method is used for the first time for this class of problems, so it required the development of appropriate algorithmic support. Heuristic algorithms are usually implemented in operating systems. Therefore, effective heuristic algorithms are proposed that use the final principle, which significantly improves the solution of the problem.

DOI 10.15588/1607-3274-2025-2-18

Results. New optimization models for the allocation of limited resources in multiprocessor systems have been constructed. Effective heuristic algorithms have been developed, which are implemented software-wise using VBA in the Excel package. Software for entering initial data for optimization models has also been developed, which simplifies their solution. The results of computational experiments are presented.

Conclusions. A new effective technology for optimal resource allocation in multiprocessor systems has been developed. Heuristic algorithms have been developed and implemented in software. Computational experiments have been conducted to confirm the effectiveness of the proposed technology for solving the problem.

KEYWORDS: multiprocessor systems, optimization models, problems with Boolean variables, heuristic algorithms, exact quadratic regularization method, final principle.

REFERENCES

1. Kosolap A. A new method for global optimization, *ESAIM: Proceedings and surveys*, 2021, Vol. 71, pp. 121–130. DOI 10.1051/proc/202171121.
2. Ramamoorthy C. V., Chandy K. M. and Gonzalez M. J. Optimal Scheduling Strategies in a Multiprocessor System, *IEEE Transactions on Computers*, 1972, Vol. C-21, No. 2, pp. 137–146. DOI: 10.1109/TC. 1972.5008918.
3. Coffman E. G., Garey Jr., M. R., and Johnson D. S. An Application of Bin-Packing to Multiprocessor Scheduling, *SIAM Journal of Computing*, 1978, Vol. 7, Iss. 1, pp. 1–17. DOI: 10.1137/0207001.
4. Garey M. R. and Johnson D. S. Complexity Results for Multiprocessor Scheduling under Resource Constraints, *SIAM Journal on Computing*, 1975, Vol. 4, Iss. 4, pp. 397–411. DOI: 10.1137/0204035.
5. Dilawar N., Zakarya M. and Rahman I. Ur A Review of Power Efficient Load Balancing Algorithms for Multicore Systems, *World Applied Sciences Journal*, 2013, Vol. 27(9), pp. 1175–1182. DOI: 10.5829/idosi. wasj. 2013.27.09.1627.
6. Vidyarthi D. P., Sarker D. K., Tripathi A. K., Yang L. T. Scheduling in Distributed Computing Systems Analysis, Design & Models. Springer Science+Business Media, LLC, 2009, 300 p.
7. Khawatreh S. A. An Efficient Algorithm for Load Balancing in Multiprocessor Systems, *International Journal of Advanced Computer Science and Applications*, 2018, Vol. 9, No. 3, pp. 160–164. DOI: 10.14569/ IJACSA.2018.090324.
8. Kermia O. and Sorel Y. Load Balancing and Efficient Memory Usage for Homogeneous Distributed Real-Time Embedded Systems, *International Conference on Parallel Processing*. Workshops, Portland, OR, USA, 2008, pp. 39–46. DOI: 10.1109/ICPP-W.2008.20.
9. Teixeira R. B., Lima G. Shared resources in multiprocessor real-time systems scheduled by RUN, *Real-Time Syst.*, 2022, No. 58, pp. 153–188. DOI 10.1007/ s11241-021-09374-3.
10. Walter R., Lawrinenko A. A characterization of optimal multiprocessor schedules and new dominance rules, *Journal of Combinatorial Optimization*, 2020, Vol 40, pp. 876–900. DOI 1007/s10878-020-00634-9.
11. Mehrabi A., Mehrabi S., Mehrabi Ali D. An Adaptive Genetic Algorithm for Multiprocessor Task Assignment Problem with Limited Memory. [Electronic resource]. Access mode: https://www.oalib.com/research/2169214
12. Revilla-Duarte U., Ramırez-Salinas M. A., Villa-Vargas L. A., Tchernykh A. Proactive Load Balancing to Reduce Unnecessary Thread Migrations on Chip Multi-Processor (CMP) System, *Computación y Sistemas*, 2024, Vol. 28, No. 2, pp. 623–645. DOI: 10.13053/CyS-28-2-4403.
13. Kellerer H., Pferschy U., Pisinger D. Knapsack Problems. Springer-Verlag Berlin Heidelberg, 2004, 554 p. DOI l0.I007/978-3-540-24777-7.
14. Hill R. R., Hiremath C. S. Generation Methods for Multidimensional Knapsack Problems and their Implications, *Systemics, Cybernetics and Informatics*, 2007, Vol. 5, № 5, pp. 59–64. DOI: 10.54808/JSCI.21.04.42.

DOI 10.15588/1607-3274-2025-2-18

UDC 004.8

METHOD FOR DEVELOPMENT MODELS OF POLYSUBJECT MULTIFACTOR ENVIRONMENT OF SOFTWARE COMPLEX'S SUPPORT

Pukach A. I. – PhD, Assistant of ACS Department, Institute of Computer Sciences and Informational Technologies, Lviv Polytechnic National University, Lviv, Ukraine.

Teslyuk V. M. – Doctor of Sciences, Professor, Head of ACS Department, Institute of Computer Sciences and Informational Technologies, Lviv Polytechnic National University, Lviv, Ukraine.

ABSTRACT

Context. The task of development the models of a polysubject multifactor environment for software's complex support is considered in this research, that ensures possibilities of taking into account the influence of various impact factors onto the supported software complexes themselves, onto their complex support's processes, as well as onto the subjects (interacting with them) who provide and implement this complex support. **The object of study** are the processes of complex support of software products, the processes of automation of this complex support, the processes of influence of impact factors onto the object and subjects of the complex support of software products, as well as the processes of perception's subjectivization of the supported object by relevant subjects of interaction with it. **The subject of study** are methods and means of artificial neural networks, in particular a multilayer perceptron, as well as a computer design and modeling. **Objective** is the development of the method for building models of a polysubject multifactor environment(s) of the complex support of software product(s).

Method. The developed method for building models of a polysubject multifactor environment of software complexes' support is proposed, which makes it possible (in an automated mode) to obtain appropriate models, based on which, later on – to investigate the strengths and weaknesses of a specific researched complex support's environment(s) of a particular investigated software product(s), in order to ensure further improvement and automation of this complex support based on the study and analysis of impact factors, which form the subjective vision and perception of this complex support by those subjects who directly provide and perform it, that is, in fact, on whom this support itself depends, as well as its corresponding qualitative and quantitative characteristics and indicators.

Results. The results of functioning of the developed method are corresponding models of investigated polysubject multifactor environments of the complex support of software products, which take into account the presence and the level of influence of relevant existing and present factors performing impact onto the subjects of interaction with supported software complexes, which (subjects) directly provide and perform the complex support for the studied software products, and also form relevant researched support environments. In addition, as an example of a practical application and approbation, the developed method was used, in particular, to solve the applied practical task of determining the dominant and the deficient factors of influence of a polysubject multifactor environment of the studied software complex's support, with presenting and analyzing the obtained results of resolving the given task.

Conclusions. The developed method resolves the problem of building models of a polysubject multifactor environment of the complex support of software products, and ensures taking into account the action of various impact factors performing influence onto the supported software complex itself, onto the processes of its support, as well as onto the subjects of interaction with it, which (subjects) provide and perform this complex support. In particular, the developed method provides possibilities for modeling and investigating a polysubject multifactor environments of the "in focus" software product's complex support, which reflect the global (or the local, it depends on the specific tasks) impact of various existing factors making influence onto the object of support itself (the supported software complex, or the processes of its complex support), as well as onto the subjects which directly carry out and implement this complex support in all its possible and/or declared manifestations. The practical approbation of the developed method has been carried out by solving specific applied practical tasks, one of which is presented, as an example, in this paper, – which is the task of determining the dominant and the deficient factors of influence of a polysubject multifactor environment of the studied software complex's support, and this approbation, actually, confirms its effectiveness in solving a stack of applied practical problems related to researching the impact of factors performing influence onto the complex support of software products, using the advantages of artificial intelligence technologies, machine learning, artificial neural networks, and multilayer perceptron in particular.

KEYWORDS: software product, complex support, software product support environment, impact factor, automation, artificial neural networks, multilayer perceptron.

ABBREVIATIONS

ANN – artificial neural networks;
DevOps – Development and Operations;
IT – information technologies;
MP – multilayer perceptron;
XML – EXtensible Markup Language.

NOMENCLATURE

$F[k][j]$ is a level of presence of the k-th impact factor within the j-th instant slice of a multifactor portrait of currently investigated subject of the complex support;

$G[i].F[j]$ is a level of presence (in a normalized form of representation) of the j-th impact factor within the obtained multifactor portrait of the i-th investigated subject of the complex support, represented by the corresponding relevant i-th unique gradient;

InflFact$[1..p][1..q]$ is a set of pre-agreed and declared impact factors, affecting the perception subjectivization of the supported object by relevant subjects, who provide and perform a complex support of/for this object;

PsMfEnvExt is a variable describing the expanded version (option) of mathematical representation of the model

DOI 10.15588/1607-3274-2025-2-19

of researched polysubject multifactor environment of complex support;

PsMfEnvGrad is a variable describing the matrix variant of interpretation of the gradient form of representation of the model of researched polysubject multifactor environment of the complex support;

PsMfEnvSimp is a variable describing the simplified version (option) of mathematical representation of the model of researched polysubject multifactor environment of complex support;

Subj[*i*]*PortInst*[*j*] is an *j*-th instant slice of a multifactor portrait of the *i*-th investigated subject of support;

Subj[*i*]*PortFull* is a full multifactor portrait of the *i*-th investigated subject of the complex support, formed on the basis of its corresponding instant slices;

SubjPercOfObj[*j*] is an *j*-th subjectivized characteristic of subjective perception of the supported object by a specific subject which provides and performs its complex support;

SupObjChars[*i*] is an *i*-th objective characteristic of the investigated object of complex support.

INTRODUCTION

The nomenclature and assortment of software complexes, as well as a wide variety of software in general, continues growing steadily, which is due to the global digitalization and informatization of an extremely huge amount of objects, processes, entities and phenomena. Thus, both the total amount of existing and developed software and its general complexity are increasing, as well as extremely high requirements for its competitiveness in the global information technology (IT) market. Accordingly, there is a need for a complex support of all these (both existing and those in-process of development) software complexes, the requirements for which (just as in case of the software itself) are constantly growing, because clients, customers and investors, as well as, directly, the development companies of the relevant software complexes, are interested in providing the highest quality, effective, efficient and competitive, complex and comprehensive, support for all these software products.

Complex support of software products is one of the most important stages of the software's life cycle, while the automation of this support is an actual scientific and applied problem, which includes a huge range of related scientific applied and practical applied tasks. At the same time, the main driving force behind the implementation of the complex support of software products – are, undoubtedly, the specialists and professionals of various fields: ranging from a software developers, to customer service specialists, and real client's users of these supported software products. All these specialists are the subjects of a complex support of software products. Besides, all of them, in one way, or another, are influenced by both internal and external impact factors, which, in different ways and different extents, affect their subjective perception of both the supported software complex itself as well as the processes related to its complex support. And also, all these subjects, as a single whole entity, form the corresponding researched polysubject multifactor environment of the complex support of software product. Thus, there is a need to research and investigate such environments, formalize their representation, and also ensure the possibilities of their reproducing and modeling.

The object of study are the processes of complex support of software products, the processes of automation of this support, the processes of influence of impact factors onto the object and subjects of the complex support of software products, as well as the processes of the perception's subjectivization of the supported object by relevant subjects interacting with it.

The subject of study are methods and means of artificial neural networks, in particular a multilayer perceptron, as well as a computer design and modeling.

The purpose of the work is a development of a method for building models of a polysubject multifactor environment of the complex support of software products, that take into account the presence and the level of influence of relevant existing impact factors onto the subjects, which (those subjects) are interacting with the supported software complexes, and which directly provide and perform the complex support for the "in focus" software products, and form the relevant researched complex support's environments.

1 PROBLEM STATEMENT

Let's consider the formalization of the researched problem of building models of a polysubject multifactor environment of the complex support of software products in the form of problem of a nonlinear poly-criteria dependence. In this case, the input variables of the problem are the objective characteristics of the supported software complex (or processes related to its complex support) as a direct object of support: *SupObjChars*[*i*] (*i*=[1..*n*]), where *n* – the number of characteristics of this object of support.

While the initial variables of this task are the subjective characteristics of perception of the same object of support by the subjects who directly provide and perform its complex support: *SubjPercOfObj*[*j*] (*j*=[1..*m*]), where *m* – the number of characteristics of the subjectivized perception of the object of support by a specific subject(s) which provides and performs its complex support.

Let there be an existing set of a pre-agreed and predeclared impact factors affecting the perception's subjectivization of the support object by the subjects, which provide and perform its complex support, thus forming a non-linear polycriteria dependence in the form like below:

$$SubjPercOfObj[1..m]= \\ =InflFact[1..p][1..q](SupObjChars[1..n]), \quad (1)$$

The main necessary criterion of the researched problem is the finiteness of this set of pre-agreed and declared impact factors, that ensures the stability of the transformation function over the entire period of the research.

DOI 10.15588/1607-3274-2025-2-19

Limitation(s) of the problem:

1. The values of the input characteristics of the investigated object of complex support *SupObjChars*[1..*n*] must be represented in the format of real numbers and necessarily in a normalized form (that is, in the range of values between 0.0 and 1.0): *SupObjChars*[1..*n*] ∈ [0..1].

Expression (1) provides the possibility of interpreting the given problem with help of a multilayer perceptron, where *SupObjChars*[1..*n*] – is interpreted by neurons of the input layer of MP ANN; *InflFact*[1..*p*][1..*q*] – is interpreted by neurons of the hidden layers of MP ANN; *SubjPercOfObj*[1..*m*] – is interpreted by neurons of the output layer of MP ANN.

However, such interpretation requires additional training and further testing of a multilayer perceptron, as well as formation of a new quality data (based on the received information) which will provide the possibility of assessing the complex influence of impact factors onto the entire support environment in general, including each of the subjects forming this environment as a single whole.

Thus raises a relevant scientific and applied task of forming and modeling a polysubject multifactor environment of the complex support of software products, in order to take into account the influence of various impact factors affecting the supported software complex itself, the processes of its complex support, as well as the subjects, who directly provide and perform this complex support, and the processes of subjectivization of their perception of the supported software complex or the processes of its complex support. In order to resolve scientific and applied problem a suitable method for building models of a polysubject multifactor environment of the complex support of software products has been developed.

The purpose of this paper is to highlight the developed method for building models of a polysubject multifactor environment of the complex support of software products, as well as the corresponding developed algorithm for building these models, which both and together provides possibilities to solve the scientific and applied problem of forming and modeling a polysubject multifactor environment(s) of the complex support software products, in order to take into account the influence of impact factors onto the objects, the processes, and the subjects of the complex support of software products.

2 REVIEW OF THE LITERATURE

The analysis of existing researches and publications was carried out in two main directions, namely: in the direction of automating the complex support of software products, as well as in the direction of the application of artificial intelligence technologies (in particular a multilayer perceptron type of artificial neural networks) in the processes of the complex support of software product.

One of the basic options for ensuring the mandatory requirements for the functionality, reliability, and competitiveness of software products is, actually, the automation of the complex support of these software products, which includes, in particular, such key points as: testing automation; DevOps automation; automation by means of knowledge bases and chatbots; automation of processing of a customer/user requests. Each of these basic directions in its own way investigates and improves the support of software products, while all of them together provide a comprehensive (complex) support for these products. At the same time, artificial (or computational) intelligence and/or machine learning technologies are increasingly becoming effective mechanisms for implementing this automation. All the information, obtained by the results of processing of each of the directions, is presented below.

In particular, authors of research [1] carried out an extended review of the current state of general research and implementation in the field of software testing with usage of machine learning, in order to identify and classify (by classification categories, by clustering and by anomaly detection) existing approaches, methodologies and tools of such use, and their application in various types of testing, such as test creation, test execution and defect prediction. The research [2] represents introductory information on the application of artificial intelligence technologies to improve the quality of implemented software, including the way by analyzing any anomalies in the behavior of the researched software complexes and systems. For example, authors of another research [3] investigate the issue of improving test automation using guided machine learning, namely the “The K nearest neighbors” method for setting priorities and configuring testing scenarios and relevant test cases. While, research [4] investigates the end-to-end automation of DevOps, emphasizing its potential for optimizing the entire life cycle of software: from the commit of correction code into the appropriate version control system’s repository, and up to deployment in the client’s main operational environment(s). In addition, author of research [5] conducts a generalized review of the application of DevOps best practices to improve the entire life cycle of software complexes, both for systems that require a high level of automation and support, and for all others, which are, actually, not characterized by the presence of highly complex processes inside of their operational routines. The research [6] examines the advantage of DevOps compared to Agile, as well as their combination, since, according to the author, Agile and DevOps function as complements, and also author emphasizes that for obtaining a better effect DevOps should be adopted rather as an organizational culture then just a technique, which allows to increase the overall efficiency of operational process and reduce costs due to cooperation improvement and tasks automation. In turn, author of research [7] reviewed the existing methods, tools, and applications for building knowledge bases, while, another author of the following considered research [8] investigated the semantic parsing of natural language phrases and sentences in such a manner that they were compatible with the used sources of structured data, such as: ConceptNet, Quasimodo, ATOMIC, and ontology like a WordNet, by extracting meaning from unstructured texts and representing it in the form of knowledge graphs, which are transformed into the first-order logical formulas that can be further used in order to answer user queries. At the same time, authors of

DOI 10.15588/1607-3274-2025-2-19

research [9] conducted a systematic study (in the context of a human-machine interaction approach) of how users interact with text chatbots, describing how users (alive people) perceive a chatbots within categories of satisfaction, involvement and trust, how and why they accept and use this technology, the issue of emotional involvement of such an interaction, as well as the issue of the disadvantages of such type of interaction. In addition, work [10] represents the results of the authors' research on the issue of automation of IT-incident's forecasting (these incidents are, in fact, the appeals of real users of software complexes, that come to the relevant customer support services of these complexes) and solving them in the shortest time, by using an artificial intelligence models. In addition, authors of research [11] proposed a neural network, based on a convolutional neural network, for the automated classification of customer support service tickets of software complexes, which provides possibilities to solve such problems of traditional ticket classifiers as sparsity, nonlinearity, overfitting and manual work of functions.

Thus, based on performed analysis of existing researches, the considerable influence of artificial intelligence and machine learning technologies, used precisely for the purpose of automating the component processes of the complex support of software products, is confirmed. However, at the same time, we also state the lack of consideration of the peculiarities of the subjects interacting with the processes of the complex support of software products, as well as various (both internal and external) impact factors which affect the supported software complex itself, the processes of its support, as well as the subjects of this support. After all, in fact, impact factors form the very environment inside of which each particular supported software complex is constantly located and exists. So, this is the way how a corresponding actual scientific-applied task of researching this polysubject multifactor environment (of the complex support of software products) arises. And one of the effective tools for its resolution is, actually, the development of an appropriate relevant model which provides possibilities for describing, researching and modeling such environments, and, accordingly, taking into account the effect of various impact factors that significantly affect the object, processes, and subjects of the complex support of software products.

3 MATERIALS AND METHODS

One of the most important components of development the method, highlighted in current one research, is the preliminary development of the algorithm for building a model(s) of a polysubject multifactor environment(s) of the complex support of software products.

The general step-by-step mechanism for building a model of a polysubject multifactor environment of the complex support of software products involves the following mandatory stages, which, actually, form the basis of the developed algorithm.

At the first stage, the construction of a generalized support model of the software complex's support is carried out, followed by the encapsulation of an artificial neural network (ANN) of the multilayer perceptron (BP) type, as well as the implementation of the corresponding training of this encapsulated ANN BP based on a previously prepared dataset(s).

At the second stage, the levels of presence of each of the impact factors (from the pre-declared set of impact factors) in the corresponding neurons of the hidden layers of the encapsulated and trained BP ANN are calculated.

At the third stage, personal multifactor portraits of the subjects of support, formed on the basis of the corresponding instant slices of these portraits, are built.

At the fourth (and the final) stage, the construction of the model of a polysubject multifactor environment of the complex support of studied software product is implemented, based on the subjects' personal multifactor portraits obtained at the previous stage, which, actually at the same time, form the researched support environment.

Thus, the implementation of these presented above four basic stages of the developed algorithm makes it possible to obtain (at the output) a corresponding model of the researched polysubject multifactor environment of the complex support of corresponding software product.

Figure 1 below represents the block diagram visualization of the developed algorithm, with a detailed representation of each of the aforementioned stages.

The developed algorithm provides both: options for representing the model of a polysubject multifactor environment of the complex support (from among two possible developed options: simplified or expanded), as well as the forms of representing the model (from among possible developed forms, such as: mathematical, linguistic and gradient). Each of these possible fluctuations of options and forms is described in more detail in the following paragraphs of current section of this research.

The next fundamental component of the developed method is, in fact, the development of a model of polysubject multifactor environment for supporting software complexes. The main feature of the developed model is that it requires preliminary decomposition into simpler components, such as:

– at the first (external) decomposition level – personal (individual) multifactor portraits of each of the subjects interacting with the object of support (the supported software complex itself, or the processes of its support);

– at the second (internal) decomposition level – instant slices of these multifactor portraits of each of the subjects interacting with the object of support.

Accordingly, in order to ensure the possibility of building a correct and complete model of a polysubject multifactor environment for supporting any software complex, it is necessary and mandatory to fully implement its two levels of decomposition, starting from the most detailed (i.e., in this case – aforementioned internal, or second, decomposition level), and ending with the least detailed (i.e., in this case – aforementioned external, or first, decomposition level).

Using the appropriate components, such as, in particular: the mathematical model presented in research [12], as well as the model of decomposed insulating dominance

DOI 10.15588/1607-3274-2025-2-19

presented in research [13], together with the information model described in research [14], it becomes possible to obtain the second (internal) level of decomposition of the developed model of a polysubject multifactor environment of the complex support of researched supported object by modeling one specific case of perception's subjectivization of this object by the relevant researched subject interacting with it.

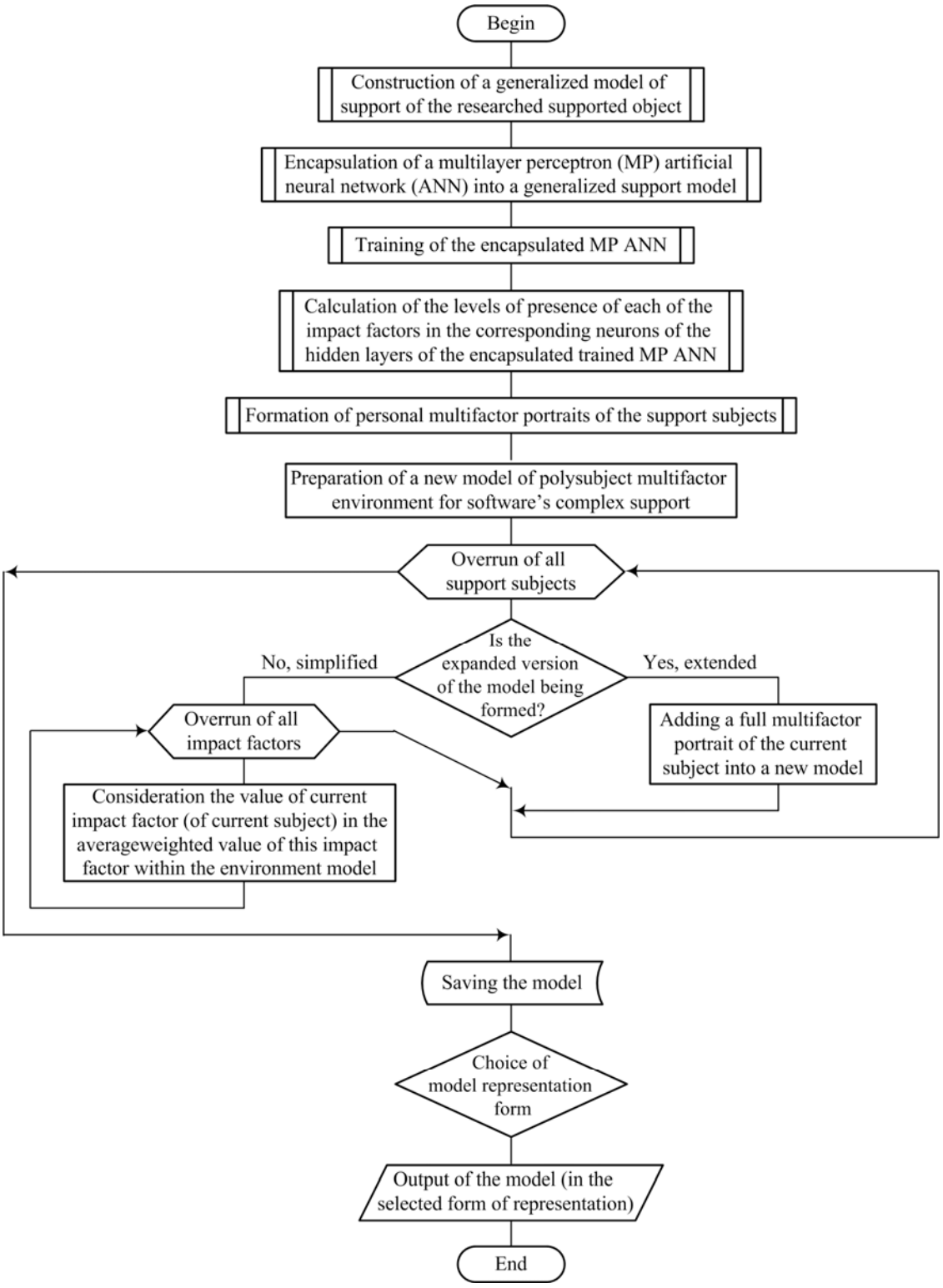

Figure 1 – Block diagram of the developed algorithm for building a model of polysubject multifactor environment of the complex support of software products

DOI 10.15588/1607-3274-2025-2-19

In turn, the set of modeling results of all available cases of perception subjectivization of the supported object by the corresponding researched subject of interaction – provides all the necessary data for building a personal (individual) multifactor portrait of this specific researched subject, which represents the first (or external) level of decomposition of the developed model of a polysubject multifactor environment of researched object's support.

Few variants of representation forms of the model of a polysubject multifactor environment of the complex support of software products have been developed and proposed, in particular, such as: mathematical form of representation; linguistic form of representation; and gradient form of representation.

At the same time, the developed model of a polysubject multifactor environment of the complex support of software products, regardless of its form of presentation, can exist in scope of two possible options of its presenting: a simplified option (in which only the average values of the presence levels of each of the impact factors in the researched environment are represented), as well as expanded option (in which there are separate values of the presence levels of each of the impact factors for each of the subjects which form the researched environment).

The mathematical form of representation of the model of a polysubject multifactor environment of the complex support of software products contains the following components, which are described in detail in the text below.

The basic fundamental unit of measurement for the future representation of any researched polysubject multifactor environment – is an instant slice of the multifactor portrait of each specific individual researched subject, represented by the following single expression:

$$Subj[i]PortInst[j](i \in 1..n)=[F1[j], F2[j], \dots Fm[j]], \quad (2)$$

where $F[k](k \in 1..m)[j]$ – the level of presence of the impact factor $F[k]$ inside the instant slice of a multifactor portrait $PortInst[j]$ of the investigated subject $Subj[i]$; n – the number of subjects forming the researched polysubject multifactor environment of complex support; m – the number of pre-agreed and declared impact factors within researched environment of complex support.

The next important component of constructing of any researched polysubject multifactor environment – is a complete multifactor portrait of the researched subject(s), formed on the basis of its instant slices, and represented by the following expression:

$$Subj[i]PortFull(i \in 1..n)=[\sum(F1[1..o]) / o, \sum(F2[1..o]) / o, \dots \sum(Fm[1..o]) / o], \quad (3)$$

where $\sum(F[j][1..o])/o$ $(j \in 1..m)$ – the average arithmetic value of the level of presence of a specific (currently considered) impact factor $F[j]$ inside the multifactor portrait of current researched subject $Subj[i]PortFull$, formed on the basis of its instant slices (with total amount of slices = o); m – the number of pre-agreed and declared impact factors within researched environment of complex support; o – the number (amount) of instant slices of the currently researched multifactor portrait.

Accordingly, on the basis of formed full multifactor portraits of subjects (which, in fact, directly form the researched environment of the complex support of software product), the simplified option of mathematical representation of the polysubject multifactor environment's model of complex support is described by following expression:

$$PsMfEnvSimp=[\sum(Subj[1..p]PortFull[F1])/p, \sum(Subj[1..p]PortFull[F2])/p, \dots \dots\sum(Subj[1..p]PortFull[Fm])/p], \quad (4)$$

where $\sum(Subj[1..p]PortFull[F[j]])/p$ $(j \in 1..m)$ – the average arithmetic value of the level of presence of a specific current impact factor $F[j]$ in the current model of the researched polysubject multifactor environment of the complex support, formed on the basis of values of presence levels of this impact factor in the available full multifactor portraits of all subjects $Subj[1..p]PortFull$, which (subject) form this specific support environment; p – the number of full multifactor portraits of subjects which form the researched support environment; m – the number of pre-agreed and declared impact factors within researched environment of complex support.

Meanwhile, the expanded option of mathematical representation of the polysubject multifactor environment model of complex support is described by the following expression:

$$PsMfEnvExt=[Subj[i]PortFull(i \in 1..n)], \quad (5)$$

where $Subj[i]PortFull(i \in 1..n)$ – are full multifactor portraits of all subjects $Subj[1..p]PortFull$, which form this specific support environment; n, p – the number of subjects, which form this specific support environment.

In other words, the expanded option of mathematical representation of the polysubject multifactor environment's model of complex support – is nothing more than just an array of pre-formed full multifactor portraits of the subjects which, in fact, form this support environment.

The main advantage of the developed and described mathematical form of representation of the polysubject multifactor environment's model of complex support – is basically its universality and uniformity, which makes it possible to use it also beyond the limits of the only particular area of software complexes' support, or even the field of information technologies as a whole.

The *linguistic form* is the next one developed and introduced form of representation of the polysubject multifactor environment model of complex support. This representation form involves the partial or full use of any existing, modified, or completely new linguistic constructions, to describe a polysubject multifactor environment(s). One of such existing variants of linguistic constructions is, in particular, XML (EXtensible Markup Language), since XML still remains as one of the most widely used and popular markup languages for representing a wide variety of objects and structures regardless of their degree of

DOI 10.15588/1607-3274-2025-2-19

complexity, so it could be used both in the classic form of representation and as a basis for various modifications, including the considered linguistic form of a polysubject multifactor environment's model representation.

Below is a variant of the linguistic representation of an instant slice of the multifactor portrait of investigated subject interacting with the supported object:

```
<Subj>
  <PortInst>
    <F1>..</F1>
    <F2>..</F2>
      ...
    <Fm>..</Fm>
  </PortInst>
</Subj>
```
(6)

At the same time, the linguistic form of representation of the full multifactor portrait of the investigated subject is described by the following expression:

```
<Subj>
  <PortFull>
    <F1>∑(<PortInst>.<F1>[1..o])/o</F1>
    <F2>∑(<PortInst>.<F2>[1..o])/o</F2>
      ...
    <Fm>∑(<PortInst>.<Fm>[1..o])/o</Fm>
  </PortFull>
</Subj>
```
(7)

Accordingly, the linguistic representation of a simplified version (option) of the polysubject multifactor support environment's model will have the following form:

```
<PsMfEnvSimp>
  <F1>∑(<Subj>[1..p].<PortFull>.<F1>)/p</F1>
  <F2>∑(<Subj>[1..p].<PortFull>.<F2>)/p</F2>
    ...
  <Fm>∑(<Subj>[1..p].<PortFull>.<Fm>)/p</Fm>
</PsMfEnvSimp>
```
(8)

While, the linguistic representation of the expanded version (option) of the model of a polysubject multifactor support environment will, accordingly, look like below:

```
<PsMfEnvExt>
  <Subj>
    <PortFull>
      <F1>∑(<PortInst>.<F1>[1..o])/o</F1>
      <F2>∑(<PortInst>.<F2>[1..o])/o</F2>
        ...
      <Fm>∑(<PortInst>.<Fm>[1..o])/o</Fm>
    </PortFull>
  </Subj>
</PsMfEnvExt>
```
(9)

The main advantage of the developed and proposed linguistic form of representing of the model of a polysubject multifactor support environment is its adaptability for use precisely within the framework of almost any possible further software implementation and/or computer simulation and modeling.

The *gradient form* is the next one developed and introduced form of representation of the models of a polysubject multifactor environment of the complex support of software products. The main idea of this form of representation is the most concise and rational numerical representation of the researched model of the complex support environment with the simultaneous selection of data by each of the subjects forming this environment.

At the same time, the data of each individual subject are represented by the range of values of its (subjects's) personal gradient, which can act as a separately taken unique segment of the numerical range of values, for example: (10.00–20.00) – the gradient of subject 1, 20.00–30.00 – the gradient of subject 2, 30.00–40.00 – the gradient of subject 3, and so on; as well as, for example, a unique combination of symbols, for example: AA – the gradient of subject 1, AB – the gradient of subject 2, AC – the gradient of subject 3, and so on.

However, the numerical values (themselves) of the levels of presence of each of the impact factors inside the formed multifactor portraits of the subjects must remain in a single common coordinate system, and also, necessarily, in a single normalized form of representation (the last one means they must be represented by real numbers in the value range [0.00 – 1.00]).

Thus, each gradient, representing a multifactor portrait of a separate subject, receives its own personal range of saturation values for each of the impact factors, however (necessarily) within the framework of a common evaluation system (coordinates) as well as a common normalized scale for comparison of data of all other gradients.

Two variants of interpretation of the gradient form of representation (of the models of polysubject multifactor support environments) have been developed and proposed in this research: the matrix variant of interpretation and the graphic variant of interpretation.

In particular, the matrix variant of interpretation of the gradient form of representation (of the models of polysubject multifactor support environments) is described using the following expression:

$$\begin{aligned} PsMfEnvGrad=(&G[1].F[1],\ G[1].F[2],\ \dots\ G[1].F[f],\\ &G[2].F[1],\ G[2].F[2],\ \dots\ G[2].F[f],\\ &G[..].F[1],\ G[..].F[2],\ \dots\ G[..].F[f],\\ &G[s].F[1],\ G[s].F[2],\ \dots\ G[s].F[f]), \end{aligned} \quad (10)$$

where $G[i].F[j]$ ($i \in 1..s$, $j \in 1..f$) – the level of presence (in a normalized form of representation) of the impact factor $F[j]$ within the formed multifactor portrait of the subject $Subj[i]$, represented by its unique gradient $G[i]$; f – the number of declared available impact factors; s – the number of subjects forming the researched polysubject multifactor support environment.

While, the graphical variant of interpretation of the gradient form of representation (of the models of polysubject multifactor support environments) can be demonstrated with the help of the Figure 2 below, at the same time, all the notations used in this figure, are absolutely the same as in the expression (10) provided above.

DOI 10.15588/1607-3274-2025-2-19

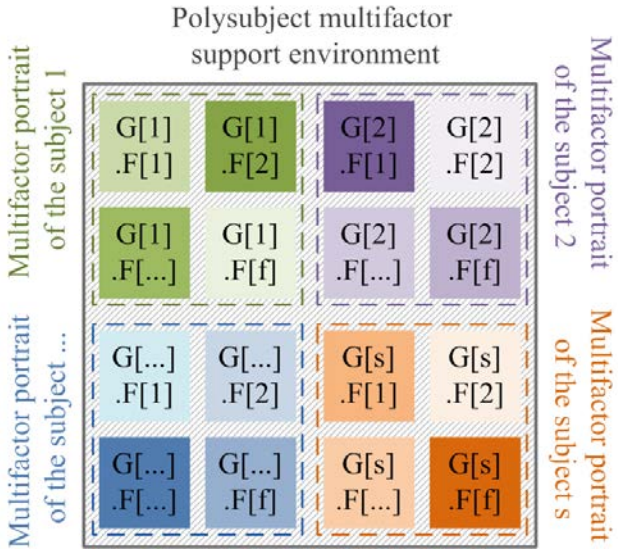

Figure 2 – Demonstration of a graphical variant of interpretation of the gradient form of the representation of a polysubject multifactor support environment's model.

The main idea of the developed and proposed graphical variant of interpretation of the gradient form of representation the support environment's model is, first of all, its simplicity of visual perception, as well as the ability to "combine" subjects in a different (and/or needed) ways/manner in order to form and obtain the necessary structure of the researched environment itself.

The gradient of each subject is indicated (in the proposed graphic variant) with a corresponding unique color, while the level of presence of each impact factor within formed multifactor portrait of this subject is represented with a gradient shades of this color. Hue saturation represents the normalized value of the presence fraction: the more saturated the hue – the closer this value is to 1, and the less saturated the hue – the closer this value is to 0.

The main advantage of the developed and described gradient form of representation of the model of a polysubject multifactor environment for supporting software complexes is its rationality, brevity, as well as dynamism and accessibility of perception, provided, among other things, by the developed and proposed graphical variant of interpretation of this form.

4 EXPERIMENTS

The experiment consists in the step-by-step execution of all the stages described in this research, namely:

– selection of an object of complex support;

– definition of the subjects of support;

– determination of existing impact factors;

– determination of the objective characteristics of the supported object;

– determination of the subjective characteristics of the perception of the supported object by relevant subjects;

– design and encapsulation of the appropriate relevant MP ANN;

– preparation of the datasets for training and testing the encapsulated MP ANN;

– formation of the instant slices of a multifactor portraits of the subjects of researched support environment;

– formation of a full multifactor portraits of the subjects of researched support environment (based on their instant slices);

– development of a model of the researched polysubject multifactor support environment based on obtained full multifactor portraits of the subjects forming this environment;

– presentation of the obtained model in an arbitrary form from among the developed, proposed and described forms of representation.

5 RESULTS

The main results of functioning of the developed method – are the appropriate models of the researched polysubject multifactor support environments for various supported software complexes. The obtained models provide opportunities both for the representation of the investigated polysubject multifactor support environment in a convenient form of representation (from a set of developed and proposed ones), as well as for any further research of such important components of the complex support of software products as: the impact of the researched support environment onto the supported object itself (directly the supported software complex itself, or the processes related to its support); the impact of individual subjects onto the researched support environment; as well as the influence of individual impact factors onto the researched support environment through prior influence onto the subjects forming the same environment.

In addition, the models of the researched polysubject multifactor support environments, obtained using the developed method, make it possible to get specific numerical values of the levels of presence of each of the impact factors within the specific researched support environment, and, therefore – the detection of any disproportions, anomalies, regularities, features, or any other characteris-

DOI 10.15588/1607-3274-2025-2-19

tics of the polysubject multifactor structure of the researched environment, in order to provide opportunities for further correction(s) of this environment, in such a manner to improve the complex support of the "in focus" software products in automated mode. In addition, the presence of the developed and proposed simplified and expanded options of representation of the obtained models ensures the variability of the detalization degree of corresponding researched polysubject multifactor structure of the simulated support environment(s). At the same time, the expanded option of representation also provides the possibility of additional clustering of the structure of researched support environment both by the criteria of support subjects and by the criteria of impact factors.

Figure 3 below presents an example of visualization of both simplified and expanded (extended) options of representation of a polysubject multifactor support environments based on relevant multifactor portraits of the subjects, which actually form these environments.

At the same time, depending on the obtained results of the complex representation of the researched polysubject multifactor support environment (obtained on the basis of processing the corresponding multifactor portraits of the subjects which form this environment) various options for the classification of such environments are possible.

In particular, the following options for the classification of support environments (of the complex support of software products) have been developed and proposed based on the level of their balance:

– perfectly balanced environments;
– well-balanced environments;
– satisfactorily balanced environments;
– non-satisfactorily balanced environments.

The main criterion for classifying the support environment(s) into one of these categories – is the average deviation (in percentages) of the indicator value of each of the impact factors, from the arithmetic mean value of this indicator across all impact factors.

Depending on specific tasks, environments, necessities or features, the specific numerical values of the thresholds of each of the categories of the developed classification may change and shift in one direction or another. As an example, as well as on the basis of conducted researches, the following values of the thresholds of each of the categories are proposed, in accordance to which:

– perfectly balanced environments – are those in which the average deviation (in percentages, rounded to the nearest integer according to generally accepted mathematical rounding rules) of the indicator value of each of the impact factors, from the arithmetic mean value of this indicator for all impact factors, varies within 1–2%;

– well-balanced environments – are those in which the average deviation (in %) of the indicator value of each of the impact factors, from the arithmetic mean value of this indicator for all impact factors, varies within 3–5%;

– satisfactorily balanced environments – are those in which the average deviation (in %) of the indicator value of each of the impact factors, from the arithmetic mean value, varies within 6–10%;

– non-satisfactorily balanced environments – are those in which the average deviation (in %) exceeds 10%.

Figure 4 below provides a visualization of examples of each of the categories of the developed classification of software product support's environments.

Thus, the developed classification provides the possibility of a flexible dynamic system of evaluation and determination of the balance category of any researched support environment of the relevant software products.

In addition, the developed method provides the possibility of studying the balance of any specific area of the researched support environment formed by the relevant subjects, as well as combining the activities of the subjects of this support environment in such a way to achieve a local balance improvement(s) within this specific area of the investigated support environment.

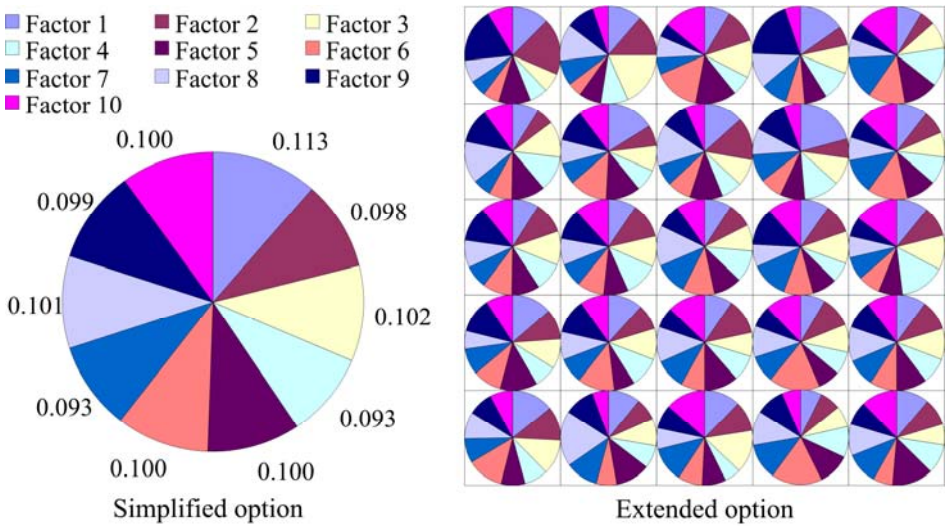

Figure 3 – Example of visualization of simplified and expanded (extended) options of representation of a polysubject multifactor support environments based on relevant multifactor portraits of the subjects which form this environment

DOI 10.15588/1607-3274-2025-2-19

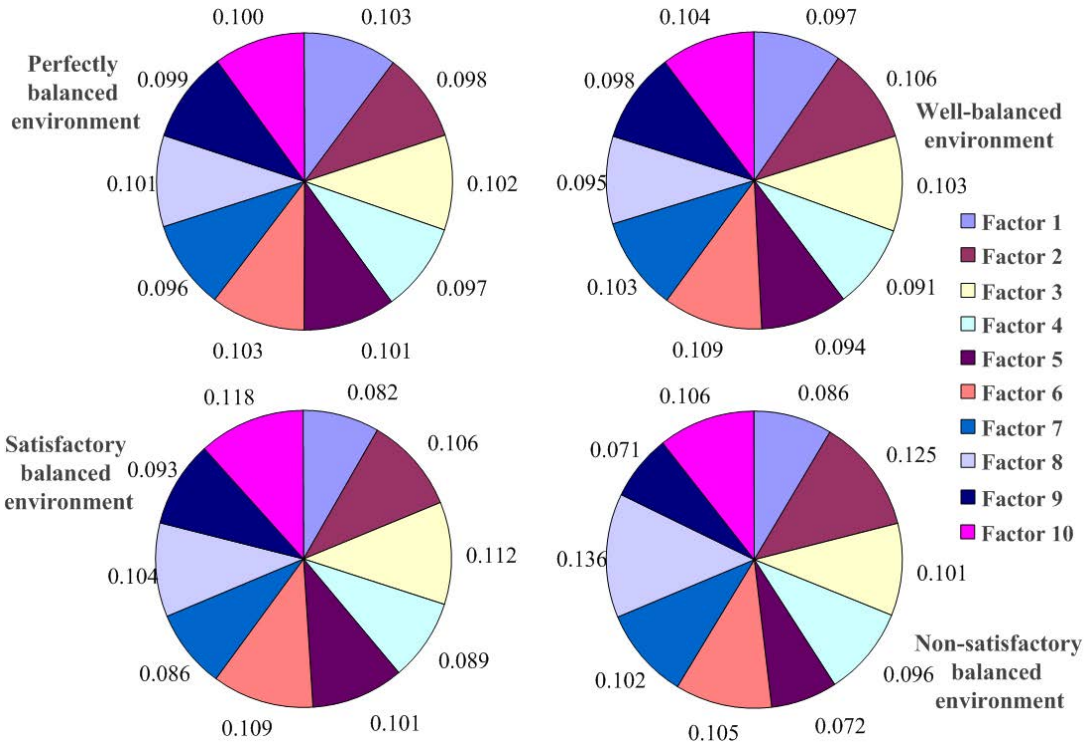

Figure 4 – Visualization examples of each of the categories of the developed classification of software product support's environments

In addition, as an example of practical application and approbation, the developed method has been used, in particular, to solve the applied practical task of determining the dominant and the deficient impact factors of a polysubject multifactor environment of the complex support of researched software product.

The resolution of the given applied practical task comes down to the application of the developed (and presented in this research) method of building models of a polysubject multifactor environment for the complex support of software products.

The formation of the model of the entire polysubject multifactor environment takes place on the basis of previously formed personal multifactor portraits of the subjects which form this support environment.

In turn, the formation of multifactor portraits of the subjects (of the support environment) is carried out on the basis of their instant slices, obtained by modeling the corresponding individual test cases of these subjects.

Figure 5 below presents the obtained results of modeling and formation of personal multifactor portraits of the subjects of the researched support environment.

While Figure 6 below presents the results of solving the given applied practical task of determining the dominant and the deficient impact factors of the polysubject multifactor environment of the complex support of the researched software product. In addition, the results of determining the balance category of the researched support environment are given, from which, by the way, another possible (alternative) way of solving the given applied practical task raises, since both the dominant and the deficient impact factors (of any researched support environment) will always have the largest indicators (in absolute equivalent) of the deviation of their value from the arithmetic mean value of all impact factors, while their polarity (that is, the real value, but not the absolute) will indicate their dominance or deficiency, which is confirmed by obtained results presented in the same Fig. 6.

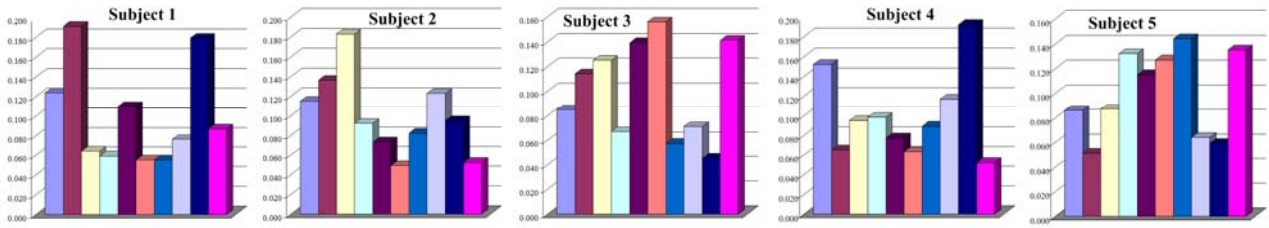

Figure 5 – Personal multifactor portraits of the subjects of the researched support environment

DOI 10.15588/1607-3274-2025-2-19

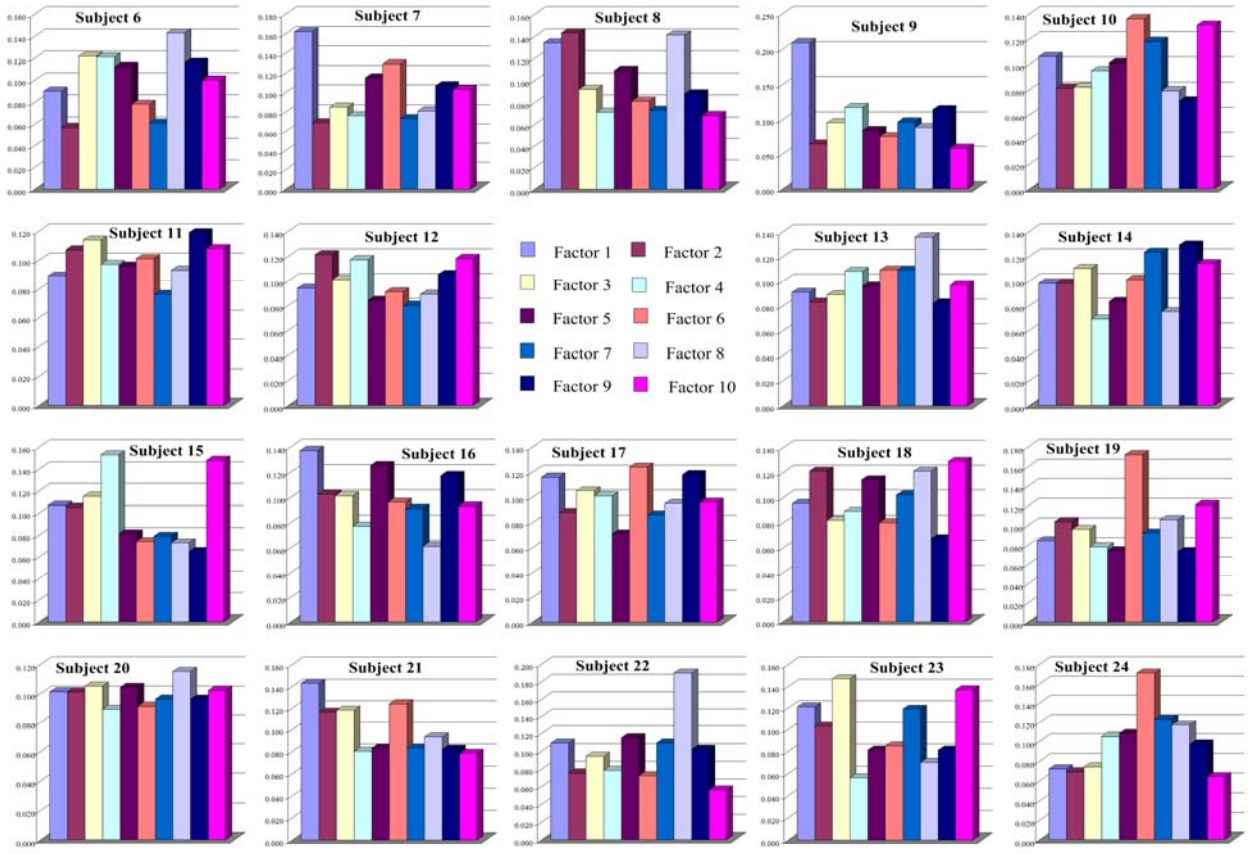

Figure 5 – Personal multifactor portraits of the subjects of the researched support environment (Continuation)

Thus, with the help of the developed method of building models of a polysubject multifactor environment for the complex support of software products, as an example of its practical application and approbation, the applied practical task of determining the dominant and the deficient impact factors of a polysubject multifactor support environment has been resolved for the specific software product. In addition, the accompanying task of identifying the balance level of the researched support environment was also resolved, which, in turn, provided the possibility of one more, additional, alternative solution to the same applied practical task.

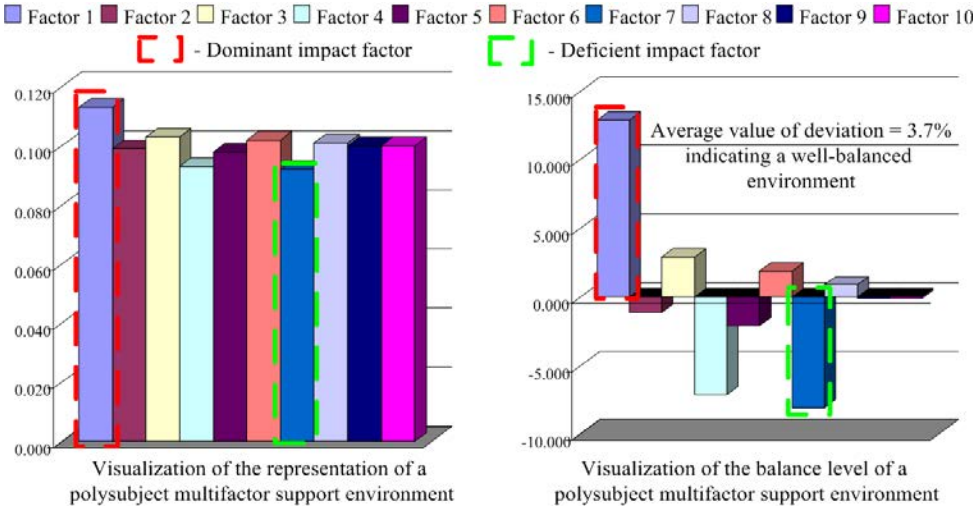

Figure 6 – Visualization of the solution of the given applied practical task

DOI 10.15588/1607-3274-2025-2-19

6 DISCUSSION

In work [15], the impact of entire procedures of Scrum and Agile technologies is studied as factors of influence onto the project management support related to the administration of development and support of software products, which takes into account, in particular, the twelve basic principles of the Agile methodology, as well as five key characteristics and three fundamental principles of the Scrum methodology, thereby demonstrating that not only external or internal separate impact factors can act as factors of influence onto the complex support of software products, but methodologies can undoubtedly be such factors as well, since each of them contains a clear list of principles that make their direct adjustments to the processes of development and complex support of software products. Another work [16] examines the influence of automated and manual testing factors onto the relevant indicators of the efficiency and effectiveness of testing the supported software product(s), where the authors take into account relevant impact factors, and as a result, it was established that only some hybrid variant of testing (which combines both manual and automated testing) makes it possible to take into account the complex influence of the impact factors of both these categories of testing, and thus obtain improvements in all indicators of efficiency and effectiveness studied by the authors. While in work [17], artificial intelligence technologies are considered as factors of influence on supported software products and their automation, and the analysis of their influence onto the automation of digital software products is carried out on example of a particular field of medical services (which is one of the most actual and profitable niches of software development nowadays) as well as the main factors affecting the implementation of artificial intelligence in systems of this class, were investigated.

Thus, in all considered cases, the relevance and significance of factors affecting supported software products, their support processes, and automation, have been confirmed. At the same time, unfortunately, the issue of a complex study of these impact factors within the framework of a single common environment of their existence and functioning remains unsolved.

At the same time, the method developed and presented in this one current research fully discloses this issue, and makes it possible to model and explore polysubject multifactor environments of the complex support of software products as a single whole indivisible entity, which directly affects the object, the processes, and the subjects of such complex support.

As at the output of the developed method, we get a model of researched polysubject multifactor environment of software's complex support, represented in a convenient form (from among those developed and proposed here in this research), which fully represents the researched environment.

As a further application of the developed method, we see the potential of its use for solving a stack of applied practical problems and tasks related to the research of a polysubject multifactor environments of the complex support of software products, which could be various investigated teams, collectives, divisions, departments, companies, or any other agglomerations of subjects interacting with the investigated object(s) of complex support. However, the potential of the developed method is not limited only to the context of software products' support, but also extends to other areas of science and practice, in which the key elements are active subjects and factors influencing their interaction. Thus, taking into account a wide range of applied problems, the expediency of further research in this direction is fully justified.

CONCLUSIONS

The method of building the models of a polysubject multifactor environment of the complex support of software products has been developed. The main scientific and applied problem solved by the developed method is the problem of forming and modeling a polysubject multifactor environment(s) of the complex support of software product(s), in order to take into account the influence of various impact factors that affect the supported software complex itself, the processes of its complex support, as well as the subjects which directly form and implement this complex support, as well as the processes of subjectivization of their (subjects') perception of the supported software complex or processes of its support. Also, the algorithm for building the model(s) of a polysubject multifactor environment(s) of the complex support of software products has been developed. In addition, several representation forms of the developed models of a polysubject multifactor environments (of the complex support of software products) have been developed and proposed, in particular, such as: mathematical form of representation (which includes additionally developed expanded and simplified representation options); linguistic form of representation; gradient form of representation (which includes additionally developed matrix and graphic versions of interpretation); and the main advantages of each of the above forms of representation are given. In addition, options for the classification of software product support's environments (based on their balance level) have been developed, which includes such categories as: perfectly balanced environments; well-balanced environments; satisfactorily balanced environments; unsatisfactorily balanced environments. The main criterion for the balance classification of the environment is the deviation average value (in percentages) of the indicator of each of the impact factors, from the arithmetic mean value of this indicator for all impact factors. The developed method provides possibility to carry out research on a polysubject multifactor environments of the complex support of software products by developing relevant models, which allows to describe, represent, investigate, and model such environments, as well as, accordingly, take into account the impact of various factors that significantly affect the object, the processes, and the subjects of the complex support of software products.

The scientific novelty consists in the development of a method for building models of a polysubject multifactor

DOI 10.15588/1607-3274-2025-2-19

environment of the complex support of software products, which provides possibility to solve the scientific and applied problem of defining, forming, and modeling a poly-subject multifactor environment(s) of the complex support of software products, in order to take into account the influence of various impact factors affecting the supported software complex itself, the processes of its complex support, as well as the subjects which directly form, provide and implement this complex support, as well as the processes of subjectivization of their (subjects') perception of the supported software complex or its relevant support's processes.

The practical significance consists in: the developed algorithm for building a model(s) of the researched poly-subject multifactor environment(s) of the complex support of software products; in the development of forms of representation of this model (in particular, such as: mathematical form of representation; linguistic form of representation; gradient form of representation); as well as in the development of an appropriate specialized classification of complex support's environments of software products based on their balance level (which includes, in particular, such categories as: perfectly balanced environments; well-balanced environments; satisfactorily balanced environments; and non-satisfactorily balanced environments).

Prospects for further research consist in the development of appropriate additional specialized algorithmic and software dedicated for modeling the researched poly-subject multifactor environments of the complex support of software products, with the aim of automating the research of the influence of various existing impact factors performing influence on the object, the processes, and the subjects of the complex support of software products, as a component of more global scientific and applied problem of automation of the complex support of software products.

ACKNOWLEDGEMENTS

This research is proactive. It was carried out as a part of the scientific activity of the authors outside of the working hours at their main positions.

REFERENCES

1. Panwar A., Peddi P. Implementation of Software Testing Using Machine Learning: A Systematic Mapping Study, *JJTU Journal of Renewable Energy Exchange*, 2023, Vol. 11, Iss. 7, pp. 58–64. – DOI: 10.58443/ijrex.11.7.2023.58-64
2. Gadani N.N. Artificial Intelligence: Leveraging Ai-Based Techniques For Software Quality, *International Research Journal of Modernization in Engineering Technology and Science*, 2024, Vol. 06, Iss. 07, pp. 757–769. – DOI: 10.56726/IRJMETS60018
3. Chaudhary J., Anand P. Predictive Modeling Of Automation In Software Testing A Machine Learning Approach For Efficient Test Case Selection [Electronic resource], *Advances in Mechanics*, 2023, Vol. 11, Iss. 2, pp. 128–139. Mode of access: https://www.advancesinmechanics.com/pdf/2023-128.pdf (date of access: 01.01.2025). – Title from screen.
4. Manchana R. The DevOps Automation Imperative: Enhancing Software Lifecycle Efficiency and Collaboration, *European Journal of Advances in Engineering and Technology*, 2021, Vol. 8, Iss. 7, pp. 100–112. DOI: 10.5281/zenodo.13789734
5. Ogala J. O. A Complete Guide to DevOps Best Practices, *International Journal of Computer Science and Information Security (IJCSIS)*, 2022, Vol. 20, No. 2, pp. 1–6. DOI: 10.5281/zenodo.6376787
6. Adnan S., Moin K., Imran J. DevOps with Agile: Best practices to improve software quality, *International Conference On Biological Research And Applied Science*, 2023, pp. 61–66. DOI: 10.37962/ibras/2023/61-66
7. Rajadhyax D. A Survey of Methods, Tools and Applications of Knowledge Base Construction (KBC) [Electronic resource], *Telecom Business Review: SIDTM Journal*, 2020, Vol. 13, Iss. 1, pp. 20–26. Mode of access: https://sidtm.edu.in/wp-content/uploads/2021/06/tbr2020.pdf#page=25 (date of access: 01.01.2025). – Title from screen.
8. Verrev M. Combining Semantic Parsing Frameworks for Automated Knowledge Base Construction [Electronic resource], *6th Workshop on Advances In Argumentation In Artificial Intelligence*, 2022, 11 pages. Mode of access: https://ceur-ws.org/Vol-3354/paper1.pdf (date of access: 01.01.2025). – Title from screen.
9. Rapp A., Curti L., Boldi A. The human side of human-chatbot interaction: A systematic literature review of ten years of research on text-based chatbots, *International Journal of Human-Computer Studies*, 2021, Vol. 151, Iss. 3, Article ID: 102630. DOI: 10.1016/j.ijhcs.2021.102630
10. Ahmed S., Singh M., Doherty B. et al. AI for Information Technology Operation (AIOps): A Review of IT Incident Risk Prediction, *9th International Conference on Soft Computing and Machine Intelligence (ISCMI)*, 2022, pp. 253–257. DOI: 10.1109/ISCMI56532.2022.10068482
11. Paramesh S. P., Shreedhara K.S. A deep learning based IT service desk ticket classifier using CNN [Electronic resource], *ICTACT journal on soft computing*, 2022, Vol. 13, Iss. 1, pp. 2805–2812. Mode of access: https://ictactjournals.in/paper/IJSC_Vol_13_Iss_1_Paper_9_2805_2812.pdf (acc. date: 02.01.2025). – Title from screen.
12. Pukach A.I. Mathematical model for analysis of influencing factors on software complexes support / A.I. Pukach, V.M. Teslyuk // Printing and Publishing. – 2024. – 1(87). – P. 75–85. – DOI: 10.32403/0554-4866-2024-1-87-75-85
13. Pukach A. I., Teslyuk V. M. Model of decomposed insulating dominance for the analysis of influencing factors of software complexes support automation, *Scientific Bulletin of UNFU*, 2024, 34(5), pp. 170–179. – DOI: 10.36930/40340521
14. Pukach A. I., Teslyuk V. M. Information model for automation of software complexes support influencing factors analysis with usage of the R-system and Python environments, *Bulletin of Lviv State University of Life Safety*, 2024, 29, pp. 54–64. – DOI: 10.32447/20784643.29.2024.06
15. Rasool N., Yousaf S., Haseeb U. et al. Scrum and the Agile procedure's impact on software project management, *Journal of Jilin University (Engineering and Technology Edition)*, 2023, Vol. 42, Iss. 2, pp. 380–392. – DOI: 10.17605/OSF.IO/MQW9P
16. Thant K. S., Tin H. H. K.The impact of manual and automatic testing on software testing efficiency and effective-

DOI 10.15588/1607-3274-2025-2-19

ness [Electronic resource], *Indian Journal of Science and Research*, 2023, Vol. 3, Iss. 3, pp. 88–93. Mode of access: https://www.ijsronline.org/issue/20230423-144118.016.pdf (acc. date: 02.01.2025). Title from screen.
17. Mehmood A. M., Murtuza A. M., Vazeer A. M. Impact of artificial intelligence on the automation of digital health system, *International Journal of Software Engineering & Applications (IJSEA)*, 2022, Vol. 13, No. 6, pp. 23–29. DOI: 10.5121/ijsea.2022.13602

Received 08.01.2025.
Accepted 18.04.2025.

УДК 004.8

МЕТОД ПОБУДОВИ МОДЕЛЕЙ ПОЛІСУБ'ЄКТНОГО МУЛЬТИФАКТОРНОГО СЕРЕДОВИЩА ПІДТРИМКИ ПРОГРАМНИХ КОМПЛЕКСІВ

Пукач А. І. – канд. техн. наук, асистент кафедри Автоматизованих Систем Управління Інституту Комп'ютерних Наук та Інформаційних Технологій Національного Університету «Львівська Політехніка», Львів, Україна.
Теслюк В. М. – д-р техн. наук, проф., завідувач кафедри Автоматизованих Систем Управління Інституту Комп'ютерних Наук та Інформаційних Технологій Національного Університету «Львівська Політехніка», Львів, Україна.

АНОТАЦІЯ

Актуальність. Розглянуто задачу побудови моделей полісуб'єктного мультифакторного середовища підтримки програмних комплексів, що забезпечує врахування дії різноманітних факторів впливу на сам підтримуваний програмний комплекс, на процеси його підтримки, а також на суб'єктів взаємодії з ним, що забезпечують та реалізують цю підтримку. **Об'єктом дослідження** є процеси комплексної підтримки програмних продуктів, процеси автоматизації цієї підтримки, процеси впливу факторів на об'єкт та суб'єкти комплексної підтримки програмних продуктів, а також процеси суб'єктивізації сприйняття об'єкта підтримки відповідними суб'єктами взаємодії з ним. **Предметом дослідження** є методи та засоби штучних нейронних мереж, зокрема багатошарового перцептрона, а також комп'ютерного проектування та моделювання. **Метою роботи** є розроблення методу побудови моделей полісуб'єктного мультифакторного середовища комплексної підтримки програмних продуктів.

Метод. Запропоновано розроблення моделей полісуб'єктного мультифакторного середовища підтримки програмних комплексів, що дає змогу, в автоматизованому режимі, отримати відповідні моделі, на основі яких, в подальшому – досліджувати сильні та слабкі сторони конкретного досліджуваного середовища комплексної підтримки того чи іншого програмного продукту, з метою забезпечення подальшого покращення та автоматизації його підтримки на основі вивчення та аналізу факторів впливу, що формують суб'єктивне бачення цієї підтримки тими суб'єктами, які її, власне, безпосередньо здійснюють, тобто, фактично, від яких залежить сама ця підтримка, а також відповідні її якісні та кількісні характеристики і показники.

Результати. Результатами роботи розробленого методу є відповідні моделі досліджуваних полісуб'єктних мультифакторних середовищ комплексної підтримки програмних продуктів, що враховують наявність та рівень впливу відповідних наявних факторів впливу на суб'єктів взаємодії з підтримуваними програмними комплексами, які (суб'єкти) безпосередньо забезпечують і реалізують цю комплексну підтримку досліджуваних програмних продуктів, та формують релевантні досліджувані середовища підтримки. Крім того, в якості прикладу практичного застосування та апробації, розроблений метод використано, зокрема, для розв'язання прикладної практичної задачі визначення домінуючого та дефіцитного факторів впливу полісуб'єктного мультифакторного середовища підтримки досліджуваного програмного комплексу, а також наведено та проаналізовано отримані результати розв'язання поставленої задачі.

Висновки. Розроблений метод вирішує поставлену задачу побудови моделей полісуб'єктного мультифакторного середовища підтримки програмних комплексів, та забезпечує врахування дії різноманітних (попередньо узгоджених та задекларованих) факторів впливу на сам підтримуваний програмний комплекс, на процеси його підтримки, а також на суб'єктів взаємодії з ним, що забезпечують та реалізують цю комплексну підтримку. Зокрема, розроблений метод дає змогу моделювати та досліджувати полісуб'єктні мультифакторні середовища комплексної підтримки програмних продуктів, що відображають глобальний (або локальний) вплив різноманітних наявних факторів як на сам об'єкт підтримки (підтримуваний програмний комплекс, чи процеси його комплексної підтримки), так і на суб'єктів, що безпосередньо здійснюють та реалізують дану комплексну підтримку в усіх її можливих та/або задекларованих проявах. Практична апробація розробленого методу здійснена на прикладі вирішення конкретних прикладних практичних задач, однією з яких є представлена в роботі задача визначення домінуючого та дефіцитного факторів впливу полісуб'єктного мультифакторного середовища підтримки досліджуваного програмного комплексу, та підтверджує його ефективність при розв'язанні стеку прикладних практичних задач дослідження впливу факторів на комплексну підтримку програмних продуктів, з використанням переваг технологій штучного інтелекту, машинного навчання, штучних нейронних мереж, та багатошарового перцептрона зокрема.

КЛЮЧОВІ СЛОВА: програмний продукт, комплексна підтримка, середовище підтримки програмних продуктів, фактор впливу, автоматизація, штучні нейронні мережі, багатошаровий перцептрон.

ЛІТЕРАТУРА

1. Panwar A. Implementation of Software Testing Using Machine Learning: A Systematic Mapping Study / A. Panwar, P. Peddi // JJTU Journal of Renewable Energy Exchange. – 2023. – Vol. 11, Iss. 7. – P. 58–64. – DOI: 10.58443/ijrex.11.7.2023.58-64
2. Gadani N. N. Artificial Intelligence: Leveraging Ai-Based Techniques For Software Quality / N.N. Gadani // International Research Journal of Modernization in Engineering Technology and Science. – 2024. – Vol. 06, Iss. 07. – P. 757–769. – DOI: 10.56726/IRJMETS60018
3. Chaudhary J. Predictive Modeling Of Automation In Software Testing A Machine Learning Approach For Efficient

DOI 10.15588/1607-3274-2025-2-19

Test Case Selection [Electronic resource] / J. Chaudhary, P. Anand // Advances in Mechanics. – 2023. – Vol. 11, Iss. 2. – P. 128–139. – Mode of access: https://www.advancesinmechanics.com/pdf/2023-128.pdf (date of access: 01.01.2025). – Title from screen.

4. Manchana R. The DevOps Automation Imperative: Enhancing Software Lifecycle Efficiency and Collaboration / R. Manchana // European Journal of Advances in Engineering and Technology. – 2021. – Vol. 8, Iss. 7. – P. 100–112. – DOI: 10.5281/zenodo.13789734
5. Ogala J. O. A Complete Guide to DevOps Best Practices / J.O. Ogala // International Journal of Computer Science and Information Security (IJCSIS). – 2022. – Vol. 20, No. 2. – P. 1–6. – DOI: 10.5281/zenodo.6376787
6. Adnan S. DevOps with Agile: Best practices to improve software quality / S. Adnan, K. Moin, J. Imran // International Conference On Biological Research And Applied Science. – 2023. – P. 61–66. – DOI: 10.37962/ibras/2023/61-66
7. Rajadhyax D. A Survey of Methods, Tools and Applications of Knowledge Base Construction (KBC) [Electronic resource] / D. Rajadhyax // Telecom Business Review: SIDTM Journal. – 2020. – Vol. 13, Iss. 1. – P. 20–26. – Mode of access: https://sidtm.edu.in/wp-content/uploads/2021/06/tbr2020.pdf#page=25 (date of access: 01.01.2025). – Title from screen.
8. Verrev M. Combining Semantic Parsing Frameworks for Automated Knowledge Base Construction [Electronic resource] / M. Verrev // 6th Workshop on Advances In Argumentation In Artificial Intelligence. – 2022. – 11 pages. – Mode of access: https://ceur-ws.org/Vol-3354/paper1.pdf (date of access: 01.01.2025). – Title from screen.
9. Rapp A. The human side of human-chatbot interaction: A systematic literature review of ten years of research on text-based chatbots / A. Rapp, L. Curti, A. Boldi // International Journal of Human-Computer Studies. – 2021. – Vol. 151, Iss. 3. – Article ID: 102630. – DOI: 10.1016/j.ijhcs.2021.102630
10. AI for Information Technology Operation (AIOps): A Review of IT Incident Risk Prediction / [S. Ahmed, M. Singh, B. Doherty et al.] // 9-th International Conference on Soft Computing and Machine Intelligence (ISCMI). – 2022. – P. 253–257. – DOI: 10.1109/ISCMI56532.2022.10068482
11. Paramesh S. P. A deep learning based IT service desk ticket classifier using CNN [Electronic resource] / S. P. Paramesh, K. S. Shreedhara// ICTACT journal on soft computing. – 2022. – Vol. 13, Iss. 1. – P. 2805–2812. – Mode of access: https://ictactjournals.in/paper/IJSC_Vol_13_Iss_1_Paper_9_2805_2812.pdf (acc. date: 02.01.2025). – Title from screen.
12. Пукач А. І. Математична модель аналізу факторів впливу підтримки програмних комплексів / А. І. Пукач, В. М. Теслюк // Поліграфія і видавнича справа. – 2024. – 1(87). – С. 75–85. – DOI: 10.32403/0554-4866-2024-1-87-75-85
13. Пукач А. І. Модель декомпонованої ізоляційної домінації для аналізу чинників впливу на автоматизацію підтримки програмних комплексів / А. І. Пукач, В. М. Теслюк // Науковий вісник НЛТУ України. – 2024. – 34(5). – С. 170–179. – DOI: 10.36930/40340521
14. Пукач А. І. Інформаційна модель аналізу факторів впливу автоматизації підтримки програмних комплексів з використанням середовищ R та Python / А. І. Пукач, В. М. Теслюк // Вісник Львівського державного університету безпеки життєдіяльності. – 2024. – 29. – С. 54–64. – DOI: 10.32447/20784643.29.2024.06
15. Scrum and the Agile procedure's impact on software project management / [N. Rasool, S. Yousaf, U. Haseeb et al.] // Journal of Jilin University (Engineering and Technology Edition). – 2023. – Vol. 42, Iss. 2. – P. 380–392. – DOI: 10.17605/OSF.IO/MQW9P
16. Thant K. S. The impact of manual and automatic testing on software testing efficiency and effectiveness[Electronic resource] / K. S. Thant, H. H. K. Tin // Indian Journal of Science and Research. – 2023. – Vol. 3, Iss. 3. – P. 88–93. – Mode of access: https://www.ijsronline.org/issue/20230423-144118.016.pdf (acc. date: 02.01.2025). – Title from screen.
17. Mehmood A. M. Impact of artificial intelligence on the automation of digital health system / A. M. Mehmood, A. M. Murtuza, A. M. Vazeer // International Journal of Software Engineering & Applications (IJSEA). – 2022. – Vol. 13, No. 6. – P. 23–29. – DOI: 10.5121/ijsea.2022.13602

DOI 10.15588/1607-3274-2025-2-19

УПРАВЛІННЯ У ТЕХНІЧНИХ СИСТЕМАХ

CONTROL IN TECHNICAL SYSTEMS

UDC 681.856.8

TERMINAL CONTROL OF QUADCOPTER SPATIAL MOTION

Yefymenko M. V. – Dr. Sc., Professor of Information Technologies of Electronic Devices Department, Zaporizhzhia Polytechnic National University, Zaporizhzhia, Ukraine.

Kudermetov R. K. – PhD, Associate Professor, Head of the Department of Computer Systems and Networks, Zaporizhzhia Polytechnic National University, Zaporizhzhia, Ukraine.

ABSTRACT

Context. Constructing quadcopter control algorithms is an area of keen interest because controlling them is fundamentally complex despite the quadcopter's mechanical simplicity. The key problem of quadcopter control systems is to effectively couple three translational and three rotational freedom degrees of motion to perform unique target manoeuvres. In addition, these tasks are relevant due to the high demand for quadcopter in various human activities, such as cadastral aerial photography for monitoring hard-to-reach areas and delivering cargo over short distances. They are also widely used in military affairs.

Objective. This work objective is to develop and substantiate novel methods for algorithms constructing the high-precision control of a quadcopter spatial motion, allowing for its autonomous operation in all main flight modes: stabilization mode, position holding mode, automatic point-to-point flight mode, automatic takeoff and landing mode.

Method. The given objective determined the use of the following research methods. Pontryagin's maximum principle was applied to develop algorithms for calculating program trajectories for transferring a quadcopter from its current state to the given one. Lyapunov functions and modal control methods were used to synthesise and analyse quadcopter angular position control algorithms. Numerical modelling methods were used to verify and confirm the obtained theoretical results.

Results. An approach for constructing algorithms for controlling the spatial quadcopter motion is proposed. It consists of two parts. The first part solves the problem of transferring a quadcopter from its current position to a given one. The second part proposes an original method to construct algorithms for quadcopter attitude control based on a dynamic equation for a quaternion.

Conclusions. The proposed quadcopter motion mathematical model and methods for constructing control algorithms are verified by numerical modelling and can be applied to develop quadcopter control systems.

KEYWORDS: quadcopter, quaternion, Pontryagin's maximum principle, Hamiltonian, Lyapunov functions.

ABBREVIATIONS

BFF is a body fixed frame;
EFF is an Earth fixed frame;
UAV is a Unmanned Aerial Vehicle.

NOMENCLATURE

D is a propeller diameter;

$\boldsymbol{F}_E$ is a vector of the sum all forces acting on quadcopter in the EFF;

$\boldsymbol{G}_E$ is a force of gravity;

H is a Hamiltonian;

$\boldsymbol{J}$ is a moment of inertia with respect to the BFF;

J_r is an inertia of the rotors;

$\boldsymbol{L}_B$ is an angular momentum in the BFF;

$\boldsymbol{M}_B$ is a moment of external forces given by projections on the BFF axes;

$\boldsymbol{M}_g$ is a gyroscopic moment;

$\boldsymbol{M}_i$ is a reactive torque from the rotation of the i-th propeller;

$\boldsymbol{M}_u$ is a control moment;

$\boldsymbol{P}_{Bi}$, is a lift force created by the i-th propeller, given by projections on BFF axes;

$\boldsymbol{P}_{Ei}$ is a lift force created by the i-th propeller, given by projections on EFF axes;

$\boldsymbol{X}_E, \boldsymbol{Y}_E, \boldsymbol{Z}_E$ are the EFF axes;

$\boldsymbol{X}_B, \boldsymbol{Y}_B, \boldsymbol{Z}_B$ are the BFF axes;

$\boldsymbol{e}$ is a pointing error;

g is a gravitational acceleration on Earth;

$\boldsymbol{h}_{Bi}$ is an angular momentum of the i-th rotor given by projections on the BFF axes;

k_m is a proportionality constants;

k_p is a proportionality constants;

ℓ is a distance from the motor rotation shaft axis to the quadcopter centre of mass;

DOI 10.15588/1607-3274-2025-2-20

m is a quadcopter mass;

$\boldsymbol{n}_B$ is a unit vector of $\boldsymbol{Y}_B$ axis;

$\boldsymbol{n}_E$ is a unit vector of the propellers' total thrust force given by the projections on the EFF axes;

$\boldsymbol{r}_E$ is a vector of the quadcopter centre mass position in the EFF;

$\boldsymbol{u}$ is a control vector;

$\boldsymbol{\Lambda}_{EB}$ is a quaternion of transition from EFF to BFF;

$\boldsymbol{\Phi}(t_0, t)$ is a transition matrix of the extended system;

α is a lift coefficient;

β_ρ is a propeller power factor;

λ_0^{EB} is a scalar part of the quaternion $\boldsymbol{\Lambda}_{EB}$;

$\boldsymbol{\lambda}_{EB}$ is a vector part of the quaternion $\boldsymbol{\Lambda}_{EB}$;

μ_i is a reactive moment on the shaft of the i-th rotor;

ρ is an air density;

φ is an Euler roll angle;

ϑ is an Euler pitch angle;

ψ is an Euler yaw angle;

$\boldsymbol{\omega}_B^{BE}$ is an angular velocity vector of BFF rotation relative to EFF, given by the projections onto the BFF axes;

ω_i is an angular speed of the i-th rotor;

$\sim$ is a conjugate quaternion notation;

$\circ$ is a quaternion multiplication operation symbol.

INTRODUCTION

Currently, work is actively underway in the field of developing new and improving existing UAV control systems. Miniature UAV multi-rotor type is an area of significant interest because of their unique features such as overall dimensions, the ability to fly in limited space and at very low speeds, vertical takeoff and landing and so on. These capabilities enable their use in various fields of activity, and for some tasks, they are indispensable. A diverse array of UAV applications can be found, for instance, in specialized literature reviews [1–3].

One of the main directions in the field of UAVs is related to increasing their flight autonomy. This, in turn, places increased demands on equipment reliability, control system intelligence, and the efficient use of power sources. On the other hand, these features ensure ease of use and reduce the cost of target tasks performed by UAVs.

This work is devoted to the development of the quadcopter spatial motion controlling algorithms, which allow autonomous implementation of its flight main modes: the stabilization mode in which the aircraft automatically maintains the zero values of roll and pitch angles and stabilizes the yaw angle; mode of keep a given position in which the UAV automatically hovers over a given point on the earth's surface; mode of automatic flight by points; automatic take-off and landing mode.

The object of the study is the process of controlling the spatial motion of a quadcopter.

The subject of the study is the synthesis of the quadcopter spatial motion control laws in the form of stationary feedback by state.

The purpose of the work is to develop algorithms for controlling the spatial motion of a quadcopter.

1 PROBLEM STATEMENT

The spatial movement of the quadcopter, a mechanical system with four propeller rotation engines and a supporting rigid frame is considered. The kinematic diagram of the quadcopter is shown in Fig. 1. On the kinematic diagram, the axes $\boldsymbol{X}_B$, $\boldsymbol{Y}_B$ and $\boldsymbol{Z}_B$ form a BFF, which is rigidly connected to the quadcopter, and the axes $\boldsymbol{X}_E$, $\boldsymbol{Y}_E$ and $\boldsymbol{Z}_E$ form the EFF, in which the observer is located. The propeller rotation engines are rigidly fixed to the quadcopter frame, and the BFF's $\boldsymbol{X}_B$ and $\boldsymbol{Y}_B$ axes intersect the centres of these engines.

The quadcopter motion control is carried out by applying control voltages to the propellers' engines. As a result of the propellers' rotation angle speeds ω_1, ω_2, ω_3 and ω_4, the lifting forces $\boldsymbol{P}_{B1}$, $\boldsymbol{P}_{B2}$, $\boldsymbol{P}_{B3}$, $\boldsymbol{P}_{B4}$ and the corresponding reaction moments $\boldsymbol{M}_1$, $\boldsymbol{M}_2$, $\boldsymbol{M}_3$ and $\boldsymbol{M}_4$ arise.

It is necessary to develop a quadcopter spatial motion mathematical model and based on it synthesize the algorithms for controlling the propeller angular velocities ω_i to transfer the quadcopter from a current position to a given one (hover point) and ensure the quadcopter's angular stabilization in this position.

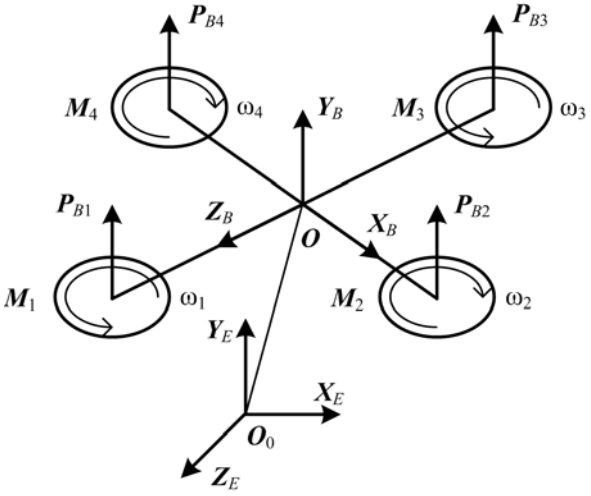

Figure 1 – The quadcopter kinematic scheme

2 REVIEW OF THE LITERATURE

The research and development of quadcopter spatial motion control have been the focus of many publications for several decades. The advances in microcontrollers, telecommunications, and quadcopter applications have

DOI 10.15588/1607-3274-2025-2-20

significantly increased the number of publications on this topic in recent years.

In studies [4–6], the control laws based on the Lyapunov function are introduced. These laws establish sufficient conditions for the asymptotic stability of a closed-loop system. and specific methodologies for determining the desired Lyapunov function are discussed. The works [7–8] discussed the use of a sliding mode control, which is simple and reliable, but requires adaptation of the switching logic to the flight modes of the quadcopter. In the work of [9], an approach that combines the method of a nonlinear observer and sliding mode control is proposed. In this approach, a nonlinear observer predicts the impact of engine failures on the quadcopter dynamics and ensures the stability of the sliding mode to uncertainties and disturbances. In work [10], a nested double-loop control scheme based on the adaptive backstepping approach concerning uncertain parameters is proposed. To avoid the analytic derivative calculation of the virtual command, a command filter is introduced into the designing procedure with a compensated signal employed in the attitude error. The backstepping-based formation control using the state transformation technique and asymptotic stability analysis based on Lyapunov's theorem is presented in the paper [11]. In [12], a highly complex controller is proposed that combines an optimal H_∞ controller with an integral predictive controller supplemented by a Kalman filter implementation. In the paper [13] a quadcopter model is developed using the Hamiltonian approach is considered and a nonlinear orientation controller for this model is proposed. In paper [14] a new nonlinear robust control algorithm with output feedback based on quaternions is presented.The work [15] is devoted to modelling a quadcopter based on certain physical parameters to build a desired model before designing a specific control system. According to the authors, this study should help save time and costs on possible errors in designing quadcopter control systems. Systematic literature reviews such as [16–18] comprehensively analyse the main modern control strategies for quadcopter UAVs.

3 MATERIALS AND METHODS

Let's assume that the origin of the coordinate system EFF coincides with the centre of mass of the quadcopter at the initial moment of movement, the EFF $\boldsymbol{Y}_E$ axis coincides with the direction of the local vertical at this point, the $\boldsymbol{X}_E$ axis is directed along the line of the given flight course, and the $\boldsymbol{Z}_E$ axis is defined as $\boldsymbol{Z}_E = \boldsymbol{X}_E \times \boldsymbol{Y}_E$. Considering the small durations of the time intervals of the quadcopter's autonomous flight, the rotation of the Earth can be neglected and the EFF coordinate system will be considered inertial (stationary) in the first approximation. The BFF axes are rigidly associated with the quadcopter body and the BFF origin coincides with the quadcopter centre of mass. Let's assume that the BFF axes coincide with the quadcopter's main central axes of inertia. In this case, the dynamic control characteristics are significantly improved and the equations of rotational motion of the quadcopter are simplified.

The relative orientation of EFF and BFF is defined as follows. The position of the coordinate system BFF relative to the coordinate system EFF is determined by the quaternion $\boldsymbol{\Lambda}_{EB}$. The BFF angular orientation relative EFF is given by three rotations: the first rotation is performed around the $\boldsymbol{X}_E$ axis by an angle φ, the second rotation is performed around the $\boldsymbol{Z}'$ axis by an angle ϑ, the third rotation is performed around the $\boldsymbol{Y}_B$ axis by an angle ψ (Fig. 2).

In this case, the quaternion $\boldsymbol{\Lambda}_{EB}$ is defined by the expression

$$\boldsymbol{\Lambda}_{EB} = \lambda_0^{EB} + \boldsymbol{\lambda}_{EB}, \tag{1}$$

where the scalar part is

$$\lambda_0^{EB} = \cos\frac{\psi}{2}\cos\frac{\vartheta}{2}\cos\frac{\varphi}{2} + \sin\frac{\psi}{2}\sin\frac{\vartheta}{2}\sin\frac{\varphi}{2}, \tag{2}$$

and the vector part is

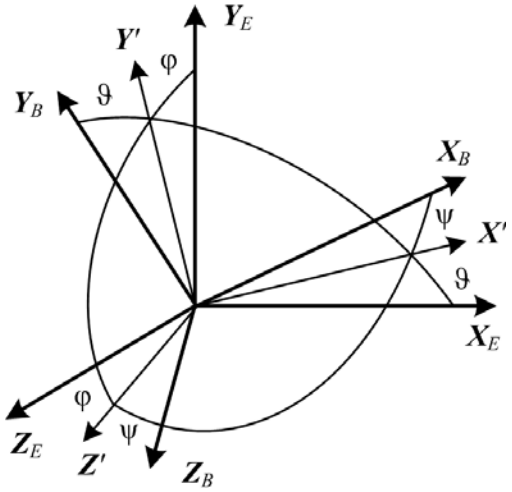

Figure 2 – Sequence of rotations for transforming from BFF to EFF

$$\boldsymbol{\lambda}_{EB} = \begin{pmatrix} \sin\frac{\varphi}{2}\cos\frac{\vartheta}{2}\cos\frac{\psi}{2} - \cos\frac{\varphi}{2}\sin\frac{\vartheta}{2}\sin\frac{\psi}{2} \\ -\sin\frac{\varphi}{2}\sin\frac{\vartheta}{2}\cos\frac{\psi}{2} + \cos\frac{\varphi}{2}\cos\frac{\vartheta}{2}\sin\frac{\psi}{2} \\ \cos\frac{\varphi}{2}\sin\frac{\vartheta}{2}\cos\frac{\psi}{2} + \sin\frac{\varphi}{2}\cos\frac{\vartheta}{2}\sin\frac{\psi}{2} \end{pmatrix}. \tag{3}$$

The system of equations for the quadcopter centre of mass motion in EFF by Newton's second law has the following form

$$m\ddot{\boldsymbol{r}}_E = \boldsymbol{F}_E. \tag{4}$$

DOI 10.15588/1607-3274-2025-2-20

Let's assume that only the thrust forces $\boldsymbol{P}_i$ of the aerodynamic propellers ($i = 1, 2, 3, 4$) and the force of gravity act on the quadcopter. In this case,

$$\boldsymbol{F}_E = \boldsymbol{P}_{E1} + \boldsymbol{P}_{E2} + \boldsymbol{P}_{E3} + \boldsymbol{P}_{E4} + \boldsymbol{G}_E = \boldsymbol{P}_E + \boldsymbol{G}_E, \quad (5)$$

where

$$\boldsymbol{G}_E = mg\begin{pmatrix} 0 \\ -1 \\ 0 \end{pmatrix}. \quad (6)$$

The direction of the force $\boldsymbol{P}_i$ coincides with the positive direction of the $\boldsymbol{Y}_B$ axis of BFF

$$\boldsymbol{P}_{Bi} = p_i \boldsymbol{n}_B. \quad (7)$$

The unit vector $\boldsymbol{n}_B$ of $\boldsymbol{Y}_B$ axis and modulus p_i of the forces $\boldsymbol{P}_i$ are determined by expressions

$$\boldsymbol{n}_B = \begin{pmatrix} 0 \\ 1 \\ 0 \end{pmatrix}, \quad (8)$$

$$p_i = \left|\boldsymbol{P}_i\right| = k_p \omega_i^2, \quad k_p = \alpha \rho D^4. \quad (9)$$

Projecting the vector $\boldsymbol{P}_{Bi}$ (7) onto the EFF axes gives

$$\boldsymbol{P}_{Ei} = p_i \boldsymbol{n}_E, \quad (10)$$

where

$$\boldsymbol{n}_E = \begin{pmatrix} -\sin\vartheta \\ \cos\vartheta\cos\varphi \\ \cos\vartheta\sin\varphi \end{pmatrix}. \quad (11)$$

Thus, the following equation describes the motion of the quadcopter centre of mass

$$m\ddot{\boldsymbol{r}}_E = k_p(\omega_1^2 + \omega_2^2 + \omega_3^2 + \omega_4^2)\boldsymbol{n}_E + \boldsymbol{G}_E. \quad (12)$$

To obtain the equation of the rotational motion of the quadcopter relative to the centre of mass, consider the equation for the angular momentum $\boldsymbol{L}$ of the "carrying body + rotors" system. This equation in BFF has the form

$$\boldsymbol{L}_B = \boldsymbol{J}\boldsymbol{\omega}_B^{BE} + J_r \boldsymbol{n}_B(\omega_1 + \omega_2 - \omega_3 - \omega_4). \quad (13)$$

According to the theorem on change of angular momentum [19], the change of the vector $\boldsymbol{L}$ in time is described by the equation

$$\dot{\boldsymbol{L}}_B = -\boldsymbol{\omega}_B^{BE} \times \boldsymbol{L}_B + \boldsymbol{M}_B, \quad (14)$$

where the moment $\boldsymbol{M}_B$ is the sum of the moments $\boldsymbol{M}_i$ created by the thrust forces $\boldsymbol{P}_{Bi}$ of the propellers. According to Fig. 1, it can be written

$$\boldsymbol{M}_B = \ell\begin{pmatrix} p_3 - p_1 \\ 0 \\ p_2 - p_4 \end{pmatrix} = k_p \ell\begin{pmatrix} \omega_3^2 - \omega_1^2 \\ 0 \\ \omega_2^2 - \omega_4^2 \end{pmatrix}. \quad (15)$$

Let us write equation (14) as follows

$$\boldsymbol{J}\dot{\boldsymbol{\omega}}_B^{BE} + J_r \boldsymbol{n}_B(\dot{\omega}_1 + \dot{\omega}_2 - \dot{\omega}_3 - \dot{\omega}_4) = \boldsymbol{M}_g + \boldsymbol{M}_B. \quad (16)$$

In equation (16), the gyroscopic moment $\boldsymbol{M}_g$ caused by the rotation of the quadcopter body and rotors is determined by the expression

$$\boldsymbol{M}_g = -\boldsymbol{\omega}_B^{BE} \times \boldsymbol{L}_B =$$
$$= -\boldsymbol{\omega}_B^{BE} \times (\boldsymbol{J}\dot{\boldsymbol{\omega}}_B^{BE} + J_r \boldsymbol{n}_B(\omega_1 + \omega_2 - \omega_3 - \omega_4)). \quad (17)$$

For the angular momentum of the *i*-th rotor, the following expression is valid

$$\boldsymbol{h}_{Bi} = J_r(\boldsymbol{\omega}_B^{BE} + \boldsymbol{n}_B\omega_i). \quad (18)$$

Therefore, taking into account (14), it can be obtained

$$J_r(\dot{\boldsymbol{\omega}}_B^{BE} + \boldsymbol{n}_B\dot{\omega}_i) + \boldsymbol{\omega}_B^{BE} \times (J_r(\boldsymbol{\omega}_B^{BE} + \boldsymbol{n}_B\omega_i)) = \boldsymbol{n}_B\mu_i, \quad (19)$$

where the reactive torque on the shaft of the *i*-th rotor is determined by the formulas

$$\mu_i = \beta_\rho D^5 \omega_i^2 = k_m \omega_i^2, \; k_m = \beta_\rho D^5 / k_p. \quad (20)$$

The presence of the torque μ_i in equation (19) reflects the fact that when the propeller rotates, due to air resistance, a moment arises that prevents this rotation. To overcome this moment, the same torque is required on the engine shaft in the opposite direction. From equation (19) it follows

$$J_r \boldsymbol{n}_B\dot{\omega}_i = \boldsymbol{n}_B\mu_i - J_r\dot{\boldsymbol{\omega}}_B^{BE} - \boldsymbol{\omega}_B^{BE} \times (J_r(\boldsymbol{\omega}_B^{BE} + \boldsymbol{n}_B\omega_i)). \quad (21)$$

Multiplying equation (21) by the vector $\boldsymbol{n}_B^T$ gives

$$\boldsymbol{n}_B^T J_r \boldsymbol{n}_B\dot{\omega}_i = \mu_i - \boldsymbol{n}_B^T J_r \dot{\boldsymbol{\omega}}_B^{BE}. \quad (22)$$

Whence, given that $\boldsymbol{n}_B^T J_r \boldsymbol{n}_B = J_r$, it follows

DOI 10.15588/1607-3274-2025-2-20

$$\dot{\omega}_i = \frac{\mu_i}{J_r} - \boldsymbol{n}_B^T \dot{\boldsymbol{\omega}}_B^{BE}. \quad (23)$$

Substituting expression (23) into equation (16) and the necessary transformations yield

$$\boldsymbol{J}\dot{\boldsymbol{\omega}}_B^{BE} = -\boldsymbol{n}_B(\mu_1 + \mu_2 - \mu_3 - \mu_4) + \boldsymbol{M}_g + \boldsymbol{M}_B. \quad (24)$$

or taking into account formula (20) it follows

$$\boldsymbol{J}\dot{\boldsymbol{\omega}}_B^{BE} = -\boldsymbol{n}_B k_m(\omega_1^2 + \omega_2^2 - \omega_3^2 - \omega_4^2) + \boldsymbol{M}_g + \boldsymbol{M}_B. \quad (25)$$

Let us introduce the following matrix into consideration

$$\boldsymbol{F} = \begin{pmatrix} -k_p\ell & 0 & k_p\ell & 0 \\ -k_m & k_m & -k_m & k_m \\ 0 & k_p\ell & 0 & -k_p\ell \end{pmatrix}. \quad (26)$$

Then equation (25) can be written in the following form

$$\boldsymbol{J}\dot{\boldsymbol{\omega}}_B^{BE} = \boldsymbol{M}_g + \boldsymbol{F}\begin{pmatrix} \omega_1^2 \\ \omega_2^2 \\ \omega_3^2 \\ \omega_4^2 \end{pmatrix}. \quad (27)$$

An equation describing the quadcopter angular orientation is needed to fully describe its spatial motion. This equation has the following form when a quaternion is used [19]:

$$\dot{\lambda}_0^{EB} = -\left(\boldsymbol{\omega}_B^{BE}\right)^T \boldsymbol{\lambda}_{EB}, \ \dot{\boldsymbol{\lambda}}_{EB} = \lambda_0^{EB}\boldsymbol{\omega}_B^{BE} + \boldsymbol{\lambda}_{EB} \times \boldsymbol{\omega}_B^{BE}. \quad (28)$$

Thus, the spatial motion of the quadcopter is described by the following system of differential equations

$$\begin{cases} m\ddot{\boldsymbol{r}}_E = k_p(\omega_1^2 + \omega_2^2 + \omega_3^2 + \omega_4^2)\boldsymbol{n}_E + \boldsymbol{G}_E; \\ \boldsymbol{J}\dot{\boldsymbol{\omega}}_B^{BE} = \boldsymbol{M}_g + \boldsymbol{M}_u; \\ \dot{\lambda}_0^{EB} = -\left(\boldsymbol{\omega}_B^{BE}\right)^T \boldsymbol{\lambda}_{EB}; \\ \dot{\boldsymbol{\lambda}}_{EB} = \lambda_0^{EB}\boldsymbol{\omega}_B^{BE} + \boldsymbol{\lambda}_{EB} \times \boldsymbol{\omega}_B^{BE}, \end{cases} \quad (29)$$

where

$$\boldsymbol{M}_u = \boldsymbol{F}\begin{pmatrix} \omega_1^2 \\ \omega_2^2 \\ \omega_3^2 \\ \omega_4^2 \end{pmatrix}. \quad (30)$$

The algorithms for controlling the spatial motion of a quadcopter were built on the assumption that on board the quadcopter there is information about the vector $\boldsymbol{r}_E$, the angular velocity vector $\boldsymbol{\omega}_B^{BE}$ and the orientation of the frame BFF relative to the frame EFF in the form of a quaternion $\boldsymbol{\Lambda}_{EB}$. The main tasks of spatial motion control are solved using the following algorithms:

– algorithm for determining the required orientation of the propellers thrust vector in the EFFs, which ensures the transfer of the quadcopter from the current position to the desired one;

– algorithm for calculating the torque, which ensures that the real direction of the thrust force coincides with the calculated one;

– algorithm for calculating the torque, which ensures stabilization of the yaw angle.

Let us introduce the following variables $\boldsymbol{x}_1 = \boldsymbol{r}_E$, $\boldsymbol{x}_2 = \dot{\boldsymbol{r}}_E$, $\boldsymbol{F}_E = \boldsymbol{u}$ and write equation (4) in Cauchy form

$$\dot{\boldsymbol{x}} = \boldsymbol{A}\boldsymbol{x} + \boldsymbol{B}\boldsymbol{u}, \quad (31)$$

where

$$\boldsymbol{A} = \begin{pmatrix} 0 & \boldsymbol{I}_3 \\ 0 & 0 \end{pmatrix}, \ \boldsymbol{B} = \begin{pmatrix} 0 \\ \boldsymbol{I}_3 \end{pmatrix}, \ \boldsymbol{x} = \begin{pmatrix} \boldsymbol{x}_1 \\ \boldsymbol{x}_2 \end{pmatrix}, \ \boldsymbol{I}_3 = \begin{pmatrix} 1 & 0 & 0 \\ 0 & 1 & 0 \\ 0 & 0 & 1 \end{pmatrix}.$$

For system (31), the following terminal control problem is formulated: *find a control* $\boldsymbol{u}$ *that transfers system* (31) *from the current state* $\boldsymbol{x}(t_0)$ *at time* t_0 *to the given state* $\boldsymbol{x}(t_1)$ *at time* t_1 *and provides the minimum of the functional* $V(\boldsymbol{u}) = \frac{1}{2}\int_{t_0}^{t_1} \|\boldsymbol{u}\|^2 dt$. *The times* t_0 *and* t_1 *are given.*

This problem can be formulated as a two-point boundary value problem, represented as a Hamiltonian system with a maximum condition for the control Hamiltonian (Pontryagin's maximum principle [20]).

To solve this problem, let us set the boundary conditions for system (31) in the form

$$\boldsymbol{x}_1(t_0) = \boldsymbol{r}_E(t_0), \ \boldsymbol{x}_2(t_0) = \dot{\boldsymbol{r}}_E(t_0), \quad (32)$$

$$\boldsymbol{x}_1(t_1) = \boldsymbol{r}_E(t_1), \ \boldsymbol{x}_2(t_1) = \dot{\boldsymbol{r}}_E(t_1), \quad (33)$$

and the Hamiltonian has the form

$$H = \frac{1}{2}\|\boldsymbol{u}\|^2 + \boldsymbol{\mu}^T(\boldsymbol{A}\boldsymbol{x} + \boldsymbol{B}\boldsymbol{u}). \quad (34)$$

In expression (34) $\boldsymbol{\mu} = \begin{pmatrix} \boldsymbol{\mu}_1 \\ \boldsymbol{\mu}_2 \end{pmatrix}$, is the related variable and $\boldsymbol{\mu}_1, \boldsymbol{\mu}_2$ are the three dimensional vectors. The optimality conditions are of the form

DOI 10.15588/1607-3274-2025-2-20

$$\frac{\partial H}{\partial \boldsymbol{x}} = -\dot{\boldsymbol{\mu}} = \boldsymbol{A}^T \boldsymbol{\mu}\,, \tag{35}$$

$$\frac{\partial H}{\partial \boldsymbol{\mu}} = \dot{\boldsymbol{x}} = \boldsymbol{A}\boldsymbol{x} + \boldsymbol{B}\boldsymbol{u}\,, \tag{36}$$

$$\frac{\partial H}{\partial \boldsymbol{u}} = \boldsymbol{u} + \boldsymbol{B}^T \boldsymbol{\mu} = 0\,. \tag{37}$$

From condition (37) it follows

$$\boldsymbol{u} = -\boldsymbol{B}^T \boldsymbol{\mu}\,. \tag{38}$$

Substituting condition (38) into equation (36) yields the equation of a two-point boundary value problem in the form of an extended system

$$\boldsymbol{Y} = \boldsymbol{Q}\boldsymbol{Y} + \begin{pmatrix} \boldsymbol{B} \\ 0 \end{pmatrix} \boldsymbol{G}_E, \boldsymbol{Y}(t) = \begin{pmatrix} \boldsymbol{x}(t) \\ \boldsymbol{\mu}(t) \end{pmatrix}, \boldsymbol{Q} = \begin{pmatrix} \boldsymbol{A} & \boldsymbol{B}\boldsymbol{B}^T \\ 0 & -\boldsymbol{A}^T \end{pmatrix}. \tag{39}$$

The solution to system (39) can be written as

$$\boldsymbol{x}(t) = \boldsymbol{\Phi}_{11}(t, t_0)\boldsymbol{x}(t_0) + \boldsymbol{\Phi}_{12}(t, t_0)\boldsymbol{\mu}(t_0), \tag{40}$$

$$\boldsymbol{\mu}(t) = \boldsymbol{\Phi}_{22}(t, t_0)\boldsymbol{\mu}(t_0)\,, \tag{41}$$

where $\boldsymbol{\Phi}(t_0, t) = \begin{pmatrix} \boldsymbol{\Phi}_{11}(t, t_0) & \boldsymbol{\Phi}_{12}(t, t_0) \\ 0 & \boldsymbol{\Phi}_{22}(t, t_0) \end{pmatrix}$ is the transition matrix of the extended system. The initial value of the vector $\boldsymbol{\mu}(t)$ is found by the formula

$$\boldsymbol{\mu}(t_0) = \boldsymbol{\Phi}_{12}^{-1}(t_1, t_0)[\boldsymbol{x}(t_1) - \boldsymbol{\Phi}_{11}(t_1, t_0)\boldsymbol{x}(t_0)]\,. \tag{42}$$

The calculated control values $\boldsymbol{u}^*$, trajectory $\boldsymbol{r}_E^*(t)$ and velocity $\dot{\boldsymbol{r}}_E^*(t)$ when moving the quadcopter from the current position to the desired one can be found as follows

$$\boldsymbol{u}^* = -\boldsymbol{B}^T \boldsymbol{\mu} = -\boldsymbol{\mu}_2\,, \tag{43}$$

$$\boldsymbol{r}_E^*(t) = \boldsymbol{x}_1(t)\,, \tag{44}$$

$$\dot{\boldsymbol{r}}_E^*(t) = \boldsymbol{x}_2(t)\,. \tag{45}$$

In this case, according to equation (4), the calculated force is determined by the expression

$$\boldsymbol{F}_E^*(t) = m\ddot{\boldsymbol{r}}_E^*(t) = m\boldsymbol{u}^*\,. \tag{46}$$

The force $\boldsymbol{F}_E^*(t)$ is the calculated total force. The real total force $\boldsymbol{F}_E(t)$ will differ from the calculated one due to the presence of disturbing forces. The difference in forces will lead to the quadcopter moving along a certain trajectory $\boldsymbol{r}_E(t)$ different from the calculated trajectory $\boldsymbol{r}_E^*(t)$. To eliminate this phenomenon, it is necessary to add a stabilizing component in the form of feedback on the state through the thrust force of the propellers. To find this component, consider the equation of the pointing error

$$\boldsymbol{e} = \boldsymbol{r}_E(t) - \boldsymbol{r}_E^*(t)\,. \tag{47}$$

This error can be found by subtracting equation (46) from equation (4):

$$m\ddot{\boldsymbol{e}}(t) = m(\ddot{\boldsymbol{r}}_E(t) - \ddot{\boldsymbol{r}}_E^*(t)) = \boldsymbol{F}_E(t) - \boldsymbol{F}_E^*(t) = \Delta\boldsymbol{F}\,, \tag{48}$$

which means

$$\boldsymbol{F}_E = \boldsymbol{F}_E^* + \Delta\boldsymbol{F}\,. \tag{49}$$

Let us choose $\Delta\boldsymbol{F}$ such that

$$\Delta\boldsymbol{F} = -m(\boldsymbol{K_1}\boldsymbol{e} + \boldsymbol{K_2}\dot{\boldsymbol{e}})\,, \tag{50}$$

where

$$\boldsymbol{K}_1 = diag(k_{1i}),\ \boldsymbol{K}_2 = diag(k_{2i}),\quad i = 1, 2, 3. \tag{51}$$

Then equation (48) can be written as

$$\ddot{\boldsymbol{e}}(t) = -(\boldsymbol{K_1}\boldsymbol{e} + \boldsymbol{K_2}\dot{\boldsymbol{e}})\,. \tag{52}$$

According to the main theorem on the asymptotic stability of a linear system, equation (52) for $k_{1i} > 0$ and $k_{2i} > 0$ is asymptotically stable and the quadcopter state vector will tend to the calculated one. In this case, the required direction of the force $\boldsymbol{P}_E(t)$ in the basis EFF will be determined by the expression

$$\boldsymbol{n}_E^*(t) = \frac{\boldsymbol{P}_E(t)}{\|\boldsymbol{P}_E(t)\|} = \frac{\boldsymbol{F}_E(t) - \boldsymbol{G}_E}{\|\boldsymbol{F}_E(t) - \boldsymbol{G}_E\|}\,. \tag{53}$$

Comparing (53) with (11), the equation for determining the required pitch ϑ^* and roll φ^* angles can be obtained:

$$\boldsymbol{n}_E^*(t) = \frac{\boldsymbol{P}_E(t)}{\|\boldsymbol{P}_E(t)\|} = \begin{pmatrix} -\sin\vartheta^* \\ \cos\vartheta^* \cos\varphi^* \\ \cos\vartheta^* \sin\varphi^* \end{pmatrix}, \tag{54}$$

$$\vartheta^*(t) = -\arcsin n_{1E}^*(t)\,, \tag{55}$$

DOI 10.15588/1607-3274-2025-2-20

$$\varphi^*(t) = -\arctan\frac{n^*_{3E}(t)}{n^*_{2E}(t)}. \quad (56)$$

In the hover mode $\ddot{\boldsymbol{r}}_E(t_1) = 0$. Then, according to expression (6), $\boldsymbol{P}_E(t_1) = -\boldsymbol{G}_E$ and

$$\boldsymbol{n}^*_E(t_1) = \frac{\boldsymbol{P}_E(t_1)}{\|\boldsymbol{P}_E(t)\|} = -\frac{\boldsymbol{G}_E(t_1)}{\|\boldsymbol{G}_E(t)\|} = \begin{pmatrix}0\\1\\0\end{pmatrix}. \quad (57)$$

Thus, when hovering, the required direction of the total thrust force of the propellers coincides with the direction of the local vertical. In this case

$$\varphi^*(t_1) = 0, \quad (58)$$

$$\vartheta^*(t_1) = 0, \quad (59)$$

and the program yaw angle $\psi^*(t)$ is a free parameter selected based on the quadcopter yaw angle requirements.

Now we will perform the synthesis of control of the angular motion of the quadcopter, ensuring the coincidence of the real direction of the thrust force of the propellers with the calculated one. Let us consider the quaternion mapping $\boldsymbol{N}^*_B$ of the vector $\boldsymbol{n}^*_B$. Its scalar part $scal(\boldsymbol{N}^*_B) = 0$, and vector part $vect(\boldsymbol{N}^*_B) = \boldsymbol{n}^*_B$. Since the quaternion $\boldsymbol{N}^*_B$ is a normalized quaternion, the quaternion equation is valid for it [21]

$$\ddot{\boldsymbol{N}}^*_B = \boldsymbol{U}_n - \left\|\dot{\boldsymbol{N}}^*_B\right\|^2 \boldsymbol{N}^*_B, \quad (60)$$

where $\boldsymbol{U}_n$ is an arbitrary quaternion with a zero scalar part, specifying which can form the required character of the change in the vector $\boldsymbol{n}^*_B$ projections on the BFF axes. In this case, the quaternion $\boldsymbol{U}_n$ satisfies the constraint

$$scal(\tilde{\boldsymbol{N}}^*_B \circ \boldsymbol{U}_n) = 0. \quad (61)$$

From constraint (61) it follows

$$(\boldsymbol{n}^*_B)^T \boldsymbol{U}_n = 0. \quad (62)$$

The vector form of equation (63) is

$$\ddot{\boldsymbol{n}}^*_B = \boldsymbol{u}_n - \left\|\dot{\boldsymbol{n}}^*_B\right\|^2 \boldsymbol{n}^*_B. \quad (63)$$

Let us represent the control $\boldsymbol{u}_n$ as follows

$$\boldsymbol{u}_n = -\boldsymbol{n}^*_B \times \boldsymbol{n}^*_B \times \boldsymbol{\tau}. \quad (64)$$

With this choice of $\boldsymbol{u}_n$, the relation (62) will hold for any $\boldsymbol{\tau}$. Taking into account (64), equation (63) can be written as

$$\ddot{\boldsymbol{n}}^*_B = -\boldsymbol{n}^*_B \times \boldsymbol{n}^*_B \times \boldsymbol{\tau} - \left\|\dot{\boldsymbol{n}}^*_B\right\|^2 \boldsymbol{n}^*_B. \quad (65)$$

Let us decompose the left-hand side of equation (65) into two components: perpendicular $\boldsymbol{n}^*_B$ and parallel $\boldsymbol{n}^*_B$:

$$-\boldsymbol{n}^*_B \times \boldsymbol{n}^*_B \times \ddot{\boldsymbol{n}}^*_B + \boldsymbol{n}^*_B \boldsymbol{n}^{*T}_B \ddot{\boldsymbol{n}}^*_B = \\ = -\boldsymbol{n}^*_B \times \boldsymbol{n}^*_B \times \boldsymbol{\tau} - \left\|\dot{\boldsymbol{n}}^*_B\right\|^2 \boldsymbol{n}^*_B. \quad (66)$$

Taking into account (64) and (65) transforming (66) gives

$$-\boldsymbol{n}^*_B \times \boldsymbol{n}^*_B \times (\ddot{\boldsymbol{n}}^*_B - \boldsymbol{\tau}) = \left(\boldsymbol{n}^{*T}_B \ddot{\boldsymbol{n}}^{*T}_B + \left\|\dot{\boldsymbol{n}}^*_B\right\|^2\right)\boldsymbol{n}^*_B = \\ = \left(-\left\|\dot{\boldsymbol{n}}^*_B\right\|^2 + \left\|\dot{\boldsymbol{n}}^*_B\right\|^2\right)\boldsymbol{n}^*_B. \quad (67)$$

From relation (67) it follows

$$\ddot{\boldsymbol{n}}^*_B = \boldsymbol{\tau} + \alpha \boldsymbol{n}^*_B, \quad (68)$$

where α is an arbitrary parameter. Since α is an arbitrary parameter, when solving various problems of controlling the motion of the vector $\boldsymbol{n}^*_B$ it can be set equal to zero ($\alpha = 0$). In this case, the dynamic model for synthesizing the control $\boldsymbol{\tau}$ takes on a simple form

$$\ddot{\boldsymbol{n}}^*_B = \boldsymbol{\tau}. \quad (69)$$

This equation is a linear equation with constant coefficients and allows the application of well-developed methods of the theory of linear systems with constant coefficients in the synthesis of control laws.

The control $\boldsymbol{u}_n$ is virtual, the real control is the control moment $\boldsymbol{M}_u$. Therefore, when using equation (69) to solve the problem of controlling the orientation of the quadcopter, it is necessary to know the dependence of the rotational moment $\boldsymbol{M}_u$ on the elements of the control vector $\boldsymbol{u}_n$. According to the work [22], this dependence has the form

$$\boldsymbol{M}_u = -\boldsymbol{M}_g - \boldsymbol{J}(\boldsymbol{n}^*_B \times (\boldsymbol{u}_n - \boldsymbol{p})), \quad (70)$$

where

$$\boldsymbol{p} = -\boldsymbol{\omega}^{BE}_B \times \left(\dot{\boldsymbol{n}}^*_B + \tilde{\dot{\boldsymbol{n}}}^*_B\right) + \ddot{\tilde{\boldsymbol{n}}}^*_B, \quad (71)$$

DOI 10.15588/1607-3274-2025-2-20

$$\dot{\boldsymbol{n}}_B^* = -\boldsymbol{\omega}_B^{BE} \times \boldsymbol{n}_B^* + \tilde{\dot{\boldsymbol{n}}}_B^*, \quad (72)$$

$$\tilde{\dot{\boldsymbol{n}}}_B^* = \tilde{\boldsymbol{\Lambda}}_{EB} \circ \dot{\boldsymbol{n}}_E^* \circ \boldsymbol{\Lambda}_{EB}, \quad (73)$$

$$\tilde{\ddot{\boldsymbol{n}}}_B^* = -\dot{\boldsymbol{\omega}}_B^{BE} \times \boldsymbol{n}_B^* + \boldsymbol{p}, \quad (74)$$

$$\ddot{\tilde{\boldsymbol{n}}}_B^* = \tilde{\boldsymbol{\Lambda}}_{EB} \circ \ddot{\boldsymbol{n}}_B^* \circ \boldsymbol{\Lambda}_{EB}. \quad (75)$$

In order for the real direction of the propellers' thrust to coincide with the calculated one, it is necessary to find the control $\boldsymbol{u}_n$ that ensures asymptotic stability of the equilibrium position

$$\boldsymbol{n}_B^* = \boldsymbol{n}_B. \quad (76)$$

To do this, we will use the equation of motion of the vector $\boldsymbol{n}_B^*$ in the form (69), and as a result

$$\ddot{\boldsymbol{n}}_B^* = \boldsymbol{\tau}. \quad (77)$$

Consider the control error

$$\boldsymbol{e} = \boldsymbol{n}_B^* - \boldsymbol{n}_B. \quad (78)$$

Given that $\boldsymbol{n}_B$ is a constant vector, the following equation is valid for the error

$$\ddot{\boldsymbol{e}}_B = \boldsymbol{\tau}. \quad (79)$$

It is obvious that the law of control

$$\boldsymbol{\tau} = -\boldsymbol{K}_1 \boldsymbol{e} - \boldsymbol{K}_2 \dot{\boldsymbol{n}}_B^* \quad (80)$$

provides asymptotic stability to the equilibrium position $\boldsymbol{e} = 0$, $\dot{\boldsymbol{e}} = 0$. In this case, the control $\boldsymbol{u}_n$ will be determined by the relation (64), and the real control moment $\boldsymbol{M}_u$ by the relation (70). To calculate the moment $\boldsymbol{M}_u$, it is necessary to know the vectors $\dot{\boldsymbol{n}}_E^*$ and $\ddot{\boldsymbol{n}}_E^*$. There are two ways to find these variables: analytical and numerical. Analytical is very cumbersome, so in this case, given that $\boldsymbol{n}_E^*$ is a smooth analytical function of time, it is easier to do it numerically.

To construct an algorithm for stabilizing the yaw angle, let us consider the quaternion $\boldsymbol{\Lambda}_{EB}$. According to [21], the following equation is valid for it

$$\ddot{\boldsymbol{\Lambda}}_{EB} = \boldsymbol{U}_\Lambda - \left\| \dot{\boldsymbol{\Lambda}}_{EB} \right\|^2 \boldsymbol{\Lambda}_{EB}, \quad (81)$$

where $\boldsymbol{U}_\Lambda$ is an arbitrary quaternion, specifying which can form the desired angular motion of the BFF relative EFF. In this case, the moment $\boldsymbol{M}_u$ is determined by the expression

$$\boldsymbol{M}_u = -2\boldsymbol{J}(\boldsymbol{\lambda}_{EB} \times \boldsymbol{u}_\Lambda) + \boldsymbol{\omega}_B^{BE} \times \boldsymbol{J}\boldsymbol{\omega}_B^{BE}, \quad (82)$$

where $\boldsymbol{u}_\Lambda$ is the vector part of a quaternion $\boldsymbol{U}_\Lambda$. The quaternion $\boldsymbol{\Lambda}_{EB}$ is a normalized quaternion and has only three independent coordinates, the fourth coordinate is determined from the condition $\left\| \boldsymbol{\Lambda}_{EB} \right\| = 1$. Let us choose its vector part $\boldsymbol{\lambda}_{EB}$ as independent coordinates and consider the equation that describes its change in time

$$\ddot{\boldsymbol{\lambda}}_{EB} = \boldsymbol{u}_\Lambda - \left(\left(\dot{\lambda}_0^{EB} \right)^2 + \dot{\boldsymbol{\lambda}}_{EB}^T \dot{\boldsymbol{\lambda}}_{EB} \right) \boldsymbol{\lambda}_{EB}. \quad (83)$$

In [21] it is shown that the control law

$$\boldsymbol{u}_\Lambda = -k_1 \boldsymbol{\lambda}_{EB} - k_2 \dot{\boldsymbol{\lambda}}_{EB}, \quad k_1 > 0, \; k_2 > 0 \quad (84)$$

ensures asymptotic stability of the equilibrium position

$$\boldsymbol{\lambda}_{EB}^T = (0 \;\; 0 \;\; 0), \quad \dot{\boldsymbol{\lambda}}_{EB}^T = (0 \;\; 0 \;\; 0), \quad (85)$$

and as a consequence the asymptotic stability of the equilibrium position

$$\boldsymbol{\Lambda}_{EB} = 1, \quad \dot{\boldsymbol{\Lambda}}_{EB} = 0, \quad (86)$$

that is, the stabilization of BFF relative to EFF.

4 EXPERIMENTS

A numerical simulation of the proposed algorithms was carried out to analyze the qualitative features of the algorithm. The parameters of the quadcopter model are presented in Table 1. The flight from the starting point to a given one with coordinates $\boldsymbol{r}_E(t_1) = (1000;\; 300;\; -4000)^T$ and hovering over it were simulated. The initial values of the quadcopter angular orientation (for which the graphs below are given) were set as follows: $\omega_B^{BE} = 0$, $\varphi = 10^\circ$, $\psi = -10^\circ$ and $\vartheta = 10^\circ$. After hovering, the quadcopter should turn around at an angle $\psi = 45^\circ$. The flight time from the starting point to the given one was chosen to be 300 seconds.

Table 1 – Quadcopter model parameters

Parameter	Description	Value	Units
g	Gravity	9.81	m/s^2
m	Mass	0.468	kg
ℓ	Distance	0.225	m
J_r	Rotor Inertia	$3.4 \cdot 10^{-5}$	$kg \cdot m^2$
J_x	Roll Inertia	$4.9 \cdot 10^{-3}$	$kg \cdot m^2$
J_y	Pitch Inertia	$4.9 \cdot 10^{-3}$	$kg \cdot m^2$
J_z	Yaw Inertia	$8.8 \cdot 10^{-3}$	$kg \cdot m^2$
k_p	Proportionality Constant	$2.9 \cdot 10^{-5}$	
k_m	Proportionality Constant	$1.1 \cdot 10^{-6}$	

DOI 10.15588/1607-3274-2025-2-20

5 RESULTS

Figure 3 shows graphs of changes in the coordinates of the centre of mass of the quadcopter over time, Fig. 4 shows graphs of changes in the centre of mass velocities over time, Fig. 5 shows the orientation angles of the quadcopter, and Fig. 6 shows the angular velocities.

6 DISCUSSION

In this study, the quadcopter was examined as a control object, its flight mechanics analyzed, and a novel methods for synthesizing algorithms for spatial motion control of the quadcopter were proposed. Based on the obtained quadcopter motion model, algorithms for controlling the quadcopter's spatial motion were developed, namely, an algorithm for determining the required direction of the propeller thrust to translate the quadcopter from its current position to the desired one and algorithms for its angular motion control.

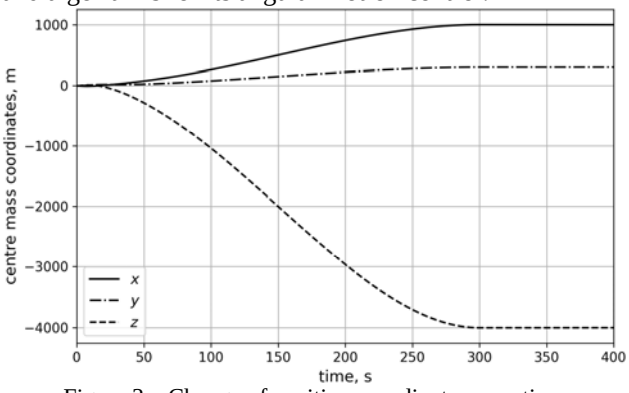

Figure 3 – Change of position coordinates over time

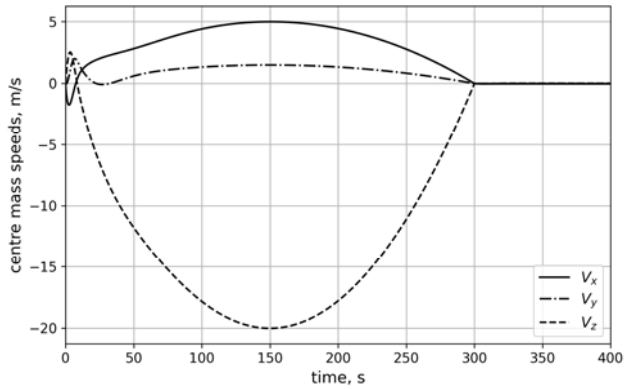

Figure 4 – Change the position coordinate velocities over time

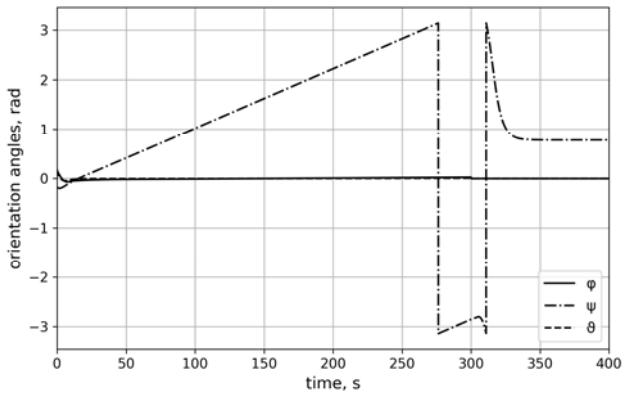

Figure 5 – Change the quadcopter orientation angles over time

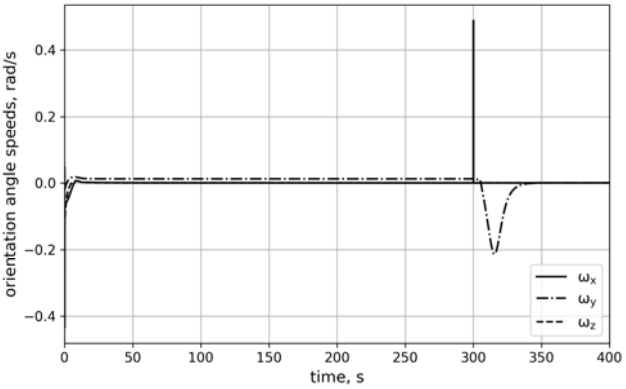

Figure 6 – Change the quadcopter angular speeds over time

The algorithm development process consists of two main parts. The first part is creating an algorithm to move a quadcopter from its current position to a specified one. For this, the approach from [23] was used, its essence is to construct an analytical solution to the boundary value problem for a linear stationary system without control constraints. This approach gives acceptable results when the system is not affected by external disturbances and there are no measurement errors. The calculated direction $\boldsymbol{n}_B^*$ of the propellers' thrust force due to disturbing forces may differ from the actual direction $\boldsymbol{n}_B$. To eliminate this phenomenon, a stabilizing component in the state feedback form was added to the analytical algorithm for solving a two-point boundary value problem.

In the second part, a novel method for constructing a quadcopter angular motion control algorithm was proposed, based on the motion of vector quaternion equation developed by authors in the works [21, 22]. The use of a dynamic quaternion equation of motion of the vector has greatly simplified control synthesis, reducing it to a set of second-order integrating links. In many cases, the control synthesis problem has an analytical solution for such systems. Control algorithms derived from this model are implemented much more simply than those synthesized from the traditional model, which includes the dynamical Euler equation and the kinematic equation for the quaternion.

The proposed algorithms were numerically simulated, and the results demonstrated that the quadcopter flew from the starting point to the target point within 300 seconds. It then turned at a 45-degree angle and hovered over the target location. The results confirmed the proposed algorithms' efficiency in controlling the quadcopter's spatial movement.

CONCLUSIONS

A mathematical model of a quadcopter motion as a control object was developed. Based on this model the algorithms for quadcopter spatial motion control were constructed. Control algorithms include determining the required direction of the propellers' thrust force to transfer the quadcopter from the current position to the given one and control angular motion, which ensures the

DOI 10.15588/1607-3274-2025-2-20

coincidence of the real direction of the propellers' thrust force with the calculated one and yaw angle stabilization.

The scientific novelty of the obtained results is that the quadcopter angular motion control algorithms developed based on the dynamic equation for the quaternion [21]. To eliminate the difference between the real direction of the thrust force and the calculated one a stabilizing component in the form of feedback on the state was added to the known analytical algorithm for solving a two-point boundary value problem. This significantly improved the accuracy of guiding the quadcopter to the given position.

The practical significance of the obtained results is that the developed algorithms allow the implementation of all main modes of quadcopter autonomous flight: stabilization mode in which the quadcopter automatically keeps zero roll and pitch angles and stabilizes the yaw angle; mode of maintaining a given position in which the quadcopter automatically hovers over a given point on the earth's surface; mode of automatic flight along points; modes of automatic takeoff and landing.

Prospects for further research will focus on studying the qualitative aspects of quadcopter control processes affected by external disturbances and onboard sensor errors and developing algorithms for autonomous navigation without using GPS information.

ACKNOWLEDGEMENTS

The study was carried out within research topics "Research, development and improvement of methods, models and subsystems of computer systems, in particular, intelligent and cyber-physical systems" (No 04821) and "Research into the specifics of Industry 4.0 technologies, particularly when used in the IT industry" (No 04814), which are carried out at the Department of computer systems and networks of Zaporizhzhia Polytechnic National University.

REFERENCES

1. Cohen A. P., Shaheen S. A., Farrar E. M. Urban air mobility: history, ecosystem, market potential, and challenges, *IEEE Transactions on Intelligent Transportation Systems*, 2021, Vol. 22, No. 9, pp. 6074–6087. DOI: 10.1109/TITS.2021.3082767
2. Nawaz H., Ali H. M., Massan S. U. R. Applications of unmanned aerial vehicles: a review, *3C Tecnología. Glosas de innovación aplicadas a la pyme. Spec, 2019*, 2019, pp. 85–105. DOI: 10.17993/3ctecno.2019.specialissue3.85-105
3. Aslan M. F., Durdu A., Sabanci K. et al. A comprehensive survey of the recent studies with UAV for precision agriculture in open fields and greenhouses, *Applied Sciences*, 2022, Vol. 12, No. 3, Article ID 1047. DOI: 10.3390/app12031047
4. Santos O., Romero H., Salazar S. et al. Real-time stabilization of a quadrotor UAV: nonlinear optimal and suboptimal control, *Journal of Intelligent & Robotic Systems*, 2013, Vol. 70, No. 1–4, pp. 79–91. DOI: 10.1007/s10846-012-9711-8
5. Liu Y., Montenbruck J. M., Stegagno P. et al. A robust nonlinear controller for nontrivial quadrotor maneuvers: approach and verification, *Intelligent Robots and Systems (IROS) : IEEE/RSJ International Conference, Hamburg, 28 September – 02 October 2015 : proceeding*, IEEE, 2015, pp. 5410–5416. DOI: 10.1109/IROS.2015.7354142
6. Zhiwei H., Lu P., Tu Z. Nonsingular terminal sliding mode control for a quadrotor UAV with a total rotor failure, *Aerospace Science and Technology*, 2020, Vol. 98. Article ID 105716. DOI: 10.1016/j.ast.2020.105716
7. Li T., Zhang Y., Gordon B. W. Passive and active nonlinear fault-tolerant control of a quadrotor UAV based on sliding mode control technique, *Proceedings of the Institution of Mechanical Engineers, Part I: Journal of Systems and Control Engineering*, 2012, Vol. 227, No. 1, pp. 12–23. DOI: 10.1177/0959651812455293
8. Elkholy H., Habib M. K. Dynamic modeling and control techniques for a quadrotor, *Unmanned Aerial Vehicles: Breakthroughs in Research and Practice*. Hershey, IGI Global, 2019, Section 1, pp. 20–66. DOI: 10.4018/978-1-5225-8365-3.ch002
9. Ahmadi K., Asadi D., Merheb A. et al. Active fault-tolerant control of quadrotor UAVs with nonlinear observer-based sliding mode control validated through hardware in the loop experiments, *Control Engineering Practice*, 2023, Vol. 137. Article ID 105557. DOI: 10.1016/j.conengprac.2023.105557
10. Gong X., Bai Y., Peng C. et al. Trajectory tracking control of a quad-rotor UAV based on command filtered backstepping, *Intelligent Control and Information Processing : Third International Conference, Dalian, 15–17 July 2012 : proceeding*. IEEE, 2012, pp. 179–184. DOI: 10.1109/ICICIP.2012.6391413
11. Lee K. U., Choi Y. H., Park J. B. Backstepping based formation control of quadrotors with the state transformation technique, *Applied Sciences*, 2017, Vol. 7, No. 11. Article ID 1170. DOI: 10.3390/app7111170
12. Pham D.-A., Han S.-H. Critically leveraging theory for optimal control of quadrotor unmanned aircraft systems, *Applied Sciences*, 2024, Vol. 14, No. 6. Article ID 2414. DOI: 10.3390/app14062414
13. Hu K., Wu Y., Sun X.-M. Attitude controller design for quadrotors based on the controlled Hamiltonian system, *Chinese Control And Decision Conference (CCDC) : 29th Chinese Conference*, Chongqing, 28–30 May 2017 : proceeding. IEEE, 2017, pp. 5137–5141. DOI: 10.1109/CCDC.2017.7979407
14. Xian B., Diao C., Zhao B.et al. Nonlinear robust output feedback tracking control of a quadrotor UAV using quaternion representation, *Nonlinear Dynamics*, 2015, Vol. 79, pp. 2735–2752. DOI: 10.1007/s11071-014-1843-x
15. Idrissi M., Annaz F. Dynamic modelling and analysis of a quadrotor based on selected physical parameters, *International Journal of Mechanical Engineering and Robotics Research*, 2020, Vol. 9, No. 6, pp. 784–790. DOI: 10.18178/ijmerr.9.6.784-790
16. Roy R., Islam M., Sadman N. et al. A review on comparative remarks, performance evaluation and improvement strategies of quadrotor controllers, *Technologies*, 2021, Vol. 9, No. 2. Artical ID 37. DOI: 10.3390/technologies9020037

DOI 10.15588/1607-3274-2025-2-20

17. Maaruf M., Mahmoud M. S., Ma'arif A. A survey of control methods for quadrotor UAV, *International Journal of Robotics and Control Systems*, 2022, Vol. 2, No. 4, pp. 652–665. DOI: 10.31763/ijrcs.v2i4.743
18. Al-Husnawy T., Al-Ghanimi A. A review of control methods for quadrotor UAV, *Kufa Journal of Engineering*, 2024, Vol. 15, No. 4, pp. 98–124. DOI: 10.30572/2018/KJE/150408
19. Wittenburg J. Dynamics of systems of rigid bodies. Stuttgart, Teubner, 1977, 224 p. DOI: 10.1007/978-3-322-90942-8
20. Sage A. P., White C. C. Optimum systems control. 2th ed. Englewood Cliffs, N.J., Prentice-Hall, 1977, 372 p.
21. Yefymenko N., Kudermetov R. Quaternion models of a rigid body rotation motion and its application for spacecraft attitude control, *Acta Astronautica*, 2022, Vol. 194, pp. 76–82. DOI:10.1016/j.actaastro.2022.01.029
22. Yefymenko N., Kudermetov R. Dynamic model motion of vector and its application in spacecraft uniaxial orientation problems, *Space Science and Technology*, 2024, Vol. 30, No. 4, pp. 24–33. DOI: 10.15407/knit2024.04.024
23. Novikov A. K. Synthesis of optimal controls based on an analytical solution of a linear stationary two-point boundary value problem, *Radio Electronics, Computer Science, Control*, 2006, No. 2, pp. 133–156.

Received 18.02.2024.
Accepted 03.04.2024.

УДК 681.865

ТЕРМІНАЛЬНЕ КЕРУВАННЯ ПРОСТОРОВИМ РУХОМ КВАДРОКОПТЕРА

Єфименко М. В. – д-р техн. наук, професор, професор кафедри інформаційних технологій електронних засобів Національного університету «Запорізька політехніка», Запоріжжя, Україна.

Кудерметов Р. К. – канд. техн. наук, доцент, завідувач кафедри комп'ютерних систем та мереж Національного університету «Запорізька політехніка», Запоріжжя, Україна.

АНОТАЦІЯ

Актуальність. Побудова алгоритмів керування квадрокоптером є областю підвищеного інтересу, оскільки керування квадрокоптером принципово складна задача, незважаючи на його механічну простоту. Ключовою проблемою систем управління квадрокоптерами є ефективне поєднання трьох поступальних та трьох обертальних ступенів свободи руху для виконання унікальних цільових маневрів. Крім того, ці задачі актуальні у зв'язку з високою затребуваністю квадрокоптерів у різних видах діяльності людини, таких як кадастрова аерофотозйомка для моніторингу важкодоступних територій, доставка вантажів на невеликі відстані, військова справа тощо.

Мета роботи – розробка та обґрунтування нових методів побудови алгоритмів високоточного керування просторовим рухом квадрокоптера, що забезпечують його автономну роботу у всіх основних режимах польоту: режим стабілізації, режим утримання положення, режим автоматичного польоту з точки в точку, режим автоматичного зльоту та посадки.

Метод. Поставлена мета зумовила використання наступних методів дослідження. Для розробки алгоритмів розрахунку програмних траєкторій переведення квадрокоптера з поточного стану в заданий застосовано принцип максимуму Понтрягіна. Для синтезу та аналізу алгоритмів керування кутовим положенням квадрокоптера використано функції Ляпунова та методи модального керування. Для перевірки та підтвердження отриманих теоретичних результатів використано методи чисельного моделювання.

Результати. Запропоновано методику побудови алгоритмів керування просторовим рухом квадрокоптера, що складається з двох частин. Перша частина містить удосконалений метод побудови алгоритма переведення квадрокоптера з поточного положення в задане. У другій частині запропоновано оригінальний метод побудови алгоритмів керування орієнтацією квадрокоптера на основі динамічного рівняння для кватерніону.

Висновки. Запропонована математична модель руху квадрокоптера та методи побудови алгоритмів керування верифіковані чисельним моделюванням та можуть бути застосовані для розробки систем керування квадрокоптерами.

КЛЮЧОВІ СЛОВА: квадрокоптер, кватерніон, принцип максимуму Понтрягіна, гамільтоніан, функції Ляпунова.

ЛІТЕРАТУРА

1. Cohen A. P. Urban air mobility: history, ecosystem, market potential, and challenges / A. P. Cohen, S. A. Shaheen, E. M. Farrar // IEEE Transactions on Intelligent Transportation Systems. – 2021. – Vol. 22, No. 9. – P. 6074–6087. DOI: 10.1109/TITS.2021.3082767
2. Nawaz H. Applications of unmanned aerial vehicles: a review / H. Nawaz, H. M. Ali, S. U. R. Massan // 3C Tecnología. Glosas de innovación aplicadas a la pyme. Spec, 2019. – 2019. – P. 85–105. DOI: 10.17993/3ctecno.2019.specialissue3.85-105
3. A comprehensive survey of the recent studies with UAV for precision agriculture in open fields and greenhouses / [M. F. Aslan, A. Durdu, K. Sabanci et al.] // Applied Sciences. – 2022. – Vol. 12, No. 3. – Article ID 1047. DOI: 10.3390/app12031047
4. Real-time stabilization of a quadrotor UAV: nonlinear optimal and suboptimal control / [O. Santos, H. Romero, S. Salazar et al.] // Journal of Intelligent & Robotic Systems. – 2013. – Vol. 70, No. 1–4. – P. 79–91. DOI: 10.1007/s10846-012-9711-8
5. A robust nonlinear controller for nontrivial quadrotor maneuvers: approach and verification / [Y. Liu, J. M.

DOI 10.15588/1607-3274-2025-2-20

Montenbruck, P. Stegagno et al.] // Intelligent Robots and Systems (IROS) : IEEE/RSJ International Conference, Hamburg, 28 September – 02 October 2015 : proceeding. – IEEE, 2015. – P. 5410–5416. DOI: 10.1109/IROS.2015.7354142
6. Zhiwei H. Nonsingular terminal sliding mode control for a quadrotor UAV with a total rotor failure / H. Zhiwei, P. Lu, Z. Tu // Aerospace Science and Technology. – 2020. – Vol. 98. – Article ID 105716. DOI: 10.1016/j.ast.2020.105716
7. Li T. Passive and active nonlinear fault-tolerant control of a quadrotor UAV based on sliding mode control technique. / T. Li, Y. Zhang, B. W. Gordon // Proceedings of the Institution of Mechanical Engineers, Part I: Journal of Systems and Control Engineering. – 2012. – Vol. 227, No. 1. – P. 12–23. DOI: 10.1177/0959651812455293
8. Elkholy H. Dynamic modeling and control techniques for a quadrotor / H. Elkholy, M. K. Habib // Unmanned Aerial Vehicles: Breakthroughs in Research and Practice. – Hershey : IGI Global, 2019. – Section 1. – P. 20–66. DOI: 10.4018/978-1-5225-8365-3.ch002
9. Active fault-tolerant control of quadrotor UAVs with nonlinear observer-based sliding mode control validated through hardware in the loop experiments / [K. Ahmadi, D. Asadi, A. Merheb et al.] // Control Engineering Practice. – 2023. – Vol. 137. – Article ID 105557. DOI: 10.1016/j.conengprac.2023.105557
10. Trajectory tracking control of a quad-rotor UAV based on command filtered backstepping / [X. Gong, Y. Bai, C. Peng et al.] // Intelligent Control and Information Processing : Third International Conference, Dalian, 15–17 July 2012 : proceeding. – IEEE, 2012. – P. 179–184. DOI: 10.1109/ICICIP.2012.6391413
11. Lee K. U. Backstepping based formation control of quadrotors with the state transformation technique / K. U. Lee, Y. H. Choi, J. B. Park // Applied Sciences. – 2017. – Vol. 7, No. 11. – Article ID 1170. DOI: 10.3390/app7111170
12. Pham D.-A. Critically leveraging theory for optimal control of quadrotor unmanned aircraft systems / D.-A. Pham, S.-H. Han // Applied Sciences. – 2024. – Vol. 14, No. 6. – Article ID 2414. DOI: 10.3390/app14062414
13. Hu K. Attitude controller design for quadrotors based on the controlled Hamiltonian system / K. Hu, Y. Wu, X.-M. Sun // Chinese Control And Decision Conference (CCDC) : 29th Chinese Conference, Chongqing, 28–30 May 2017 : proceeding. – IEEE, 2017. – P. 5137–5141, DOI: 10.1109/CCDC.2017.7979407
14. Nonlinear robust output feedback tracking control of a quadrotor UAV using quaternion representation / [B. Xian, C. Diao, B. Zhao et al.] // Nonlinear Dynamics. – 2015. – Vol. 79. – P. 2735–2752. DOI: 10.1007/s11071-014-1843-x
15. Idrissi M. Dynamic modelling and analysis of a quadrotor based on selected physical parameters / M. Idrissi, F. Annaz // International Journal of Mechanical Engineering and Robotics Research. – 2020. – Vol. 9, No. 6. – P. 784–790. DOI: 10.18178/ijmerr.9.6.784-790
16. A review on comparative remarks, performance evaluation and improvement strategies of quadrotor controllers / [R. Roy, M. Islam, N. Sadman et al.] // Technologies. – 2021. – Vol. 9, No. 2. – Artical ID 37. DOI: 10.3390/technologies9020037
17. Maaruf M. A survey of control methods for quadrotor UAV / M. Maaruf, M. S. Mahmoud, A. Ma'arif // International Journal of Robotics and Control Systems. – 2022. – Vol. 2, No. 4. – P. 652–665. DOI: 10.31763/ijrcs.v2i4.743
18. Al-Husnawy T. A review of control methods for quadrotor UAV / T. Al-Husnawy, A. Al-Ghanimi // Kufa Journal of Engineering. – 2024. – Vol. 15, No. 4. – P. 98–124. DOI: 10.30572/2018/KJE/150408
19. Wittenburg J. Dynamics of systems of rigid bodies / J. Wittenburg – Stuttgart : Teubner, 1977. – 224 p. DOI: 10.1007/978-3-322-90942-8
20. Sage A. P. Optimum systems control. 2th ed. / A. P. Sage, C. C. White. – Englewood Cliffs, N.J. : Prentice-Hall, 1977. – 372 p.
21. Yefymenko N. Quaternion models of a rigid body rotation motion and its application for spacecraft attitude control / N. Yefymenko, R. Kudermetov // Acta Astronautica. – 2022. – Vol. 194. – P. 76–82. DOI:10.1016/j.actaastro.2022.01.029
22. Yefymenko N. Dynamic model motion of vector and its application in spacecraft uniaxial orientation problems / N. Yefymenko, R. Kudermetov // Space Science and Technology. – 2024. – Vol. 30, No. 4. – P. 24–33. DOI: 10.15407/knit2024.04.024
23. Novikov A. K. Synthesis of optimal controls based on an analytical solution of a linear stationary two-point boundary value problem / A. K. Novikov // Radio Electronics, Computer Science, Control. – 2006. – No. 2. – P. 133–156.

DOI 10.15588/1607-3274-2025-2-20

Наукове видання

Радіоелектроніка,

інформатика,

управління

№ 2/2025

Науковий журнал

Головний редактор – д-р техн. наук С. О. Субботін

Заст. головного редактора – д-р техн. наук Д. М. Піза

Комп’ютерне моделювання та верстання С. В. Зуб
Редактор англійських текстів С. О. Субботін

Оригінал-макет підготовлено у редакційно-видавничому відділі НУ «Запорізька політехніка»

Реєстрація суб’єкта у сфері друкованих медіа:
Рішення Національної ради України з питань телебачення і радіомовлення № 3040 від 07.11.2024 року
Ідентифікатор медіа: R30-05582

Підписано до друку 29.05.2025. Формат 60×84/8.
Папір офс. Різогр. друк. Ум. друк. арк. 28,25.
Тираж 300 прим. Зам. № 481.

69063, м. Запоріжжя, НУ «Запорізька політехніка», друкарня, вул. Жуковського, 64

Свідоцтво суб’єкта видавничої справи
ДК № 6952 від 22.10.2019.